Molecular and functional characterisation of Müller glia derived from retinal organoids formed by human pluripotent stem cells (hPSCs)

Weixin Wang

Thesis submitted to University College London for the degree of Doctor of Philosophy

Institute of Ophthalmology

Faculty of Brain Sciences

University College London

Novermber 2020

Declaration

I, Weixin Wang, confirm that the work presented in this thesis is my own. Where information has been derived from other sources, I confirm that this has been indicated in the thesis.

London, 2020

Acknowledgement

This thesis would not have been possible without the generous support of my supervisors Prof Astrid Limb and Prof Pete Coffey. I am particularly grateful to Astrid for offering me the opportunity to explore a research project on translational study and regenerative medicine for the past three and half years. Her invaluable support, patience and guidance always enlighten me and encourage me to seek for resilience to tackle challenges during this PhD study. Astrid's mentorship is far beyond science, she is a role model with enthusiasm on life and arts, and her beautiful characters have been the attributes that I have been looking up to and they will continue to influence me in the future. My learning experience on RNA-seq and critical thinking was supported by Dr Nick Owen, who offered valuable feedback; and Naheed, Joanne and Sudershana who have been warmly encouraging and helpful on handling admin works.

I am very fortunate to have made this Ph.D. journey an unforgettable memory with my 'Spare Limbs' buddies. Thank you Karen for taking my hands to make organoids and all the lab skills, and I really loved our lunch chat on anime, Japanese food and cats. My gratitude also goes to Erika, Will and Josh who have been always supportive on lab work and have brough enormous fund to our team. I've made a group of wonderful friends at IoO, and the research challenges were thankfully lightened up by these amazing 'Second and Third Floor people': I-Hui, He, Carla, Rita, Ashkon, Tiago, Yann, Christin, Qian, Yuyi, Kwan, Rintra and Meng-Chen. I will always remember those beautiful trips and parties we had in London, Baltimore, Hawaii, Barcelona and Vancouver. I am sure our friendships will last and we will remain connected wherever we are in the world.

Lastly, I am in debt to my parents who have been unconditionally supporting me to explore the world and to become the person I want to be. Thank you both for always backing me whenever I lose my confidence, and for encouraging me that all the hard work can be realised. I have been well supported by my partner Bobby. Thank you for always being there for me and going through all the ups and downs, despite the 8600km distance. Our morning calls, coffee brews, yoga lessons and everything you have taught me, have made me always stay curious and grow old with you. This thesis is dedicated to my family.

Abstract

Previous studies have shown that transplantation of human Müller glia into animal models of retinal degeneration improves visual functions, possibly due to their neuroprotective ability. Since sourcing Müller glia from adult donor retinae is not acceptable for therapeutic use, differentiating Müller glia from human pluripotent stem cells (hPSCs) constitutes an attractive approach for developing cell-based therapies to treat retinal degenerative diseases. However, it is important to examine the molecular and functional characteristics of Müller glia derived from retinal organoids and compare these with cells isolated from adult retina before they can be considered for development of cell therapies. The transcriptomic profile of Müller glia isolated from retinal organoids formed by hPSCs was also examined and compared to that of the well-characterised adult Müller cell line MIO-M1. In addition, the effect of cytokines on the neuroprotective response of these cells, as well as the neuroprotective functionality of culture supernatants on rat retinal ganglion cells (RGCs) were assessed.

RNA-sequencing revealed that hPSC-derived cells exhibited Müller glia-like transcriptomic profiles as compared to MIO-M1 and expressed a broad spectrum of genes known to confer neuroprotection. Short-term culture with TNF-α elicited a pleiotropic transcriptomic response in MIO-M1, with significant downregulation of gliotic genes and upregulation of antioxidant enzymes and immune mediators. Similarly, TNF-α significantly increased expression and release of several antioxidant enzymes in hPSC-derived Müller glia-like cells. Treatment of both, hPSC-derived or MIO-M1 cells with TGF-β1 did not change the expression of antioxidative enzymes in these cells *in vitro*. Culture supernatants of hPSC-derived cells induced neuroprotection of rat RGCs subjected to glutamate excitotoxicity, as shown by their better survival and structural integrity when compared to controls cultured without neurotrophic factors. Improved RGC survival was supported by the presence of various neuroprotective factors in the culture supernatants.

In conclusion, the present study demonstrates that hPSC-derived cells displayed Müller glia-like characteristics and neuroprotective potential, which has laid a solid foundation to accelerate the clinical translation of Müller glia cell therapies.

Impact Statement

The increase of ageing population coincides with the prevalence of visual degenerative diseases, with cataract and glaucoma representing the most common diseases leading to permanent loss of vision. The irreversible nature of retinal degeneration limits the current clinical management to delay the disease progress in these patients, whilst further development of visual impairments cannot be mitigated. Thanks to the ongoing study on Müller glia, the principal glial cells in the neural retina, scientists have developed a novel approach to target retinal degeneration using their neuroprotective potential. Evidence from research findings in the hosting laboratory identified that transplantation of human Müller glia into animal models of retinal degeneration have significantly improved visual function. These observations have been attributed to the release of various antioxidant enzymes and neurotrophins by Müller glia, however sourcing Müller glia from adult donor retinae is not acceptable for therapeutic risks use due to pathogenic and histocompatibility. On this basis, differentiating Müller glia from human pluripotent stem cells (hPSCs) constitutes a feasible approach for developing cell-based therapies to treat retinal degenerative diseases. However, human Müller glia with full molecular characterisation have yet been investigated nor the neuroprotective profile of these cells. This work capitalised on the pluripotency of human pluripotent stem cells to derive a well characterised cell type, and advances on protocols for three-dimensional retinal organoid formation to derive Müller cells suitable for clinical use. Retinal organoid-derived Müller glia were expanded *in vitro* and full characterisation on these cells was performed using immunohistochemical techniques, as well as *in vitro* models of retinal neural damage and next-generation sequencing. Established markers of Müller glia and the ability of these cells to produce neuroprotective molecules were detected using molecular biology tools to understand the similarity of these cells to human adult Müller glia isolated from cadaveric donors. This study has also explored both the change of global transcriptomics and neuroprotective profiles in response to inflammatory cytokines. Most importantly, the neuroprotective function of retinal organoid-derived Müller glia on retinal ganglion cells was examined. It was observed that the morphological features and viability of rat RGCs were maintained when these cells were subjected to neurotoxicity in the presence of conditioned medium collected from retinal

organoid-derived Müller glia. These findings collectively suggested that Müller glia have the therapeutic potential to release trophic factors to promote the survival of retinal cells.

The data reported in this PhD study has both academic and translational potential to the understanding of retinal degeneration and cell-based therapy development. It has added novel ideas of how Müller cells response to various stress conditions during retinal degeneration and highlight its neuroprotective profiles. Transcriptomic data on the analysis on Müller glia may contribute to future studies to investigate endogenous regeneration of the retina and its neuroprotection by Müller cells. In summary, this study provides important observations to allow further exploration of the therapeutic potential of Müller glia.

Table of Contents

Declaration 1
Acknowledgement 2
Abstract 3
Impact Statement 4
Table of Contents 6
Table of Figures 15
Table of Tables 20
Abbreviations 21
CHAPTER 1 General introduction 25
1.1 Anatomy of the human eye 25
1.1.1 The retina 26
1.1.2 Retinogenesis 28
1.2 Müller glia and its roles in the neural retina 30
1.2.1 Development of Müller glia 30
1.2.2 Characteristics of Müller glia 32
1.2.3 Implications of Müller glia in retinal regeneration and degeneration 33
1.2.4 Müller glia constitute the source of cytokines in retinal degeneration 37
1.3 Retinal degeneration and perspective therapies 38
1.3.1 Retinal degenerative diseases 38
1.3.2 Potential of cell-based therapies to treat retinal degeneration 41
1.4 Application of stem cells in cell-based therapies 43
1.4.1 Embryonic stem cells 43
1.4.2 Induced pluripotent stem cells 45
1.4.3 Adult tissue-specific stem cells 46
1.5 Objectives of this thesis 47

CHAPTER 2 Isolation of Müller glia from retinal organoids derived from human pluripotent stem cells 49

2.1 Introduction 49

2.1.1 *In vitro* generation of retinal organoids 49

2.2 Retinal organoids constitute an important tool to understand retinal development and for disease modelling *in vitro* 51

2.3 The application of transcriptomic profiling in retinal biology 52

2.4 Objectives and experimental outline 55

2.5 Results 58

2.5.1 Differentiation of hPSCs into retinal organoids 58

2.5.2 Presence of Müller glia markers within retinal organoids 61

2.5.3 Isolation of CD29-positive cells from retinal organoids and their *in vitro* propagation 65

2.5.4 Molecular characterisation of cells isolated from hPSC-formed retinal organoids 67

2.5.5 Characterisation of cells dissociated from retinal organoids by FACS analysis 70

2.5.6 Transcriptomic profiling of retinal organoid-derived Müller glia-like cells 74

2.5.6.1 Overview of RNA-seq libraries of hiPSC-MG1, hESC-MG1 and MIO-M1 cells 74

2.5.6.2 Gene ontology (GO) enrichment analysis of DEGs in hiPSC-MG1 and hESC-MG1 cells 78

2.5.6.3 Expression of markers of undifferentiated stem cells and other retinal cells in hiPSC-MG1 and hESC-MG1 90

2.5.6.4 Expression of characteristic Müller glia markers by hiPSC-MG1 and hESC-MG1 92

2.5.6.5 hiPSC-MG1 and hESC-MG1 expressed genes coding for proteins implicated in neurotrophic supports 97

2.5.6.6 Validation of RNA-seq data by qRT-PCR 102

2.6 Discussion 104
2.6.1 *In vitro* development of hPSCs-formed retinal organoids recapitulated major events of retinogensis 104
2.6.2 Cells isolated from hPSCs-formed retinal organoids acquired developing Müller glia-like fate 104
2.6.3 Differences in the formation of retinal organoids by pluripotent stem cells are reflected in their specific transcriptomes 109
2.6.4 Limitation of study 110
CHAPTER 3 Examination of the effect of TNF-α on Müller glia neuroprotective responses as revealed by transcriptomic analysis 111
3.1 Introduction 111
3.1.1 TNF-α and its signalling components 111
3.1.2 TNF-α signalling in neurodegeneration 115
3.1.3 TNF-α signalling and neuroprotection 117
3.2 Objectives and experimental outline 119
3.3 Results 122
3.3.1 Overview of transcriptomes profile of MIO-M1 cells following short-term culture with TNF-α 122
3.3.2 Gene ontology analysis of the differentially expressed genes 128
3.3.3 Genes involved in the TNF-α signalling pathway are upregulated in Müller glia by treatment with this cytokine 132
3.3.4 Genes mediating neuroinflammation were increased in MIO-M1 cells by TNF-α 135
3.3.5 Genes coding for neuroprotective factors were upregulated in Müller glia by TNF-α 139
3.3.6 TNF-α modulation of genes controlling Müller cell gliosis 140
3.3.7 Modulation of novel transcripts comprised of non-coding RNAs in Müller glia cultured with TNF-α 142
3.3.8 Validation of RNA-seq data by qPCR 145
3.4 Discussion 146

3.4.1 Activation of TNF-α and NFkB signalling pathways in Müller glia by TNF-α 146

3.4.2 Upregulation of inflammatory markers by TNF-α accompanied by upregulation of pro-survival genes in MIO-M1 cells 148

3.4.3 Downregulation of Müller glia genes associated with reactive gliosis suggests a novel *in vitro* neuroprotective effect of TNF-α on these cells 150

3.4.4 Non-coding DEGs might contribute to transcriptional regulation 152

3.4.5 Limitation of study 153

CHAPTER 4 Müller glia constitute an important source of antioxidants in the human retina 154

4.1 Introduction 154

4.1.1 Oxidative stress in the retina 154

4.1.2 Key antioxidant molecules in the retina 155

4.1.3 Transcriptional regulation of antioxidant enzymes 157

4.1.4 Pro-inflammatory cytokines promote oxidative stress 158

4.2 Objectives 159

4.3 Results 161

4.3.1 Human Müller glia express key antioxidant enzymes..... 161

4.3.2 Müller glia is the source of antioxidant enzymes in human retina 161

4.3.3 Effect of TNF-α on the expression of antioxidant enzymes by human Müller glia 165

4.3.4 Effect of TGF-β1 on the expression of antioxidant enzymes by human Müller glia..... 171

4.4 Discussion..... 175

4.4.1 Human Müller glia constitute a rich source of antioxidant enzymes in the neural retina 175

4.4.2 TNF-α treatment led to upregulation of neuroprotective factors . 176

4.4.3 TGF-β1 did not significantly modify anti-oxidative capacity in human Müller glia 180

4.4.4 Limitation of study 181

CHAPTER 5 Evaluation of the neuroprotective effect of retinal organoid-derived Müller glia on retinal ganglion cells 182

5.1 Introduction 182

5.1.1 Early development of mammalian RGCs 182

5.1.2 Morphological and molecular features of RGCs 183

5.1.3 Glutamate excitotoxicity as a cause of glaucoma 184

5.1.3.1 RGC involvement in glaucoma 184

5.1.3.2 Current treatments for glaucoma 185

5.1.3.3 Neuroprotection of RGCs 185

5.1.4 Available culture models for RGC degeneration 187

5.1.4.1 Retinal explant cultures 187

5.1.4.2 RGC cell lines 187

5.1.4.3 Primary RGC culture 188

5.1.5 Protocols to establish primary RGC culture 189

5.1.5.1 Flow cytometry sorting 189

5.1.5.2 Two-step immunopanning (TIP) 190

5.2 Objectives and experimental outline 192

5.3 Results 195

5.3.1 Standardisation of rat RGC culture by currently available protocols 195

5.3.1.1 Purification of rat RGCs using flow cytometry sorting 195

5.3.1.2 Viability and morphology of purified RGCs upon *in vitro* culture 202

5.3.2 Establishment of primary rat RGCs culture using TIP 202

5.3.2.1 Identification and morphology of rat RGCs 202

5.3.3 Glutamate mediated excitotoxicity in RGCs 205

5.3.4 Supernatants from cultured hESC-MG promoted RGC survival following glutamate excitotoxicity 207

5.3.4.1 Supernatants from cultured hESC-MG promoted RGC viability following glutamate exposure 207
5.3.4.2 Supernatants from cultured hESC-MG protected surviving RGC dendritic projection 211
5.3.5 Identification and quantification of key neuroprotective factors in hESC-derived Müller glia supernatants 215
5.4 Discussion 217
CHAPTER 6 General discussion 223
6.1 Retinal organoids constitute a source of cells committed to the Müller glia-like fate with substantial neuroprotective potential 224
6.2 Pleiotropic transcriptomic responses of human adult Müller glia induced by TNF-α 226
6.3 hPSC-derived Müller glia constitute a source of neuroprotective antioxidant enzymes in response to cytokine stimulation 228
6.4 hESC-derived Müller glia release neuroprotective factors for RGCs subjected to early glutamate excitotoxicity 229
6.5 Conclusions 231
CHAPTER 7 MATERIALS AND METHODS 232
7.1 Isolation of Müller glia from retinal organoids derived from human pluripotent stem cells 232
7.1.1 Culture of human pluripotent stem cells 232
7.1.1.1 Freezing and defrosting of hiPSC and hESC 233
7.1.2 Generation of retinal organoids from human iPSCs and ESCs 233
7.1.3 Dissection of retinal organoids 235
7.1.4 Isolation and propagation of Müller glia from retinal organoids 235
7.1.5 *In vitro* propagation of isolated Müller glia 236
7.1.6 Fluorescent cell sorting analysis (FACS) 237
7.1.7 Characterisation of retinal organoids and Müller glia 237
7.1.7.1 Fixation and dehydration 238

7.1.7.2 Embedding and cryosectioning of retinal organoids 238
7.1.7.3 Immunohistological and immunocytochemical staining 238
7.1.7.4 Confocal microscopy and image analysis 239
7.2 Culture and cytokine treatment of Müller glia stem cells 239
7.2.1 Cryopreservation of cells 240
7.2.2 Müller glia cell culture with cytokines 240
7.2.2.1 Preparation of recombinant cytokines 241
7.2.2.2 TNF-α treatment of human Müller glia 241
7.2.2.3 ELISA analysis for antioxidant production and activity 241
7.3 Reverse transcription (RT) polymerase chain reaction (PCR) 242
7.3.1 RNA extraction 242
7.3.2 Reverse transcription 242
7.3.3 Polymerase chain reaction (PCR) 243
7.3.4 Gel electrophoresis 243
7.3.5 Imaging and statistics analysis 244
7.4 Transcriptomic analysis using RNA sequencing technique 244
7.4.1 Extraction of genomic-DNA depleted total RNA 244
7.4.2 Quality control and assurance of total RNA 244
7.4.3 Preparation of cDNA library 245
7.4.4 RNA-Sequencing 245
7.4.5 Data analysis 245
7.4.6 Validation of RNA-seq findings by Real-time polymerase chain reaction (qPCR) 246
7.4.7 Reaction mix preparation 246
7.4.8 qPCR 246
7.4.9 Data analysis 247
7.5 Western blotting 247
7.5.1 Protein extraction 247

7.5.2 BCA protein assay 247
7.5.3 Protein gel electrophoresis 248
7.5.4 Semi-dry gel transfer 249
7.5.5 Immunoblotting 250
7.5.6 Re-probing with different antibodies 250
7.5.7 Image analysis 250
7.6 Establishment of primary rat retinal ganglion cells in vitro 251
7.6.1 Overnight preparation of culture and panning plates 251
7.6.2 Tissue acquisition 251
7.6.3 Dissection and dissociation of retinae 252
7.6.4 Enrichment for viable RGCs by flow cytometry 252
7.6.5 Enrichment of RGCs by two-step immunopanning 253
7.6.5.1 Trituration of retinae 253
7.6.5.2 Panning 253
7.6.5.3 Trypsination and plating of RGCs 254
7.6.6 *In vitro* culture of primary rat RGCs 254
7.6.7 Assessment of neuroprotective potential of human Müller glia to RGCs against glutamate excitotoxicity 255
7.6.7.1 24-hour dose response of primary RGCs to glutamate neurotoxicity 255
7.6.7.2 Assessment of morphological features of RGCs 255
7.6.7.3 Preparation of human Müller glia conditioned medium 256
7.6.7.4 Induction of 24-hour glutamate excitotoxicity 256
CHAPTER 8 References 257
Appendix 286
Appendix 1 Antibodies 286
Appendix 2 RT-PCR Primers 288
Appendix 3 Taqman qRT-PCR Probes 289

Appendix 4 Preparation of stock reagents for isolation of primary RGCs 289
Appendix 5 Complete list of DEGs in the transcriptome of MIO-M1 cells treat with TNF-α for 24 hours 292
Publications.....300

Table of Figures

Figure 1.1 Anatomy of the human eye. 26
Figure 1.2 The Architecture of neural retina. 27
Figure 1.3 Generation sequence of retinal neurons from retinal progenitor cells (RPCs). 29
Figure 1.4 Morphology of human Müller glia. 31
Figure 1.5 Common retinal degenerative disorders and the affected cells. 40
Figure 1.6 Source of stem cells with therapeutic potential for treating retinal degeneration. 44
Figure 2.1 Formation of various types of organoid tissues by PSCs. 50
Figure 2.2 Illustration of the workflow for RNA sequencing. 53
Figure 2.3 Experimental outline. 57
Figure 2.4 Schematic illustration of generation of retinal organoids from hPSCs. ..58
Figure 2.5 Generation of retinal organoids. 60
Figure 2.6 Immunohistological characterisation of retinal organoids derived from the hESC line RC-9. 62
Figure 2.7 Immunohistological characterisation of retinal organoids derived from hiPSC line BJ. 63
Figure 2.8 Immunohistological characterisation of 3D cell aggregates derived from the hESC line Shef 6. 64
Figure 2.9 Morphological characteristics of cells isolated from retinal organoids formed by (A) hiPSC BJ at day 90, (B) hESC Shef 6 at day 121 and (C) hESC RC-9 at day 70. 66
Figure 2.10 Expression of mRNAs and proteins coding for Müller glia markers in cells isolated from hiPSC- and hESC-derived retinal organoids. 68
Figure 2.11 Expression of characteristic Müller glia markers GS, nestin, vimentin, CD29 and CD44 in (A) BJ Day 90 cells and (B) RC-9 Day 70 cells. 69
Figure 2.12 FACS analysis of the adult human Müller glial cell line MIO-M1 stained for characteristic Müller cell surface markers. 71
Figure 2.13 FACS analysis of BJ Day 90 cells stained for stained for characteristic Müller cell surface markers, pluripotent stem cell markers and epithelial cell markers. 72

Figure 2.14 FACS analysis of RC-9 Day 70 cells stained for stained for characteristic Müller cell surface markers, pluripotent stem cell markers and epithelial cell markers. 73
Figure 2.15 RNA-seq read alignment metrics of transcriptomic libraries from MIO-M1, hiPSC-M1 and hESC-MG1....75
Figure 2.16 Overview of transcriptomic libraries of all cell preparations examined. 77
Figure 2.17 Expression levels of transcripts for markers of undifferentiated stem cells and other retinal cell fates in the three cell preparations analysed.....91
Figure 2.18 Expression levels of transcripts for Müller glia (MG) markers in the three cell preparations analysed. 94
Figure 2.19 Expression levels of transcripts for anti-oxidative factors in the three cell preparations analysed.....99
Figure 2.20 Expression levels of transcripts for trophic factors in three cell preparations. 101
Figure 2.21 Correlation of gene expressions between qPCR and RNA-seq methods in the detection of gene expression in (A) MIO-M1, (B) hiPSC-MG1 cells and (C) hESC-MG1.....103
Figure 3.1 TNF-α signalling components and downstream signalling cascades triggered by TNF-α.....114
Figure 3.2 Experimental outline. MIO-M1 cells were cultured with 50 ng/mL TNF-α for 24 hours (yellow box).....121
Figure 3.3 Bright field images showing the representative morphological features of MIO-M1 cells before and after culture with 50 ng/mL of TNF-α for 24 hours (bottom panel), as compared with untreated cells (top panel).....122
Figure 3.4 RNA-seq read alignment overview of transcriptomic libraries from MIO-M1 treated or untreated with TNF-α. 123
Figure 3.5 Overview of transcriptomic libraries of TNF-α-treated and untreated MIO-M1 cells.....125
Figure 3.6 Overview of differentially expressed genes (DEGs) in MIO-M1 cells treated with and without TNF-α. 126
Figure 3.7 Hierarchically clustered heatmap showing DEGs between TNF-α treated (orange boxes) and control (blue boxes) MIO-M1 cells.....127

Figure 3.8 Gene ontology analysis by biological processes of DEGs induced by TNF-α in MIO-M1 cells. 129
Figure 3.9 The directed acyclic graph (DAG) of interactive relationship of GO terms based on biological processes. 131
Figure 3.10 Expression levels of DEGs coding for TNF-α and NFκB signalling pathways in control and TNF-α-treated MIO-M1 cells. 134
Figure 3.11 Expression levels of DEGs related to neuroinflammation in control and TNF-α-treated MIO-M1 cells. 138
Figure 3.12 Expression levels of DEGs coding for pro-survival factors in MIO-M1 cells treated with TNF-α. 140
Figure 3.13 Expression levels of DEGs associated with reactive gliosis by MIO-M1 cells treated with TNF-α. 142
Figure 3.14 Expression levels of non-coding DEGs in MIO-M1 cells treated with TNF-α. 144
Figure 3.15 Correlation of gene expressions between qPCR and RNA-seq. 145
Figure 4.1 Representative (A) RT-PCR bands and (B) western blotting bands showing expression of mRNA and protein coding for key antioxidant molecules by the human adult Müller glia cell line MIO-M1 cell (left), hiPSC-MG cells (middle) and hESC-MG cells (right). 162
Figure 4.2 Distribution of the antioxidant enzymes PRDX6 (A) and HO1 (B) in normal human retina. 163
Figure 4.3 Distribution of the antioxidant enzymes GCPII (A) and PON2 (B) in normal human retina. 164
Figure 4.4 Effect of TNF-α on the expression of antioxidant enzymes in MIO-M1 cells. 166
Figure 4.5 Effect of TNF-α on the expression of antioxidant enzymes in hiPSC-MG cells. 167
Figure 4.6 Effect of TNF-α on the expression of antioxidant enzymes in hESC-MG cells. 168
Figure 4.7 Mean protein levels of PRDX6 (ng/mL) detected by ELISA kit in culture supernatants of human Müller glia cultures. 169
Figure 4.8 Mean protein levels of HO1 (pg/mL) detected by ELISA kit in culture supernatants of human Müller glia cultures. 170

Figure 4.9 Effect of TGF-β1 on the expression of antioxidant enzymes in MIO-M1 cells. 172
Figure 4.10 Effect of TGF-β1 on the expression of antioxidant enzymes in hiPSC-MG cells. (A) hiPSC-MG cells exhibited characteristic bipolar morphology before (0 hour) and after (24 hours) 173
Figure 4.11 Effect of TGF-β1 on the expression of antioxidant enzymes in hESC-MG cells. 174
Figure 4.12 Schematic illustration of molecular crosstalk between cytokine (TNF-α/TGF-β1) -mediated ROS, NRF2, and NFκB on the expression of antioxidant enzymes. 179
Figure 5.1 Work flow of purifying rat RGCs by flow cytometry sorting (A) and two-step immunopanning (B). 191
Figure 5.2 Experimental outline 194
Figure 5.3 Analysis of retinal cell suspension analysis after papain dissociation. 196
Figure 5.4 Gating parameters used in flow cytometry sorting of CD90-PE^{+} RGCs from retinal cell suspensions. 197
Figure 5.5 Gating parameters used in flow cytometry sorting of CD90-PE^{+} RGCs from retinal single cell suspension. 198
Figure 5.6 Gating parameters used in flow cytometry sorting of CD90-PE^{+} RGCs from retinal single cell suspension. 199
Figure 5.7 Gating parameters used in flow cytometry sorting of CD90-PE^{+} RGCs from retinal single cell suspension. 200
Figure 5.8 Summary of RGC purification by flow cytometry. 201
Figure 5.9 Identification of rat RGCs enriched by flow cytometry sorting. 203
Figure 5.10 Identification of rat RGCs purified by TIP. 204
Figure 5.11 Glutamate induces a concentration-dependent damage to RGCs. 206
Figure 5.12 Morphological features of RGC populations exposed to 24-hours glutamate excitotoxicity. 209
Figure 5.13 Neuroprotective effect of hESC-MG supernatants on RGCs with neurites following 24-hour glutamate excitotoxicity. 210
Figure 5.14 Representative morphological features of surviving individual RGC exposed to glutamate for 24 hours. 212

Figure 5.15 Neuroprotective effect of hESC-MG supernatants as determined by the mean length (μm) of the longest neurite per RGCs following 24-hour glutamate excitotoxicity. 213
Figure 5.16 Neuroprotective effect of hESC-MG supernatants on dendritic projections of RGCs following 24-hour glutamate excitotoxicity. 214
Figure 5.17 Analyses of the mean concentration of key neuroprotective factors in the hESC-MG supernatants. 216

Table of Tables

Table 2.1 List of retinal organoids and harvesting time points used for immunohistochemical analysis. 61
Table 2.2 List of retinal organoids and time points of dissociation. 65
Table 2.3 Gene ontology (GO) analysis by cellular component of DEGs in pairwise analysis of hESC-MG1 vs MIO-M1 (left column), hiPSC-MG1 vs MIO-M1 (middle column) and hiPSC-MG1 vs hESC-MG1 (right column). 80
Table 2.4 Gene ontology (GO) analysis by molecular function of DEGs in pairwise analysis of hESC-MG1 vs MIO-M1 (left column), hiPSC-MG1 vs MIO-M1 (middle column) and hiPSC-MG1 vs hESC-MG1 (right column). 84
Table 2.5 Gene ontology (GO) analysis by biological process of DEGs in pairwise analysis of hESC-MG1 vs MIO-M1 (left column), hiPSC-MG1 vs MIO-M1 (middle column) and hiPSC-MG1 vs hESC-MG1 (right column). 89
Table 2.6 hPSC-derived cell preparations used for RNA-seq and validation by qRT-PCR. 102
Table 3.1 GO Overrepresentation analysis on the DEGs identified in the study. 128
Table 7.1 Medium components for retinal organoids culture 234
Table 7.2 Reagents required for retinal organoid dissociation 236
Table 7.3 Plans for in vitro propagation of isolated Müller glia 237
Table 7.4 MIO-M1 cell culture medium 240
Table 7.5 List of ELISA kits used for quantification of anti-oxidation molecules produced by Müller glia cells 242
Table 7.6 Molecular weight of the proteins of interest and the corresponding types of gel and running buffer used in protein gel electrophoresis. 248
Table 7.7 Culture conditions of primary RGCs for induction of 24-hour glutamate neurototoxicity. At the end of the 24-hour treatment, RGCs were harvested and RGC survival was analysed as described in 7.6.7.2. 256

Abbreviations

AMD	Age-related macular degeneration
ASCL1A	Achaete-scute homolog 1 A
ATP	Adenosine Tri-phosphate
BCA	Bicinchoninic acid
BDNF	Brain derived neurotrophic factor
bFGF	Basic fibroblast growth factor
bHLH	Basic Helix-Loop-Helix
cAMP	Cyclic adenosine monophosphate
cGMP	Cyclic guanosine monophosphate
CDK	Cyclin-dependent kinase
CNS	Central nervous system
CNTF	Ciliary neurotrophic factor
CRALBP	Cellular retinaldehyde binding protein
CSF	Colony-stimulating factor
DAPI	4',6-diamidino-2-phenylindole
DMEM	Dulbecco's Modified Eagle Medium
DNA	Deoxyribonucleic acid
EB	Embryoid body
ECM	Extracellular matrix
EGF	Epidermal growth factor
ELISA	Enzyme-Linked Immunosorbent Assay
ERG	Electroretinogram
ERK	Extracellular signal-regulated kinases
FACS	Fluorescence-activated cell sorting
FCS	Fetal calf serum
FGF	Fibroblast growth factor
GCL	Ganglion cell layer
GDNF	Glial cell-derived neurotrophic factor

GFAP	Glial fibrillary acidic protein
GLAST	Glutamate-aspartate transporter
GO	Gene ontology
hESC	Human embryonic stem cell
hESC-MG	Human embryonic stem cell-derived Müller glia
hiPSC	Human induced pluripotent stem cell
hiPSC-MG	Human induced pluripotent stem cell-derived Müller glia
hPSC	Human pluripotent stem cell
IF	Intermediate filament
IFN	Interferon
IGF	Insulin like growth factor
IL	Interleukin
ILM	Inner limiting membrane
INL	Inner nuclear layer
IOP	Intraocular pressure
IPL	Inner plexiform layer
JAK	Janus kinase
MAPK	Mitogen-activated protein kinases
MIO-M1	Moorfields/Institute of Ophthalmology-Müller 1
MMP	Matrix metalloproteinases
mRNA	Messenger ribonucleic acid
NAC	N-acetyl-L-cysteine
NFκB	Nuclear factor kappa-light-chain-enhancer of activated B cells
NGF	Nerve growth factor
NFL	Nerve fibre layer
NAC	N-acetyl-L-cysteine
NMDA	N-Methyl-D-aspartic acid
NR2E3	Nuclear receptor subfamily 2, group E, member 3
NRF2	Nuclear factor erythroid 2-related factor 2

O.D	Optical density
OLM	Outer limiting membrane
ONL	Outer nuclear layer
OPL	Outer plexiform layer
PBS	Phosphate buffered saline
PCR	Polymerase chain reaction
PDL	Poly-D-lysine
PE	Phycoerythrin
PDGF	Platelet-derived growth factor
PEDF	Pigment epithelium-derived factor
PFA	Paraformaldehyde
PVDF	Polyvinylidene difluoride
PVR	Proliferative vitreoretinopathy
RGC	Retinal ganglion cell
RIPA	Radioimmunoprecipitation assay buffer
RNA	Ribonucleic acid
RPE	Retinal pigment epithelium
RT-PCR	Reverse transcriptase polymerase chain reaction
SD	Sprague Dawley
Shh	Sonic hedgehog
STAT	Signal transducer and activator of transcription
TBS	Tris buffered saline
TIP	Two-step immunopanning
TIPM	Two-step immunopanning-magnetic
TGF	Transforming growth factor
TNF	Tumour necrosis factor
TrK	Tyrosine receptor kinases
VEGF	Vascular endothelial growth factor
WNT	Wingless-type MMTV integration site family

Work Contributed by lab members:

Dr C Murray-Dunning	Figure 2.5 (C)
Dr K Eastlake	Figure 5.17- BDNF and PEDF data

CHAPTER 1 General introduction

1.1 Anatomy of the human eye

The eye globe is located in a bony cavity of the skull known as the orbit, which protects the eye with tissues such as fat, supportive fascia and extraocular muscle. The orbit is divided anatomically into three layers and two segments, known as the anterior and posterior segments (Figure 1.1). The anterior segment refers to the lens and tissues anterior to it. The outermost layer, known as the sclera is attached to the transparent cornea that allows the entry of the light into the eye. The anterior iris, ciliary body and the posterior choroid form the middle layer. The pigmented iris functions as a shutter that regulates the amount of light entering the eye through contraction and dilation of the muscles innervating the pupil. The ciliary body is rich in blood vessels and connective tissue and responsible for producing the aqueous humor. It consists of blood plasma, enzymes and metabolite lactates from cornea and lens, and circulates throughout the eye globe from the pupil to the AC and leaves through an angle created by the root between the iris and the peripheral corneal vault. This process maintains and regulates intraocular pressure (IOP), which results from the fluid dynamics of aqueous humor draining from the trabecular meshwork (TM) to the canal of Schelmm. Aqueous humor is also important for nutrients supply and helps forming the pathway for light entering the retina. The anterior chamber (AC) is located between the cornea and the iris, whilst the posterior chamber (PC) is described as the cavity posterior to the iris and sits between suspensory ligament and lens. The innermost layer of the anterior segment is the lens, which is found behind the iris and bathed in aqueous, allowing light being refracted into the eye. The posterior segment consists of vitreous, choroid and retina. The weight and volume of the eye globe is ascribed to the vitreous cavity that encloses a pool of the vitreous gel. Many other molecules and proteins including salts and extracellular matrix proteins form the components of vitreous gel and the presence of collagen gives a viscosity higher than the aqueous humor. The choroid is sandwiched between the retina and the sclera, nourishing the photoreceptor rods and cones and the retinal pigmented epithelium (RPE) (Lens, 1999).

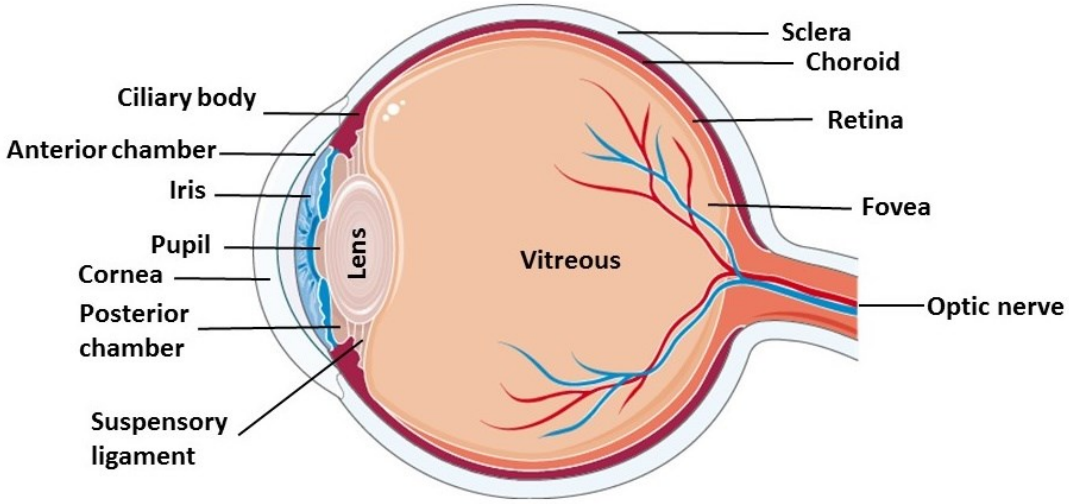

Figure 1.1 Anatomy of the human eye.
Figure shows a transverse section of the eye globe illustrating the different anatomical structures of the eye. This image was produced using Servier Medical Arts (https://smart.servier.com).

1.1.1 The retina

Lining the posterior section of the eye, the transparent retina contains all the neurons responsible for the conversion of photochemical information to neurological signals that are transmitted to the brain. The neural retina is layered by RPE, which constitutes a single layer of pigmented cells that confers protection to the underlying sensory retina, not only by absorbing excessive light but also by restraining the entry of choroidal fluids (Lens, 1999). The neural retina is subdivided into i) the RGC layer (GCL), where amacrine and RGC somata are found, ii) the inner nuclear layer (INL) that houses Müller glia and the somata of bipolar, amacrine and horizontal cells, and iii) the outer nuclear layer (ONL) that harbours the photoreceptor rods and cones (Figure 1.2). The highly polarised photoreceptor rods and cones are capable of converting the electromagnetic radiation energy from light into nerve impulses (Wassle, 2004). The rods are responsible for scotopic (vision in dim light) and peripheral vision due to their peripheral location in the retina, whilst the cones, which constitute only one twentieth of the photoreceptor population, critically provide coloured vision and fine resolution. Depending on the light intensity, depolarising of off-bipolar cells and hyperpolarising of on-bipolar cells occur at dim illumination, and depolarising of on-bipolar cells and hyperpolarising of off-bipolar cells take place at

high illumination. This is caused by a series of biochemical reactions mediated by cGMP and polarisation of membrane potential by the pigment rhodopsin in rods and three different photopsins in cones. Amacrine and horizontal cells present in the INL act as signal coordinators and integrate signals from photoreceptors. Upon receiving signal from the synapses formed at the IPL, RGCs are activated and generate distinctive action potentials, relaying details of visual information in terms of colour, intensity and movement (Wassle, 2004). While having the somata in the GCL, axons of RGCs bundle up and form the nerve fibre layer (NFL) which further converge towards the optic nerve, sending action potentials to the visual centre in the brain. Müller glia are the major macroglial cells of the neural retina, span across the entire retina and interact with all retinal neurons. In addition to offer metabolic support to the neural retina, Müller glia actively participate in retinal development, regeneration and pathological functions (Bringmann and Wiedemann, 2012). Astrocytes constitute another type of macroglia in the neural retina, mainly present in the inner retina, which regulate the ionic homeostasis in the NFL (Goldman, 2014).

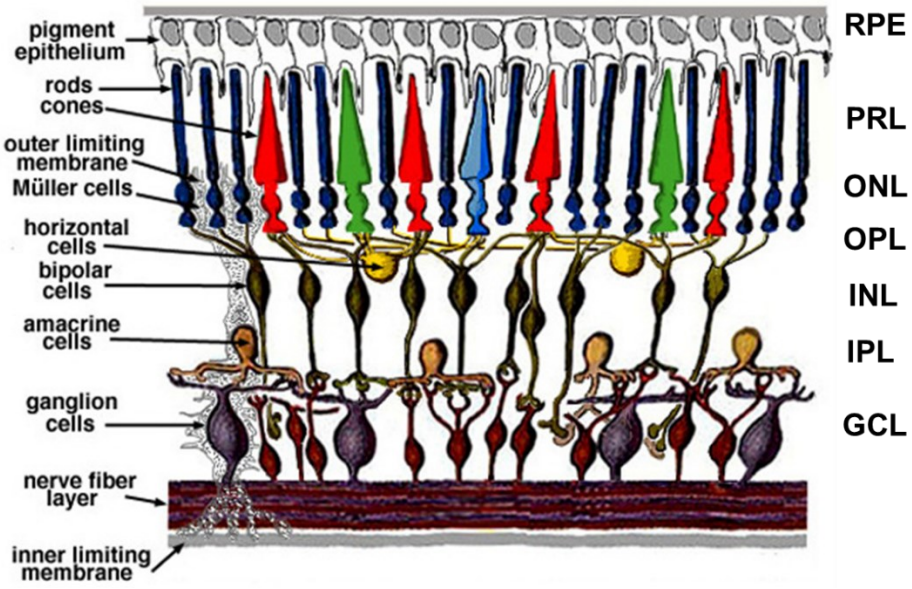

Figure 1.2 The Architecture of neural retina.
Photoreceptor rods (dark blue) and cones (red, green and light blue) are found at the outermost photoreceptor layer (PRL) and their somata are located at the outer nuclear layer (ONL) of the neural retina, lining against the retinal pigment epithelium (RPE). Interneurons The inner nuclear layer (INL) contains the Müller glia and the somata of interneurons. RGC cell bodies form the innermost ganglion cell layer (GCL) and their axons form bundles of nerve fibre layer (NFL). Complex synaptic interactions between different types of retinal neurons are found in the outer plexiform layer (OPL) and inner plexiform layer (IPL). This image was adapted from Kolb, 2011 (https://webvision.med.utah.edu/book/part-i-foundations/simple-anatomy-of-the-retina).

1.1.2 Retinogenesis

As an extension of the central nervous system (CNS), the eye shares the same embryonic origin of the neural tube that gives rise to the CNS. Retinogenesis is a conserved process in many species and begins at embryonic day 10 in the rat and between 6.5 weeks to 18 weeks of human gestation (Masland, 2001). The specification process is orchestrated by intrinsic transcription factors and external cues, gradually restricting progenitors towards the retinal fate (

Figure 1.3).

Under the synergistic regulation of Noggin which inhibits both wingless (WNT) and bone morphogenetic protein (BMP), and basic fibroblast growth factor (bFGF) and insulin-like growth factor (IGF), the anterior neural plate generates the optic vesicles via invagination in both sides of the forebrain (Livesey and Cepko, 2001, Heavner and Pevny, 2012). These events lead to the formation of the optic cup and contribute to the formation of the retinal progenitor cell (RPC) populations caused by the interactions between the ectoderm and optic vesicles. This developmental process is under the control of eye field transcription factors (EFTFs) including Pax6, Rax, Lhx2 and Sxi3 (Zuber et al., 2003, Heavner and Pevny, 2012). At the beginning, an enlargement at the site occurs, due to many rounds of cell divisions of the early pluripotent RPCs, which determine the size of the retina (Vaney, 2002). This extensive proliferation of early progenitor cells is mastered by the transcription factor Pax6, as demonstrated by knock-out studies on Pax6 expression in mouse embryo, which inhibit a full spectrum of retinal neurogenesis (Zagozewski et al., 2014). Another transcription factor, sex determining region (SRY)-box 2(Sox2), is an important neural fate inducer that reinforces the commitment of early progenitors, as indicated by Sox2 mutants that have small or absent eyes (Ragge et al., 2005). This is followed by a period of asymmetric division at which post-mitotic and mitotic daughter cells are produced. From this point onwards, the retinal neurons are generated in a temporal manner (Sinn and Wittbrodt, 2013). At the end of this proliferation phase, the post mitotic daughter cells exit the cell cycle, initiate the differentiation process and become one of photopic retinal neurons, which develop in the following order: firstly RGCs, followed by horizontal cells, photoreceptor cones and amacrine cells (Xiang, 2013). Other neurons that are required for scotopic vision

such as photoreceptor rods, bipolar cells and Müller glia derive from the late-born RPCs which have retained the mitotic potential and remain in division before fate commitment (Rapaport et al., 2004b). As development proceeds, one of the progenies of the late-born RPCs becomes the radial glial cell and gives rise to Müller glia as the last retinal cells produced in the neural retina (Elliott et al., 2008).

Shortly after the birth of RGCs, their differentiation is commenced by projecting radial processes towards the basal lamina followed by the migration of nuclei to the innermost site where they would eventually reside. This initial differentiation terminates when the axons of RGCs start projecting in the direction of the future optic nerve and align with the endfeet of radial glial cells (Xiang, 2013, Zagozewski et al., 2014). Similar to the guidance-free translocation of RGCs, horizontal cells also travel in the same direction but less far. Photoreceptor cones do not necessarily leave but rather stay at their birthplace (Masland, 2001). As the growing retinal neuroepithelium becomes wide and complexed with various cells, the late-born amacrine and bipolar cells rely on the radial glial cells for their migration to the developing INL (Sinn and Wittbrodt, 2013). At the end of this dynamic translocation process, synapses between retinal neurons are formed and the final retinal mosaic is created, with three nuclear layers interfaced by two plexiform layers (Rapaport et al., 2004a). The final retinogenesis stage aids in the maintenance of retinal shape that enlarges during additional postnatal development events.

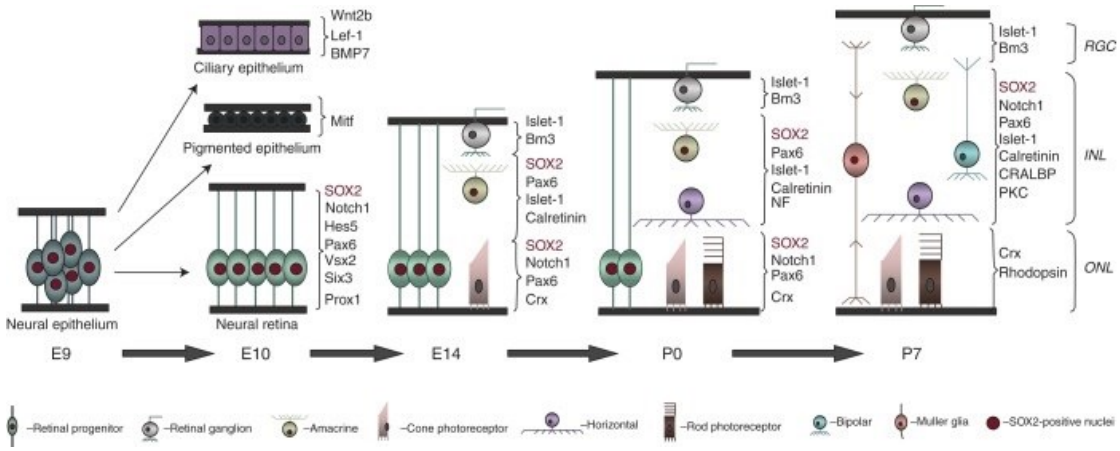

Figure 1.3 Generation sequence of retinal neurons from retinal progenitor cells (RPCs).
Expression of Sox2 and Notch is required to maintain the fate of RPCs. As retinal development proceeds, a small set of RPCs leaves the cell cycle and express genes that are lineage-specific. The temporal order of genesis of retinal cells follows the sequence of RGCs, horizontal cells,

photoreceptor cones, amacrine cells, photoreceptor rod, bipolar cells and finally Müller glia. This figure was partially adapted from (Heavner and Pevny, 2012).

1.2 Müller glia and its roles in the neural retina

1.2.1 Development of Müller glia

Müller glia are thought to be the last group of retinal cells produced during retinogenesis, although its exact developmental process remains unclear. To date, it has been proposed that RPCs driving towards Müller glia fate involves a complex group of signalling factors and cascades. In addition to Rax, Notch 1 and its downstream effector Hes1 are of paramount importance to drive the differentiation of RPCs towards the Müller glia phenotype (Furukawa et al., 2000). There is evidence that cell cycle progression tightly regulates retinogenesis via interactions between the cyclin-dependent kindase (CDK) and the Notch signalling pathway. The expression of the CDK inhibitor $p27^{Xic1}$ in mammalian retina synchronises with Müller glia development and is required for proper lamination of the retina, as demonstrated by the knockout of $p27^{kip1}$ in mice, which leads to disruption of retina lamination. In contrast, overexpression of $p27^{kip1}$ in Xenopus results in an increased Müller glia population (Nakayama et al., 1996, Ohnuma et al., 1999). Overexpression of the epidermal growth factor receptor (EGF-R) and its ligand transforming growth factor-α (TGF-α) induces an increase in Müller glia, demonstrating that limited availability of this receptor could potentially influence cell fate (Lillien, 1995). Overexpression of the bHLH transcription factor NeuroD leads to an increased population of photoreceptor rods and amarine cells at the cost of Müller glia, while its depletion lead to more Müller glia generation (Morrow et al., 1999). In addition, it has been shown that members of the high-mobility group (HMG) box transcription factors Sox2 and Sox9 critically determine Müller glia fate. The morphology and population density of Müller glia seem to be affected as a result of disrupted Sox2 expression in mice while overexpression of Sox2 expanded Müller glia population in mouse retinal explants (Lin et al., 2009, Surzenko et al., 2013). Sox9 over-expression has been reported to restrict Müller glia development in the inner nuclear layer, whilst its deletion exclusively impacts on Müller glia development, suggesting a central role for this factor on Müller glia fate determination (Poche et al., 2008). Cytoskeletal elements are considerably important for the development, functionality and identification of Müller glia. The maturation of Müller glia is

associated with the expression of a heterogeneous group of intermediate filaments (IFs) in the cytosol. Amongst them, vimentin and nestin which are normally expressed by neural progenitor cells, are co-expressed in developing Müller glia, and the polymerisation of nestin cannot take place without vimentin. The dominant expression of vimentin at the inner cell process with downregulation of nestin is a hallmark of mature Müller glia (Reichenbach and Bringmann, 2010).

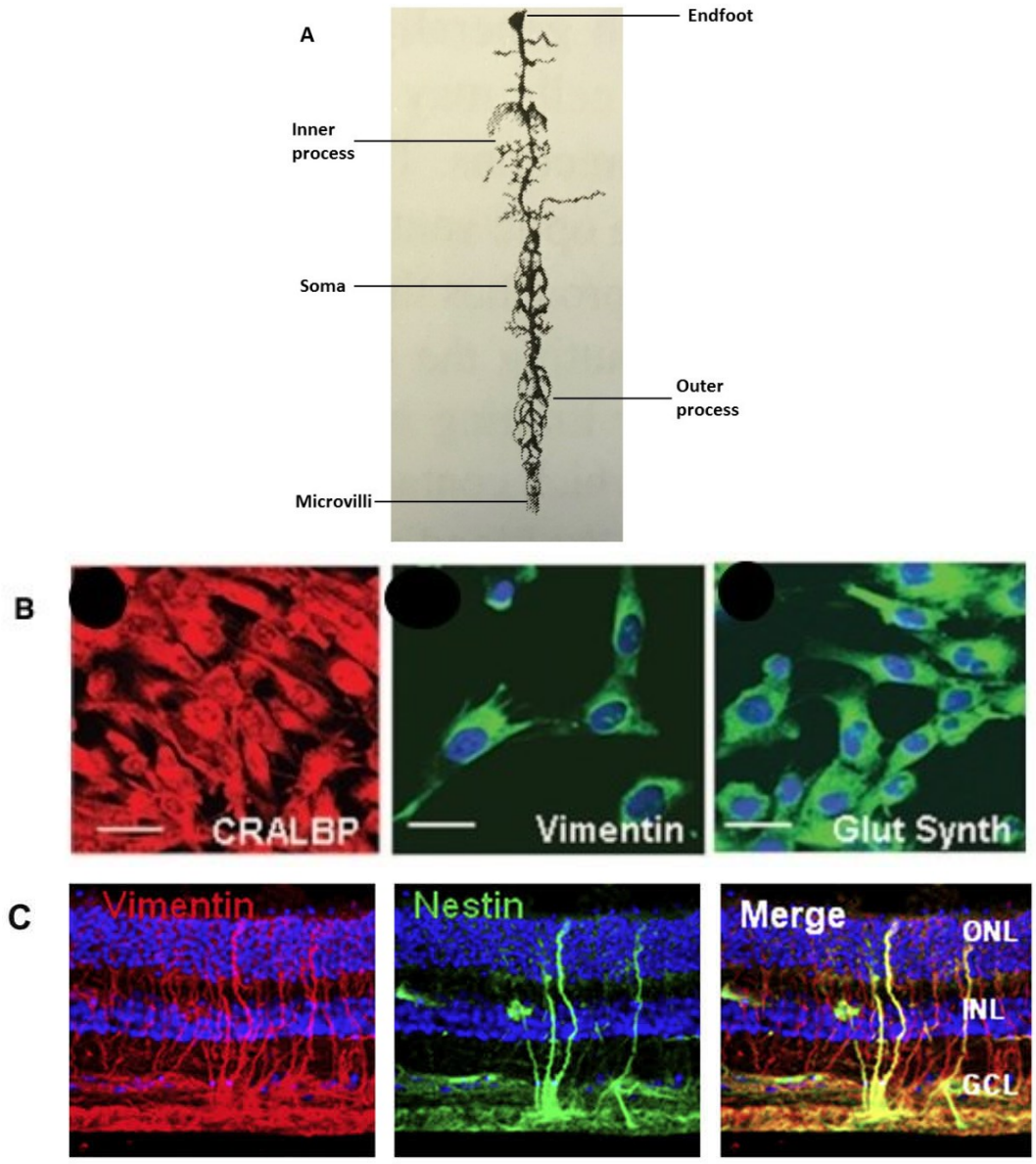

Figure 1.4 Morphology of human Müller glia.
(A) Spanning from the outer nuclear layer to the ganglion cell layer of the retina, the soma of Müller glia is found in the inner nuclear layer. The processes of Müller glia interact with different retinal cells, with the inner process extending towards the vitreous and the outer process reaching the subretinal space. This image was adapted from (Reichenbach and Bringmann, 2010). **(B)** Immunofluorescence staining of molecular markers of Müller glia: CRALBP, vimentin and GS. This image was adapted from (Lawrence et al., 2007). **(C)** Confocal images showing that a small population of Müller glia co-

express vimentin and nestin (merge) in human retinal sections while all Müller glia population are positive for vimentin. This image was partially adapted from (Bhatia et al., 2009).

1.2.2 Characteristics of Müller glia

First identified by Heinrich Müller in 1851, Müller glia are recognised as the main glial cells of the retina and span across this tissue, interacting with all neural cells. Resembling the radial glial cells in the CNS, the bipolar morphology of Müller glia is characterised by the presence of many functional processes and sizes approximately up to 200μm *in vivo* (Bringmann and Wiedemann, 2012*)*.

The somata of Müller glia locate in the INL while the major inner and outer cytoplasmic processes are found projecting bi-directionally from the basal lamina between the vitreous and the subretinal space, displaying finer structural branches such as microvilli and endfeet (Figure 1.4A). The intracellular organelles of Müller glia are specifically localised and contained proteins which are now well accepted as markers for Müller glia to assist the designated Müller cell-neuron interactions, offering both physical support and metabolic products and nutrients to the surrounding neurons. For example, the cellular powerhouse mitochondria are located at the end of the microvilli where oxygen availability is at the optimum, enabling efficient ATP production in Müller cells. Modulation of water flux across Müller glia is mediated by aquaporin 4 (AQP4), as ATP production and IOP constantly contribute to water retention in the cytosol (Newman and Reichenbach, 1996). Endfeet found at the inner processes is thought to act as a spatial buffering element to potassium ions for the neighbouring neurons via the inward rectifying potassium pump Kir2.1 and Kir4.1. These potassium channels actively modulate the ion flux and regulate membrane conductance to ensure the low membrane potential in Müller cells (Bringmann et al., 2006). Golgi apparatus and the adjoining multi-vesicular bodies are responsible for the release of growth factors, cytokines and a potent antioxidant glutathione (GSH) and their intracellular trafficking is regulated by microtubules in Müller glia (Bringmann and Wiedemann, 2012). Smooth endoplasmic reticulum, glycogen-containing vesicles and bundles of IFs such as vimentin, nestin and glial fibrillary acidic protein (GFAP) are found at the thicker inner process. These structures have a prominent cytoplasmic surface-to-volume ratio, favouring the contact with retinal neurons.

There are other well-known Müller glia-enriched proteins responsible for various Müller glia metabolic activity. The glia-specific carbonic anhydrase II (CA2) regulate homeostasis of CO_2, a metabolic by-product released by other retinal neurons, by converting CO_2 to HCO_3^- before releasing into blood vessels or further utilising it for lipid biosynthesis (Newman, 1996). Another metabolic support by Müller glia is the recycling of extracellular neurotransmitter glutamate by L-glutamate-L-aspartate transporter (GLAST) and convert it to glutamine by glutamine synthetase (GS), found in the somata and lateral branches. Similarly, the metabolism of the inhibitory neurotransmitter γ-aminobutyric acid (GABA) is regulated by the GABA plasma membrane transporter GAT-3 which catalyses GABA to glutamate (Johnson et al., 1996). Glutamate is fed into the GS pathway and is released as GSH, reducing neurotoxicity in neighbouring cells caused by excessive glutamate (Bringmann and Reichenbach, 2001). In addition, recycling and conversion of the bleached photopigment all-trans-retinal to 11-cis-retinol takes place in Müller glia and regulated by the cytosolic cellular retinaldehyde-binding protein (CRALBP) (Saari and Bredberg, 1988).

Under normal physiological condition, Müller glia continuously produce a broad spectrum of trophic factors including neurotrophins, antioxidants and growth factors for the survival and normal function of retinal neurons. Neurotrophins such as brain derived neurotrophic factor (BDNF), ciliary neurotrophic factor (CNTF) and pigment epithelium-derived factor (PEDF) (Huang and Reichardt, 2001, Eichler et al., 2017), anti-oxidative molecules which include small molecule antioxidant GSH and a diverse group of antioxidant enzymes as scavengers of free radicals (Eastlake et al., 2019a), as well as growth factors such as fibroblast growth factor 2 (FGF2) (O'Driscoll et al., 2008, Yafai et al., 2013) and vascular endothelial growth factor (VEGF) (Foxton et al., 2013, Miller et al., 2013) form a neuroprotective network in the neural retina.

1.2.3 Implications of Müller glia in retinal regeneration and degeneration

As well as offering structural and homeostatic support to the neural retina, stem cell features of Müller glia have been identified in all vertebrates and their potential to

regenerate retina has been extensively studied in various model organisms. In response to almost all harmful stimuli, Müller glia immediately undergo an activation process called gliosis which comprises of a series of complex cellular events such as proliferation and is accompanied by various changes in cell morphology, gene expression and tissue re-organisation.

Gliosis is often considered as the initial attempt of Müller glia to halt further damage, promoting tissue repair and preserving tissue function. Although this response is universal across nearly all vertebrates, gliosis could induce either protective or degenerative consequences and is species-dependent (Reichenbach and Bringmann, 2010). In zebrafish, upregulation of cytokines as represented by the pro-inflammatory tumour necrosis factor (TNF)-α from dying photoreceptors acts as essential signalling cues to activate Müller glia, inducing them to proliferate, migrate to injury site followed by differentiation to replace the damage retinal cells (Nelson et al., 2013). During gliosis, Müller glia also become hypertrophic in their morphology and upregulate the expression of characteristic GFAP (Thomas et al., 2016). At the early phase of injury, hypertrophic Müller glia have been demonstrated to respond to the stimulating cues from dying neurons and support synaptic remodelling by releasing a variety of neurotrophic factors and growth factors which favour the survival of retinal neurons (Bessero and Clarke, 2010, Langmann, 2007). For example VEGF is released to limit oxidative damage to retinal vasculatures while TNF-α, FGF2 and CNTF promote the survival of RGCs and photoreceptors (Tezel, 2008, Miller et al., 2013, Harada et al., 2002). Gliosis is regarded as the pre-condition of retina regeneration in zebrafish as Müller glia only stay in this reactive status temporarily and rapidly exhibit genes prompting stem cell characters. Preceding to differentiation of Müller glia towards the type of damaged retinal neurons, extensive modification of gene expression and signalling changes represents another characteristic of gliotic response in Müller glia. For example, the proliferative potential of Müller glia is normally regulated by several members of progenitor genes and signalling pathways including Pax6, Stat3, Notch and WNT families (Fausett and Goldman, 2006, Ramachandran et al., 2011, Nelson et al., 2012) while downregulating Müller glia-specific genes such as GFAP and GS is necessary for entry into cell cycle (Thummel et al., 2008). Initially activation of Notch pathway is required to acquire neural progenitor potential while its suppression is

necessary for Müller glia to commit to photoreceptor fate as accompanied by migration to injury site (Yurco and Cameron, 2005).

While retinal regenerative potential of zebrafish is fully retained throughout life, Müller glia in higher order vertebrates such as chick and rodents only possess limited regenerative capacity during early postnatal stage (Fischer and Reh, 2003, Ooto et al., 2004). Human retina is also known to harbour a subpopulation of Müller cells with neural stem cell characteristics (Lawrence et al., 2007) which acquire gene expression profiles of RGCs and photoreceptors upon culturing with appropriate inducing factors *in vitro* (Singhal et al., 2012, Jayaram et al., 2014b). Nevertheless instead of regeneration, human Müller glia undergo reactivity and contribute to various retinal pathogenesis including proliferative retinopathy (PVR), retinal detachment and glaucoma (Tezel and Wax, 2000, Verardo et al., 2008, Hoerster et al., 2014). There are some similarities and differences between the activation of Müller glia in zebrafish and higher vertebrates. Activation of Müller glia commonly relies on cytokines and in mouse gliosis is also triggered by endothelin 2 from dying photoreceptors (Rattner and Nathans, 2005). In contrast, one distinctive behaviours of Müller glia in higher vertebrates is the persistent gliotic response unlike in zebrafish at which Müller glia undergo a transient gliotic phase before quickly transitioning towards stem cell-like. It is evident that Müller glia were held at gliotic stage after treating zebrafish retina with a chemical to halt cell cycle (Thomas et al., 2016). Whereas in mouse retina, downregulation of the cell cycle regulator protein $p27^{Kip1}$ permitted activated Müller glia entering into mitosis whereas inhibition of cyclin D3 by $p27^{Kip1}$ did not encourage Müller glia from exiting cell cycle (Dyer and Cepko, 2000). These evidences suggest that prolonged gliosis might be a result of dysregulated Müller glia proliferation and might be one of the underlying factors preventing mammalian retina regeneration.

In addition, persistent gliosis is accompanied by increased production of cytokines and reduced metabolic support by Müller glia to the damaged neurons, which might exacerbate retinal degeneration. These responses at early phase of injury appear to be protective and limit injury from further spreading and seem to be detrimental when persisting in higher vertebrates. For instance, reduction of Kir4.1 conductance at early phase is associated with neuroprotection as it is thought to be a prerequisite to facilitate de-differentiation of Müller glia (Bringmann et al., 2000). However

prolonged downregulation or even mislocalisation of Kir4.1 could induces potassium ion accumulation in Müller glia and subsequently increased osmotic pressure and cell death, which is well documented in large body of degenerative disorders (Pannicke et al., 2004, Amin et al., 1997, Erickson et al., 1987).

Reactive Müller glia in nearly all model organisms are accompanied by immediate GFAP upregulation (Sethi et al., 2005, Lewis and Fisher, 2003, Erickson et al., 1987, Lenkowski et al., 2013). Interestingly, this IF subsequently becomes downregulated in zebrafish which coincides with the regeneration phase while remaining highly expressed in all higher vertebrates (Fimbel et al., 2007). In these vertebrates, reactive Müller cells subsequently become stiffened at their inner processes and endfeet as a result of accumulation of IFs, generating glia scars to fill the space where the deceased retinal neurons used to be (Lu et al., 2011). In normal physiology, Müller glia function as a soft substrate that favours neurite outgrowth and neuronal migration during development owning to its low elasticity (Lu et al., 2006). However this biomechanical property is altered and becomes detrimental to retinal regeneration following gliosis, as glial scar not only further distorts the remaining retina but also forms an obstacle that hinders neurite growth, cell migration and cell-cell interactions essential for synaptic regeneration (Lu et al., 2011). Specifically, the stiffened Müller glia become mechanically impaired such that anormal blood vessels form extension into the vitreous (Lundkvist et al., 2004) and neurite outgrowth is suppressed (Flanagan et al., 2002, Franze et al., 2009). Consequently, these cellular events lead to impaired photo-transduction to the visual cortex and loss of visual function (Bringmann et al., 2006). It is noteworthy that GFAP is not the only component of glial scar as additional cytoskeletal proteins including vimentin, nestin and synemin are also found in the scarring tissue (Luna et al., 2010, Wilhelmsson et al., 2004). Rodents with Müller glia deficient of GFAP and vimentin did not have a significant different rigidity as compared to those in wildtype rodents with fewer neovasculatures formed at the vitreous following gliosis (Lu et al., 2011). These observations suggest that other IFs might be responsible for the mechanical response of reactive Müller glia and suppression of glia scar-related IFs might facilitate retinal regeneration.

1.2.4 Müller glia constitute the source of cytokines in retinal degeneration

Gliosis is believed as an endogenous protective mechanism of Müller glia pathological insults, however it is observed in virtually all retinal degenerative disorders, such as proliferative retinopathy (PVR), glaucoma and diabetic retinopathy (Tezel and Wax, 2000, Hoerster et al., 2014, Amin et al., 1997, Muether et al., 2013). Another common observation in these conditions was the upregulation of multiple inflammatory mediators. Source of these factors in the neural retina are thought to be heterogeneous, as multiple types of cells including RPE, microglia and Müller are capable of producing these molecules (Holtkamp et al., 2001, Reichenbach and Bringmann, 2010, Pastor et al., 2016, Todd et al., 2019, Langmann, 2007). Nevertheless, Müller glia constitute a rich source of a broad range of cytokines and growth factors, into the local retina microenvironment (Lewis and Fisher, 2003, Bringmann et al., 2009)

Müller glia constitutively produce a broad spectrum of inflammatory mediators including tumour necrosis factor (TNF)-α (Yoshida et al., 2004), interleukin (IL)-6 (Yoshida et al., 2001), transforming growth factor-β (TGF-β) and VEGF. Pro-inflammatory cytokine TNF-α was originally identified as an endotoxin-induced factor released by macrophages and evidence from various organisms showed that Müller cells is the main source of TNF-α in the neural retina (Fischer, 2005, Eastlake et al., 2018, Yoshida et al., 2004, Lebrun-Julien et al., 2009, Tezel and Wax, 2000). Interestingly, a recent study suggested that microglia are the only source of pro-inflammatory cytokines IL-1 and TNF-α in acutely damaged mammalian retina (Todd et al., 2019). Elevation of TNF-α is found in various retinal diseases such as PVR, diabetic retinopathy, glaucoma and retinal detachment (Limb et al., 1991, Suzuki et al., 2011, Ghanem AA, 2010, Rasier et al., 2010, Pennock et al., 2014). In response to injury, IL-6 is increased and drives the activation of JAK-STAT signalling and Müller glia reprogramming in zebrafish (Zhao et al., 2014). Similarly following microglia activation, mammalian Müller glia showed elevated production of IL-6 (Wang et al., 2011, Hauck et al., 2007). It is also found significantly increased in PVR patients (Eastlake et al., 2018) and has shown to potentiate the expression of enzymes regulating ECM homeostasis such as matrix metalloproteinase (MMP)-1 and tissue inhibitor of metalloproteinases (TIMP)-1 (Symeonidis et al., 2011,

Pennock et al., 2014). Another member of the IL-6 family CNTF was also released by Müller glia in response to exogenous CNTF stimulation (Harada et al., 2002) and correlated to GFAP upregulation (Walsh et al., 2001). Transforming growth factor-β (TGF-β) signalling is known to induce a broad range of biological responses including immune response, cell proliferation and differentiation and apoptosis (Meng et al., 2016). Although it acts as a cytostatic signal to suppress the proliferative potential of mammalian Müller glia during retinal development (Kimchi et al., 1988, Close et al., 2005), TGF-β1 is found upregulated in gliosis and in PVR patients (Limb et al., 1994, Hoerster et al., 2014, Bringmann et al., 2009). In addition, TGF-β1 plays a pivotal role in the development of fibrotic scarring (Close et al., 2005, Bringmann et al., 2009) and is believed to be mediated by the canonical Smad pathway, or the non-canonical mitogen activated protein kinase (MAPK) or Rho-like GTPase pathways (Liu and Desai, 2015). In addition, the angiogenic growth factor VEGF family which consists of three protein subtypes acts as a pivotal mediator of angiogenesis and increasing vascular permeability (Foxton et al., 2013, Miller et al., 2013). Its release in Müller glia could be elicited by bFGF and hyperglycemia (Hollborn et al., 2004, Sun et al., 2013) and is found substantially increased in gliotic human retina (Eastlake et al., 2018, Limb et al., 1994).

1.3 Retinal degeneration and perspective therapies

1.3.1 Retinal degenerative diseases

Epidemiology data published by the World Health Organisation have predicted that the world population affected by visual impairment by 2020 would reach 285 million, with 39 million people suffering from complete blindness (Organization, 2017). With the increasing average lifespan brought by improved healthcare and life quality, the impact of these diseases would continuously get more severe, putting an enormous economic burden to the world healthcare system.

Retinal degeneration comprises a diverse group of ocular disorders that affect retinal cells found in the posterior segment and choroid, and the most commonly seen diseases are age-related macular degeneration (AMD), retinitis pigmentosa (RP), diabetic retinopathy (DR) and glaucoma (Figure 1.5). These conditions are

often characterised by pathological alterations of the surrounding vasculature due to ischaemia and leakage, which contribute to the progressive degeneration of the retina. Both AMD and RP share a characteristic loss of photoreceptors, although they differ in their pathogenesis. Secondary dysfunction of photoreceptors owning to the atrophy of RPE population leads to the development of AMD (Figure 1.5A). Early manifestation of AMD is characterised by lipid-containing drusen deposition in the space between RPE and choroid. Depletion of the central visual acuity appears when the macula is affected. Depending on the type of AMD, pharmacological treatment may vary. Neovascular AMD is managed by inhibition of angiogenesis and neovascularisation. Intravitreal injection of antivascular endothelial growth factor (anti-VEGF) drugs and factors targeting the maturation and remodelling of vasculature have been gradually introduced into clinical practice (Bandello *et al*., 2017). Whereas geographic atrophy has drawn much research, only a few anti-inflammatory drug candidates have been tested in clinical trials. These include a C3 inhibitor POT-4, which has passed phase I clinical trial, and Lampalizumab, a humanised monoclonal antibody targeting complement factor D, which has been reported to effectively delay disease progression (Potentia Pharmaceuticals, 2017; Genentech, 2017). Unlike AMD, RP is a hereditary condition that leads to malfunction and subsequent apoptosis of photoreceptors and RPE, with a high susceptibility of rods deterioration than that of cones (Figure 1.5B). DR is regarded as one of the complications associated with diabetes mellitus that has been poorly managed or had a prolonged course (Figure 1.5C).

Glaucoma is characterised by a progressive loss of RGCs and constitutes the second most prevalent cause of irreversible vision loss in the world, affecting approximately 12.3% of the world population (Figure 1.5D) (Pascolini and Mariotti, 2012, Organization, 2017). It is recognised as a heterogeneous optic neuropathy (Gauthier and Liu, 2017) and is commonly thought to be associated with increased IOP, as a result of excessive inflow of aqueous humour. Other risk factors include nitric oxide (NO)-mediated toxicity (Neufeld AH, 2002) and glutamate excitotoxicity (Hahn et al., 1988). Loss of visual field in this condition starts at the periphery and gradually spread towards the centre when the disease progresses. Control of glaucoma progression by lowering IOP both surgically and pharmacologically is the current management of this condition. Pharmacological approaches target the ciliary body and the TM by suppressing the production of aqueous humor and promoting

outflow from the TM. Topical eye drops of α-agonists, β-adrenoceptor antagonists, carbonic anhydrase inhibitors, cholinergic agents and prostaglandin analogues are considered as neuroprotective agents as they collectively reduce oxidative stress and neuro-inflammation caused by high IOP on the optic nerve (Gauthier *et al*., 2017). They are the commonly prescribed drugs as the first-line treatment but have been strongly associated with side effects, increasing incidence of ocular surface disease in old age patients. The alternative surgical invention aims to divert drainage of aqueous humor into the subconjunctival space by laser treatment. At present, new candidate molecules are being investigated to induce neuroprotection of the optic nerve by means of eliminating toxic molecules such as glutamate and NO by chemical inhibitors (Sena and Lindsley, 2017). Antioxidants glutathione and Coenzyme Q10, α-lipoic acid, superoxide dismutase have been identified to promote RGC survival (Gauthier and Liu, 2017) and constitute good candidates for therapeutic development.

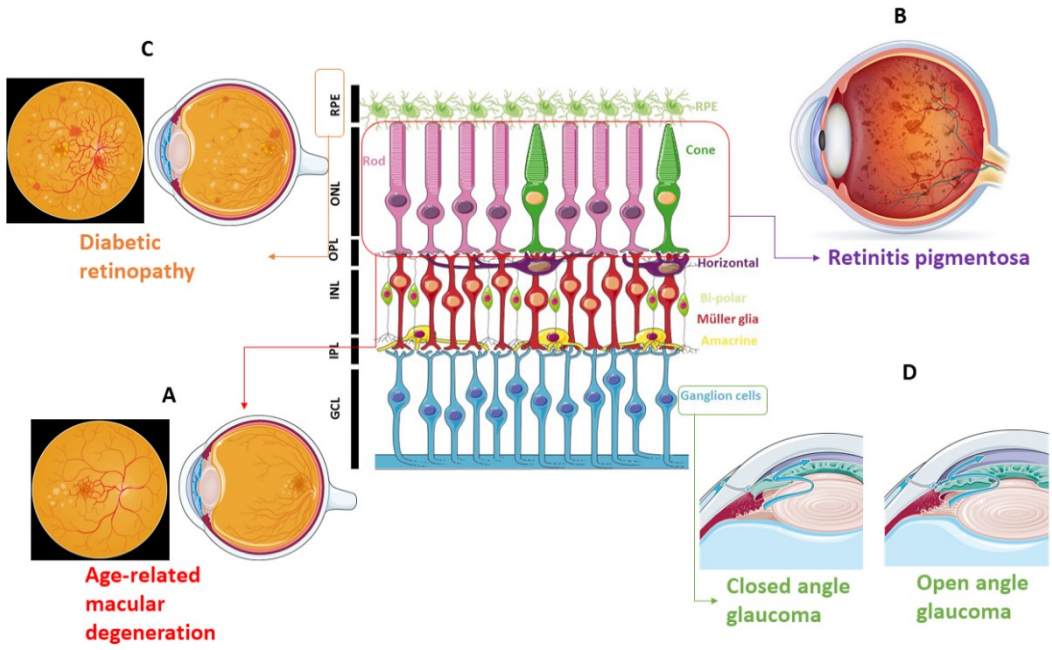

Figure 1.5 Common retinal degenerative disorders and the affected cells.
Degenerations of various retinal cells lead to distinctive retinal disorders. Age-related macular degeneration (AMD) **(A)** and retinitis pigmentosa (PR) **(B)** often involve initial defects in RPE cells and lead to dysfunctional photoreceptors. Diabetic retinopathy (DR) **(C)** occurs as a complication of diabetic mellitus, leading aberrant vascularisation in the retina. Loss of retinal ganglion cells due to increased IOP leads to open-angle glaucoma or sudden increase of IOP as closed angel glaucoma **(D)**. This imaged was produced using Servier Medical Arts (https://smart.servier.com/).

1.3.2 Potential of cell-based therapies to treat retinal degeneration

Investigations on the aetiology of retinal degenerative conditions have made significant improvement due to a better understanding of the underlying mechanisms of these disorders. However, the existing therapies could not repair the damaging neurons but only limiting the disease progression. Therefore, there is still much research needed to design new therapeutic approaches that can provide effective treatments to prevent development and/or progression of irreversible blindness in these patients.

The increasing popularity of retinal cell-based therapies by transplantation of cells into the diseased retina has been a subject of intensive research in recent years. The notion behind this idea is to deliver therapeutic cells in a formulation of single cell suspensions or cells attached to substrates made of appropriate biomaterials for subretinal or intravitreous delivery. These approaches aim to preserve the remaining visual function and/or improve such function by either cell replacement or trophic support.

The success of cell replacement would critically rely on establishing structural integration and appropriate synaptic re-establishment between the graft and the retina. While migration into the designated location of the host neural retina and sustained viability of grafted cells could be facilitated by appropriate injection methods, grafted cells should not develop aberrant synapses or disrupt existing architecture within the neural retina (Fariss et al., 2000). A few studies have shown that abnormal integration of transplanted cells could potentiate the existing retinal degeneration and fail to offer visual improvement (Fisher et al., 2005, Marc et al., 2003). Therefore, replacement approaches seem to have narrow therapeutic scope, as only patients who have already developed degeneration could benefit from this approach.

A more realistic therapeutic objective would be to provide trophic support from the transplanted cells. The sophistication of this approach is conceived from the promising results of transplanting RPCs obtained from foetal and postnatal retina (Mansergh et al., 2014). They were initially thought to have the potential to differentiate into retinal cells and to establish synapses with the host retina and visual cortex (Trese et al., 2012). However, studies involving subretinal injections of

foetal RPCs showed that the improved visual function was mainly attributed to the trophic supplementation from the graft, whilst only one study reported weak host-graft integration (Ludwig et al., 2019). RPCs have a gene expression profile of immature retinal markers (Qiu et al., 2007) and can be transplanted as allografts with minimal immunological response, although this privilege of safety is compromised due to low cell proliferation (Klassen et al., 2008). Nevertheless, these pioneer studies have laid down the concept of neuroprotective approaches for visual function improvement.

Several factors could limit the development and application of cell-based therapies to treat retinal degenerative disorders. The local retinal environment critically determines the success of transplantation. For example, dystrophic retina creates a non-permissive environment due to the presence of inflammatory cytokines and immune cells, while the accumulation of abnormal extracellular matrix in the damaged retina could hinder graft migration and integration. Most importantly, the source of cells used for transplantation critically drives the application of cell-based therapies. Ideally, autologous or heterologous population of cells should be readily available for *in vitro* expansion and elicit minimal immunological response to the recipient. In addition, the use of autologous cells would prevent adverse immune responses against the grafted cells. Unfortunately, current research findings cannot fulfil the above criteria and alternative cell source with unlimited proliferation and differentiation potential might constitute a promising source for cell-based therapies.

1.4 Application of stem cells in cell-based therapies

Increasing evidence suggests that human pluripotent stem cells (hPSCs) including human embryonic stem cells (hESCs) and human induced pluripotent stem cells (hiPSCs), as well as adult tissue-specific stem cells, such as bone marrow and mesenchymal stem cells (MSCs) could be potentially used in cell-based therapies to treat retinal diseases.

1.4.1 Embryonic stem cells

Pluripotent ESCs are derived from the inner cell mass of the developing embryo at blastocyst stage and can be sourced from embryos donated from *in vitro* fertilisation treatment (
Figure 1.6). Their infinitive *in vitro* propagation and generation of abundant linage-specific cells when exposed to appropriate inducing factors constitute an ideal cell source for retinal therapies. Many studies have successfully generated cells from ESC that are found in the retina, including RPE cells (Hirano et al., 2003) and $Pax6^{+}$ radial glial cells (Bibel et al., 2004).The feasibility of neural differentiation for transplantation of ESC-derived retinal progenitors was initially observed with non-human ESCs. Zhao and colleagues successfully generated photoreceptors from neural progenitors derived from mouse ESCs (Zhao et al., 2002) and this has laid a solid foundation for other groups who studied the transplantation of ESC-derived neural precursors into mouse models of retinal degeneration. In addition to expressing the expected neural markers within the host retina (Schraermeyer et al., 2001, Meyer et al., 2006), these cells have been reported to have limited integration ability but are able to improve or delay retinal degeneration. Comparable transplantation studies using primate ESCs co-cultured with RPE in the presence of retinoic acid, have also revealed cell integration and the presence of rhodopsin positive cells within the graft (Haruta et al., 2004, Takahashi and Haruta, 2006). Transplantation of photoreceptors derived from hESCs into mouse models of retinal degeneration have shown long term graft survival (Lamba et al., 2009). After initiation of neuronal differentiation, the expression of human leukocyte antigen (HLA) class I barely increased while class II remained absent on the ESC-derived cells (Drukker et al., 2006). As such, these cells were thought to be immune

privileged and would only elicit weak immune responses. However recent studies found that T cells and natural killer (NK) cells were activated by ESCs-derived grafts (Wu et al., 2008), suggesting that this privilege should be carefully reviewed when planning for *in vivo* transplantation.

Developing a defined protocol for retinal neuron derivation from ESCs with the appropriate inducing factors has always been a great challenge. In addition, the use of ESCs arises ethical issues for application as an allogenic cell source for therapies. Limitations arise from the uncontrolled cell growth observed in some cases due to genetic abnormalities which could lead to teratoma formation (Hentze et al., 2007, Yue et al., 2010). Most importantly, life-long immunosuppressive treatment would be required to keep the host-versus-graft response minimal. These factors suggest that further in-depth investigation is required to look into the application of ESCs as a cell source for retinal therapies.

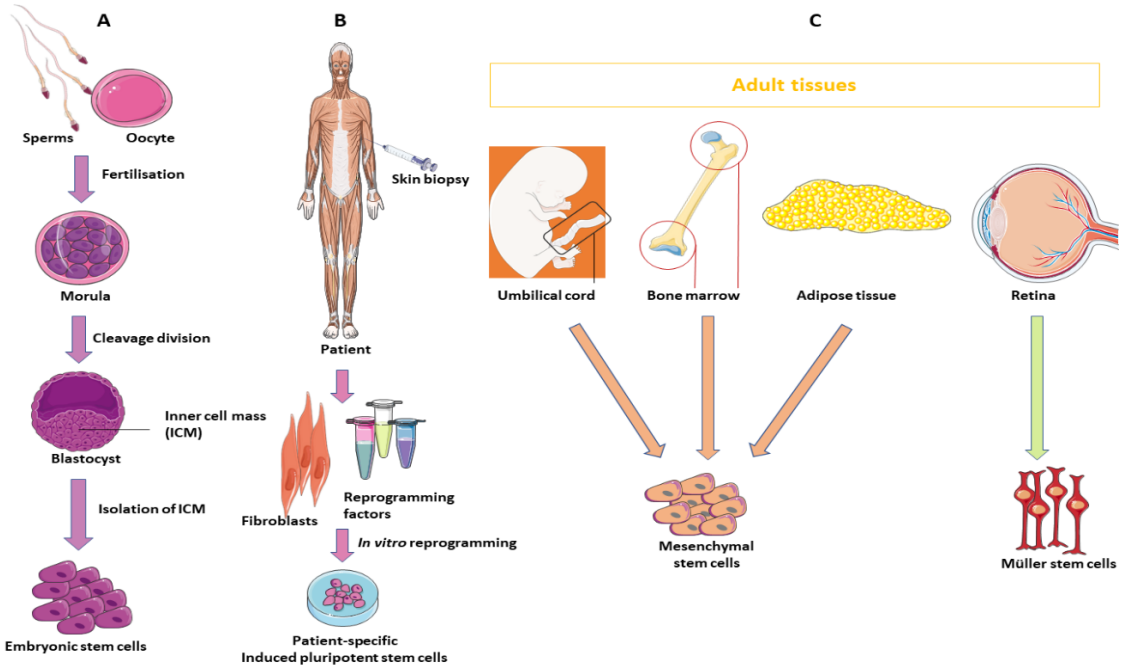

Figure 1.6 Source of stem cells with therapeutic potential for treating retinal degeneration. Stem cell pools could be obtained from **(A)** embryonic stem cells, **(B)** induced pluripotent stem cells from terminally differentiated cells by in vitro reprogramming, or **(C)** tissue-specific stem cell reservoirs located in adult specific tissues. This figure was produced using Servier Medical Arts (https://smart.servier.com/).

1.4.2 Induced pluripotent stem cells

Researchers have addressed the hurdle of lack of availability of tissue-specific progenitors for autologous transplantation. The idea of adult cells acquiring pluripotency was pioneered by Nobel Prize laureate Shinya Yamanaka, who reprogrammed terminally differentiated adult somatic cells to a state resembling pluripotent ESCs, both morphologically and functionally (Takahashi and Yamanaka, 2006, Wernig et al., 2007). Removing epigenetic and genetic modifications constitutes the first step of the reprogramming protocol, while later manipulations involve progression to pluripotency and confirmation of continuous autonomous pluripotency (

Figure 1.6) (Niwa, 2015, Takahashi and Yamanaka, 2016). The introduction of the Yamanaka protocol that originally utilised retroviral vectors to transfect fibroblasts with exogenous pluripotency genes, including Sox2, Oct4, c-Myc and Klf4, has been proven to be necessary to achieve the reprogramming objective. New generation approaches have been developed using non-viral delivery based on mRNA and chemical reprogramming, and have contributed to the upscale of *in vitro* iPSCs culture, implying that novel personalised cell therapies could become feasible (Prasad et al., 2017). Similar to ESCs, iPSCs have the plasticity to differentiate into a variety of cells including neurons, muscles and bones (Bonfanti et al., 2012). Both mouse (Hirami et al., 2009) and hiPSCs (Buchholz et al., 2009, Liao et al., 2010) could acquire photoreceptor progenitor fate under the influence of WNT and Nodal antagonists, and express RPE cell markers when further cultured with retinoic acid and taurine. In 2014, transplantation of autologous RPE sheets derived from a patient-specific iPSCs into a Japanese patient with AMD demonstrated the potential use of these cells for retinal therapies (UMIN000011929) (Kamao et al., 2014, Mandai et al., 2017, Garber, 2015). Further experimental studies have been focused on the development of photoreceptor cell therapies using cells derived from hiPSCs and have shown some success when transplanted into mouse retina *in vivo* (Lamba et al., 2010). Tumourigenecity has been associated with iPSCs, and teratoma formation was observed by two studies conducted by Tucker et al. (Tucker et al., 2013, Tucker et al., 2015), albeit significant integration within the host and enhancement of retinal functions was observed. To this extend, iPSCs may carry some advantages over ESCs, but weak and inconsistent differentiation potential and functionality should be evaluated against the unique benefits of these cells.

1.4.3 Adult tissue-specific stem cells

Although there is very little evidence of spontaneous regeneration occurring in most of the developmentally matured human tissues, few of them such as skeletal muscle, bone marrow and gut still maintain a limited pool of multipotent stem cells (MSCs) aiding in a limited maintenance of tissue turnover. MSCs can be found in bone marrow, umbilical cord and adipose tissue (
Figure 1.6). Although mouse and cat bone marrow mesenchymal stem cells (BM-MSCs) can acquire glial morphology *in vitro,* transplantation into the subretinal space only revealed prolonged survival of degenerating neurons without cell integration or axonal regeneration (Inoue et al., 2007, Junyi et al., 2015). Likewise, a study led by Rezanejad observed the expression of the neural progenitor marker Pax6 in adipose-tissue derived stem cells (ADSCs) (Rezanejad et al., 2014) and further work employing transgenic human ADSCs observed good survival of retinal cells in a rat model of retinal degeneration (Li et al., 2016b). It is noted that in addition to lack of immunoreactivity, transplantation of MSCs does not replace the lost retinal neurons but rather offers trophic support by providing anti-apoptotic and anti-inflammatory factors to the degenerated retinal cells (Xu et al., 2014, Li et al., 2016a). Clinical trials using intravitreal injection of BM-MSCs to treat RP have shown a slight enhancement in the quality of life for patients after three months, but no difference was observed after 12 months. However, there was no indication that the visual function of these patients was improved (Siqueira et al., 2013, Siqueira et al., 2015).

1.5 Objectives of this thesis

Human retina harbours Müller glia with neuroprotective potential to retinal neurons. Previous work in the host laboratory reported that animal models of retinal degeneration had their visual functions significantly improved after transplantation of human adult Müller glia, and might be owning to the trophic factors including antioxidant enzymes, neurotrophins and growth factors. This has led to the idea that a cell-based therapy of Müller glia could constitute an alternative to support the visual function of patients with retinal degeneration. Whilst obtaining cells from allogenic donors for therapeutic use is not feasible, recent studies have shown that hPSCs can be differentiated into retinal organoids that contain most of the retinal cell types including Müller glia, but studies on developing this approach and on the characteristics and functionality of these cells require further investigation.

This thesis aimed to generate Müller glia from hPSC-formed retinal organoids and to study the phenotypic and molecular functions of these cells. It also compared the Müller glia-like characteristics of hPSC-derived cells to the adult-derived Müller cell line MIO-M1. Characteristics of these hPSC-derived cells in terms of the mRNA transcriptome, molecular and cellular markers of Müller glia were investigated. The pleiotropic response of human adult Müller glia MIO-M1 cells cultured with the inflammatory cytokine TNF-α examined by RNA-sequencing techniques, and the molecular responses of hPSC-derived cells to TNF-α and TGF-β1 were compared to those of MIO-M1 cells. The neuroprotective functionality of hPSC-derived cells was assessed by establishing a glutamate excitotoxicity assay on primary rat RGCs treated with culture supernatants collected from these cells.

The specific aims of this thesis were therefore:

1) Generate retinal organoids from various hPSC sources based on an established *in vitro* retinal differentiation protocol:
    i. To identify the chronological appearance of Müller glia within these three-dimensional structures;
    ii. To isolate Müller glia from retinal organoids and propagate these cells *in vitro*.

2) Examine the molecular characteristics of the isolated hPSC-derived cells:
   i. To confirm the purity of the isolated cells based on the expression of Müller glia surface markers;
   ii. To compared the mRNA transcriptome of hPSC-derived Müller cells with the well-characterised human adult Müller glia cell line MIO-M1.

3) Assess the neuroprotective potential of hPSC-derived and MIO-M1 cells by examining:
   i. The expression of various key antioxidant enzymes under normal culture conditions;
   ii. The effect of the cytokines TNF-α and TGF-β1 on the anti-oxidative profile of Müller glia using RNA-sequencing techniques and molecular biology analysis;
   iii. To assess the neuroprotective potential of culture supernatants collected from hPSC-derived cells oo primary rat RGCs following glutamate excitotoxicity.

CHAPTER 2 Isolation of Müller glia from retinal organoids derived from human pluripotent stem cells

2.1 Introduction

2.1.1 *In vitro* generation of retinal organoids

Organoids are spontaneously self-organised three-dimensional (3D) structures formed by pluripotent stem cells (PSCs) with the support of extracellular matrix (ECM). Formation of organoids exploits the unlimited proliferation potential of PSCs and their differentiation potential to give rise to cell lineages from the three germ layers. Organoid induction protocols utilise ECMs including collagen, vitronectin, laminin, and hyaluronic acids (Ravi et al., 2015) to mimic the mechanical stiffness and permeability of the native ECM (Morrison and Spradling, 2008). Not only do ECMs allow re-aggregation of PSCs to form initial cell aggregates known as embryoid bodies (EBs), but they also facilitate proliferation, differentiation and interaction of these structures (Ader and Tanaka, 2014, Ravi et al., 2015). The specificity of organoid formation from EBs is also dictated by various differentiation and growth factors that participate in different stages of early embryonic development (Figure 2.1A). With the appropriate growth factors, it is possible to drive specific differentiation processes that generate organoids such as cerebellar, neural tube, hippocampus cortex, neural retina, optic cup and liver buds amongst others (Figure 2.1A) (Kuwahara et al., 2015, Chambers et al., 2013, Muguruma et al., 2015, Ranga et al., 2016, Sakaguchi et al., 2015, Takebe et al., 2014). For example, Activin A is required for mesoderm induction and with other growth factors such as WNT3 and FGF4, intestinal organoids can be produced while renal organoid development is driven by bone morphogenetic protein 4 (BMP4) and retinoic acid (RA). By varying the concentrations of serum-free alternative knockout serum replacement (KSR) and Matrigel, it is possible to derive neuroectoderm tissues such as cerebral and retinal organoids.

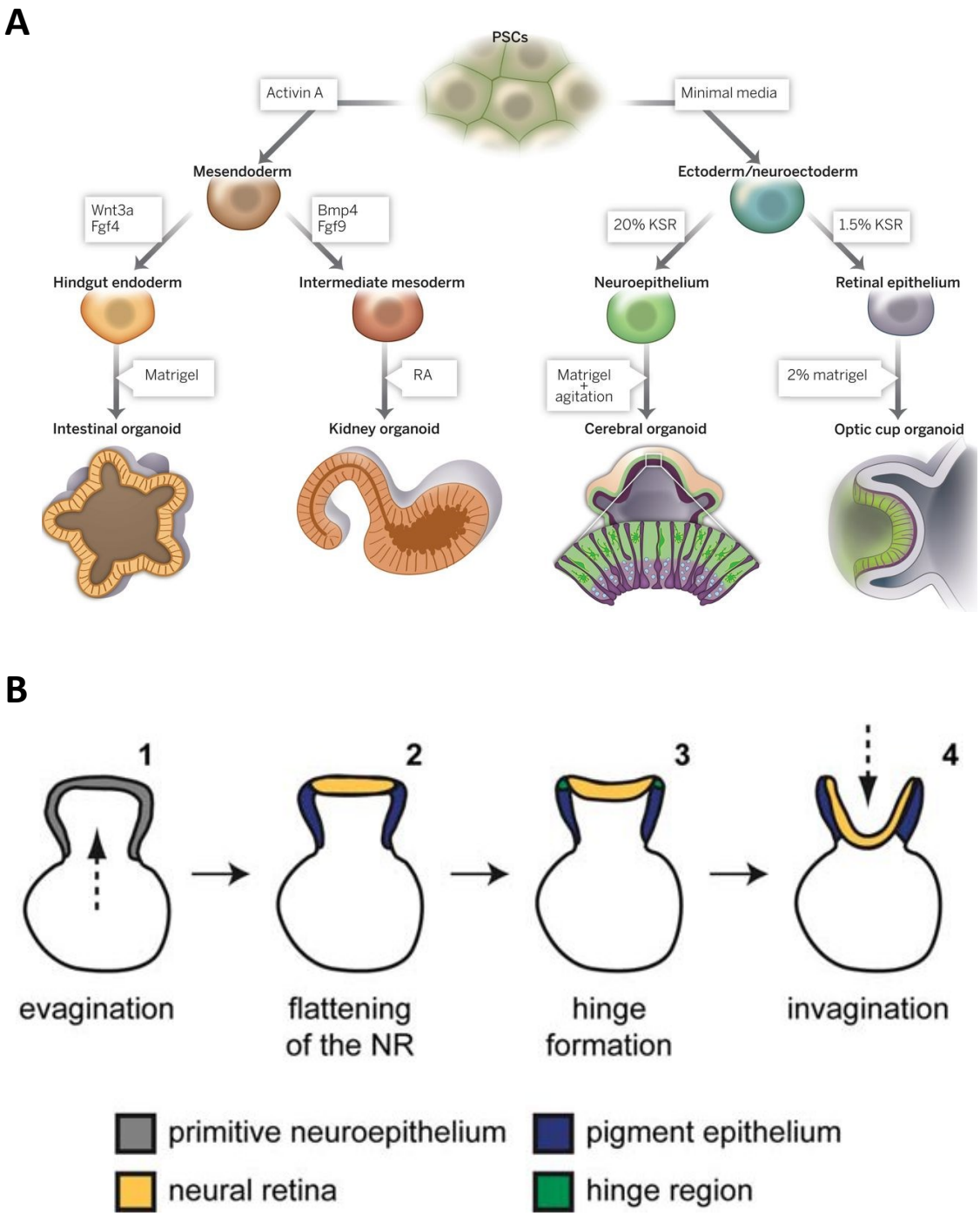

Figure 2.1 Formation of various types of organoid tissues by PSCs.
(A) Growth and differentiation factors and ECMs drive the differentiation of PSCs into organoids. PSCs cultured with a combination of factors and ECM can generate 3D tissues derived from the three germ layers. This figure was partially adapted from (Lancaster and Knoblich, 2014). **(B)** Illustration of optic cup formation *in vitro* 1). The primitive neuroepithelium (top grey region) evaginate from EBs (white region); 2 & 3). Distal region gives rise to the future neural retina (yellow), a hinge section (green) becomes the ciliary marginal zone and pigmented epithelium (blue) appears. 4). Invagination of the neural retina. This figure was partially adapted from (Karus et al., 2014).

The protocols used for generating retinal organoids are based on the induction of a retinal lineage that mimics neural differentiation by inhibiting morphogen BMP and WNT. This allows the activation of eye field transcription factors such as PAX6, RAX and VSX2 (Watanabe et al., 2005). By culturing PSCs in Matrigel medium containing Sonic hedgehog (Shh) agonist and WNT inhibitor, EBs undergo a spontaneous invagination process, in which optic cup-like structures emerge of these structures. This process is driven by the actomyosin contraction in the local cells and shows a close resemblance of retinogenesis *in vitro* (Figure 2.1B) (Eiraku and Sasai, 2011). In this process, evagination first occurs at the primitive neuroepithelium of the EBs (Figure 2.1B-1), followed by the flattening of the distal region of this structure, forming a two-walled structure separated by a hinge region which then becomes the future ciliary marginal zone (Figure 2.1B-2). The future neural retina derives from the inner wall while the outer wall gives rise to the pigmented epithelium (Figure 2.1B-3). Finally, optic cups become polarised as the invagination of the neural retina occurs (Figure 2.1B-4). Upon long-term *in vitro* culture in medium containing RA and N2 supplement, retinal organoids develop a characteristic stratification of the neural retina (Durston et al., 1989, Li et al., 2018), with the correct alignment and topology of retinal cells (Eiraku and Sasai, 2011).

2.2 Retinal organoids constitute an important tool to understand retinal development and for disease modelling *in vitro*

Retinal organoids constitute a powerful tool for a better understanding of the eye development (Wei et al., 2017). Previous studies have demonstrated both spatial and temporal expression of rods- and cones-specific genes, with CRX first appearing at the basal region of the neural retina as early as day 37 in culture (Kaewkhaw et al., 2015). Expression of the rod-specific gene neural retina leucine zipper protein (NRL) coincided with the late expression of CRX and peaked at day 90. Pioneering work has used iPSCs derived from patients to generate organoids for disease modelling (Xia et al., 2013) and to study pharmacokinetics of novel drug candidates (Takebe et al., 2014). By applying CRISPR-Cas9 system, Parffit and his co-workers have introduced introns into the gene encoding RP2 protein in iPSCs-derived RPE cells and studied disease mechanisms of retinal ciliopathy (Parfitt et

al., 2016). Retinal organoids can also serve as *in vitro* models to study photoreceptor degeneration and evaluate the protective effects of putative drug candidates (Ito et al., 2017).

Differentiation protocols can be manipulated to generate region-specific or population-enriched cells at the cost of other cell types, favouring the therapeutic aims on replacing degenerated tissue structures. So far, protocols developed to generate minicorneal organoids and cell enrichment for RPE and photoreceptors have been very successful (Wei et al., 2017, Kuwahara et al., 2015, Eiraku and Sasai, 2011, Reichman et al., 2017, Susaimanickam et al., 2017, Li et al., 2018). Cells found at the outer segment region of retinal organoids have shown responses to light stimuli, which is akin to photoreceptor rods *in vivo* (Zhong et al., 2014). Some groups have taken a step forward by performing transplantation of retinal cells derived from retinal organoids. This is illustrated by studies in which transplantation of 3D retinal outer nuclear layers, comprising mature photoreceptors derived from mouse ESCs and iPSCs, into a retinal degeneration mouse model, has showed structural integrations of these retinal sheets with the host retina (Assawachananont et al., 2014). Similarly, photoreceptors derived from mouse ESCs have been transplanted into the subretinal space of a rhodopsin-depleted mouse model. The transplanted cells appeared to show integration within the host retina as evidenced by the expression of synaptic markers (Santos-Ferreira et al., 2016). Furthermore, transplantation of RPE derived from iPSCs in a retinal dystrophic rat model has offered both short-term and long-term protective phagocytosis of photoreceptor outer segments (Carr et al., 2009), providing evidence for the feasibility of cell replacement by PSC-derived cells in the near future.

2.3 The application of transcriptomic profiling in retinal biology

The complete collection of molecular constituents and their expression levels in cells or tissues under physiological changes or diseases is known as the transcriptome. Over the last two decades, several sequencing methodologies have been developed to acquire transcriptomes and these include the hybridisation-based method microarray analysis (Royce et al., 2007), the sequence-based approach serial analysis of gene expression (SAGE), as well as the latest next-generation RNA-sequencing (RNA-seq) technology (Wang et al., 2009b). The high-throughput

RNA-seq overcomes several hurdles associated with microarray and SAGE, as it works by the principle of DNA amplification that can generate reads with high fidelity, reproducibility and low background signals (Marioni et al., 2008). The principle of RNA-seq is similar as other sequencing methodologies. This involves the construction of a cDNA library using a small amount of RNA, before undergoing fragmentation by hydrolysis or nebulisation (Figure 2.2A) (Mortazavi et al., 2008). Adaptors are ligated to one or both ends of cDNA fragments, which serve as templates for generating millions of short nucleotide sequences called reads (Figure 2.2B). Computational analysis starts by conducting quality assurance of the pre-alignment data including removing data contaminants such as vector, adapter and ribosomal reads (Figure 2.2C). This is followed by mapping the processed reads to exons of each gene in a reference genome and quantification of their expression levels. Differential gene analysis is carried out on genes that reach a threshold for significance and can be clustered to perform statistically analysis (Wang et al., 2009b, Marioni et al., 2008).

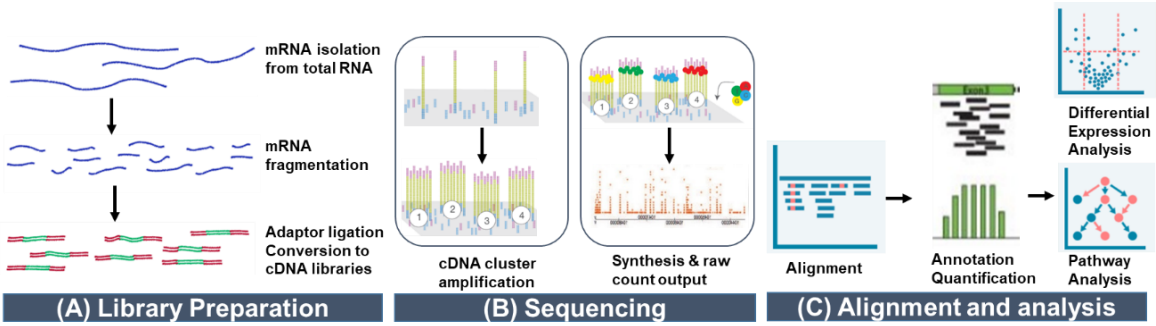

Figure 2.2 Illustration of the workflow for RNA sequencing.
(A) mRNAs are purified from total RNA and fragmented, followed by adaptor (red) ligation at the end of each fragment and conversion into cDNA. **(B)** Prepared cDNA libraries are loaded to a flow cell surface where they are amplified into small clusters by bridge amplification. Fluorescently labelled nucleotides are incorporated during the sequencing cycles and the emission of signals during synthesis process are recorded. **(C)** Using bioinformatics tools, raw reads are aligned to a reference genome sequence, followed by annotation and quantification of each gene. These data enable in-depth interpretation on the differential expression of genes and pathway analysis. This figure was partially adapted from the protocols published by Illumina® (https://emea.illumina.com) and GeneVia Technologies (https://geneviatechnologies.com/).

In retinal biology, transcriptomic profiling is useful to reveal key developmental states and signalling pathways during retinogenesis. Genes and the underlying

signalling cascades involved in the development of murine retinal cells at multiple time points have been investigated. Specifically, it has been observed that the expression pattern of genes found in mitotic neural progenitors is highly similar to that of the developing Müller glia, highlighting the endogenous regenerative potential of these cells (Blackshaw et al., 2004). A recent single cell RNA-seq (scRNA–Seq) study on RPCs isolated from hESC-derived retinal organoids identified two subgroups of RPCs with pluripotent and neurogenic potential (Mao et al., 2019). Similar approaches have also helped to interrogate the emergence of various types of retinal cells within the developing hESC-formed retinal organoids (Welby et al., 2017, Collin et al., 2019a). RNA-seq is also employed to address the spatially varied expressions of the molecular determinants in human retinae, as supported by the distinctive low expression of gene BEST1 and MAK in the macular region, and the explicit expression of matrix Gla protein (MGP) in RPE/choroid (Whitmore et al., 2014). The molecular heterogeneity of human retina is illustrated by another scRNA–Seq study that revealed 18 distinct clusters of cells expressing characteristic markers of retinal cells (Lukowski et al., 2019).

Other studies have explored the transcriptomic dynamics of mammalian retinae following pathological changes. It has been reported that genes encoding proteins of the anti-oxidative and immune responses are upregulated in the transcriptome of murine retinae following axonal damage (Yasuda et al., 2014). Pathway analysis in this study also reported that those differentially expressed genes actively drive cell death and survival pathway, suggesting a pleiotropic response mediated during early stages of axonal injury. Phototoxicity induced by UVB irradiation in mouse models has also shown to lead to upregulation of selective gene clusters responsible for cellular stress and chromatin regulation (An et al., 2018). Whilst transcriptomic profiling from patients with early and late stage of AMD have revealed an overlap of 15 key genes that might serve as putative biomarkers for AMD diagnosis (Newman et al., 2012, Whitmore et al., 2013), many studies have also focused on elucidating the transcriptomes of a specific cell types in the neural retina. In-depth analysis on the human RPE transcriptome has addressed the strong link between five miRNAs and mutated genes commonly identified in retinitis pigmentosa (Donato et al., 2018). The transcriptome of the freshly isolated murine Müller glia was shown to contain several clusters of highly expressed transcripts that dictate known functions of Müller glia (Roesch et al., 2008). In addition, many

transcripts enriched in this transcriptome revealed to be coding for factors produced by Müller cells such as chemokines, growth factors and novel transcripts. Transcriptomic libraries of human Müller cells examined by SAGE analysis showed that gene expression profiles of human Müller cells sourced from normal and diabetic patients exhibited substantial difference on gene clusters related to metabolism, transcription, as well as synthesis and transport of proteins (Lupien et al., 2007). In summary, many transcriptomic findings, including novel transcripts, post-transcriptional modification of transcripts, alternative splicing events and single nucleotide polymorphisms (SNPs), as well as the non-coding RNAs have been uncovered in human retinae (Wang et al., 2009b, Sultan et al., 2008, Farkas et al., 2013). In-depth exploration of these transcriptional regulatory events could contribute to knowledge on the regulation of chromatin accessibility and ultimately pathogenesis of retinal disorders.

2.4 Objectives and experimental outline

Obtaining Müller glia from retinal organoids derived from hPSCs may facilitate the development of allogeneic cell therapies using these cells. Therefore, the aim of this chapter was to generate retinal organoids formed by hPSCs and to isolate and characterise Müller glia from these structures. Isolated cells were examined for their characteristic markers of Müller glia using molecular and immunohistochemical analyses. These cells were compared with the adult human Müller glia cell line MIO-M1, which has shown experimental impact on improving visual functions in animal models of retinal degeneration.

The specific aims of this chapter were:

1. To generate retinal organoids from different hPSC sources and to identify the developmental stage of retinal organoids at which Müller glia emerge within these structures;
2. To isolate Müller glia from retinal organoids and expand them *in vitro;*
3. To characterise isolated cells for their characteristic markers of Müller glia;
4. To confirm the Müller cell nature of the isolated cells by examination of their transcriptomic phenotype.

Experimental design:

i. A summary of the experimental design is illustrated in Figure 2.3. Generation of retinal organoids was initiated by seeding single cell suspensions of hPSCs into v-bottomed 96-well plates and inducing their retinal differentiation using a protocol adapted from Nakano et al. (Figure 2.4) (Nakano et al., 2012). At various time points after initiation of differentiation, organoids were harvested to identify the emergence of Müller glia by immunohistological and molecular analyses.

ii. Between 70 to 121 days after initiation of differentiation, retinal organoids were enzymatically dissociated into single cell suspensions before plating in culture flasks pre-coated with fibronectin. Adherent cells were propagated *in* vitro to obtain confluent monolayers after several passages. The localisation of Müller glial markers was analysed for immune-staining of cell monolayers.

iii. The purity of isolated cells was examined by FACS analysis.

iv. Cell pellets were collected for total RNA and protein extraction to investigate the expression of Müller glia markers using RT-PCR and western blotting techniques.

v. For mRNA transcriptomic analysis, three consecutive passages of isolated cell preparations from hiPSC and hESC sources and the human adult Müller cell MIO-M1 cells were collected as biological replicates. RNA-sequencing was performed by 75 bp pair-end sequencing on an Illumina® HighSeq 3000 platform by UCL Genomics. Bioinformatics analysis was performed in collaboration with Dr Nicholas Owen at the Institute of Ophthalmology. Differential gene expression and gene ontology (GO) analysis were performed on a pairwise comparison between the three cell preparations. Statistical analysis was performed by programming software R environment. RNA-sequencing findings were validated by Taqman™ qRT-PCR.

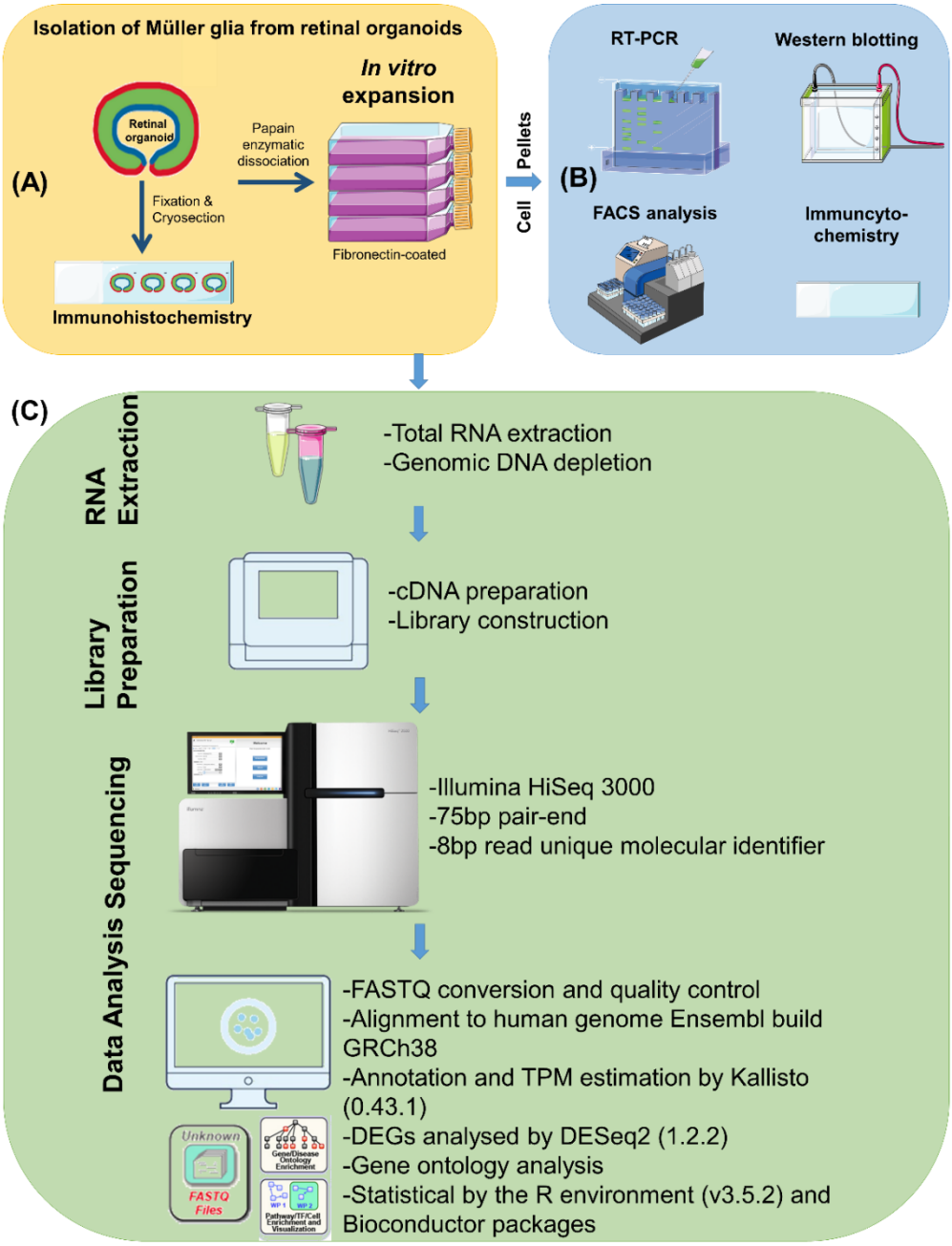

Figure 2.3 Experimental outline.
(A) Differentiation of hPSCs into retinal organoids was initiated using a protocol adapted from a previously published work (Nakano et al., 2012). Retinal organoids were cryosectioned for immunohistological analysis. Organoids were also dissociated to single cell suspensions and plated onto fibronectin-coated culture flasks for in vitro expansion. **(B)** Expanded cells were collected for RNA and protein extraction and subsequent RT-PCR, western blotting analysis, as well as for immunocytochemistry to examine Müller cell markers. **(C)** Cell pellets were collected for RNA-sequencing. This image was produced using Servier Medical Arts (http://smart.servier.com).

2.5 Results

2.5.1 Differentiation of hPSCs into retinal organoids

In this study, three hPSC lines were used to generate retinal organoids: the hiPSC line BJ (kind gift of Dr Amanda Carr, UCL) and the hESC lines Shef 6 and RC-9 both obtained from the UK Stem Cell Research Bank. The differentiation protocol used to generate retinal organoids was a modification of the protocol published by Nakano et al. (Nakano et al., 2012) and modified in the host laboratory at the Institute. A schematic illustration of this process is summarised in Figure 2.4.

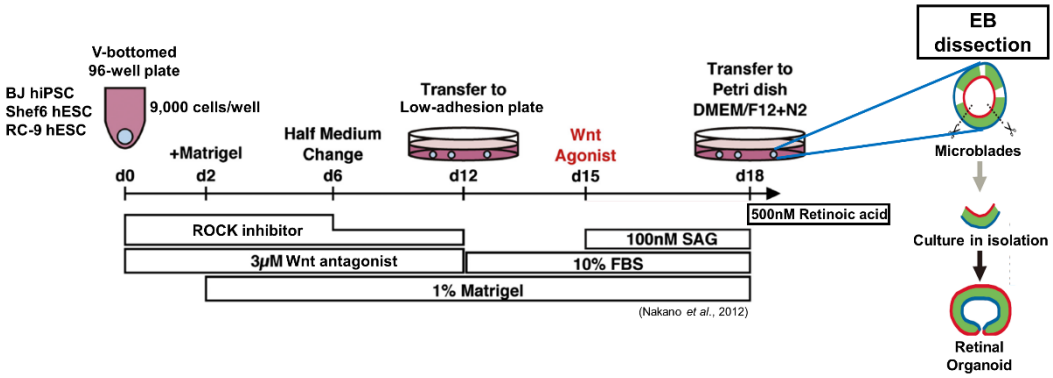

Figure 2.4 Schematic illustration of generation of retinal organoids from hPSCs.
Retinal organoid formation involved a few stages of culturing of hPSCs with combinations of different inducing and growth factors and Matrigel at critical time points (marked on the timeline). Manual dissection of EBs with surgical microblade was used to purify and encourage growth of retinal organoids up to 70-121 days in culture. hiPSC: human induced pluripotent stem cells; hESC: human embryonic stem cell; d: day; SAG: Smoothened agonist; EB: embryoid body. This image was adapted from Nakano et al., 2012.

Briefly, before initiation of EB formation, colonies of hPSCs showing the best growth parameters were selected, based on the criteria of round colonies with clean margin and no differentiation (Figure 2.5, 1st row). Spherical EBs were observed two days after initiation of retinal differentiation and became denser as the differentiation progressed (Figure 2.5, 2nd row). The size of the EBs gradually increased as the culture developed and small protrusion of 'mantle'-like structures started to emerge approximately at day 12 (not shown). By day 18, optic cups with characteristic retinal lamination became visible at the distal region (not shown). From day 21 to 31, these retinal structures were isolated manually by microblade dissection under a microscope and cultured in low-adhesion plates with medium containing retinoic acid (Figure 2.5, 3rd row). These neural retina structures persisted for up to 70 - 121 days (the time points at which organoids were processed for cell isolation) (Figure 2.5, 4th and 5th rows). Additional dissections were performed in several retinal organoids to encourage their expansion. Generation of retinal organoids was repeated for multiple batches for different hPSC sources and more than 10 batches of organoids were successfully generated using BJ and RC-9 cells, as shown by their distinctive retina 'mantle'. In contrast, only two batches of organoids were formed by Shef 6 cells out of five batches of attempts, and few of them displayed lamination structures at the periphery. This might be attributable to the quality of hiPSC colonies which was observed with spontaneous differentiation during *in vitro* maintenance and might also reflect the variability of hPSC when subjected to retinal differentiation protocols.

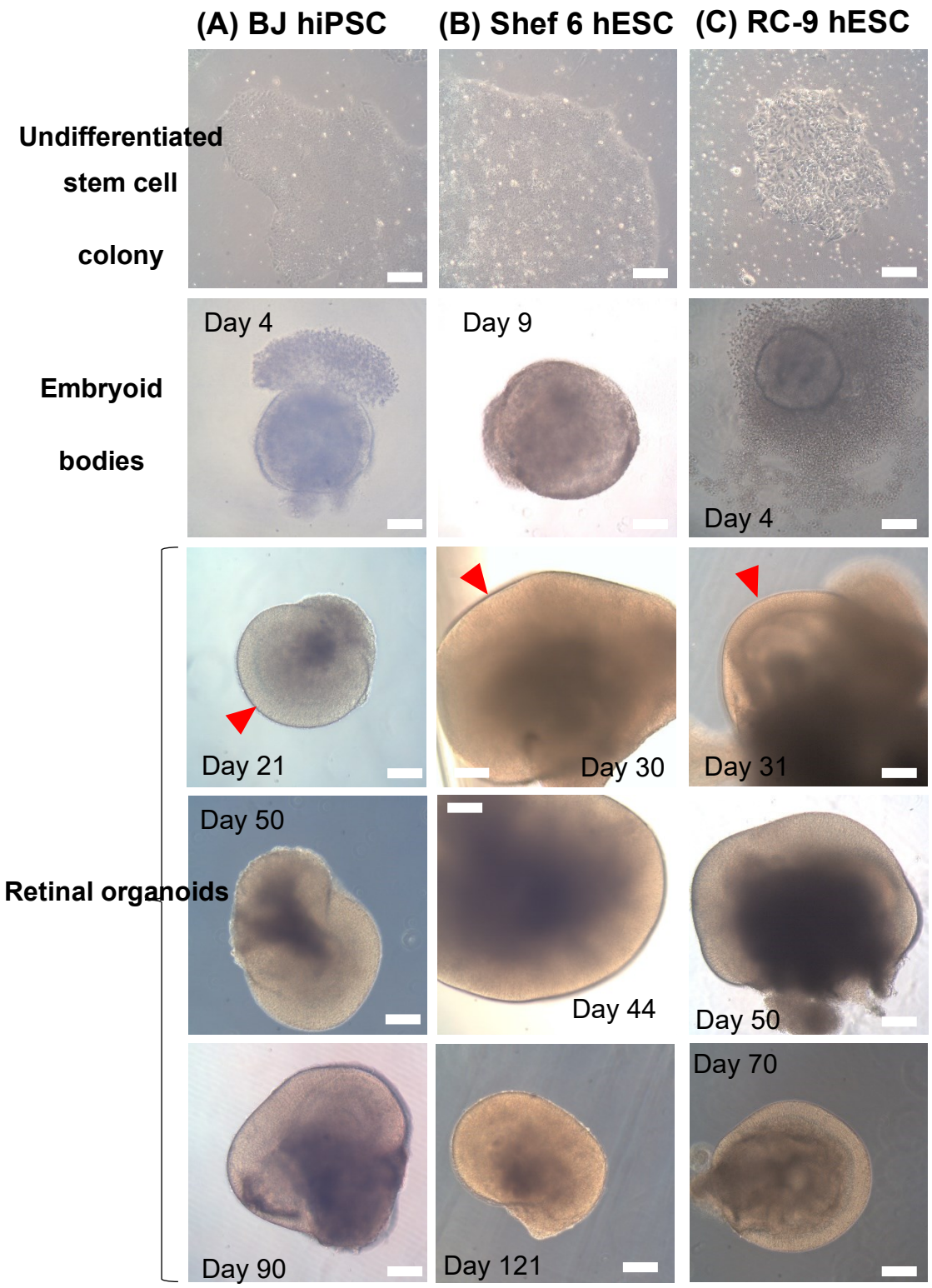

Figure 2.5 Generation of retinal organoids.
Images show representative phase microscopy images of undifferentiated stem cell colonies formed by (A) the hiPSC line BJ and **(B, C)** the hESC lines Shef 6 and RC-9, before and after initiation of retinal differentiation. Aggregates of hPSCs resembling embryoid bodies (EBs) were observed as between day 4 to 9 after initiation of differentiation. The characteristic neural retina 'mantle' at the periphery of the retinal organoids were clearly visible after microblade isolation of retinal organoids from the EBs (day 20-31; red arrows). Retinal organoids became enlarged as the differentiation proceeded towards long-term maturation (day 40 onwards), after which some retinal organoids were repeatedly dissected and cultured for up to 121 days. Scale bars = 20μm.

2.5.2 Presence of Müller glia markers within retinal organoids

Retinal organoids derived from each hPSC source were examined at different time points to assess the appearance of Müller glia. Retinal organoids analysed at various time points after stem cell differentiation are shown in Table 2.1.

Retinal organoid	hPSC source	Harvest day after initiation of retinal differentiation
BJ Day 32	hiPSC BJ	32
BJ Day 52		52
BJ Day 70		70
BJ Day 90		90
RC9 Day 10	hESC RC-9	10
RC9 Day 16		16
RC9 Day 51		51
RC9 Day 84		84
Shef 6 Day 121	hESC Shef 6	121

Table 2.1 List of retinal organoids and harvesting time points used for immunohistochemical analysis.

Immunohistological staining of retinal organoids formed by the RC-9 cells revealed that the Müller glia surface marker CD29 mainly appeared at the periphery of the well-organised neural retina, as early as day 10 after initiation of retinal differentiation (Figure 2.6 & Figure 2.7). As the organoid maturation continued (examined at days 16, 51 and 84), other Müller markers including vimentin, nestin and glutamine synthetase (GS) were identified spanning the entire width of the retina 'mantle'. This indicated the localisation of Müller cells within the neural retina. Similarly in retinal organoids formed by BJ cells at various time points after initiation of retinal differentiation, immunoreactivity for the Müller glia markers vimentin and nestin was detected when examined at days 32, 52, 70 and 90 (Figure 2.7). CRALBP was not detected in all the retinal structures observed. Following retinal differentiation, the majority of the Shef 6 cells did not form retinal organoids but rather remained as disorganised cell aggregates, despite cells within these structures being positive for GS and CD29 (Figure 2.8). Together, the localisation of Müller cells within the BJ- and RC-9-formed retinal organoids are in line with the *in vivo* observation that Müller glia extend across the mammalian retinae.

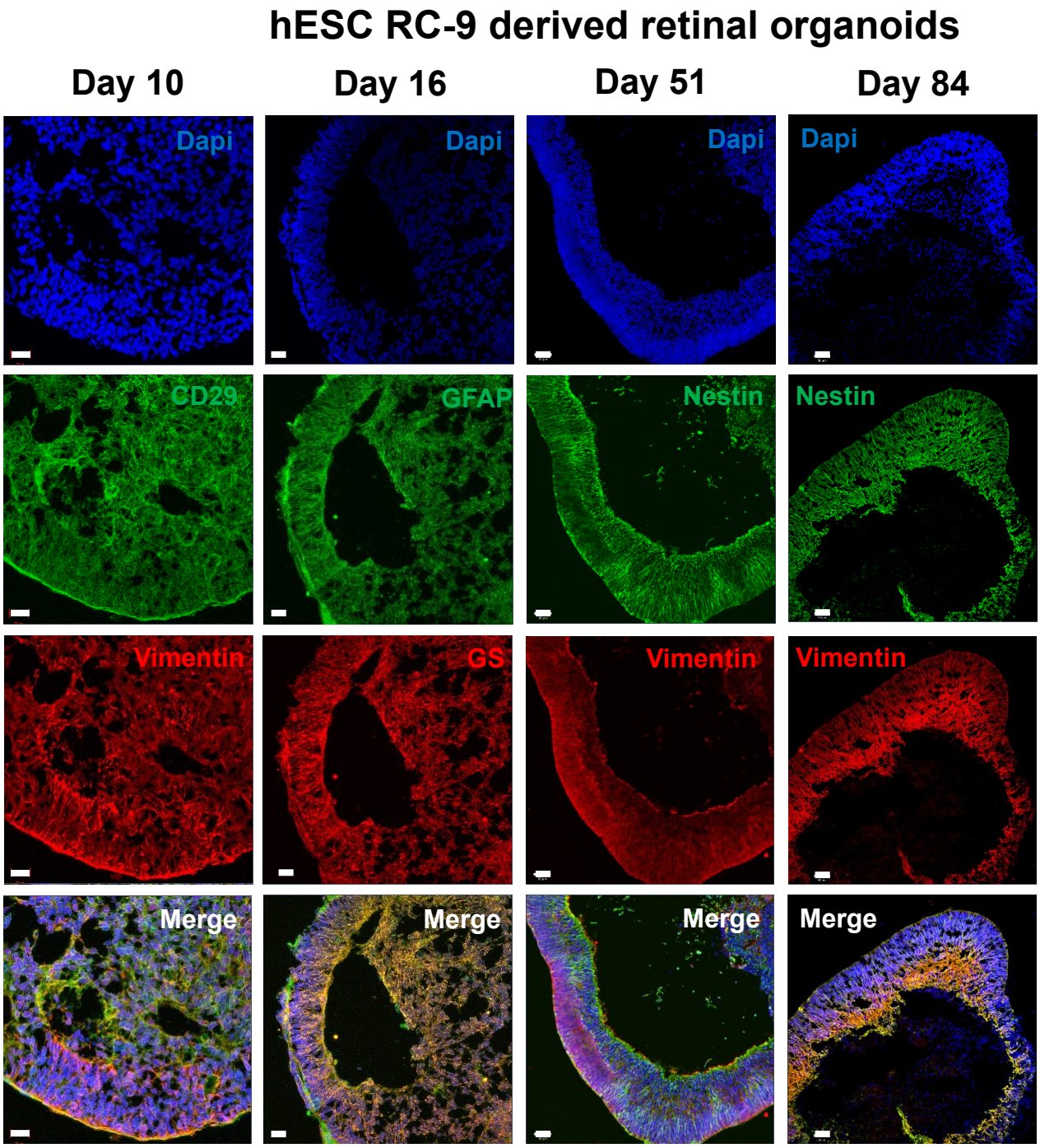

Figure 2.6 Immunohistological characterisation of retinal organoids derived from the hESC line RC-9.
Representative images of retinal organoids showing immunostaining for the Müller glia markers CD29, vimentin, GFAP, GS and nestin at days 10, 16, 51 and 84 after initiation of differentiation. Antibodies used for detection are indicated by the corresponding colours: Green-Alexa Fluor® 488; Red-Alexa Fluor® 555; Blue-DAPI. Scale bars = 50µm.

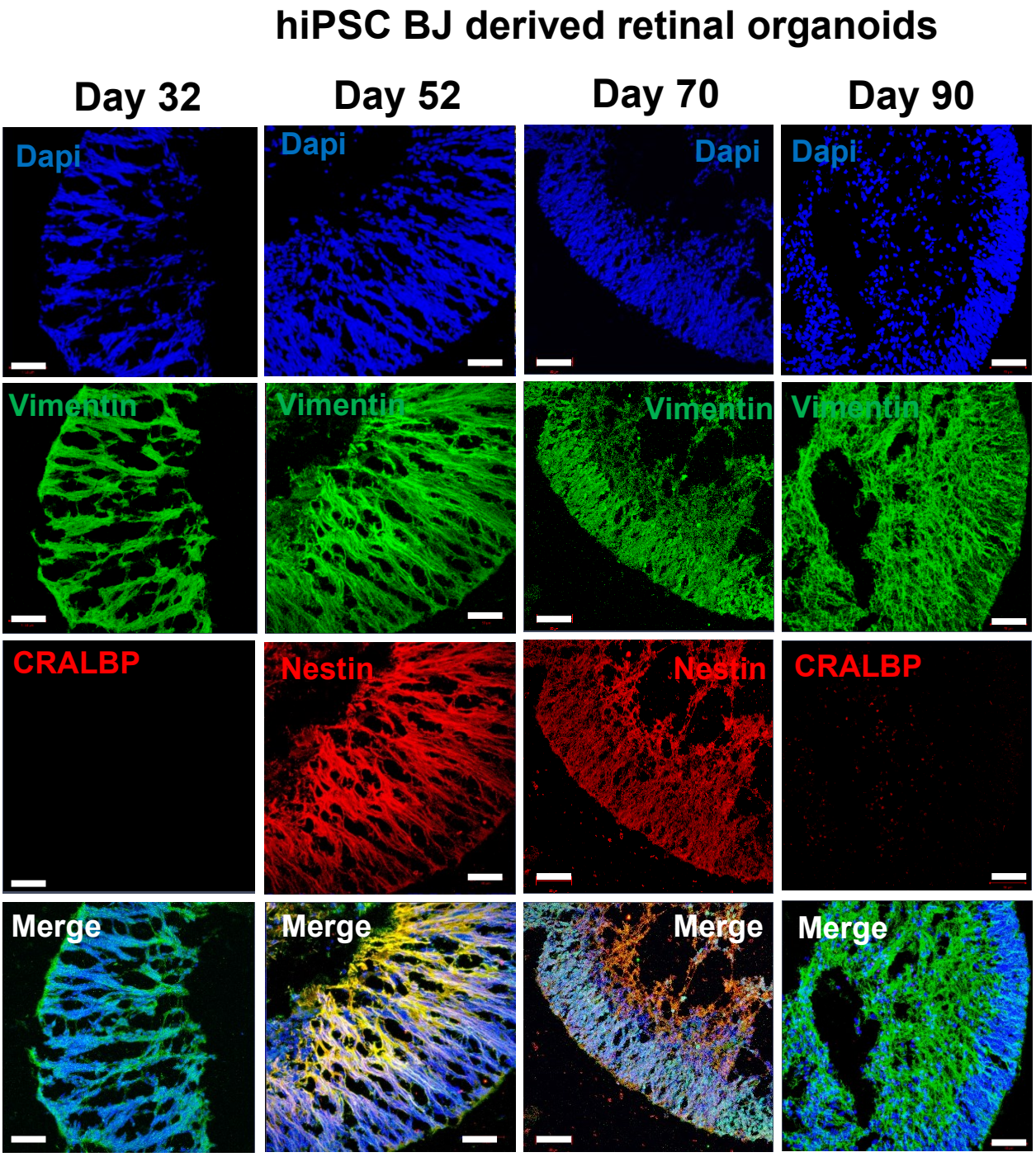

Figure 2.7 Immunohistological characterisation of retinal organoids derived from hiPSC line BJ.

Representative images of retinal organoids showing immunostaining for the Müller glia markers vimentin, CRALBP and nestin at days 32, 52, 70 and 90 after initiating of organoid formation. Antibodies used for detection are indicated by the corresponding colours: Green-Alexa Fluor® 488; Red-Alexa Fluor® 555; Blue-DAPI. Scale bars = 50µm.

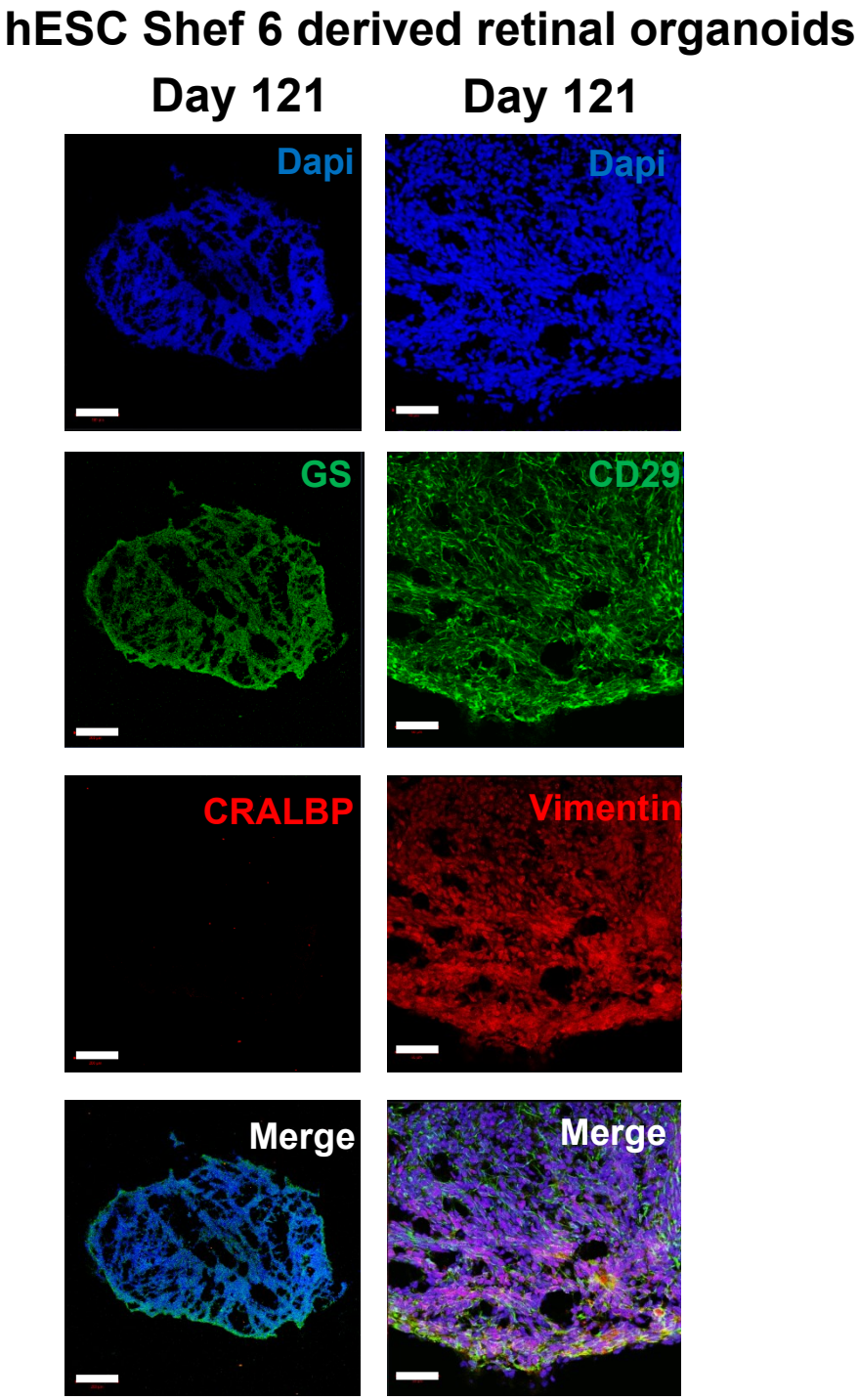

Figure 2.8 Immunohistological characterisation of 3D cell aggregates derived from the hESC line Shef 6.

Representative images of disorganised cell aggregates formed by Shef 6 cells showing that cell aggregates immunostained for the Müller glia markers CD29, vimentin, and CRALBP at days 121 after initiating differentiation. However, cells present in the aggregates did not exhibit the characteristic Müller glia morphology. Antibodies used for detection are indicated by the corresponding colours: Green-Alexa Fluor® 488; Red-Alexa Fluor® 555; Blue-DAPI. Scale bars = 50µm.

2.5.3 Isolation of CD29-positive cells from retinal organoids and their *in vitro* propagation

Retinal organoids showing neural retinal 'mantles' were dissociated between days 70 to 121 after initiating retinal differentiation. They were dissociated into a single cell suspension using papain followed by trituration in a protein solution containing BSA and ovomucoid (see Materials and Methods). After centrifugation, cells were seeded in flasks pre-coated with human fibronectin. The principle of isolating Müller glia was based on the binding of the Müller glia cell surface marker CD29 (β-integrin 1) to its substrate fibronectin. Dissociated cells were cultured in medium containing epidermal growth factor (EGF) and fibroblast growth factor (FGF) to promote cell growth. Previous work in the hosting laboratory indicates that EGF promotes proliferation of freshly isolated Müller cells, and that cells would otherwise acquire terminally differentiated morphology in the absence of EGF. Table 2.2 lists the most representative retinal organoids from each hPSC source at which CD29-positive cells were successfully isolated:

Isolated cells	hPSC source	Retinal differentiation days
BJ Day 90	hiPSC BJ	90
RC-9 Day 70	hESC RC-9	70
Shef 6 Day 121	hESC Shef 6	121

Table 2.2 List of retinal organoids and time points of dissociation.

The Müller glia morphology of cells isolated from BJ organoids at day 90 (hereafter refer as BJ Day 90 cells) was consistent up to passage 6 (Figure 2.9A). These cells were smaller than MIO-M1 cells used as a reference (Figure 2.9D). Dissociated cells in culture formed small clusters that resemble neurospheres when cultured with FGF. During early passages, the morphological features of cells isolated from Shef 6 organoids at day 121 (hereafter refer as Shef 6 Day 121 cells) resembled epithelial-like cells (Figure 2.9B). However, upon reaching passage 6, they became very irregular and formed small clusters that after subsequent passages did not proliferate. Cells isolated from RC-9 organoid at day 70 (hereafter refer as RC-9 Day 70 cells) showed a distinctive bipolar morphology (Figure 2.9C), which persisted throughout *in vitro* propagation and highly resembled MIO-M1 cells.

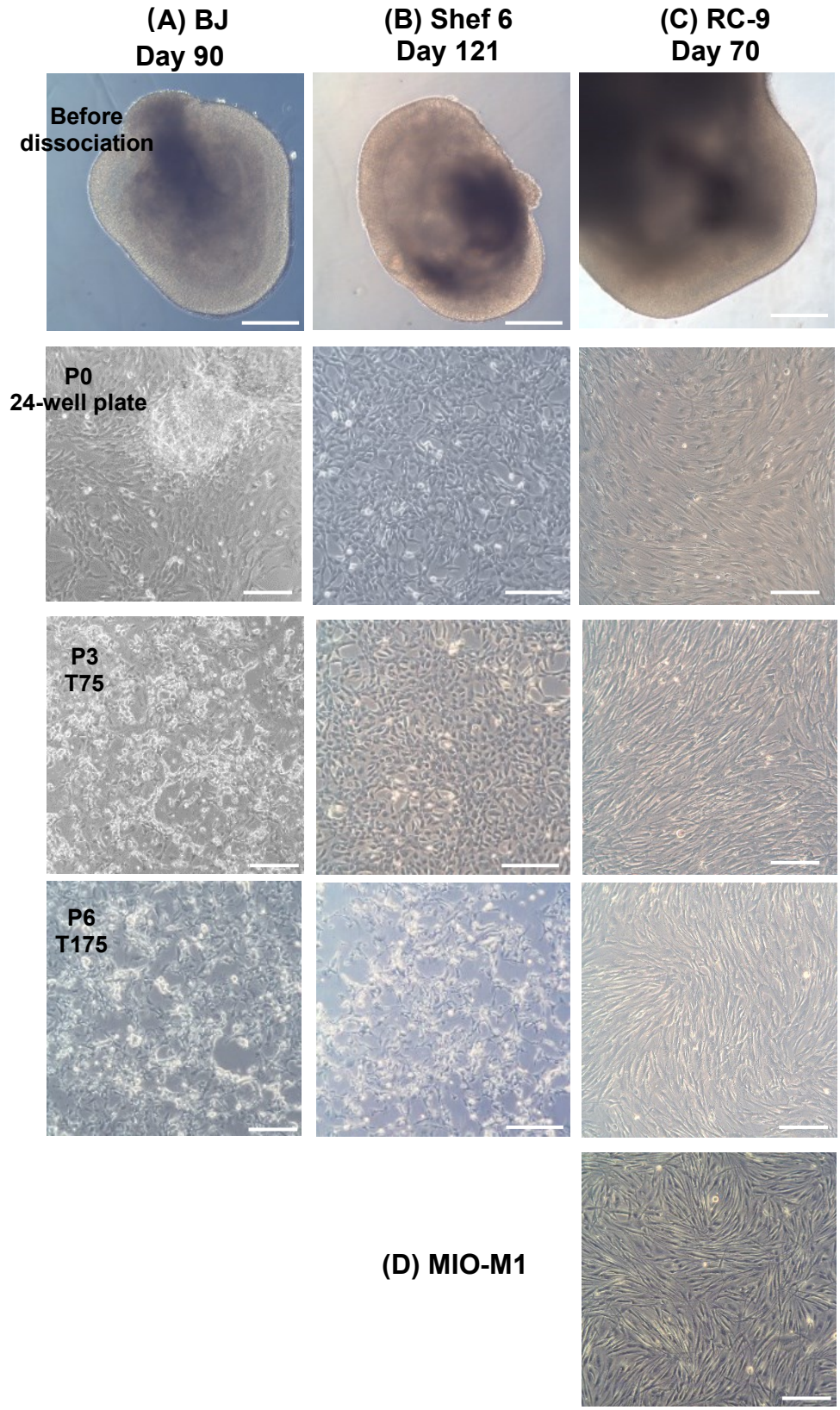

Figure 2.9 Morphological characteristics of cells isolated from retinal organoids formed by (A) hiPSC BJ at day 90, (B) hESC Shef 6 at day 121 and (C) hESC RC-9 at day 70.
Brightfield images show the retinal organoids derived from each hPSC source at various time points after initiating retinal differentiation (1st row). The morphological appearance of isolated cells from each hPSC source were shown at confluency in a 24-well plate (passage 0), T75 culture flask (Passage 3) and T175 culture flask (Passage 6). (D) MIO-M1 cells were used a reference. Scale bar = 50µm.

2.5.4 Molecular characterisation of cells isolated from hPSC-formed retinal organoids

Following *in vitro* propagation for several passages, the expression profile of genes coding for Müller cell markers was examined by RT-PCR and western blotting. The Müller glia markers investigated included GS, GFAP, vimentin and the neural progenitor markers were Sox2, Sox9, nestin, Pax6, Notch1, WNT2B and WNT5B. The results showed that cells isolated from each hPSC source showed specific expressions of Müller glia markers, as compared with the expression profile of the well-characterised adult Müller cell line MIO-M1 (Figure 2.10). BJ Day 90 cells showed mRNA expression of all the abovementioned markers except Sox2. Semi-quantitative western blotting analysis of protein isolated from these cells confirm the mRNA expression of these markers. Similarly, analysis of Shef 6 Day 121 cells revealed that they expressed mRNA coding for all markers examined, except for Sox2. Consistent with the BJ- and Shef 6-derived cells, RC-9 Day 70 cells expressed all genes and proteins investigated, except Sox2. Unlike the hPSC-derived cells, MIO-M1 cells expressed mRNA and protein coding for Sox2, which might reflect the nature of a cell line that proliferates indefinitely *in vitro*.

Staining of BJ Day 90 cells and RC-9 Day 70 cells with antibodies against CD29, CD44, GS and vimentin showed co-staining for surface and intracellular Müller markers (

Figure 2.11). Strong immunostaining for CD29 and CD4 outlined the bipolar morphology of these cells, which showed prominent intracellular expressions of GS and vimentin. However, Shef 6 Day 121 cells showed an irregular and flattened morphology and lost their *in vitro* proliferative potential upon passage 6, these cells were not examined immunochemically.

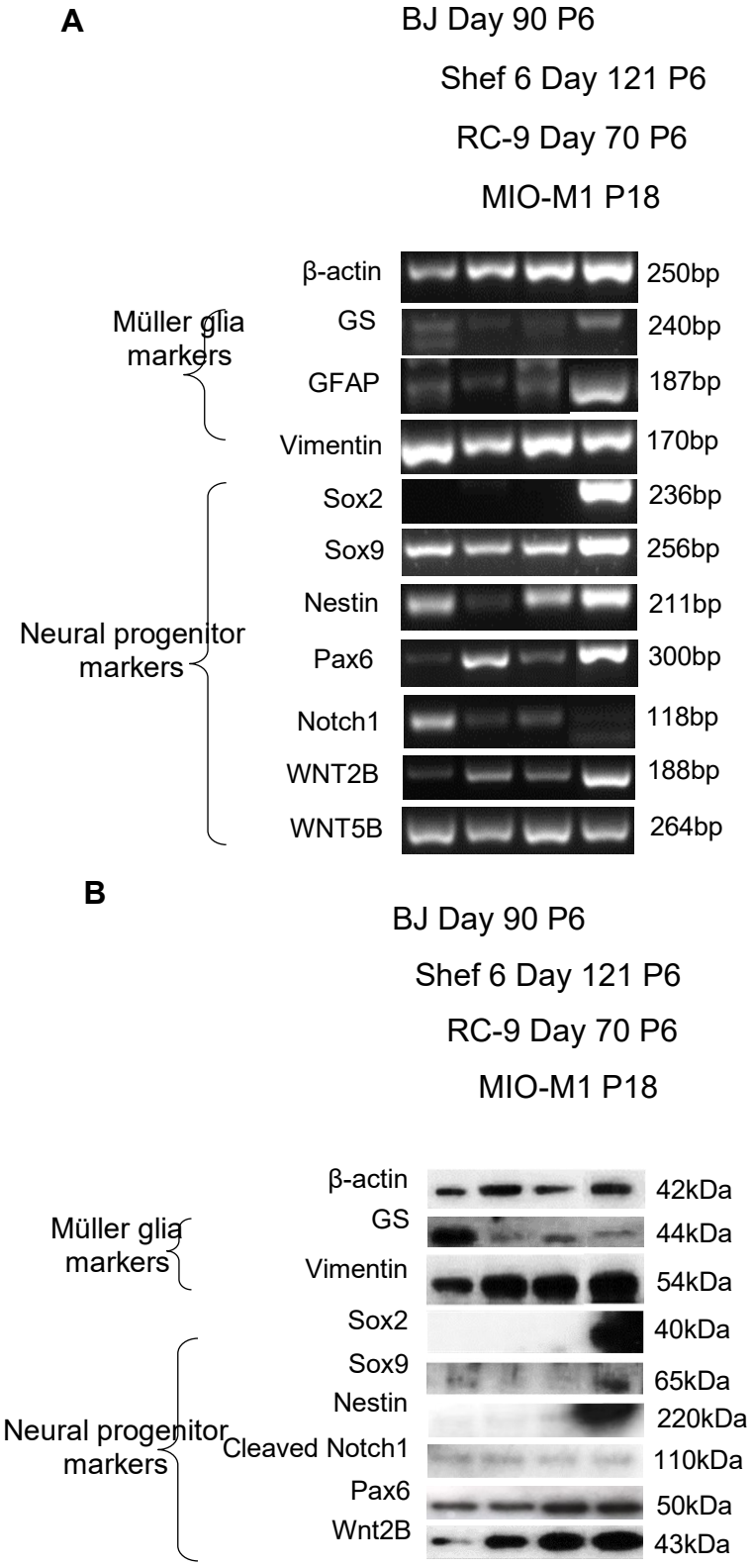

Figure 2.10 Expression of mRNAs and proteins coding for Müller glia markers in cells isolated from hiPSC- and hESC-derived retinal organoids.

(A) Representative RT-PCR bands and **(B)** western blotting bands represent the expression of mRNAs and proteins coding for Müller glia and neural progenitor factors in cells isolated from retinal organoids at different times points after initiation of retinal differentiation. The expression profile of the human adult Müller glial cell line MIO-M1 served as reference. β-actin was used as the house-keeping gene/protein. bp, base pairs; kDa, kilo dalton.

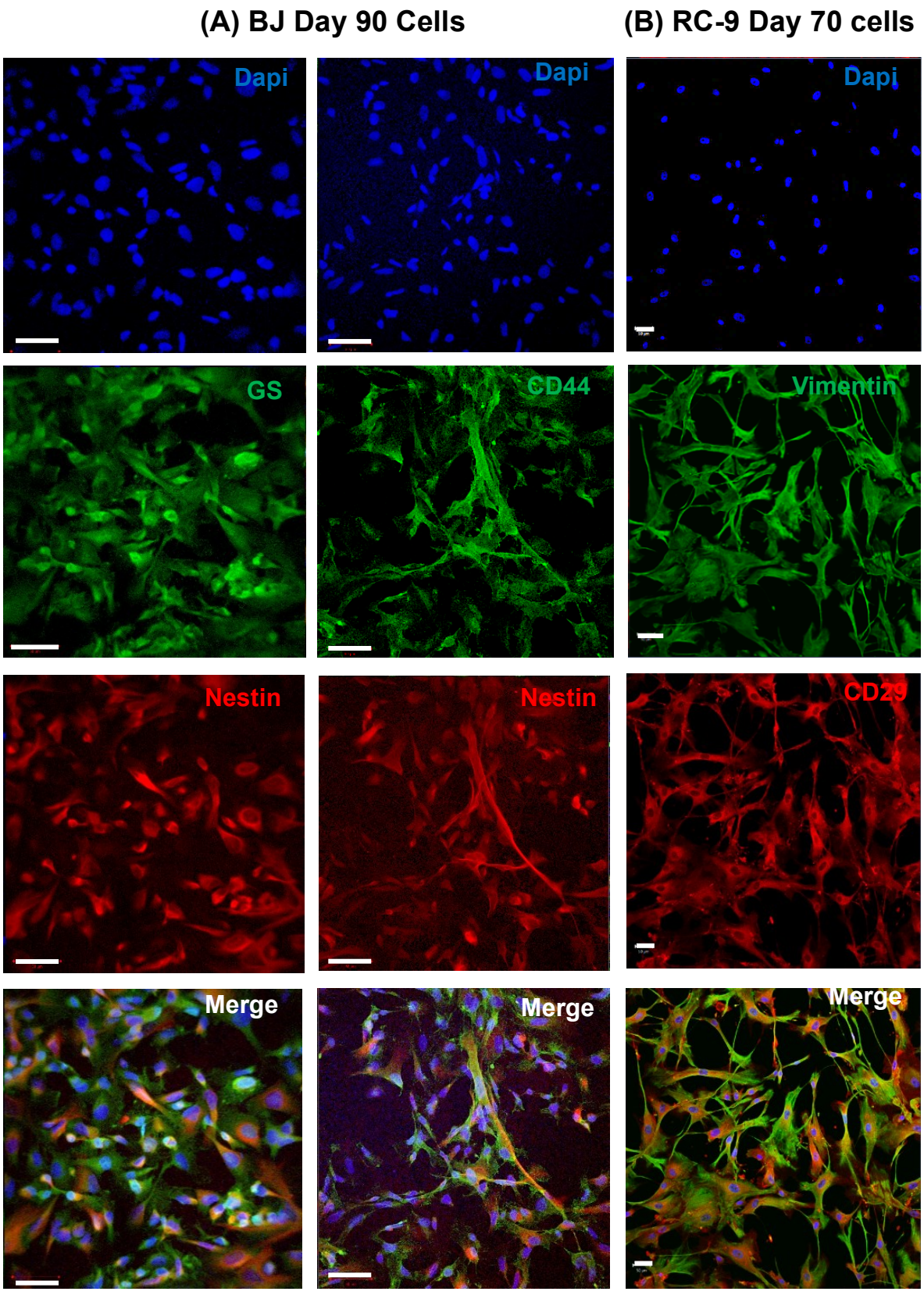

Figure 2.11 Expression of characteristic Müller glia markers GS, nestin, vimentin, CD29 and CD44 in (A) BJ Day 90 cells and (B) RC-9 Day 70 cells.
Antibodies against specific proteins of interest are indicated by the corresponding colour as follows: Green-Alexa Fluor® 488; Red-Alexa Fluor® 555; Blue-DAPI. Scale bars = 50μm.

2.5.5 Characterisation of cells dissociated from retinal organoids by FACS analysis

After limited propagation *in vitro*, the percentage of BJ Day 90 cells and RC-9 Day 70 cells expressing the Müller glia surface markers CD29 and CD44 was examined using FACS analysis. The Müller cell line MIO-M1 cells was used as a reference. To set up the gating parameters, cell suspensions that were unstained (i,

Figure 2.12-

Figure 2.14) and single stained with antibodies against CD29 (ii,

Figure 2.12-

Figure 2.14) and CD44 (iii,

Figure 2.12-

Figure 2.14) served as negative and positive controls respectively. Single-stained cell suspensions from four cell preparations consistently showed high expression of CD29 (> 98.9%) and CD44 (>97.9%). FACS analysis showed a 99.9 % of purity of the MIO-M1 cells co-expressing both Müller surface markers (iv,

Figure 2.12). The co-expression of CD29 and CD44 by BJ Day 90 cells was 99.7% (iv, Figure 2.13) and that of RC-9 Day 70 cells was 99.9% (iv,

Figure 2.14). The expression of the pluripotent stem cell marker stage-specific human embryonic antigen-4 (SSEA-4) and an epithelial cell marker cytokeratin-18 were also examined in BJ Day 90 cells and RC-9 Day 70 cells to assess their

differentiation status and lineage. Only 0.2% of BJ Day 90 cells (v, Figure 2.13) and 1.8% of RC-9 Day 70 cells (v,

Figure 2.14) were positive for SSEA-4, whilst 0.7% of BJ Day 90 cells (vi, Figure 2.13) and 0.6% of RC-9 Day 70 cells (vi,

Figure 2.14) expressed cytokeratin-18. These results indicate that hPSC-derived cells have fully switched off their pluripotency capacity and correctly differentiated into the Müller glia cell-like fate by taking up Müller cell surface markers.

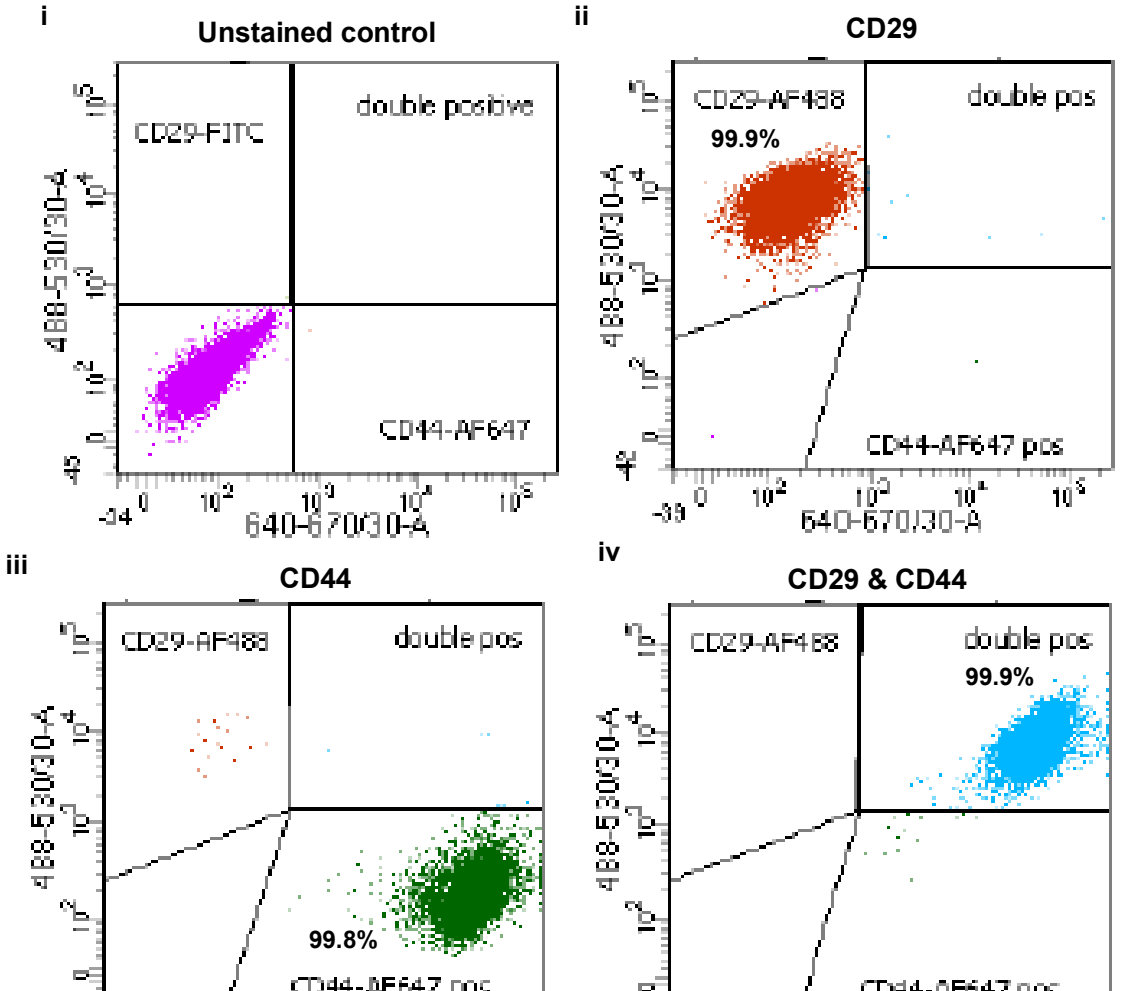

Figure 2.12 FACS analysis of the adult human Müller glial cell line MIO-M1 stained for characteristic Müller cell surface markers.
(i) Unstained MIO-M1 cells were used as negative control to set up the gating parameters. Flow cytometry analysis of MIO-M1 cells showed that **(ii)** 99.9% of the cells expressed CD29, **(iii)** 99.8% were positive for CD44, and **(iv)** 99.9% co-expressed both markers.

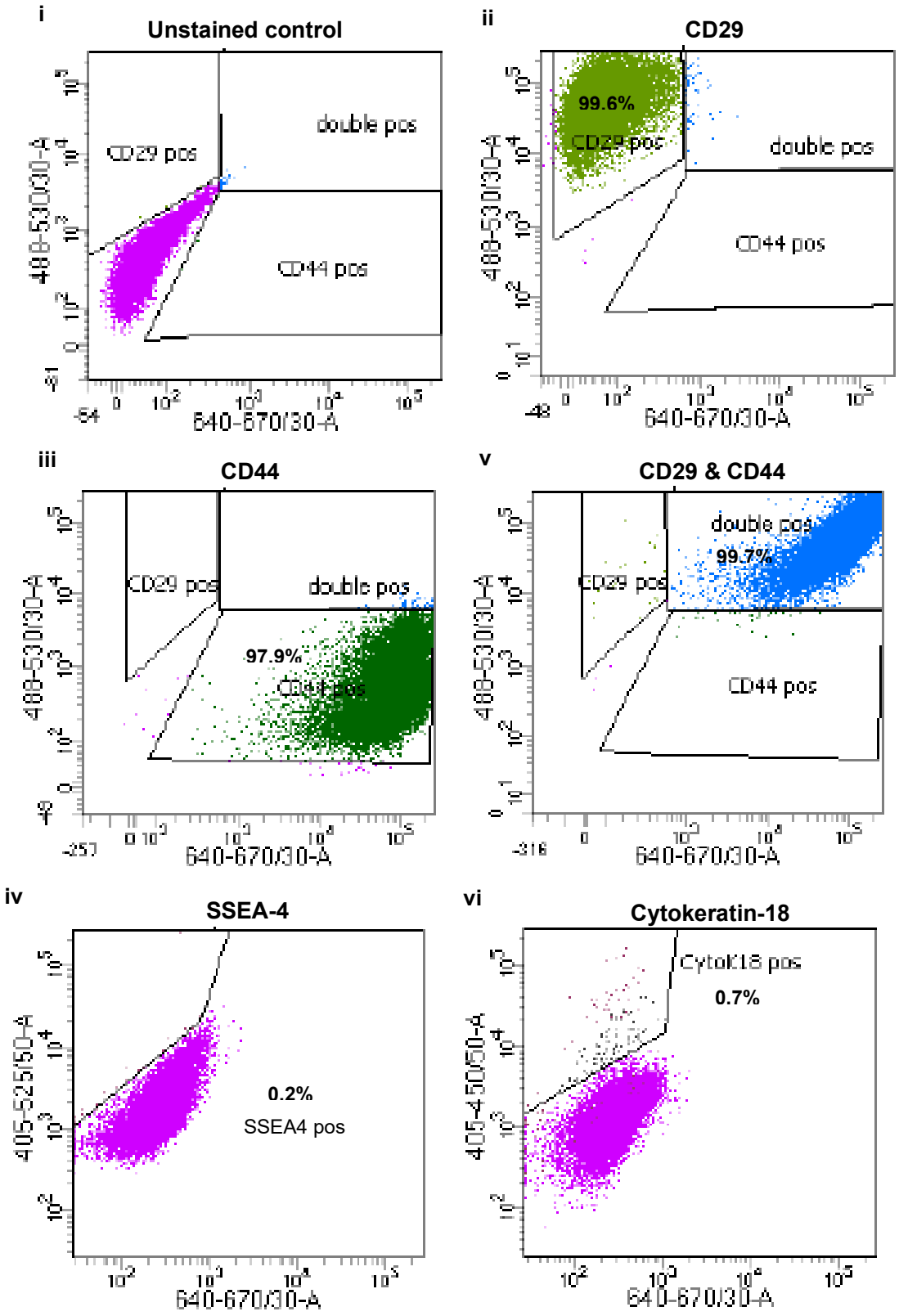

Figure 2.13 FACS analysis of BJ Day 90 cells stained for stained for characteristic Müller cell surface markers, pluripotent stem cell markers and epithelial cell markers.
(i) Unstained cells were used as negative control to set up the gating parameters. Flow cytometry analysis of BJ Day 90 cells showed that **(ii)** 99.6% of the cells expressed CD29, **(iii)** 97.9% of the cells expressed CD44, **(iv)** 99.7% co-expressed both markers, **(v)** 0.2% of the cells expressed stem cell marker SSEA-4, and **(vi)** 0.7% of the cells were positive for the epithelial marker cytokeratin-18.

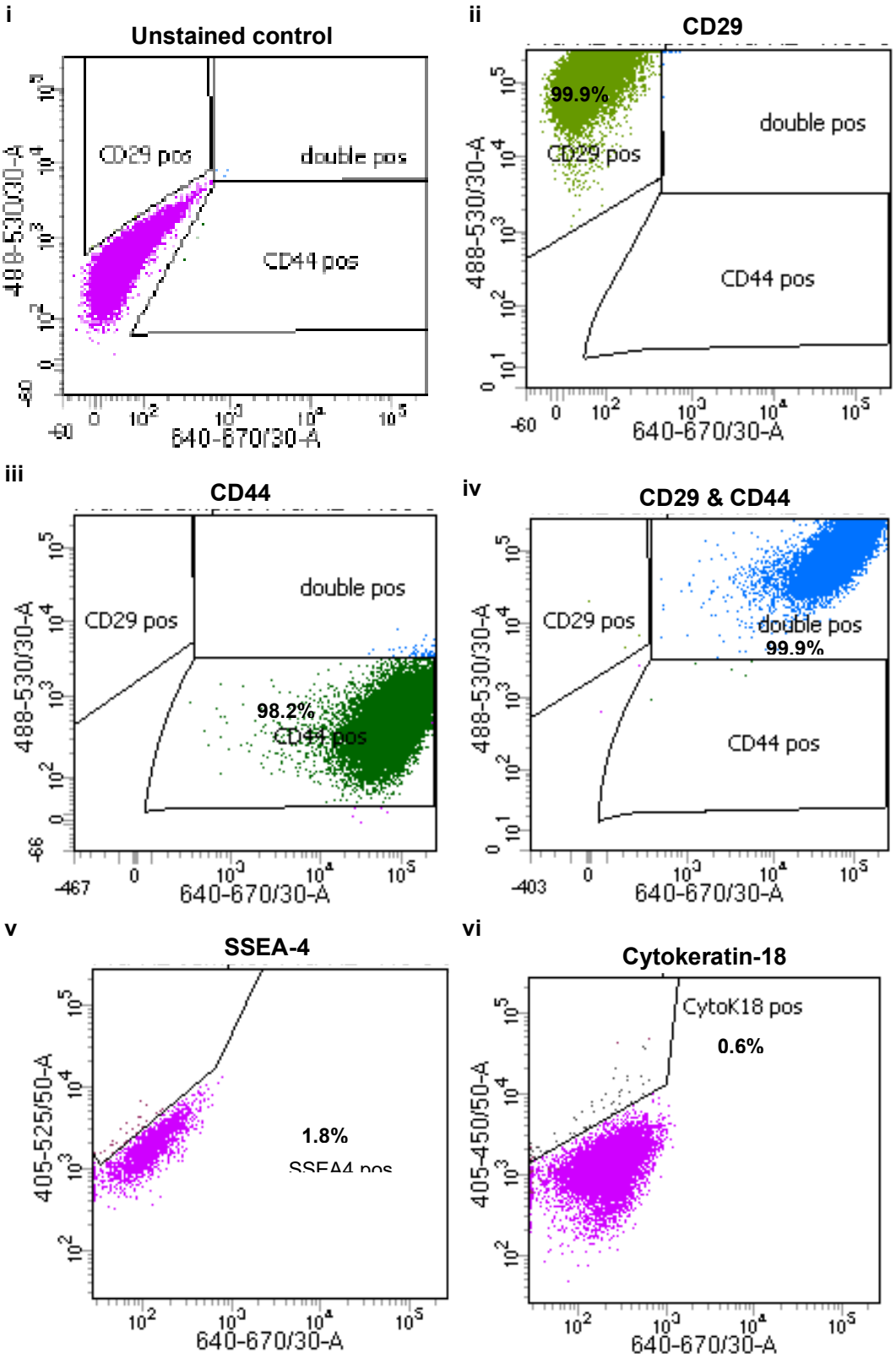

Figure 2.14 FACS analysis of RC-9 Day 70 cells stained for stained for characteristic Müller cell surface markers, pluripotent stem cell markers and epithelial cell markers.
(i) Unstained cells were used as negative control to set up the gating parameters. Flow cytometry analysis of RC-9 Day 70 cells showed that **(ii)** 99.9% of the cells expressed CD29, **(iii)** 98.2% of the cells expressed CD44, **(iv)** 99.9% co-expressed both markers, **(v)** 1.8% of the cells expressed stem cell marker SSEA-4, and **(vi)** 0.6% of the cells were positive for the epithelial marker cytokeratin-18.

2.5.6 Transcriptomic profiling of retinal organoid-derived Müller glia-like cells

The mRNA transcriptome of retinal organoid-derived Müller glia-like cells was investigated by a RNA-sequencing technique to gain a more comprehensive and systematic understanding on the molecular signatures of these cells when compared to the adult human Müller glia cell line MIO-M1. BJ Day 90 cells represents the hiPSC-derived Müller glia-like cells and are named hereafter as hiPSC-MG1. RC-9 Day 70 cells represents the hESC-derived Müller glia-like cells and are named hereafter as hESC-MG1. Cell pellets from three continuous passages of hiPSC-MG1 and hESC-MG1 were harvested as biological replicates. MIO-M1 cells were cultured in the same *in vitro* conditions as hiPSC-MG1 and hESC-MG1. Total RNA was extracted from cell pellets and depleted from genomic DNA before assessing the integrity of RNA samples as described in detail in the Materials and Methods section. The quality of all RNA samples was assessed by the RNA integrity number (RIN), which showed that RNA samples contained a relatively high proportion of mRNA with minimal degradation (RIN > 8). This is followed by cDNA libraries preparation and sequencing. Sequencing data of RNA subjected to transcriptomic analysis revealed that the read depth was of high quality.

2.5.6.1 Overview of RNA-seq libraries of hiPSC-MG1, hESC-MG1 and MIO-M1 cells

The read alignment metrics reported by RNA-seq are summarised in

Figure 2.15. In general, the pattern of alignment and uniquely mapped reads for all samples remained similar, achieving high percentage of unique alignment to at least 85% and 22 million of uniquely mapped reads (

Figure 2.15). For each library, the total read counts were first normalised to gene length in kilobase, followed by sequencing depth using scaling factor in millions. Gene expression levels were then converted to transcript per kilobase millions (TPM), although raw counts were utilised for subsequent differential analyses. Fold changes of gene expressions of each cell preparation were calculated in log2 base (log2FC).

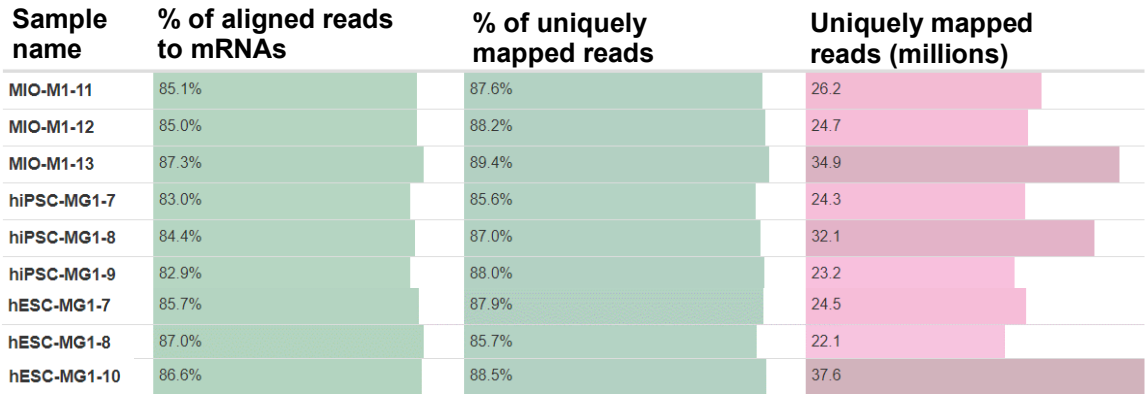

Figure 2.15 RNA-seq read alignment metrics of transcriptomic libraries from MIO-M1, hiPSC-M1 and hESC-MG1.

The percentage (%) of aligned reads overlapping UTRs and coding regions of mRNAs, the percentage (%) of uniquely mapped reads and uniquely mapped reads in millions were tabulated for each sequenced sample using MultiQC, an online bioinformatic visualising tool developed by (Ewels et al., 2016).

Principle component analysis (PCA) was firstly performed to identify the correlation of triplicates from each cell preparations (Figure 2.16A). Strong clustering was observed in biological replicates of each cell preparation while the different graphical patterns varied between different cells sources. The largest principal component (PC1) with a proportion of variance at 0.24, was likely attributed to the source of the cells analysed, capturing almost a quarter of the variance in the reported data. The tight clustering of biological replicates within each cell preparation suggests that the transcriptomes remained relatively consistent as the *in vitro* culture proceeded to later passage. To understand the differential gene expression profiles in hiPSC-MG1 and hESC-MG1 with reference to MIO-M1, differentially expressed genes (DEGs), showing differences with the adjusted p-value < 0.05, were examined. This brought the number of DEGs in each pair analysis to 2,397 (hiPSC-MG1 vs MIO-M1) and 1,912 (hESC-MG1 vs MIO-M1). Additionally, using the same criteria, hiPSC-MG1 had 2,231 DEGs when compared to hESC-MG1. Further filtering DEGs that had a log2FC > 2 or < -2 reduced the number of DEGs in each pairwise analysis to 2,103, 1,772 and 1,929, respectively. The similarity of filtered DEGs between each pair analysis was illustrated by a Venn diagram (Figure 2.16B). With reference to MIO-M1, there are 551 DEGs distinctively expressed in hiPSC-MG1, while 1552 DEGs are commonly found in both cell preparations (green circle). Similarly, hESC-MG1 cells also uniquely expressed 441 DEGs whilst the remaining 1331 DEGs were also identified in the transcriptomic libraries of MIO-M1 (blue circle). When comparing to hESC-MG1, hiPSC-MG1 had distinctively expressed 441 DEGs whilst both cell preparations had 1488 DEGs in common (yellow circle). In addition, 181 DEGs were universally found in all the three cell preparations analysed (central overlap area).

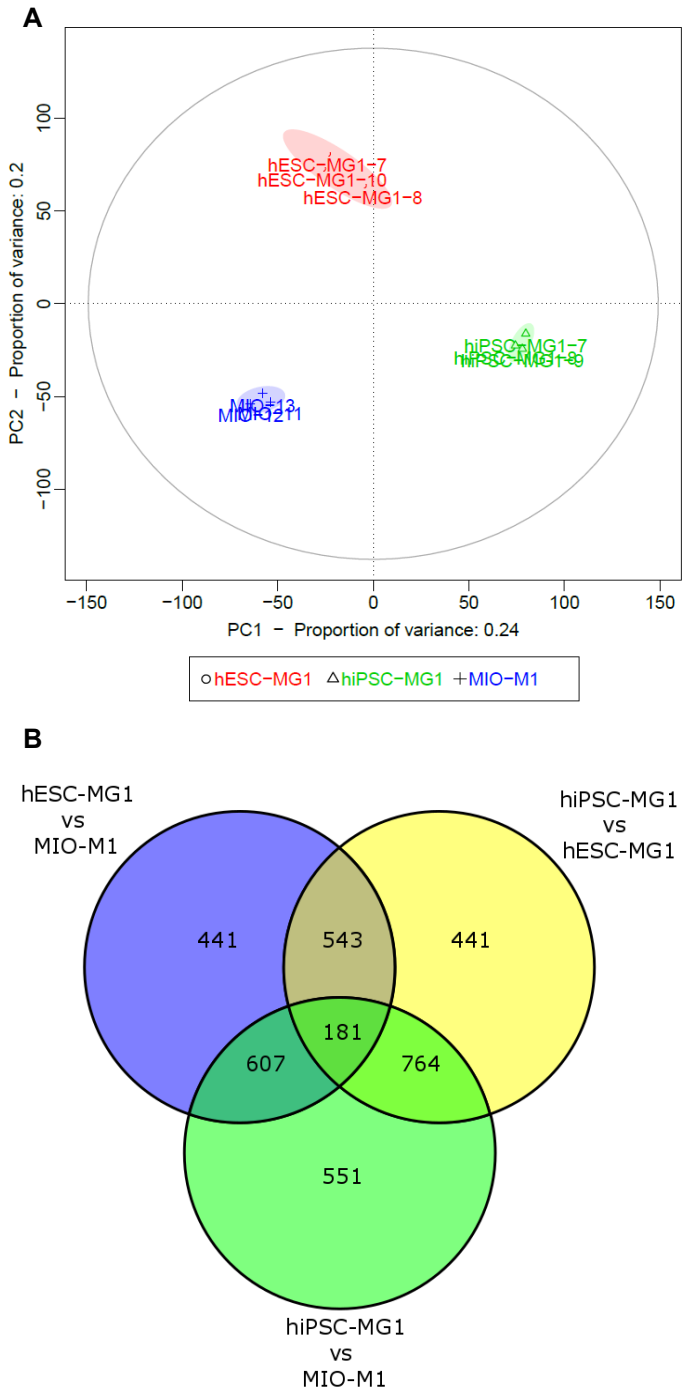

Figure 2.16 Overview of transcriptomic libraries of all cell preparations examined.
(A) Principal component analysis (PCA) plot shows clustering of the analysed RNA-seq libraries. PCA was performed using DESeq2 on the regularised log transformed count data. Plot shows the clustering of each transcriptome representing individual biological replicates of hESC-MG1 (red circles), hiPSC-MG1 (green triangles) and MIO-M1 (blue crosses). Passage number was indicated following the cell line name. **(B)** Venn diagram showing overlap of DEGs between pair analyses of Müller glia cell preparations. Venn diagram show the number of filtered DEGs commonly and differentially expressed in hiPSC-MG1 referenced to MIO-M1 (green), hESC-MG1 referenced to MIO-M1 (blue), and hiPSC-MG1 referenced to hESC-MG1 (yellow).

2.5.6.2 Gene ontology (GO) enrichment analysis of DEGs in hiPSC-MG1 and hESC-MG1 cells

The annotations of these significantly differentiated expressed genes were subsequently subjected to overrepresentation analysis using gene ontology (GO) method. By referencing to the transcriptomes of MIO-M1 cells, DEGs of hESC-MG1 and hiPSC-MG1 were classified into appropriate functional groups including cellular component, molecular function and biological processes. Similar pairwise comparison was also made between hiPSC-MG1 and hESC-MG1 to understand the transcriptomic differences attributable to the nature of hPSCs.

Firstly, overrepresentation by cellular component was given a cut-off value of the false discovery rate (FDR) at 0.05 and the top 30 GOs from each pair were tabulated based on the negative value of FDR on a log10 basis (log10 *p*-value) (Table 2.3). Amongst these, the most significant GOs included ’cytoplasm’ (GO: 0005737), ‘anchoring junction’ (GO: 0070161), ‘cell junction’ (GO: 0030054), ‘focal adhesion’ (GO: 0005925), ‘cell-substrate junction’ (GO: 0030055), and ‘extracellular matrix’ (GO: 0031012) were found commonly overrepresented in all three pair analyses (each GO was colour coded in the table). The *in vitro* expansion of these cells involved ECM supplementation and it was not surprising that genes regulating these cellular events were differentially expressed. In addition, GOs regulating trafficking of neurotrophic factors to the extracellular environment including ‘membrane-bound organelles’ (GO: 0043227), ‘vesicle’ (GO: 0031982) and ‘extracellular exosome’ (GO: 0070062) were observed. These observations suggest that extracellular release of trophic factors by hPSC-derived Müller cells might be associated to the expressions of genes regulating formation and release of exosomes.

hESC-MG1 vs MIO-M1			hiPSC-MG1 vs MIO-M1			hiPSC-MG1 vs hESC-MG1		
term_ID	**description**	**log10 *p*-value**	**term_ID**	**description**	**log10 *p*-value**	**term_ID**	**description**	**log10 *p*-value**
GO:0005737	cytoplasm	-15.75	GO:0005737	cytoplasm	-22.25	GO:0005737	cytoplasm	-17.99
GO:0070161	anchoring junction	-15.50	GO:0070161	anchoring junction	-20.29	GO:0005622	intracellular	-14.65
GO:0030054	cell junction	-14.96	GO:0005925	focal adhesion	-17.21	GO:0031012	extracellular matrix	-12.42
GO:0005925	focal adhesion	-14.48	GO:0030055	cell-substrate junction	-17.11	GO:0043227	membrane-bounded organelle	-10.05
GO:0030055	cell-substrate junction	-13.98	GO:0030054	cell junction	-14.77	GO:0043226	organelle	-9.84
GO:0031012	extracellular matrix	-11.35	GO:0031012	extracellular matrix	-13.84	GO:0043231	intracellular membrane-bounded organelle	-8.52
GO:0045202	synapse	-9.56	GO:0031982	vesicle	-10.68	GO:0043229	intracellular organelle	-8.48
GO:0022626	cytosolic ribosome	-9.24	GO:0005622	intracellular	-10.35	GO:0070161	anchoring junction	-7.69
GO:0005829	cytosol	-8.51	GO:0070062	extracellular exosome	-10.25	GO:0012505	endomembrane system	-7.61
GO:0012505	endomembrane system	-8.45	GO:0043230	extracellular organelle	-10.16	GO:0005829	cytosol	-6.53

GO:0043226	organelle	-8.35	GO:1903561	extracellular vesicle	-9.85	GO:0005925	focal adhesion	-6.04
GO:0005622	intracellular	-7.12	GO:0043226	organelle	-9.51	GO:0031974	membrane-enclosed lumen	-5.92
GO:0043227	membrane-bounded organelle	-6.46	GO:0043227	membrane-bounded organelle	-9.50	GO:0070013	intracellular organelle lumen	-5.92
GO:0099572	postsynaptic specialization	-6.43	GO:0012505	endomembrane system	-8.82	GO:0043233	organelle lumen	-5.92
GO:0014069	postsynaptic density	-6.16	GO:0045202	synapse	-8.78	GO:0030055	cell-substrate junction	-5.69
GO:0032279	asymmetric synapse	-5.95	GO:0043005	neuron projection	-8.10	GO:0005604	basement membrane	-5.56
GO:0022625	cytosolic large ribosomal subunit	-5.61	GO:0005829	cytosol	-7.70	GO:0045121	membrane raft	-5.54
GO:0031982	vesicle	-5.37	GO:0042995	cell projection	-7.68	GO:0030054	cell junction	-5.54
GO:0070062	extracellular exosome	-5.35	GO:0005794	Golgi apparatus	-7.11	GO:0005788	endoplasmic reticulum lumen	-5.49
GO:0043230	extracellular organelle	-5.21	GO:0005604	basement membrane	-6.83	GO:0098857	membrane microdomain	-5.49

Table 2.3 Gene ontology (GO) analysis by cellular component of DEGs in pairwise analysis of hESC-MG1 vs MIO-M1 (left column), hiPSC-MG1 vs MIO-M1 (middle column) and hiPSC-MG1 vs hESC-MG1 (right column).
The results of the gene ontology (GO) analysis of DEGs for regulating cellular components in each pair analysis were filtered using false discovery rate (FDR) ≤ 0.05 and the top 30 most significant GOs was tabulated based on with –log10 FDR (log10 *p*-value; 2 decimal places). GOs commonly overrepresented across three pairs of analysis were colour coded.

Based on molecular function, common GOs across three pair analyses were also identified. Applying a cut-off value of FDR at 0.05 significantly reduced representative GOs and the top 20 GOs from each pair were tabulated based on the negative value of FDR on a log10 basis (log10 *p*-value) (Table 2.4). Here, the majority of the GOs identified belonged to cell-matrix binding groups such as 'protein binding' (GO:0005515), 'integrin binding' (GO:0005178), 'extracellular matrix binding' (GO:0050840), 'collagen binding' (GO: 0005518), as well as 'growth factor binding' (GO: 0019838) and 'protein binding involved in cell adhesion' (GO: 0098631). These observations were in line with the experimental conditions at which hPSC-derived Müller glia cell cultures were treated with fibronectin, EGF and FGF, indicating that the *in vitro* culture conditions might have an impact on their transcriptomes. The differential expressions of cell binding factors might be important for the continuous expansion of Müller glia *in vitro*.

hESC-MG1 vs MIO-M1			hiPSC-MG1 vs MIO-M1			hiPSC-MG1 vs hESC-MG1		
term_ID	**description**	**log10 *p*-value**	**term_ID**	**description**	**log10 *p*-value**	**term_ID**	**description**	**log10 *p*-value**
GO:0005515	protein binding	-9.50	GO:0005515	protein binding	-8.35	GO:0005515	protein binding	-11.27
GO:0005178	integrin binding	-7.85	GO:0050839	cell adhesion molecule binding	-7.11	GO:0005201	extracellular matrix structural constituent	-9.39
GO:0005198	structural molecule activity	-7.80	GO:0005201	extracellular matrix structural constituent	-6.36	GO:0019899	enzyme binding	-6.69
GO:0050840	extracellular matrix binding	-7.24	GO:0050840	extracellular matrix binding	-5.75	GO:0050839	cell adhesion molecule binding	-6.60
GO:0005518	collagen binding	-5.19	GO:0005518	collagen binding	-5.14	GO:0005518	collagen binding	-4.89
GO:0098631	protein binding involved in cell adhesion	-5.11	GO:0005178	integrin binding	-4.57	GO:0019838	growth factor binding	-4.37
GO:0003735	structural constituent of ribosome	-5.02	GO:0005198	structural molecule activity	-4.53	GO:0005488	binding	-3.85
GO:0019838	growth factor binding	-3.62	GO:0019899	enzyme binding	-4.18	GO:0005178	integrin binding	-3.62
GO:0005201	extracellular matrix structural constituent	-3.48	GO:0043167	ion binding	-3.88	GO:0044877	macromolecular complex binding	-3.57

GO:0098632	protein binding involved in cell-cell adhesion	-3.38	GO:0019838	growth factor binding	-3.82	GO:0019900	kinase binding	-3.31
GO:0005488	binding	-3.21	GO:0098631	protein binding involved in cell adhesion	-3.82	GO:0098631	protein binding involved in cell adhesion	-2.84
GO:0044877	macromolecular complex binding	-3.18	GO:0044877	macromolecular complex binding	-3.66	GO:0042802	identical protein binding	-2.71
GO:0050839	cell adhesion molecule binding	-3.03	GO:0005488	binding	-3.62	GO:0043167	ion binding	-2.35
GO:0086080	protein binding involved in heterotypic cell-cell adhesion	-2.79	GO:0005509	calcium ion binding	-3.17	GO:0019901	protein kinase binding	-2.26
GO:0001968	fibronectin binding	-2.38	GO:0019904	protein domain specific binding	-3.08	GO:0098632	protein binding involved in cell-cell adhesion	-2.00
GO:0031994	insulin-like growth factor I binding	-1.64	GO:0043169	cation binding	-2.93	GO:0030020	extracellular matrix structural constituent conferring tensile strength	-1.95
GO:0030234	enzyme regulator activity	-1.63	GO:0046872	metal ion binding	-2.63	GO:0019798	procollagen-proline dioxygenase activity	-1.95

GO:0098772	molecular function regulator	-1.50	GO:0002020	protease binding	-1.83	GO:0046332	SMAD binding	-1.67
GO:0051371	muscle alpha-actinin binding	-1.44	GO:0060090	binding, bridging	-1.73	GO:0060090	binding, bridging	-1.46
GO:0019843	rRNA binding	-1.39	GO:0001968	fibronectin binding	-1.68	GO:1901681	sulfur compound binding	-1.44

Table 2.4 Gene ontology (GO) analysis by molecular function of DEGs in pairwise analysis of hESC-MG1 vs MIO-M1 (left column), hiPSC-MG1 vs MIO-M1 (middle column) and hiPSC-MG1 vs hESC-MG1 (right column).
The results of the gene ontology (GO) analysis of DEGs for regulating molecular function in each pair analysis were filtered using false discovery rate (FDR) ≤ 0.05 and the top 20 most significant GOs was tabulated based on with –log10 FDR (log10 *p*-value; 2 decimal places). GOs commonly overrepresented across three pairs of analysis were colour coded.

Most importantly, by overrepresentation on biological processes and using the same cut-off criteria, the most significant 30 GOs were tabulated with commonly identified GOs uniquely colour coded (Table 2.5). For example, GOs involved in early morphological development of CNS tissues were found across three pairs, and these consisted of ‘system development’ (GO: 0048731), ‘anatomical structure morphogenesis’ (GO: 0009653), ‘anatomical structure development’ (GO: 0048856) and ‘developmental process’ (GO 0032502). In addition, when referencing to MIO-M1 cells, DEGs of hESC-MG1 appeared to be associated with neuronal development, as evident by six out of 30 GOs identified that were related to early generation and differentiation of neurons, such as ‘nervous system development (GO: 0007399), ‘neuron development’ (GO: 0048666), ‘generation of neurons’ (GO: 0048699), ‘neurogenesis’ (GO: 0022008), ‘neuron differentiation’ (GO: 0030182), and ‘neuron projection development’ (GO: 0031175). In contrast, in comparison to MIO-M1 cells, hiPSCs have less DEGs overrepresented in GOs relating to neuronal development and only two GOs represented by ‘nervous system development (GO: 0007399) and ‘neurogenesis’ (GO: 0022008) were observed in the top 30 GOs. These observations may indicate that the differentiation of hESC-MG1 appeared to be more inclined to neuron like genotype than that of hiPSC-MG1. This is more striking when pairwise comparison was made between hESC-MG1 cells and hiPSC-MG1 cells, which had significantly less GOs involving in neuronal development (‘nervous system development (GO: 0007399), supporting the view that the differentiation of hiSPC-MG1 was less profound towards neural cells as compared to hESC-MG1 cells.

hESC-MG1 vs MIO-M1			hiPSC-MG1 vs MIO-M1			hiPSC-MG1 vs hESC-MG1		
term_ID	**description**	**log10 *p*-value**	**term_ID**	**description**	**log10 *p*-value**	**term_ID**	**description**	**log10 *p*-value**
GO:0048731	system development	-14.61	GO:0009653	anatomical structure morphogenesis	-21.74	GO:0009653	anatomical structure morphogenesis	-19.01
GO:0009653	anatomical structure morphogenesis	-14.35	GO:0022610	biological adhesion	-18.15	GO:0048731	system development	-15.00
GO:0007155	cell adhesion	-12.86	GO:0007155	cell adhesion	-18.14	GO:0048856	anatomical structure development	-14.37
GO:0022610	biological adhesion	-12.62	GO:0048731	system development	-16.23	GO:0007275	multicellular organism development	-13.05
GO:0007275	multicellular organism development	-12.42	GO:0048856	anatomical structure development	-16.07	GO:0010646	regulation of cell communication	-12.96
GO:0007399	**nervous system development**	-12.10	GO:0007399	**nervous system development**	-14.56	GO:0023051	regulation of signaling	-12.84
GO:0048856	anatomical structure development	-12.03	GO:0030198	extracellular matrix organization	-14.43	GO:0022610	biological adhesion	-12.73
GO:0032502	developmental process	-10.07	GO:0032502	developmental process	-14.38	GO:0007155	cell adhesion	-12.69

GO:0072359	circulatory system development	-8.87	GO:0043062	extracellular structure organization	-14.35	GO:0072359	circulatory system development	-12.18
GO:0048519	negative regulation of biological process	-8.52	GO:0007275	multicellular organism development	-13.86	GO:0032502	developmental process	-12.11
GO:0030198	extracellular matrix organization	-8.44	GO:0010646	regulation of cell communication	-12.31	GO:0009888	tissue development	-11.75
GO:0048468	cell development	-8.40	GO:0023051	regulation of signaling	-12.15	GO:0016477	cell migration	-11.74
GO:0070887	cellular response to chemical stimulus	-8.39	GO:0051239	regulation of multicellular organismal process	-10.55	GO:0030198	extracellular matrix organization	-11.42
GO:0043062	extracellular structure organization	-8.38	GO:0050793	regulation of developmental process	-10.52	GO:0043062	extracellular structure organization	-11.35
GO:0048513	animal organ development	-8.37	GO:0032989	cellular component morphogenesis	-10.11	GO:0048646	anatomical structure formation involved in morphogenesis	-11.11
GO:0051239	regulation of multicellular organismal process	-7.63	GO:0000902	cell morphogenesis	-9.74	GO:0050793	regulation of developmental process	-10.91
GO:0048666	**neuron development**	-7.55	GO:0035295	tube development	-9.42	GO:0035239	tube morphogenesis	-10.78

GO:0048699	**generation of neurons**	-7.43	GO:0031589	cell-substrate adhesion	-9.35	GO:0007167	enzyme linked receptor protein signaling pathway	-10.71
GO:0022008	**neurogenesis**	-7.40	GO:0030155	regulation of cell adhesion	-9.21	GO:0035295	tube development	-10.52
GO:0051179	localization	-7.35	GO:0072359	circulatory system development	-9.20	GO:0001501	skeletal system development	-10.51
GO:0030182	**neuron differentiation**	-7.34	GO:0048468	cell development	-8.97	GO:0009966	regulation of signal transduction	-10.41
GO:0010033	response to organic substance	-7.20	GO:0009888	tissue development	-8.96	GO:0030334	regulation of cell migration	-10.31
GO:0000902	cell morphogenesis	-7.18	GO:0035239	tube morphogenesis	-8.83	GO:0048514	blood vessel morphogenesis	-10.19
GO:0050793	regulation of developmental process	-7.17	GO:0009966	regulation of signal transduction	-8.49	GO:0007399	**nervous system development**	-10.19
GO:0071310	cellular response to organic substance	-7.10	GO:0022008	**neurogenesis**	-8.48	GO:0051270	regulation of cellular component movement	-9.87
GO:0031175	**neuron projection development**	-7.10	GO:0048869	cellular developmental process	-8.44	GO:0008283	cell proliferation	-9.70
GO:0007166	cell surface receptor signaling pathway	-6.97	GO:0048513	animal organ development	-8.05	GO:0048513	animal organ development	-9.48

GO:0006614	SRP-dependent cotranslational protein targeting to membrane	-6.94	GO:2000026	regulation of multicellular organismal development	-8.05	GO:0016043	cellular component organization	-9.38
GO:0032989	cellular component morphogenesis	-6.88	GO:0048646	anatomical structure formation involved in morphogenesis	-7.71	GO:0001568	blood vessel development	-9.23
GO:0009888	tissue development	-6.63	GO:0001503	ossification	-7.63	GO:0001944	vasculature development	-8.97

Table 2.5 Gene ontology (GO) analysis by biological process of DEGs in pairwise analysis of hESC-MG1 vs MIO-M1 (left column), hiPSC-MG1 vs MIO-M1 (middle column) and hiPSC-MG1 vs hESC-MG1 (right column).
The results of the gene ontology (GO) analysis of DEGs for regulating biological process in each pair analysis were filtered using false discovery rate (FDR) ≤ 0.05 and the top 30 most significant GOs was tabulated based on with –log10 FDR (log10 *p*-value; 2 decimal places). GOs commonly overrepresented across three pairs of analysis are colour coded. Neuronal related GOs are bold.

2.5.6.3 Expression of markers of undifferentiated stem cells and other retinal cells in hiPSC-MG1 and hESC-MG1

Analysis of specific gene clusters associated with pluripotency and undifferentiated states of stem cells was also carried out on hPSC-derived cells. These genes are normally expressed in PSCs at high levels to maintain the unlimited proliferation potential of stem cells whilst their downregulation is necessary for cell fate commitment. Transcripts of master pluripotency genes nanog homeobox (NANOG), telomerase reverse transcriptase (TERT), undifferentiated embryonic cell transcription factor 1 (UTF1) and teratocarcinoma-derived growth factor 1 (TDGF1) were not detected in all cell preparations (TPM = 0). When compared to MIO-M1, another pluripotency regulator Oct3/4 (POU5F1) was significantly higher in hiPSC-MG1 (log2FC=7.6), while transcripts of podocalyxin like genes (PODXL) that encode tumour rejection antigen-1–60 and (TRA-1-60) and 1–81 (TRA-1-81) were significantly lower

(

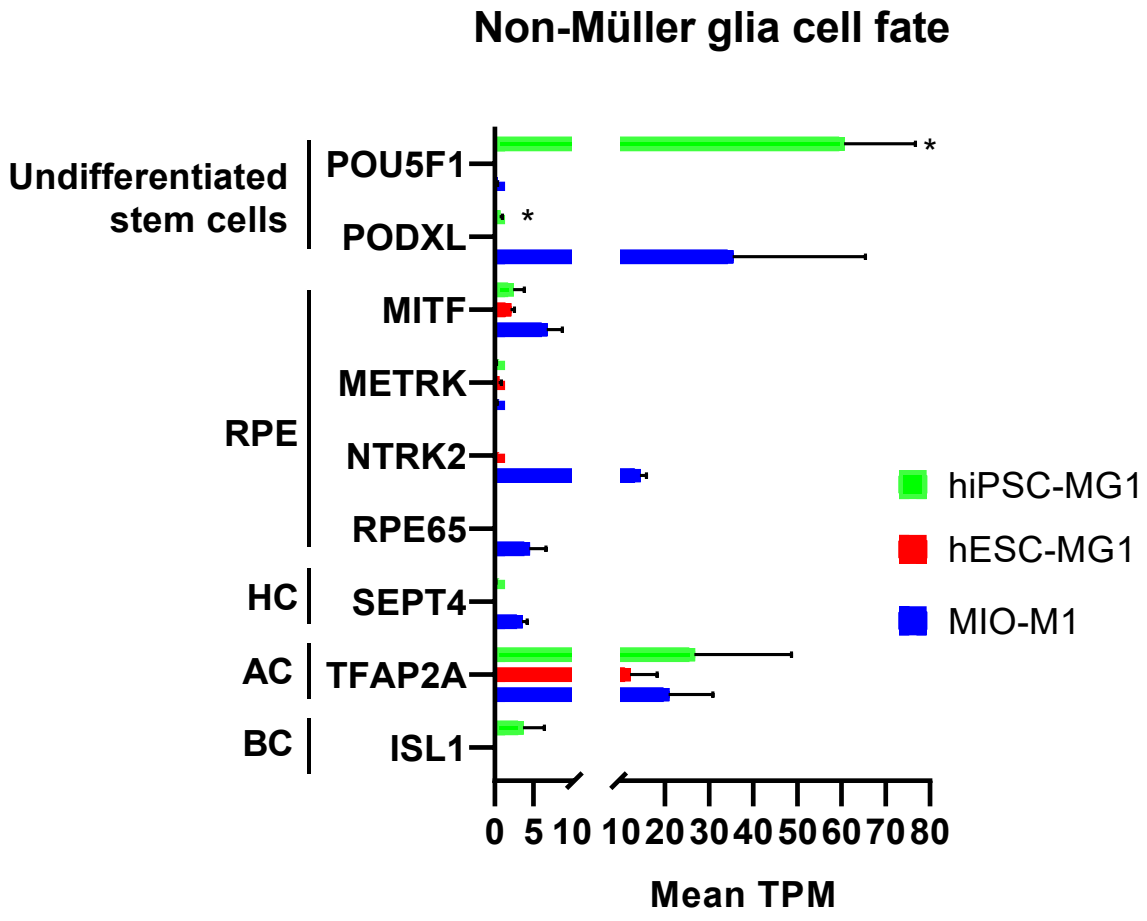

Figure **2.17**). Both genes were not expressed in hESC-MG1 cells (TPM =0). Collectively these results suggest that following neural differentiation and long-term culture in medium containing inducing factors that maintaining retinal fate, hiPSC-MG1 and hESC-MG1 cells have significantly downregulated markers governing the pluripotency of stem cells.

The concern that hiPSC-MG1 and hESC-MG1 did not acquire other retinal cell fates is corroborated by the levels of expression of markers specific to RPE, photoreceptors, horizontal cells (HC), amacrine cells (AC) and bipolar cells (BC) (

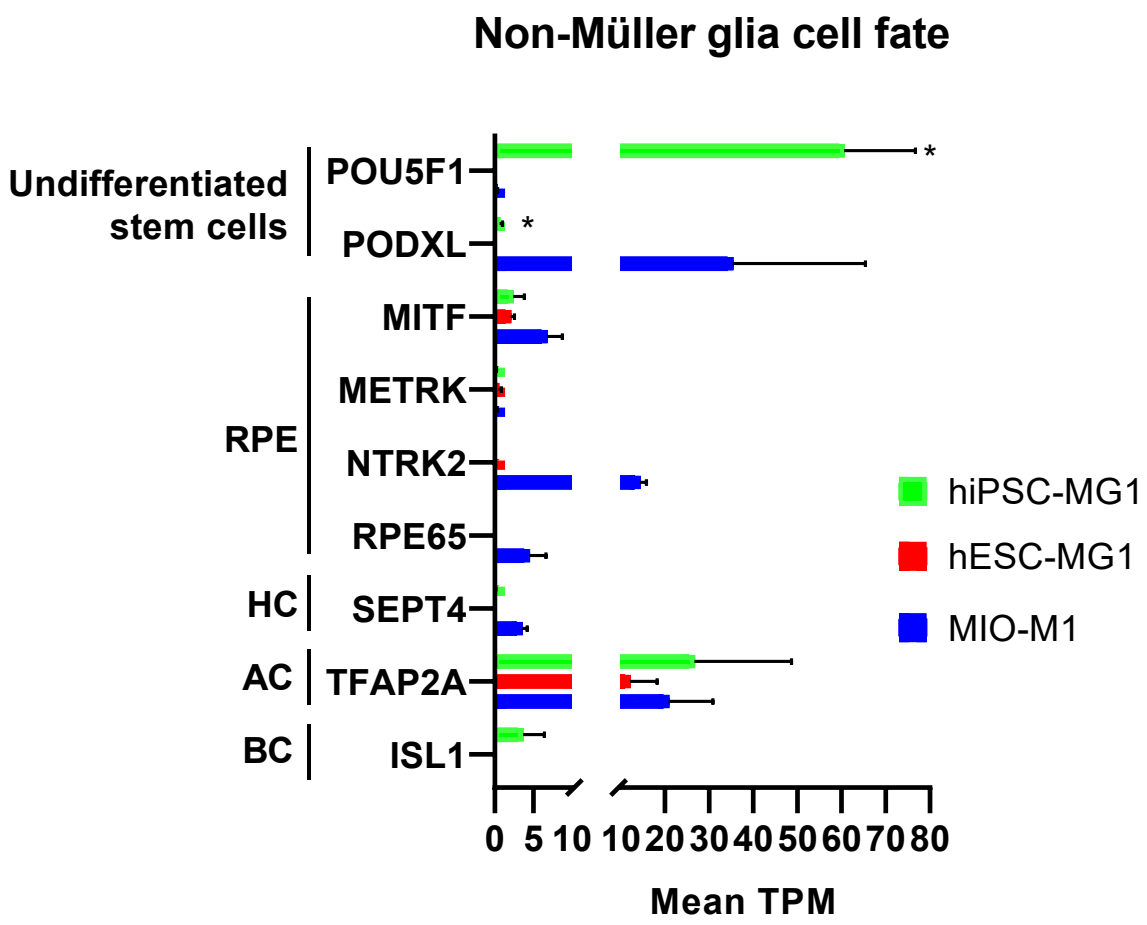

Figure **2.17**). RPE cell fate is dictated by expression of melanocyte inducing transcription factor (MITF) and several functional markers including MER proto-oncogene tyrosine kinase (MERTK), neurotrophic receptor tyrosine kinase 2 (NTRK2) and retinoid isomerohydrolase (RPE65). MITF transcripts were detected in all cells at minimum levels (TPM < 10), whilst MERTK transcripts were not detected in any of the three libraries. Expression of NTRK2 and RPE65 were confirmed absent in hiPSC-MG1 and hESC-MG1 preparations.

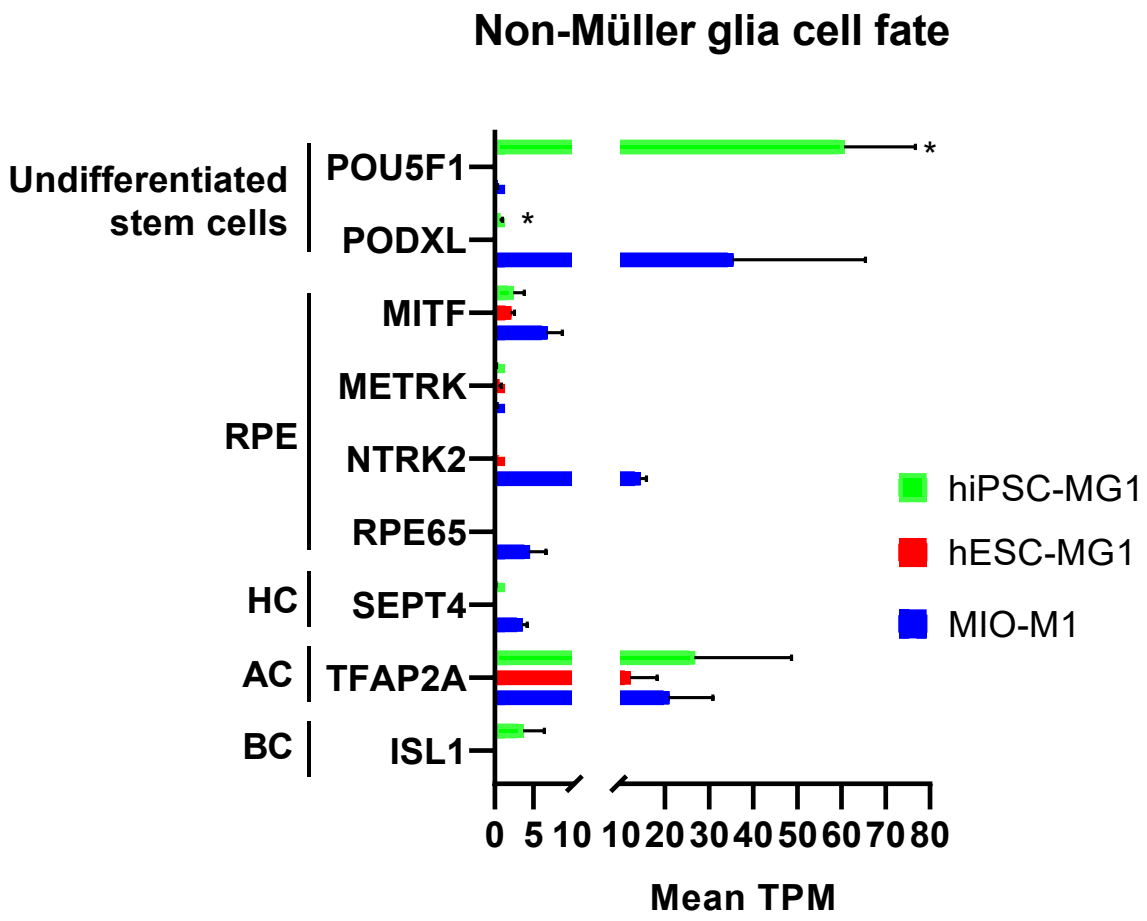

Figure 2.17 Expression levels of transcripts for markers of undifferentiated stem cells and other retinal cell fates in the three cell preparations analysed.
Histograms showing the mean TPMs of transcripts of undifferentiated stem cell markers (POU5F1 and PODXL), and other retinal cell fates including RPE (MITF, METRK, NTRK2, RPE65), HC (SEPT4), AC (TFAP2A) and BC (ISL1). hiPSC-MG1 (green); hESC-MG1 (red); and MIO-M1 cells (blue). * adjusted *p*-value < 0.05 for pair analysis with MIO-M1 cells. Respective log2FC is shown above the *p*-value.

Genes that determine photoreceptor fate such as orthodenticle homeobox 2 (OTX2), nuclear receptor subfamily 2 group E member 3 (NR2E3), neural retina leucine zipper (NRL) and cone-rod homeobox (CRX), were not detected in all transcriptomic libraries. In addition, photoreceptor functional markers such as rhodopsin (RHO), recoverin (RCVRN), opsin 1 medium wave sensitive (OPN1MW), and arrestin (ARR3) (Chen et al., 2014, Collin et al., 2019b) were not detected in all cell preparations, nor transcripts of genes associated with HC differentiation including neurofilament 160 kDa (NEFM), LIM homeobox 1 (LHX1) and calbindin 1 (CALB1) (Wassle et al., 1998, Singh et al., 2015, Blackshaw et al., 2004) were absent in all

three cell preparations. Whilst another HC functional marker septin 4 (SEPT4) were absent in hiPSC-MG1 and hESC-MG1 but expressed significantly higher in MIO-M1 (

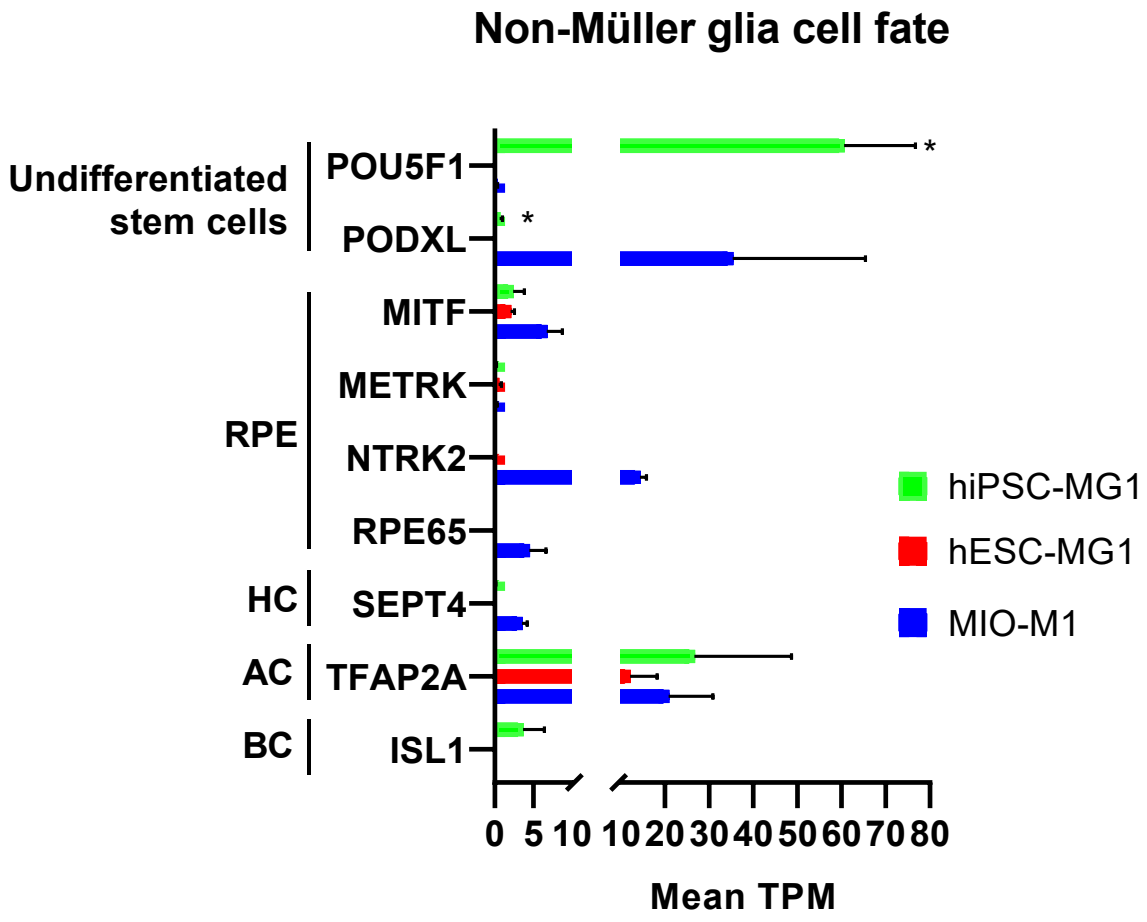

Figure 2.17). It was noted that bHLH gene SIX homeobox 3 (SIX3) (Jin et al., 2015), neuronal differentiation factor 1-4 (NEUROD1-4) (Inoue et al., 2002), and calretinin (CALB2) (Singh et al., 2015) that are required for AC development did not their transcripts detected in all libraries. The transcription factor activating protein-2 (TFAP2A) (Hicks et al., 2018, Jain et al., 2018) was expressed at similar levels (TPM < 30)

(

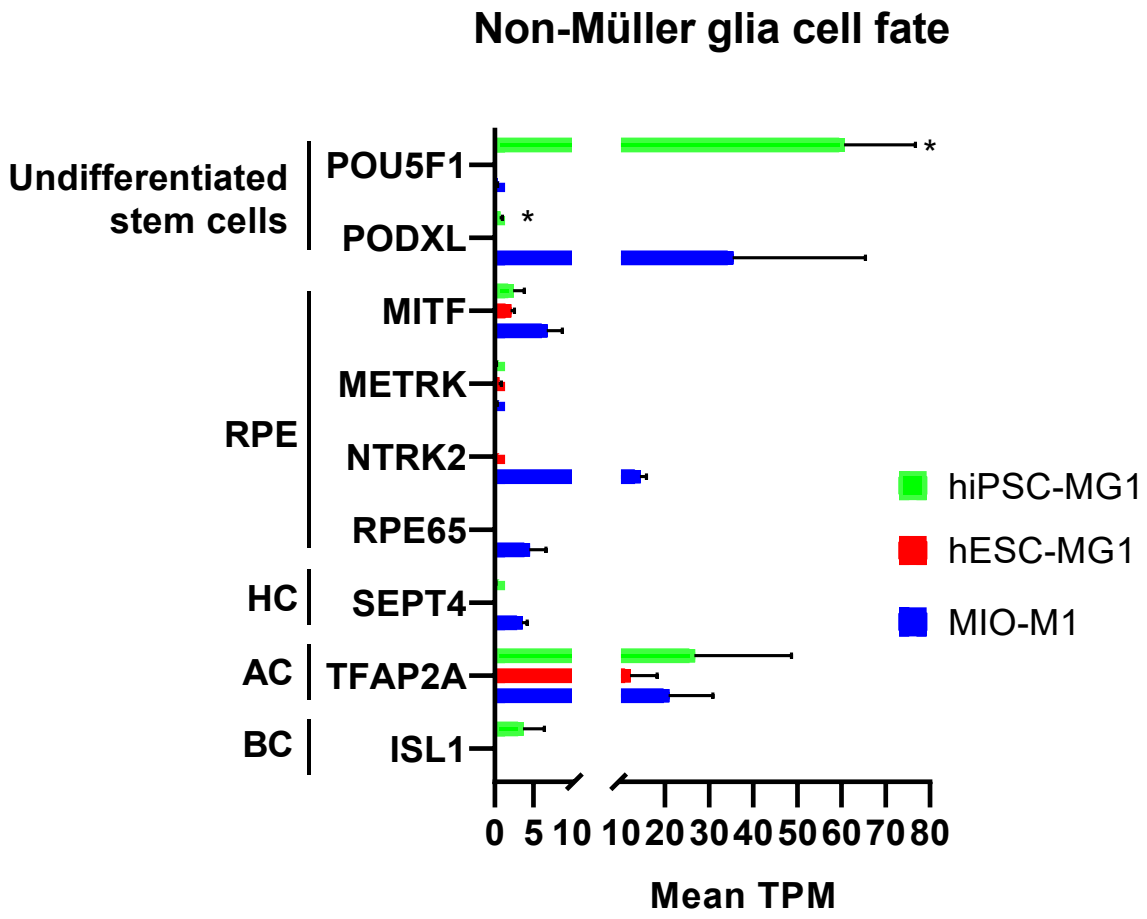

Figure **2.17**) in all three cell preparations. Previous studies have reported that a small subpopulation of developing Müller glia express transcription factors specifying BC fate such as Chx10 (VSX2), LIM homeobox3 (LHX3), islet-1 (ISL1) (Fischer et al., 2008, Elshatory et al., 2007), as well as GLI Family Zinc Finger 1 and 2 (GLI1 & GLI2) (Blackshaw et al., 2004). However, with exception of ISL1 which was only expressed in hiPSC-MG1 (TPM < 3)

(

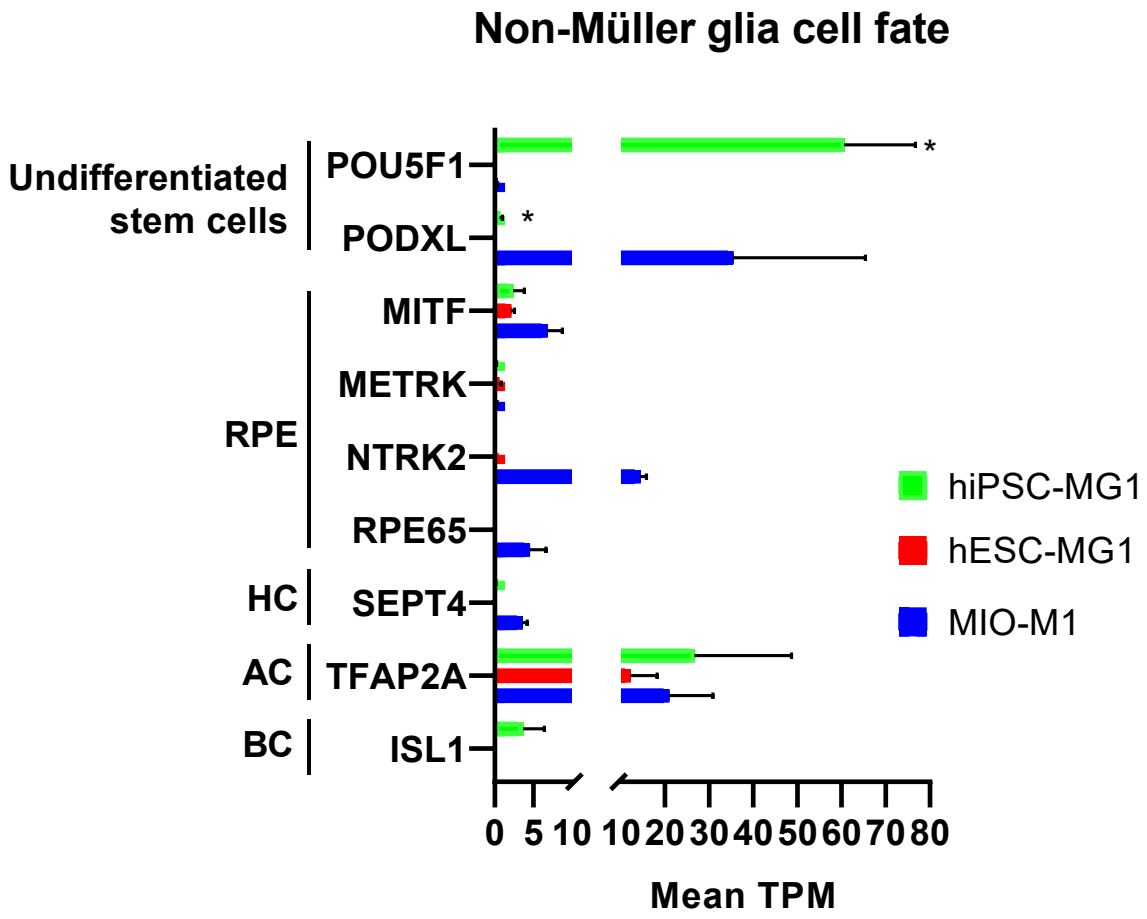

Figure **2.17**), these genes were not detected in any of the cell preparations examined. Similarly, transcripts coding for functional markers of BC including the transmembrane metabotropic glutamate receptor 6 (GRM6), and glutamate ionotropic receptor kainate type subunit 1 (GRIK1) (Liu et al., 2019), were not detected in any of the cell preparations. Lastly, transcripts of RGC markers including transcription factors BRN3A (POU4F1) and BRN3B (POU4F2) were also absent in all transcriptomic libraries. Taken these observations together, hiPSC-MG1 and hESC-MG1 did not show significant molecular signatures of the abovementioned retinal phenotypes.

2.5.6.4 Expression of characteristic Müller glia markers by hiPSC-MG1 and hESC-MG1

The following analysis aimed to identify whether hiPSC-MG1 and hESC-MG1 expressed Müller glia phenotype. The first set of analysis focused on the examination of the expression levels of Müller glia markers in both hPSC-derived cell preparations when compared with MIO-M1 cells (Eastlake et al., 2018). The most abundant Müller glia markers in all three cell preparations were vimentin (VIM), glutamine synthetase (GLUL), CD29 (ITGB1) and CD44 (Figure 2.18A). Based on TPM values, VIM was the highest expressed Müller glia marker in all three preparations. Pairwise analysis showed that the levels of VIM expression in hESC-MG1 were similar to that of MIO-M1 cells, whilst significantly lower levels of this transcript were seen in hiPSC-MG1 when compared with MIO-M1 cells (log2FC=-1.9). The abundancy of GLUL transcripts followed a similar pattern to VIM, with significant downregulation in hiPSC-MG1 (log2FC=-2.5) and no difference in hESC-MG1 when compared with MIO-M1 cells. Pairwise analyses revealed that when compared to MIO-M1, CD44 transcripts were significantly lower in hiPSC-MG1 (log2FC=-4.7) but were at similar levels in hESC-MG1. CD29 (ITGB1) expression was similar in hiPSC-MG1 and MIO-M1 cells, but significantly higher in hESC-MG1 (log2FC=2.2).

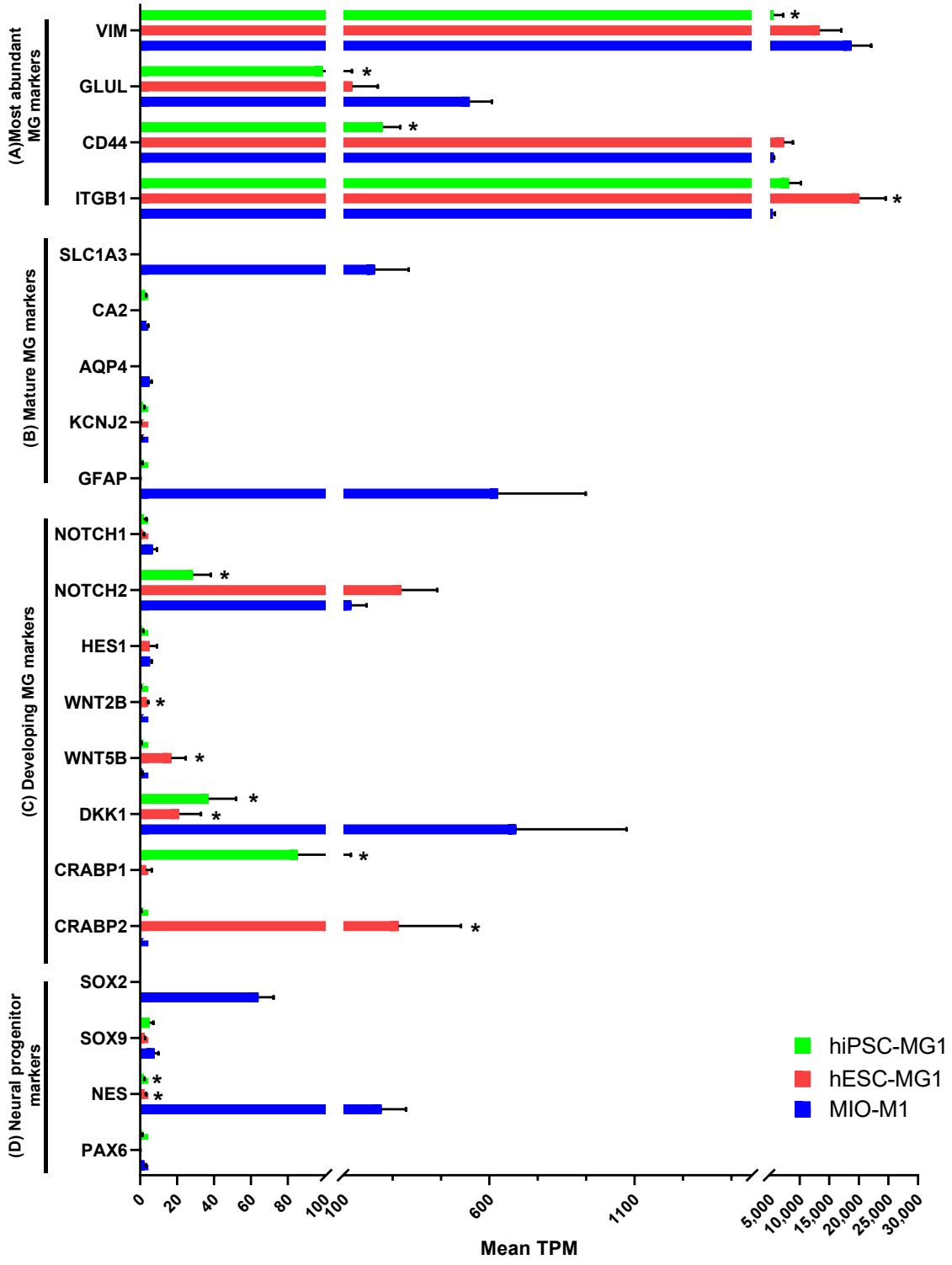

Figure 2.18 Expression levels of transcripts for Müller glia (MG) markers in the three cell preparations analysed.

Histograms show the mean TPM of transcripts of **(A)** the most abundant MG markers (VIM, GLUL, ITGB1, CD44), **(B)** mature Müller glia markers (SLC1A3, CA2, AQP4, KCNJ2, GFAP), **(C)** developing MG markers (NOTCH1/2, WNT2B/5B, HES1, DKK3, CRABP1/2), and **(D)** neural progenitor markers (SOX2, SOX9, NES, PAX6). hiPSC-MG1 (green); hESC-MG1 (red); and MIO-M1 (blue). * adjusted *p*-value < 0.05 for pair analysis with MIO-M1 cells.

In contrast, several markers that are normally identified in Müller glia from adult retina and responsible for regulation of glutamate metabolism, fluid flux, conductance of potassium current and intermediate filaments were significantly or absent in most samples (Figure 2.18B). These included glutamate transporter GLAST (SLC1A3), carbonic anhydrase II (CA2) (Vardimon et al., 1986), aquaporin 4 (AQP4) and potassium channels Kir2.1 (KCNJ2) and Kir4.1 (KCNJ10). Transcripts of SLC1A3 and AQP4 were not detected in either hiPSC-MG1 or hESC-MG1, whilst these were expressed at much higher levels in MIO-M1. CA2 showed comparable levels of expression in hiPSC-MG1 and MO-M1 but absent in hESC-MG1 (TPM=0). KCNJ2 were very low in all three cell preparations, whereas none of the cells expressed KCNJ10 (TPM=0; not shown). The cytoskeletal component intermediate filament GFAP was hardly identified in hPSC-derived cells (hiPSC-MG1: log2FC=-9.8; hESC-MG1: log2FC=-12.2), whereas the reference MIO-M1 cells showed a significantly higher expression. An important function of mature Müller glia is the regulation of intracellular availability of the light-sensitive intermediate substrate 11-*cis*-retinal, a retinoic acid derivative at which its biosynthesis between the *trans* and *cis* forms is critical for the phototransduction cascade that converts light to photochemical signals (Wang et al., 2009a, Saari, 2016). In humans, CRALBP is coded by RLBP1 and is a reported marker of Müller glia (Saari and Bredberg, 1988). However, it was noticed that no reads for RLBP1 were recovered in any of the three Müller glia preparations (TPM =0). Low expression of mature Müller markers may suggest that the hiPSC-MG1 and hESC-MG1 preparations were perhaps at a pre-mature stage and therefore not functionally active. That MIO-M1 did not show RLBP1 expression might be related to its long-term *in vitro* adaption following spontaneous immortalisation and this requires further investigation.

Considering the time points at which these cells were harvested from retinal organoids, it was important to examine the expression levels of genes that might determine their developing status (Figure 2.18C). During retinogenesis, the NOTCH pathway is required for maintaining undifferentiated progenitors and promoting Müller glia cell fate (Ghai et al., 2010). The transcriptomes of hiPSC-MG1 and hESC-MG1 indeed contained genes associated with developing Müller glia, such as of NOTCH receptors 1 and 2 (Furukawa et al., 2000) and its downstream effector hairy and enhancer of split-1 (HES1) (Hatakeyama and Kageyama, 2004). Transcripts of NOTCH1 and HES1 were statistically similar in the three cell

transcriptomes, whilst NOTCH2 was significantly downregulated in hiPSC-MG1 (log2FC=-2.4) when compared with MIO-M1 cells. In addition, WNT signalling is a major regulator of neurogenesis and retinal development (van Raay and Vetter, 2004) and mammalian Müller glia express the WNT ligands WNT2B, WNT5B and an inhibitor of WNT signalling Dickkopf-related protein 1 (DKK1) (Bernardos et al., 2007, Lawrence et al., 2007). In the presented transcriptomes, WNT2B and WNT5B, albeit their relative low expression, were significantly increased in hESC-MG1 as compared with MIO-M1 cells (WNT2B: log2FC=5.3; WNT5B: log2FC=3.9). However, their levels in hiPSC-MG1 were similar to those in MIO-M1 cells. DKK1 was significantly downregulated in hiPSC-MG1 (log2FC=-4.4) and hESC-MG1 (log2FC=-3.5), when comparing to MIO-M1. In additionally, it was observed that expression of two isoforms of the cellular retinoic-acid binding proteins (CRBPs), CRABP1 and CRABP2, were uniquely expressed in hiPSC-MG1 cells and hESC-MG1 cells, but were not found in MIO-M1 cells. CRBPs bind to the transcriptionally active derivative of retinoic acid called all-trans retinoic acid (atRA) (Blaner, 2019), one of the major transcriptional factors that functions as a morphogen for the pattern establishment of the inner retina during development (Maden et al., 1988). Translocation of atRA from the cytosol into the nucleus is executed by CRBPs, which directly interacts with the nuclear receptor of atRA, leading to activation of downstream signalling cascades (Budhu and Noy, 2002, Al Tanoury et al., 2013). *In vitro* studies on ESCs have revealed that CRBP is required for regulating G1-S transition of cell cycle by activation of the ERK1/2 pathway (Persaud et al., 2013). Given the long-term culture needed for retinal organoid maturation, the addition of retinoic acids to the culture medium and the harvesting time points of hiPSC-MG1 and hESC-MG1, it can be postulated that the transcript levels of CRABP1 and CRABP2 may be associated with the development and maturation of these cells within the retinal organoids.

Lastly, to determine whether hPSC-derived cells exhibited neuronal progenitor-like phenotypes, the expression levels of the neural progenitor markers SOX2, SOX9, PAX6, nestin (NES) were examined (Figure 2.18D). Transcripts of the progenitor master regulator SOX2 were absent in hiPSC-MG1 and hESC-MG1 but present in MIO-M1 cells, whilst the expression of SOX9 was similar in all cell preparations. Both hiPSC-MG1 and hESC-MG1 showed a low but similar expression of NES, whilst a significant higher expression of this transcripts was observed in MIO-M1

cells (hiPSC-MG1: log2FC=-6.9; hESC-MG1: log2FC=-6.4). PAX6 was expressed in hiPSC-MG1 and statistically no different to MIO-M1, but its transcripts were not detected in hESC-MG1. Based on the above results, it can be concluded that hiPSC-MG1 and hESC-MG1 have acquired the right cell lineage towards a developing Müller glia-like fate, although the levels of expression of characteristic Müller glia markers varied between cell sources.

2.5.6.5 hiPSC-MG1 and hESC-MG1 expressed genes coding for proteins implicated in neurotrophic supports

To gain further insights into the transcriptional landscape on the trophic support mechanism of Müller cells derived from hPSCs, the expression of a broad spectrum of anti-oxidative factors and trophic factors were highlighted in the transcriptomes of hiPSC-MG1 and hESC-MG1.

Analyses of these transcriptomes revealed that hPSC-derived Müller cells exhibited a wide range of genes coding for anti-oxidative enzymes whose expression profiles were highly comparable to the adult cell line MIO-M1 (Figure 2.19A). Amongst these genes, the peroxiredoxin (PRDX) family member PRDX1 and PRDX6 (Kang et al., 1998, Patenaude et al., 2005) represented the most abundant isoforms, with PRDX1 being expressed at similar levels across the three cell preparations examined. PRDX6 expression however, was significantly lower, in hiPSC-MG1 (log2FC=-1.9) when compared with hESC-MG1 and MIO-M1 cells. Genes coding for another differentially expressed antioxidant enzyme, the heme oxygenase 1 (HMOX) (Everse and Coates, 2009), were also observed in all cell preparations, albeit at lower level, but significantly higher in hiPSC-MG1 (log2FC=2.9) as compared with MIO-M1 cells. Pairwise analysis of this gene expression did not identify a statistical significance on its expression in hESC-MG1 when benchmark to MIO-M1 cells. Various genes coding for the common phase II anti-oxidative enzymes such as NAD(P)H Quinone Dehydrogenase 1 (NOQ1) (Talalay et al., 1995), superoxide dismutase (SOD) family member SOD1 and SOD2 (Inarrea et al., 2014, Azadmanesh et al., 2017), as well as a peroxidation ameliorating protein paraoxonase 2 (PON2) (Draganov et al., 2005, Grosche et al., 2016) were expressed at similar levels in all three cell preparations investigated. Furthermore,

transcripts for the mitochondrial enzymes coenzyme Q-binding protein homolog 10A (COQ10A) and COQ10B, which are associated with anti-oxidative and anti-apoptotic activities (Lee et al., 2014a), as well as the lipoic acid synthetase (LIAS) that catalyses the biosynthesis of α-lipoic acid, another a small-molecule antioxidant (Inman et al., 2013), detected at similar levels across the three transcriptomes. In addition, the differentially expressed putative antioxidant gene clusterin (CLU) (Ruzafa et al., 2018), coding for a glycoprotein that has been strongly suggestive of neuroprotective potential (Trougakos et al., 2009), was found at similar levels in both hESC-MG1 and MIO-M1, but expressed at significantly lower levels in hiPSC-MG1 (log2FC=-4.4) when compared with the above cells.

An enzyme family responsible for the small-molecule antioxidant glutathione (GSH) biosynthesis was also identified in the transcriptomes of the three call preparations (Figure 2.19B) (Forman et al., 2009). All cell expressed had similar levels of glutathione synthetase (GSS) transcripts whilst hiPSC-MG1 produced significantly higher levels of glutathione disulfide reductase (GSR) (Log2FC = 2.3) as compared to hESC-MG1 and MIO-M1 cells. The bioavailability of GSH is also under the regulation of several glutathione S-transferases (GSTs) that conjugate with a reduced form of GSH to form a wide ranges of exogenous and endogenous hydrophobic electrophiles (Chatterjee and Gupta, 2018). Amongst them, the transcript levels of GST-A4 (GSTA4), GST-C-terminal domain containing (GSTCD), GST-Kappa 1 (GSTK1), GST-Omega 1 (GSTO1) and GST-P1 (GSTP1) in hiPSC-MG1 and hESC-MG1 were not statistically different to those expressed in MIO-M1. Some GST isoforms including GST-Mu 3 (GSTM3) (Log2FC = 4.3) and GST-Zeta 1(GSTZ1) (Log2FC = 2.5) were found upregulated in hiPSC-MG1, whilst GST-Theta 2B (GSTT2B) was uniquely expressed in hESC-MG1 (Log2FC= 5.3) as compared to MIO-M1 cells.

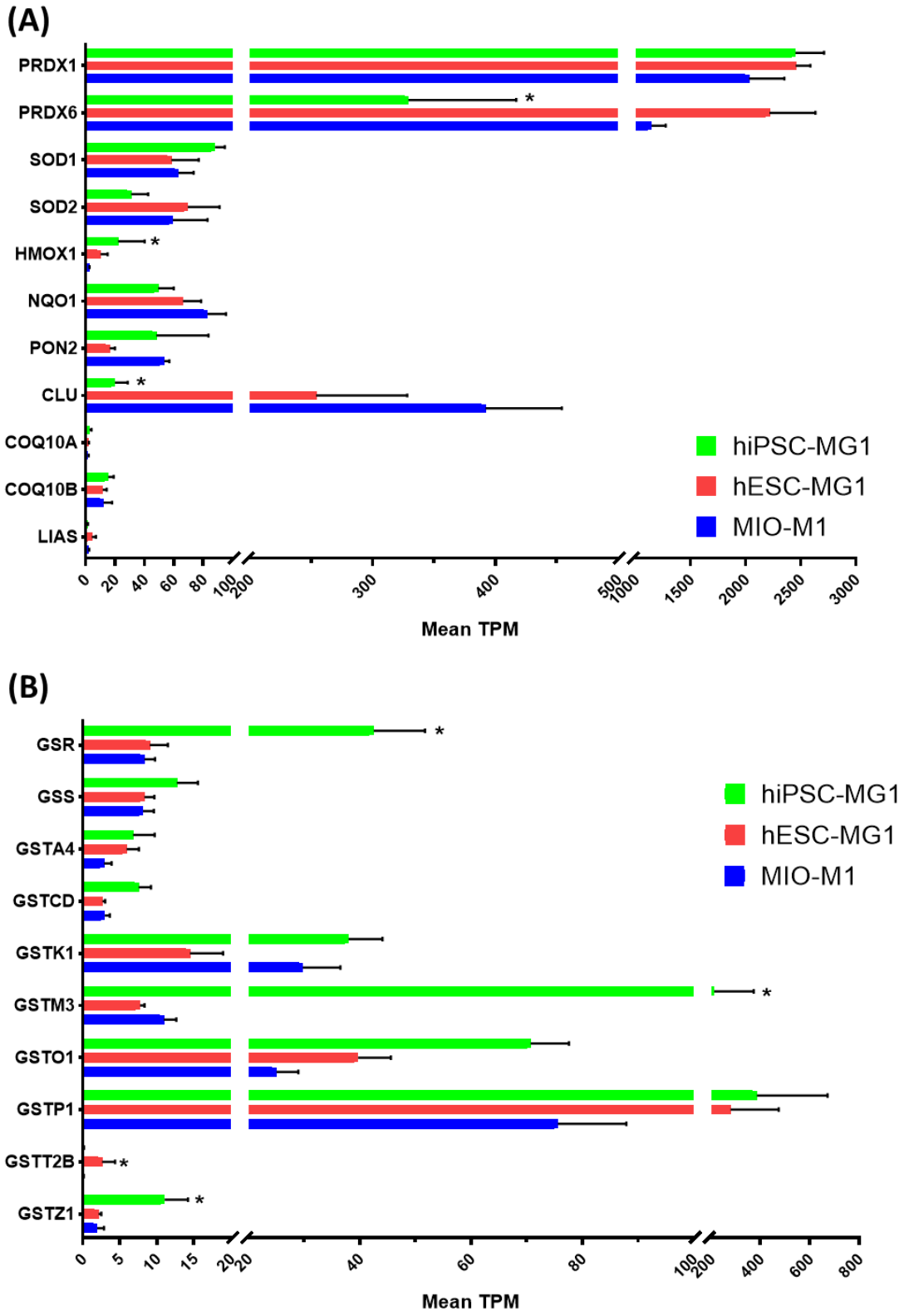

Figure 2.19 Expression levels of transcripts for anti-oxidative factors in the three cell preparations analysed.

Histograms show the mean TPM of transcripts for **(A)** antioxidant enzymes (PRDXs, SODs, HMOX1, NQO1, ALDH2, CLU, COQ10, LIAS) and **(B)** enzymes involved in glutathione biosynthesis (GSS, GSR, GSTs). hiPSC-MG1 (green); hESC-MG1 (red); and MIO-M1 (blue). * adjusted p-value < 0.05 for pair analysis with MIO-M1 cells**.**

Further analyses identified transcripts coding for various trophic factors such as neutrophins (Figure 2.20A) that have demonstrated neuroprotective effects in both *in vitro* and *in vivo* studies (Wurzelmann et al., 2017, Eichler et al., 2017, Price et al., 2007, Huang and Reichardt, 2001) in the transcriptomes of hiPSC-MG1 and hESC-MG1. Strikingly, hiPSC-MG1 and hESC-MG1 revealed distinctive upregulation of neutrophins. In comparison with the other two cell lines, whilst hiPSC-MG1 exhibited significant increase in neurotrophin-3 (NTF3) gene expression (Log2FC=10.6), hESC-MG1 showed significant upregulation of brain-derived neurotrophic factor (BDNF) gene expression (Log2FC=8.3), with reference to MIO-M1 cells. Nerve growth factor (NGF) transcripts were present in both hiPSC and hESC-derived cells but absent in MIO-M1. Another trophic factor, the pigment epithelium derived factor (SERPINF1) was detected at significantly higher levels in hESC-MG1 cells (Log2FC=6.4) when compared with the other two cell preparations. Moreover, other important genes coding for growth factors, including EGF, heparin binding EGF like growth factor (HBEFG), FGF, platelet derived growth factor (PDGF) and vascular endothelial growth factor (VEGF) that have been shown to be expressed by MIO-M1 cells (Eastlake et al., 2018), were enriched and some were differentially expressed at different levels in hiPSC-MG1 and hESC-MG1 (Figure 2.20B). Notably, transcripts of EGF and HBEGF were detected at similar levels in hESC-MG1 and MIO-M1, whereas hiPSC-MG1 did not express these transcripts. FGF family members including FGF1, FGF2 and FGF12 were expressed at abundant levels in all cell preparations, with FGF2 and FGF12 showing unique enrichment in hESC-MG1 (log2FC=2.6) and hiPSC-MG1 (log2FC=3.7) respectively, whilst FGF1 levels were statistically similar across all samples. Three isoforms of the PDGF family were selectively observed in some cell preparations, with PDGFA and PDGFD increased in MIO-M1 cells when compared with hPSC-derived cells (hiPSC-MG1: log2FC=-5.1; hESC-MG1: log2FC=-3.4). Similarly, differential expression of the gene coding for the VEGF family isoform VEGFA in hiPSC-MG1 transcriptomes was identified (log2FC=-2.5) when comparing to MIO-M1 cells, whilst other isoforms VEGFB and VEGFC did not show significant differences on their transcript levels between different cell preparations.

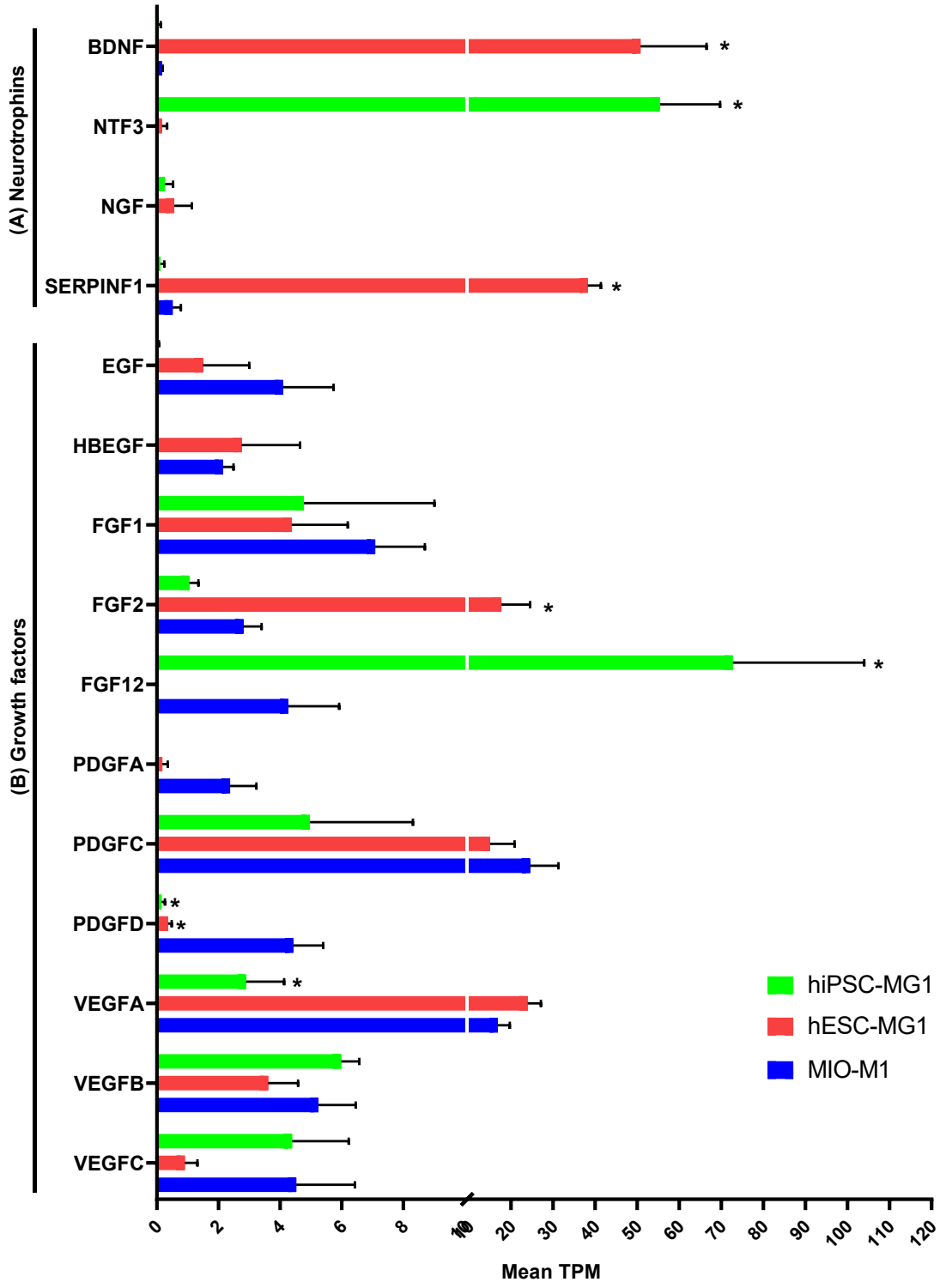

Figure 2.20 Expression levels of transcripts for trophic factors in three cell preparations. Histograms showing the mean TPM of transcripts of **(A)** neurotrophins (BDNF, NTF3, NGF, SERPINF1) and, **(B)** growth factors (EGF, HBEGF, FGFs, PDGFs, VEGFs). hiPSC-MG1 (green); hESC-MG1 (red); and MIO-M1 (blue). * adjusted *p*-value < 0.05 for pair analysis with MIO-M1 cells.

2.5.6.6 Validation of RNA-seq data by qRT-PCR

Fold-change of several Müller glia markers detected by RNA-seq that showed differential or selective gene expression. including BDNF, CRABP1/2, GFAP, GLUL, NES, PRDX6, SLC1A3, SOX2 and VIM was validated using Taman® quantitative RT-PCR (qRT-PCR). Cell preparations derived from biologically independent samples using the same hPSC source (hereafter referring as hiPSC-MG2 and hESC-MG2 respectively) were used to corroborate RNA-seq findings (Table 2.6). Subretinal injection of hiPSC-MG2 (Eastlake et al., 2019b) or hESC-MG2 (Eastlake et al., unpublished) into a NMDA-damaged animal model of retinal degeneration significantly improved the scotopic response corresponding to RGC function in these animals, demonstrating their *in vivo* neuroprotective functionalities to the damaged RGCs. Therefore, assessing the transcriptomic similarity of the hiPSC-MG2 and hESC-MG2 to their corresponding counterparts might shed light to the observed *in vivo* neuroprotective ability of these cells.

Experiment	**RNA-seq**			**qRT-PCR**		
Sample	hESC-MG1	hiPSC-MG1	MIO-M1	hESC-MG2	hiPSC-MG2	MIO-M1
***In vivo* transplantation**				Unpublished	(Eastlake et al., 2019b)	(Jayaram et al., 2014a, Becker et al., 2016)
Differentiation time (days)	70	90	Adult retina	70	281	Adult retina
Passage	P7,8,10	P7,8,9	P11,12,13	P8	P11	P18

Table 2.6 hPSC-derived cell preparations used for RNA-seq and validation by qRT-PCR. Three biological replicates of each cell preparation were subjected to RNA-seq analysis. Samples used for qRT-PCR validation were cells isolated from retinal organoids from different batches using the same hPSC source.

The consistency of gene expression levels detected in each cell preparation by the two methodologies was examined by Spearman's correlation coefficient. The log2FC values in the majority of genes detected by qRT-PCR in all cell preparations are in accordance with the RNA-seq findings (Figure 2.21). All correlations coefficients were statistically significant (p<0.005), with MIO-M1 cells showing the highest correlation coefficient (R^2=0.7653), followed by hiPSC-MG1 (R^2=0.7268) and hESC-MG1 (R^2=0.6581). This suggests that for majority of the genes, the RNA-

seq findings carry high reliability and accuracy on capturing the genome-wide molecular signatures of hiPSC-MG1 and hESC-MG1.

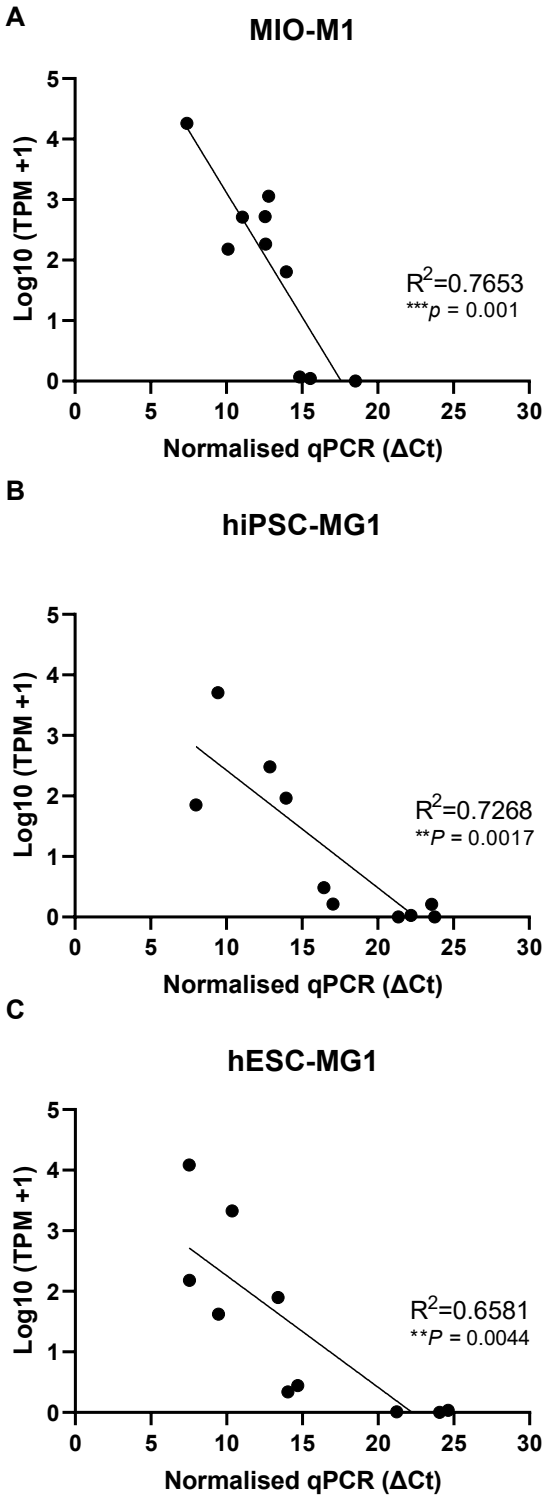

Figure 2.21 Correlation of gene expressions between qPCR and RNA-seq methods in the detection of gene expression in (A) MIO-M1, (B) hiPSC-MG1 cells and (C) hESC-MG1.
Plots show gene expression abundancies determined by qRT-PCR and RNA-seq for the Müller glia markers BDNF, CRABP1, CRABP2, GFAP, GLUL, NES, PRDX6, SLC1A3, SOX2 and VIM. The correlation coefficients (R^2) and the corresponding p-values are shown within the plot.

2.6 Discussion

2.6.1 *In vitro* development of hPSCs-formed retinal organoids recapitulated major events of retinogenesis

In this study, three hPSC sources were used to generate EBs and under the current differentiation protocol, the major steps of retinogensis *in vivo* including the emergence of optic vesicle were recapitulated in this study (Karus et al., 2014). The specification and maturation of retinal organoids followed the spatial-temporal process, agreeing with other studies using hPSCs (Nakano et al., 2012, Li et al., 2018). Retinal organoids represent a powerful tool to study retinal development and tracking the emergence and localisation of retinal cells (Wei et al., 2017), as evident by the appearance of a distinctive lamination characteristic of the neural retina. This is initiated by the formation of a 'mantle' at the periphery of the EBs, which upon dissection developed as a retina that could be clearly visualised under light microscopy. Multiple dissections of individual mantles appeared to be effective in obtaining several retinal organoids from a single EB in this study. Immuno-histochemical analysis of retinal organoid formed by hiPSC revealed the localisation of Müller glia as determined by a strong vimentin staining throughout retinal differentiation and was consistent with previous reports (Zhong et al., 2014). It was interesting that early appearance of CD29 in the periphery of EBs between days 10 to 16 after initiation of retinal differentiation, was observed in cells expressing the Müller glia markers vimentin and nestin. It is important to note that while the proper retinal architecture was demonstrated in retinal organoids, whether retinal cells within these 3D structures are functionally active remains unknown. Future investigation on the response of retinal organoids to electrical stimulation by patch clamp approach should be merited.

2.6.2 Cells isolated from hPSCs-formed retinal organoids acquired developing Müller glia-like fate

The isolation of Müller glia exploits the binding of Müller glia surface marker CD29 to its ligand fibronectin (Matsuyama et al., 1989), positively selecting Müller cells from the rest of retinal cell suspension and further propagating *in vitro* with supplementation of growth factors EGF and FGF. The isolated cells exhibited the

characteristic bipolar morphology of Müller glia as previously described (Limb et al., 2002, Lawrence et al., 2007). The molecular and cellular signatures of hiPSC- and hESC-derived Müller glia were examined by multiple approaches to validate their nature and the efficiency of retinal differentiation protocol. Majority of Müller glia markers and neural progenitor markers were confirmed in the hiPSCs and hESCs-derived Müller glia at both mRNA and protein levels. FACS analysis showed that nearly all of the hiPSC-MG1 (99.5%) and the hESC-MG1 (99.9%) showed comparable purity for Müller surface markers CD29 and CD44 to MIO-M1. The enrichment of Müller glia population was clearly owning to the effective retinal differentiation protocol across three different hPSCs and the binding of CD29 to fibronectin. These results demonstrated that plating cells isolated from retinal organoids on fibronectin is an effective method to isolate Müller glia and promoted the enrichment of these cells.

Characterisation of hiPSC-MG1 and hESC-MG1 by commonly used molecular genetic approach was further validated by capturing the genome-wide molecular signature of hiPSC-MG1 and hESC-MG1. Performing pairwise analyses with reference to the transcriptomes of MIO-M1 cells is appropriate to the research interest of this study that focuses on neuroprotective potential of hPSC-derived cells, as supported by the strong evidence on the neuroprotective competency of MIO-M1 cells (Singhal et al., 2012, Jayaram et al., 2014b). The differentiated status of hiPSC-MG1 and hESC-MG1 was confirmed through both FACS analysis and transcriptomic profiling on key pluripotency genes. SSEA-4 is expressed at the early stage of embryonic development and is useful for identifying cells of embryonic origin that are potentially tumorigenic (West et al., 2010). Less than 1% of hiPSC-MG1 and hESC-MG1 were positive for SSEA-4 expression, and the absence of this pluripotency gene in their transcriptomes highlights the exit of pluripotency in hPSC-derived cells as a result of retinoic acid-driven neural induction (Fenderson et al., 1987, Andrews et al., 1996, Draper et al., 2002). Most importantly, these findings augment the minimal teratogenic risk of these cells (Semrau et al., 2017). Additionally, overrepresentation analysis through investigating gene ontology (GO) by biological process also indicate that many significant GOs in the transcriptomes of hiPSC-MG1 and hESC-MG1 are involved in neuronal development and differentiation, with hESC-MG1 showing a more neuronal like development than hiPSC-MG1 did. These observations implied that differentiation of these Müller cells

was indeed towards the right neural lineage. In addition, the absence of majority of markers for retinal cell phenotypes including RPE, photoreceptors, HC, AC and BC confirmed that hiPSC-MG1 and hESC-MG1 did not acquire these phenotypes. Together, these evidences highlighted the robustness of the differentiation protocol to drive hiPSC-MG1 and hESC-MG1 exited pluripotency and have undergone the right lineage commitment.

The observations that retinal differentiation protocol specifying Müller glia-like cell fate was significantly robust within 90 days of organoid differentiation, as supported by the emergence of gene clusters associated with Müller glia cell fate. The Müller glia-like identity of hiPSC-MG1 and hESC-MG1 is supported by the strong expression of VIM, GLUL, ITGB1 and CD44. It is noteworthy that Müller glia marker panel is not definitive and is established based on previous immunohistological studies that reported localisation of these markers in Müller glia within the neural retina (Milam et al., 1990, Vardimon et al., 1986, Lawrence et al., 2007), especially for CRALBP (Fischer et al., 2001, Pfeiffer et al., 2016, Frenkel et al., 2018). In the data presented herein, some of well-established mature Müller glia markers such as RLBP1, AQP4, SCL1A3 and KCNJ2/10 were absent or expressed at minimal levels in some or all transcriptomic libraries. These findings were not surprising as it might be possible that at this organoid stage, Müller glia might not have acquired functions associated with a fully developed retina. A key weakness in this study is that the maturity of hiPSC-MG1 and hESC-MG1 was not assessed and represents a common obstacle in *in vitro* formed retinal organoids (DiStefano et al., 2018). There is no evidence that cells present in retinal organoids are functionally active or that stages of retinal organoid development mimic human embryonic development. A recent study showed that long-term cultured (205 days) hPSC-derived retinal organoid closely resembled cell composition of human foetal retina at day 125 of gestation, with Müller glia cluster positive for RLBP1, AQP4 and SCL1A3 (Sridhar et al., 2020). Since the cells examined in this study were obtained from retinal organoids cultured for only 90 days, this might explain the lack of detection of functional genes coding for mature functions. During mouse embryonic development, CRALBP is limited to RPEs at E15.5 and co-localised with GFAP in astrocytes (Johnson et al., 1997). Its presence in the Müller glia endfeet is not detected until birth and its levels continuously increase from the first week of postnatal stage until adulthood, implying that CRALBP appears in Müller glia at late

developmental stages. Therefore, it can be speculated that hPSC-derived cells isolated at day 90 were at a much earlier stage of retinal development and functional markers have yet been fully expressed, which do not necessarily deny their phenotypes as Müller glia-like.

During embryonic development, subtle regulation of retinoic acid is critical for organogenesis and preventing toxicity (Hyatt et al., 1996, Johnson et al., 1997, Snodgrass, 1992). This is thought to be achieved by multiple intracellular binding proteins expressed by astrocytes and Müller glia such as CRALBP and CRBP (Snodgrass, 1992). Interestingly, coding genes of the latter CRABP1 and CRABP2 showed cell-type specific abundancy in hiPSC-MG1 and hESC-MG1 respectively, but were absent in MIO-M1. CRBPs have shown exclusive immunoreactivity in Müller glia of human and primate retinae while some amacrine cells in murine and feline retina are also positive for these proteins (Milam et al., 1990). This is in concordance with our hypothesis that CRABP may be required for maintaining the nuclear transport of retinoic acid and might be indicative of Müller cell development.

The expression of NOTCH and WNT signalling components in Müller glia derived from retinal organoids formed by hPSC-derived cells further support the differentiated phenotype. It also remains obscure that the neuronal progenicity regulators SOX2, SOX9 and PAX6 showed absent or low expressions in hiPSC-MG1 and hESC-MG1. A possible explanation could be that the downregulated expression of Müller glia markers might be owning to the caveat of pro-longed *in vitro* culture. Johnsen and colleagues reported that cells isolated from human peripheral retinae had all retinal cell markers including CRALBP and GFAP significantly declined within two weeks of *in vitro* propagation (Johnsen et al., 2018). Indeed, by biological processes, GO overrepresentation identified several GO groups regulating early anatomical and morphological development, implying that these Müller cells were indeed still at developing stage. For MIO-M1, it might be possible that the spontaneous immortalisation process might have an impact on their Müller glia characteristics, as supported by studies showing that immortalisation of primary cultures by manual transformation could lead to dedifferentiation of cells and reduction of specific cellular markers (Sippl and Tamm, 2014).

Most importantly, genes governing the fundamental functions of Müller glia as represented by the broad spectrum of trophic and growth factors were identified in the transcriptome analysis of hiPSC-MG1 and hESC-MG1. However, not all genes coding for these factors were observed in all cells. This is illustrated by the observation that whilst relatively high level of transcripts NTF3 but low or no levels for BDNF or SERPINF1 were observed in hiPSC-MG1, hESC-MG1 expressed almost imperceptible levels of NT3 but high levels of BDNF and SERPINF1 transcripts. It is noted that BDNF and NTF3 are homologous to NGF, which are also exclusively found in the transcriptome of hPSC-derived cells. During CNS development, NT3 is the most abundant neurotrophin and its expression drastically reduces when neuronal maturation takes place, which is accompanied by upregulation of BDNF (Maisonpierre et al., 1990a). Perhaps that the enrichment of BDNF in hESC-MG1 might indicate that these cells were at a more advanced stage of maturation than hiPSC-MG1 which exclusively expressed hiPSC-MG1. Whilst it is widely recognised that neurotrophins offer critical support to cell survival and function via tyrosine kinase (TrK)-driven signalling, it seems that the enrichment of BDNF or NT3 in hPSC-derived cells are essential for maintaining the proliferative potential and the differentiated phenotypes of neurons in the CNS (Maisonpierre et al., 1990b, Snider and Johnson, 1989). Other trophic factors. including PEDF (Pang et al., 2007, Eichler et al., 2017), PDGF (Osborne et al., 2018), FGF (Otto et al., 1989), EGF (Duarte et al., 2016), HBEGF (Wan et al., 2012) and VEGF (Foxton et al., 2013) are essential to promote survival and possibly regeneration of damaged neurons. In addition, the significant rescue of RGC scotopic responses in animal models of NDMA damage by Müller cell obtained from hPSC-derived retinal organoids (Eastlake et al., 2019b) (Eastlake et al., unpublished) offers evidence of the trophic support of these Müller glia-like cells *in vivo*. Interestingly, many GO groups by cellular component were associated with the formation of membrane-bound organelle and extracellular exosome, which might be responsible for the extracellular delivery of these trophic factors (Kalani et al., 2014). Taken Together, these observations further reiterate the hypothesis that hiPSC-MG1 cells and hESC-MG1 indeed harboured promising neuroprotective potential to support survival and functions of retinal neurons.

In summary, the retinal differentiation protocol and the methods used in this study provide sufficient evidence that homogenous populations of Müller glia can be

isolated from hPSCs-derived retinal organoids. An important and simplified step constitutes the binding of CD29 positive cells to fibronectin, which proved effective to produce a highly pure cell population. The abundancy of several Müller glia markers and enrichment of a broad range of neuroprotective genes in these cells are sufficiently encouraging to suggest that hPSC-derived Müller cells might constitute a viable cell source for therapies to treat retinal degeneration.

2.6.3 Differences in the formation of retinal organoids by pluripotent stem cells are reflected in their specific transcriptomes

Throughout the retinal differentiation of hPSC process and during *in vitro* propagation of isolated Müller cells from retinal organoids, striking differences were observed depending on the sources of hPSC used to derive the organoids. More than 16 independent passages of hiPSC BJ and hESC RC-9 successfully formed retinal organoids, whilst cell aggregates resembling EBs were only formed by hESC Shef 6 in two occasions, and these did not develop into morphologically identifiable retinal organoids. The success rate of proliferation of isolated Müller cells from different hPSC sources also varied, with majority of Müller cells derived from BJ and RC-9 cell lines could be propagated up to 10 passages, but cells isolated from the Shef 6 organoid-like structures failed to expand beyond passage 6. The importance of the hPSC source used is further demonstrated by the cell-type specific variation on the morphology and transcriptomic profiles. Consistent variations in the expression of gene clusters associated with Müller cell markers, anti-oxidative enzymes and trophic factors including PRDX6, BDNF and SERPINF1, as well as CRABP and components of NOTCH and WNT pathways, were observed amongst the different cell preparations according to the hPSC source. The molecular distinction between hiPSC and hESC in their ability to form retinal organoids and generate retinal cells with unique molecular identity is yet to be investigated and it is possible that their genetic and epigenetic variation might dictate the differences between the Müller cells formed by them. This is supported by observations that the epigenetic signatures of hPSCs may be have implicated in their propensity to respond to inducing factors (Osafune et al., 2008, Sun et al., 2018). In particular, hypermethylation at certain loci and maintenance and biological source of hPSCs

might also influence the successful formation of retinal organoids by these cells. Future studies involving karyotyping and identification of epigenetic features on different hPSC sources may aid in the understanding of the response of these cells to retinal differentiation.

2.6.4 Limitation of study

This study focused on the mRNA transcriptomes of hPSC-derived Müller cells and did not capture the full complexity of the transcriptomes on the non-coding repertoire. Appreciating the influence of the non-coding RNAs is important as they could interfere in the conversion of transcriptome to proteosome by interacting with mRNAs at both transcriptional and post-transcriptional levels. Many studies have addressed the implication of microRNAs (miRNAs) in the development, maturation and functions of neurons (Lagos-Quintana et al., 2002, Xiao et al., 2014), therefore investigating the miRNAs repertoire in hPSC-derived cells may facilitate the understanding of their *in vivo* functionality. In addition, the maturation of hPSC-derived cells cannot be fully addressed by the transcriptome of cells isolated at a single time-point. Future studies could explore the temporal transcriptomic changes on cells isolated at multiple time points over the course of retinal organoid differentiation. Together with the dataset presented here, insights generated from these potential investigations could optimise the robustness of the retinal differentiation protocols and perhaps, proposing appropriate time points to isolate Müller glia with the right maturation.

To conclude, transcriptomic analysis revealed that isolated hiPSC-MG1 and hESC-MG1 cells exhibited significant overlap on the morphological characteristics and molecular signatures associated with trophic support as compared to the adult human Müller glia cell line MIO-M1. This study has therefore demonstrated that Müller glia-like cells isolated from hPSC-derived retinal organoids can be consistently produced, providing a traceable source for their application in the development of cell therapies to treat retinal diseases.

CHAPTER 3 Examination of the effect of TNF-α on Müller glia neuroprotective responses as revealed by transcriptomic analysis

3.1 Introduction

3.1.1 TNF-α and its signalling components

Upregulation of TNF-α expression is well documented in various retinal disorders such as retinal detachment (Rasier et al., 2010), diabetic retinopathy (Kern, 2007, Suzuki et al., 2011), glaucoma (Kondkar et al., 2018, Ghanem AA, 2010) and age-related macular degeneration (Al-Gayyar and Elsherbiny, 2013, Mimura et al., 2019). High level of TNF-α is hallmark of traumatic retina at which gliosis of Müller glia is the universal event in the abovementioned disorders. However, Müller glia is not the only cell type releasing TNF-α and in fact microglia (Langmann, 2007) also contribute to the production of TNF-α. In acute injury, a recent study suggested that microglia is proposed as the only source of TNF-α (Todd et al., 2019) while Müller glia is widely accepted as the major inducible reservoir of this cytokine in many retinal degenerative conditions.

TNF-α exists as a 26kDa-transmembrane pro-form of homotrimer and is cleaved by the metalloproteinase TNF-α-converting enzyme (TACE) to become the soluble 17kDa molecule (

Figure 3.1) (Ruuls et al., 2001). Upon binding of TNF-α to its cell surface receptors, both forms of TNF-α are shown to trigger signalling mechanisms that activate cellular functions including proliferation, differentiation, migration, survival and apoptosis (Pfeffer, 2003, Vandenabeele et al., 1995). The transmembrane TNF-α receptors (TNFRs) can form two types of complexes including TNFR1/p55 and TNFR2/75 which show variations in terms of expression pattern, ligand type and structural differences (Agarwal and Agarwal, 2012). These expression patterns of TNFRs vary depending on cell types. TNRF1 constitutes the constitutive receptor and TNFR2 is found in a subpopulation of T regulatory cells, endothelial cells and CNS cells (Salomon et al., 2018). The soluble TNF-α is the main ligand for TNFR1

which can also be activated by the membrane-bound form of this cytokine. In contrast, TNFR2 predominantly responds to the membrane-bound TNF-α (

Figure 3.1) (Locksley et al., 2001). Structurally, both receptors show high similarity on the extracellular domains, whilst the intracellular domain of TNFR1 has a death domain which is not found in TNFR2. Both types of TNFRs however do not have catalytic activity and TNF-α signalling is conducted by activated TNFRs engaging adaptor proteins which act as effectors to prompt additional signalling pathways (Locksley et al., 2001, Ruuls et al., 2001). In addition to transducing TNF-α signalling, the ectodomains of TNFRs become soluble receptors (sTNFR) following cleavage by TACE, which act as an intrinsic regulatory mechanism to alleviate TNF-α toxicity (Fischer *et al*., 2015). By competing with the transmembrane TNFRs for the circulating TNF-α, sTNFRs are thought to induce delayed TNF-α activation, ensuring no exacerbated TNF-α responsiveness (

Figure 3.1).

Following TNF-α binding, TNFR1 undergo trimerization and conformational changes and the death domain becomes exposed following dissociation of the inhibitory protein silencer of death domains (SODD) (

Figure 3.1). Subsequently, several signal transducers including the TNFR1-associated death domain (TRADD), receptor interacting protein kinases (RIPKs) and the TNF receptor associated factor 2 (TRAF2) are recruited (Ruuls et al., 2001). Amongst them, TRADD appears to be the switchboard of downstream signalling and could activate apoptosis via engagement of the Fas-associated death domain (FADD) and pro-apoptotic protein caspase 8 and 10, inducing auto-proteolysis and pro-apoptotic signalling (Urschel and Cicha, 2015). TRAF2 can also be activated by TNFR2, inducing a non-receptor tyrosine kinase family member epithelial tyrosine kinase (ETK) that activates the phosphatidylinositol 3-kinase (PI3K) signalling pathway and induces pro-survival responses including migration, proliferation and angiogenesis (Agarwal and Agarwal, 2012).

Interestingly, signalling cascades mediated by TNFR1 and TNFR2 can crosstalk to each other via the nuclear factor kappa-light-chain-enhancer of activated B cells (NFκB), another protein complex that interacts with TRADD (Tezel, 2008). NFkB is a transcription factor complex that comprises of NFκB1/p105 and NF-κB2/p100

(Baldwin, 1996). NFκB1 and NFκB2 proteins are synthesised as the large subunit p105 and p100 respectively and are cleaved to become p50 and p52, whilst their respective inhibitory subunit IκBα remains bound in quiescent state (

Figure 3.1). NFκB complexes can be induced by the canonical or alternative pathways, leading to a diverse range of cellular responses. Stress stimuli such as TNF-α and other cytokines activate the classic canonical pathway and normally produce pro-apoptotic outcomes. Upon activation of TNFRs, TRADD promotes TRAF2 and RIP binding which in turn recruit and activate the IκB kinase (IκK), leading to phosphorylation and proteomic degradation of IκBα. Free NFκB1/p50 and NFκB2/p52 are no longer sequestered and form dimers before nuclear translocation. In contrast, alternative pathways including the non-canonical and atypical pathways are IKKβ independent. As a consequence, these pathways might be associated with modification of NFκB subunits and their target genes (Perkins and Gilmore, 2006). It is noteworthy that depending on the type of cells, stimuli and timing exposure to stimuli, NFκB dimerisation might vary and therefore the plethora of effects mediated by this transcription factor could be linked to neurodegeneration and/or neuroprotection.

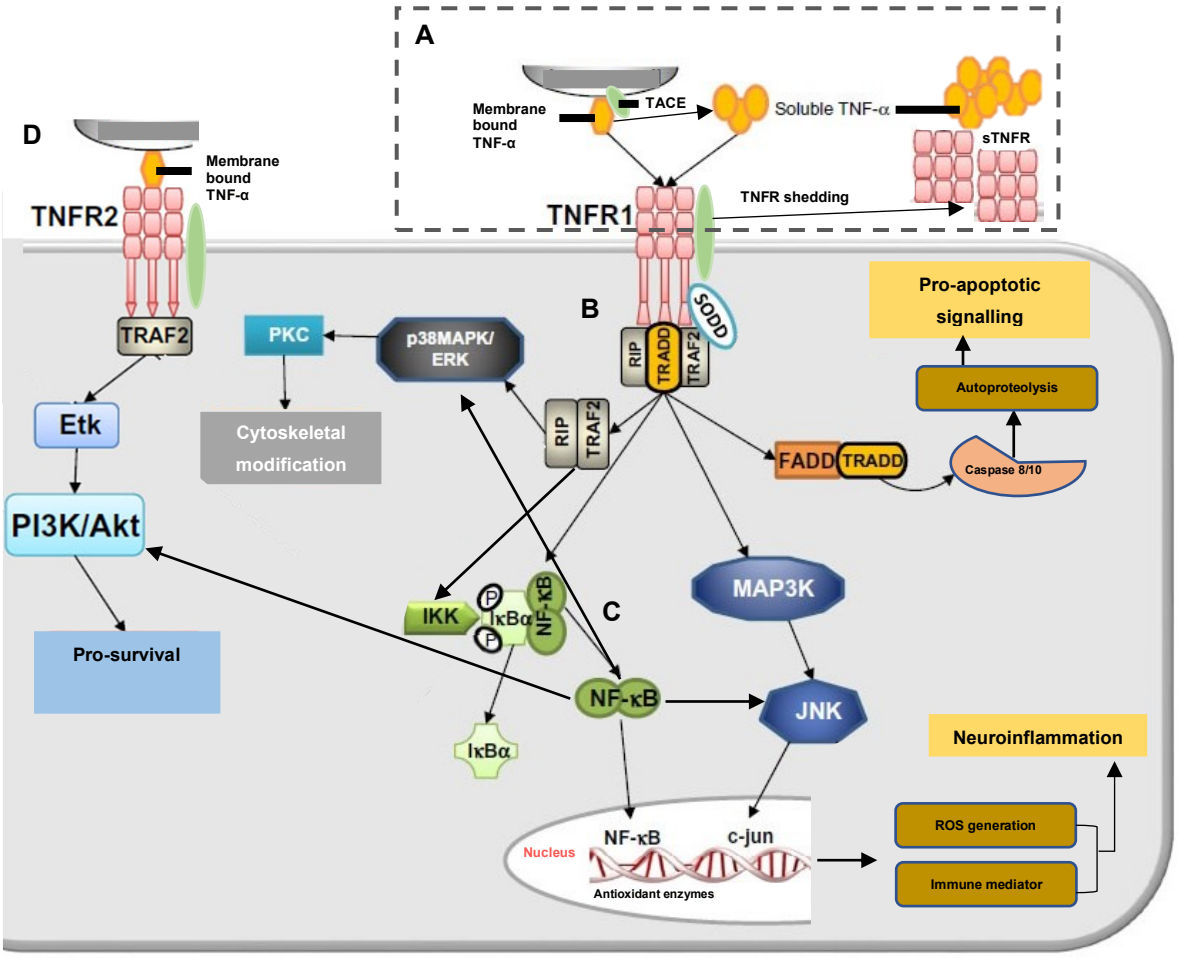

Figure 3.1 TNF-α signalling components and downstream signalling cascades triggered by TNF-α.
(A) TNF-α can be found as a membrane-bound form or as a free-floating protein following cleavage from the cell membrane by TACE. This enzyme also catalyses the shedding of the TNFRs ectodomain to release soluble TNFRs act as intrinsic inhibitors of TNF-α signalling and regulate the bioavailability of this cytokine to TNFRs. **(B)** Soluble TNF-α is the main ligand of TNRF1 and following binding, silencer of death domains (SODD) dissociates away from the TNFR1, allowing TRAF2 and TRADD binding to its intracellular death domain. TRADD forms a transcriptional complex with FADD which activates caspase 8/10, leading to activation of autoprotelolysis and pro-apoptotic signalling. (C) Activated TRAF2 interacts with NFκB complex and drive its conformational change. Dissociation of the inhibitory subunit IκBα allows the NFκB subunit translocation to the nucleus and drives the transcription of various genes involved in ROS generation, anti-oxidative and neuroinflammatory signalling. (D) TNFR2 activation is primarily mediated by membrane-bound TNF-α and upon binding, TRAF2 dissociates from the TNFR2 complex and activates the PI3K/Akt pathway, leading to induction of a pro-survival signalling. This figure was partially adapted from (Urschel and Cicha, 2015).

3.1.2 TNF-α signalling in neurodegeneration

TNFR1-mediated signalling involves induction of inflammation, oxidative stress and neuronal cell death. These cellular events are driven by mainly three types of mitogen-activated protein kinases (MAPKs) including the c-Jun N-terminal kinases (JNKs), the p38-MAPKs and the extracellular signal-regulated kinase (ERK). Their activation can involve NFκB signalling in parallel to the upstream TNFR/TRADD (Perkins and Gilmore, 2006, Sabio and Davis, 2014).

p38-MAPKs and ERKs provoke less potent cellular reactions such as upregulation of the gliotic intermediate filament GFAP, one of the immediate neurodegenerative features of the acute phase of TNF-α-mediated neuroinflammation (

Figure 3.1). GFAP upregulation has been reported to be effectively attenuated when treating retinal explants with anti-TNF-α monoclonal antibodies (Fernandez-Bueno et al., 2013, Martínez-Fernández de la Cámara et al., 2014). Moreover, these cytoskeletal modifications are driven by p38MAPK/ERK pathway activation, which is effected by PKC signalling (Perkins and Gilmore, 2006, Tezel, 2008). This activation has been further confirmed in an experimental model of retinal detachment as absence of GFAP showed reduction in ERK activation as compared to wildtype mice (Nakazawa et al., 2007).

NFκB-mediated cJNKs activation represents the strongest response of TNFR1 signalling (

Figure 3.1), further conveying inflammatory response by promoting the expression of cytokines, chemokines and their receptors and inducing migration of immune cells to the damage sites. Ruuls and colleagues revealed that binding of the soluble TNF-α to TNFR1 prompted neuroinflammation manifested as leukocyte infiltration (Ruuls et al., 2001). Another target of TNFR1 signalling is JAK/STAT signalling which induces inflammatory response in the CNS and the expression of many components of this signalling is identified elevated in glaucomatous conditions (Yang et al., 2011, Wang et al., 2000). The chemotactic property of TNF-α signalling increases is witnessed by the upregulation of cell adhesive molecules vascular cell adhesion protein 1 (VCAM1) and intercellular cell adhesion protein 1 (ICAM1), and those regulating ECM homeostasis including matrix metalloproteases (MMPs), tissue

inhibitor of metalloproteinase (TIMPs) (Perkins, 2004). Inflammasome assembly as characterised by aggregation of multiple immune proteins stimulate caspase 1 which in turn further promotes secretion of potent pro-inflammatory cytokines IL-1β and IL-18 (Ogura et al., 2006).

During neuroinflammation, oxidative stress is another consequence of TNF-α signalling (

Figure 3.1). Reactive oxygen species (ROS) such as free radicals or peroxides ROS accumulate within mitochondria following TNF-α stimulation. This results from NFκB-mediated activation of the pro-oxidative gene NADPH oxidase (NOX) member NOX (Anrather et al., 2006). Prolonged NOX activation can impair mitochondrial oxidative phosphorylation following the transfer of electrons to oxygen molecules mediated by NOX, leading to generation of superoxide which can disrupt mitochondria morphology and membrane potential (Fiers et al., 1999). Evidence from co-culture of Müller glia with RGCs under stress conditions mimicking ischemia and glaucoma revealed that Müller glia-derived TNF-α elicited a series of intracellular events in RGCs including oxidative stress-mediated mitochondrial dysfunction (Tezel and Wax, 2000). This is recognised as the immediate result of prolonged MAPK signalling (Sakon et al., 2003) or persistent JNK signalling, which forms a positive feedback loop that further promotes ROS production within mitochondria (Blaser et al., 2016).

Evidence that TNF-α amplifies cell death is witnessed in retinal ischemia and glaucoma models, while neutralisation of TNF-α promotes neuronal survival (Nakazawa et al., 2007, Berger et al., 2008). Cell death could be the direct consequence of TNFR1 activation or chronic neuroinflammation. TNFR1-driven signalling directly activate apoptosis by TRADD and FADD inducing caspase-8/10 mediated autoproteolysis, further inducing effector caspases to execute apoptosis (

Figure 3.1). Additionally, a prolonged inflammatory response with chronic oxidative stress elicited by TNF-α/TNFR1 activation, that can aggravate neurodegeneration by activating several downstream signalling pathways leading to neuronal cell death. For example, the p38-MAPK pathway can engage key factors regulating caspases and proteolytic components, indirectly inducing apoptosis (Tobiume et al., 2001). TNFR1 knockdown has been shown to mitigate NMDA-mediated RGC damage

(Takeda et al., 2018), whilst neuronal loss in TNFR1 deficient mice is significantly halted, with this rescue being lost when PI3K signalling is arrested (Fontaine et al., 2002). TNFR1 also recruits JNKs (Wei et al., 2002) and induces RGC cell death following optic nerve crush, as evident by inhibition of JNK in wild type rodents, which leads to RGC survival comparable to with the loss of TNFR1 (Tezel et al., 2004).

3.1.3 TNF-α signalling and neuroprotection

The earliest evidence supporting a neuroprotective effect of TNF-α signalling was observed in zebrafish, in which TNF-α released by dying photoreceptors is regarded as the first signalling molecule to activate Müller glia as determined by GFAP upregulation (Thomas et al., 2016), followed by subsequent downregulation (Thummel et al., 2008). Additionally, it was reported that TNF-α deficiency failed to activate the proliferative regulators signal transducer and activator of transcription 3 (STAT3) and Achaete-Scute family bHLH transcription factor 1 (ASCL1a), which drive Müller glia entering the cell cycle to regenerate the damaged zebrafish retina (Nelson et al., 2013, Conner et al., 2014). The protective effect of TNF-α is evident in rodents receiving exogenous TNF-α prior to optic nerve injury, which show less RGC loss and post-injury injection do not exacerbate further damage (Mac Nair et al., 2014).

It is well accepted that TNFR2 signalling antagonises degenerative processes evoked by TNFR1 and promotes neuroprotection by engaging effectors TRAF1 and TRAF2 to activate NFκB and additional signalling cascades (

Figure 3.1) (Yeh et al., 1999, Bouwmeester et al., 2004). This is supported by a previous study that was showed that retinal ischemia in mice with TNFR2 deficiency causes profound cell death as compared to wildtype animals (Fontaine et al., 2002). In another study, primary cortical neurons that lack of TNRF2 were more susceptible to glutamate excitotoxicity (Marchetti et al., 2004). Interestingly, several studies have highlighted that TNFR2-dependent continuous activation of NFκB is important to induce cell survival and in contrast, the transient elicitation of NFκB by TNFR1 might be associated with neurodegeneration (Fontaine et al., 2002, Marchetti et al.,

2004, Mac Nair et al., 2014). TNFR2-dependent neuroprotection is linked to several kinase-mediated cascades. PI3K-depedent activation of protein kinase B (PkB/Akt) promotes angiogenesis and cell survival (Yuan and Yankner, 2000). In addition, pro-survival signalling could be driven by NFκB interfering with the pro-apoptotic JNK signalling (Tang et al., 2001) and by induction of PI3K signalling by BDNF (Klocker et al., 2000, Marchetti et al., 2004). TNFR2 signalling also modulate the neuroinflammatory response by promoting the activity of granulocyte colony-stimulating factor (G-CSF) which might also influence neuronal survival following cerebral ischemia (Xiao et al., 2007, Veroni et al., 2010). This neuroprotective effect is accompanied by significant upregulation of sTNFR2 rather than sTNFR1 as shown by *in vitro* studies, implying the importance of this regulatory mechanism to reinforce TNFR2-mediated neuroprotection (Veroni et al., 2010). In addition, TNFR1 drives neuroinflammation and disrupting oxidative balance within the cell, it has revealed that mitochondria-derived ROS could is necessary for NFκB activation and subsequent anti-apoptotic response (Hughes et al., 2005). ROS elevation leads to a transcriptional activation of an intrinsic anti-oxidative defence mechanism driven by a master transcription factor nuclear factor erythroid 2-related factor 2 (NRF2) (Navneet et al., 2019). Subsequently, a series of anti-oxidative enzymes including superoxide dismutase 2 (SOD2) and heme oxygenase 1 (HO1) scavenge ROS to prevent protein- and lipid-rich organelles from oxidation (Blaser et al., 2016, Xiong et al., 2015).

TNFR2 also appears enhance the TNFR1-driven apoptotic signalling (Ruuls et al., 2001). Following N-Methyl-d-aspartate (NMDA) stimulation, Müller glia-derived TNF-α has been implicated in RGC apoptosis via NFκB and blockade of TNF-α signalling by Etanercept which is structurally akin to TNFR2 rescued RGC death (Lebrun-Julien et al., 2009). It has also been reported that the pro-form of NGF could bind to TNFR2, causing RGC death by increasing TNF-α release from glial cells (Lebrun-Julien et al., 2010).

3.2 Objectives and experimental outline

Müller glia are the principal glial cells that offer structural and homeostatic support to the neural retina (Oku et al., 2002, Bringmann et al., 2006). In response to external insults such as pro-inflammatory cytokines, Müller glia undergo reactive gliosis and become hypertrophic with significant upregulation of GFAP (Erickson et al., 1987, Bringmann and Reichenbach, 2001). Although this reactive response is believed to be a protective mechanism in the mammalian eye to limit damage to the neural retina, it fails to promote regeneration of the human retina and instead, further potentiates the retinal inflammatory response and retinal degeneration (Lewis and Fisher, 2003). In addition, extensive research *in vitro* has revealed the effect of TNF-α on retinal cells including astrocytes (Santos et al., 2017) and photoreceptors (Xie et al., 2017). Genome-wide studies have provided knowledge on the transcriptomic modifications that occur during experimentally induced retinal degeneration (Lupien et al., 2007, Suga et al., 2014). However much remains unknown on the transcriptomic impact of TNF-α on Müller cells. To understand the molecular manifestations induced by this cytokine in MIO-M1 cells, a high-throughput sequencing technique was utilised to examine the transcriptomic profile of these cells following an acute exposure to this cytokine.

The specific aims of this chapter were:

1. To investigate the transcriptomic response of human adult Müller glia cell line MIO-M1 to TNF-α using RNA-sequencing technique.

Experimental design:

i. A summary of the experimental design is illustrated in Figure 3.2.

ii. Human MIO-M1 cells were seeded at 1 million cells in T25 flasks containing 5mL of DMEM with 10% FCS and allowed to adhere for 24 hours before replacing culture medium with fresh medium containing 50ng/mL TNF-α and incubated for 24 hours at 37^{o}C. Untreated cells served as controls. The working concentration of 50ng/mL was selected based on previous work in

the hosting laboratory where this was the minimal concentration that induce significant modulation on the expression of antioxidant enzymes.

iii. Cell pellets were collected at the end of treatment for total RNA extraction, followed by genomic DNA depletion (See Materials and Methods for detailed protocol). This was followed by cDNA library preparation and sequencing. Three culture passages were collected as biological replicates.

iv. RNA-sequencing was performed by 75bp pair-end sequencing on an Illumina® HighSeq 3000 platform. Bioinformatics analysis was performed in collaboration with Dr Nicholas Owen from the Institute of Ophthalmology. Differential gene expression, gene enrichment and pathway analysis were performed on a pair-wise comparison between control and treated samples.

v. Statistical analysis was achieved by programming software R environment.

vi. Biological findings from RNA-seq experiments were validated using RNA samples from other independent experiments in which MIO-M1 cells were cultured with 50ng/mL TNF-α for 24 hours. Fold-changes of representative differentially expressed genes (DEGs) from RNA-seq findings were validated by qRT-PCR.

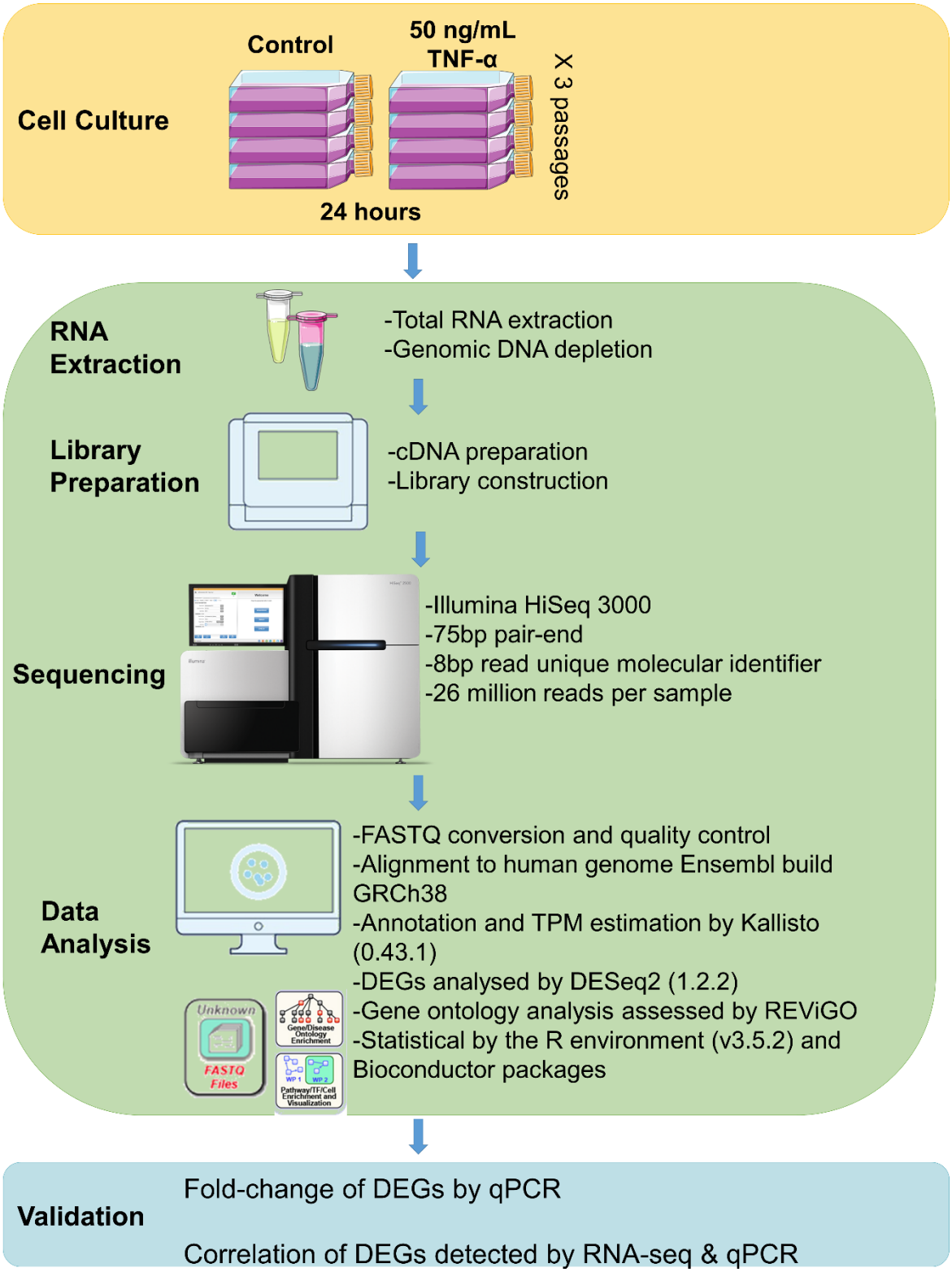

Figure 3.2 Experimental outline. MIO-M1 cells were cultured with 50 ng/mL TNF-α for 24 hours (yellow box).
Cell pellets were collected for total RNA extraction and subsequent preparation of cDNA library. Sequencing was performed by UCL Genomics and data analysis was performed in total RNA samples from three biological replicates (green box). Independent experiments were used to validate RNA-seq findings by qPCR (blue box). This image was produced using Servier Medical Arts (http://smart.servier.com).

3.3 Results

3.3.1 Overview of transcriptomes profile of MIO-M1 cells following short-term culture with TNF-α

Following culture of MIO-M1 cells with 50 ng/mL of TNF-α for 24 hours, no morphological changes were observed in these cells. They maintained their characteristic bipolar morphology and viability as compared to untreated cells (Figure 3.3).

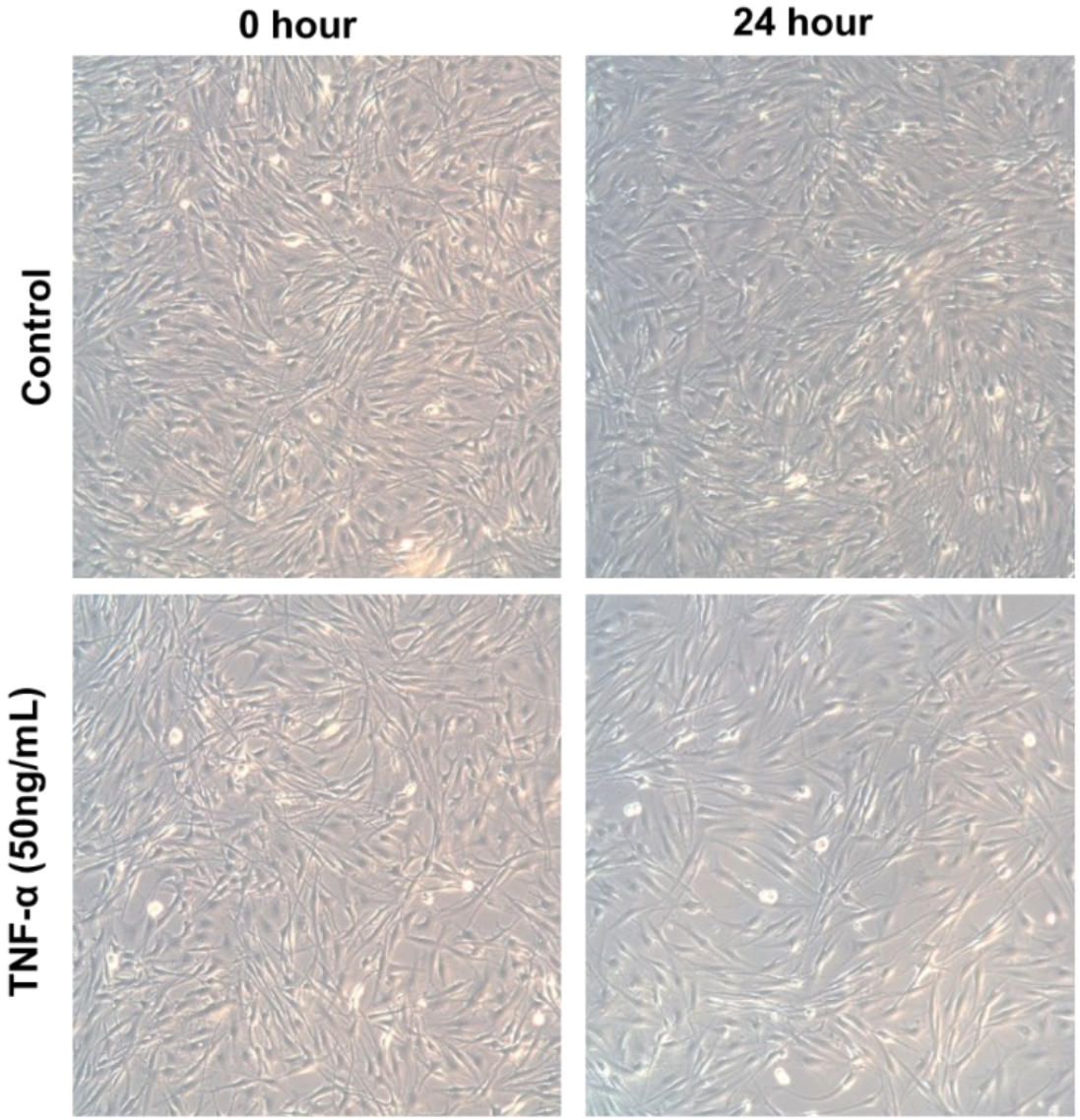

Figure 3.3 Bright field images showing the representative morphological features of MIO-M1 cells before and after culture with 50 ng/mL of TNF-α for 24 hours (bottom panel), as compared with untreated cells (top panel).

All RNA samples were confirmed of high quality as measured by the RNA integrity number (RIN), which showed that RNA samples contained a relatively high proportion of mRNA with minimal degradation (RIN > 8). Sequencing data of RNA subjected to transcriptomic analysis revealed that the read depth was of high quality. In general, the pattern of alignment and uniquely mapped reads within two groups of samples remained similar, achieving high percentage of unique alignment to at least 86% (Figure 3.4). The transcriptome of one of the TNF-α-treated cell preparations (passage 12) showed the lowest uniquely mapped reads (14.8 million) and this variation between biological replicates might have been attributed to technology artefacts, such as imprecise quantitation of cDNA library concentrations or varied levels of rRNA in each library. For each library total read counts were first normalised to gene length in kilobase, followed by sequencing depth using scaling factor in millions.

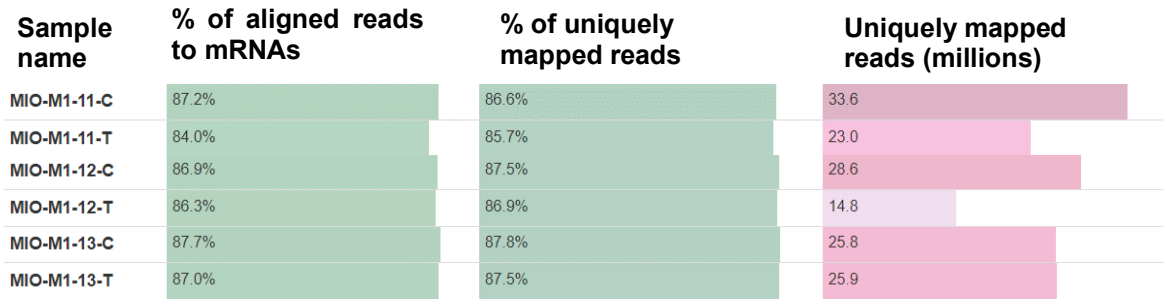

Figure 3.4 RNA-seq read alignment overview of transcriptomic libraries from MIO-M1 treated or untreated with TNF-α.
The percentage (%) of aligned reads overlapping UTRs and coding regions of mRNAs, as well as the percentage (%) of uniquely mapped reads and uniquely mapped reads in millions were tabulated for each sequenced sample using MultiQC, an online bioinformatic visualising tool developed by (Ewels et al., 2016). C: control and T: TNF-α.

Gene expression levels were converted to transcript per kilobase millions (TPM), although raw counts were utilised for subsequent differential analyses. Fold changes of gene expressions between control and TNF-α treated group were calculated in log2 base. As visualised using a principal component plot (PCA) (

Figure 3.5A), there was a clear segregation between the transcriptomes of TNF-α-treated MIO-M1 and those of untreated cells. The first principal component (PC1) separated the TNF-α-treated samples from controls, accounting for 29% of the widespread transcriptomic changes in this study (proportion of variance=0.29), whilst the second principal component (PC2) separated two groups with 22% of variability (proportion of variance=0.22). The overall similarity between each transcriptomes was further assessed and illustrated using a dendrogram with the hierarchical linkage and distance between each sample (

Figure 3.5B). Based on Euclidean distance, transcriptomes of P11 and P12 within the control groups were tightly clustered and distinctively separated from P13 sample. Whereas in the TNF-α-treated group, P11 and 13 samples were more similar than that of P12. When comparing between treatment groups, a discrete variability was observed and was in line with the PCA analysis, indicating that biological variation might also contribute to the detected transcriptomic variation.

Processed sequence data discussed in this this chapter has been uploaded to an open access resource for fast and easy quantitative interrogation of the RNA-seq gene expression data (bit.ly/WWang2019). Gene level analysis identified 13837 transcripts that were mapped to the human reference genome; of these, 899 were differentially expressed at high significance (adjusted *p*-valued ≤ 0.05) and the complete list can be retrieved from the link above. The global overview of the

differentially expressed genes (DEGs) are presented in a MA plot with the log2-fold change (log2FC) over averaged normalised counts for each transcript (

Figure 3.6A). Amongst the 899 DEGs, 445 were upregulated and 454 were downregulated. Of those, 839 were protein-coding transcripts, and 43 were marked non-protein coding transcripts such as long intergenic noncoding RNAs (lincRNAs), processed pseudogenes and antisense RNAs (AS). Using the criteria of log2FC ≥ 2 or ≤ -2, the number of protein-coding transcripts with significant up- or down-regulation was reduced to 364 and 361, respectively (

Figure 3.6B). Further filtering protein-coding DEGs using more stringent cut-off criteria of log2FC at 4 or -4, and 8 or -8, were narrowed down to smaller groups as shown in

Figure 3.6B. These findings indicated that majority of DEGs were rapidly modified for higher fold change ($2 \leq log2FC \leq 4$ or $-4 \leq log2FC \leq -2$) by TNF-α within 24 hours.

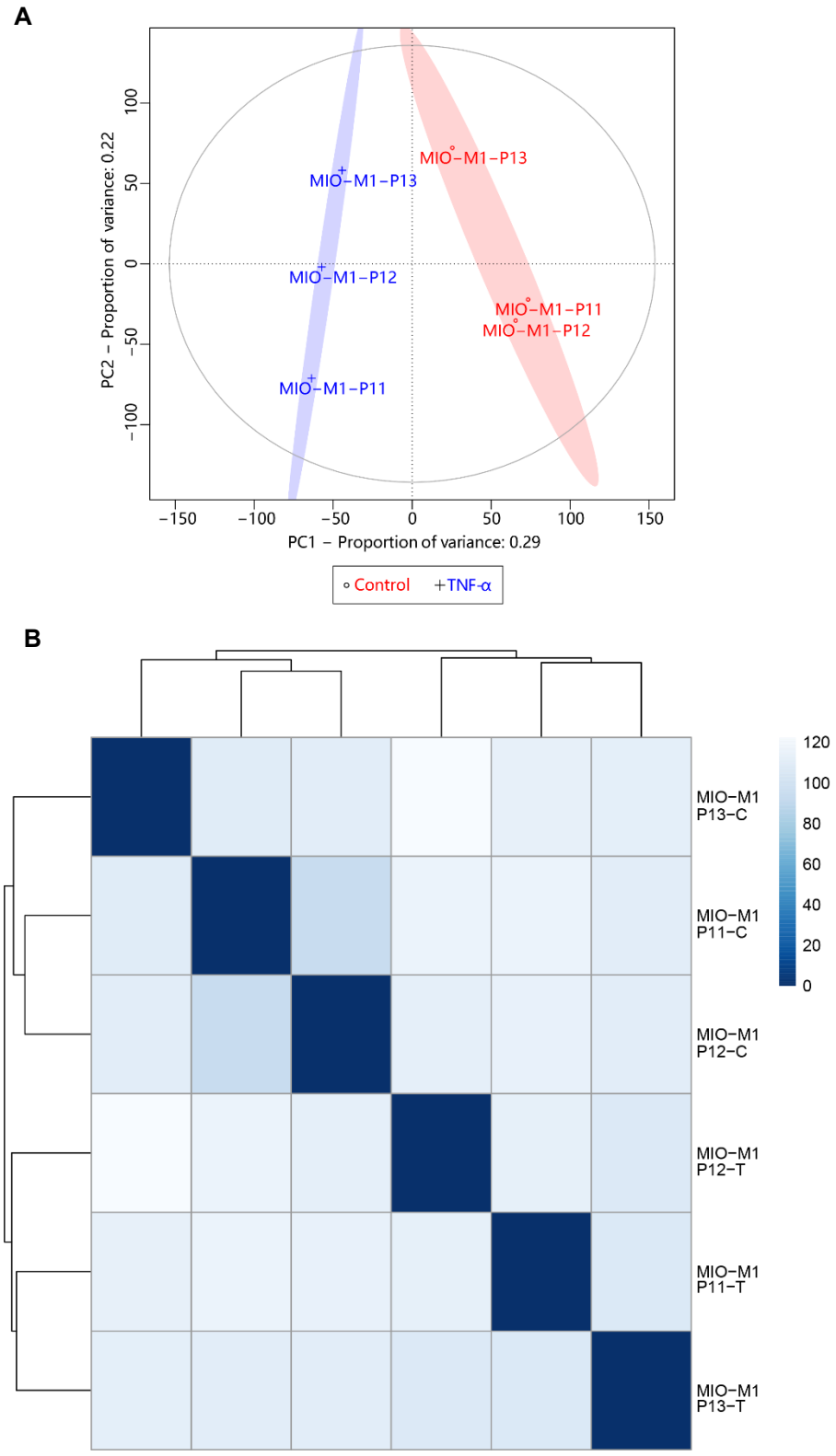

Figure 3.5 Overview of transcriptomic libraries of TNF-α-treated and untreated MIO-M1 cells. **(A)** Principal component analysis (PCA) plot shows clustering of each transcriptome representing MIO-M1 cells treated with TNF-α (blue) and control cells (red) from three independent cell culture passages (P11, 12, 13). PCA was performed using DESeq2 on the normalised log transformed count data. **(B)** Dendrogram illustrates sample-to-sample variation with hierarchical clustering and the Euclidean distance (x-axis) plotted against different samples (y-axis) was calculated using DESeq2. C: control; T: TNF-α.

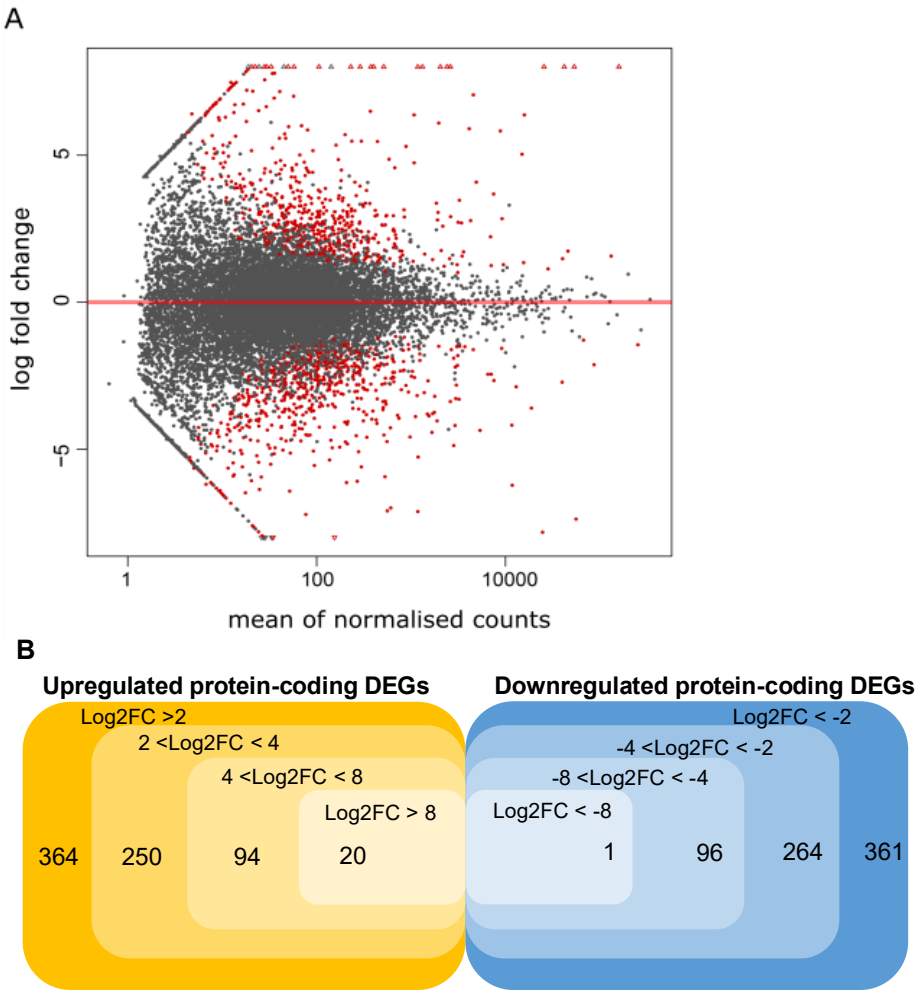

Figure 3.6 Overview of differentially expressed genes (DEGs) in MIO-M1 cells treated with and without TNF-α.
(A) MA plot reveals the dispersion of log2FC (y-axis) as a function of mean normalised counts (x-axis) for each transcript. Significantly DEGs (adjusted p-value ≤ 0.05) were highlighted in red. **(B)** Venn diagram depicts the distribution of up- and down-regulated protein-coding DEGs expressed by MIO-M1 cells in response to TNF-α. DEGs were filtered by log2FC more than 4 and 8, or less than -4 and -8.

Given the abundancy of the DEGs, the top 100 DEGs were therefore ranked and their expression pattern and correlation were visualised in a heat map. The unbiased hierarchical cluster analysis grouped DEG events in four distinct clusters between control and TNF-α cells, illustrating their functional or regulatory correlation (Figure 3.7). In relation to the gene expression in control cells, TNF-α induced upregulation of two clusters of DEGs associated with neuroinflammation, pro-cell survival, TNF-α signalling components and ECM-cell binding. In contrast, TNF-α-induced downregulation of DEGs observed in the other two clusters are associated with gliotic responses, cell-cell interaction and other functions which have not been previously studied in retinal biology.

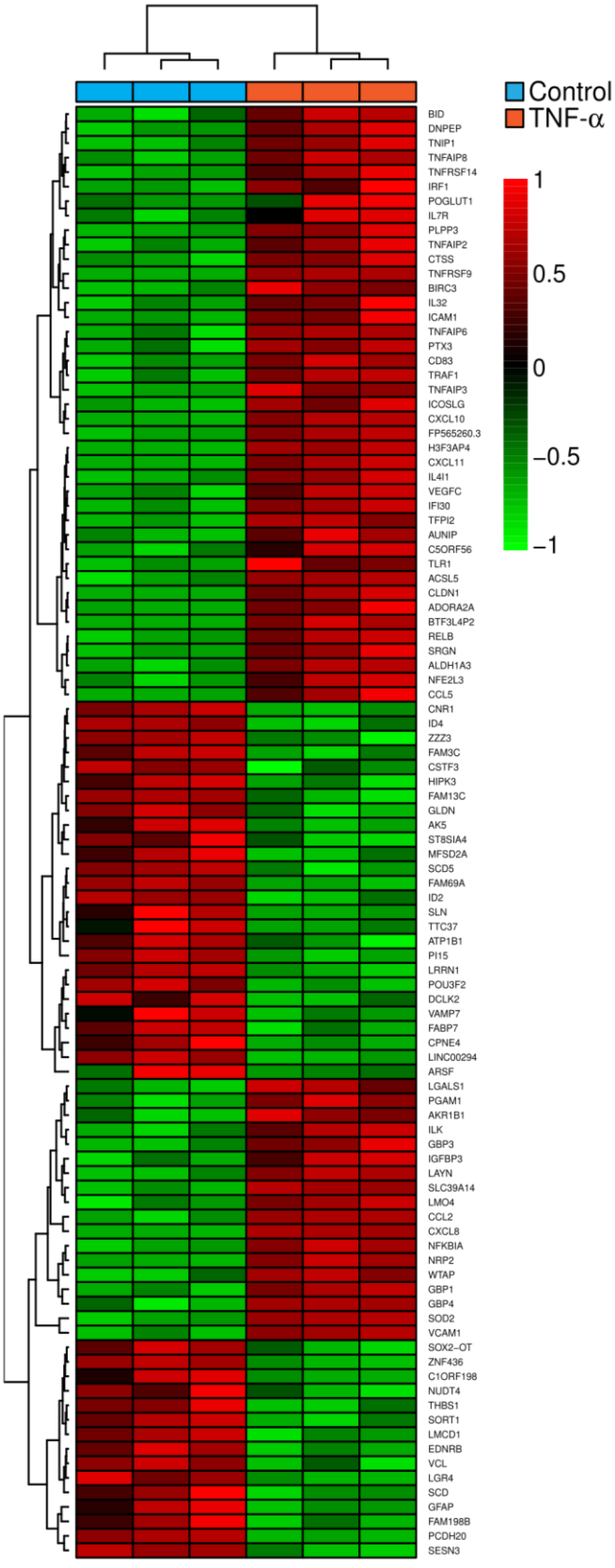

Figure 3.7 Hierarchically clustered heatmap showing DEGs between TNF-α treated (orange boxes) and control (blue boxes) MIO-M1 cells.

The top 100 DEGs shown in the heat map indicate the top 50 genes found up-regulated and the top 50 down-regulated genes by TNF-α. Genes were clustered using a hierarchical average linkage clustering and Euclidean distances using the R package. Colour scale indicated on the right representing the standard deviation from the base mean for each DEG.

3.3.2 Gene ontology analysis of the differentially expressed genes

To further confirm the annotations of the highly regulated genes, overrepresentation analysis by gene ontology (GO) was applied to all 899 DEGs identified. Of these, 798 DEGs were classified into appropriate functional groups including cellular component, molecular function and biological processes.

Overrepresentation by cellular component of the observed DEGs belonged to 'side of membrane' (GO:0098552), 'extracellular space' (GO:0005615) and 'tertiary granule lumen' groups (GO:1904724) (Table 3.1). Using false discovery rate adjusted *p*-value (FDR) ≤ 0.05 as cut-off criteria, none of these groups were statistically significant. Based on the molecular function of overrepresentation analysis, the 'chemokine activity' (GO:0008009) and 'chemokine receptor binding' groups (GO:0042379) were identified but did not show statistical significance (FDR>0.05) (Table 3.1).

Gene ontology overrepresentation analysis				
Ontology	**Gene ontology term**	**Description**	**Over-represented *p*-value**	**false discovery rate adjusted *p*-value**
Cellular component	GO:0098552	side of membrane	3.08E-04	0.264
	GO:0005615	extracellular space	4.12E-04	0.176
	GO:1904724	tertiary granule lumen	8.70E-04	0.248
Molecular function	GO:0008009	chemokine activity	2.75E-04	0.379
	GO:0042379	chemokine receptor binding	2.75E-04	0.189

Table 3.1 GO Overrepresentation analysis on the DEGs identified in the study.
Gene ontology analysis by Cellular component and Molecular function and the respective GO term, description, over-represented p-value and over-represented adjusted q-value are listed.

In addition, overrepresentation by biological processes showed that out of 50 GOs identified (not shown), 13 GOs were found significantly associated to specific functions (FDR≤0.05) and they were plotted against their FDR on a $-\log_{10}$ basis (Figure 3.8). The 'defence response' (GO:0006952) was the most overrepresented GO group ($-\log_{10}$FDR=2.127) and contained 21 DEGs, and this was followed by

'cellular response to tumour necrosis factor' (GO:0071356) with 9 DEGs (-$\log_{10}$FDR=1.967). There were also 9 DEGs enriched in 'second-messenger-mediated signalling' (GO:0019932) (-$\log_{10}$FDR=1.650) and 19 DEGs belong to 'regulation of cell activation' (GO:0050865) (-$\log_{10}$FDR=1.607). Whilst the rest of GOs clusters shared similar significance (1.384≤-$\log_{10}$FDR≤1.450), amongst them 'response to external stimulus' (GO:0009605) had the most abundant DEGs (47) and 'regulation of cell proliferation' (GO:0042127) encompassed 39 DEGs. The remaining 9 GO groups had less than 30 DEGs in the respective biological functions.

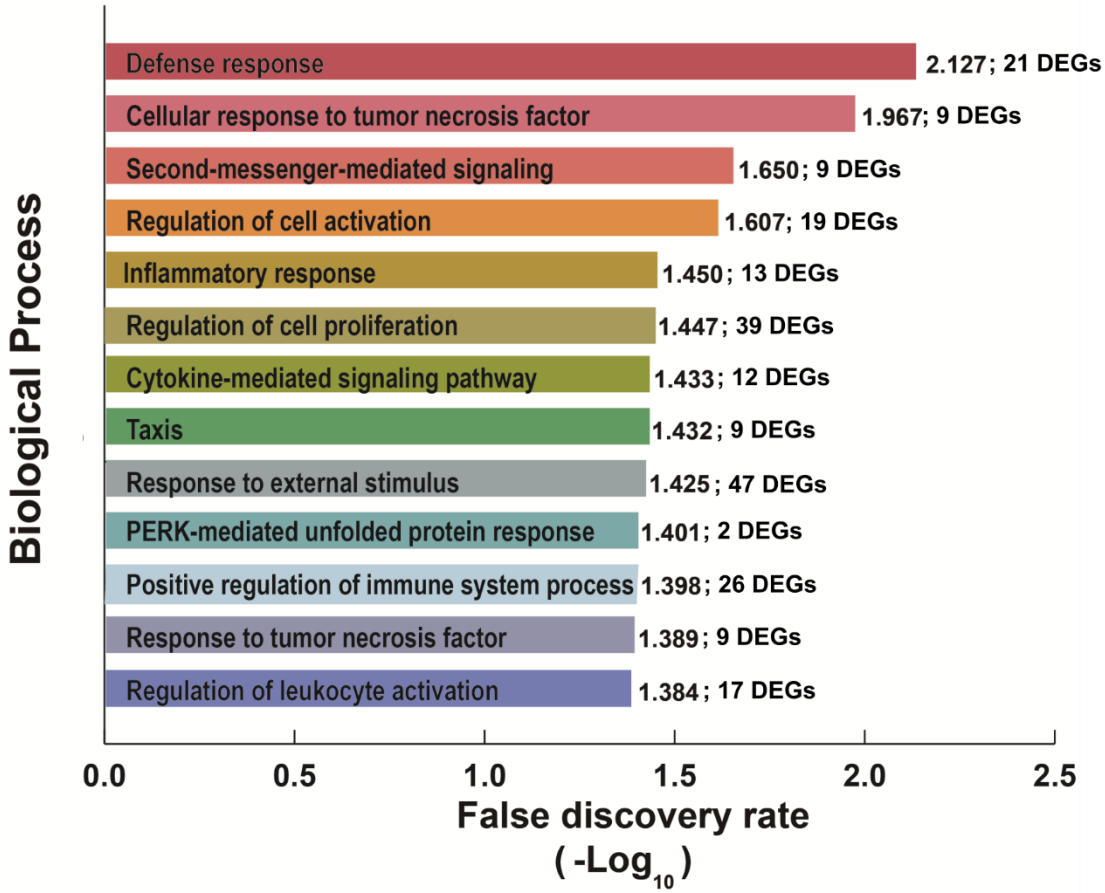

Figure 3.8 Gene ontology analysis by biological processes of DEGs induced by TNF-α in MIO-M1 cells.

The results of the gene ontology (GO) analysis of DEGs for regulating biological process in Müller glia were filtered using false discovery rate (FDR). 13 out of 50 GO clusters were found to be significant (FDR ≤ 0.05) and plotted with -$\log_{10}$FDR. The respective FDR and number of DEGs in each GO cluster are indicated on the right.

The interactive relationships between the 13 GOs found to be significantly associated to specific functions, as well as the parent ontology that they might be associated with, were visualised using a web-based tool GoView (Figure 3.9). It was observed that 6 top GOs ('defence response', 'inflammatory response', 'response to tumour necrosis factor', 'cellular response to tumour necrosis factor', 'response to external stimulus' and 'taxis') were closely clustered under the higher ancestral GO 'response to stimulus' (GO: 0050896). Similarly, the ancestral GOs of 'positive regulation of immune system process' (GO:0002684), 'regulation of cell activation' (GO:0050865) and 'regulation of leukocyte activation' (GO:0002694) are likely to be 'immune system process' (GO: 0002376), 'biological regulation' (GO: 0065007) and/or 'cellular process' (GO: 0009987). The possible ancestral GO terms for 'regulation of cell proliferation', 'cytokine-mediated signalling pathway' (GO:0019221) and 'second-messenger-mediated signalling' were likely to be 'signalling' or the five higher ancestral GO terms mentioned above. In summary, this ancestor chart shows that 24-hour TNF-α elicited profound biological response related to immune regulation and signal transduction.

Amongst the DEGs in the abovementioned GO clusters, VCAM1 and CCL2 were the most common transcripts and appeared in 12 GOs. The chemokines and inflammation associated genes CCL5, CXCL10, CXCL11, ICAM1, IRF1, THB1, and TNFAIP3 were frequently seen in several GOs (between 6 and 10 GOs). The following sections will further discuss the expression and implication of these DEGs and associated genes in the context of TNF-α activation of Müller glia *in vitro.*

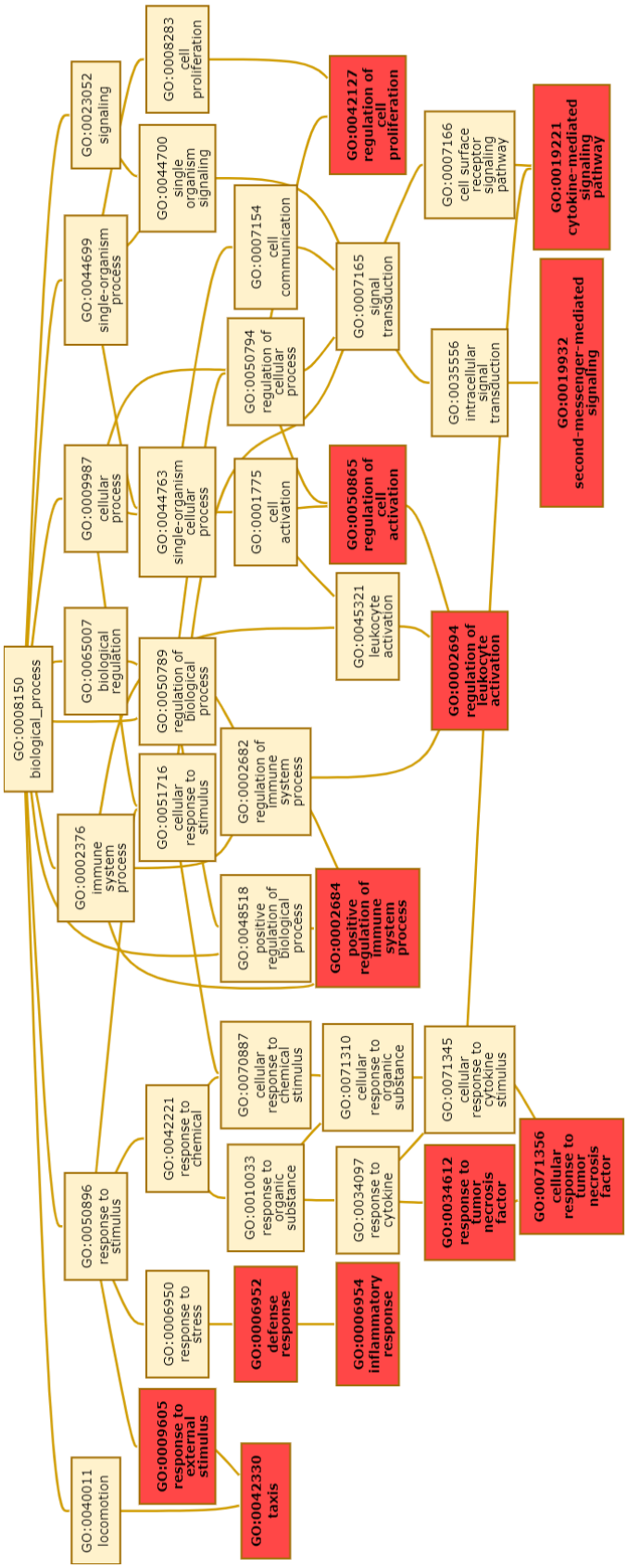

Figure 3.9 The directed acyclic graph (DAG) of interactive relationship of GO terms based on biological processes.

Red nodes indicate the 13 significantly overrepresented GO terms by filtering the FDR *q*-value < 0.05. Yellow nodes represent the ancestors of these terms. The line between two nodes represents the interactive pathway. This GO DAG was generated using GoView: http://www.webgestalt.org/2017/GOView/).

3.3.3 Genes involved in the TNF-α signalling pathway are upregulated in Müller glia by treatment with this cytokine

Following culture with TNF-α, it is understandable that many members of the TNF-α signalling components showed universal upregulation with significant overrepresentation in 8 GOs based on biological processes.

Binding of soluble TNF-α to the TNFR1, a receptor associated with neuroinflammation did not induce its transcriptional upregulation (TNFRSF1A; not shown), although its signal transducers TRAF2 and RIPK2 showed significant upregulation (log2FC=5.0 & 3.1 respectively) (

Figure 3.10A-i). Other transducers such as FADD, TRADD and pro-apoptotic caspase (not shown) remained unchanged (adjusted *p*-value > 0.05), whilst the BH3-interacting domain death agonist (BID) (Debernardi et al., 2018) was the only pro-apoptotic regulator upregulated (log2FC=3.6) as a result of TNFR1 activation. Other TNFR super family members and their ligands that mediate neuroinflammatory events were over-represented in several Go clusters upon TNF-α stimulation. There included TNFRSF9 (log2FC=15.0) and TNFRSF14 (log2FC=4.1), which are implicated in T cell response via TRAF interactions (Marsters et al., 1997). However, ligands for these TNFRs were not identified in the DEGs. Interestingly, TNFRSF10B and its ligand TNF superfamily member 10 (TNFSF10) were similarly upregulated (log2FC=3.1). TNFSF10 is also known as TNF-related apoptosis-inducing ligand (TRAIL) and formation of this ligand-receptor complex is related to induction of apoptosis and NFκB activation (Mongkolsapaya et al., 1999). Other TNFSF members that were differentially expressed included TNFSF4 (log2FC=3.2), TNFSF13B (log2FC=4.0) and TNFSF18 (log2FC=6.4), which are linked to the activation NFκB and immune cells, as well as stimulation of VCAM1 and ICAM1 upregulation (Chattopadhyay et al., 2007). In addition, TNF-α-induced protein (TNFAIP) family member TNFAIP2 was highly upregulated (log2FC=8.5). This protein can be primarily activated at transcriptional levels and has an important role on mediating inflammation and angiogenesis (Sarma et al., 1992).

Surprisingly, treating Müller cells with soluble TNF-α led to significant upregulation of the neuroprotective TNFR2 (TNFRSF1B; log2FC=5.4) and its signal transducer TRAF1 at a similar fold-change (log2FC=5.3) (

Figure 3.10A-ii). Whilst TRAF2 can also be activated by TNFR2, it remains unclear whether TRAF2 increase was a result of co-stimulation of both types of TNFRs. Interestingly, counteractive upregulation of potent apoptosis suppressors baculoviral inhibitor of apoptosis proteins (IAPs) repeat containing proteins (BIRC), BIRC2 and BIRC3 (log2FC=10.3 & 3.4 respectively) were detected at higher transcriptional levels than BID. This is important as these multifunctional anti-apoptotic factors could suppress TRAF1-induced inflammatory response, ubiquitinate RIPK to prevent activation death complexes (Bertrand et al., 2011), as well as activating the canonical NFκB pro-survival signalling (Wang et al., 2012, Varfolomeev et al., 2008). TNFAIP3, also known as the A20 zinc finger protein, was identified in 7 GOs (log2FC=6.5). This anti-apoptotic protein has potency to interfere with TNFR1-mediated activation of JNKs and caspase 8 (He and Ting, 2002), and also antagonises ubiquitination and proteasomal enzymes upstream of NFκB activation (Song et al., 1996), therefore modulating neuroinflammation and apoptosis (Vereecke et al., 2009, He and Ting, 2002). Similarly, TNFAIP6 (log2FC=5.5) which was overrepresented in 2 GOs including ‘defense response’ and ‘inflammatory response’, has an anti-inflammatory potential (Wisniewski et al., 1996), whilst the negative regulator of apoptosis TNFAIP8 (You et al., 2001) also showed significant upregulation at similar fold-change (log2FC=5.5). These

observations suggest that in response to TNF-α, neuroprotective and pro-survival signalling cascades were activated in MIO-M1 cells.

Several components of NFκB signalling were also found significantly upregulated as a result of TNF-α activation (

Figure 3.10B). Increased NFκB2 (log2FC=4.0; adjusted *p*-value <0.05) was over-represented by GO 'response to external stimulus', although its counterpart NFκB1 remained unchanged (not shown). NFκB2 upregulation may have likely led to significantly increased transcription of the inhibitor IkB family at higher TPMs, including IkB zetta (NFκBIZ, log2FC=3.0) and IkB epsilon (NFκBIE, log2FC=2.1),

with IkB alpha (NFκBIA) (log2FC=6.1) as the most prominently upregulated member and over-represented in four GO clusters. These findings might indicate that TNF-α-induced NFκB activation was well controlled by its constitutive inhibitors and further signalling downstream of NFκB cascade was analysed in the following section based on their implication in neuroinflammation or neuroprotection.

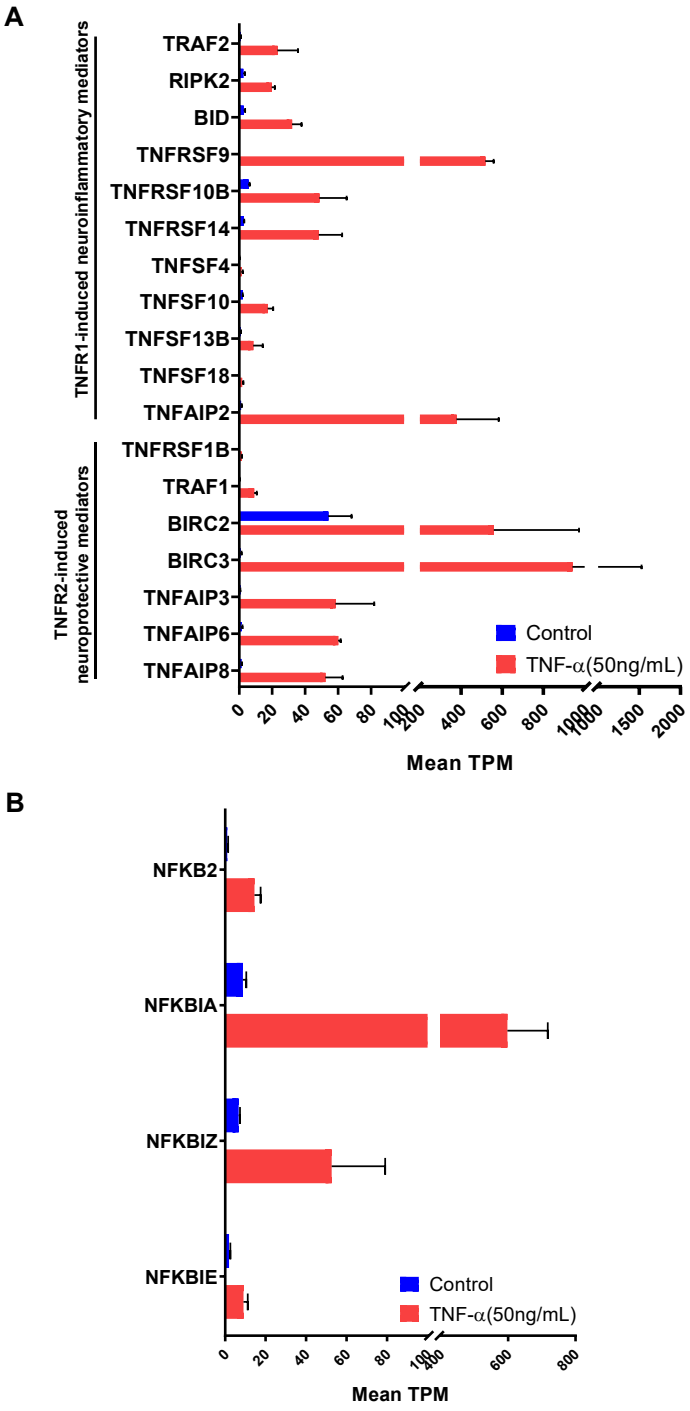

Figure 3.10 Expression levels of DEGs coding for TNF-α and NFκB signalling pathways in control and TNF-α-treated MIO-M1 cells.

(A) Histograms show the mean TPM of transcripts coding for TNFR1-induced inflammatory mediators and TNFR2-induced neuroprotective mediators of the TNF-α signalling pathway**. (B)** Mean TPM of transcripts coding for NFκB signalling components. Transcriptomes of control cells are shown in blue and TNF-α-treated cells are shown in red. TPM: transcript per kilobase millions.

3.3.4 Genes mediating neuroinflammation were increased in MIO-M1 cells by TNF-α

Downstream of TNFR1-driven signalling, a plethora of genes involved in leukocyte migration, extracellular matrix remodelling and cell-matrix interaction were activated. Accordingly, genes related to ‘defence response’ (GO:0006952) and ‘inflammatory response’ (GO: GO:0006954) were over-represented in this dataset and showed significant overlap with some DEGs over-represented in GOs terms ‘cellular response to tumour necrosis factor’ (GO:0071356) and ‘response to tumour necrosis factor’ (GO:0034612). These included ICAM1, THBS1, CLDN1, VCAM1, CCL5 and CCL2 commonly identified in neuroinflammatory events occurring in various retinal diseases.

In this dataset, two clusters of genes coding for proteins that promote leukocyte trafficking were examined. The first cluster (

Figure 3.11A) showed universal upregulation of genes coding for chemotactic factors including α chemokines C-C motif chemokine ligand (CCL) 2/MCP-1 and CCL5/RANTES, which showed a similar fold-change (log2FC=9.2 and 9.5, respectively) (

Figure 3.11A). Of importance, upregulation of these proteins has been associated with microglia activation (Ramesh et al., 2013). In addition, β chemokines as represented by C-X-C motif chemokine (CXCL) 8, CXCL10 and CXCL11 (log2FC=15.1, 11.5 and 9.3, respectively). These chemotactic factors are mainly responsible for recruitment of several types of leukocytes (Rutar and Provis, 2016, Galimberti et al., 2006), and are often seen in retinal disease (Newman et al., 2012, Rutar et al., 2011, Chiu et al., 2010). Similarly, cytokines including IL24 and IL32 were noticeably upregulated (log2-FC = 11.9, and 8.4, respectively). IL32 is an important pro-inflammatory cytokine release by macrophages (Kim et al., 2005). IL24 was expressed at much lower TPM, has been recently classified as an IL10 family member; however, its cellular functions remain largely unexplored (Borish and Steinke, 2003). Interferon regulatory factor 1 (IRF1), a transcription factor that can be induced by interferons, also showed a transcriptional increase (log2FC=5.5). It is believed to regulate the expression of the apoptosis-related TNFSF10/TRAIL gene (Honda and Taniguchi, 2006), which also upregulated by TNF-α in MIO-M1 cells (

Figure 3.10A). In addition, the transcription of colony-stimulating factor 1 (CSF1) and CSF2 genes was significantly increased (log2FC=2.6 and 6.7, respectively). Both factors are known to regulate the survival and proliferation of macrophages and granulocytes and consequently mediate inflammation (Chitu and Stanley, 2006), and recent studies propose that they could be neuroprotective by modulating T helper cell differentiation (Xiao et al., 2007). In this study, the vascular endothelial growth factor (VEGF) isoform C (VEGFC) was found to be upregulated in TNF-α-treated Müller glia (log2FC=5.6). VEGF mediates angiogenesis and vascular permeability has been described as the pivotal mediators of macular oedema in many retinal disorders (Miller et al., 2013). A second cluster examined (

Figure 3.11A) consisted of genes promoting leukocyte infiltration to inflammatory sites and included leukocyte binding ligands. Short exposure of Müller cells to TNF-α resulted in high-level upregulation of mRNAs coding for leukocyte binding ICAM1 and VCAM1 (log2FC=11.3 and 8.5, respectively). Their roles in promoting leukocyte trafficking into the retina have been well documented in several studies (Chen et al., 2012, Bharadwaj et al., 2017, Zhang et al., 2011). Furthermore, upregulation of the beta-galactoside-binding protein galectin 1 (LGALS1) gene was observed (log2FC=2.8). This polysaccharide is widely distributed both intracellularly and extracellularly and has multiple roles such as T cell adhesion and survival (Camby et al., 2006). Interestingly, reduced expressions of additional binding ligands including integrin subunit β5 (ITGB5) and thrombospondin 1 (THBS1) (log2FC=-2.4 and -3.8, respectively) were also seen in this study. ITGB5 represents a subunit of the cell surface receptor integrin which promotes cell attachment to vitronectin and fibronectin (Smith et al., 1990), whereas THBS1 binds to multiple ECM components including fibronectin and collagen and seems to mediate mechanical stress in the

eye, as evident by knockout THBS1 led to reduced IOP in mice (Vittal et al., 2005, Wallace et al., 2014).

Leukocyte trafficking also requires dynamic ECM remodelling to facilitate their migration and infiltration into the tissues. In this study, one of the most pleiotropic transcriptional modifications were observed in genes coding for ECM components (

Figure 3.11B) and those responsible for their homeostasis (

Figure 3.11B). Reduced TPM levels of several genes belonging to the collagen family, such as collagen type I alpha 2 chain (COL1A2) and collagen type XXI alpha 1 chain (COL21A1) (log2FC=-1.4 and -3.5, respectively), and significant upregulation of collagen type VI alpha 1 chain (COL6A1) genes were observed

(log2FC=3.0). Other ECM components such as fibronectin 1 (FN1) and laminin subunit alpha 3 (LAMA3) were also found upregulated by TNF-α in Müller glia (log2FC=3.1 and 7.2, respectively).

Analysis was also undertaken on genes controlling ECM homeostasis (

Figure 3.11B). Pronounced upregulation of genes coding for MMP1 (log2FC=8.5) and its inducer TFPI2 (log2FC=7.8) was noticed in the TNF-α-treated cells, whilst genes coding for the MMP1 inhibitor TIMP4 had its mRNA transcripts significantly downregulated (log2FC=-3.5). The zinc-dependent endopeptidases MMPs promote ECM remodelling by cleaving fibronectin and collagen and in the context of eye physiology, MMPs play a critical role on maintaining aqueous humour flow and intraocular pressure (Wallace et al., 2014). MMPs activity are regulated by TIMPs and a serine protease inhibitor called tissue factor pathway inhibitor 2 (TFPI2) (Nita et al., 2014, Rao et al., 1999). In addition, within the same cluster of ECM homeostasis, connective tissue growth factor (CTGF), which is also known as cellular communication network factor 2 (CCN2) showed transcriptional downregulation (log2FC=-2.7) by TNF-α. This factor promotes heparin-dependent adhesion of fibroblasts and endothelial cells (Ball et al., 2003) and its upregulation by TGF-β has been revealed to accelerate aberrant fibrosis and ECM deposit (Sato et al., 2000, Lang et al., 2008). A common manifestation of TNF-α-elicited neuroinflammation in many retinal degenerative disorders is characterised by a compromised blood-retinal barrier (BRB), as infiltration of microglia and lymphocytes are preceded by the downregulation of tight junction proteins (TJs) (Morcos et al., 2001). Surprisingly, one of the TJPs claudin 1 (CLDN1) was significantly upregulated by TNF-α (log2FC=8.7), whilst other TJPs such as zonula occludens (ZOs) and occludin were not differentially expressed (not shown). In summary, these observations highlighted the complex response of MIO-M1 genes coding for ECM remodelling and intercellular interactions as a result of TNF-α activation.

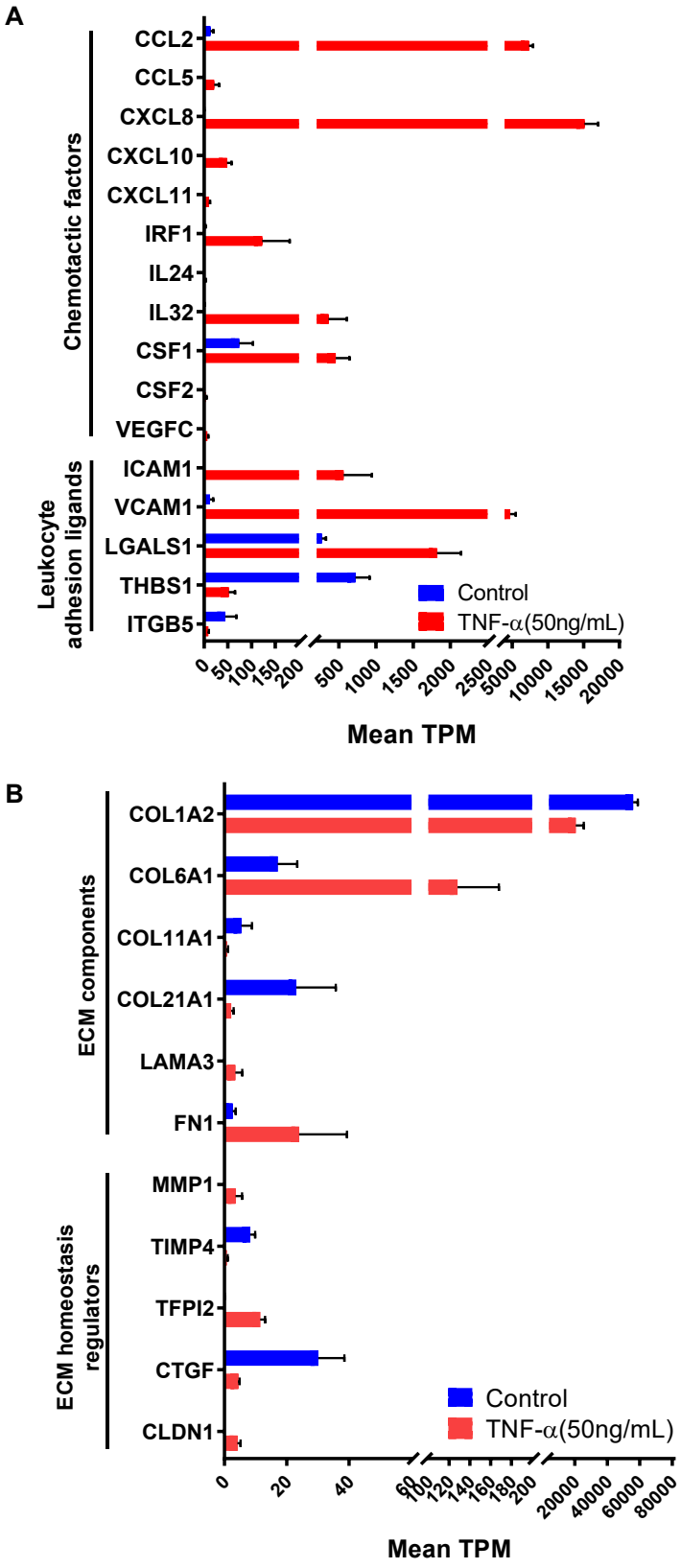

Figure 3.11 Expression levels of DEGs related to neuroinflammation in control and TNF-α-treated MIO-M1 cells.

Histograms showing the mean TPM of transcripts coding for **(A)** chemoattractant factors and leukocyte adhesion ligands that mediate leukocyte trafficking and**, (B)** ECM components and ECM homeostasis regulators of ECM remodelling. Transcriptomes of control cells are shown in blue and TNF-α-treated cells are shown in red. TPM: transcript per kilobase millions.

3.3.5 Genes coding for neuroprotective factors were upregulated in Müller glia by TNF-α

Due to the pro-inflammatory nature of TNF-α, activation of MIO-M1 cells by this cytokine may also lead to upregulation of genes involved in regulating oxidative stress, therefore these were specially analysed. It was observed that the oxidative master regulator NRF2 gene (NFE2L2) was not significantly modified by TNF-α (not shown). However, its downstream anti-oxidative genes showed significant transcriptional modification (Figure 3.12A), as illustrated by the significantly increased expression (log2FC=8.5) of the mitochondria-bound SOD2, an important antioxidative gene, which mediates the conversion of superoxide to hydrogen peroxide (Joe et al., 2015). Similarly, other genes coding for NFE2L2-regulated antioxidant enzymes including peroxiredoxin 6 (PRDX6) and aldehyde dehydrogenase 1 family member A3 (ALDH1A3) showed significant upregulation (log2FC=1.4 and 4.8 respectively) following TNF-α treatment. PRDX6 is an important mediator of the anti-oxidative response against reactive oxygen species generated during gliosis (Zha et al., 2015), whilst ALDH1A3 encodes an isoform of the cytosolic aldehyde dehydrogenase family 1 and oxidises retinal to the corresponding carboxylic acid to reduce oxidative stress (Duong et al., 2017). It was also observed that in the present transcriptomic analysis, a few NFE2L2-regulated genes such as NOQ1, PON2 and HMOX1, as well as the putative neuroprotective factor CLU demonstrated a trend of mRNA upregulation despite not showing any statistical significance (not shown). Additionally, several neurotrophic factors were present in the transcriptomic libraries and showed transcriptional upregulation (Figure 3.12B). Platelet derived growth factor C (PDGFC) and neurotrophin BDNF genes were markedly increased (log2FC=2.8 and log2FC=3.8, respectively), whilst NGF showed a slight but not significant increase (not shown). PDGF is found essential to promote the survival and possibly regeneration of damaged neurons (Osborne et al., 2018), whilst BDNF is capable of activating multiple molecular pathways overlapping with anti-oxidative and anti-apoptotic responses, as well as inhibiting autophagy through activation of tropomyosin-related kinase (Trk) receptor or the p75NTR receptor expressed on retinal cells (Chen et al., 2017, Garcia and Vecino, 2003).

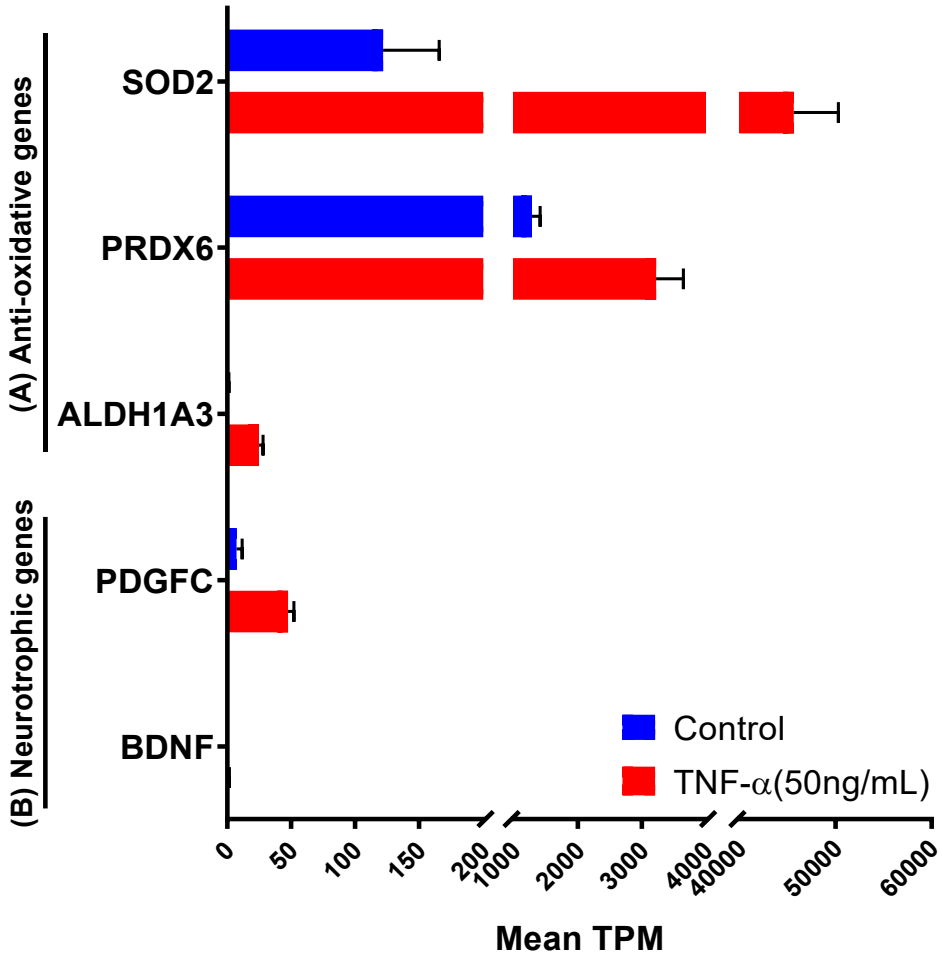

Figure 3.12 Expression levels of DEGs coding for pro-survival factors in MIO-M1 cells treated with TNF-α.
Histograms showing the mean TPM of transcripts relevant to **(A)** anti-oxidative factors and **(B)** neurotrophic factors in transcriptomes of control (blue) and TNF-α-treated (red) Müller cells. TPM: transcript per kilobase millions.

3.3.6 TNF-α modulation of genes controlling Müller cell gliosis

It is equally important to evaluate the gliotic response of MIO-M1 cells by examining gene clusters related to reactivity, proliferation and function of Müller glia. Reactive Müller glia with aberrant proliferation and overexpression of GFAP is recognised as a hallmark of gliosis, and is driven by an intrinsic transcriptional regulatory network. Here, 'regulation of cell activation' (GO:0050865) and 'regulation of cell proliferation' (GO:0042127) highlighted several genes responsible for gliotic responses (Figure 3.8). Following TNF-α exposure, a negative regulator of STATs activation known as suppressor of cytokine signalling (SOCS) protein SOCS2 (Kubo et al., 2003), was

significantly downregulated (log2FC=-2.1)

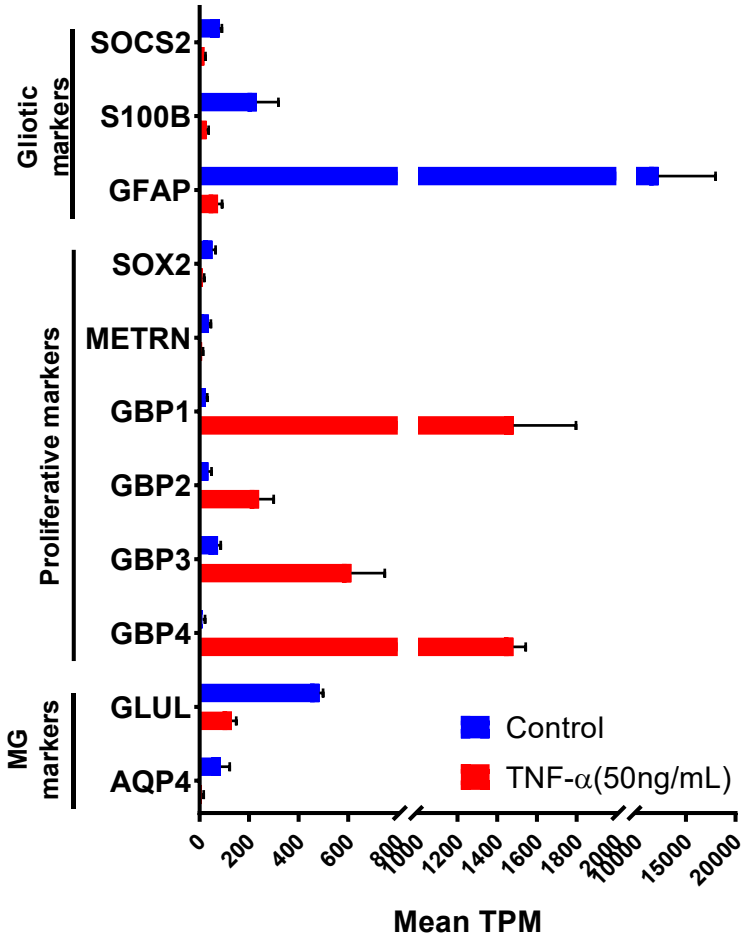

(

Figure 3.13). However, the transcription factors LIM homeobox 2 (LHX2) and STAT3 (Okada et al., 2006) did not show differential expression (not shown). Importantly, the significant reduction of the S100 calcium binding protein B (S100B) (log2FC=-

3.0) was accompanied by the highest fold downregulation (log2FC=-7.4) of the key

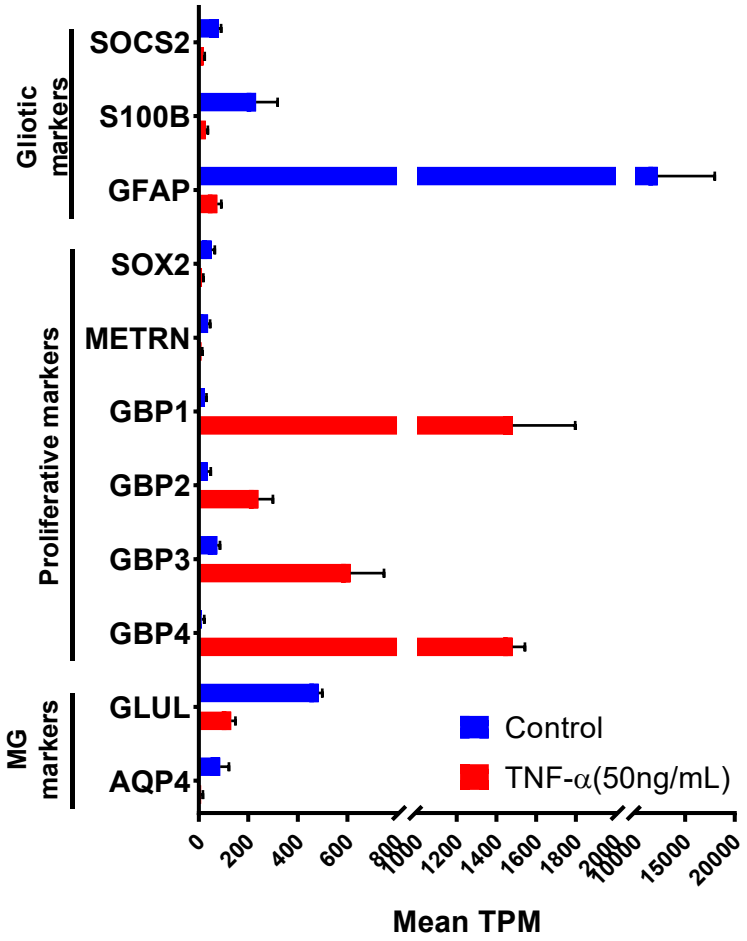

gliotic marker GFAP (

Figure 3.13). These are known markers of reactive gliosis occurring during retinal degeneration and it is important that is downregulating their expression (Escher et al., 2008, Brozzi et al., 2009, Hippert et al., 2015, Galindo et al., 2018, Walker et al., 2019). This strongly indicates that that MIO-M1 reactivity might be significantly suppressed following TNF-α stimulation.

Transcriptomic data also showed that genes governing Müller cell progenicity and proliferation, such as the neuronal progenitor marker SOX2, and meteorin (METRN), a transcription factor required for proliferation and maintenance of progenicity in Müller cells during development (Nishino et al., 2004, Lee et al., 2010a), were

significantly downregulated at similar fold levels (log2FC=-1.9 and -1.8 respectively)

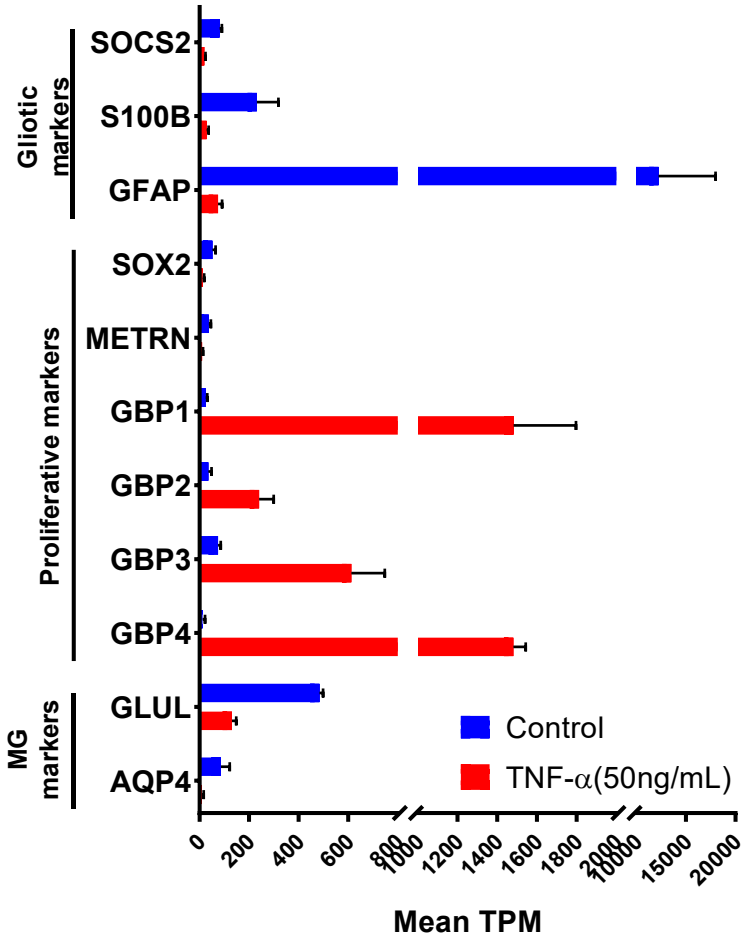

(

Figure 3.13). This is also true for several members of the human guanylate-binding proteins (GBPs), including GBP1-4, which were consistently upregulated in TNF-α-treated MIO-M1 cells (log2FC=5.9, 2.7, 3.1 and 7.0, respectively). The expression of these guanosine triphosphatase (GTPases) are mainly driven by TNF-α and/or interferon-induced NFκB1/p50 (Naschberger et al., 2004). Particularly, previous studies have shown that GBP1, which is linked to 'cellular response to tumour necrosis factor' (GO:0071356) and 'response to tumour necrosis factor' (GO:0034612), is anti-proliferative and anti-angiogenic as suggested by their ability to suppress MMP-1 expression in endothelial cells (Guenzi et al., 2001, Guenzi et al., 2003). Similarly, GBP2 is found phenocopying the inhibitory effect of interferon on AKT-driven cell spreading on fibronectin (Messmer-Blust et al., 2010). Interestingly, expression of common Müller glia function markers such as glutamine synthetase (GLUL) and the fluid flux-regulator aquaporin 4 (AQP4) were significantly

downregulated by TNF-α(log2FC=-1.9 and -3.3, respectively)

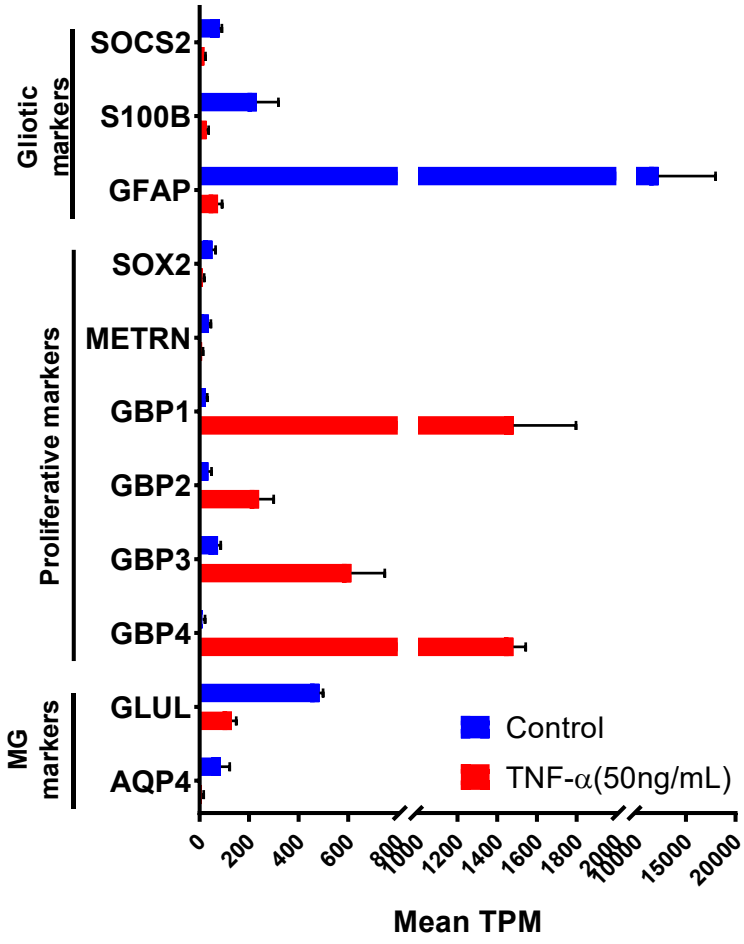

(

Figure 3.13), whilst other Müller cell function genes were unchanged (not shown). GLUL genes encode proteins that regulate glutamine metabolism and AQP4 the bidirectional transport of free water, maintaining the osmotic homeostasis within the neural retina (Reichenbach and Bringmann, 2010, Verkman et al., 2017). These observations suggest that the significant downregulation of gliotic markers by Müller cells following TNF-α treatment might represent a protective mechanism *in vitro*.

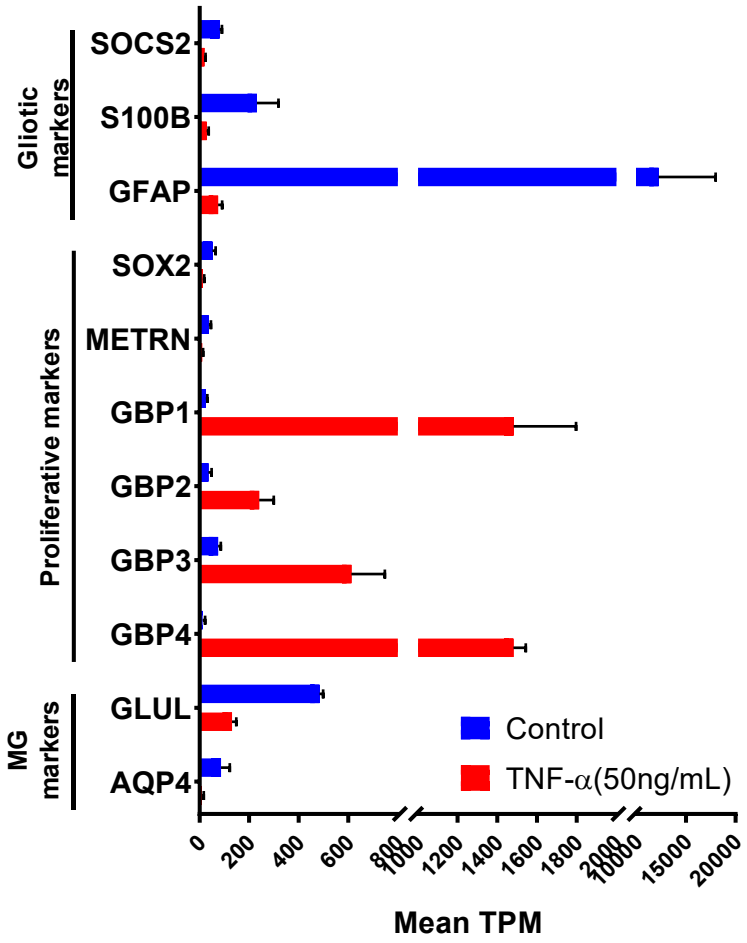

Figure 3.13 Expression levels of DEGs associated with reactive gliosis by MIO-M1 cells treated with TNF-α.
Histograms showing the mean TPM of transcripts associated with gliosis, proliferation and other Müller glia functions in transcriptomes of control (blue) and TNF-α-treated (red) cells. TPM: transcript per kilobase millions.

3.3.7 Modulation of novel transcripts comprised of non-coding RNAs in Müller glia cultured with TNF-α

In addition to protein-coding DEGs, 43 non-coding DEGs were observed in the transcriptome of Müller glia treated with TNF-α. These were classified into three categories: lincRNAs, antisense RNAs (AS) and processed pseudogenes. Only a few of them were annotated to known functions while others were regarded as putative genes. LincRNAs represent a subclass of long non-coding RNAs (lncRNAs) with more than 200 nucleotides (St Laurent et al., 2012, Jarroux et al., 2017). Similar to mRNA, lincRNAs are transcribed by RNA polymerase II and associated with functions of transcriptional enhancement and regulation by direct interaction with

DNA, RNA and proteins by base pairing or structural interference (Wang and Chang, 2011). In this study, lincRNAs account for more than half of the top 10 lincRNAs based on their transcriptional abundancy are presented (Figure 3.14A). Several lincRNAs such as MIR99AHG, LINC00511, SOX21-AS1 and GLIDR have been related to various carcinomas (Emmrich et al., 2014, Sun et al., 2016, Lu et al., 2017, Zhang et al., 2017), whereas annotation of the other lincRNAs remains unexplored. Because of the nature of the spontaneous immortalisation of MIO-M1 cells, it is not surprising that cancer-related lincRNAs were differentially expressed in their transcriptome.

AS is another subclass of lncRNA genes and originates from the DNA strand opposite the sense strand that serves as the template of mRNA. The biological activities of the AS genes include induction of transcriptional enhancers, inhibition of mRNA splicing, facilitation of miRNA binding and modulate enzyme activities (Ambros, 2004, Zucchelli et al., 2019). These functions are exerted by combining with sense sequences to form sense/antisense (S/AS) pairing (Katayama et al., 2005). Six of these genes were found significantly upregulated and another six were significantly downregulated (Figure 3.14B). Of these, SERTAD4-AS1, which has been shown to regulate TNFAIP3 activity (Trynka et al., 2009, Banks et al., 2016) was found downregulated (log2FC=-4.2) by TNF-α. Others such as ATP6V0E2-AS1, AC008622.2, SMAD1-AS1, USP30-AS1 and AL357060.3 were uniquely expressed in TNF-α-treated Müller glia. No studies have investigated their biological functions. SMAD1-AS1 was the only upregulated AS that has been previously associated to congenital heart disease (Song et al., 2013), whilst its target SMAD1 mRNA, an important component of BMP signalling pathway, was not identified as differentiability expressed in the current transcriptome study. It remains unclear if the increased SMAD1-AS1 might have any biological impact in MIO-M1 cells.

In addition, three processed pseudogenes were significantly upregulated while four were significantly downregulated (Figure 3.14C). Originating from protein-coding genes, pseudogenes differ from their functional counterparts due to sequence degeneration and can be classified to duplicated, processed and unitary pseudogenes (Liu et al., 2016, Balakirev and Ayala, 2003, Zhang et al., 2010). Processed pseudogenes exist in higher amounts as compared to duplicated counterparts in mammalian genomes (Zhang et al., 2002), and in this study majority

of processed pseudogenes were not annotated to known functions, whereas the Rac Family Small GTPase 1-derived RAC1P2 and the histone H3-derived H3F3AP4 were briefly studied (Kugler et al., 2004, Ederveen et al., 2011) and no comprehensive annotations are available to interpret their roles in this study.

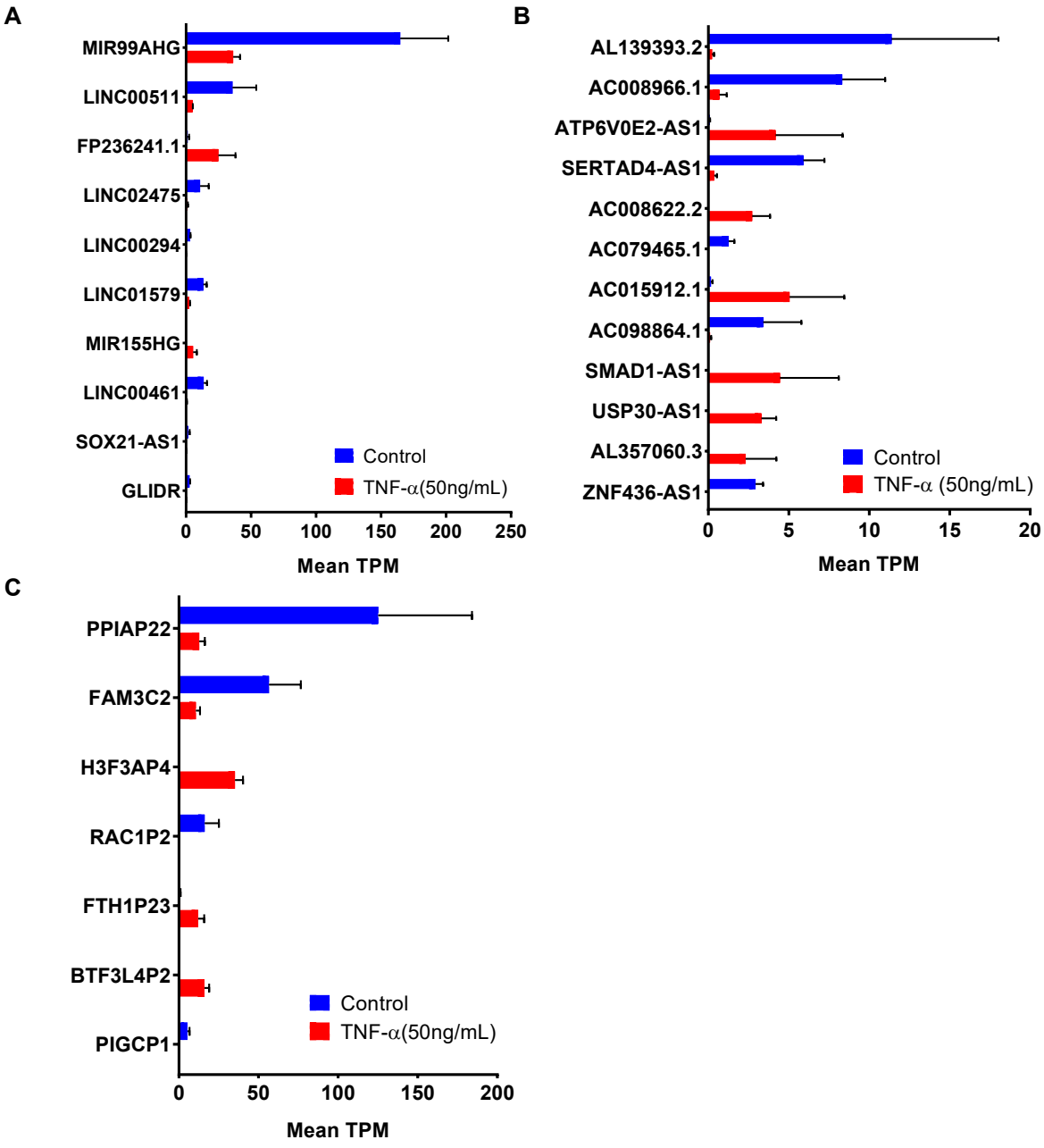

Figure 3.14 Expression levels of non-coding DEGs in MIO-M1 cells treated with TNF-α. Histograms showing the mean TPM of non-coding DEGs of **(A)** the top 10 lincRNAs, **(B)** antisense RNAs (AS), and **(C)** processed pseudogenes in transcriptomes of control (blue) and TNF-α-treated (red) cells.

3.3.8 Validation of RNA-seq data by qPCR

The expression levels of 6 selected DEGs on MIO-M1 cells from independently experiments was validated using Taman® quantitative RT-PCR (qRT-PCR). These genes included the upregulated BDNF, SOD2, PRDX6 and the downregulated GFAP, GLUL and SOX2, which are associated with Müller glia functions. The Spearman's correlation coefficient analysis was also applied to determine the consistency of log2-FC of the above DEGs reported by both methods. For the these genes, there is a strong correlation between the RNA-seq and qPCR, as evidenced by a significant Spearman's correlation coefficient 0.9344 ($p < 0.0001$) (Figure 3.15), underpinning the high reliability of the biological findings drawn from the reported RNA-seq data was observed.

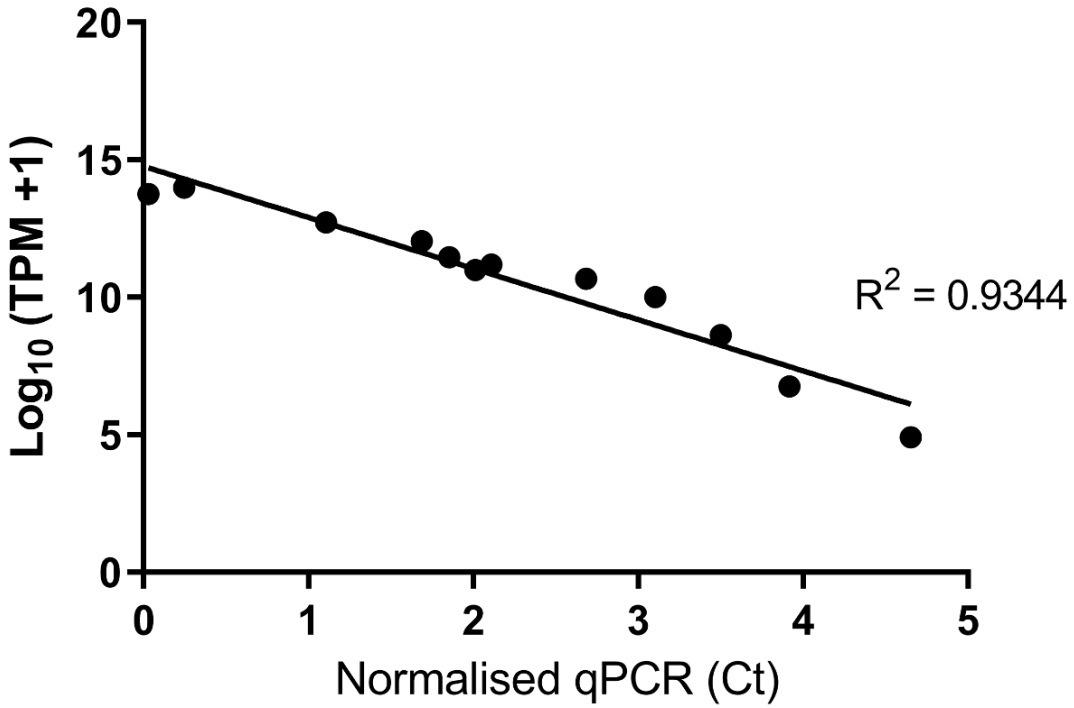

Figure 3.15 Correlation of gene expressions between qPCR and RNA-seq.
The plot shows gene expression abundancies determined by qPCR and RNA-seq for the upregulated BDNF, SOD2, PRDX6 genes, and the downregulated GFAP, GLUL and SOX2 genes, associated with Müller glia functions. The linear regression analysis and Pearson correlation coefficient (R^2 = 0.9344, $p < 0.0001$) is shown.

3.4 Discussion

Extensive efforts have been made to understand the implication of TNF-α effects on astrocytes (Santos et al., 2017) and photoreceptor cells (Xie et al., 2017) in the neural retina. However, the transcriptomic profiling of human adult Müller glia in response to TNF-α has not been investigated. Therefore, this study attempted to map the genome-wide expression of the human adult Müller glial cell line MIO-M1 upon short-term exposure to TNF-α. RNA-seq analysis revealed that following 24-hour culture with this cytokine, a large number of genes are significantly modified in MIO-M1 cells with similar number of genes shown to be up- and down-regulated by this cytokine. The top DEGs contain not only genes coding for TNF-α and NFkB signalling that drive further molecular modifications, whilst the remaining DEGs represent a pleiotropic response of MIO-M1 cells to TNF-α. These responses can be categorised as neuroinflammatory and neuroprotective based on interpretation of the existing literature. The neuroinflammatory functions are identified by the elevation of various immune mediators, whilst neuroprotective functions are supported by an increase in genes coding for neuroprotective factors and the decrease in genes coding for gliotic functions. The following sections will interpret the possible impact of genes under those two categories.

3.4.1 Activation of TNF-α and NFkB signalling pathways in Müller glia by TNF-α

It is not surprising that several genes coding for components of the TNF-α signalling pathways were substantially increased in Müller glia following overnight culture with this cytokine. Binding of exogenous soluble TNF-α to its higher affinity receptor TNFR1 (TNFRSF1A) did not modify the mRNA levels of this receptor, instead TNFR2 (TNFRSF1B) which directs TNF-α signalling between neighbouring cells (Horiuchi et al., 2010), showed significant upregulation. Previous studies showed that increased TNFR1 in RGCs is associated with higher susceptibility to cell death, whilst Müller glia that express lower levels of TNFR1 withstand TNF-α insult (Tezel et al., 2001, Agarwal and Agarwal, 2012). In contrast, TNFR2 has higher affinity to membrane-bound TNF-α and activation of TNRF2 induced anti-inflammatory response has been previously recorded in microglia (Veroni et al., 2010).

Importantly, TNFR2 mediated TNF-α signalling between neighbouring cells, enhancing activation of the constitutive NFκB pathway and consequently cell survival (Sedger and McDermott, 2014). Although it is not clear if MIO-M1 cells could 'crosstalk' and activate neuroprotective signals in adjacent cells, the present findings suggest that MIO-M1 cells did not respond to TNF-α in a detrimental manner and instead this cytokine elicited a protective response on these cells. In this study, shedding of TNFR2 into the extracellular environment might have occurred and this has been observed in the host laboratory. As a consequence, neutralisation of exogenous TNF-α might have reduced availability of TNF-α binding for TNFR1 and may explain why mRNA coding for this receptor remained unchanged.

It should be noted that activation of both types of TNFR simultaneously induces a reciprocal regulatory mechanism. For example, within the TNF-α superfamily, factors that initiate apoptosis including TNFSF10 and TNFRSF10B, as well as those that execute apoptosis such as BID showed significant upregulation. In addition, the anti-apoptotic genes BIRC2 and BIRC3, as well as the apoptosis negative regulator TNFAIP3 (Yang et al., 2011) and TNFAIP8 (You et al., 2001) showed significant counteractive upregulation at much higher TPMs and perhaps could be considered as an endogenous regulatory mechanism to attenuate cell death. This is supported by the findings that in the presence of this cytokine Müller cells did not show morphological changes and remained viable. This is in agreement with other reports showing unaffected astrocyte viability upon culture with TNF-α (Edwards and Robinson, 2006). Similarly, upregulation of genes coding for the NFκB2 signalling pathway was accompanied by increase in genes coding for its three endogenous inhibitors NFκBIA, NFκBIE and NFκBIZ, indicating an autoregulatory feedback loop (Thompson et al., 1995). In particular, upon activation of the NFκB gene complex (Chiao et al., 1994), IκBα protein which is coded by NFκBIA is firstly phosphorylated by RIPKs before subjecting to degradation, inducing further mRNA productions, in order to regulate NFκB signalling (Brown et al., 1993).

Taken together, the above analyses support the hypothesis that activation of both TNF-α and NFκB signalling cascades in Müller glia are well regulated and did not induce profound destructive transcriptomic profile characteristic of uncontrolled cell death.

3.4.2 Upregulation of inflammatory markers by TNF-α accompanied by upregulation of pro-survival genes in MIO-M1 cells

Cellular events such as leukocyte infiltration into the inflammatory sites and ECM remodelling represent common manifestations of inflammation. Transcriptional upregulation of major effectors appeared to be counterbalanced by modification of other genes implicated in similar functions. For instance, upstream of pro-inflammatory effector genes, elevated TNFAIP2 which mediates inflammation and angiogenesis (Sarma et al., 1992) appears to be counterbalanced by upregulation of the anti-inflammatory TNFAIP6 gene (Wisniewski et al., 1996). The current observations that genes coding for α and βchemokines exhibited the highest fold-change are consistent with other reports that increased levels of these inflammatory mediators are promoted by TNF-α (Horuk, 1994, Oh et al., 1999). It is noteworthy to emphasise that these chemotactic factors are also important to support survival of retinal cells under cellular stress. Some studies have proposed that CCL2 could confer some neuroprotection to RGCs by restoring IGF1 levels (Chiu et al., 2010), and primary cortical neurons pre-treated with CCL5 show better survival after exposure to neurotoxic agents. The underlying mechanism is thought to be mediated by the G protein coupled receptor GPR74 (Tripathy et al., 2010, Ignatov et al., 2006). Similarly, Veroni and colleagues speculated that the initial upregulation of several angiogenic and chemoattractant factors such as CSFs may be associated with neuroprotection (Xiao et al., 2007, Veroni et al., 2010).

Upregulation of chemotactic factors was accompanied by extensive transcriptional modification of genes coding for leukocyte binding factors and ECM components. Hence, upregulation of VCAM1 and ICAM1 that facilitate cell-matrix interaction and leukocyte migration to inflammatory sites (White et al., 2013) was accompanied by increased expression of LGALS1 genes, which are often triggered in proliferating Müller glia by photoreceptor damage or degeneration in zebrafish (Craig et al., 2010) and rodent (Uehara et al., 2001). It has been proposed that increased LGALS1 expression might be a protective mechanism to promote attachment of the neural retina to RPE during gliosis (Alge et al., 2006), whilst downregulation of the cell-ECM binding factors ITGB5 and THBS1 genes may potentially reduce leukocyte migration to reduce neuroinflammation.

Aberrant ECM stiffening by active synthesis and crosslink of collagens are key features of the gliotic response and leads to scar formation (Wallace et al., 2014, Nita et al., 2014). In this study, several collagen family members and non-structural matricellular proteins CTGF, fibronectin and LAMA3 that promote cell adhesion to ECM and aberrant ECM deposition (Sato et al., 2000, Lang et al., 2008, Ball et al., 2003) exhibited substantial downregulation. These findings might indicate that suppressing ECM synthesis represent an endogenous regulatory mechanism to halt leukocyte infiltration. Interestingly, COL6A1 was the only collagen gene that showed upregulation, and this might be associated with its function of binding and modulating the biological activities of PDGF (Somasundaram and Schuppan, 1996). Perhaps the transcriptional upregulation of COL6A1 might be necessary to facilitate the trophic function of PDGFC (Osborne et al., 2018). In this study, upregulated MMP1 and its inducer TFPI2 with downregulated inhibitor TIMP4 might suggest that TNF-α potentiates MMP1 activity to suppress aberrant ECM formation. Interestingly, upregulated MMP1 has different implications in various organisms. For example, MMP upregulation is required for regeneration of CNS and retina in axolotl and zebrafish (Lemmens et al., 2016, Verslegers et al., 2013, Chernoff et al., 2000), however in human, its elevation is found contributing to PVR by promoting neuroinflammation (Symeonidis et al., 2011), as MMP1-driven angiogenic proteolysis is a prerequisite of neovasculature formation in the ECM (Seandel et al., 2001). Nevertheless, upregulation of the anti-proliferative and anti-angiogenic GBP1 is possibly a counteractive response to the upregulated VEGF and MMP1 (Guenzi et al., 2001, Guenzi et al., 2003) and the inhibitory potential of GBP2 on cell spreading on fibronectin may be considered as another regulatory mechanism to supress leukocyte adherence on fibronectin (Messmer-Blust et al., 2010).

The hypothesis that upregulated TNFR2 induce expeditious response to TNFR1-mediated neuroinflammation is augmented by the increased TPM of anti-oxidative and neurotrophic factors including SOD2 (Joe et al., 2015), PRDX6 (Zha et al., 2015), ALDH1A3 (Duong et al., 2017), BDNF (Chen et al., 2017) and PDGFC (Osborne et al., 2018). These findings are in accordance with previous studies that have documented TNF-α mediated upregulation of neurotropic factors in astrocytes (Saha et al., 2006) and in Müller glia (Toft-Kehler et al., 2016), indicating a neuroprotective attempt of MIO-M1 cells to abrogate oxidative stress induced by neuroinflammatory response and promote cell survival. The overall biological impact

of TNF-α on MIO-M1 cells is difficult to interpret whether the neuroinflammatory upregulation might overwhelm the neuroprotective effects under an *in vitro* context. They remain to be resolved in future studies that should explore proteomic analysis on these genes.

3.4.3 Downregulation of Müller glia genes associated with reactive gliosis suggests a novel *in vitro* neuroprotective response in these cells

A major observation in this study was the reduced expression of genes associated with gliosis by MIO-M1 cells in response to TNF-α. Surprisingly, repressed expression of the gliosis transcription factor SOCS2 and reactivity marker S100B, as well as the gliotic marker GFAP in MIO-M1 cells induced by TNF-α is a novel observation in this study. Overexpression of GFAP in reactive Müller cells during gliosis and its contribution to the gliotic scar is a hallmark of gliosis in higher vertebrates (Lewis and Fisher, 2003, Sethi et al., 2005). As a result, accumulation of these intermediate filament proteins at their inner processes and endfeet, fills the space left by deceased retinal neurons. This causes stiffening of Müller cells, generating glial scars that hinder subsequent regeneration events (Lu et al., 2011, Franze et al., 2007). Together with the downregulation of the proliferation-associated genes SOX2 and METRN, the present findings suggest that entering the reactive proliferative state is not an immediate response of Müller cells. Transcriptional expression of GFAP is primarily regulated by the JAK/STAT3 signalling pathway (Herrmann et al., 2008) which can be activated by TNF-α via the MAPK pathway (Kahn et al., 1997, Zhang et al., 2000). Notably in this study, SOCS2 and METRN genes acting upstream of JAK/STAT3 pathway were found significantly upregulated. The SOCS family of genes initiates a negative feedback loop that prevents STAT3 activation and attenuate JAK signalling cascades (Kubo et al., 2003), whilst SOCS2 influences the proliferation and survival of hippocampal neurons. Its overexpression significantly promotes cell survival whilst its knockout reduces cell proliferation (Basrai et al., 2017, Basrai et al., 2016). This perhaps is relevant to the suppression by TNF-α of METRN and SOX2 that regulate the progenicity and proliferation of Müller glia. METRN is a ligand for the gp130 co-receptor that activates the

JAK/STAT3 and is reported to induced astrocytes reactivity increasing their expression of SOX2 and GFAP (Nishino et al., 2004, Gotz and Barde, 2005). Downregulation of SOCS2 may indicate that the biological activity of STAT3 could be increased, whereas METRN downregulation may modulate STAT3-driven GFAP expression. In addition, crosstalk between multiple signalling cascades at STAT3 could also influence downstream transcription. A good example is the compensatory mechanism between GFAP and VEGF which are commonly regulated by NFκB and JAK/STAT3 pathways (Sun et al., 2013). Compensatory expression of one gene by another has been observed during VEGF deprivation (Kahn et al., 1997, Valapala et al., 2015, Gaddini et al., 2016) and depletion of VEGF in primary retinal *in vitro* has been shown to enhance GFAP expression in Müller cells through STAT3 activation (Gaddini et al., 2016). Whether GFAP downregulation in Müller glia could be caused by VEGFC downregulation is not known, and subsequent investigations could exploit siRNAs targeting VEGFC to examine this compensatory regulation hypothesis. Taken together, it remains unclear how these transcription factors have interacted to induce mRNA downregulation of GFAP, nevertheless these observations provide the basis for further investigations on the regulation of GFAP expression.

Increased levels of TNF-α have been implicated in disrupting BRB integrity attributed to the loss of tight junction proteins (TJs) by increased MMP activities leading to influx of ion, water and immune cells across the BRB into the retina (Tsuge et al., 2010). This is suggested by other studies that indicate that AQP4 potentiates neuroinflammation by facilitating infiltration of immune cells (Li et al., 2011), as well as promoting glial scar formation by increasing cellular fluid permeability driven by actin polymerisation (Oster and Perelson, 1987). This might also help the outgrowth of reactive Müller glia to fill the subretinal space and replace the dying cones after insults, such as retinal detachment (Lewis and Fisher, 2000). Therefore, the novel observation of CLDN1 upregulation and AQP4 downregulation in response to TNF-α might also suggest an additional neuroprotective function with elevated barrier-regulating response to impede BRB leakage and mitigate leukocyte infiltration and gliotic scarring, as evident by studies attenuating BRB breakdown consistently reported improved CLDN1 levels (Tian et al., 2014, Mei et al., 2019) and that AQP4-null rodent had impairment of astroglia migration (Saadoun et al., 2005).

Surprisingly, the observed downregulation of GFAP, GLUL and AQP4 in this study was similar to findings previously reported in zebrafish and chick during retinal regeneration, which constitute a pre-requisite for Müller glia to undergo proliferation (Fimbel et al., 2007, Thummel et al., 2008, Nelson et al., 2013, Fischer and Reh, 2003). These findings suggest that reducing GFAP expression in Müller cells might promote migration and differentiation of these cells during endogenous regeneration of neural retina.

3.4.4 Non-coding DEGs might contribute to transcriptional regulation

The core analysis of this chapter targeted on protein-coding transcripts and further studies should seek to investigate the impact of the non-protein coding repertoire on transcriptomic regulation. In addition to the regulatory roles of non-coding transcripts from mRNA processing to cell signal modulation, lincRNAs are also reported functioning as either enhancer or suppressor in NFκB-induced inflammatory response (Mathy and Chen, 2017). In this study the downregulated SERTAD4-AS1 was previously identified as a NFκB-induced lncRNAs and may be involved in the regulatory role of TNFAIP3 (Trynka et al., 2009, Banks et al., 2016). In the context of neurodegenerative disorders, many AS are linked to neurodegenerative disease-causing genes and might interfere with the expression of neuroprotective genes such as BDNF and GDNF (Zucchelli et al., 2019). Whilst no definitive candidates could be identified in the current transcriptomic data, it is likely that those novel transcripts might carry similar functions. Processed pseudogenes with regulatory potential remain under ongoing debate, and emerging evidence from rodent transcriptomes suggest that these non-autonomous transcriptional products might function similarly to AS (Pink et al., 2011, Watanabe et al., 2008). While the interpretation of some of the non-coding transcripts reported in this study is built upon annotation from the current literature, the lack of knowledge restricts the identification of the role of novel transcripts identified in this study (Costa et al., 2013). It is hoped that the continuously expanded database on non-coding RNAs would facilitate the understanding of the activity of identified novel lncRNAs in the reported transcriptomic libraries.

3.4.5 Limitation of study

Although a pleiotropic response of Müller glia to a short-term exposure to TNF-α was identified, there are limitations to the study design and data interpretation. RNA-sequencing was only applied to Müller cells under acute exposure to TNF-α, but their transcriptomic landscape upon chronic cytokine stimulation remains unanswered. In addition, it is still unclear whether the global transcriptional landscape of MIO-M1 cells would be predisposed towards a neuroinflammatory or neuroprotective status without relating the transcriptomic observations to actual protein levels and functions. This is because transcriptomic modification might not immediately feed into the proteasome of cells, and discrepancies between transcript and protein levels due to post-transcriptional modification mechanisms have been well documented (de Sousa Abreu et al., 2009, Vogel and Marcotte, 2012). On this basis, it would be important to compile a comprehensive proteomic study of MIO-M1 cells under the same experimental conditions, to correlate with the transcriptome, which might shed light on the post-transcriptional regulation of the transcriptome in these cells.

In summary, despite the limitations discussed, this transcriptomic study captured molecular signatures associated with both neuroinflammatory and neuroprotective responses in the human adult Müller glia cell line upon acute response to TNF-α-mediated stress. The functional characteristics of several DEGs discussed in this study could be further exploited to help elucidate the mechanisms that underpin *in vivo* gliotic or *in vitro* neuroprotective responses.

CHAPTER 4 Müller glia constitute an important source of antioxidants in the human retina

4.1 Introduction

4.1.1 Oxidative stress in the retina

Oxygen is a metabolite that participates in essential cell activities such as glycolysis and the citric acid cycle (Yu and Cringle, 2005). During this process, oxygen is reduced to a broad range of highly reactive intermediates which are collectively known as reactive oxygen species (ROS). These include free radicals, singlet oxygen and peroxides (Brantley and Sternberg, 2013). Common free radicals comprise the potent oxidising molecules hydroxyl radical (OH^-) and superoxide anion ($O_2^{-}\bullet$) that can take additional electrons from other compounds for its unpaired electron, causing cytotoxic damage. Hydrogen peroxide (H_2O_2) and singlet oxygen ($^1O_2$) are in an unstable state and could induce cellular damage when they undergo biochemical reactions (Beatty et al., 2000). Endogenous ROS are primarily produced within the mitochondria and factors such as ageing, inflammation and smoking could accelerate their production (Beatty et al., 2000, Jones et al., 2002, Hanus et al., 2015). ROS can diffuse out of the mitochondria into the cytosol, where protein- and lipid-rich organelles reside (Wahlig et al., 2018). Oxidisation of cytosolic and mitochondrial proteins and DNA could lead to dysfunctional cell signalling and malfunction of electron transport chain in the mitochondria. This eventually activates apoptosis as the damage accumulates in the cell (Hurley et al., 2015).

Retina is amongst the tissues that require enormous amount of oxygen for their metabolism. It is highly susceptible to oxidative stress as its primary activity of converting physical light to electrophysiological action potentials demands a high rate of oxygen consumption (De La Paz and Anderson, 1992). This neurosensory tissue is rich in polyunsaturated fatty, which makes it highly susceptible to oxidative burden and lipid peroxidation (Cai et al., 2000). Photoreceptors represent one of the most susceptible retinal cells to oxidative stress because of their continuous exposure to light and oxygen (Hanus et al., 2015). In addition, RPE and RGCs are also vulnerable to oxidative damage. RPE cells steadily phagocytose photo pigments shed from rods and cones (Kuse et al., 2014), while RGCs are constantly

under the stimulation of glutamatergic signalling pathway that generates electrical impulses (Quinlan et al., 2013).

4.1.2 Key antioxidant molecules in the retina

Under normal physiological conditions, the equilibrium of generation and elimination of ROS in the retina is well regulated by intrinsic defence mechanisms comprised of small-molecule antioxidants and enzymes to keep ROS levels at low concentrations. Vitamins C and E are small antioxidants that can directly quench hydroxyl radicals. Glutathione (GSH) is a tripeptide that contains subunits of cysteine, glycine and glutamine and constitutes the most abundant low molecular weight antioxidant (Forman et al., 2009). The ROS scavenger capacity of GSH is ascribed to the cysteine subunit which allows GSH to act as a reducing agent to detoxify electrophiles and eliminate lipid peroxidation and hydrogen peroxide (Meister, 1992). The biosynthesis of GSH is a two-step reaction catalysed by glutamate cysteine ligase (GCL) and glutathione synthetase (GSS), sequentially adding cysteine to glutamate and finally glycine. Whereas glutathione reductase (GSR) is capable of releasing GSH from its metabolic derivative and maintaining GSH in its reduced form (Forman et al., 2009).

Unlike the natural antioxidants that directly neutralise ROS, antioxidant enzymes initiate a series of biochemical reactions to convert highly active particles to a more stable form. Within the mitochondria, several enzymes form the first line of anti-oxidative defence and most of the superoxide anions generated by these organelles are immediately metabolised by superoxide dismutase 2 (SOD2) localised at their inner membrane to a less harmful form of hydrogen peroxide (Candas and Li, 2014) (Beatty et al., 2000). The activity of SOD2 requires magnesium ion and it actively binds to superoxide byproducts of oxidative phosphorylation such as hydrogen radicals (H^+), converting these into hydrogen peroxide and diatomic oxygen (Inarrea et al., 2014, Azadmanesh et al., 2017). SOD2 is present in many types of tissues and in the eye is mainly found within the trabecular meshwork cells (Joe et al., 2015). Another mitochondria-bound enzyme, the lipoic acid synthetase (LIAS), catalyses the biosynthesis of α-lipoic acid, which could also directly scavenge ROS and activate additional antioxidant genes in RGCs (Inman et al., 2013). Found in the

mitochondrial inner membrane and matrix, the coenzyme Q-binding protein homolog 10A (CQ10A) is required by coenzyme Q and serves as a chaperone in the respiratory chain. Its anti-oxidative and anti-apoptotic effects are evident in the nervous system, despite its underlying mechanism remaining elusive (Lee et al., 2014a).

Upon ROS released into the cytoplasm, several cytosolic antioxidant enzymes are responsible for regulating the redox balance and prevent oxidative damage to other organelles. The peroxiredoxin (PRDX) family is one of the thioredoxin enzyme systems that prevents disulfide bonds forming between proteins, as well as promoting the conversion of hydrogen peroxide, short-chain organic hydroperoxides and fatty acids into water and alcohols (Kang et al., 1998, Patenaude et al., 2005). Among the six members of peroxiredoxin family, the isoform 6 (PRDX6) is expressed at the highest level in mammalian retina and is the only member that has one catalytically active cysteine site (Grosche et al., 2016). The ability of PRDX6 to reduce hydrogen peroxide to water and repair membrane phospholipids requires GSH (Ralat et al., 2006). PRDX6 is highly concentrated within the lysosomes and can be released into cytoplasm, although it might sporadically be found within the secretory organelles in lung cells (Chen et al., 2000, Wood et al., 2003). Another defence enzyme against oxidative stress is the heme oxygenase 1 (HO1) which can be induced by hypoxia, cytokine and heat shock (Maines, 1988, Yong et al., 2010). It is found within microsomes, endoplasmic reticulum, cytosol and even as a membrane-bound form (Gottlieb et al., 2012). Heme is found in oxidases and peroxidases and mediates the production of superoxide and hydrogen peroxide (Everse and Coates, 2009). HO1 cleaves the heme ring at the alpha methene bridge to produce biologically active end products including biliverdin, CO and ferrous ion (Cheng and Rong, 2017). The bioactive gaseous CO has been suggested to control vascular tone and promote cell survival and growth, whereas biliverdin, which is reduced by biliverdin reductase to form bilirubin is another potent antioxidant (Baranano et al., 2002). NAD(P)H: quinone oxidoreductase 1 (NQO1) is another important enzyme that catalyses the reduction of the unstable quinone to a more stable state known as hydroquinone, preventing free radicals from reacting with quinone (Talalay et al., 1995).

Peroxidation of the low-density lipoprotein (LDL) is ameliorated by a transmembrane protein paraoxonase/arylesterase 2 (PON2) which is widely expressed in various tissues with normally experience high oxidative stress , such as brain, heart and retina (Ng et al., 2001, Bharathidevi et al., 2017). Binding to its cofactor calcium ion, PON2 reverses the oxidation process by hydrolysing lactones and aromatic carboxylic acid esters, although some literature suggests that it could be acting as a cytosolic enzyme (Draganov et al., 2005, Grosche et al., 2016). Moreover, oxidative stress could arise following N-methyl-d-aspartate (NMDA) receptor activation by the neuropeptide N-acetyl-aspartyl-glutamate (NAAG) released from neurons (Puttfarcken et al., 1993). Rodent Müller glia express a type II single-pass transmembrane protein called glutamate carboxypeptidase 2 (GCPII) (Grosche et al., 2016, Berger et al., 1999), which has an N-acetylated-alpha-linked-acidic dipeptidase (NAALADase) activity that cleaves NAAG to N-acetyl-aspartate and glutamate (Ghosh and Heston, 2003). Coded by the gene folate hydrolase 1 (FOLH1) in humans (Mesters et al., 2006), GCPII activity is essential to terminate the excitatory activity of NAAG, although NAAG could also partially antagonise NMDA receptors and decrease glutamate binding (Puttfarcken et al., 1993).

4.1.3 Transcriptional regulation of antioxidant enzymes

The expression of many antioxidant enzymes including SODs, PRDXs, HO1 and NQO1 is mainly regulated by a master transcription factor called nuclear factor erythroid 2 related factor 2 (NRF2). In the inactive stage, NRF2 is constitutively bound to its cytoplasmic protein Kelch-like ECH-associated protein 1 (Keap1) and this complex is ubiquitinated before proteasomal degradation. Upon elevation of intracellular oxidative stress, ROS induces conformational changes of NRF2 by interacting with the cysteine residues on NRF2, to release it from Keap1 (Dinkova-Kostova et al., 2002). The transcriptional activity of NRF2 can also be indirectly promoted by the autophagy-adaptor protein p62, which facilitates the proteosomal degradation of Keap1 (Ichimura et al., 2013). Free NRF2 accumulates in the nucleus and forms a transcriptional complex with additional transcriptional co-activators such as CREB-binding protein (CBP) and small Maf proteins (sMaf) (Wardyn et al., 2015). CBP has a histone acetyl transferase domain and is important for loosening chromatin and exposing DNA for subsequent transcription (Sun et al., 2009),

whereas sMaf acts as a scaffolding protein to promote NRF2 acetylation by CBP (Hwang et al., 2013).

The NRF2-CBP-sMaf protein complex binds to the DNA promoter sequence called antioxidant response element (ARE) at the promotor site of target genes and drives the expression of numerous antioxidant enzymes to regulate cellular oxidative balance (Ma, 2013, Jaiswal, 2004). The anti-oxidative response of retinal cells can be abolished in mice with NRF2 deletion, which manifest in severe oxidative stress and degenerative conditions (Pittala et al., 2017, Ramos-Gomez et al., 2001, Navneet et al., 2019), addressing the importance of NRF2 on regulating neuroprotective gene expression.

4.1.4 Pro-inflammatory cytokines promote oxidative stress

The physiological oxidative balance is disrupted when the level of pro-oxidative species exceeds the anti-oxidative capacity of the cells, leading to DNA damage and metabolic suppression. It has been hypothesised that oxidative stress plays a crucial role in retinal degeneration and is implicated in a great number of retinal pathologies. In diabetic retinopathy, ROS production results from accelerated oxidation of fatty acids and mitochondrial dysfunction due to hyperglycaemia (Calderon et al., 2017), whilst in trabecular meshwork from patients with primary open-angle glaucoma, ROS has been shown to promote oxidative DNA damage (Pinazo-Duran et al., 2015). Interestingly, oxygen metabolism has been proposed to be increased in retinal degenerative conditions, where retinal neurons and supporting cells undergo an inflammatory response which further potentiates the dysregulation of the oxidative balance (Anderson, 1968).

Pro-inflammatory cytokines play an important role in the pathogenesis of retinal degeneration, with the activation of downstream signalling cascades mediated by TNF-α and TGF-β being the cause of ROS production. ROS accumulates within the mitochondria following TNF-α stimulation, due to activation of the pro-oxidative gene NADPH oxidase (NOX) member NOX2 via its signalling mediator NFκB (Anrather et al., 2006). Prolonged NOX2 activation can impair mitochondrial oxidative phosphorylation, leading to disruption of mitochondria morphology and membrane

potential (Fiers et al., 1999). This is recognised as the immediate result of prolonged activation of mitogen activated protein kinase (MAPK) downstream of TNF-α signalling (Sakon et al., 2003).

TGF-β exists as a pro-form when bound to its binding protein latent TGF-β binding proteins (LTBP), and following proteolytic cleavage by plasmin, ROS and thrombospondin-1, it is freed from LTBP and association to their cell surface receptors activates downstream canonical and non-canonical signalling cascades (Roberts, 1998). It is believed that TGF-β increases ROS production by activating NOX4 via the canonical Smad pathway, or the non-canonical phosphatidylinositol 3-kinase (PI3K) or MAPK pathways (Michaeloudes et al., 2011, Ismail et al., 2009, Tobar et al., 2014). Interestingly, there is a reciprocal regulation between TGF-β and ROS, in which TGF-β induces mitochondrial and cytosolic ROS, while ROS can further potentiate the release of endogenous TGF-β (Liu and Desai, 2015, Michaeloudes et al., 2011).

4.2 Objectives

The specific aims of this chapter were:

1. To identify whether Müller glia present in the human retina express neuroprotective antioxidant proteins;

2. To examine the expression of genes and proteins coding for antioxidant enzymes in Müller glia derived from human adult retina and Müller glia derived from hPSC-formed retinal organoids. hiPSC-derived Müller glia 1 (hiPSC-MG1) is referred to hereafter as hiPSC-MG cells. hESC-derived Müller glia 1 (hESC-MG1) is referred to hereafter as hESC-MG cells;

3. To investigate the effect of cytokine TNF-α on the expression of antioxidant enzymes in Müller glia derived from human adult retina and Müller glia derived from hPSC-formed retinal organoids;

4. To investigate the effect of cytokine TGF-β1 to the antioxidant enzymes expressed by Müller glia derived from human adult retina and Müller glia derived from hPSC-formed retinal organoids.

Experimental design:

i. Normal human retinae were obtained from cadaveric donors from Moorfield Eye Bank upon local ethical approval, fixed and embedded for histological tissue sectioning at 12μm. Retinal sections were immune-stained with antibodies specific to key antioxidant enzymes PRDX6, SOD2, PON2, HO1, NQO1, GCPII, GSS, GSR, COQ10A and LIAS and Müller glia markers GS and vimentin and imaged by confocal microscopy.

ii. Human adult Müller glial cell line MIO-M1 cells, hiPSC-MG cells and hESC-MG cells were seeded at 1 million cells and allowed attachment for 24 hours before replacing culture medium to fresh medium containing 50 ng/mL TNF-α or 50 ng/mL TGF-β1 for 24 hours. Untreated cells served as controls.

iii. At the end of the treatment, cell pellets were collected for extraction of RNA and proteins. Total RNA was reversed transcribed into cDNA and subjected to RT-PCR analysis. Extracted proteins were used to examine the expression of the antioxidant enzyme proteins using western blotting analysis.

iv. Culture supernatants were collected from cells undergoing TNF-α treatment and control untreated cells, and briefly centrifuged to remove floating cells before storing in small aliquotes at -80°C. Working aliquots were defrosted on ice before proceeding to quantitative enzyme-linked immunosorbent assay (ELISA) analysis to determine the mean concentrations of PRDX6 and HO1 released by these Müller cells.

4.3 Results

4.3.1 Human Müller glia express key antioxidant enzymes

The expression of mRNA coding for several antioxidant enzymes in the hPSC-formed retinal organoid-derived hiPSC-MG cells, hESC-MG cells and the human adult Müller cell line MIO-M1 cells was determined by RT-PCR (Figure 4.1A). These genes included PRDX6, SOD2, PON2, HO1, NQO1, GCPII, GSS, GSR, COQ10A and LIAS. The mRNA expression of the majority of these genes was consistently observed at comparable levels in all three Müller glia samples, with exception of mRNAs coding for NQO1 and GCPII, which were found strongly expressed in MIO-M1 cells, but weakly expressed in hiPSC-MG and hESC-MG cells (Figure 4.1A). Similarly, proteins coding for PRDX6, SOD2, PON2, HO1, NQO1, GCPII, GSS and GSR in hiPSC-MG, hESC-MG and MIO-M1 cells were confirmed by western blotting (Figure 4.1B). These findings indicated that human Müller glia constitute a rich source of antioxidant enzymes.

4.3.2 Müller glia is the source of antioxidant enzymes in human retina

Amongst the above antioxidant enzymes, the subcellular expression patterns of PRDX6 (

Figure 4.2A), HO1 (

Figure 4.2B), GCPII (

Figure 4.3A) and PON2 (

Figure 4.3B) in the normal human neural retina were examined by co-immunolabelling with the intracellular Müller glia markers GS or vimentin (red channel). These antioxidant enzymes were found distributed across the entire retina, and predominantly followed the pattern of Müller glia distribution. In addition, GCPII and PON2 staining extended to the photoreceptor outer segments (

Figure 4.3). Strong expression of all these four antioxidant enzymes was observed in the never fibre layer, with perinuclear staining for GCPII often observed in RGCs (arrows,

Figure 4.3A).

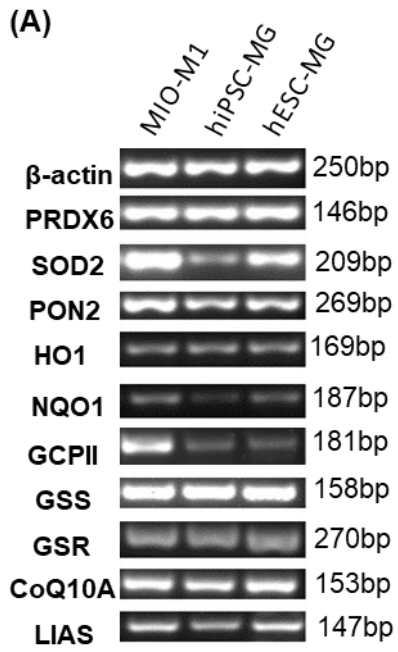

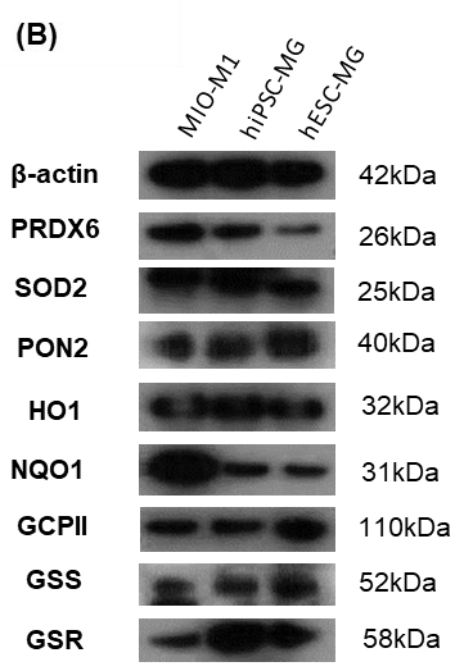

Figure 4.1 Representative (A) RT-PCR bands and **(B)** western blotting bands showing expression of mRNA and protein coding for key antioxidant molecules by the human adult Müller glia cell line MIO-M1 cell (left), hiPSC-MG cells (middle) and hESC-MG cells (right).
β-actin was used as the house-keeping marker. kb, kilo base; kDa, kilo Dalton.

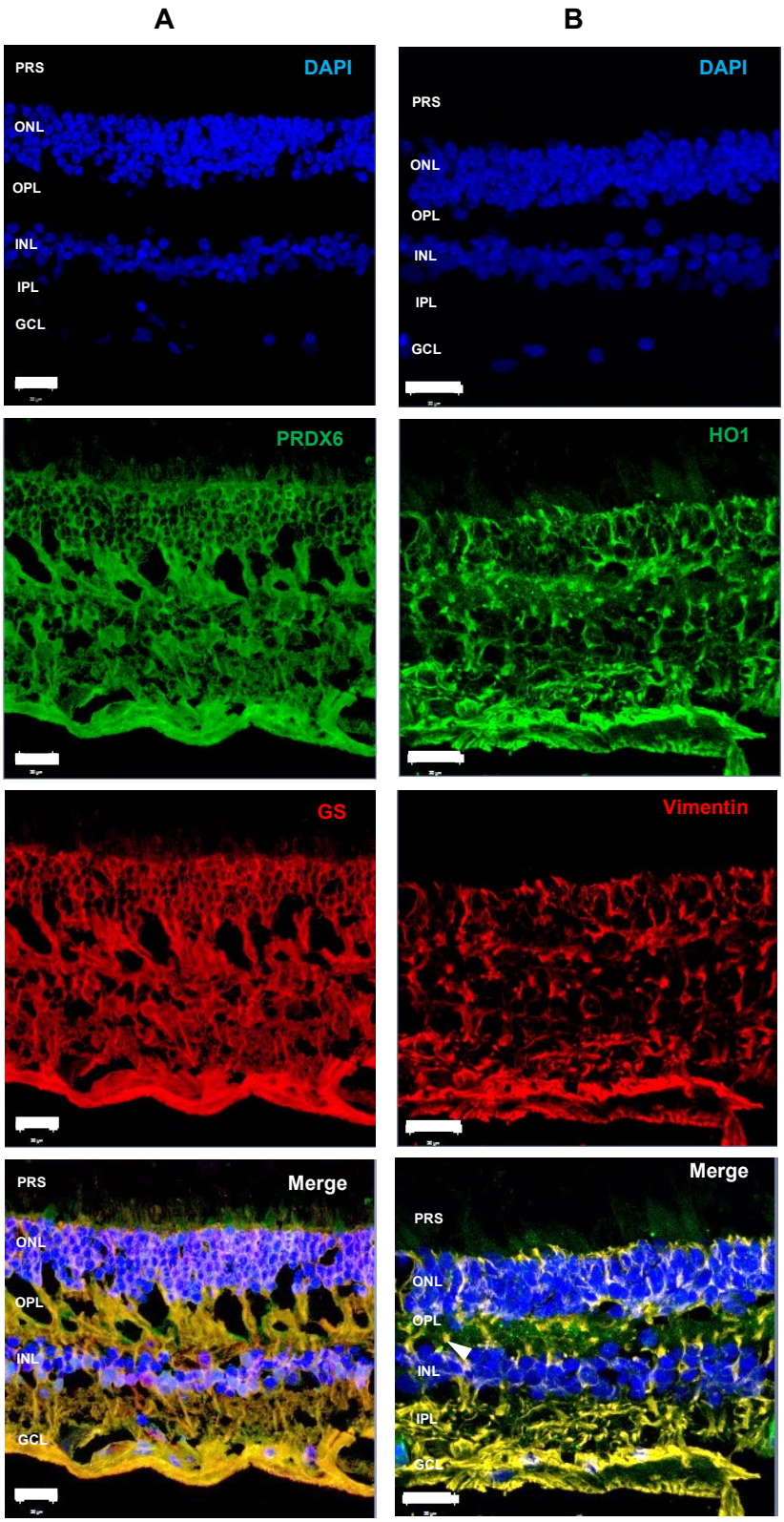

Figure 4.2 Distribution of the antioxidant enzymes PRDX6 (A) and HO1 (B) in normal human retina.

(A) Immunostaining of retinal section shows that PRDX6 (Green; Alexa Fluor® 488) is present in the neural retina and co-localised with Müller glia marker GS (Red; Alexa Fluor® 555). **(B)** HO1 (Green; Alexa Fluor® 488) is found throughout the neural retina and showed strong co-localisation with Müller glia marker vimentin (Red; Alexa Fluor® 555). Nucleus is counterstained with DAPI (blue). Scale bar = 20 µm. PRS, photoreceptor segment; ONL, outer nuclear layer; INL, inner nuclear layer; IPL, inner plexiform layer; GCL, ganglion cell layer.

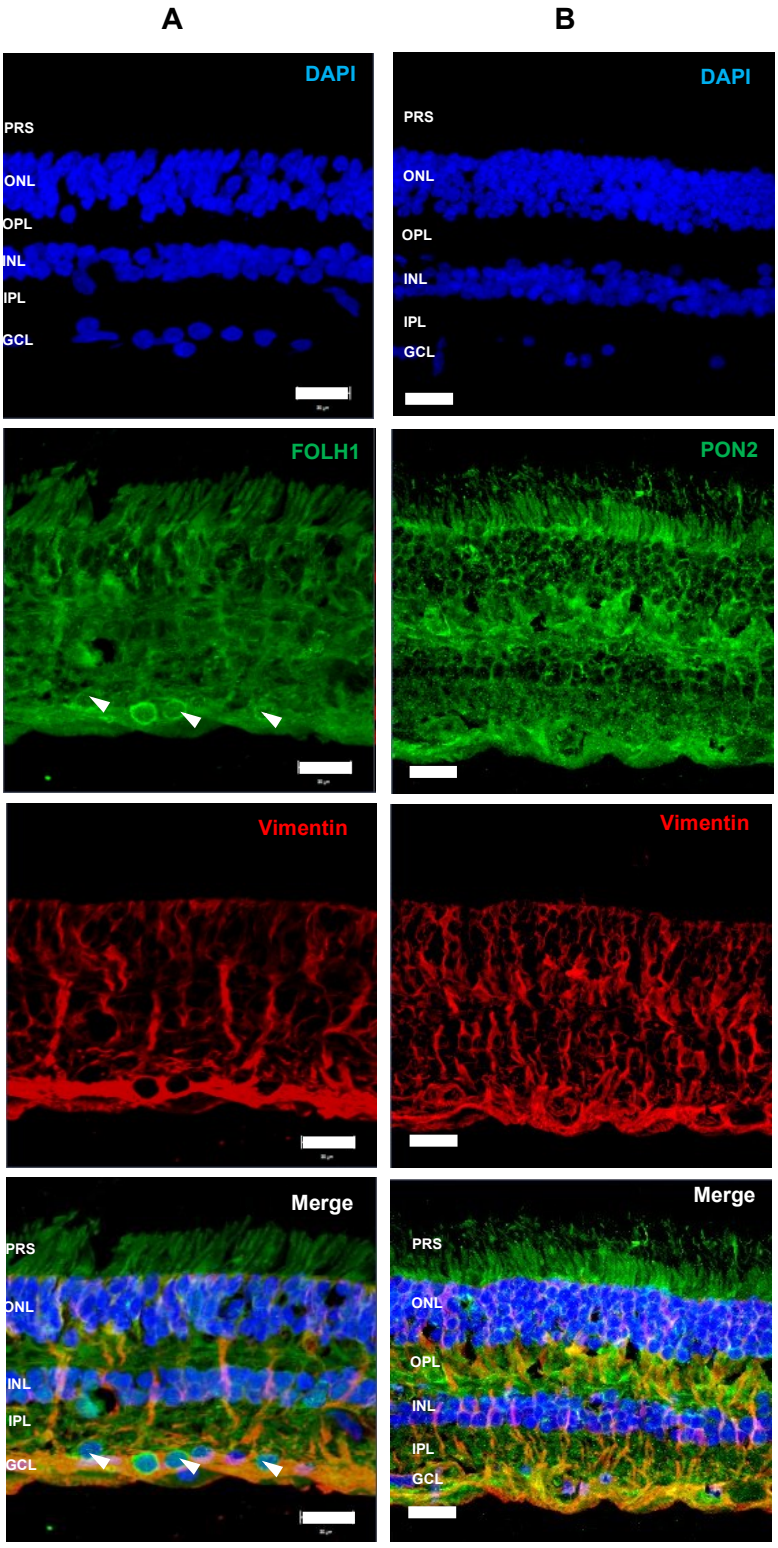

Figure 4.3 Distribution of the antioxidant enzymes GCPII (A) and PON2 (B) in normal human retina.

(A) Immunostaining of human retinal section shows that GCPII (Green; Alexa Fluor® 488) is localised along the outer stem of Müller glia (vimentin; Red; Alexa Fluor® 555) near the PRS and concentrated at the nerve fibre layer and surrounding RGCs (white arrows). **(B)** The distribution of PON2 follows the morphology of Müller glia (vimentin; Red; Alexa Fluor® 555) and extends to the outer PRS. Nucleus is counterstained with DAPI (blue). Scale bar = 20 µm. PRS, photoreceptor segment; ONL, outer nuclear layer; INL, inner nuclear layer; IPL, inner plexiform layer; GCL, ganglion cell layer.

4.3.3 Effect of TNF-α on the expression of antioxidant enzymes by human Müller glia

The human adult Müller glia cell line MIO-M1, hiPSC-MG cells and hESC-MG cells were cultured with 50 ng/mL TNF-α for 24 hours. Light-phase images of MIO-M1 cells (

Figure 4.4A), hiPSC-MG cells (

Figure 4.5A) and hESC-MG cells (

Figure 4.6A) showed that they retained their characteristic bipolar morphology following 24-hour exposure to TNF-α, as compared to untreated cells. Cell pellets and culture supernatants were collected to investigate the gene and protein expressions, as well as the release of neuroprotective antioxidant enzymes by these cells. Cell viability was examined by trypan blue exclusion to assess cytotoxicity induced by TNF-α. The results showed that TNF-α did not exert cytotoxicity to these cells.

Gene expression of the transcriptional regulator NRF2 and the neuroprotective mediator NFκB2 was studied using RT-PCR. As compared to untreated cells, TNF-α did not modify the mRNA expression of NRF2, but NFκB2 showed a slight but not significant upregulation in MIO-M1 cells (

Figure 4.4B) and hESC-MG cells (

Figure 4.6B). Interestingly, hiPSC-MG cells treated with TNF-α showed significant upregulation of NFκB2, although NRF2 remained unchanged (

Figure 4.5B). On this basis, the expression of antioxidant enzymes downstream of NRF2, including SOD2, PRDX6, HO1, GCPII and PON2 was analysed by RT-PCR and their protein expression confirmed by western blotting. TNF-α treatment caused significant upregulation of both mRNA and protein coding for SOD2 in MIO-M1 cells (

Figure 4.4B&C), hiPSC-MG cells (

Figure 4.5B&C) and hESC-MG cells (

Figure 4.6B&C). While the mRNA levels of PRDX6 were significantly increased by TNF-α in hiPSC-MG cells, a slight but not significant increase in the protein level of PRDX6 was observed (

Figure 4.5B&C). However, the levels of mRNA and protein coding for PRDX6 remained unchanged in MIO-M1 cells (

Figure 4.4B&C), and hESC-MG cells (

Figure 4.6B&C), regardless treatment conditions. Furthermore, TNF-α did not modify the expression of the antioxidant enzymes HO1, GCPII and PON2 in any of the three Müller glia preparations (

Figure 4.4B&C,

Figure 4.5B&C and

Figure 4.6B&C).

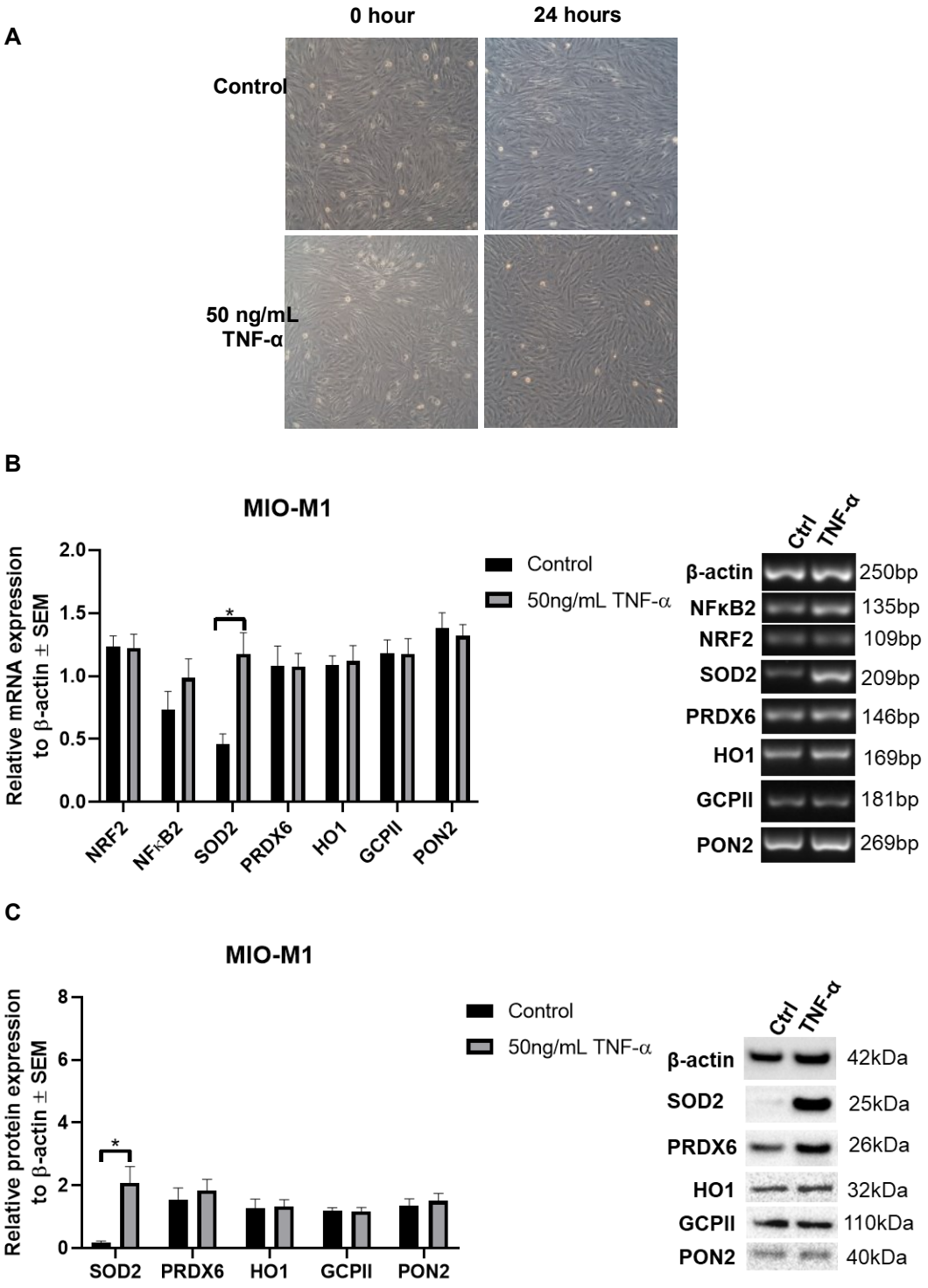

Figure 4.4 Effect of TNF-α on the expression of antioxidant enzymes in MIO-M1 cells.
(A) MIO-M1 cells exhibited characteristic bipolar morphology before (0 hour) and after (24 hours) treatment with 50 ng/mL TNF-α. Untreated cells served as controls. **(B)** Histograms represent the mean expression of mRNA coding for the antioxidant enzyme ± standard error of the mean (SEM), from the optical density of RT-PCR bands normalised to β-actin. Representative RT-PCR bands and the respective molecular weights (bp) of antioxidant of interest are shown on the right. **(C)** Histograms represent the mean protein expression coding for antioxidant enzyme ± SEM from the optical density of western blotting bands normalised to β-actin. Representative western blotting bands and the respective molecular weights (kDa) of antioxidant enzymes are shown on the right. N=3, parametric t-test, *$p < 0.05$.

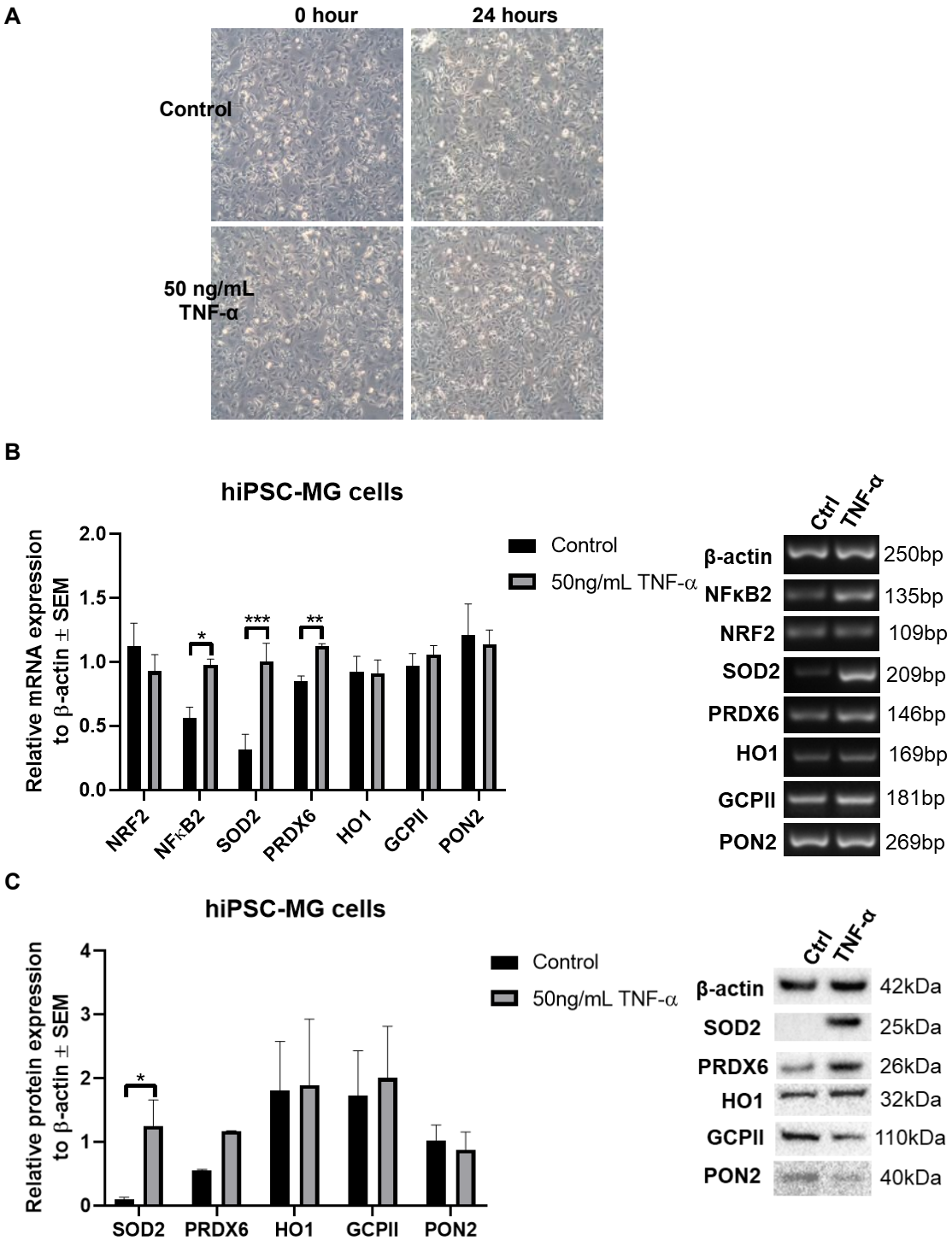

Figure 4.5 Effect of TNF-α on the expression of antioxidant enzymes in hiPSC-MG cells. **(A)** hiPSC-MG cells exhibited characteristic bipolar morphology before (0 hour) and after (24 hours) treatment with 50 ng/mL TNF-α. Untreated cells served as controls. **(B)** Histograms represent the mean expression of mRNA coding for the antioxidant enzyme ± SEM, from the optical density of RT-PCR bands normalised to β-actin. Representative RT-PCR bands and the respective molecular weights (bp) of antioxidant of interest are shown on the right. **(C)** Histograms represent the mean protein expression coding for antioxidant enzyme ± SEM from the optical density of western blotting bands normalised to β-actin. Representative western blotting bands and the respective molecular weights (kDa) of antioxidant enzymes are shown on the right. N=3, parametric t-test, *$p < 0.05$, **$p < 0.03$, ***$p < 0.01$.

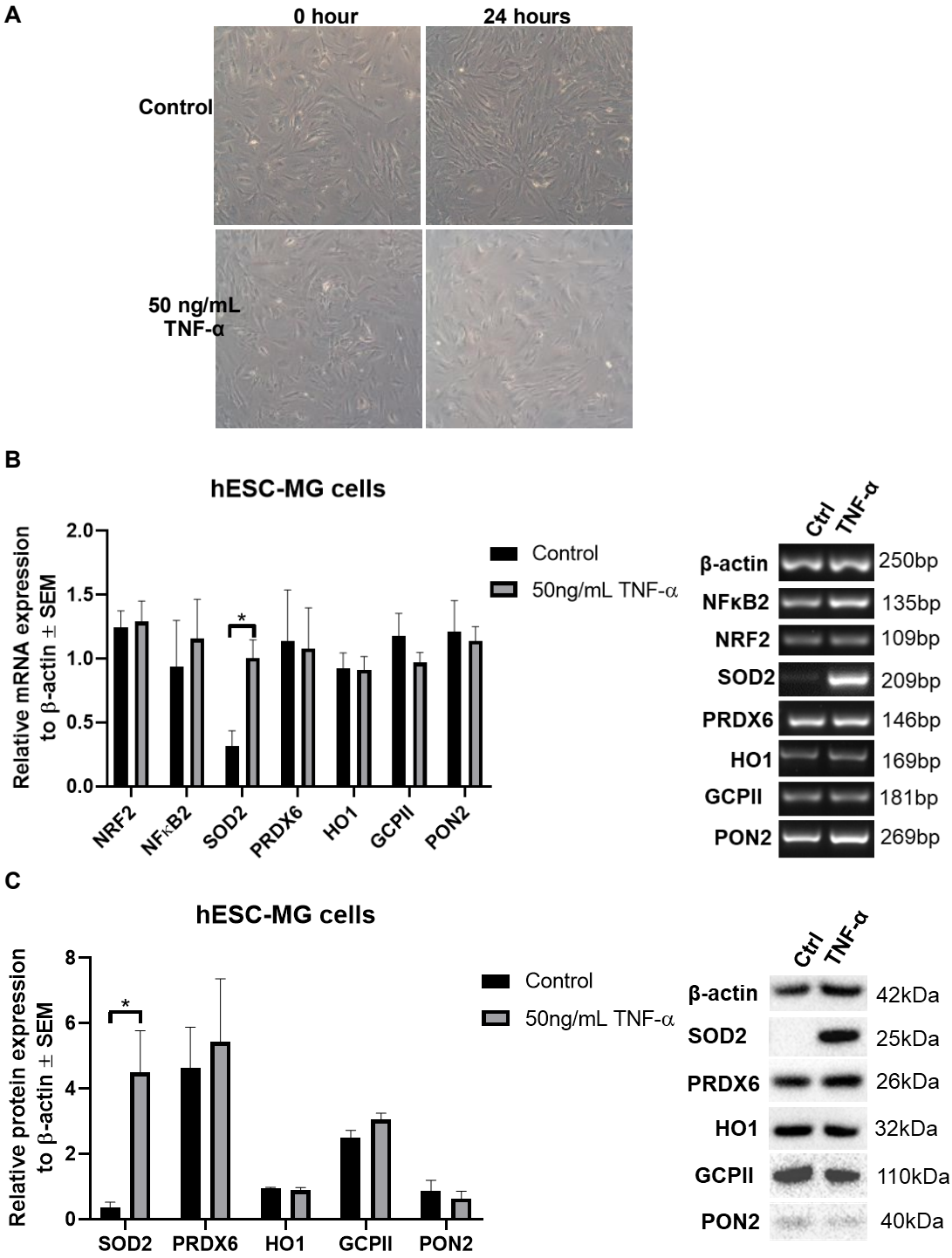

Figure 4.6 Effect of TNF-α on the expression of antioxidant enzymes in hESC-MG cells.
(A) hESC-MG cells exhibited characteristic bipolar morphology before (0 hour) and after (24 hours) treatment with 50 ng/mL TNF-α. Untreated cells served as controls. **(B)** Histograms represent the mean expression of mRNA coding for the antioxidant enzyme ± SEM, from the optical density of RT-PCR bands normalised to β-actin. Representative RT-PCR bands and the respective molecular weights (bp) of antioxidant of interest are shown on the right. **(C)** Histograms represent the mean protein expression coding for antioxidant enzyme ± SEM from the optical density of western blotting bands normalised to β-actin. Representative western blotting bands and the respective molecular weights (kDa) of antioxidant enzymes are shown on the right. N=3, parametric t-test, *$p < 0.05$.

ELISA kits were used to quantify the mean concentration of the soluble antioxidant enzymes PRDX6 (

Figure 4.7) and HO1 (

Figure 4.8) in culture supernatants of Müller glia following overnight culture with 50 ng/mL TNF-α. As determined by ELISA methods, similar levels of PRDX6 were detected in the supernatants of 1×10^6 MIO-M1 cells treated (8.9 ± 1 ng/mL) or untreated (8.4 ± 1 ng/mL) with TNF-α. Although slightly higher levels of PRDX6 secretion was observed in supernatants of 1×10^6 hiPSC-MG cells (17.9 ± 10 ng/mL) and hESC-MG cells (17.9 ± 7 ng/mL) cultured with TNF-α, these were not significantly different from untreated cells (11.8 ± 5 ng/mL for hiPSC-MG cells and 16.6 ± 7 ng/mL for hESC-MG cells).

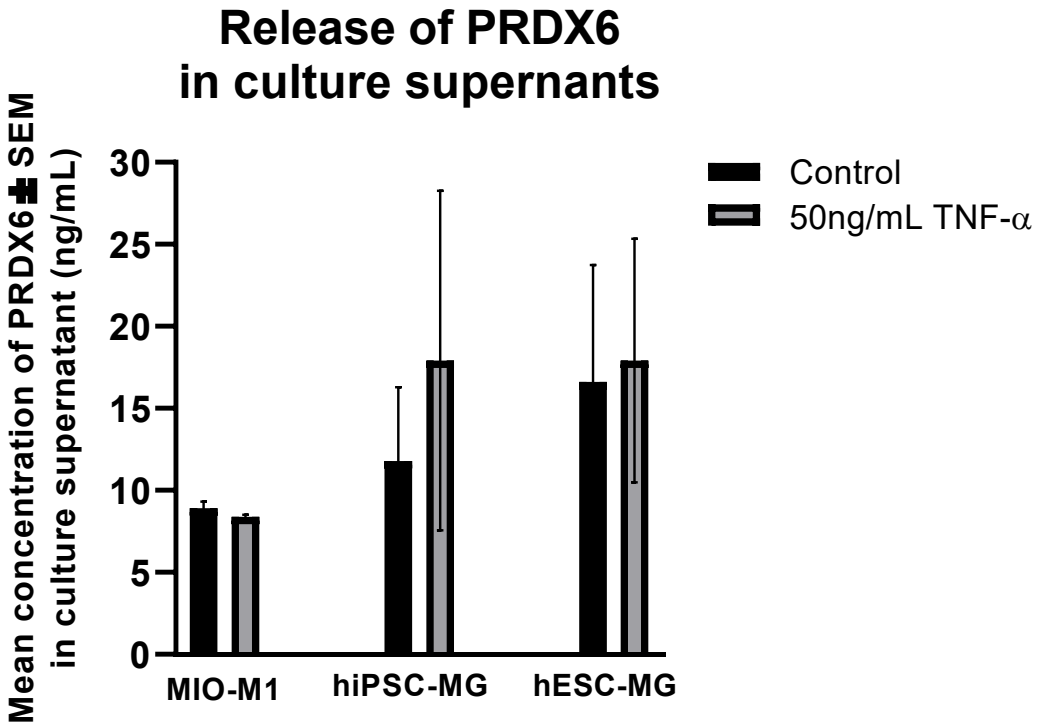

Figure 4.7 Mean protein levels of PRDX6 (ng/mL) detected by ELISA kit in culture supernatants of human Müller glia cultures.

Histogram represents the mean concentrations of PRDX6 ± SEM in culture supernatants of 1×10^6 cells of MIO-M1 cells (left), hiPSC-MG cell (middle) or hESC-MG cells (right) cultured with and

without 50 ng/mL TNF-α for 24 hours. No significant differences ($p > 0.05$) between the two conditions were observed; N=3.

Moreover, soluble HO1 was minimally detected (> 1pg/mL) by ELISA in control and TNF-α-treated MIO-M1 cells and there was no difference between these two conditions (

Figure 4.8). In contrast, both hiPSC-MG1 cells and hESC-MG1 cells secreted significantly higher levels of HO1 into supernatants at 15.1 ± 2 pg/mL and 30.2 ± 2 pg/mL for 1×10^6 cells respectively, when compared with MIO-M1 cells. In addition, a trend of upregulated release of HO1 was observed in hiPSC-MG1 cells (27.2 ± 5 pg/mL) and hESC-MG1 cells (49.2 ± 13 pg/mL) treated with TNF-α, despite no statistical significance was found as compared to their respective untreated cells.

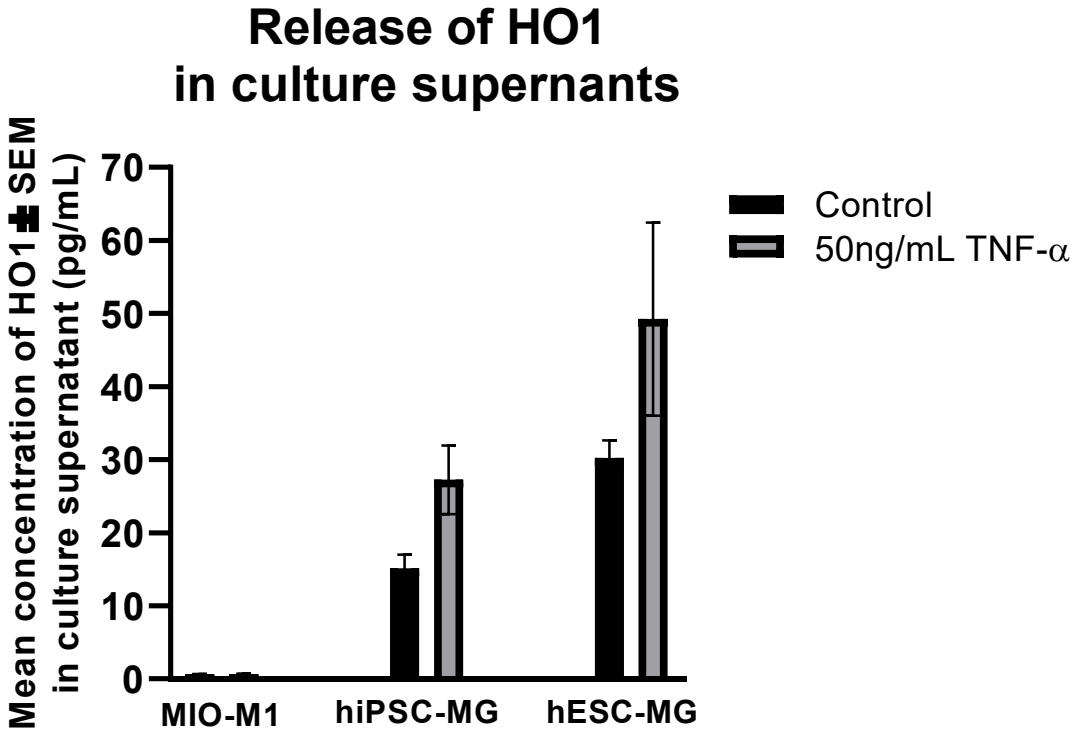

Figure 4.8 Mean protein levels of HO1 (pg/mL) detected by ELISA kit in culture supernatants of human Müller glia cultures.

Histogram represents the mean concentrations of HO1 ± SEM in culture supernatants of 1×10^6 cells of MIO-M1 cells (left), hiPSC-MG cell (middle) or hESC-MG cells (right) cultured with and without 50 ng/mL TNF-α for 24 hours. No significant differences ($p > 0.05$) between the two conditions were observed; N=3.

4.3.4 Effect of TGF-β1 on the expression of antioxidant enzymes by human Müller glia

MIO-M1, hiPSC-MG and hESC-MG cells were cultured with in the presence of 50 ng/mL of TGF-β1 for 24 hours. Light-phase images of the three Müller glia cultures showed that the characteristic bipolar morphology of MIO-M1 cells (

Figure 4.9A), hiPSC-MG cells (

Figure 4.10A), and hESC-MG cells (

Figure 4.11A) remained unchanged at the end of 24-hour culture. As revealed by trypan blue staining on cell pellets collected from the three Müller glia preparations, no cytotoxicity was induced in these cells by overnight incubation with TGF-β1.

Transcriptional modification of the neuroprotective and anti-oxidative regulators NRF2 and NFκB2 in three Müller glia preparations were firstly examined using RT-PCR analysis. A slight but not significant decrease in mRNA levels of NRF2 and NFκB2 were observed in MIO-M1 cells receiving TGF-β1 treatment (

Figure 4.9B). None of the antioxidant enzymes showed modification in both mRNA and protein levels in TGF-β1-treated MIO-M1 cells (

Figure 4.9B & C). Similarly, hESC-MG cells also exhibited a slight but not significant decline of mRNAs and proteins coding for NRF2 and NFκB2, as well as the antioxidant enzymes analysed following overnight culture with TGF-β1 (

Figure 4.11B & C). In hiPSC-MG cells, mRNA expressions of NRF2, NFκB2, SOD2, PRDX6, HO1, GCPII and PON2 were not modified by TGF-β1 (

Figure 4.10B) and western blotting analysis revealed consistent findings on the protein levels of all these antioxidant enzymes remained unchanged by TGF-β1 (

Figure 4.10C). In summary, these findings suggest that activation of TGF-β1 signalling did not significantly change the expression of antioxidant enzymes in MIO-M1, hiPSC-MG and hESC-MG cells.

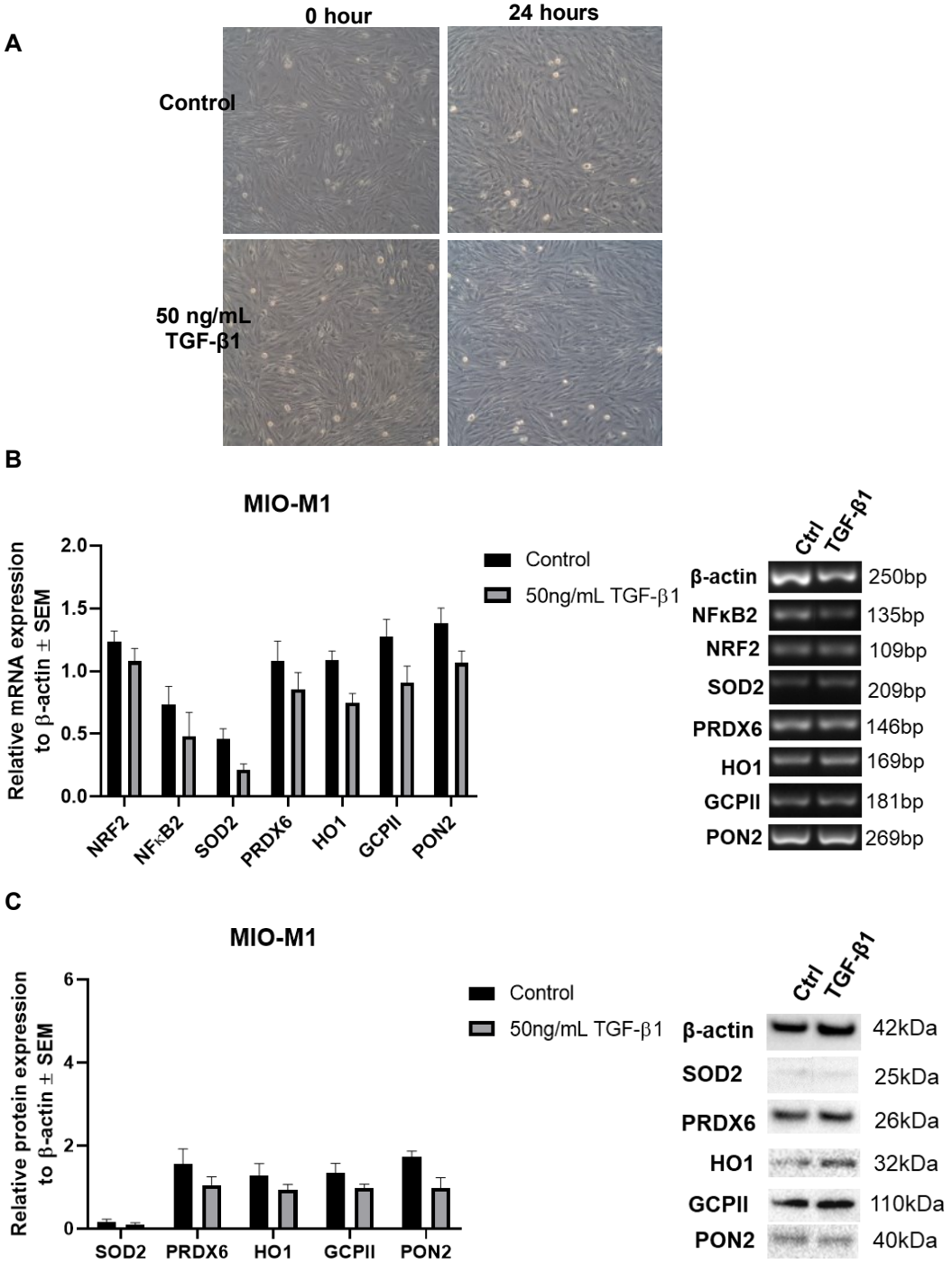

Figure 4.9 Effect of TGF-β1 on the expression of antioxidant enzymes in MIO-M1 cells.
(A) MIO-M1 cells exhibited characteristic bipolar morphology before (0 hour) and after (24 hours) treatment with 50 ng/mL TGF-β1. Untreated cells served as controls. **(B)** Histograms represent the mean expression of mRNA coding for the antioxidant enzyme ± SEM, from the optical density of RT-PCR bands normalised to β-actin. Representative RT-PCR bands and the respective molecular weights (bp) of antioxidant of interest are shown on the right. **(C)** Histograms represent the mean protein expression coding for antioxidant enzyme ± SEM from the optical density of western blotting bands normalised to β-actin. Representative western blotting bands and the respective molecular weights (kDa) of antioxidant enzymes are shown on the right. N=3, parametric t-test, $p > 0.05$.

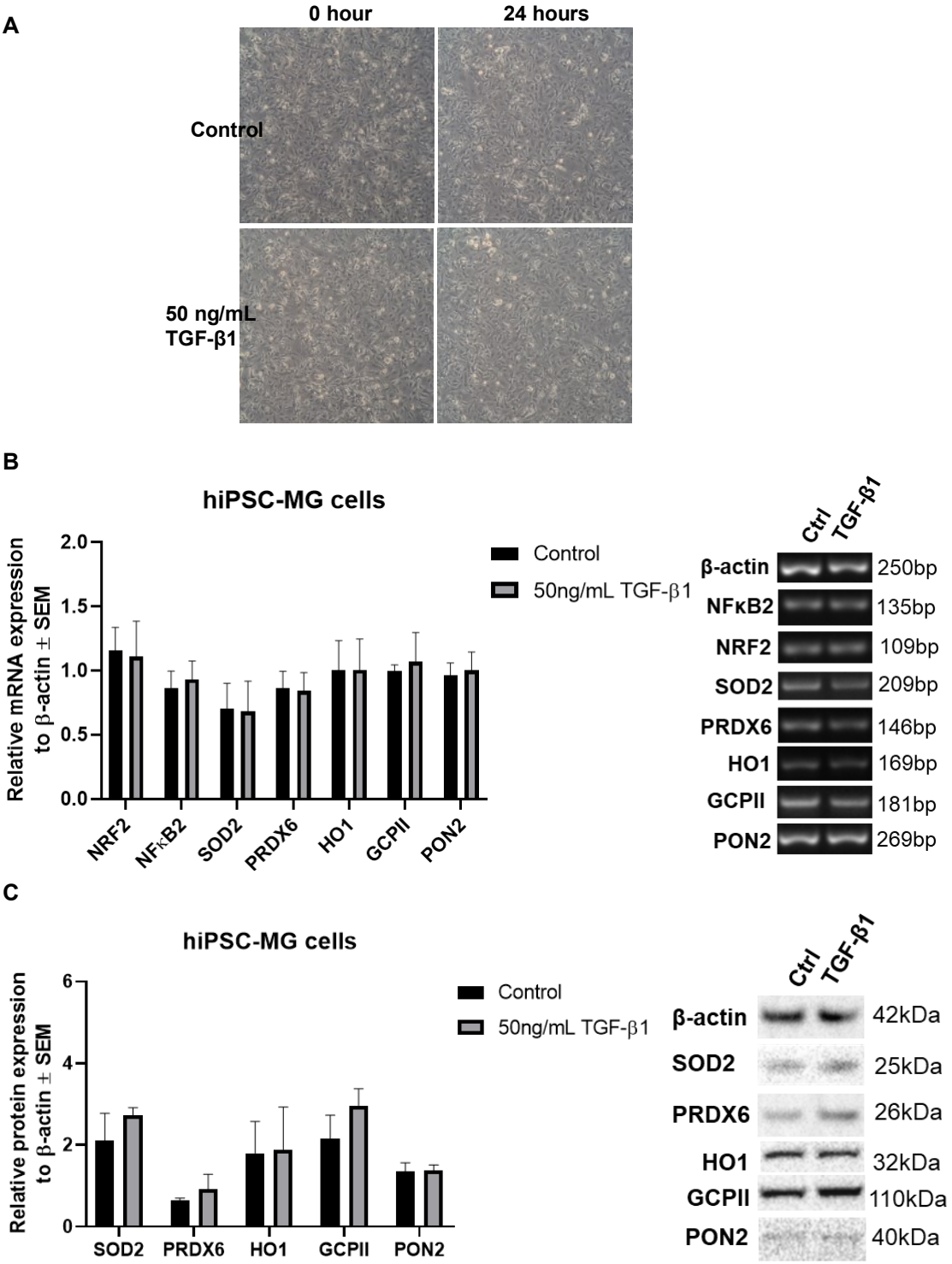

Figure 4.10 Effect of TGF-β1 on the expression of antioxidant enzymes in hiPSC-MG cells. (A) hiPSC-MG cells exhibited characteristic bipolar morphology before (0 hour) and after (24 hours) treatment with 50 ng/mL TGF-β1. Untreated cells served as controls. **(B)** Histograms represent the mean expression of mRNA coding for the antioxidant enzyme ± SEM, from the optical density of RT-PCR bands normalised to β-actin. Representative RT-PCR bands and the respective molecular weights (bp) of antioxidant of interest are shown on the right. **(C)** Histograms represent the mean protein expression coding for antioxidant enzyme ± SEM from the optical density of western blotting bands normalised to β-actin. Representative western blotting bands and the respective molecular weights (kDa) of antioxidant enzymes are shown on the right. N=3, parametric t-test, $p > 0.05$.

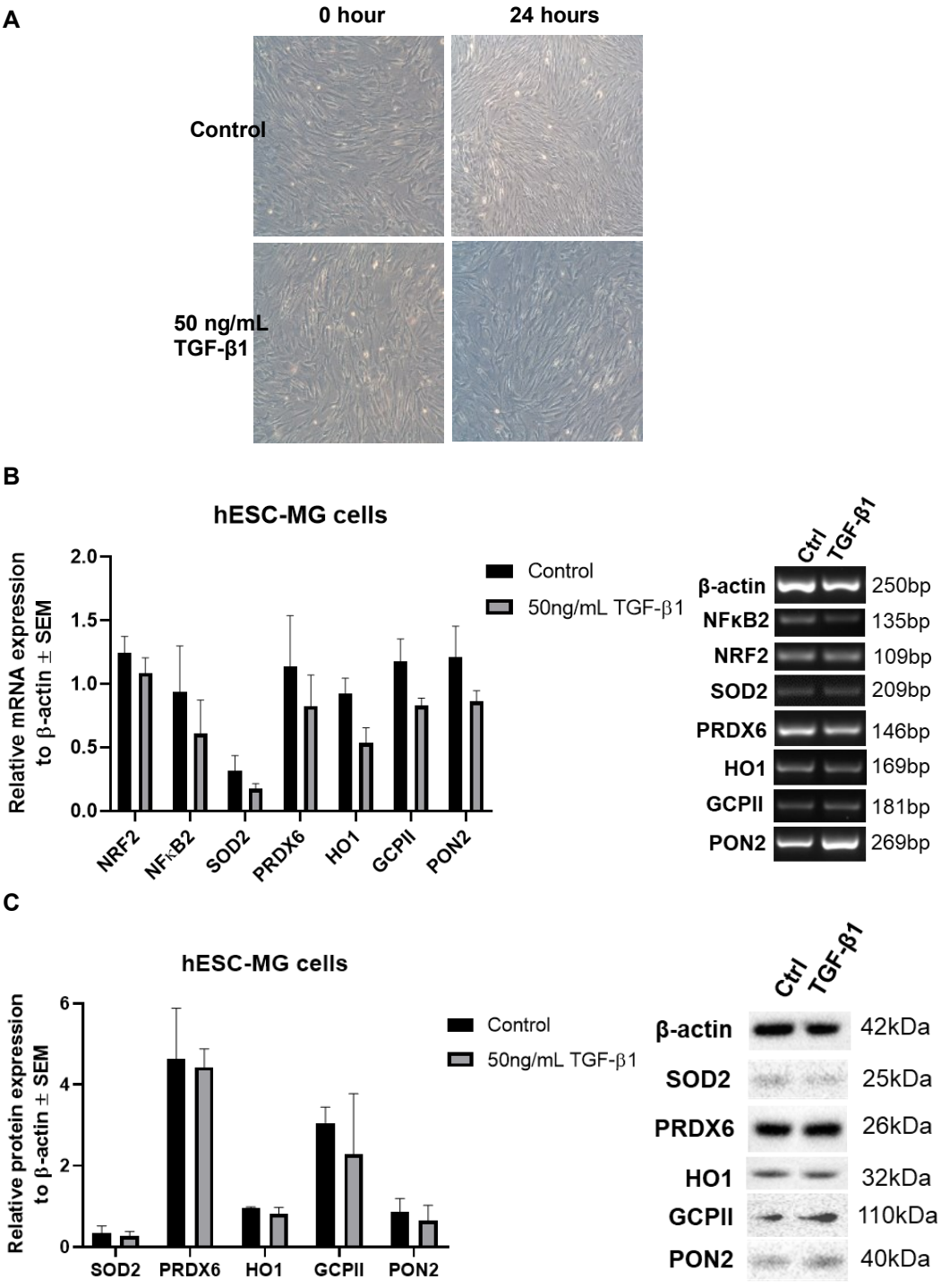

Figure 4.11 Effect of TGF-β1 on the expression of antioxidant enzymes in hESC-MG cells. **(A)** hESC-MG cells exhibited characteristic bipolar morphology before (0 hour) and after (24 hours) treatment with 50 ng/mL TGF-β1. Untreated cells served as controls. **(B)** Histograms represent the mean expression of mRNA coding for the antioxidant enzyme ± SEM, from the optical density of RT-PCR bands normalised to β-actin. Representative RT-PCR bands and the respective molecular weights (bp) of antioxidant of interest are shown on the right. **(C)** Histograms represent the mean protein expression coding for antioxidant enzyme ± SEM from the optical density of western blot bands normalised to β-actin. Representative western blot bands and the respective molecular weights (kDa) of antioxidant enzymes are shown on the right. N=3, parametric t-test, $p > 0.05$.

4.4 Discussion

4.4.1 Human Müller glia constitute a rich source of antioxidant enzymes in the neural retina

Müller glia have been known to maintain the homeostasis of cells in the neural retina by producing various neuroprotective factors (Reichenbach and Bringmann, 2010). In this study, Müller glia has been isolated from retinal organoids formed by hPSCs *in vitro,* for which is important to further explore the neuroprotective profile of these cells under normal conditions and upon stimulation with pro-inflammatory cytokines. The principle objective of this chapter was to examine the capacity of hiPSC-MG cells and hESC-MG cells to produce and release antioxidant enzymes when compared with Müller glia derived from human adult retina. Many antioxidant enzymes have previously described in experimental animal models, but their expression, localisation and sources have yet to been identified in human retina. The results from this chapter demonstrated that Müller glia constitutively produce a wide spectrum of antioxidant enzymes. Moreover, immunohistological staining of normal human retinal sections revealed that key antioxidant enzymes, including PRDX6, GCPII, PON2 and HO1 were distributed throughout the neural retina, overlapping the morphology of Müller glia as evident by GS and vimentin staining. The distinctive subcellular localisation of GCPII at the endfeet of Müller glia forming the nerve fibre layer might reflect their designated metabolic function, at which conversion of NAAG to glutamate primarily takes place at this site (Robinson et al., 1987). The enrichment of these antioxidant enzymes throughout the neural retina was not surprising as they are essential for maintaining the normal physiological function of the neural retina and most importantly for promoting cell survival during retinal degeneration. Extensive research has shown the importance of these neuroprotective factors for the normal function and survival of retinal neurons. For example, SOD2 deletion in animal models of glaucoma and AMD induces highly levels of oxidative stress and severely disrupts retinal cell functions (Biswal et al., 2016, Joe et al., 2015). Murine lens epithelial cells (LEC) are more susceptible to ROS-induced apoptosis as a result of PRDX6 deficiency (Fatma et al., 2011, Fatma et al., 2005), while overexpression of PRDX6 delivers neuroprotection to RGC cultured under hypoxia (Tulsawani et al., 2010). Loss of HO1 significantly induces

RPE degeneration (Pittala et al., 2017), and PON2 silencing significantly suppresses the resistance of RPE to oxidative stress, whereas its overexpression robustly reduces intracellular oxidative stress in HeLa cells treated with hydrogen peroxide (Ng et al., 2001, Jasna et al., 2014).

4.4.2 TNF-α treatment led to upregulation of neuroprotective factors

The previous chapter has unfolded the transcriptomic modification of human adult Müller cell line MIO-M1 cells by cytokine TNF-α and identified the activation of neuroprotective responses in these cells. The current chapter investigated the neuroprotective response of hiPSC-MG cells and hESC-MG cells to TNF-α and TGF-β1, in comparison with MIO-M1 cells. Both cytokines are present in the vitreous and the retina in various retinal degenerative disorders (Limb et al., 1991, Limb et al., 1994, Hoerster et al., 2014) and constitute an important trigger of oxidative stress in the neural retina (Yu and Welge-Lussen, 2013).

It has been previously reported that TNF-α released during retinal disease or injury induce Müller cells to secrete neurotrophic factors (Tezel and Wax, 2000). On this basis, this study compared the effect of this cytokine on the expression of antioxidant enzymes produced by MIO-M1, hiPSC-MG and hESC-MG cells. Unlike a previous study which reported upregulation of NRF2 mRNA in murine Müller cells stimulated by homocysteine within 24 hours (Navneet et al., 2019), in this study TNF-α did not modify NRF2 expression in human Müller glia derived from all sources investigated. Nevertheless, human Müller glia rapidly responded to TNF-α as evident by NFκB2 upregulation. The TNF-α-induced SOD2 upregulation observed in all Müller cell preparations was likely to be associated with the nuclear translocation of NRF2 (Jaiswal, 2004). Importantly, increased SOD2 is a sign of neuroprotective response of Müller glia to oxidative stress in the mitochondria (Fiers et al., 1999) and has been associated with neuroprotection. This is supported by an improved RGC survival and function observed in a rat model of glaucoma following SOD2 dietary supplementation or SOD2 overexpression (Nebbioso et al., 2013, Xiong et al., 2015). Overexpression of SOD2 in a mouse model of diabetic retinopathy also mitigates the reduction of GSH and total anti-oxidative capacity, protecting the retina from increased oxidative damage (Kowluru et al., 2006).

Moreover, the present results showed that expression of cytosolic and membrane-bound antioxidant enzymes such as PRDX6, HO1, PON2 and GCPII was not significantly altered in MIO-M1, hiPSC-MG and hESC-MG cells by TNF-α, although a consistent tendency for upregulation was observed. Given the possibility that ROS might diffuse out of the mitochondria into the cytosol, it may be possible that these constitutively expressed cytosolic antioxidant enzymes are sufficient to regulate the oxidative stressed in the cytosol, while SOD2 upregulation may be required to scavenge local ROS in mitochondria induced by electron transport chain (Nishikawa et al., 2000). Interestingly, several studies have reported that PRDX6 accumulation in the mitochondria can be stimulated by hypoxia-induced ROS (Ma et al., 2016, Eismann et al., 2009). It might be possible that in this study, recruitment of the constitutively expressed PRDX6 into the mitochondria might be sufficient to limit ROS within these organelles to regulate redox balance in Müller cells. Additionally, elevated HO1 and PON2 expressions have been documented in retinal neurons stimulated by oxidative stress, further reinforcing the hypothesis that TNF-α activated a neuroprotective response in Müller glia (Inman et al., 2013, Yong et al., 2010, Jasna et al., 2014).

The experimental observations presented in this chapter indicated that there appears to be a complex regulation of antioxidant enzymes in human Müller glia following acute treatment with TNF-α. Indeed, complex crosstalk between ROS, NFκB2 and NRF2 on regulating antioxidant enzyme expression has been extensively discussed (Figure 4.12) (Morgan and Liu, 2011, Wardyn et al., 2015). Firstly, multiple transcription regulators could modulate the expression of a single antioxidant enzyme. NRF2, NFκB and cell-type specific transcription factors co-regulate the expression of PRDX6 (Sharma et al., 2003, Fatma et al., 2005, Kubo et al., 2006), SOD2 (Das et al., 1995, Djavaheri-Mergny et al., 2004), HO1 (Lin et al., 2007) and NQO1 (Yao et al., 1997). In most cases, NFκB is shown crosstalking to JNK pathway which sustains the transcription of target genes with anti-oxidative and pro-survival properties (Morgan et al., 2008). However, NFκB could also activate pro-oxidative genes such as p53 and NOX2 which may result in cell death (Gloire et al., 2006, Perkins and Gilmore, 2006). Specifically, activation of anti-oxidative genes is mediated by the p65 subunit of NFκB complex and the crosstalk between NRF2 and NFκB involves proteins that commonly interact with both

signalling mediators including CBP, p62 and sMaf (Figure 4.12) (Wardyn et al., 2015). The scaffolding protein p62 could feed into NFκB signalling pathway by activating TNF-α receptor associated protein 6 (TRAF6), further enhancing NRF2 activity (Wooten et al., 2005). In addition to its acetylation activity, CBP has a higher affinity to binding the phosphorylated p65 and with the help of sMaf which promotes acetylation of p65 by CBP, this protein complex might drive activation of NFκB signalling (Sun et al., 2009, Liu et al., 2008). Therefore, the competition between p65 and NRF2 might be important to influence the cytokine-induced oxidative stress or neuroprotective effects. Crosstalk could also occur between antioxidant enzymes to modulate their anti-oxidative activity. This is illustrated by studies in which supplementation of CQ10A in the diet to a mouse model of glaucoma significantly delayed the oxidative stress-induced degeneration of RGCs, as evident by increased expression of HO1 and SOD2, as well as reduction of proteins involved in apoptosis is ameliorate increased (Lee et al., 2014b). Induction on the expression and activity of HO1 results in elevated levels of SOD and catalase in the endothelial cells of a diabetic rat model (Turkseven et al., 2005), it might be possible that similar effects might be elicited by cytokines in Müller glia.

In this study, quantitative ELISA analysis of soluble PRDX6 and HO1 in culture supernatants of three Müller glia cell preparations showed that in addition to constitutively releasing both trophic factors into the extracellular environment, hiPSC-MG and hESC-MG cells also showed incremental production of these antioxidant enzymes in response to TNF-α stimulation. The capacity of Müller glia to release neuroprotective factors during degenerative processes might contribute to the survival of neighbouring retinal cells, as a result of uptaking these factors. Although extracellular release of PRDX6 has yet to be documented, there is evidence that PRDX6 translocation to cell membrane occurs following external stimuli in corneal endothelial cells and neutrophils (Ambruso et al., 2012, Ding et al., 2014). Supplementation of PRDX6 effectively alleviates oxidative damage generated by hypoxia, cytokine-mediated inflammation, UV exposure and hyperglycaemia and reduces apoptosis of RPE (Zha et al., 2015), retinal pericytes (Kubo et al., 2009) and RGCs (Fatma et al., 2008, Tulsawani et al., 2010). Co-culturing mesenchymal stem cells overexpressed with HO1 with RGCs attenuates apoptotic RGC death (Li et al., 2017), indicating that hydrogen peroxide-induced

ROS mitigation might possibly be achieved by extracellular release of HO1. Moreover, the observation that hiPSC-MG cells and hESC-MG cells showed higher extracellular release of PRDX6 and HO1 than that MIO-M1 cells suggests that retinal organoid-derived Müller glia might have a better neuroprotective capacity than human adult cells. In summary, it can be concluded that the *in vitro* responses of hiPSC-MG cells and hESC-MG cells to TNF-α on the expression of antioxidant enzymes were highly similar to the biological responses of MIO-M1 cells, and an immediate endogenous neuroprotective mechanism was identified in these cells.

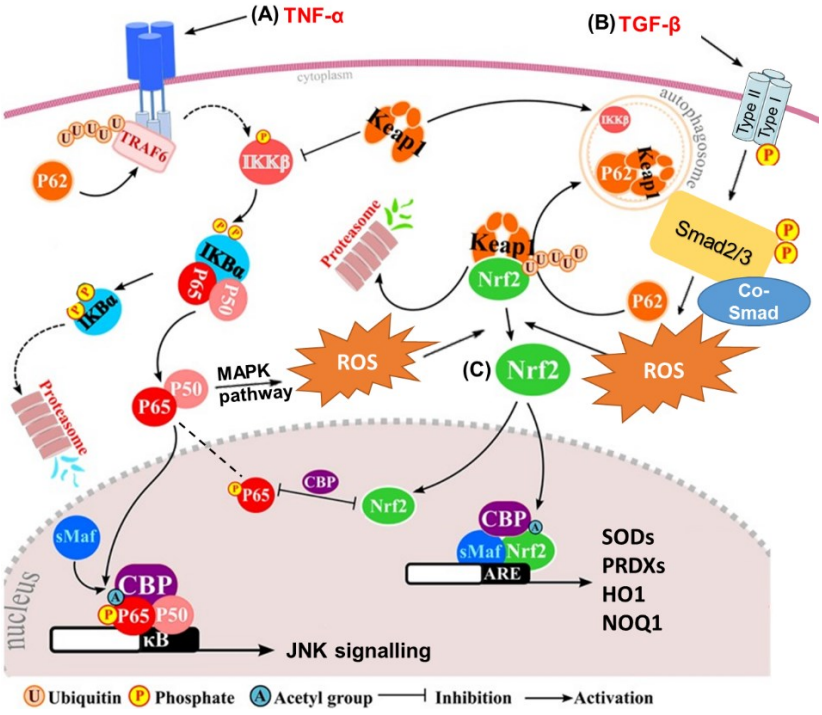

Figure 4.12 Schematic illustration of molecular crosstalk between cytokine (TNF-α/TGF-β1) - mediated ROS, NRF2, and NFκB on the expression of antioxidant enzymes.
(A) TNF-α binding to its receptors results in phosphorylation of the inhibitory complex IκB, releasing the NFκB complex consisting of p65 and p50. Activation of NFκB complex induces prolonged activation of MAPK pathway and elevation intracellular ROS. **(B)** Binding of TGF-β1 ligands to type II receptor induces formation of type II and type I receptor complex, with activating of the type II kinase activity that phosphorylates type I receptor. Subsequently the kinase domain on the type I receptor kinase phosphorylates Smad2/3 followed by binding to its co-factor Co-Smad, before activating ROS generation via canonical or non-canonical signalling cascades. **(C)** NRF2 normally binds to Keap1 and the ubiquitinated complex undergoes proteasome degradation. Cytokine-induced ROS causes structural modification of Keap1 and releases NRF2 which then translocates to the nucleus. NRF2 forms a complex with CBP and sMaf, which binds to the ARE at the promotor site, driving the downstream anti-oxidative genes such as SODs, PRDXs, HO1 and NQO1. ROS induced by NFκB (A) and Smad (B) activates NRF2 (C) and the crosstalk between these signalling pathways is possibly mediated by CBP, p62 and sMaf. This figure was partially adapted from (Wardyn et al., 2015) and reproduced using Servier Medical Arts (https://smart.servier.com).

4.4.3 TGF-β1 did not significantly modify anti-oxidative capacity in human Müller glia

The highly similar neuroprotective expression profiles of MIO-M1, hiPSC-MG and hESC-MG cells was also observed in the investigation involved TGF-β1 treatment and the findings indicated that this cytokine did not significantly modify anti-oxidative capacity of these Müller glia cells within 24 hours. Although the underlying regulatory mechanism on the modification of antioxidant enzymes mediated by TGF-β1 remains unknown, previous studies using other human airway smooth muscle cells and murine LECs suggested that TGF-β1 influence the expression of antioxidant enzymes by activating its downstream canonical Smad pathway (Figure 4.12) (Michaeloudes et al., 2011, Fatma et al., 2009a, Liu and Desai, 2015). Following binding of TGF-β1 to its transmembrane type II receptor, ROS production by TGF-β1 signalling is mainly mediated by Smad2/3 and its co-factors which in turn induce NRF2 nuclear translocation. Although direct activation of NFκB by TGF-β1 signalling is not documented, interestingly, other studies reported that TGF-β1 is likely to interfere PRDX6 expression via NFκB2, as previous studies reported that NFκB2 point mutation abrogates PRDX6 expression (Gallagher and Phelan, 2007, Fatma et al., 2009a). Nevertheless, TGF-β1-mediated reduction of antioxidant enzymes does not necessarily suggest that MIO-M1, hiPSC-MG and hESC-MG cells did not exhibit neuroprotective response against TGF-β1 signalling. For example, despite its downregulation by TGF-β1, the constitutively expressed PRDX6 nevertheless reduced oxidative stress in trabecula meshwork cells (Fatma et al., 2009b). Therefore, future study should also incorporate measurements of the metabolism of antioxidant enzymes to facilitate the understanding on the *in vitro* relationship between the enzymatic activities of these factors to the incremental intracellular ROS levels following cytokine treatment. The findings discussed here add to knowledge of how the complex gene network is changed during oxidative stress and should merit further investigation to understand the underlying mechanism of TGF-β1 regulating antioxidant enzyme expression in Müller glia upon long-term culture.

4.4.4 Limitation of study

The majority of the experimental work presented in this chapter has attempted to validate the expressions of antioxidant enzymes in Müller glia caused by TNF-α and TGF-β1 upon short-term stimulation. A limitation in the experimental design was that it did not examine the effect of these cytokines in a long-term culture. Further studies may seek to evaluate the expression and release of these antioxidant enzymes in hiPSC-MG cells and hESC-MG cells following longer incubation (3-6 days) with TNF-α and TGF-β1. Elucidation of the factors that regulate the transcription and release of these antioxidant enzymes may aid in the identification of targets to support the application of hiPSC-MG cells and hESC-MG cells as cell-based therapies to deliver neuroprotection to degenerative retinae.

CHAPTER 5 Evaluation of the neuroprotective effect of retinal organoid-derived Müller glia on retinal ganglion cells

5.1 Introduction

5.1.1 Early development of mammalian RGCs

Receiving, processing and relaying visual information from amacrine and bipolar cells to the lateral geniculate nucleus (LGN) and superior colliculus in the central nervous system (CNS) is the primary responsibility of RGCs. These cells constitute one of the most important cell types within the neural retina, yet only account for less than 1% of the total neural retinal cell population (Masland, 2012, Smith and Chauhan, 2015).

RGCs are the earliest retinal neurons formed during embryonic development. In rodents, their first appearance has been reported to occur during embryonic (E) day 10 in mouse (Muzyka et al., 2018) and E14 in rat (Reese and Colello, 1992). Once RGC progenitors migrate to the designated GCL, their fate specification into various subtypes is driven by transcription factors including Brn3A, Islet2, Tbr2, Satb1 and Satb2 (Sweeney et al., 2019, Muzyka et al., 2018). Following differentiation, dendritic outgrowth of RGCs occur as the same time as their synaptogenesis with other retinal cells develop (Sernagor et al., 2001). The establishment of synapses between RGCs and the superior colliculus occurs between E16 and P5 in rats (Reese and Colello, 1992). The survival of RGCs is signal-dependent and the underlying mechanism is regulated by neurons competing for limited availability of surviving signals by sending axons to form synapses with target neurons in the brain (Meyer-Franke et al., 1995, Acheson et al., 1995). The peak at which RGCs that fail to synapse with the superior colliculus commit suicide is at P3-5 (Schmid and Guenther, 1996) and P2-5 (Young, 1984) in rat and mouse respectively.

5.1.2 Morphological and molecular features of RGCs

The heterogeneity of RGCs has been demonstrated by histological and electrophysiological studies on the CNS. Classification of RGCs has been revised by various studies using improved intracellular tracing and imaging techniques that enables in-depth illustration of RGC dendritic patterns and that has led to newly discovered RGC subtypes (Masland, 2012). Three major subclasses of rat RGCs are grouped according to features of soma area, projection patterns of dendritic field and response to electrophysiological stimuli (Sanes and Masland, 2015). However, these physiological properties show some overlap and have therefore posed challenges for accurate characterisation. Rat RGCs with large soma and large dendritic field fall in group A (RG_A) or type I, while group B (RG_B) or type II contains cells with small soma and small dendritic distribution which accounts for the most common RGC subclass (Thanos, 1988). Smaller RGCs are classified as group C (RG_C) or type III that represents RGCs with small soma but large dendritic field (Sun et al., 2002).

Healthy RGCs normally display characteristic features with continuous plasma membranes, no signs of vacuolation in the round soma, and well-developed neuritic processes with 2-5 primary branches of neurites (Sun et al., 2002). The number of bifurcations at which secondary and fine neurites branch out from major dendrites and form expansion of dendritic processes are good indications of neuritogenesis and structural integrity of RGCs. A group of molecular markers has been extensively used for illustrating RGC morphology which can be modified by external insults including glutamate excitotoxicity, facilitating the evaluation of neuronal injury using these molecular features. Membrane integrity and intracellular features could be visualised by staining with the neural specific β-III tubulin (TUJ), that identifies the microtubules of the cytoskeleton (Jiang et al., 2015). Broken processes or loss of neurites, presence of vacuole structures in the cytoplasm and membrane discontinuity are the common characteristics of damaged RGCs and can be illustrated by TUJ. Another pan-RGC surface marker is the glycoprotein Thy-1/CD90. Initially identified in the somata and dendrites of neurons dissected from rodent brain, the Thy-1 surface antigen was shown to mediate intercellular interactions (Barclay and Hyden, 1979). Its enriched expression on rat RGCs was later confirmed by

subsequent studies (Beale and Osborne, 1982). DAPI counterstain in these cells is useful for assessing nuclear changes such as condensation, fragmentation and pyknosis that are normally associated with glutamate toxicity (Kritis et al., 2015). Apart from the abovementioned transcription factor Brn3A that constitutes a nuclear marker, there are additional RGC markers that have been increasingly identified and used in more studies. For example, γ-synuclein can be found in the cytoplasm of RGCs in human and rat RGCs (Surgucheva et al., 2008), while RNA-binding protein with multiple splicing (RBPMS) is expressed in the nucleus and cytoplasm of RGCs (Rodriguez et al., 2014).

5.1.3 Glutamate excitotoxicity as a cause of glaucoma

5.1.3.1 RGC involvement in glaucoma

One of the most prevalent retinal degenerative disorders associated with progressive and irreversible loss of RGCs is glaucoma (Tham et al., 2014). Elevation of the IOP constitutes a major risk factor associated with this condition, but other risk factors include nitric oxide (NO)-mediated toxicity (Neufeld AH, 2002) and glutamate excitotoxicity (Hahn et al., 1988). Despite the contribution of these factors being recognised, the underlying molecular mechanisms responsible for the pathogenesis of glaucoma remain poorly understood.

Glutamate excitotoxicity is thought to result from a prolonged excitatory stimulation by the endogenous excitatory neurotransmitter glutamate, which mediates a variety of neurotransmission activities in mammalian CNS (Fonnum, 1984), including learning and memory (Zhou and Danbolt, 2014). Within the retina, glutamate constitutes the principal neurotransmitter and stimulates the ionotrophic N-methyl-D-aspartate (NMDA) receptors on RGCs to produce excitatory responses. Upon glutamate binding, NMDA receptor allows the entry of calcium ion on a non-selective basis into RGCs, causing depolarisation of the resting potential of RGCs from -65 mV to nearly 0 mV (Seki and Lipton, 2008). The increased intracellular concentration of calcium acts as a secondary messenger to induce an additional signalling cascade (Kritis et al., 2015). Overstimulation by glutamate affects nearly all retinal

neurons (Mehta et al., 2013) and RGCs are the most sensitive to glutamate (Li et al., 1999). This process leads to excessive calcium influx and mitochondrial dysfunction, as well as increased oxidative stress and the release of pro-apoptotic factors by RGCs (Li et al., 1999, Mehta et al., 2013, Ju et al., 2015).

5.1.3.2 Current treatments for glaucoma

To date, no effective treatment is available to prevent RGC loss or reverse the damage on RGCs. The control of glaucoma progression by lowering IOP through surgical and pharmacological intervention constitutes the current management. Pharmacological approaches target the ciliary body and the trabecular meshwork (TM) by suppressing the production of aqueous humour and promoting fluid drainage from the anterior chamber through the TM. Topical eye drops of α-agonists, β-adrenoceptor antagonists, carbonic anhydrase inhibitors, cholinergic agents and prostaglandin analogues are commonly used as neuroprotective agents as they reduce oxidative stress on the optic nerve and neuro-inflammation caused by high IOP (Gauthier and Liu, 2017). They are prescribed drugs as the first-line treatment but have been strongly associated with side effects. Alternative surgical procedures aim to divert drainage of aqueous humour into the subconjunctival space by laser treatment.

5.1.3.3 Neuroprotection of RGCs

RGC survival could be promoted by neuroprotective strategies as evidenced by early studies showing that neurotrophin supplementation promotes RGC survival and prevents apoptosis *in vitro* (Meyer-Franke et al., 1995). Using *in vitro* glutamate excitotoxicity on RGC cultures, the therapeutic potential of small molecules that eliminate toxic molecules such as glutamate and NO have produced promising results on the optic nerve (Sena and Lindsley, 2017). Small molecules including antioxidant glutathione and Coenzyme Q10, α-lipoic acid and superoxide dismutase have been shown to promote RGC survival and are thought to have potential for therapeutic development (Gauthier and Liu, 2017). RGCs treated with the

glycoprotein erythropoietin (EPO) improve their survival upon glutamate-induced neurotoxicity. The underlying mechanism is thought to be due to activation of the STAT5/JAK signalling cascade that leads to anti-apoptosis and anti-oxidation (Siren and Ehrenreich, 2001, Chang et al., 2013). PEDF derived from RPE and Müller glia has also shown to confer protection to RGCs (Ogata et al., 2001, Pang et al., 2007). Moreover, the neuroprotective effect of an acetylcholinesterase (AChE) inhibitor bis(7)-tacrine was suggested to be owning to its interference on the binding of glutamate to NMDA receptors (Fang et al., 2010). Another synthetic IOP-lowering agent, known as Brimonidine has shown neuroprotective properties by targeting the α2-adrenergic receptors on RGCs and promoting RGC survival upon glutamate and hypoxia neurotoxicity (Lee et al., 2010c).

Another source of neurotrophic factors is the cell-free conditioned medium (CM) concentrated with a broad spectrum of endogenous factors including cytokines, growth factors, antioxidants and exosomes (Monsel et al., 2016, Duarte et al., 2016). CM can be harvested from the supernatants of monolayer cultures in either serum-rich or serum-free medium, under either normoxic or hypoxic conditions (Veronesi et al., 2018). Early studies showed that the CM derived from human stem cells delivers trophic support to damaged cells relying on the paracrine mechanism, promoting anti-inflammatory and proliferative response in the recipient cells (Baraniak and McDevitt, 2010). Studies showed that Müller glia supernatants contain a panel of known growth factors and cytokines that are common constituents of CM derived from hESCs (Araujo et al., 2018). For example, TNF-α, IL-1β, IL-6, TSP-1 and VEGF were described by several studies while proteins regulating ECM homeostasis including MMP2 (Rodrigues et al., 2013) and MMP9 (Chau et al., 2008) were also found released by human Müller cells. Co-culture of rat Müller glia with rat RGCs have demonstrated the survival of these cells following neurotoxicity induced by glutamate and NO, which presumably was associated with glutamate uptake and release of neuroprotective factors by Müller glia (Kawasaki et al., 2000). Recently, an in-depth mass spectrometry analysed the proteomic content of porcine Müller glia CM and identified several key factors that promote survival of RGCs (Ruzafa et al., 2018). Amongst them, basigin and osteopontin were shown to promote RGC survival by promoting normal neuronal function and neuroprotection to photoreceptors. Therefore, CM collected from factor-rich cell cultures such as

Müller glia may harbour promising therapeutic prospect for retinal degeneration with the advantage of low risk on immunogenicity.

5.1.4 Available culture models for RGC degeneration

Several culture models of RGCs have been used to explore RGC survival and axon regeneration. Most common models include retinal explant cultures, purified primary RGC cultures and proliferative RGC cell lines. Each model examines different aspects of RGC and have some limitations.

5.1.4.1 Retinal explant cultures

Because of the limited availability of post-mortem human retina, retinas isolated from various mammalian animal models have been favoured for *ex vivo* culture. Several factors influence the success of retinal explant culture, for example substrates such as ECM proteins (Hopkins and Bunge, 1991) or culture inserts (Carter and Dick, 2004) aid to maintain the intact structure of retinal explants, whilst supplementation with growth factors, serum and antimicrobial agents promote better cell growth (Osborne et al., 2016). However, many physiological features of the neural retina, including intraocular pressure and blood circulation cannot be recapitulated in retinal explants *in vitro* (Murali et al., 2019). For example, the macula found in human retina is absent in rodent and feline retinas (Murali et al., 2019). Another striking anatomical variation between human and rodent retina is the density of RGCs per unit area, with the average RGC population in human retina being at least 3 times denser as compared to rat retina (Curcio and Allen, 1990, Danias et al., 2002).

5.1.4.2 RGC cell lines

Mammalian cell lines constitute an important research tool owning to their close resemblance to cells *in vivo*. Over 200 studies investigating the neurobiology of RGCs (Tanwar et al., 2010, Lee et al., 2010b) have employed the RGC-5 cell line.

This immortalised cell line was transformed from primary rat RGC culture using adenovirus (Krishnamoorthy et al., 2001) and shows markers of characteristic RGCs, including expression of the surface marker Thy-1 and dependency on neurotrophins for survival (Agarwal et al., 2007). However, the nature of RGC-5 cell line has been questioned as many studies failed to produce glutamate excitotoxicity in RGC-5 cells and its origin was later confirmed to be a mouse photoreceptor cell line (Van Bergen et al., 2009). This leads to retraction of the original paper and widely misled the research community and funding authorities. It is suspected that the mischaracterisation of RGC-5 was due to cross-contamination from the mouse 661W photoreceptor cell line (Krishnamoorthy et al., 2013). Unfortunately, to date there is no other mammalian RGC line available, and the challenge of producing one such cell line is limited by the nature of RGCs, which lose their proliferation potential after making axonal synapses during retinal development (Galvao et al., 2018).

5.1.4.3 Primary RGC culture

Primary RGC culture purified from rodent retina is commonly used for the development of novel neuroprotective therapeutics targeting optic neuropathies. Despite the laborious procedure to isolate these cells, establishing primary RGC culture has some advantages. Rodent RGCs have shown both morphological and physiological similarly to human RGCs and is thought to constitute the most appropriate *in vitro* model to study RGCs. Primary RGCs can be obtained using a well-defined protocol in which enriched RGC populations are purified from retinal tissue based on the surface antigen Thy-1/CD90 (known as CD90) on RGCs. It is noteworthy that Thy-1/CD90 is not an exclusive marker for RGC as macrophages and amacrine cells also express Thy-1/CD90 (Barres et al., 1988), therefore relying on surface antigen recognition of Thy-1 produces an enriched population of RGC rather than a truly purified population. One drawback of primary rodent RGC culture is the short culture period as the survival of these primary cells is limited to up to 3-4 weeks maximum (Fang et al., 2018). Extensive remodelling of the dendritic network of RGCs is commonly known as ‘pruning’ after long-term culture *in vitro*. Nevertheless, primary RGC culture is useful for testing the neuroprotective effect of

putative agents during short *in vitro* incubation periods for up to a week (Gao et al., 2016).

5.1.5 Protocols to establish primary RGC culture

The most commonly used rat species to obtain RGCs are Sprague Dawley (SD) rats (Ruzafa et al., 2018), as these are albino rodents that have melanin-free RPE (Huxlin and Goodchild, 1997). The age of donor pups is crucial for the long-term survival of purified RGCs in culture. Early work from Goldberg's group (Corredor et al., 2012, Steketee et al., 2014) used early postnatal (P1-9) SD rats as it was shown that P5 retinae would give a larger yield of enriched RGC cells as compared with P8 retinae. This is due to the building of extracellular matrix during early postnatal development, which makes the dissection more difficult after P5 (Steketee et al., 2014). Another work by Ma and Taylor compared the yield of RGCs isolated from neonatal pup retinae at P0, 4, 8 to that of adult retinae and reported that both the yield and survival of RGCs dropped as the animals grow. Moreover, early postnatal RGCs can exhibit extended neurite features much quicker than the adult counterparts (Ma and Taylor, 2010).

5.1.5.1 Flow cytometry sorting

The rationale behind flow cytometry sorting is such that retinae are firstly dissociated to single cell suspension and macrophages are excluded using a specific macrophage monoclonal antibody before cell sorting using a conjugated antibody specific to the surface antigen Thy-1/CD90 (

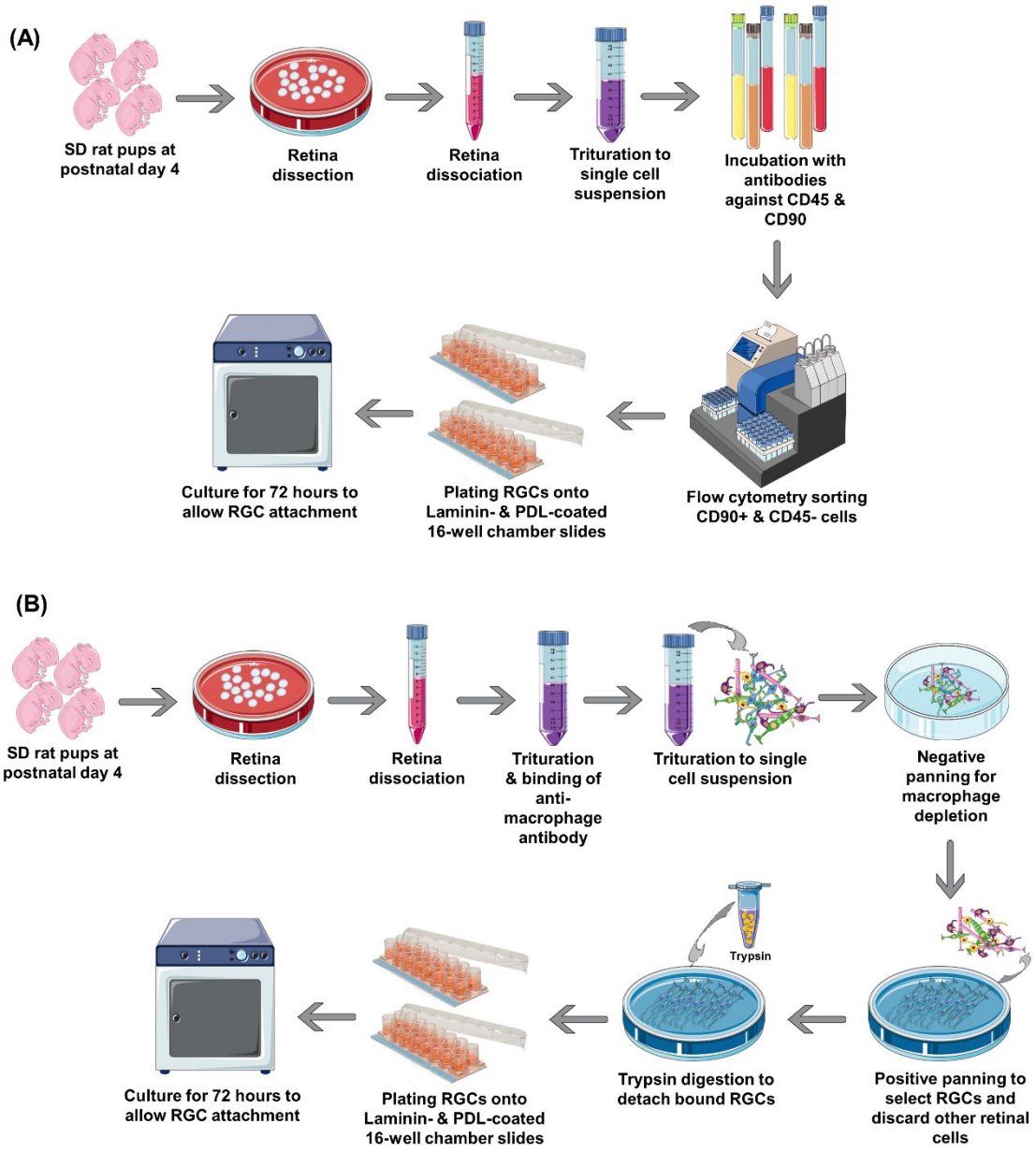

Figure 5.1A). A highlight of this approach is that a purified RGC population can be sorted from mix population of retinal cell suspension within a relative short period. However, tuning the gating to ensure population purity requires expertise and knowledge. Flow cytometry sorting is least favoured among other alternatives as the process sacrificed cell viability. This is due to the treatment of retinae cell suspensions with flow cytometry antibodies on ice and most importantly, to the later mechanical stress caused by the sorting process. Despite these issues, flow cytometry sorting is suitable for conducting in-depth content analysis of biochemical and morphological characteristics of RGCs (Chang et al., 2012).

5.1.5.2 Two-step immunopanning (TIP)

The original protocol introduced by Barres and colleagues in 1988 (Barres et al., 1988) has been improved by various groups according to specific rodent types (Winzeler and Wang, 2013a). TIP method consists of dissociating retinae of perinatal rats to a single cell suspension, followed by a series of negative and positive selection of cell populations by antibodies against unwanted cells and RGCs (

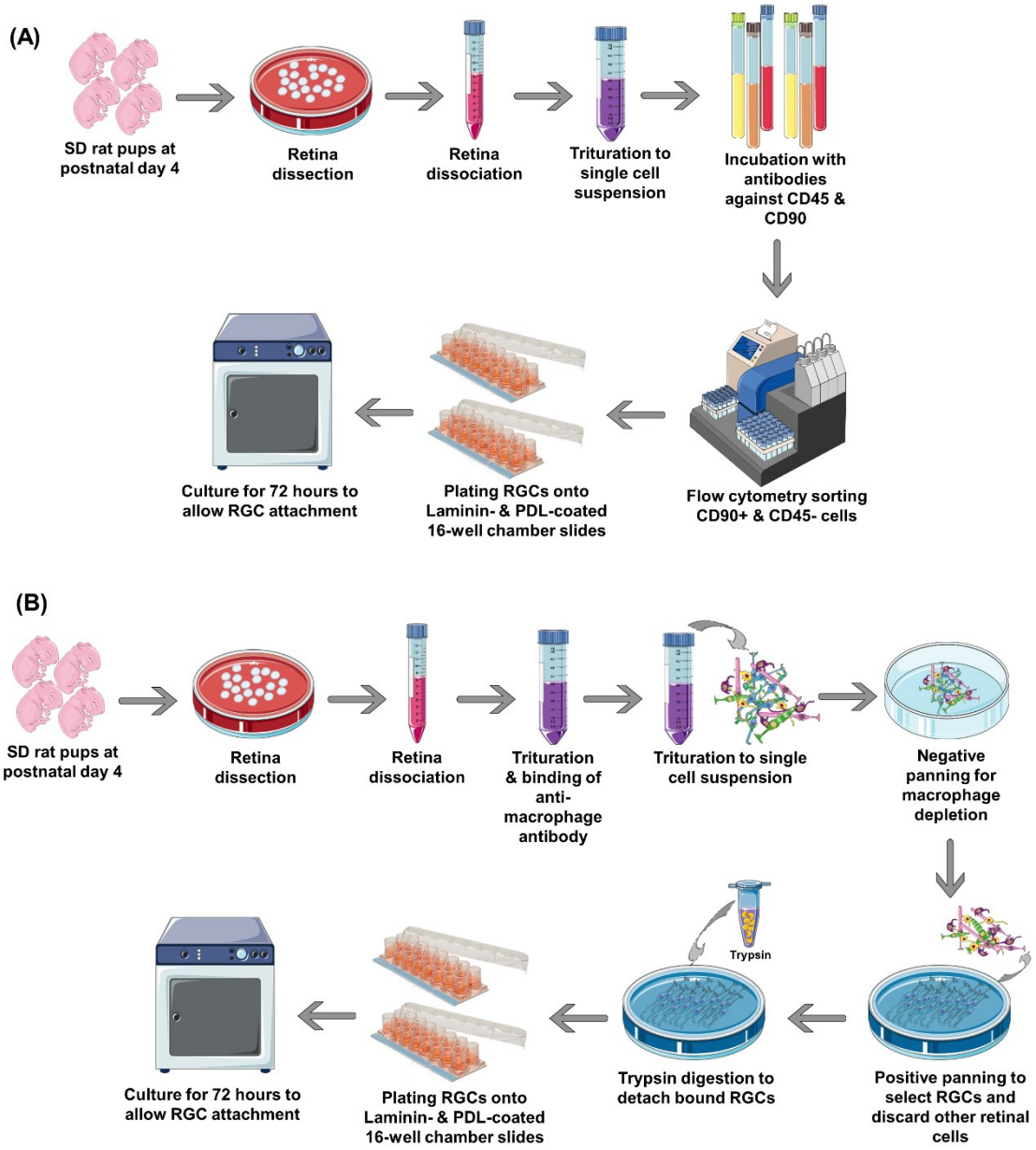

Figure 5.1B). Firstly, single cell suspensions are triturated with low percentage protein solution containing anti-macrophages antibodies. This is followed by two negative

panning step which removes unwanted cells such as amacrine and macrophages by incubating single cell suspensions in lectin-coated plates pre-coated with secondary antibody specific to anti-macrophages antibodies. Next, macrophage-depleted suspension is transferred to a positive panning plate pre-coated with Thy-1/CD90 antibody to bring down RGCs. TIP produces a rather enriched RGC population while other Thy-1^{+}-cells including macrophages and amacrine cells might be still present in the culture. The morphology of purified RGCs is also much improved compared to those purified by flow cytometry, displaying long dendrites and uniform somata as early as 24 hours following plating (Gao et al., 2016).

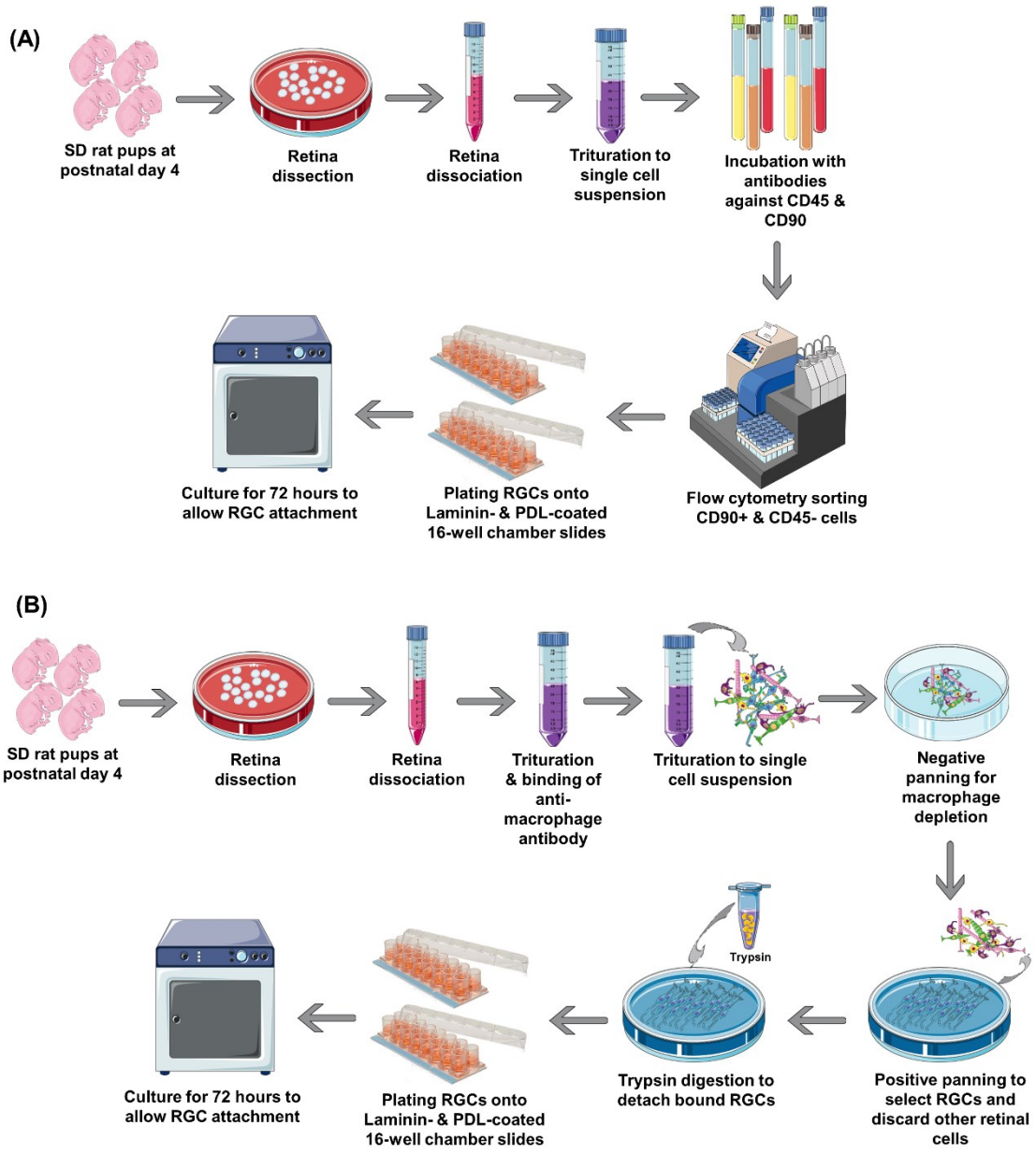

Figure 5.1 Work flow of purifying rat RGCs by flow cytometry sorting (A) and two-step immunopanning (B).

(A) Retinae from P4 SD rat pups were isolated and transparent membrane with blood vessels coursing through was removed. Retinae were dissociated and triturated to single cell suspension which was incubated with conjugated antibodies specific to CD45 and CD90. Cell suspension was sorted through a flow cytometry facility, isolating only $CD45^{-}$&$CD90^{+}$ cells. Purified cells were plated to pre-coated culture chambers and cultured for 72 hours in recommended serum-free medium before further treatment. **(B)** Retinae were dissected and isolated as described in (A), followed by gentle trituration by protein solution containing anti-macrophage antibody. Binding of antibody to macrophage was encouraged by further trituration before plating single cell suspension to negative panning plate pre-coated with specific secondary antibody. Unbound cell suspension was transferred to positive panning plate pre-coated with Thy-1 antibody for selection of Thy-1^{+}-RGCs. Bound cells were detached by trypsin digestion and plated as described above. This image was produced using Servier Medical Arts (http://smart.servier.com).

5.2 Objectives and experimental outline

Examination of the neuroprotective characteristics of hESC-MG1 on RGCs can be facilitated by the use of cells isolated from the new-born rodent retinae. Therefore, the objectives of this chapter were as follows:

1. To assess the feasibility of available protocols to establish an enriched and healthy primary rat RGC culture;
2. To examine the neuroprotective effects of hESC-MG culture supernatants on enriched rat RGCs subjected to 24-hour glutamate excitotoxicity;
3. To determine the concentration of known neuroprotective factors in the supernatants of hESC-MG that can potentially promote RGC survival.

Experimental design:

i. A summary of the experimental design is illustrated in Figure 5.2.

ii. To compare flow cytometry sorting and two-step immunopanning assay to determine the most appropriate method to purify rat RGCs.

iii. To determine a suitable dosage of glutamate to induce RGC damage by exposing RGCs to various concentrations of glutamate for 24 hours. This was assessed by staining RGCs with known RGC markers and performing immunocytochemical analysis by confocal microscopy for at least 18 random fields per experimental condition. The concentration of glutamate at which resulted in at least 50% of RGCs with neurites was used for the following neuroprotective functionality assessment.

iv. To investigate the neuroprotective effect of culture supernatants collected from hESC-MG1 to RGCs following 24-hour exposure to glutamate. For this purpose, the culture supernatants of hESC-MG1 were collected after replacing normal culture medium of hESC-MG1 to DMEM containing 10% KOSR for 24 hours. Culture supernatants were briefly centrifuged to remove floating cells. The appropriate concentration of glutamate as determined in iv) was introduced to Basal medium, Basal medium containing neurotrophins or

hESC-MG1 supernatants, and cultured with RGCs for 24 hours before harvesting for immunocytochemical analysis as described above. RGC survival was determined by quantifying several morphological features of RGCs. Statistical analysis was performed to assess the significant difference of RGCs cultured in various experiment conditions.

v. The remaining culture supernatants were stored in small aliquotes at -80°C. Working aliquot was defrosted on ice before proceeding to quantitative enzyme-linked immunosorbent assay (ELISA) analysis to quantify concentration of BDNF, PEDF, PRDX6, SOD2 and HO1.

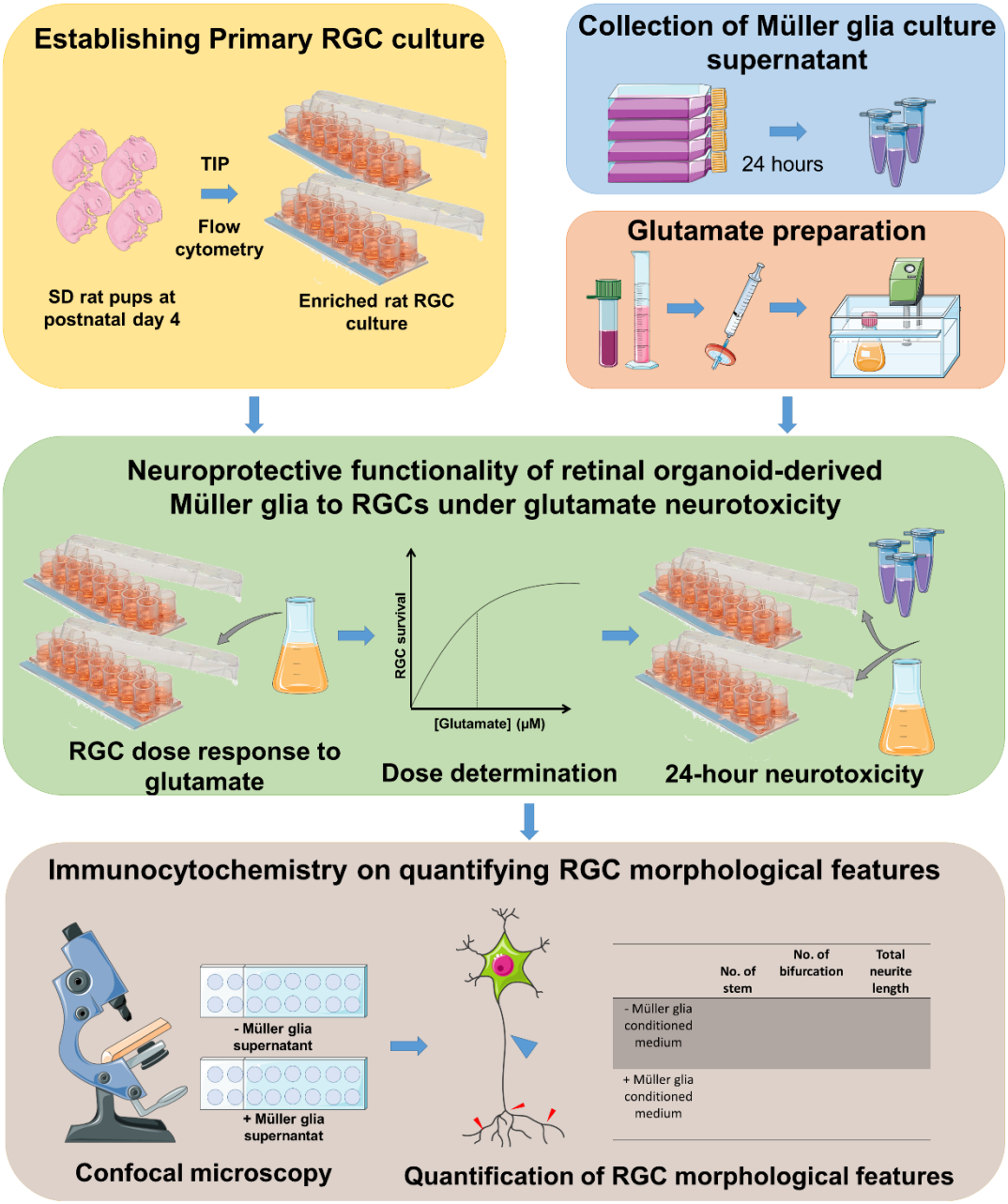

Figure 5.2 Experimental outline.
Primary RGC culture was established from SD rat pups (yellow box). Müller glia supernatant was collected from hESC-MG1 culture overnight (blue box). Glutamate was prepared and pre-warmed before use (orange box). The appropriate glutamate concentration was determined by exposing RGCs to various concentration of glutamate for 24 hours. RGC survival was assessed by confocal microscopy and the appropriate concentration of glutamate was selected for subsequent excitotoxicity treatment (green box). Neuroprotective effect of hESC-MG1 supernatant was examined by culturing RGCs in hESC-MG1 supernatant containing the appropriate concentration of glutamate for 24 hours (green box). RGC survival was examined by quantifying the morphological features of RGCs (beige box). This image was produced using Servier Medical Arts (http://smart.servier.com).

5.3 Results

5.3.1 Standardisation of rat RGC culture by currently available protocols

Purification of rat RGCs by two commonly used protocols, flow cytometry sorting and two-step immunopanning (TIP) were performed and the feasibility of each protocol was assessed to determine the most appropriate approach for this study.

5.3.1.1 Purification of rat RGCs using flow cytometry sorting

Retinae were isolated from SD rat pups at postnatal day 4 within 30 minutes of animal euthanasia and collected in pre-warmed sterile D-PBS. Under a dissection microscope, a semi-transparent membrane with blood vessels coursing through was gentle removed. This step was essential to effectively deplete macrophages that contribute to *in vitro* cytotoxicity and survival of RGCs. The remaining macrophages can be further exhausted by antibodies specific to macrophages. Dissociating retinae by papain enzyme followed by trituration with protein solutions and filtration through 40µm filter cone enabled generating a single cell suspension while preserving cell viability. The recovered cells were collected in serum-free Basal medium containing essential factors including SATO supplement (Winzeler and Wang, 2013b), thyroxine (T3), NS21 supplement (Chen et al., 2008), forskolin, BDNF and CNTF for their best survival (See Materials and Methods and Appendix 4).

The population count and viability of the retinal single cell suspension were determined by an automated cell counter (Beckman Coulter). A single experiment yielded 132.95 million cells dissociated from 28 retinae. Cells showed 99.0% viability and cell diameters were estimated to be between 10µm to 20µm according to data generated by the cell counter (Figure 5.3). Half a million of retina cell suspension was prepared as an unstained (Figure 5.4A), CD45-AF647 (Figure 5.4B), and CD90-PE (Figure 5.4C), single-stained samples for calibration and setting up the appropriate gating, and the rest of cells were double stained and used for sorting CD90-PE^{+} cells from CD45-AF647^{-} population (Figure 5.4D).

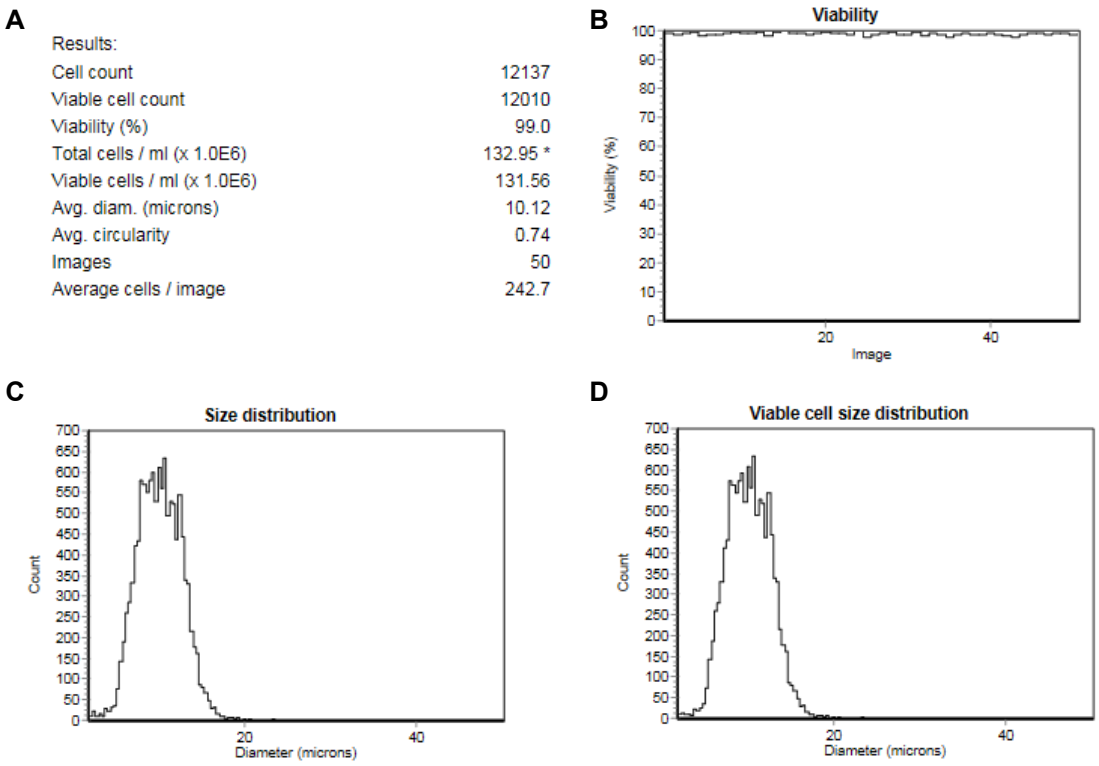

Figure 5.3 Analysis of retinal cell suspension analysis after papain dissociation.
(A) Summary of the total cell count, viability and viable cell count of the retinal cell suspension. **(B)** Distribution plots show the cell viability and size distribution (µm) **(C, D)** of the retinal cell suspension and of the viable cells respectively.

The viability and percentage of cells expressing CD90 and/or CD45 in each sample were determined by coupling the fluorescent signal emitted by SYTOX™ Blue dead cell stain to the signals released by respective fluorophores upon excitation at 480nm and 647nm. The percentage of live cells to overall cell population in all samples was from 59.03% to 80.85% (Figure 5.4i-Figure 5.7i). Within 2 hours, 1,097,899 cells were purified from 129.5 million of retinal cells double stained with CD45-AF647 and CD90-PE (

Figure **5.8**A). Upon completion of flow cytometry sorting, purity of recovered CD90-PE^{+} cells was shown as 48% (

Figure **5.8**B-vi). The recovered cells were collected in Basal medium containing BDNF and CNTF for their best survival and seeded at 10,000 cells/well in a PDL & laminin-coated 16-well glass chamber.

Unstained retinal cell suspension

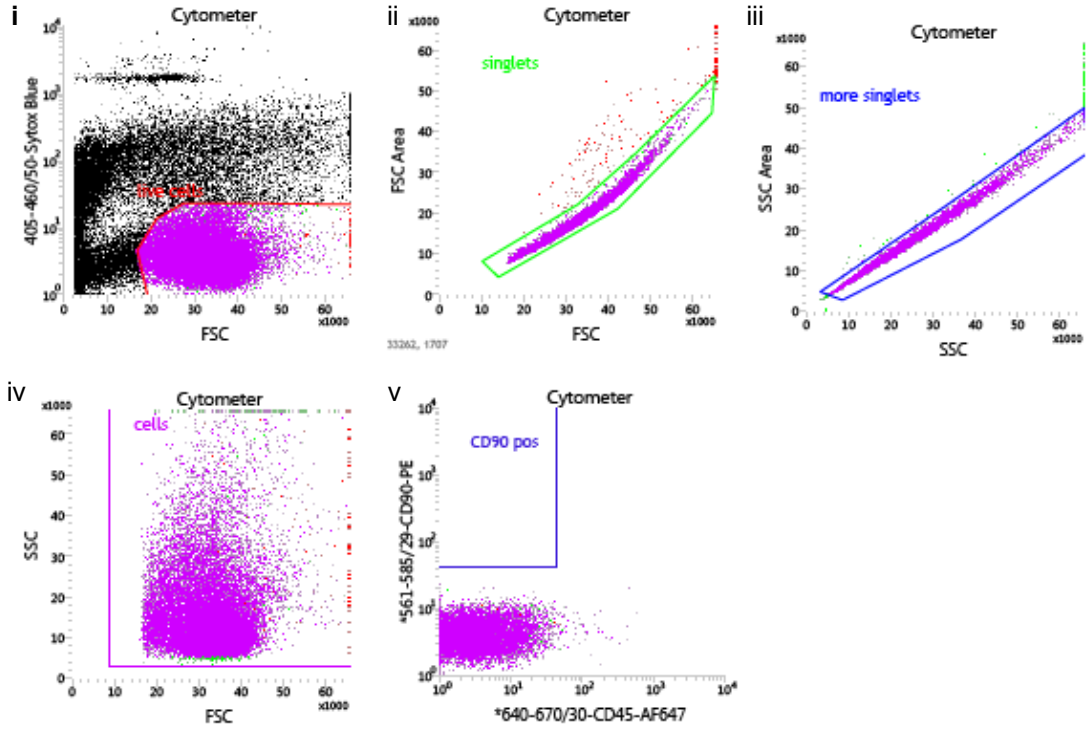

vi

Populations: Cytometer

Populations	Even...	% Total	% Parent
All Events	50,000	100.00%	####
live cells	29,517	59.03%	59.03%
singlets	29,345	58.69%	99.42%
more singlets	29,048	58.10%	98.99%
cells	29,048	58.10%	100.00%
CD90 pos	0	0.00%	0.00%

Figure 5.4 Gating parameters used in flow cytometry sorting of CD90-PE^{+} RGCs from retinal cell suspensions.
An unstained retinal cell suspension was used as a negative control. **(i)** Retinal cell suspensions were firstly gated by uptake of the live-dead stain SYTOX^{TM} Blue to exclude dead cells; **(ii)** cells were gated by forward scatter (FSC) to separate live cells, followed by side scatter (SSC) **(iii)** to eliminate aggregated cells. Alive singlet cells were further gated **(iv)**, before selecting cells based on the fluorescence emitted from CD90-PE antibodies bound on the surface. This was conducted using a 261-585/29 bandpass filter. **(v)** Cells positive for CD45-AF647 were excluded using a 640-670/30 bandpass filter. **(vi)** Cytometer event table shows a summary of the percentage of analysed sample showing positivity to CD90 (0.00%).

CD45-AF647 single-stained sample

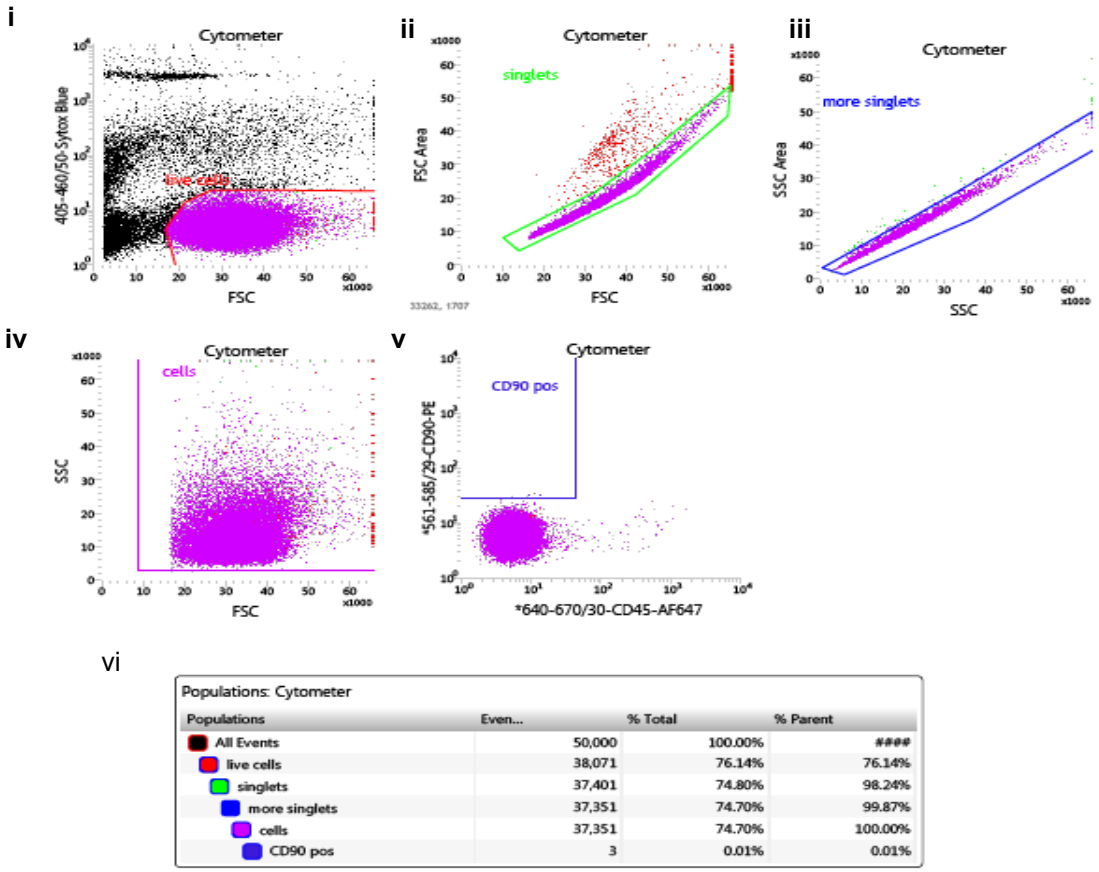

Figure 5.5 Gating parameters used in flow cytometry sorting of CD90-PE^{+} RGCs from retinal single cell suspension.
Retinal cell suspension single stained with CD45-AF647 was used as positive control to set gating for flow cytometry. **(i)** Retinal cell suspensions were firstly gated by uptake of the live-dead stain SYTOX^{TM} Blue to exclude dead cells; **(ii)** cells were gated by forward scatter (FSC) to separate live cells, followed by side scatter (SSC) **(iii)** to eliminate aggregated cells. Alive singlet cells were further gated **(iv)**, before selecting cells based on the fluorescence emitted from CD90-PE antibodies bound on the surface. This was conducted using a 261-585/29 bandpass filter. **(v)** Cells positive for CD45-AF647 were excluded using a 640-670/30 bandpass filter. **(vi)** Cytometer event table shows a summary of the percentage of analysed sample showing positivity to CD90 (0.01%).

CD90-PE single-stained sample

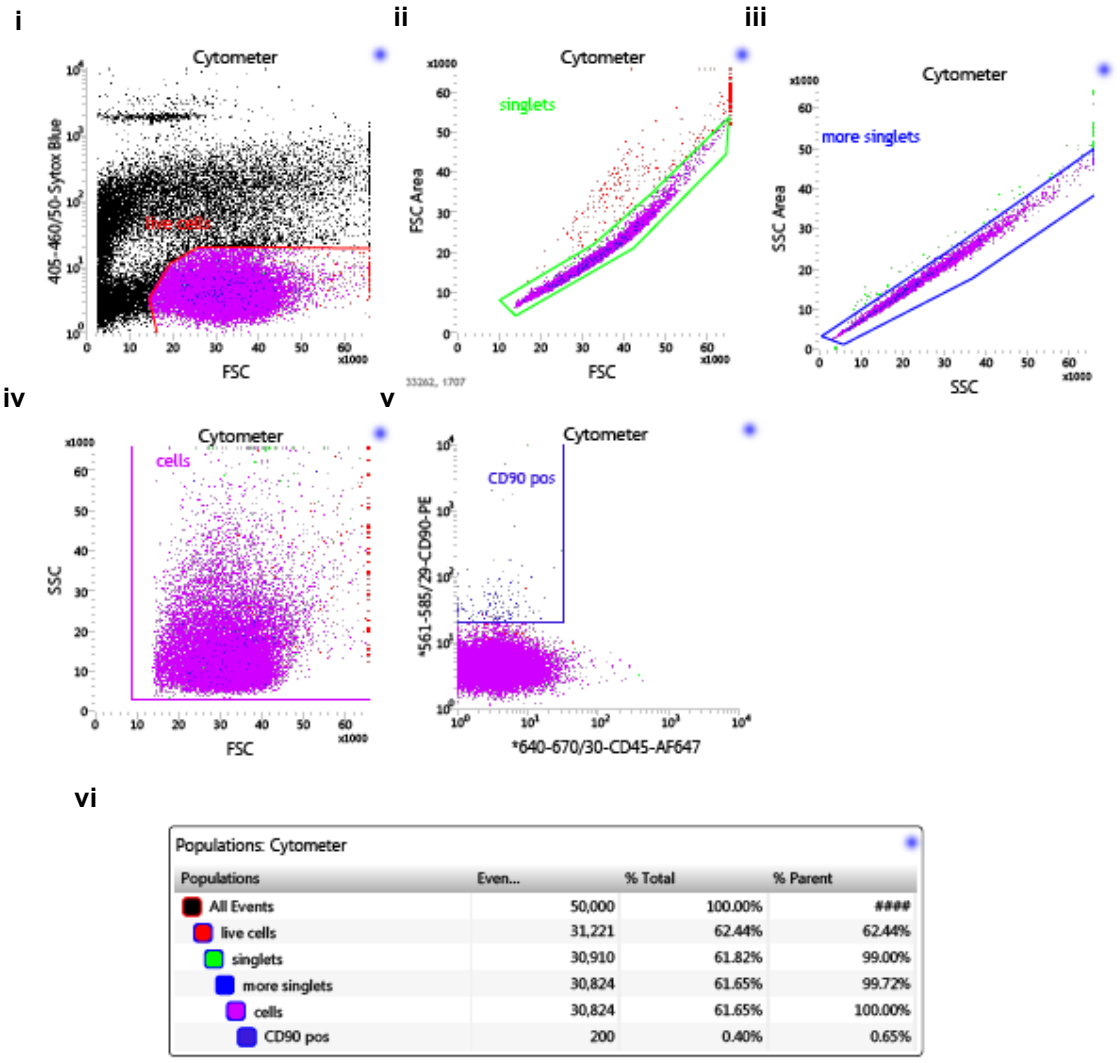

Figure 5.6 Gating parameters used in flow cytometry sorting of CD90-PE^{+} RGCs from retinal single cell suspension.
Retinal cell suspension single stained with CD90-PE was used as positive control to set gating for flow cytometry. **(i)** Retinal cell suspensions were firstly gated by uptake of the live-dead stain SYTOX^{TM} Blue to exclude dead cells; **(ii)** cells were gated by forward scatter (FSC) to separate live cells, followed by side scatter (SSC) **(iii)** to eliminate aggregated cells. Alive singlet cells were further gated **(iv)**, before selecting cells based on the fluorescence emitted from CD90-PE antibodies bound on the surface. This was conducted using a 261-585/29 bandpass filter. **(v)** Cells positive for CD45-AF647 were excluded using a 640-670/30 bandpass filter. **(vi)** Cytometer event table shows a summary of the percentage of analysed sample showing positivity to CD90 (0.65%).

CD45-AF647 & CD90-PE double-stained sample

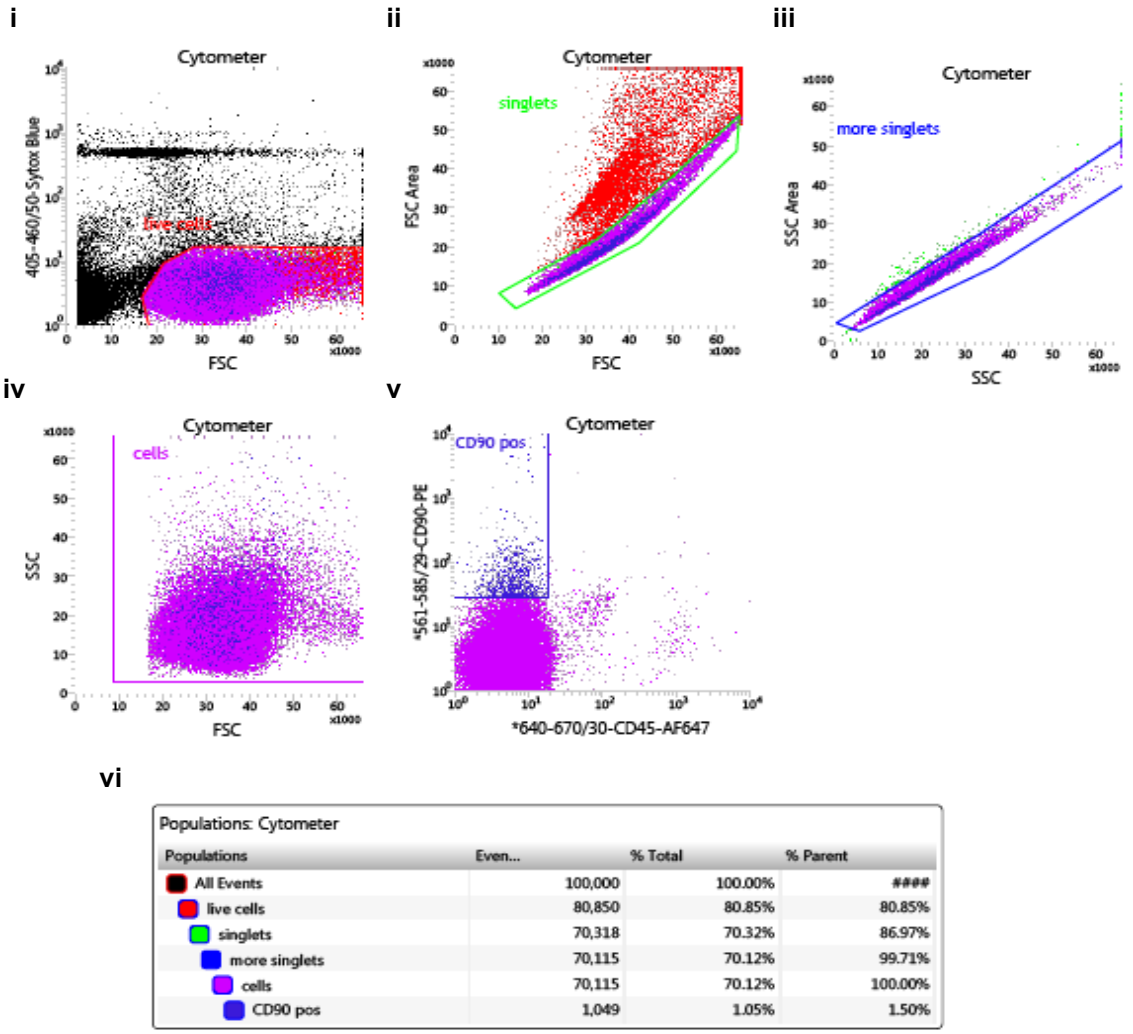

Populations: Cytometer

Populations	Even...	% Total	% Parent
All Events	100,000	100.00%	####
live cells	80,850	80.85%	80.85%
singlets	70,318	70.32%	86.97%
more singlets	70,115	70.12%	99.71%
cells	70,115	70.12%	100.00%
CD90 pos	1,049	1.05%	1.50%

Figure 5.7 Gating parameters used in flow cytometry sorting of CD90-PE^{+} RGCs from retinal single cell suspension.
Retinal cell suspension double stained with CD45-AF647 and CD90-PE was used to sort RGCs. **(i)** Retinal cell suspensions were firstly gated by uptake of the live-dead stain SYTOX^{TM} Blue to exclude dead cells; **(ii)** cells were gated by forward scatter (FSC) to separate live cells, followed by side scatter (SSC) **(iii)** to eliminate aggregated cells. Alive singlet cells were further gated **(iv)**, before selecting cells based on the fluorescence emitted from CD90-PE antibodies bound on the surface. This was conducted using a 261-585/29 bandpass filter. **(v)** Cells positive for CD45-AF647 were excluded using a 640-670/30 bandpass filter. **(vi)** Cytometer event table shows a summary of the percentage of analysed sample showing positivity to CD90 (1.50%).

A **Summary of purification by flow cytometry**

Sort Report

System

Sort Start:	11/30/2018 1:52:49 PM	Server:	Utopex
Application:	BD FACS™ Sortware	Build:	1.2.0.107
Version:	1.2.0.124	Cytometer Model:	BD Influx System
ValComp:	7.5.1.3.16	Cytometer Serial #:	X64650000112

Details

Data Source:	Cytometer	Sort Mode:	1.0 Drop Pure
Nozzle Diameter (µm):	0.00	Drop Envelope:	1.0 Drop
Sheath Pressure (PSI):	0.00	Sort Objective:	Purify
Sort Device:	4 Tube Holder - 4 Way Sort	Phase Mask:	16/16
Piezo Amplitude:	12.93	Extra Coincidence Bits:	4
Drop Delay:	37.5625	Drop Frequency (kHz):	60.00

Sort Details

Name	Population	Event Limit	Event Count	Sort Count	Sort Rate	Aborts	Abort Rate	Efficiency	Time (sec)
Far Left	-	-	-	-	-	-	-	-	-
Left	CD90 pos	Unlimited	147,702,350	1,097,899	161	407,517	59	72.9%	6,800
Right	-	-	-	-	-	-	-	-	-
Far Right	-	-	-	-	-	-	-	-	-

B **Recovered CD45-AF647^{-} & CD90-PE^{+} cells**

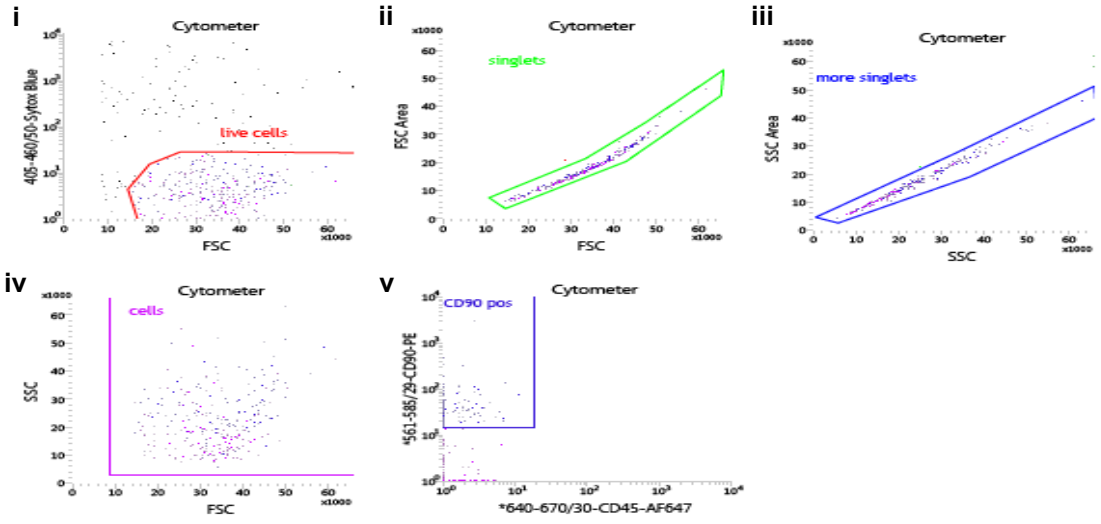

vi

Populations: Cytometer

Populations	Even...	% Total	% Parent
All Events	382	100.00%	####
live cells	281	73.56%	73.56%
singlets	280	73.30%	99.64%
more singlets	277	72.51%	98.93%
cells	277	72.51%	100.00%
CD90 pos	133	34.82%	48.01%

Figure 5.8 Summary of RGC purification by flow cytometry.
(A) Sort report showing sort count, efficiency and time taken to complete the sorting task. **(B)** The purity of recovered RGCs by flow cytometry was validated by live/dead fluorescent dye **(i)**, FSC **(ii)**, and SSC **(iii)**. Alive singlet cells were further gated and CD90^{+} cells were check by a 640-670/30 bandpass filter **(v)**. **(vi)** Cytometer event table shows a summary of the percentage of sorted cell sample showing positivity to CD90 (48.01%).

5.3.1.2 Viability and morphology of purified RGCs upon *in vitro* culture

Following 72-hour culture of enriched populations of RGC obtained by flow cytometry sorting in Basal medium containing BDNF and CNTF, cells were identified by immunostaining for the intracellular RGC marker TUJ and the nuclear marker BRN3A. Confocal images showed that the characteristic features of RGCs including radial dendritic trees and fine neurites were absent (

Figure 5.9A). TUJ^+ structures were only limited to soma and only a very small proportion of TUJ^+ cells stained for BRN3A (Arrowheads, merge images,

Figure 5.9A). Quantitative analysis showed that approximately 22.2% of cells were stained for TUJ and 10.2% for BRN3A, and about 9.09% of cells co-stained for both TUJ & BRN3A (

Figure 5.9B). These observations suggested that the recovered RGCs were severely damaged and did not survive after *in vitro* culture.

5.3.2 Establishment of primary rat RGCs culture using TIP

5.3.2.1 Identification and morphology of rat RGCs

RGCs were isolated according to a modified protocol from Winzeler and Wang (2013), as described in the Materials and Methods. Following retinae dissociation and immunopanning, RGCs were plated at the density of 10,000 cells/well in 16-well chamber slides pre-coated with PDL and laminin as ECM. 72 hours after culturing in serum-free medium containing BDNF and CNTF, purified RGCs were cultured as described above before immunocytochemical analysis. It was observed that the TIP protocol yielded approximately 75.0± 4% of RGCs (TUJ^+ cells/$DAPI^+$ cells). Adhered RGCs exhibited healthy RGC morphology including a round soma, continuous plasma membranes with no signs of vacuolation, and well-developed dendritic processes (

Figure 5.10A). In addition, radial dendritic trees with 2-5 long primary neurites of approximately 20–50μm in length (Arrow,

Figure 5.10A), and various axonal bifurcations with fine neurites were clearly visualised by TUJ staining (Arrowhead,

Figure 5.10A). DAPI counterstain revealed no nuclear fragmentation in RGCs (

Figure 5.10C), indicating that TIP produced an enriched and healthy RGC culture.

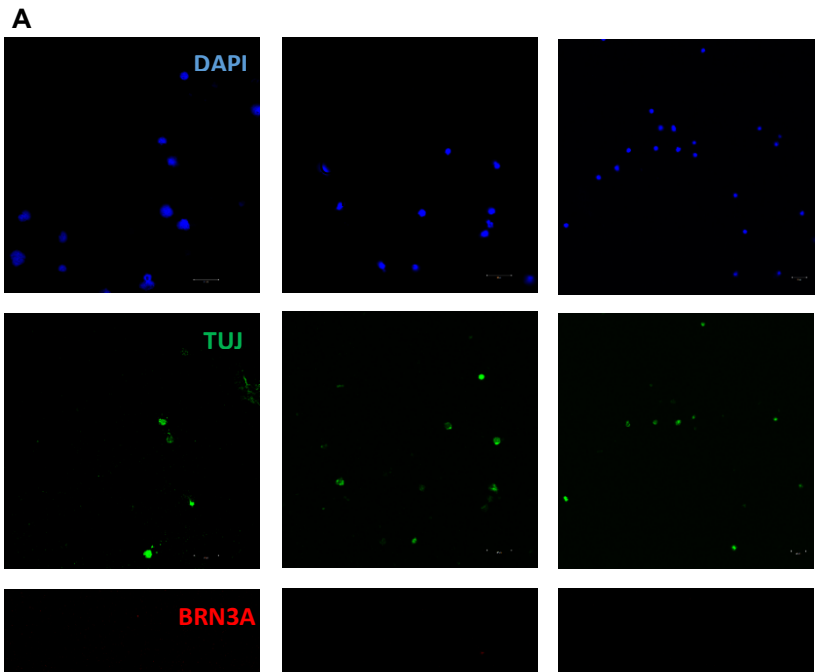

Figure 5.9 Identification of rat RGCs enriched by flow cytometry sorting.
Following 72 hours of culture, RGCs were immunostained with anti-β-tublin III/TUJ antibody (Alexa 488, green), anti-BRN3A antibody (Alexa 555, red), DAPI (blue) and merged images. Arrows show cells positive for TUJ and BRN3A. Scale bar =20μm. **(B)** Mean number of recovered RGCs positive for TUJ, BRN3A and both by manual microscopic counting the number of cells stained for each of the above markers.

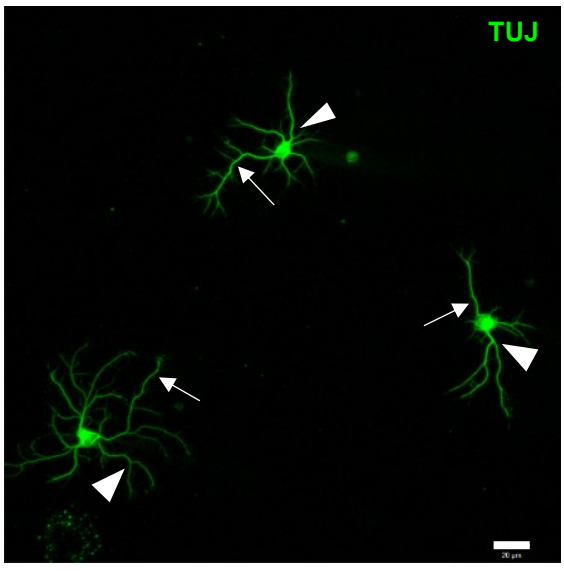

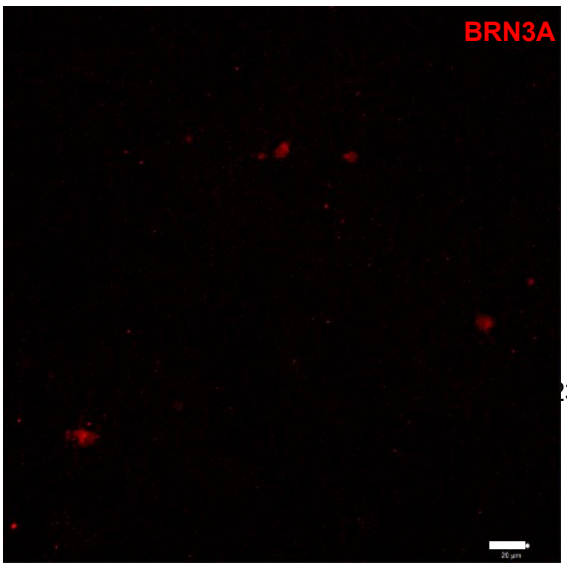

Figure 5.10 Identification of rat RGCs purified by TIP.
Characteristic morphology of RGCs following 72 hours culture at 37ºC. The majority of cells immunostained with anti-β-tublin III/TUJ antibody (Alexa 488, green), anti-BRN3A antibody (Alexa 555, red), DAPI (blue) and merged images. Arrows show primary RGC neurites; arrowheads indicate neuronal bifurcations in these cells. Scale bar =20μm.

5.3.3 Glutamate mediated excitotoxicity in RGCs

To determine the appropriate concentration of glutamate that could induce partial neurotoxicity without causing RGC death and would therefore allow neurotrophic rescue by hESC-MG1 supernatants, various concentrations of glutamate (25μM, 37.5μM and 50μM) were added to the Basal medium containing BDNF and CNTF and cells were cultured for 24 hours. Cells cultured in same medium without glutamate served as control. These cells showed characteristics of healthy RGC as previously described (Figure 5.11A). Cells received glutamate treatment showed various degree of damage as illustrated by loss of structural integrity, with more profound damage observed when the higher concentrations of glutamate were added to the culture medium. Cells cultured with 25μM glutamate showed RGC viability of 56.6±2% (****$p < 0.0001$, Figure 5.11B). These RGCs showed some signs of glutamate excitotoxicity, as indicated by smaller dendritic projections than those seen in cells cultured without glutamate (Figure 5.11A). When higher concentrations of glutamate (37.5μM or 50μM) were added to the culture medium, a significant loss of dendritic networks in RGCs was observed (Figure 5.11A). In addition, 37.5μM glutamate caused a significant reduction in RGC viability (41.3±9%, **$p = 0.0026$, Figure 5.11B). However surviving cells showed better axonal ramifications when compared with cells cultured with 50μM glutamate (Figure 5.11A). Using 50μM glutamate, caused a more severe damage to RGCs, which showed a significantly lower viability (1.6±1.5%, ****$p < 0.0001$, Figure 5.11B) as compared with control cells. Damaged RGC predominantly showed absence of primary neurites and dendritic processes. These observations suggest that the viability and morphological changes in RGCs were dependent on the concentrations of glutamate added to the culture medium. Most importantly, the response of RGCs to BDNF and CNTF in the Basal medium was critically affected by the excitotoxicity induced by glutamate, suggesting that the optimal glutamate concentration should not significantly deprive the response of RGCs to neuroprotective factors while inducing appropriate RGC damage. Therefore, 25μM was considered to be an appropriate concentration that could induce partial neurotoxicity that could be rescued by neurotrophic factors.

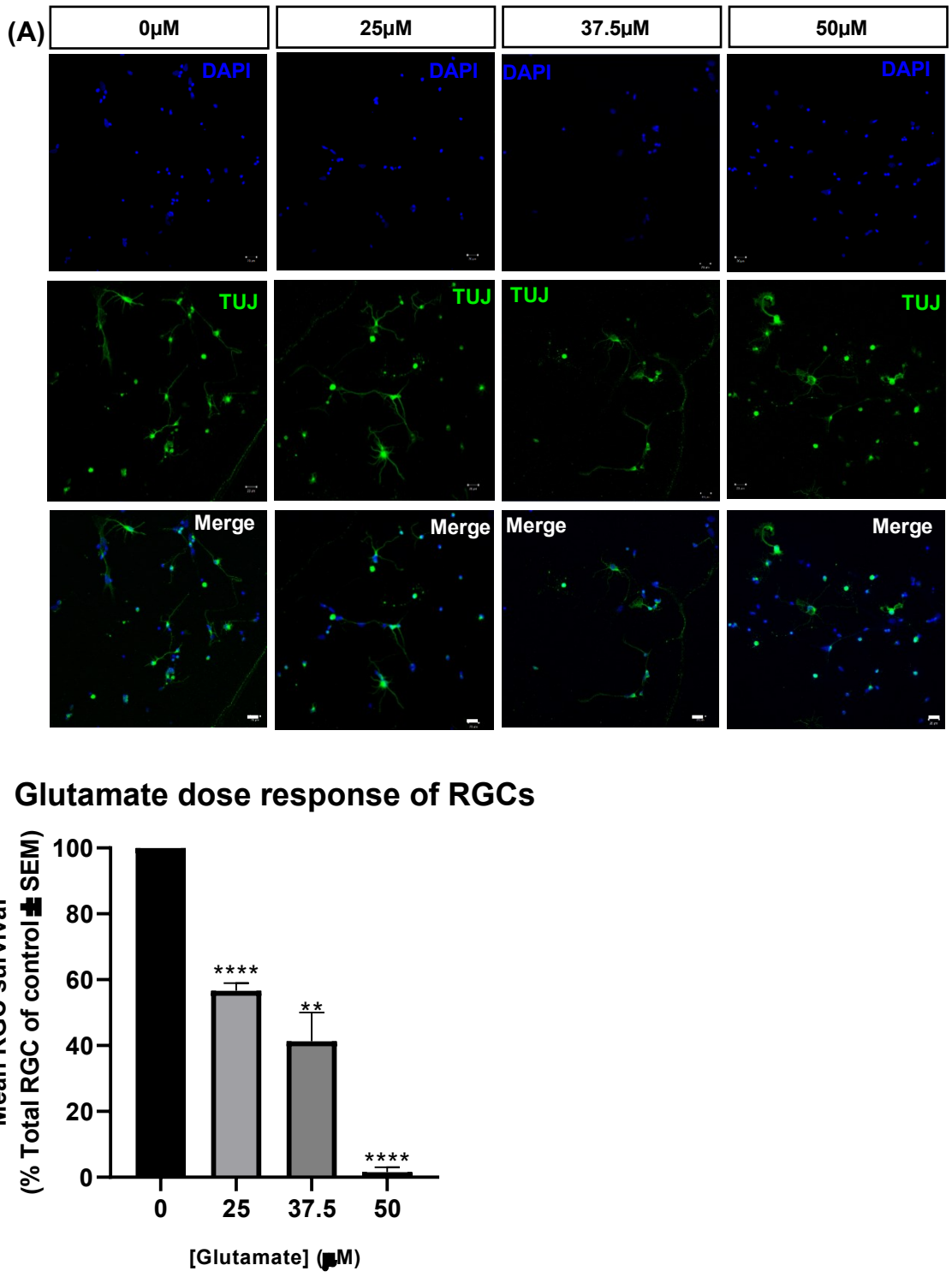

Figure 5.11 Glutamate induces a concentration-dependent damage to RGCs.
(A) Representative immunocytochemical images of RGCs following 24-hour exposure to 25μM, 37.5μM and 50μM glutamate. RGCs were co-stained with anti-β-tubulin III antibody (Alexa 488, green) and DAPI (blue). **(B)** Bar chart showing the percentage of RGC survival (represented by the presence of neurites) in response to increasing glutamate concentrations in culture. Survival rate of RGCs was presented as mean ± standard error of the mean (SEM, n =3), and estimated as percentages of the control group by D'Agostino-Pearson test followed by Mann-Whitney test. ***p* = 0.0026 and *****p* < 0.0001.

5.3.4 Supernatants from cultured hESC-MG promoted RGC survival following glutamate excitotoxicity

The neuroprotective effect of hESC-MG supernatants on RGCs following 24-hour exposure to 25μM glutamate was investigated by firstly assessing the viability of RGC population after glutamate exposure. Two control conditions included culture of RGCs with Basal medium containing BDNF and CNTF, or Basal medium without supplements. RGC viability was analysed by quantifying percentage of TUJ-positive RGCs lacking of neurites which represented several structural damages induced by glutamate. The surviving cells with primary neurites were also examined by determining the percentage of surviving RGCs with a) the longest primary neurite under 50μm length, b) the longest primary neurite between 50 and 100μm length, and c) the longest primary neurite above 100μm length.

5.3.4.1 Supernatants from cultured hESC-MG promoted RGC viability following glutamate exposure

The viability of RGCs after a 24-hour glutamate treatment was assessed by quantification of the percentage of cells with primary neurites. As represented in Figure 5.12, absence of neurites was generally observed in RGCs cultured with Basal medium containing 25μM glutamate. In contrast, more RGCs maintained primary neurites when they were cultured with 25μM glutamate in Basal medium supplemented with BDNF and CNTF and in hESC-MG supernatants. Quantification of RGC numbers showed that the percentage of RGC lacking neurites was significantly higher in cultures containing glutamate and Basal medium alone (48.5±5%) when compared with RGC cultured in the same medium supplemented with BDNF and CNTF (37.6±4%) (*$p < 0.05$; Figure 5.13A). Similarly, RGC cultured with hESC-MG supernatants containing glutamate showed a slightly lower but not significant proportion of cells lacking neurites as compared to those cultured with medium supplemented with BDNF and CNTF (32.1±4%) ($p < 0.05$; Figure 5.13A).

Whereas for the surviving RGCs displayed primary neurites, the population was heterogeneous and was classified into three groups based on the length of the longest primary neurites. The percentage of surviving RGCs with the longest primary neurite < 50μm long were slightly more abundant in cultures containing hESC-MG supernatants (45.4±5%) than in cultures had Basal medium without BDNF and CNTF (35.9±3%), despite of no statistical significance ($p > 0.05$, Figure 5.13B). The proportion of cells showing the longest primary neurite <50μm long was statistically no different between the cultures containing Basal medium with (35.9±3%) or without neurotrophins (35.9±3%) ($p > 0.05$; Figure 5.13B).

The proportion of RGCs with the longest primary neurite between 50 μm and 100μm (Figure 5.13C) and >100μm long (Figure 5.13D) constituted the smallest cell population. Quantification of surviving RGCs showed that a significantly higher proportion of RGCs exhibited the longest primary neurites between 50 μm and 100μm when cultured in Basal medium with BDNF and CNTF (17.2±3%), as compared to those treated with Basal medium alone (9.6±3%) (****$p < 0.0001$; Figure 5.13C). The percentage of RGCs with the longest primary neurite found 50-100μm constituted 13.8±3% of cells cultured in hESC-MG supernatants, which was also significantly more abundant than those in Basal medium alone (9.6±3%) (*$p < 0.05$; Figure 5.13C). Interestingly, a statistical significance on the proportion of RGCs showed similar length of the longest primary neurite was observed between RGCs cultured with hESC-MG supernatants and those had neurotrophins in Basal medium (*$p < 0.05$; Figure 5.13C).

The other category of surviving RGCs were those had the longest primary neurite >100μm. Statistical analysis revealed that the least percentage of RGCs was found in culture containing glutamate and Basal medium only (6.9±3%) and was statistically less than those found in culture containing Basal medium supplemented with BDNF and CNTF (11.1±3%) (**$p < 0.05$; Figure 5.13D). Similarly, RGCs with the longest primary neurite more than 100μm cultured in hESC-MG supernatants (12.9±3%) was significantly more than those did not have neurotrophins in Basal medium (*$p < 0.05$; Figure 5.13D). When comparing between the two groups of RGCs cultured with either neurotrophin supplementation in Basal medium or in

hESC-MG supernatants, no significant difference was revealed ($p > 0.05$; Figure 5.13D).

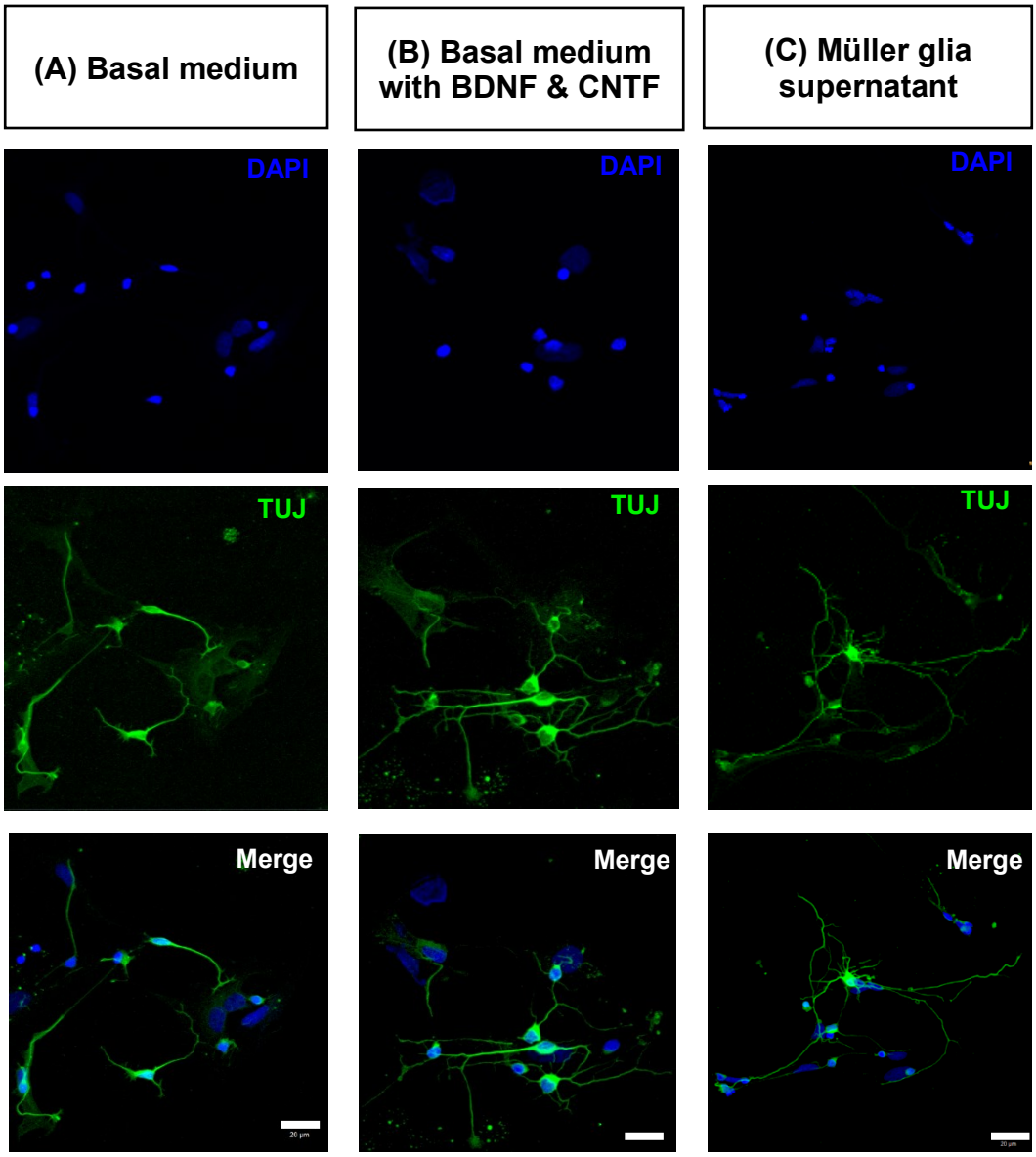

Figure 5.12 Morphological features of RGC populations exposed to 24-hours glutamate excitotoxicity.
Representative images of RGCs cultured in **(A)** Basal medium, **(B)** Basal medium supplemented with BDNF and CNTF, **(C)** hESC-MG supernatants. All cells were cultured in the presence of 25μM glutamate for 24 hours. RGCs were immunostained with anti-β-tubulin III antibody (TUJ, Alexa 488, green) and DAPI (blue). Scale bar = 20μm.

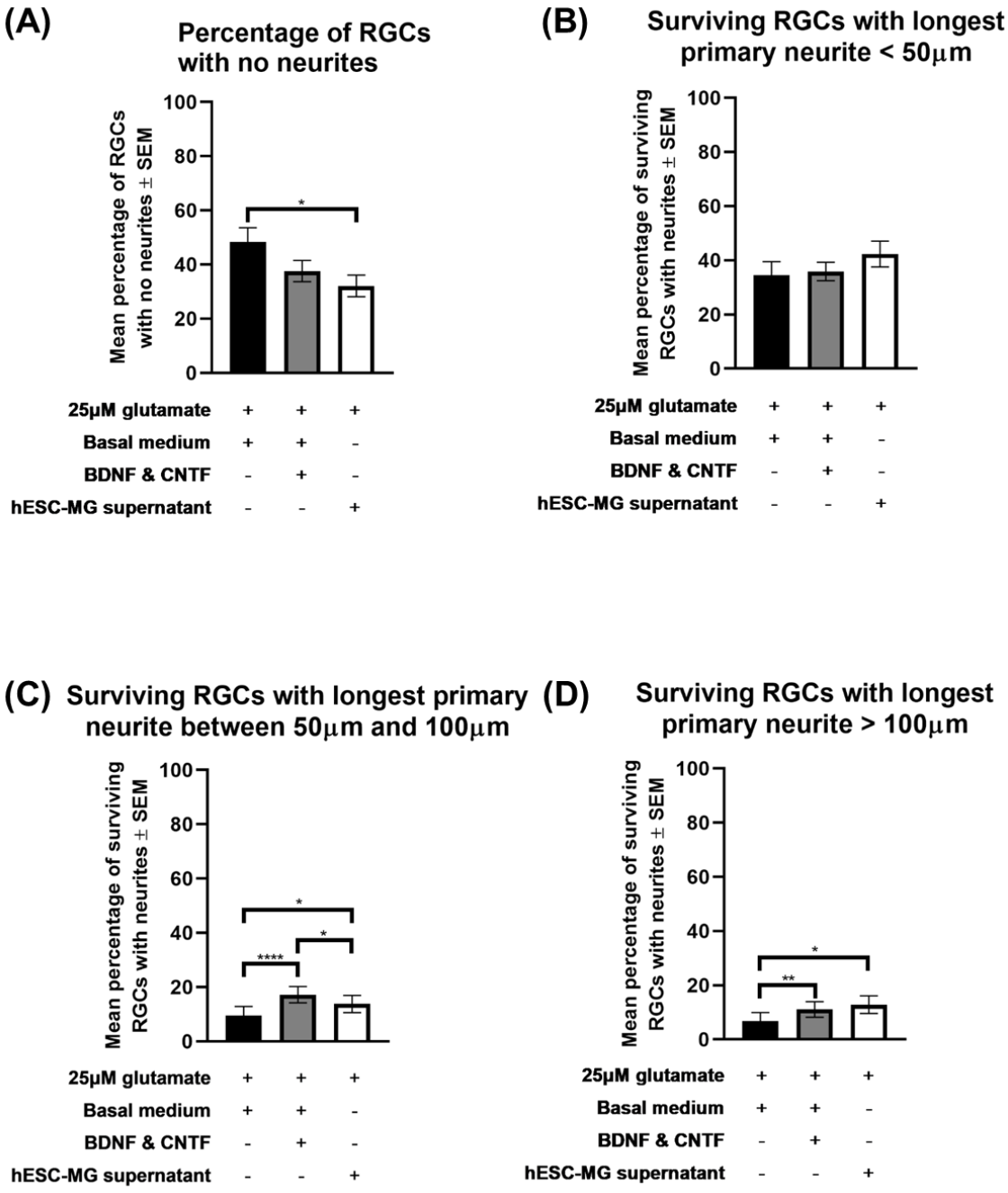

Figure 5.13 Neuroprotective effect of hESC-MG supernatants on RGCs with neurites following 24-hour glutamate excitotoxicity.

Histogram shows **(A)** the mean percentage of RGCs lacking neurites, **(B)** the mean percentage of RGCs with the longest primary neurite < 50μm, **(C)** the mean percentage of RGCs with the longest primary neurites between 50-100μm, and **(D)** the mean percentage of RGCs with the longest primary neurite >100μm. Culture conditions were shown below histogram. Data are presented as mean ± standard error of the mean (SEM, n =4), and analysed by D'Agostino-Pearson test followed by Mann-Whitney test. *p < 0.05 and ****p < 0.0001.

5.3.4.2 Supernatants from cultured hESC-MG protected surviving RGC dendritic projection

In addition, the surviving RGCs with neurites were further quantified for the following structural features to understand the neuroprotective effect of hESC-MG supernatants:

i. The length (μm) of the longest primary neurite per RGC;
ii. The number of primary neurites per RGC;
iii. The number of bifurcations at which two dendrites branched from primary neurites per RGC.

The mean length of the longest primary neurite projected from the soma of the surviving RGCs was determined by manually tracing the longest neurite length of individual cells and averaging these values to the number of RGCs assessed for each culture condition. The representative immunofluorescent images of representative RGCs were shown in Figure 5.14. The mean length of the longest neurite per RGC cultured in Basal medium containing BDNF and CNTF was 1.4-fold longer (52.9±3 μm) than that of RGCs cultured in Basal medium without supplements (39.0±3 μm) (**$p < 0.05$, Figure 5.15). This suggests that both trophic factors were essential for maintaining the dendritic projection of RGCs. Pair-wise comparison showed that the mean length of the longest neurite per RGC cultured with hESC-MG supernatants (62.5±7 μm) was 1.6-fold longer than that of RGCs cultured in Basal medium without neurotrophin supplementation (**$p < 0.05$, Figure 5.15). Interestingly, RGCs cultured in Basal medium with BDNF and CNTF supplements showed neurites with a similar mean length to those cells cultured with hESC-MG supernatants with no statistical significance ($p > 0.05$, Figure 5.15), indicating that Müller glia supernatants contain neuroprotective factors to promote RGC survival following glutamate insult.

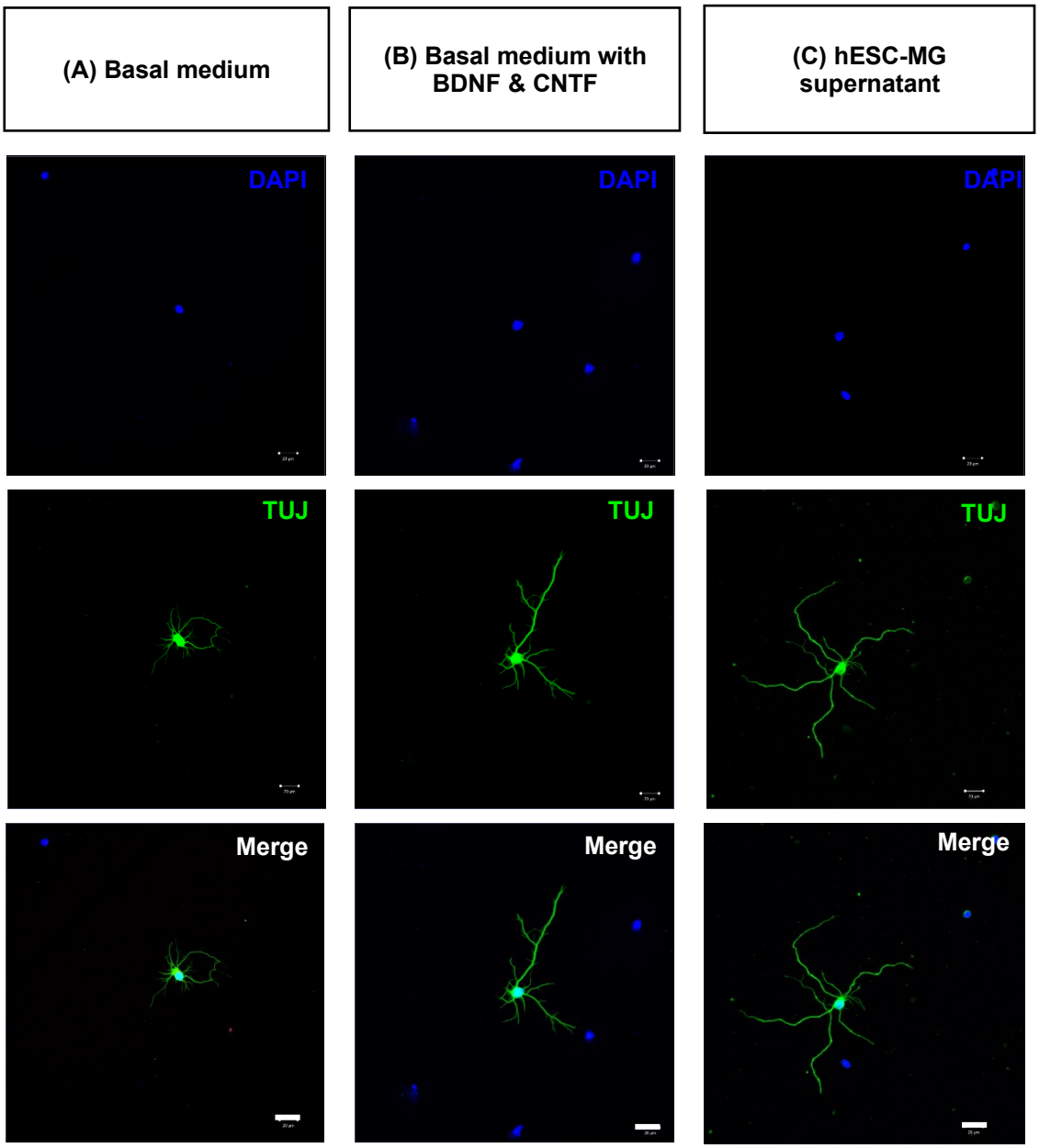

Figure 5.14 Representative morphological features of surviving individual RGC exposed to glutamate for 24 hours.

Representative images of surviving RGCs cultured in (A) Basal medium, (B) Basal medium supplemented with BDNF and CNTF, (C) hESC-MG supernatants. All cells were cultured in the presence of 25μM glutamate for 24 hours. RGCs were immunostained with anti-β-tublin III antibody (TUJ, Alexa 488, green) and DAPI (blue). Scale bar = 20μm.

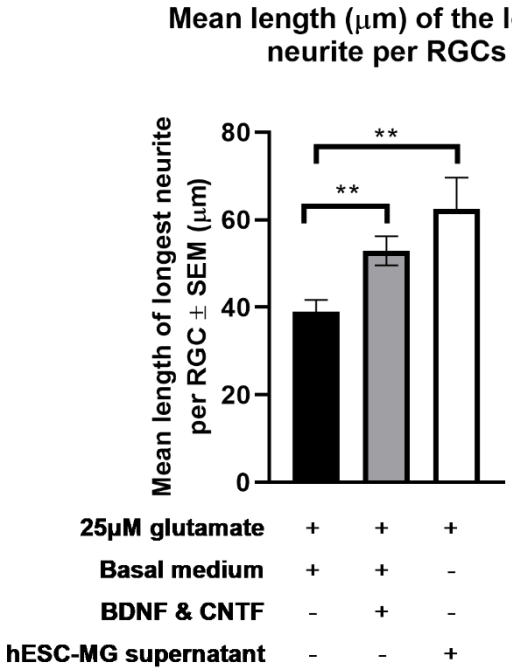

Figure 5.15 Neuroprotective effect of hESC-MG supernatants as determined by the mean length (μm) of the longest neurite per RGCs following 24-hour glutamate excitotoxicity.
Histogram shows the mean length of the longest neurites per RGC ± SEM (μm). Culture conditions were shown below histogram. Data are presented as mean ± standard error of the mean (SEM, n =4), and analysed by D'Agostino-Pearson test followed by Mann-Whitney test. ** $p < 0.005$.

Examination of the mean number of primary neurites per RGC in cell populations subjected to glutamate toxicity showed a similar number of primary neurites across the three culture conditions ($p > 0.05$; Figure 5.16A), suggesting that RGCs surviving glutamate excitotoxicity did not have a significant axonal damage. However, it was observed that RGCs cultured in Basal medium supplemented with BDNF and CNTF showed a higher number of bifurcations per RGC (2.9-fold, 8.5±1 bifurcations per RGC, *** $p < 0.05$, Figure 5.16B) in comparison with cells cultured in Basal medium alone (2.8±1 bifurcations per RGC, Figure 5.16B). A significant protective effect on the number of bifurcations was also observed in RGC cultured with hESC-MG supernatants (1.8-fold increase, 5.2±1 bifurcations per RGC, * $p < 0.05$, Figure 5.16B) when compared with RGCs cultured in Basal medium without neurotrophin supplementation. No statistically significant difference was observed between RGC cultured with hESC-MG supernatants and Basal medium supplemented with BDNF and CNTF (Figure 5.16B). These observations indicate that induced damage to

surviving RGC by glutamate exposure was limited to the distal region of RGC dendritic trees.

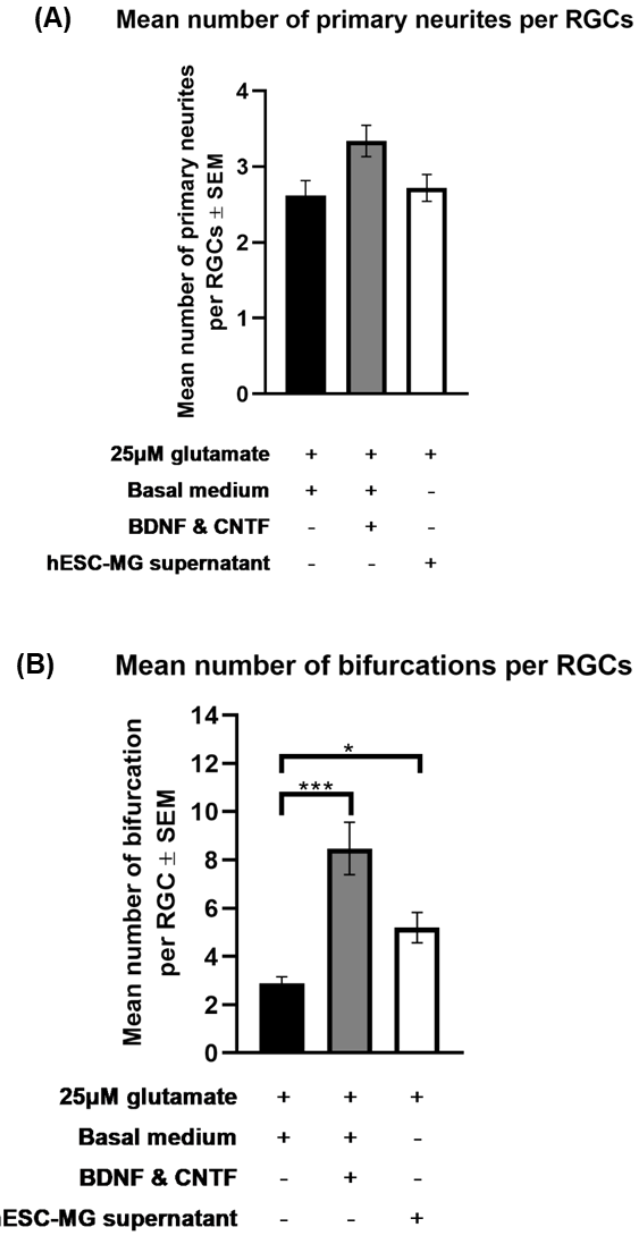

Figure 5.16 Neuroprotective effect of hESC-MG supernatants on dendritic projections of RGCs following 24-hour glutamate excitotoxicity.
Histogram shows **(A)** the mean number of primary neurites per RGC ± SEM, and **(B)** the mean number of bifurcations per RGC ± SEM. Culture conditions were shown below histogram. Data are presented as mean ± standard error of the mean (SEM, n =4), and analysed by D'Agostino-Pearson test followed by Mann-Whitney test. *$p < 0.05$, **$p < 0.005$ and ****$p < 0.0001$.

In summary, under glutamate excitotoxicity RGCs cultured with hESC-MG supernatants showed a higher survival than cells cultured in Basal medium only. Of the surviving cells, similar percentages of RGCs exhibited primary neurites and small dendritic processes in both Müller glia supernatants and in Basal medium containing BDNF and CNTF, when compared to RGCs cultured in Basal medium alone. These observations indicate that preservation of axonal integrity was dependent on exogenous neurotrophins.

5.3.5 Identification and quantification of key neuroprotective factors in hESC-derived Müller glia supernatants

The concentrations of the neuroprotective factors BDNF, PEDF, PRDX6, HO1 and SOD2 were examined in hESC-MG supernatants, using quantitative ELISA analyses (Figure 5.17). The mean concentrations of neurotrophin BDNF and PEDF in hESC-MG supernatants were 1487.0±18 pg/mL and 191.0±20 ng/mL respectively. Similarly, the antioxidant enzymes PRDX6, HO1 and SOD2 were present in hESC-MG supernatants at concentrations of 9.3±2 ng/mL, 266.8±99 pg/mL and 838.7±229 pg/mL, respectively. The presence of these neuroprotective factors supported the hypothesis that hESC-derived Müller glia release various neuroprotective factors which might be uptaken by RGCs and contribute to their survival following glutamate excitotoxicity.

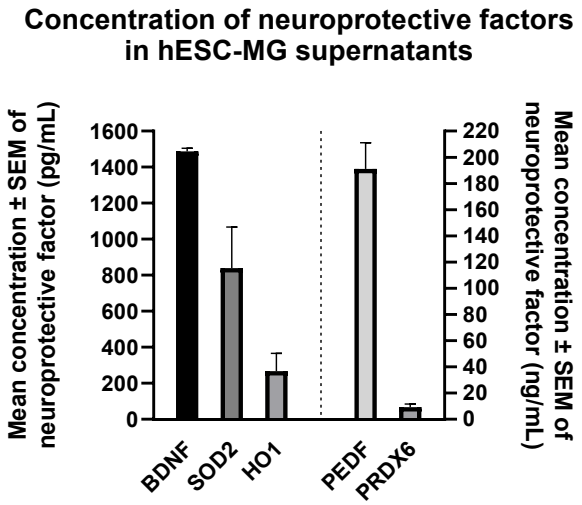

Figure 5.17 Analyses of the mean concentration of key neuroprotective factors in the hESC-MG supernatants.

Histograms show mean concentration of the neurotrophins BDNF (pg/mL) and PEDF (ng/mL), as well as the antioxidants PRDX6 (ng/mL), HO1 (pg/mL) and SOD2 (pg/mL) in hESC-MG supernatants, as determined by quantitative ELISA assays. Columns on the left show protein concentrations in pg/mL and columns on the right show concentrations in ng/mL Data are presented as mean ± standard error of the mean (SEM, n =3 cell passages in culture).

5.4 Discussion

The aim of this chapter is to investigate the neuroprotective potential of hESC-MGs to RGCs following glutamate excitotoxicity. Given that RGC lines are not available, primary RGC culture is the most appropriate experimental model to study the neuroprotection of Müller glia *in vitro*. In this study, the feasibility of flow cytometry and TIP were evaluated to assess the optimal recovery of healthy RGCs for subsequent *in vitro* neuroprotective studies of hESC-MG supernatants on RGCs. The sorting strategy of flow cytometry aimed to separate RGCs from macrophages using a leukocyte-specific surface marker CD45 (Pilling et al., 2009). The survival of purified RGCs was directly dependent on the viability of retinal suspensions. Conjugated antibodies diluted in RGC Basal medium containing neurotrophins were incubated with dissociated retinal cells and recovered cells were collected in the same medium to promote survival. It was observed that using this medium, long sorting process posed mechanical pressure on cells when passing through tubes in a non-favourable temperature and atmospheric environment. This led to poor survival of the recovered RGCs as shown by that the low cell viability of RGCs after 72 hours. This observation has been reported by Gao et al. whilst using this method (Gao et al., 2016). Other studies have also shown that limiting sorters to a very narrow gate using antibodies to CD90 to isolate RGCs is prone to errors as CD90 is also found on amacrine cells (Perry et al., 1984). This was reflected in the heterogeneity of recovered cells after purity check, as the sorter could have failed to distinguish the weak Thy-1/CD90^{+} signal from fine microfluidics and discard Thy-1/CD90^{-} cells (

Figure **5.8**). Reduction of flow rate and gating of sorters could reduce but not overcome such discrepancy. Given that the purity of the recovered cells could not be guaranteed and that the cell viability was not ideal, it was considered that flow cytometry could not be used to establish primary rat RGCs for this study.

TIP constituted a better approach to isolated rat RGCs. The principle behind TIP is that it relies on the affinity of cell surface molecule to its specific antibody while incubating retinal cell suspensions in a protein solution favouring their survival. Effectively negative panning by pulling down antibody-bound macrophages to secondary antibody-coated plates removed macrophages, despite some retinal

cells being lost during this process (Gao et al., 2016). Further purification of RGCs included the attachment of RGCs to anti-Thy-1 antibody bound onto plates via positive panning. In this study, it was observed that several factors could influence the success of positive panning. Firstly, binding affinity of anti-Thy-1 antibody to petri dishes could be weak. Swirling of panning plate during incubation aimed to encourage binding of cells to tethered anti-Thy-1 antibody may wash off the weakly bound RGCs. Furthermore, the pH of coating and panning buffer appears to critically control the binding affinity of RGCs to anti-Thy-1 antibody. Therefore, a good practice of reagent preparation and experimental skills was necessary to ensure the efficacy and consistency of RGC purification and survival. In this study, the purity and morphology of RGCs were in agreement with previous reports (Pang et al., 2007, Gao et al., 2016). Most importantly, the viability of RGCs purified by TIP was much higher than that of by flow cytometry, and facilitated the observation of the morphological features of RGCs, so that these cells could be systemically quantified. Therefore, acquiring an enriched and healthy RGC population was very important for this study.

The dose response of RGCs to glutamate was assessed by determining the suitable concentration of this neurotransmitter that caused a sub-optimal damage to RGCs but that allowed their survival upon exposure to neuroprotective factors present in Müller glia supernatants. It was observed that the survival rate of RGCs cultured with 37.5μM and 50μM glutamate was significantly lower than untreated cells and the structural integrity of RGCs were severely disrupted (

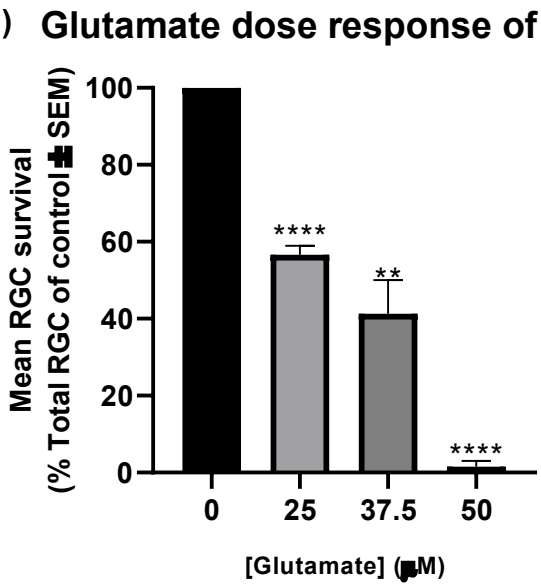

Figure 5.11), This is in agreement with other studies reporting apoptotic cell death as early as 12 hours after exposure of RGCs to 50μM glutamate (Fang et al., 2010). Therefore, 25μM glutamate was considered as an optimal concentration to induce partial RGC damage in this study. The chosen concentration is in line with other reports which show that as little as 20μM glutamate is sufficient to induce partial RGCs cytotoxicity *in vitro* (Otori et al., 1998, Lee et al., 2010c, Chang et al., 2013) with an average survival rate at 67% (Kawasaki et al., 2000, Lee et al., 2010c). Importantly, using 25μM glutamate, RGCs still displayed dendritic projections so that the effect of neuroprotective factors in Müller cell supernatants could be assessed. It has been reported that apoptotic cell death is inevitable following major axonal injury to RGCs (Shen et al., 1999, Goldberg & Barres, 2000), implying that external insult to axons should not deprive the ability of RGCs to respond to neuroprotective treatment.

Using retrograde labelling, the RGC survival following glutamate excitotoxicity and the neuroprotection effect of small molecules on RGCs have been assessed by calculation of the proportion of RGCs surviving after glutamate treatment when compared with control conditions (Lee et al., 2010c, Fang et al., 2010, Chang et al., 2013, Pang et al., 2007). Attempts have been also made to analyse the

morphological features of RGCs using these labelling methods, as fine structures of RGC neurites are only affected following transient insult (Morgan et al., 2006, Williams et al., 2010). Although recent studies have examined the morphological heterogeneity and axonal lengths of RGCs (Ruzafa et al., 2018, Mead and Tomarev, 2017), the fine bifurcation structures have not been examined. In this study, the length of the longest neurite per RGC which indicates the dimension of RGC dendritic projection and the number of primary neurites and bifurcation per RGC were examined, as they are good indicators of neuritogenesis and structural integrity of RGCs. These quantifiable parameters can be easily reproduced across different experimental conditions. This analysis is important because the morphological dimension of the dendritic field is coupled to the innervation property of these cells, with large RGCs having fast conductance and small cells relaying slow action potentials (Huxlin and Goodchild, 1997). Interestingly, it was observed that RGCs treated with glutamate in hESC-MG supernatants had longer primary neurites and more burfications when compared to control cells treated with glutamate in the absence of BDNF and CNTF. In this study, while the number of primary neurites per RGC remained significantly no different in all culture conditions, significant abundancy on the number of bifurcations per RGC was noticed in cells cultured with neurotrophin supplements or hESC-MG supernatants when compared to control cells. These observations indicate that neuroprotective factors in these culture conditions might be important to preserve distal structures of RGC neurites following early exposure to glutamate. This hypothesis is in line with early studies, which suggested that structural modification of RGC axonal terminals was a sign of early degeneration of RGC dendritic trees (Weber et al., 1998) and might be ascribed to superoxide burst induced by external insults (Swanson et al., 2005, Kanamori et al., 2010).

The observations from this study, that hESC-MG supernatants have partially rescued the axonal degeneration of RGCs induced by glutamate excitotoxicity, suggested that the proteomic content of hESC-MG supernatants might be enriched by neuroprotective factors. Given the transcriptomic evidence presented in Chapter 2 that highlights the enrichment of various neuroprotective genes in hESC-MG1, concentrations of proteins coding for several key trophic factors were further confirmed by ELISA analysis, which showed that hESC-MG supernatants contained

not only BDNF and PEDF, but also antioxidant enzymes PRDX6, HO1 and SOD2. These findings confirmed that neuroprotective factors present in hESC-MG supernatants may be partially responsible for the promotion of RGC survival observed in this study. This is supported by existing evidence that BDNF is uptaken in a retrograde direction (Horch et al., 1999) and enhances RGC survival through activation of the TrKB signalling pathway (Ma and Taylor, 2010, Uchida et al., 2003, Harada et al., 2002, Meyer-Franke et al., 1995). PEDF has shown to confer neuroprotection in a specific dose-dependent manner to a wide spectrum of retinal neurons including photoreceptors subjected to glutamate and TNF-α neurotoxicity (Cao et al., 2001) and RGCs (Ogata et al., 2001, Pang et al., 2007). In addition, it has been reported that binding of Müller glia-derived PEDF to its correspondent receptors in RGCs leads to activation of the STAT3-dependent signalling cascade in these cells and this is a mechanism thought to contribute to RGC survival (Eichler et al., 2017).

Neuroprotective molecules present in the Müller glia supernatants may not be limited to neurotrophins, and it is possible that other secreted factors including growth factors, antioxidants and membrane-bound microvesicles (MVs) present in the supernatants (Duarte et al., 2016, Monsel et al., 2016) could account for the promotion of RGC survival observed in this study. Glutamate excitotoxicity is accompanied by generation of reactive oxygen species (ROS) and nitric oxide (Mehta et al., 2013) which contribute to neuronal death, therefore the presence of antioxidants in the Müller cell supernatants may have contributed to the regulation of the redox balance, resulting in attenuation of ROS in RGCs. As confirmed by ELISA analysis, the presence of the antioxidants PRDX6, HO1 and SOD2 in hESC-MG supernatants might have contribute to the observed RGC protection. Although PRDX6 is also expressed by RGCs, its abundancy undergoes significant reduction following glutamate excitotoxicity and exogenous supplementation of PRX6 is critical for RGC survival (Fatma et al., 2008). This is supported by evidence that resistance to hypoxia-induced cell death has been found in RGCs overexpressing PRDX6 (Tulsawani et al., 2010, Pacifici et al., 2014). HO1 has been shown to decrease glutamate- (Lee et al., 2014b) or injury-induced (Davis et al., 2017) oxidative stress in rodent models of glaucoma. Deletion of SOD2 in RPE and RGCs in experimental animals has led to elevated oxidative stress and dysfunction of

these cells (Biswal et al., 2016, Joe et al., 2015), suggesting that this superoxide scavenger plays a critical role in RGC survival. Other trophic factors such as nerve growth factor (NGF) (Giardino et al., 1998) and NT3 (LaVail et al., 1992), as well as small molecules such as basigin, osteopontin, and antioxidants such as glutathione S transferase (GST1) (Harada et al., 2007), that have shown neuroprotective effects *in vitro*. It is therefore possible that similar factors may be present in hESC-MG supernatants and this merits further investigations.

As suggested above, in addition to neurotrophic factors and antioxidants, hESC-MG supernatants may also contain MVs carrying bioactive molecules such as mRNA and microRNA (Huynh et al., 2016). In this study, it is possible that MVs present in hESC-MG supernatants may have been uptaken by RGCs, causing changes in their molecular signatures, leading to improved survival after glutamate-induced damage (Kalani et al., 2014, Santos-Ferreira et al., 2016, Waldron et al., 2018). This is supported by previous demonstrations that RGCs exposed to MVs harvested from mesenchymal stem cells exhibit a better survival after injury (Mead et al., 2018, Mead and Tomarev, 2017), for which it would be important to investigate the presence of these microstructures in Müller glia supernatants.

Whilst the neuroprotection potential of hESC-MG supernatants on preserving the structural integrity of RGCs was demonstrated in this study, the physiological functionality on RGCs has yet to be examined. Future studies should consider conducting patch clamp experiments to assess membrane potential of RGCs responding to electrical stimuli. In addition, it remains elusive whether the RGC heterogeneity between rat and human are similar. Overlap of RGC subtypes of similar morphology have made discriminating RGC subtypes extremely imprecise and impractical (Rheaume et al., 2018). Nevertheless, RGCs have shown subtype-specific susceptibility to degeneration in rodents (Thanos, 1988, Feng et al., 2013), with type II RGCs showing small dendritic projections being primarily affected and large RGCs (type I and III) being less sensitive to degeneration (Thanos, 1988). Therefore, when translating the current results towards therapy development, researchers should also consider species differences. Moreover, this *in vitro* glutamate excitotoxicity model only represented a simplified model of RGC damage *in vitro* which is far from the actual damage observed in glaucoma *in vivo,* where

RGC damage gradually progresses over years and involves multiple cellular responses. Further efforts should be aimed at validating the *in vivo* findings from this chapter in experimental models of RGCs, such as the commonly used NMDA-induced glaucoma-like rat model.

In summary, this chapter has demonstrated that culture supernatants collected from hESC-MG have promising neuroprotective potential that promotes survival of RGCs following acute glutamate excitotoxicity. This study showed that Müller glia derived from retinal organoids constitute a source of neuroprotective factors including BDNF, PEDF, PRDX6, HO1 and SOD2, which might have contributed to the viability and structural integrity of RGCs subjected to glutamate damage. These findings suggest that Müller glia may constitute a viable cell-based approach to deliver neuroprotection to retinal neurons against retinal degeneration and merits further studies.

CHAPTER 6 General discussion

Many retinal diseases including glaucoma, AMD and diabetic retinopathy are common manifestations of retinal degeneration and accounts for the most common causes of visual impairment and blindness in the world. Despite the continuous advances on disease diagnosis and management, no effective treatments are yet available to offer functional protection to damaged retinal neurons. Previous wok in the hosting laboratory showed that transplanting human Müller glial cells into the eye of animal models of retinal degeneration significantly improved their visual function (Jayaram et al., 2014b, Becker et al., 2016), with the underlying mechanisms attributed to the trophic factors released by these cells that promote the survival of the host retinal cells. Human Müller glia may constitute an invaluable source of cells for neuroprotective therapies, however sourcing Müller glia from allogenic donors has been deemed unsuitable for the development of cell-based therapies, due to the infectious risks that adult human tissue poses and to the immunological responses that they can elicit due to histocompatibility. The ongoing advancements of stem cell differentiation techniques have offered alternatives to source cells from adult tissues, for which deriving Müller cells from hPSCs might circumvent the limited availability of suitable retinal tissues. Many studies using hPSC-derived cells have witnessed the unlimited potential and therapeutic benefits of these cells generating neural retina with laminated structure and whole retinal cell populations (Li et al., 2018, Nakano et al., 2012), as well as enhancement of visual functions in animal models receiving cell transplants using these cells (Gagliardi et al., 2018, Carr et al., 2009). The primary objective of this thesis was therefore to investigate the potential of deriving retinal organoids from hPSCs to isolate Müller glial cells. The novelty of this thesis is that it has taken the advantage of retinal organoids mimicking embryonic development of neural retina *in vitro*, and isolating Müller glia by specific binding of their cell surface marker CD29 to the ECM protein fibronectin. The majority of this work was to further demonstrate the proof of concept of this methodology by assessing the characteristics of the isolated Müller glia-like cells such as their native and cytokine-induced transcriptomic profiles, as well as their neuroprotective functionality using an *in vitro* model of RGC excitotoxicity.

6.1 Retinal organoids constitute a source of cells committed to the Müller glia-like fate with substantial neuroprotective potential

In this chapter, various hPSC sources were subjected to *in vitro* retinal differentiation and formed retinal organoids with distinctive 'mantle'-like structures. This process recapitulated major events of retinogensis *in vivo* and the emergency of Müller glia cells within these structures were clearly illustrated over 70 days of differentiation, offering guidance for isolating and propagating CD29+ cells *in vitro.* The transcriptomic analyses of the isolated cells using a differentiation protocol modified in the host laboratory indicates that this method is highly robust to induce retinal differentiation of hPSCs into retinal organoids. In addition, the isolation and *in vitro* propagation techniques used are efficient to produce a highly homogenous population of Müller glia-like cells. Using RNA-seq, the absent pluripotent markers in hPSC-derived cells highlighted that hiPSC-MG1 and hESC-MG1 cells show minimal risk of teratogenic risk that they were committed towards Müller glia-like phenotype. In-depth pairwise analyses revealed that they showed some similarities to the reference cell line MIO-M1, whilst showing some differential variation, notably evident by the expression of mature and developing Müller markers, as well as several neuroprotective factors. The Müller glia-like phenotype of hiPSC-MG1 and hESC-MG1 was supported by the substantial expression of Müller glia markers, including VIM, GLUL, ITGB1 and CD44, despite of the absence or low expression of the mature markers RLBP1, AQP4, KCNJ2/10 and SLC1A3. It is possible that hPSC-derived cells upon isolation were at a developing stage, as shown by the high expression of components of NOTCH and WNT pathways, and the retinoic acid-binding protein CRBPs. This was in line with a latest study which showed that the presence of mature Müller glia markers within retinal organoids were detected at a more advanced differentiation stage (Sridhar et al., 2020). However, it may be possible that acquisition of mature markers may be the result of mature functionality upon neural maturation induced by visual stimuli such as light (Wang et al., 2009a, Saari, 2016). Indeed, GO analysis revealed that many DEGs found in the transcriptomes of hPSC-derived Müller cells were associated with early neuronal development, although hESC-MG1 was more well differentiated towards neural

phenotype than hiPSC-MG1. The highly upregulated neuroprotective signatures of these cells represent the most striking findings in this chapter, underpinning the invaluable therapeutic potential of novel hPSC-derived Müller cells for retinal degenerative therapies. Furthermore, *in vivo* transplantation of hPSC-derived cells into an animal model of glaucoma-like disease reported significantly improvement in RGC functions (Eastlake et al., 2019b), corroborating the neuroprotective functionality of these cells. Future studies on CD29+ cells isolated at later stages of organoid development are needed to understand if mature Müller glia markers could be detected in those cells, and to assess whether the molecular landscape of trophic functions in these cells would be associated to the maturation of Müller glia.

Moreover, hiPSCs and hESCs have shown cell specific responses to the retinal differentiation protocol used, as shown by the varied success rate at forming retinal organoids and the morphological and transcriptomic differences of the isolated cells. Future examinations on karyotyping and epigenetics of hPSCs may elucidate these differences observed. While hiPSCs represents the ideal source to obtain allogenic cells because they could minimise the host immune response to cell transplantation, many studies still highlight the unpredicted risk of teratoma associated with reprogramming approaches or the pathogenic features of virus vectors that might be used for preparation of hiPSCs (Higuchi et al., 2017). In contrast, hESCs are free from engineered pluripotency and accessible from major stem cell banks which have performed thorough and regular monitor on their genome stability (Singh et al., 2018). They have demonstrated valid safety and robustness for their use in therapies as observed in a recent clinical trial developed for AMD (da Cruz et al., 2018). The validity of the transcriptomic landscape shown in this study may provide data to explore the molecular determinants of Müller glia phenotype and to revise retinal differentiation protocols for cell isolation. Additionally, the acceleration of this work towards pre-clinical studies would require the retinal differentiation protocol to comply with the Good Manufacture Practice (GMP) guidelines. Many reagents and culture conditions described in this study such as Matrigel and β-mercaptoethanol contain xenogeneic components. For which replacing those components to GMP-grade alternatives would be necessary.

In summary, this study presents a solid proof of concept on the feasibility of producing a highly homogenous population of Müller glia-like cells from hPSC-formed retinal organoids.

6.2 Pleiotropic transcriptomic responses of human adult Müller glia induced by TNF-α

Upregulation of inflammatory cytokines such as TNF-α, constitutes a well-known feature of many retinal degenerative diseases (Nakazawa et al., 2006, Al-Gayyar and Elsherbiny, 2013). The response of Müller glia to these factors, which is often manifested as reactive gliosis in mammalian retinae, plays a major role in the pathogenesis of these diseases (Reichenbach and Bringmann, 2010). Although reactive gliosis is considered as an attempt of Müller glia to restrict damage, this process further increases inflammatory damage, and there are no studies demonstrating the early transcriptomic changes of human Müller glial response to TNF-α (Thomas et al., 2016, Bringmann and Reichenbach, 2001). This study mapped the transcriptomic landscape of human adult Müller cells within 24 hours *in vitro* exposure to this cytokine, using RNA-seq approach.

Activation of TNF-α signalling induced a well-regulated mechanism of signalling cascades, such as TNFR2-driven activation of anti-apoptotic regulators due to TNFR1-induced apoptosis genes. By clustering DEGs related to neuroinflammation, neuroprotection and Müller cell functions, a plethora of gene clusters was found differentially expressed and showed contrasting expression in MIO-M1 cells. For example, upregulation of neuroinflammatory events including leukocyte trafficking factors was generally associated with TNFR1 activation (Yang et al., 2011), and these were counterbalanced by significant upregulation of TNFR2 (Veroni et al., 2010), demonstrating enhanced neuroprotective response as shown by upregulation of neurotrophins and antioxidant factors. Similarly, TNF-α promoted extensive modification of ECM components and their homeostasis regulators, representing another feature of well-regulated transcriptomic response of MIO-M1 cells under acute stimulation by TNF-α.

Importantly, RNA-seq also identified several genes that did not indicate reactivity of MIO-M1 cells, such as gliotic response mediators, proliferative markers and GFAP

downregulation upon TNF-α treatment. Importantly, this study identified that an important transcriptional mediator of GFAP expression, STAT3 (Herrmann et al., 2008) had its upstream regulators LHX2, SOCS2 and METRN differentially expressed (de Melo et al., 2012, Basrai et al., 2017, Lee et al., 2010a), which might indicate that underlying signalling pathways such as JAK/STAT3 and MAPK pathways regulating gliotic response and GFAP expression are highly complex and might involve the simultaneous activation of multiple signalling cascades (Zhang et al., 2000, Sabio and Davis, 2014). Interestingly, simultaneous downregulation of GFAP and GLUL in MIO-M1 cells *in vitro* closely resembled the *in vivo* behaviours of these cells re-entering cell cycles in zebrafish and chicks (Fischer and Reh, 2003, Thummel et al., 2008), and perhaps suggests that the retinal microenvironment might be the underlying factor limiting regeneration of the human retina. Elucidation of the underlying signalling pathway regulating GFAP downregulation by targeting SOCS2 and/or METRN using overexpression tools in MIO-M1 cells, may aid to bridge the existing knowledge gap on the molecular differences between *in vitro* and *in vivo* Müller glia response to TNF-α that lead to differences in GFAP expression.

Taken together, the current findings support the notion that TNF-α does not acutely induce neurodegenerative effects on Müller glia, but that instead, elicits pleotropic expression of genes regulating neuroinflammation and neuroprotection. Nevertheless, the highly dynamic nature of the transcriptome, the complex post-transcriptional modification observed, possibly regulated by novel non-protein coding transcripts (Trynka et al., 2009, Banks et al., 2016, Mathy and Chen, 2017), and the retinal microenvironment, indicates underpins that this dataset provides limited information on the transcriptional response of Müller cells to prolonged exposure to TNF-α. However, to our knowledge, this study represents the first report presenting a global view on the pleiotropic response of Müller glial cells following acute TNF-α stimulation *in vitro*. The current findings added mounting evidence that Müller glia do not respond acutely to TNF-α in a degenerative manner but that in fact, this cytokine induces some neuroprotective behaviours on these cells and merits further investigations.

6.3 hPSC-derived Müller glia constitute a source of neuroprotective antioxidant enzymes in response to cytokine stimulation

In previous chapters, the transcriptomic similarities between human retinal organoid-derived Müller glia and adult cells were revealed by RNA-seq, and using similar techniques, the neuroprotective response of a human adult Müller glia cell line to TNF-α was also identified. On this basis, it was important to validate the expression of neuroprotective antioxidant enzymes by hPSC-derived Müller cells and understand if they would exhibit similar response to inflammatory cytokines *in vitro*.

The results presented in this thesis demonstrate that hPSC-derived Müller glia constitutively express a broad spectrum of antioxidant enzymes and represent the source of neuroprotection for the diseased neural retina. This study compared the anti-oxidative response of hiPSC-MG, hESC-MG and MIO-M1 cells exposed to TNF-α and TGF-β1, two cytokines that have been shown to play important roles in retinal degenerative disorders (Bringmann et al., 2006, Limb et al., 1991), as well as inducing oxidative stress during the pathogenesis of these conditions (Yu and Welge-Lussen, 2013, Anrather et al., 2006). A highly similar *in vitro* response of hiPSC-MG1 and hESC-MG1 to both cytokines as compared to adult retinal derived cells (MIO-M1 cells) was observed. When culturing these cells with TNF-α overnight, significant upregulation of SOD2 was accompanied by a slight increase of other antioxidant enzymes, as well as increased release of PRDX6 and HO1 into culture supernatants. Thus, it may be possible that the oxidative stress triggered by TNF-α can be effectively balanced by the production of antioxidant enzymes and trophic factors, in addition to upregulating SOD2 expression in mitochondria. In contract, TGF-β1 did not significantly modify the expression of antioxidant enzymes in human Müller glia within 24 hours. Although the inhibitory effect of this cytokine to antioxidant enzyme expression has been reported in both ocular and non-ocular cells (Michaeloudes et al., 2011, Fatma et al., 2009a).

The modification of mRNAs coding for antioxidant enzymes in Müller glia might be under the influence of transcriptional regulators NRF2 and NFκB2. Many papers in

the literature suggest that there seems to be a very complex and sophisticated signalling network including but not limited to the NFκB pathway of the TNF-α signalling and the canonical Smad pathway of the TGF-β1 signalling (Michaeloudes et al., 2011, Fatma et al., 2009a, Liu and Desai, 2015, Wardyn et al., 2015). Therefore, further investigations into the crosstalk between NRF2 and NFκB2 by knockout approaches may give light into the regulatory antioxidant potential of Müller cells. This study specifically investigated the response of Müller glia following transient exposure to a single cytokine and showed that Müller glia exhibits plasticity to modify its molecular profile towards neuroprotection. However, given the highly complex degenerative microenvironment which may involve chronic exposure to multiple cytokines, future work should examine the response of Müller glia upon long-term exposure to multiple cytokines.

Taken together, the results presented in this study suggest that Müller glia constitute an important source of antioxidant enzymes in the neural retina during normal physiology and retinal degeneration. Targeting the extracellular release of these factors by Müller glia may represent a valid approach to deliver neuroprotection to retinal neurons.

6.4 hESC-derived Müller glia release neuroprotective factors for RGCs subjected to early glutamate excitotoxicity

The current findings showed that primary rat RGC cultures could be effectively enriched by a two-step immunopanning assay (TIP) to study structural modification of RGCs by glutamate excitotoxicity *in vitro*. Addition of glutamate to RGC Basal medium supplemented with BDNF and CNTF elicited RGC cytotoxicity following overnight culture and structural damage of RGCs. This damage became more profound when glutamate concentration was increased. It was observed that when treating RGCs with 25μM glutamate for 24 hours, the overall viability as determined by presence of primary neurites, was significantly higher in cells receiving supernatants collected from hESC-MG1 cells, as compared to those cultured with BDNF and CNTF. The structural integrity of RGCs including neurite length and distal dendritic projections was significantly preserved by hESC-MG1 supernatants. The

improved RGC survival and structural integrity might be attributed but not limited to the released neuroprotective factors BDNF, PEDF, PRDX6, SOD2 and HO1 by hESC-MG1 cells. Uptake of these Müller glia-derived trophic factors by RGCs might either activate the cell survival signalling cascade (Horch et al., 1999, Eichler et al., 2017), or directly upregulate scavenging ROS induced by glutamate excitotoxicity (Mehta et al., 2013, Fatma et al., 2008, Lee et al., 2014b, Joe et al., 2015). Future studies should demonstrate the transfer of these factors from Müller cells to RGCs *in vivo*. Additional investigations to fully elucidate the proteomic contents of culture supernatants may help identify novel neuroprotective candidates produced by Müller glia that contribute to the observed neuroprotective effects *in vitro*. Exosomal vesicles that may contain regulatory components such as miRNAs released by Müller glia might also contribute to the anti-apoptotic signalling activation in RGCs following glutamate overstimulation (Kalani et al., 2014, Santos-Ferreira et al., 2016, Waldron et al., 2018).

In conclusion, supernatants from hESC-derived Müller glia have demonstrated neuroprotective effect on rat RGCs following an early phase of glutamate excitotoxicity. In-depth investigation of the neuroprotective signatures of hESC-derived Müller glia would help to understand the therapeutic potential associated with these cells.

6.5 Conclusions

This work has demonstrated that hiPSC and hESC could undergo retinal differentiation and form retinal organoids *in vitro*, and that Müller glia can be successfully isolated and propagated from these organoids. Comparative studies on the transcriptomes of the hiPSC-MG and hESC-MG cells demonstrated that these cells presented highly comparable molecular signatures as compared to that of Müller glia isolated from adult human retina. Analysis on transcriptomic modifications of adult Müller glia by TNF-α revealed that a pleiotropic response consisting of neuroprotective and neurodegenerative genes could be elicited in these cells. In addition, hiPSC-MG and hESC-MG cells were confirmed as the source of neuroprotective antioxidant enzymes in the neural retina and their *in vitro* exposure to TNF-α and TGF-β1 further added evidence that hiPSC-and hESC-derived Müller glia responded to exogenous cytokine stimulation by modifying their anti-oxidative profile. It would be important to further investigate the neuroprotective plasticity of Müller glia following chronic stimulation by these cytokines to build insights on their long-term neuroprotective potential. The *in vitro* treatment of rat RGCs with culture supernatants of hESC-MG cells further supports the hypothesis that Müller glia are capable of promoting the survival of RGCs following glutamate excitotoxicity by releasing a broad spectrum of neuroprotective factors. Further investigation into the *in vivo* functionality of the hiPSC-MG and hESC-MG cells in pre-clinical models of retinal degeneration would accelerate the clinical translation of cell-based therapies utilising these cells.

CHAPTER 7 MATERIALS AND METHODS

7.1 Isolation of Müller glia from retinal organoids derived from human pluripotent stem cells

7.1.1 Culture of human pluripotent stem cells

The human iPSC line BJ and the ESC line Sheffield human embryonic stem cell 6 (Shef 6) were provided by Professor Pete Coffey from the UCL Institute of Ophthalmology. The human ESC line RC-9 was provided by The Roslin Institute (University of Edinburgh). The generation of hiPSC line from BJ fibroblasts (Stemgent, UK) and the generation of Shef-6 and RC-9 embryonic stem cells were previously described by various groups (Carter et al., 2016, De Sousa et al., 2016, Aflatoonian et al., 2010). These cell lines were previously shown as presenting a normal karyotyping profile and free of contamination. The following culture procedures are applied to both the human iPSC line BJ, the ESC line Shef 6 and RC-9.

hiPSCs/hESCs were cultured as feeder-free colonies in 6-well plates pre-coated with human qualified Matrigel (Catalogue no. 734-0269; VWR) with TeSR-Essential 8 (E8) media (Catalogue no. 05940; Stem Cell Technologies) containing 50 μM gentamycin (Catalogue no. G1397; Sigma-Aldrich). Cell cultures were checked and fed daily to assess the colony morphology and confluency. Differentiated cells were removed with pipette tips under an EVOS microscope in a tissue culture hood. Weekend feeding medium Essential 8 Flex medium (Catalogue no. A2858501; Invitrogen) was used on Friday and replaced with weekday medium TeSR-E8 medium on the following Monday.

When 60-70% confluency of colonies was observed, culture media were aspirated, and colonies were washed with PBS briefly before individual colonies were incubated in 1 mL of PBS containing 0.5 mM EDTA (Catalogue no. AM9260G; Invitrogen) for up to 5 minutes at room temperature. EDTA solution was removed when cell colonies started to break to small clusters and cells were gently washed off from plates using 2 mL of TeSR-E8 medium. Cell suspension was split at 1:6 and the new passage of cells was seeded in a 6-well plate pre-coated with Matrigel.

7.1.1.1 Freezing and defrosting of hiPSC and hESC

Cells could be frozen after removal of EDTA solution as described above. Colonies from a single 6-well plate were collected in 6 mL of mFreSR cryopreservation medium (Catalogue no. 05854; Stem Cell Technologies) and allioquted as 1 mL suspension in a cryovial. These cells were frozen at -80^{o}C using a cell freezing container filled with isopropanol before transfer to liquid nitrogen. Upon defrosting, 6-well plates were pre-coated with Matrigel for a few hours prior seeding of cells. Cryovials were thawed in a 37^{o}C water bath for a few minutes and cell suspension was collected in 2 mL of TeSR-E8 medium containing 10 µM ROCK inhibitor (ROCKi) (Catalogue no. A11001-5; Biosciences) before centrifugation at 300 g for 3 minutes. The supernant was aspirated and the cell pellet was resuspended and plated in 2 mL of TeSR-E8 medium containing 10 µM ROCKi and 50 µm gentamicin.

7.1.2 Generation of retinal organoids from human iPSCs and ESCs

The protocol used to generate retinal organoids was adapted from a published protocol (Nakano et al., 2012). hiPSCs and ESCs were cultured in a series of culture media containing different neuronal differentiation factors and growth factors (**Error! R eference source not found.**).

At Day 0, human iPSCs/ESCs were washed with 1X PBS (Catalogue no. Cat 6505; Calbiochem) and dissociated to single cells using 1 mL of Triple^{TM} containing 10 µM ROCKi and 0.5 mg/mL DNase (Catalogue no. 1010459001; Sigma-Aldrich) at 37°C for 3 minutes. Cell suspension was collected using 5 mL of embryoid body (EB) culture medium (Table 7.1) and centrifuged at 300 g for 5 minutes. The supernatant was discarded and the cell pellet resuspended in 2 mL of EB culture medium containing 10 µM ROCKi. Cell numbers were counted, and concentration was calculated to make up 9000 cells per well for a 96-well plate. The appropriate volume of cell suspension was added to retinal differentiation medium containing 10mL EB culture medium with 20 µM ROCKi and 3 µM WNT antagonist. 100 µL of cell suspension was added to each well of a low-cell-adhesion V-bottomed conical 96-well plate (Catalogue no. MS-9096VZ; Sumitomo Bakelite) to re-aggregate cells.

Embryoid body (EB) culture medium	**Glasgow´s minimal essential medium (GMEM) with L-glutamine** Catalogue no. 21710-025; Invitrogen
	1% 100x penicillin-streptomycin Catalogue no. 15070-063; Gibco
	20% knockout serum replacement (KOSR) Catalogue no. 10828-028; Invitrogen
	1mM non-essential amino acids (NEAA) Catalogue no. 11400-050; Invitrogen
	1mM sodium pyruvate Catalogue no. 11360-039; Invitrogen
	0.1mM 2-mercaptoethanol Catalogue no. 31350-010; Invitrogen
EB2/FCS medium	**EB Culture medium**
	10% Fetal calf serum (FCS) Catalogue no. FB-1001; Biosera
	1% Matrigel Catalogue no. 734-0269; VWR
Neural retina (NR) culture medium	**DMEM-F12-Glutamix medium** Catalogue no. 31331-028; Invitrogen
	1% 100x penicillin-streptomycin Catalogue no. 15070-063; Gibco
	10% FCS Catalogue no. FB-1001; Biosera
	1% N2 supplement Catalogue no. 16502-048; Invitrogen
	500 nM Retinoic acid Catalogue no. R2625-50; Sigma-Aldrich

Table 7.1 Medium components for retinal organoids culture

At Day 2, 100 µL of fresh EB medium and 2% Matrigel (growth-factor-reduced; BD Biosciences) was topped up to each well using a multichannel pipette. Every 4 days, 100 µL of medium were carefully removed without disturbing the growth of EBs and replaced with 100 µL of fresh EB medium until Day 12 of differentiation (Figure 2.5).

At Day 12, EBs were transferred to a squared low-adhesion 25-well plates (Catalogue no. 103; Thermo Fisher), using a tip-cut 1000 µL pipette and cultured in EB2/FCS medium (Table 7.1) and 100 nM smoonthened ligand SAG (Catalogue no. ALX-270-426-M001; Enzo Life Sciences). Medium change was performed every 4 days until Day 18 (Figure 2.5). At Day 18, EBs were cultured in neural retina (NR) culture medium (Table 7.1) and retinal organoids with distinctive layered ‘mantle’ became visible under the microscope. Culture medium was changed every 4 days.

7.1.3 Dissection of retinal organoids

From Day 30 onwards, retinal organoids with distinctive neural retinal layers were dissected with a microblade under a dissecting microscope to encourage further expansion of optic cups. Isolated structures were cultured in a separate well in NR medium.

7.1.4 Isolation and propagation of Müller glia from retinal organoids

Müller glia were isolated from retinal organoids cultured for 30 days to 121 days. A few hours prior to organoid dissociation, a few wells of a 24-well plate were coated with human fibronectin (Catalogue no. 356008; Corning®) at the working concentration of 50 µg/mL from 5 mg stocking with extracellular matrix buffer. Excess fibronectin was aspirated immediately before plating cell suspension.

Retinal organoids were incubated in 500 µL of dissociation mix (Table 7.2) in a 1.5 mL Eppendorf tube with the cap opened to displace air up to 10 minutes at 37°C, using vigorous pipetting every 5 minutes to help the organoid break up. At the end of incubation, the organoid suspension was collected in a 15 mL Falcon tube and centrifuged at 300 g for 5 minutes at room temperature. During centrifugation the resuspension solution (Table 7.2) was prepared. For every organoid, supernatant was discarded and cell pellet was resuspended in 400 µL of resuspension solution. Cell suspension was then carefully layered on the top of 1 mL of ovomucoid inhibitor solution and centrifuged at 300 g for 6 minutes at room temperature. Supernatant was discarded and immediately resuspended in 1 mL of culture medium for isolated Müller glia. Cell suspension was plated in one well of a 24-well plate to allow cell attachment and propagation (Figure 2.5).

Basic reagents				
Final solution	**Chemical**	**Dissolvent**	**Sterile filtration**	
3 units/mg Papain solution	6.7 mg Papain lyophilised powder (Catalogue no. 76220-25G; Sigma-Aldrich)	1 mL Earls balanced salt solution (EBSS) (Catalogue no. 24010043; Thermo-fisher)	22 µm filter (Catalogue no. SLGP003RS; Millex®)	
10mg/mL ovomucoid inhibitor solution	Ovomucoid inhibitor (Catalogue no. T9253; Sigma-Aldrich)	1 mL EBSS	22 µm filter	
1M L-Cysteine solution	610 mg L-Cysteine (Catalogue no. C7352; Sigma-Aldrich)	5 mL MilliQ water	22 µm filter	
Dissociation mix				
20 units/mL papain solution	1 mM L-cysteine	0.5 mM EDTA pH8.0 (Catalogue no. AM9260G; Invitrogen)	20 units/mL DNase	
Resuspension solution				
1.35 mL EBSS	150 µL ovomucoid inhibitor solution	7.5 µL DNase		
Culture medium for isolated Müller glia				
DMEM	1% penicillin-streptomycin	10% FCS	20 ng/mL EGF	20 ng/mL FGF

Table 7.2 Reagents required for retinal organoid dissociation

7.1.5 *In vitro* propagation of isolated Müller glia

Upon confluency of a 24-well plate, Müller glia isolated from retinal organoids were passaged and re-plated into a 6-well plate pre-coated with human fibronectin and cultured in the medium described in Table 7.2. Cells were further propagated up to passage 6 (P6) according to Table 7.3. This was to prepare enough populations of cells for cell surface marker analysis using fluorescent cell sorting analysis (FACS). Upon confluency of P6 culture, some cells were stored in freezing medium at -80°C while further continuous passages of three (P7-9) were continued in T25 culture flasks until confluent monolayers for collection of cell pellet samples for transcriptomic analysis.

Passage	P0	P1	P2	P3	P4	P5	P6
Culture Flask	24-well plate	6-well plate	T25	T75	T175	T175*2	T175*4
Split	1:1	1:1	1:1	1:1	1:1	1:2	1:4

Table 7.3 Plans for in vitro propagation of isolated Müller glia

7.1.6 Fluorescent cell sorting analysis (FACS)

The isolated cell population was examined for expression of the Müller glia cell surface markers CD29 and CD44, the negative markers including the undifferentiated stem cell marker SSEA-4 and epithelial cell surface marker cytokeratin-18, using FACS analysis. Upon confluency, cells were detached using Triple™ and cell pellets were obtained by centrifugation at 500 g for 5 minutes followed by washing in PBS twice. Cell pellets containing $2.5x10^5$ cells were incubated in 500 µL of PBS containing either single primary antibody against the above surface markers with conjugated respective fluorophores at the recommended dilution for 30 minutes on ice in the dark (Appendix 1). For unconjugated primary antibodies, primary antibodies were washed off with PBS 3 times and incubated with corresponding secondary antibodies for 30 minutes on ice in the dark (Appendix 1). Cell suspensions were washed three times in PBS by centrifugation at 500 g for 5 minutes and the supernatants discarded. At the end of the third wash, cell pellets were resuspended in 500 µL of PBS. Corresponding isotype controls and an unstained cell suspension were used as negative controls. FACS analysis for the prepared cell suspensions was performed using a LSRFortessa™ X-20 cell analyser (BD Biosciences).

7.1.7 Characterisation of retinal organoids and Müller glia

Between Day 30 and Day 121, retinal organoids were harvested for immunohistochemical characterisation. Isolated Müller glia were cultured onto glass coverslips pre-coated with human fibronectin. Cell pellets were also collected to obtain RNA and proteins to identify the expression of Müller glia-specific and progenitor cell markers using RT-PCR and western blotting, respectively. The

general procedures were described as follows and might apply as a general protocol for other experiments. The information of specific genes and proteins can be found in Appendix 1 & 2.

7.1.7.1 Fixation and dehydration

Each organoid was collected in an Eppendorf tube with a 5 mL pipette to avoid destruction of organoid structure. Residual culture medium was substituted by 250 µL of 4% paraformaldehyde (PFA) using a fume hood, and incubated for 20 minutes at room temperature, followed by addition of 250 µL of 30% sucrose to the 4% PFA and incubation for another 20 minutes. The mix solution was removed and substituted with 500 µL of fresh 30% sucrose and incubated for 20 minutes. This cryoprotection was completed by a final incubation with fresh 30% sucrose for at least an hour.

Isolated Müller glia were cultured in a 24-well plate on sterile glass cover slips coated with human fibronectin prior to use. Upon cell confluency, culture media was aspirated and cells were washed with sterile PBS before fixation with 4% PFA for 5 minutes. PFA was then aspirated under a fume hood and 30% sucrose was added for 15 minutes for dehydration. All liquid was aspirated and plate was left air dry for 15 minutes and sealed with Parafilm (Catalogue no. BR701605; Sigma-Aldrich) for storage at -20°C until use.

7.1.7.2 Embedding and cryosectioning of retinal organoids

Dehydrated organoids were placed in a cryosectoning tissue mould and embedded in OCT (optimum cutting temperature) embedding matrix (Catalogue no. KMA-0100-00A; CellPath) and snap frozen on dry ice. Embedded organoids were stored at -20°C before being sectioned at a thickness of 14µm using a cryostat (Leica CM1850). A series of organoid slices were placed on microscopic slides (Catalogue no. ECN631-1550; VWR) and stored at -20°C until use.

7.1.7.3 Immunohistological and immunocytochemical staining

Prior to staining, cells and organoid sections were defrosted for 30 minutes at room temperature and washed with tris buffered saline (TBS: 0.05M Trisma base+

0.145M NaCl) 3 times for 10 minutes each, followed by incubation with blocking solution consisting of 0.3% Triton (X100; Catalogue no. 9002-93-1; Sigma-Aldrich) and 5% donkey serum (Catalogue no. 017-000-121; Jackson ImmunoResearch Laboratories Inc.).

Antibodies used for the characterisation of human Müller glia are listed in Appendix 1. Primary antibodies were diluted in blocking solution and incubated with cells overnight at 4°C on a shaker. A control section was incubated with no primary antibody to check for non-specific staining. Cells were washed 3 times with TBS for 5 minutes and incubated with secondary bodies (Alexa-Fluor fluorochromes; Jackson ImmunoResearch Laboratories Inc.) diluted with TBS containing 0.3% Triton 1: 500 for 3 hours at room temperature in the dark (Appendix 2). Cells were washed three times in TBS for 5 minutes before counterstaining with DAPI (4', 6-diamidino-2-phenylindole; Catalogue no. D9542; Sigma-Aldrich) diluted in TBS 1:5000 for 2 minutes. Coverslips were then rinsed with distilled water and mounted with the cell side down on microscope slides using Vectashield mounting medium (Vector Laboratories). Cover slips were sealed with nail varnish before imaging.

7.1.7.4 Confocal microscopy and image analysis

Fluorescence images were acquired using a Zeiss confocal laser scanning microscope (LSM 700/710). The objectives 10X, 20X and 40X (oil immersion for LSM 700 and water immersion for LSM 710) were used according to the resolution acquired. Exposure times in milliseconds were set for individual filters without bleaching. Images were taken using Zeiss Zen Imaging Software and were analysed using ImageJ software. The results were processed by Excel and GraphPad Prism as described above.

7.2 Culture and cytokine treatment of Müller glia stem cells

Our laboratory has previously established an immortalised Müller glia stem cell line MIO-M1 (Moorfields Institute of Ophthalmology-Müller1) (Lawrence et al., 2007) which was used in this study. Müller glia were cultured in DMEM culture medium supplemented with foetal calf serum (FBS) and antibiotics as detailed in Table 7.4. Cells were incubated at 37°C with 5% CO_2. Upon confluency, cells were passaged

by aspirating culture media and detaching from the culture flask with 1X TrypLE™ Express Enzyme (Catalogue no. 12604; Gibco) by incubation for up to 5 minutes at 37°C. Cell Suspension was collected in DMEM with 10% FCS and centrifuged at 1500 rpm for 5 minutes to pellet cells. The supernatant was aspirated and the cell pellet was re-suspended in fresh DMEM supplemented with 10% FBS. To assess cell number, 10 µL of cell suspension was collected and mixed with 10 µL of Trypan Blue solution (Catalogue no. T8154; Sigma Aldrich). Cells were counted using a haemocytometer under an inverted phase-contrast light microscope. A fraction was re-plated at the appropriate concentration according to size of the culture flask and top up with the corresponding volume of media.

MIO-M1 Culture Medium	**Dulbecco's Modified Eagle Media (DMEM, high glucose, GlutaMAX™, pyruvate)** Catalogue no. 31966-047; Gibco
	10% FCS Catalogue no. FB-1001; Biosera
	1% 100x Penicillin-streptomycin Catalogue no. 15070-063; Gibco

Table 7.4 MIO-M1 cell culture medium

7.2.1 Cryopreservation of cells

Cell suspensions were centrifuged and pellets re-suspended in 1mL of freezing medium (50% DMEM, 40% FCS and 10% Dimethyl Sulfoxide (DMSO; Catalogue no. D4540; Sigma-Aldrich). Cell suspensions were aliquoted in cryovials and transferred to an isopropanol freezing container at -80°C for 24 hours for slow freezing before transferring to a liquid nitrogen tank at -150°C for long-term storage.

7.2.2 Müller glia cell culture with cytokines

MIO-M1 cells, hiPSC-MG1 and hESC-MG1 were cultured with the human pro-inflammatory recombinant cytokine Tumour Necrosis Factor-α (TNF-α; Catalogue no. 300-01A; Peprotech) and human recombinant Transforming Growth Factor-β1 (TGF-β1, Catalogue no. 100-21; Peprotech) for 24 hours to assess the modification of neuroprotective antioxidants produced by these cells.

7.2.2.1 Preparation of recombinant cytokines

Lyophilised TNF-α and TGF-β1 were reconstituted in sterile tissue-culture grade water (Catalogue no. 7732-18-5; Sigma-Aldrich) and further diluted to working concentrations (100 µg/mL) in sterile 0.1% Bovine Serum Albumin (BSA; Acros Organics, Thermo Fisher Scientific) diluted in phosphate buffered saline (PBS) according to the manufacturer's instructions and frozen at -20°C.

7.2.2.2 TNF-α treatment of human Müller glia

MIO-M1 cells, hiPSC-MG1 and hESC-MG1 were seeded at 1 million cells in T25 flasks for at 24 hours before cultured with TNF-α in 2 mL of culture medium at the final concentration of 50 ng/mL for 24 hours. Cell culture without cytokines were used control. Culture supernatants were collected in aliquots of at 500µL and centrifuged at 2000rpm for 10 minutes at 4°C to remove floating cells before frozen at -80°C for ELISA analysis. Cell pellets were collected for analysis of transcriptome (MIO-M1 cells only), gene and protein expression.

7.2.2.3 ELISA analysis for antioxidant production and activity

Supernatants were defrosted on ice and each aliquot was only used once for ELISA analysis and discarded to avoid multiple freezing and thawing. The following ELISA kits were purchased and relevant technical information were listed below and performed according to the manufacturer's instructions.

All ELISA analysis were performed in 96-well plates and a set of serially diluted standard proteins were used to provide a standard curve. Each sample and standard were performed in duplication. At the end of the ELISA analysis, the absorbance of the reagent mix in each well were read at the suggested wavelength (Table 7.5) using a SAFIRE plate reader (TECAN, Switzerland). Readings for samples and standards were normalised to control. A standard curve was plotted using Microsoft Excel and plotted using GraphPad Prism and the concentrations of proteins were extrapolated from the standard curve.

ELISA kit	Method	Detection range	Absorbance reading wavelength	Supplier	Catalogue no.
Human HO1 ELISA kit	Quantitative sandwich ELISA	23.44 pg/ml - 1500 pg/ml	450 nm	Abcam	Ab207261
Human PRDX6 ELISA kit	Quantitative sandwich ELISA	0.31 ng/mL - 20 ng/mL	450 nm	Cloud Clone	ABIN421344
Human SOD2 ELISA kit	Quantitative sandwich ELISA	0.78 ng/mL - 50 ng/mL	450 nm	Abnova	ABIN418871
Human BDNF ELISA kit	Quantitative sandwich ELISA	15.6 pg/mL- 1000 pg/mL	450 nm	Abcam	Ab212166
Human PEDF ELISA kit	Quantitative sandwich ELISA	0.9 ng/mL – 62.5 ng/mL	450 nm	Abcam	Ab246535

Table 7.5 List of ELISA kits used for quantification of anti-oxidation molecules produced by Müller glia cells

7.3 Reverse transcription (RT) polymerase chain reaction (PCR)

7.3.1 RNA extraction

RNA isolation was performed using the RNeasy Plus Mini Kit (Catalogue no. 74134; Qiagen). Upon cell confluency, culture media was aspirated and cells were washed with sterile PBS to remove residual serum and detached with a cell scraper. Cell suspensions were collected in one unit (350 µL for a T25 flask) of Buffer RLT Plus with β-mercaptoenthanol diluted at 1:100 and frozen overnight at -21°C for complete cell lysis and homogenisation. RNA extraction was then performed according to the manufacturer's instructions. Cell lysates were centrifuged at 2000 rpm for 5 minutes at 4°C before being transferred to a gDNA Eliminator Spin Column to remove genomic DNA. Lysates were homogenised with 70% ethanol and loaded onto a RNeasy Mini Spin Column and contaminants were eluted by washing with the supplied buffer RW1 and RPE. The concentrated RNA was eluted in 30 µL of the supplied RNase-free water and the concentration was determined using a spectrophotometer (Nanodrop-1000, Thermo Scientific). RNA samples were stored at -80°C and thawed on ice prior to use.

7.3.2 Reverse transcription

Prior to RT, the concentration of cDNA to be transcribed (either 1000 ng or 500 ng) was determined by the RNA concentration and the volume of RNA required for RT.

A home-made RT kit was used as follows: For every RT reaction, 1 µL dNTP mix (Catalogue no. U151A; Promega) and 1 µL Oligo d(T)12-18 primer (Catalogue no. 18418-012; Life Technologies) were mixed with the appropriate volume of RNA required. Ultrapure™ RNase-free water (Catalogue no. 10977-3; Invitrogen) was added to achieve a final volume of 11.5 µL. The RT mix was then transferred to a thermocycler (Mastercycler® Gradient; Eppendorf) which was heated to 65°C for 5 minutes and then cooled down to 4°C for 1 minute, before a mix of 1 µL 100 mM DTT, 1µL SuperScript® IV reverse transcriptase (Catalogue no. 18090010; SuperScript® IV First-Strand Synthesis System; Life Technologies), 4 µL 5X SuperScript® IV Buffer and 0.5 µL RNasin® Plus RNase inhibitor (Catalogue no. N2611; Promega) were added to the RT mix. The RT reaction was continued by another heating phase at 55°C for 10 minutes and at 80°C for 10 minutes. The cDNA product was used a PCR reaction or stored at -20°C for future use.

7.3.3 Polymerase chain reaction (PCR)

For each PCR reaction, a reaction mix was prepared as follows: 10 µL of GoTaq® Green Master Mix (Catalogue no. M712; Promega), 1 µL of forward and 1 µL of reverse primers diluted at a working concentration of 10 µM, 1 µL of sample cDNA at 1000 ng or 2 µL for cDNA at 500 ng, topping up to a final volume of 20 µL with DNase-free water. The reaction mix was transferred to a thermocycler with the following settings for PCR: an initial incubation at 95°C for 6 minutes, a further incubation at annealing temperature for 1 minute and an extension step of 72°C for 1 minute. This cycle was repeated for an appropriate number of cycles according to each primer pair. PCR reaction was terminated before a final extension phase at 72°C for 5 minutes and cooling at 4°C. PCR products were then stored at -4°C overnight or immediately separated by gel electrophoresis. Primer sequences, annealing temperature and run cycles recommended were listed in Appendix 2.

7.3.4 Gel electrophoresis

Prior to eletrophoresis, 2% agarose gel was prepared as follows: 2 g of agarose powder dissolved in 100 mL of 1X TAE buffer (40X) with nucleic acid gel stain GelRed™ (Catalogue no. 41003; Biotium Inc.) at the working concentration of 1 in 15,000. 10 µL of PCR product and 2.5 µL of 100 bp DNA ladder (Catalogue no.

G210; Promega) was loaded in the agarose gel and subjected to 100 V for 60 minutes. At the end of the electrophoresis, PCR products were visualised under UV light at appropriate exposure level and images taken using Genesnap Image Acquisition Software (www.syngene.com).

7.3.5 Imaging and statistics analysis

The intensity of the PCR bands was analysed by transforming intensity to peaks and measuring the area under each peak using the software ImageJ (Java). The measurements of gene-of-interest were normalised to the expression of the control house-keeping gene β-actin. For quantitative statistical analysis, cells from 3 or more passages were used as repeats and data analysis was performed using Microsoft Excel and plotted using GraphPad Prism. Comparison of up- or downregulation of genes-of-interest was performed using a paired Student's t-test with a *p*-value less than 0.05 indicating statistical significance.

7.4 Transcriptomic analysis using RNA sequencing technique

7.4.1 Extraction of genomic-DNA depleted total RNA

Extraction of genomic-DNA depleted total RNA followed similar steps described in section 7.3.1. Cell pellets collected from cell cultures prepared in section 7.1.5 were processed using RNeasy Plus Micro Kit (Catalogue no. 74034; Qiagen) which could remove genomic DNA through gDNA Eliminator spin columns. Concentrated RNA was eluted in 14 µL of the supplied RNase-free water and the concentration was determined using a spectrophotometer (Nanodrop-1000, Thermo Scientific). RNA samples were stored at -80°C and transported on dry ice to UCL Genomics for processing and sequencing.

7.4.2 Quality control and assurance of total RNA

Assessment on quality and quantity of extracted RNA were examined using a 2200 RNA ScreenTape system (Catalogue no. G2964AA; Agilent Technologies). RNA integrity was quantified by Agilent software and presented using RIN score. cDNA libraries were prepared from at least 100 ng of total RNA with high quality score using the KAPA mRNA HyperPrep Kit (Catalogue no. KK8580; KAPA Biosystems).

7.4.3 Preparation of cDNA library

mRNA transcripts with poly-adenylated were pulled out from total RNA using Oligo dT beads and fragmented by chemical hydrolysis before priming with random hexamers. First strand of cDNA was generated in strand-specific fashion by reverse transcriptase in the presence of Actinomycin D to favour RNA-dependent synthesis over DNA-dependent synthesis. The second cDNA strand was then synthesised and marked using dUTP. The final cDNA was added with A-tail at 3' end for prevention of self-ligation and adaptor dimerization. The A-tailed cDNA was then ligated with full length xGen adaptors (IDT) containing two unique 8bp sample specific indexes, a unique molecular identifier (N8) and a T overhang. The first-strand of ligated cDNA were amplified with 12 cycles of PCR with high fidelity polymerase which cannot extend dUTP-marked second-strand.

7.4.4 RNA-Sequencing

cDNA libraries were pooled in equimolar quantities and validated by the Agilent Technologies 2200 Bio-analyzer (Agilent Technologies). Paired-end sequencing of 75 bases with a corresponding 8bp UMI read was performed on an Illumina® HiSeq 3000 system for an average read of 26 million per sample.

7.4.5 Data analysis

Run data were processed to FASTQ files using Illumina's bcl2fastq Conversion Software (v2.19). The FASTQ files were filtered on quality and processed for adapter sequences. High quality reads were processed against the human reference genome Ensembl build GRCh38 using RNA-STAR 2.5.2b and UMI deduplicated using Je-suite (v1.2.1). Reads per transcript were counted using FeatureCounts and counts were estimated to transcript per million base (TPM) data based upon the index build from the human transcriptome. Differential gene expression (DEG) analysis was carried out using the BioConductor package SARTools, a DESeq2 wrapper (1.2.2) and subjected to gene ontology (GO) overrepresentation analysis using GOSeq. Statistical analysis and plots were carried out using the R environment (v3.5.2) and Bioconductor packages.

7.4.6 Validation of RNA-seq findings by Real-time polymerase chain reaction (qPCR)

Total RNAs collected from samples of independent experiments were used to validate the biological findings from RNA-seq data. The cDNA produced at 1000 ng using first-strand synthesis system as previously described in 7.3.2, was further diluted with RNase-free water 300 ng to for use.

7.4.7 Reaction mix preparation

Quantitative RT-PCR (qPCR) was performed using the TaqMan Gene Expression Assays following protocols from the manufacturer (Life Technologies). Each reaction mix consisted of 10 µL TaqMan™ Universal PCR Master Mix (Catalogue no. 4364338; Thermo Fisher), 1 µL TaqMan® Gene Expression Assay specific to genes of interest or endogenous control (Appendix 3) and 4 µL RNase-free water to make up for 15 µL. Duplicate of each conditions were prepared for analysis. Reaction mix for each reaction was loaded into a MicroAmp® Optical 96-Well Reaction Plate (Catalogue no. N8010560; Thermo Fisher) and 5µL of the diluted cDNA at 10ng per reaction added to each well for a total of 20 µL. All reactions were prepared on a StarChill PCR chiller (Catalogue no. E2396-2006; Starlab) and plates sealed with a MicroAmp™ Optical adhesive film (Catalogue no. 4311971; Thermo Fisher) to avoid evaporation.

7.4.8 qPCR

QuantStudio™ 6 Flex Real-Time PCR System (Applied Biosystems™) was used for qPCR run. Prior to loading, plates were centrifuged to bring down reaction mix to the bottom of the well and get rid of bubble. The thermo cycling conditions were set as follows: 50°C for 2 minutes, 95°C for 10 minutes followed by 40 cycles of 95°C for 15 seconds and 60°C for 1 minute and finished with a melt curve step of 95°C for 15 seconds, and 60°C for 1 minute. Fluorescent signal emitted between 60°C and 72°C of each cycle was recorded by the reader sensor.

7.4.9 Data analysis

At the end of the run, the threshold cycle (Ct) value was exported from the QuantStudio™ 6 Flex Real-Time PCR software (v1.1). Ct value represents the number of cycles at which the of the amplified PCR product reaches the threshold level. The data were analysed using the $2^{-\Delta\Delta Ct}$ method as fold change relative to endogenous control 18S. The following step indicates quantification procedures:

1. Normalise Ct values of gene of interest to that of endogenous control: ΔCt = Ct (gene of interest) – Ct (endogenous control 18S)
2. Normalise Ct values of experimental sample to calibrator as fold difference:
   $\Delta\Delta Ct = \Delta Ct$ (sample) – ΔCt (untreated control)
   Where $\Delta\Delta Ct > 0$ indicates upregulation and < 0 suggests downregulation.
3. Calculate fold change: Fold change = $2^{-\Delta\Delta Ct}$

7.5 Western blotting

7.5.1 Protein extraction

Cells were washed with PBS and detached using Triple™ before centrifuging to a cell pellet. To obtain a whole cell lysate for one sample, 100 µL of ice-cold Radio Immunoprecipitation Assay (RIPA) lysis buffer (Catalogue no. R0278; Sigma-Aldrich) mixed with 10 µL of protease inhibitor cocktail (Catalogue no. P8340; Sigma-Aldrich), 3 mM Sodium Orthovanadate (Na_3VO_4), 0.5 mM Dithiothreitol (DTT) and 1mM Phenyl Methyl Sulphonyl Fluoride (PMSF) was prepared. The cell pellet was vortexed vigorously in RPA buffer to reach homogenization and placed on ice for 5 minutes before centrifugation at 10,000 rpm for 5 minutes to separate cell debris.

7.5.2 BCA protein assay

Protein concentrations were measured using the Thermo Scientific Pierce™ BCA (Bicinchoninic Acid) Protein Assay Kit (Catalogue no. 23225; Life Technologies). This colorimetric assay works on the basis of measuring the generation of the coloured end-product bicinchoninic acid upon the reduction of Cu^{2+} ion to Cu^{1+} by the protein of interest by spectrophotometry at 562 nm. The absorbance of the end-product is linearly proportional to the protein concentration.

According to the manufacture's protocol, proteins to be tested were diluted in water, standards were diluted in lysis buffer, a blank containing only water and zero containing lysis buffer and water were prepared in duplicates in a 96-well plate as per manufacturer's instructions. BCA reagent mix was prepared as per manufacturer's instructions and loaded to each well. Plates were incubated at 37°C for 30 minutes and absorbance at 562 nm was measured using a SAFIRE plate reader (TECAN). Readings for proteins of interest and standards were normalized to blank and zero respectively. A standard curve was plotted and the concentrations of proteins were extrapolated from the standard curve.

7.5.3 Protein gel electrophoresis

NuPAGE® (Life Technologies) electrophoresis using precast Novex® gels with 15 wells and the corresponding 1X Running Buffer were employed to separate proteins between 15 kDa to 260 kDa. The molecular weight of proteins-of-interest in this study and the corresponding types of gels and running buffer to separate them were listed below (Table 7.6).

Protein	Molecular weight (kDa)	Type of gel	Running buffer
β-actin	42	4-12% Bis-Tris polyacrylamide gel (Catalogue. no NP0336BOX; Life Technologies)	MOPS SDS running buffer (Catalogue. no NP0001; Life Technologies)
CD29	110		
Vimentin	54		
Glutamine synthase	44		
Sox9	65		
Sox2	40		
Pax6	50		
WNT2b	43		
Cleaved Notch 1	110		
Nestin	220	3-8% Tris-acetate gel (Catalogue. no EA03755BOX; Life Technologies)	Tris-acetate SDS running buffer (Catalogue. no LA0041; Life Technologies)
NQO1	31	4-12% Bis-Tris polyacrylamide gel	MES SDS running buffer (Catalogue. no NP0002; Life Technologies)
HO1	32		
PRD6	26		
FOLH1	110		
SOD2	25		
GSR	50-65		
GSS	52		
PON2	40		

Table 7.6 Molecular weight of the proteins of interest and the corresponding types of gel and running buffer used in protein gel electrophoresis.

Prior to loading, for every sample (15 µL), 3.75 µL of loading buffer (LDS 4X; Catalogue no. NP0007; Life Technologies) and 1.5 µL of reducing agent (10X; Catalogue no. NP0009; Life Technologies) were mixed with 9.75 µL of extracted protein giving a mass of 5 µg or 2 µg and topped up with the corresponding volume of water, depending on the protein concentration, to a final volume of 15 µL. This mixture was gently vortexed and centrifuged before protein denaturation in a heat block set at 80°C for 10 minutes.

To set up the gel electrophoresis system, precast gels were removed from packaging and rinsed with water to remove soaking liquid. Combs and seal tape were removed before securing the gels to an XCell SureLock™ Mini-Cell Electrophoresis System (Life Technologies) tank. 200 mL of running buffer containing 500 µL of antioxidant (Catalogue no. NP0005; Life Technologies) was poured into the inner compartment while 600 mL was poured into the outer compartment of the tank. Protein samples and 5 µL of pre-stained protein standard ladder (ranging between 11 and 190 kDa; Catalogue no. P7706; New England Biolabs) were loaded into the wells. The gel was then run at 180 V for 60 minutes.

7.5.4 Semi-dry gel transfer

Appropriately sized 0.45 µm Poly VinyliDene Fluoride (PVDF) membranes (Immobilon-FL PVDF, Catalogue no. IPFL00010; Merck Millipore) were soaked in methanol and rinsed with distilled water before placing in transfer buffer. 20X transfer buffer (Catalogue no. NP0006; Life Technologies) was diluted with 15% methanol in 100 mL of distilled water to make up for 1X working transfer buffer and was used for rinsing gels and wetting filter paper and membrane (Catalogue no. 1703968; Bio-Rad Laboratories). Upon the completion of gel electrophoresis, the gel was removed from its cast and rinsed in transfer buffer. The transfer system was set up as such that the pre-wet filter paper was placed on the bottom platinum anode of the Trans-Blot® SD Semi-Dry Transfer Cell (Bio-Rad Laboratories), followed by the PVDF membrane. The gel was then placed faced-down, followed by another piece of pre-wet filter paper. The top cathode was placed in contact with the top filter paper and the transfer was carried out at 10 V for 30 minutes.

7.5.5 Immunoblotting

A blocking solution containing Tris-buffered Saline (TBS) with 0.1% Tween-20, 5% milk and 5% FCS was prepared. PVDF membranes were blocked in the said blocking solution for 2 hours at 37°C. The primary antibody (Appendix 1) was diluted appropriately in the blocking agent and incubated with the PVDF membrane overnight at 4°C on a shaker. The membrane was washed 3 times for 30 minutes in TBS with 0.1% Tween-20 on a shaker at room temperature. This was followed by incubation with secondary antibodies (Jackson ImmunoResearch Laboratories Inc.) specific for the primary antibodies and diluted 1:5000 in blocking agent. Membranes were then incubated at room temperature for 1 hour. The membrane was washed for another three times in TBS with 0.1% Tween-20 on a shaker at room temperature. Luminata Western HRP Substrate (Catalogue no. WBLUC0500; Millipore) was added onto the membrane for 2 minutes before removing access liquid and sealing the membrane in a plastic cassette. Proteins-of-interest were visualised using Fuji X-ray film (Catalogue no. AUT-300-040D; Thermo-Fisher Scientific) developed in a dark room.

7.5.6 Re-probing with different antibodies

To visualise other proteins-of-interest with primary antibodies, previously bound primary antibodies could be stripped off by incubating PDVF membranes with TBS followed by washing in stripping buffer containing 200 mM glycine and 5 mM NaCl at pH 2.5 for half an hour at room temperature. This was followed by washing the membrane in TBS 3 times for 5 minutes each at room temperature. Membrane were then re-probbed with other primary antibodies or stored in TBS at 4°C up to two weeks for future use.

7.5.7 Image analysis

X-ray films were scanned and optical density of bands was measured using ImageJ. Statistical analysis was performed in GraphPad Prism as described in section of PCR analysis.

7.6 Establishment of primary rat retinal ganglion cells in vitro

RGCs were isolated from Sprague Dawley rat pups from postnatal day 4 using two-step immunopanning protocol modified from (Winzeler and Wang, 2013b). The preparation of reagent stocks and working solution was detailed in Appendix 3-4.

7.6.1 Overnight preparation of culture and panning plates

The following reagents are prepared prior to the day of dissection of rat pup eyes. Nunc™ Lab-Tek™ Chamber Slide System Coverglass for 16-well chamber slides (Catalogue no. 178599PK; Thermo Fisher Scientific) were coated with 1x PDL (Appendix 4.2-1)) at room temperature overnight. Culture chambers were gently swirled to ensure proper coverage of the surface. In the following morning, 1x PDL was aspirated and culture chambers were rinsed with sterile H_2O three times. An aliquot of 10 µL mouse laminin (1 mg/mL) (Appendix 4.2-2)) was thawed at 4°C and was diluted with 5 mL of Neurobasal medium to a final concentration of 50 µg/mL. 100 µL of the laminin working solution was added to each coverslip. Culture chambers were incubated at 37°C for at least two hours and rinsed with sterile water for three times before use.

The negative and positive panning solution were prepared (Appendix 4.2-10)) and added into 2 of the 15-cm Petri dish and 1 of the 10-cm Petri dish, respectively. The plates were swirled gently for even coating with antibody-Tris solution and were transferred to a 4°C fridge for overnight coating for best results. In the following morning prior to tissue dissection, 0.2 % BSA working solution (Appendix 4.1-7) and panning buffer were prepared (Appendix 4.1-11)). 15 mL of EBSS were warmed in an incubator at 37°C for at least 2 hours. The positive panning plate was rinsed with D-PBS once. D-PBS containing anti-thy1.1 (Appendix 1) at a dilution of 1:25 and 0.2% BSA was prepared and swirled gentle to coat the plate evenly. The plates were left at room temperature for at least 2 hours.

7.6.2 Tissue acquisition

Pregnant female Sprague Dawley (SD) rats obtained from Charles Rivers Fish facility and the new-born postnatal pups were maintained at the UCL Biological Service Unit. Procedures involving animals were performed in accordance to the

guidelines described in the ARVO Statement for the Use of Animals in Ophthalmic and Vision Research. The use of animals for this study was approved by the Ethics Committee at University College London Institute of Ophthalmology and the U.K. Home Office.

7.6.3 Dissection and dissociation of retinae

The key to achieve high yield of RGC isolation is to dissect intact retinae as much as possible as small pieces could be lost in later steps. Retinae were collected from pups euthanised by cervical dislocation at postnatal day 4. Heads were removed by a sterilised scissors and transferred to a dissection hood. The skin overlaying the eyeball was cut away using a small scissor. The eye balls were pushed out by pressing down the tissues around using forceps and a Swann-Morton surgical scalpel (Catalogue no. 233-5364; VWR). While the eyeball was exposed, the exposed cornea was sliced across by the scalpel. The lens and vitreous humour were removed with the back of scalpel with a gentle squeeze by the forceps. The retinae were gently detached using a small flat spatula and transferred to a 6-cm Petri dish containing pre-warmed Earle's balanced salt solution (EBSS) for pooling. Under a dissection microscope, membranes having blood vessels visibly through the retina were removed by forceps. Retinae were transferred gently to 10 mL of papain dissociation solution (Catalogue no. LK003178; Worthington Biochemicals) containing 100 µL of DNase I stock (0.4%) (Appendix 4.2-4)) and incubated at 37°C for 30 minutes. The falcon was shaken every 15 minutes.

7.6.4 Enrichment for viable RGCs by flow cytometry

Retinal suspension was triturated with low ovomucoid working solution (Appendix 4.2-5)) by gentle pipetting before passing through a sterile 40-µm nylon mesh (Catalogue no. 352340; Corning) placed on top of a 50-mL Falcone tube. Cell counts were performed using an automated cell counter Vi-cell (Beckman Coulter). Each ½ million cells were taken as blank, single stained with CD45-Alexa fluorescence (AF) 647 and CD90- Phycoerythrin (PE) respectively (Appendix 1). The rest of retinal cell suspension was double stained with both antibodies in the dark on ice for 30 minutes. Prepared samples were briefly incubated with SYTOX^{TM} Blue Dead

Cell Stain (Catalogue no. S34857; Invitrogen) before sorting by a BD Influx™ flow cytometer system (BD Biosicences) to recover $CD45^-$ & $CD90^+$ RGCs.

7.6.5 Enrichment of RGCs by two-step immunopanning

The previous steps from tissue acquisition to retinal dissociation were shared by both methodologies.

7.6.5.1 Trituration of retinae

Low (low-ovomuocid) and high (high-ovomucoid) working solutions were prepared (Appendix 4.2-5) while papain digestion was ongoing. 4 mL of low solution was added to retinal suspension and incubated at room temperature for 1 minute. 80 µL of rabbit anti-rat macrophage polyclonal antibody (Appendix 4.2-7) was then added to the remaining 6 mL of low solution.

After 1-minute incubation, the low solution was aspirated and 2 mL of the low + anti-macrophage solution was added to the cell suspension. Using a P1000 pipette, gently triturate the cell suspension was gently triturated for three to four times and settled for 1 minute. Note that bubbles must be avoided and pipette gently to allow optimal cell health. After incubation, the supernatant was transferred to a new 15-mL Falcon tube. 1 mL of the low + anti-macrophage solution was added and gentle triturated and 1 min-settlement as previously described was repeated for 4 times, until the low + anti-macrophage solution was used. At the end of last repeat, retinal suspension was incubated at room temperature for 10 minutes to allow binding of macrophage antibody to cells. Cell suspension was centrifuged at 1000 rpm for 12 minutes at 25°C. Supernatant was aspirated and cell pellet was resuspended in high solution, followed by centrifugation at 1000 rpm for 12 minutes at 25°C.

7.6.5.2 Panning

Supernatant was aspirated and the cell pellet was resuspended in 15 mL of panning buffer. Cell suspension was filtered through a sterile 40-µm nylon mesh placed on top of a 50-mL Falcone tube. 1 mL of the cell suspension was transferred through the mesh filter and repeat until the all suspension was filtered. The mesh was rinsed with the remaining panning buffer.

The prepared two negative selection plates were rinsed three times with D-PBS. The cell suspension was transferred to the 1st negative panning plate placed on a flat surface and incubated for 20 minutes. The cell suspension was then transferred to the 2nd negative panning plate and incubated for 45 minutes. The plate was shaken every 15 minutes. Before transferring the cell suspension from the 2nd negative panning plate, the positive panning plate was aspirated to remove the Thy1 antibody solution and rinsed with D-PBS for three times. The cell suspension was transferred to the positive panning plate and incubated for 45 minutes. The plate was shaken every 15 minutes. While waiting for the incubation, the RGC Complete Culture Medium was prepared (Appendix 4.3-4.6) and warmed at 37°C.

7.6.5.3 Trypsination and plating of RGCs

For the last 15 minutes of panning, 100 µL of trypsin stock (30,000 U/mL) (Appendix 4.2-6) was added to 4 mL of pre-warmed EBSS. The positive panning plate was washed 6 times with DPBS and checked under the microscope to ensure only adherent cells attached. The plate was washed with the remaining 6 mL of EBSS, rinsed again with the trypsin solution and incubated at 37°C for 4 minutes. While waiting, 30% FCS in D-PBS was prepared as follows: 6 mL of FCS was filtered through a 0.22-µm filter and collected into 14 mL of D-PBS. 2 mL of 30% FCS was gently squirted against the plate to rinse off the adherent RGCs. The solution was transferred to a new 50-mL Falcon tube containing 1 mL of 30% FCS. Another 5 mL of 30% FCS was gently squirted against the plate and the solution was also transferred to the same tube. This was repeated until all the 30% FCS was used. The plate was checked under the microscope to ensure the adherent cells have been detached. The cell suspension was gently homogenised and centrifuged at 1000 rpm for 12 minutes. The cell pellet was then resuspended in prewarmed RGC Complete Medium and cell count using trypan blue was performed to estimate RGC population.

7.6.6 *In vitro* culture of primary rat RGCs

Collected cells were seeded at 10,000 cells /well in PDL-laminin-coated 16-well chamber. The culture condition of purified rat RGCs wereperfomred under normoxic

conditions with 20% O_2, 5% CO_2, 75% N_2 at 37 °C, as suggested by (Lee et al., 2010c) for 72 hours in RGC complete medium before further treatment.

7.6.7 Assessment of neuroprotective potential of human Müller glia to RGCs against glutamate excitotoxicity

7.6.7.1 24-hour dose response of primary RGCs to glutamate neurotoxicity

Glutamate was prepared by dissolving L-glutamic acid (Catalogue no. G1251; Sigma-Aldrich) in sterile tissue-culture grade water which was pre-warmed at 37°C to a final concentration of 10 mM and filtered through a 0.22-µm filter. Sterile 10 mM glutamate stock was diluted to respective volume of RGC Complete Medium to achieve dose curve of final concentrations 25 µM, 37.5 µM and 50 µM. 100 µL of each concentration was added to a well of primary RGC culture for 24 hours. RGCs cultured with RGC Complete Medium only served as controls. At least three wells of replicates were prepared for each concentration of glutamate. RGC survival was assessed by quantifying the percentage of healthy RGC with morphological features showing round soma with complete membrane integrity and 2-5 primary branches of neurites. The concentration of glutamate that achieves 70-80% of survival was considered as the minimal concentration of neurotoxicity.

7.6.7.2 Assessment of morphological features of RGCs

Upon completion of the dose response experiment, RGCs were fixed with 4% PFA and dehydrated in 30% sucrose solution. Morphological features of RGCs were examined by staining with antibodies specific to markers of RGC, including beta III tubulin (TUJ), BRN3A and DAPI (Appendix 1). Fluorescence images with Z-stacks were acquired using a Zeiss confocal laser scanning microscope (LSM 700/710) at 40x and image analysis were performed on images processed for maximum intensity projection. Images were taken for at least 18 random fields per well.

Quantitative features including number of RGCs per field, total dendritic length in µm per RGC, number of primary neurite (stem) and bifurcation (branches) per RGC were quantified by a tracing pad connected to ImageJ. Statistical analysis of RGC

features at each culture condition were performed using t-test on Graphpad Prism 5.

7.6.7.3 Preparation of human Müller glia conditioned medium

As described previously in section 7.1.5 and 7.2, MIO-M1 and hESC-MG1 were seeded at 1 million in a T25 culture flask pre-coated fibronectin. The culture media consisted of DMEM containing 10% KOSR and P/S. Cells were cultured for 24 hours before harvesting of conditioned medium. Culture supernatants was collected and briefly centrifuged to remove floating cells.

7.6.7.4 Induction of 24-hour glutamate excitotoxicity

72 hours after seeding, 100 µL of each of the following culture media (Table 7.7) were replaced in each well of RGC culture to induce glutamate excitotoxicity.

Condition	Negative Control	Test 1	Test 2	Positive Control
[Glutamate] (µM)	0	25	25	25
Culture Medium	DMEM + 10% KOSR + P/S	RGC Basal Medium	hESC-MG1 conditioned medium	RGC Complete Medium

Table 7.7 Culture conditions of primary RGCs for induction of 24-hour glutamate neurototoxicity. At the end of the 24-hour treatment, RGCs were harvested and RGC survival was analysed as described in 7.6.7.2.

CHAPTER 8 References

ACHESON, A., CONOVER, J. C., FANDL, J. P., DECHIARA, T. M., RUSSELL, M., THADANI, A., SQUINTO, S. P., YANCOPOULOS, G. D. & LINDSAY, R. M. 1995. A BDNF autocrine loop in adult sensory neurons prevents cell death. *Nature,* 374**,** 450-3.

ADER, M. & TANAKA, E. M. 2014. Modeling human development in 3D culture. *Curr Opin Cell Biol,* 31**,** 23-8.

AFLATOONIAN, B., RUBAN, L., SHAMSUDDIN, S., BAKER, D., ANDREWS, P. & MOORE, H. 2010. Generation of Sheffield (Shef) human embryonic stem cell lines using a microdrop culture system. *In Vitro Cell Dev Biol Anim,* 46**,** 236-41.

AGARWAL, N., AGARWAL, R., KUMAR, D. M., ONDRICEK, A., CLARK, A. F., WORDINGER, R. J. & PANG, I. H. 2007. Comparison of expression profile of neurotrophins and their receptors in primary and transformed rat retinal ganglion cells. *Mol Vis,* 13**,** 1311-8.

AGARWAL, R. & AGARWAL, P. 2012. Glaucomatous neurodegeneration: An eye on tumor necrosis factor-alpha. *Indian Journal of Ophthalmology,* 60**,** 255-261.

AL-GAYYAR, M. & ELSHERBINY, N. 2013. Contribution of TNF-α to the development of retinal neurodegenerative disorders. *European cytokine network,* 24**,** 27-36.

AL TANOURY, Z., PISKUNOV, A. & ROCHETTE-EGLY, C. 2013. Vitamin A and retinoid signaling: genomic and nongenomic effects. *J Lipid Res,* 54**,** 1761-75.

ALGE, C. S., PRIGLINGER, S. G., KOOK, D., SCHMID, H., HARITOGLOU, C., WELGE-LUSSEN, U. & KAMPIK, A. 2006. Galectin-1 influences migration of retinal pigment epithelial cells. *Invest Ophthalmol Vis Sci,* 47**,** 415-26.

AMBROS, V. 2004. The functions of animal microRNAs. *Nature,* 431**,** 350-5.

AMBRUSO, D. R., ELLISON, M. A., THURMAN, G. W. & LETO, T. L. 2012. Peroxiredoxin 6 translocates to the plasma membrane during neutrophil activation and is required for optimal NADPH oxidase activity. *Biochim Biophys Acta,* 1823**,** 306-15.

AMIN, R. H., FRANK, R. N., KENNEDY, A., ELIOTT, D., PUKLIN, J. E. & ABRAMS, G. W. 1997. Vascular endothelial growth factor is present in glial cells of the retina and optic nerve of human subjects with nonproliferative diabetic retinopathy. *Invest Ophthalmol Vis Sci,* 38**,** 36-47.

AN, M. J., KIM, C. H., NAM, G. Y., KIM, D. H., RHEE, S., CHO, S. J. & KIM, J. W. 2018. Transcriptome analysis for UVB-induced phototoxicity in mouse retina. *Environ Toxicol,* 33**,** 52-62.

ANDERSON, B., JR. 1968. Ocular effects of changes in oxygen and carbon dioxide tension. *Trans Am Ophthalmol Soc,* 66**,** 423-74.

ANDREWS, P. W., CASPER, J., DAMJANOV, I., DUGGAN-KEEN, M., GIWERCMAN, A., HATA, J., VON KEITZ, A., LOOIJENGA, L. H., MILLAN, J. L., OOSTERHUIS, J. W., PERA, M., SAWADA, M., SCHMOLL, H. J., SKAKKEBAEK, N. E., VAN PUTTEN, W. & STERN, P. 1996. Comparative analysis of cell surface antigens expressed by cell lines derived from human germ cell tumours. *Int J Cancer,* 66**,** 806-16.

ANRATHER, J., RACCHUMI, G. & IADECOLA, C. 2006. NF-kappaB regulates phagocytic NADPH oxidase by inducing the expression of gp91phox. *J Biol Chem,* 281**,** 5657-67.

ARAUJO, R. S., SANTOS, D. F. & SILVA, G. A. 2018. The role of the retinal pigment epithelium and Muller cells secretome in neovascular retinal pathologies. *Biochimie,* 155**,** 104-108.

ASSAWACHANANONT, J., MANDAI, M., OKAMOTO, S., YAMADA, C., EIRAKU, M., YONEMURA, S., SASAI, Y. & TAKAHASHI, M. 2014. Transplantation of embryonic and induced pluripotent stem cell-derived 3D retinal sheets into retinal degenerative mice. *Stem Cell Reports,* 2**,** 662-74.

AZADMANESH, J., TRICKEL, S. R., WEISS, K. L., COATES, L. & BORGSTAHL, G. E. 2017. Preliminary neutron diffraction analysis of challenging human manganese superoxide dismutase crystals. *Acta Crystallogr F Struct Biol Commun,* 73**,** 235-240.

BALAKIREV, E. S. & AYALA, F. J. 2003. Pseudogenes: are they "junk" or functional DNA? *Annu Rev Genet,* 37**,** 123-51.

BALDWIN, A. S., JR. 1996. The NF-kappa B and I kappa B proteins: new discoveries and insights. *Annu Rev Immunol,* 14**,** 649-83.

BALL, D. K., RACHFAL, A. W., KEMPER, S. A. & BRIGSTOCK, D. R. 2003. The heparin-binding 10 kDa fragment of connective tissue growth factor (CTGF) containing module 4 alone stimulates cell adhesion. *J Endocrinol,* 176**,** R1-7.

BANKS, C. A., BOANCA, G., LEE, Z. T., EUBANKS, C. G., HATTEM, G. L., PEAK, A., WEEMS, L. E., CONKRIGHT, J. J., FLORENS, L. & WASHBURN, M. P. 2016. TNIP2 is a Hub Protein in the NF-kappaB Network with Both Protein and RNA Mediated Interactions. *Mol Cell Proteomics,* 15**,** 3435-3449.

BARANANO, D. E., RAO, M., FERRIS, C. D. & SNYDER, S. H. 2002. Biliverdin reductase: a major physiologic cytoprotectant. *Proc Natl Acad Sci U S A,* 99**,** 16093-8.

BARANIAK, P. R. & MCDEVITT, T. C. 2010. Stem cell paracrine actions and tissue regeneration. *Regen Med,* 5**,** 121-43.

BARCLAY, A. N. & HYDEN, H. 1979. Localization of the Thy-1 antigen by immunofluorescence on neurons isolated from rat brain. *J Neurochem,* 32**,** 1583-6.

BARRES, B. A., SILVERSTEIN, B. E., COREY, D. P. & CHUN, L. L. 1988. Immunological, morphological, and electrophysiological variation among retinal ganglion cells purified by panning. *Neuron,* 1**,** 791-803.

BASRAI, H. S., CHRISTIE, K. J., TURBIC, A., BYE, N. & TURNLEY, A. M. 2016. Suppressor of Cytokine Signaling-2 (SOCS2) Regulates the Microglial Response and Improves Functional Outcome after Traumatic Brain Injury in Mice. *PLoS One,* 11**,** e0153418.

BASRAI, H. S., TURBIC, A., CHRISTIE, K. J. & TURNLEY, A. M. 2017. Suppressor of Cytokine Signalling 2 (SOCS2) Regulates Numbers of Mature Newborn Adult Hippocampal Neurons and Their Dendritic Spine Maturation. *Cell Mol Neurobiol,* 37**,** 899-909.

BEALE, R. & OSBORNE, N. N. 1982. Localization of the Thy-1 antigen to the surfaces of rat retinal ganglion cells. *Neurochem Int,* 4**,** 587-95.

BEATTY, S., KOH, H., PHIL, M., HENSON, D. & BOULTON, M. 2000. The role of oxidative stress in the pathogenesis of age-related macular degeneration. *Surv Ophthalmol,* 45**,** 115-34.

BECKER, S., EASTLAKE, K., JAYARAM, H., JONES, M. F., BROWN, R. A., MCLELLAN, G. J., CHARTERIS, D. G., KHAW, P. T. & LIMB, G. A. 2016. Allogeneic Transplantation of Muller-Derived Retinal Ganglion Cells Improves Retinal Function in a Feline Model of Ganglion Cell Depletion. *Stem Cells Transl Med,* 5**,** 192-205.

BERGER, S., SAVITZ, S. I., NIJHAWAN, S., SINGH, M., DAVID, J., ROSENBAUM, P. S. & ROSENBAUM, D. M. 2008. Deleterious role of TNF-alpha in retinal ischemia-reperfusion injury. *Invest Ophthalmol Vis Sci,* 49**,** 3605-10.

BERGER, U. V., LUTHI-CARTER, R., PASSANI, L. A., ELKABES, S., BLACK, I., KONRADI, C. & COYLE, J. T. 1999. Glutamate carboxypeptidase II is expressed by astrocytes in the adult rat nervous system. *J Comp Neurol,* 415**,** 52-64.

BERNARDOS, R. L., BARTHEL, L. K., MEYERS, J. R. & RAYMOND, P. A. 2007. Late-Stage Neuronal Progenitors in the Retina Are Radial Müller Glia That Function as Retinal Stem Cells. *The Journal of Neuroscience,* 27**,** 7028-7040.

BERTRAND, M. J., LIPPENS, S., STAES, A., GILBERT, B., ROELANDT, R., DE MEDTS, J., GEVAERT, K., DECLERCQ, W. & VANDENABEELE, P. 2011. cIAP1/2 are direct E3 ligases conjugating diverse types of ubiquitin chains to receptor interacting proteins kinases 1 to 4 (RIP1-4). *PLoS One,* 6**,** e22356.

BESSERO, A. C. & CLARKE, P. G. 2010. Neuroprotection for optic nerve disorders. *Curr Opin Neurol,* 23**,** 10-5.

BHARADWAJ, A. S., STEMPEL, A. J., OLIVAS, A., FRANZESE, S. E., ASHANDER, L. M., MA, Y., LIE, S., APPUKUTTAN, B. & SMITH, J. R. 2017. Molecular Signals Involved in Human B Cell Migration into the Retina: In Vitro Investigation of ICAM-1, VCAM-1, and CXCL13. *Ocul Immunol Inflamm,* 25**,** 811-819.

BHARATHIDEVI, S. R., BABU, K. A., JAIN, N., MUTHUKUMARAN, S., UMASHANKAR, V., BISWAS, J. & ANGAYARKANNI, N. 2017. Ocular distribution of antioxidant enzyme paraoxonase & its alteration in cataractous lens & diabetic retina. *Indian J Med Res,* 145**,** 513-520.

BHATIA, B., SINGHAL, S., LAWRENCE, J. M., KHAW, P. T. & LIMB, G. A. 2009. Distribution of Müller stem cells within the neural retina: Evidence for the existence of a ciliary margin-like zone in the adult human eye. *Experimental Eye Research,* 89**,** 373-382.

BIBEL, M., RICHTER, J., SCHRENK, K., TUCKER, K. L., STAIGER, V., KORTE, M., GOETZ, M. & BARDE, Y. A. 2004. Differentiation of mouse embryonic stem cells into a defined neuronal lineage. *Nat Neurosci,* 7**,** 1003-9.

BISWAL, M. R., ILDEFONSO, C. J., MAO, H., SEO, S. J., WANG, Z., LI, H., LE, Y. Z. & LEWIN, A. S. 2016. Conditional Induction of Oxidative Stress in RPE: A Mouse Model of Progressive Retinal Degeneration. *Adv Exp Med Biol,* 854**,** 31-7.

BLACKSHAW, S., HARPAVAT, S., TRIMARCHI, J., CAI, L., HUANG, H., KUO, W. P., WEBER, G., LEE, K., FRAIOLI, R. E., CHO, S. H., YUNG, R., ASCH, E., OHNO-MACHADO, L., WONG,

W. H. & CEPKO, C. L. 2004. Genomic analysis of mouse retinal development. *PLoS Biol,* 2**,** E247.
BLANER, W. S. 2019. Vitamin A signaling and homeostasis in obesity, diabetes, and metabolic disorders. *Pharmacol Ther,* 197**,** 153-178.
BLASER, H., DOSTERT, C., MAK, T. W. & BRENNER, D. 2016. TNF and ROS Crosstalk in Inflammation. *Trends Cell Biol,* 26**,** 249-261.
BOUWMEESTER, T., BAUCH, A., RUFFNER, H., ANGRAND, P. O., BERGAMINI, G., CROUGHTON, K., CRUCIAT, C., EBERHARD, D., GAGNEUR, J., GHIDELLI, S., HOPF, C., HUHSE, B., MANGANO, R., MICHON, A. M., SCHIRLE, M., SCHLEGL, J., SCHWAB, M., STEIN, M. A., BAUER, A., CASARI, G., DREWES, G., GAVIN, A. C., JACKSON, D. B., JOBERTY, G., NEUBAUER, G., RICK, J., KUSTER, B. & SUPERTI-FURGA, G. 2004. A physical and functional map of the human TNF-alpha/NF-kappa B signal transduction pathway. *Nat Cell Biol,* 6**,** 97-105.
BRANTLEY, M. A. & STERNBERG, P. 2013. Chapter 22 - Mechanisms of Oxidative Stress in Retinal Injury. *In:* RYAN, S. J., SADDA, S. R., HINTON, D. R., SCHACHAT, A. P., SADDA, S. R., WILKINSON, C. P., WIEDEMANN, P. & SCHACHAT, A. P. (eds.) *Retina (Fifth Edition).* London: W.B. Saunders.
BRINGMANN, A., FRANCKE, M., PANNICKE, T., BIEDERMANN, B., KODAL, H., FAUDE, F., REICHELT, W. & REICHENBACH, A. 2000. Role of glial K(+) channels in ontogeny and gliosis: a hypothesis based upon studies on Muller cells. *Glia,* 29**,** 35-44.
BRINGMANN, A., IANDIEV, I., PANNICKE, T., WURM, A., HOLLBORN, M., WIEDEMANN, P., OSBORNE, N. N. & REICHENBACH, A. 2009. Cellular signaling and factors involved in Muller cell gliosis: neuroprotective and detrimental effects. *Prog Retin Eye Res,* 28**,** 423-51.
BRINGMANN, A., PANNICKE, T., GROSCHE, J., FRANCKE, M., WIEDEMANN, P., SKATCHKOV, S. N., OSBORNE, N. N. & REICHENBACH, A. 2006. Müller cells in the healthy and diseased retina. *Progress in Retinal and Eye Research,* 25**,** 397-424.
BRINGMANN, A. & REICHENBACH, A. 2001. Role of Muller cells in retinal degenerations. *Front Biosci,* 6**,** E72-92.
BRINGMANN, A. & WIEDEMANN, P. 2012. Muller glial cells in retinal disease. *Ophthalmologica,* 227**,** 1-19.
BROWN, K., PARK, S., KANNO, T., FRANZOSO, G. & SIEBENLIST, U. 1993. Mutual regulation of the transcriptional activator NF-kappa B and its inhibitor, I kappa B-alpha. *Proceedings of the National Academy of Sciences,* 90**,** 2532-2536.
BROZZI, F., ARCURI, C., GIAMBANCO, I. & DONATO, R. 2009. S100B Protein Regulates Astrocyte Shape and Migration via Interaction with Src Kinase: IMPLICATIONS FOR ASTROCYTE DEVELOPMENT, ACTIVATION, AND TUMOR GROWTH. *J Biol Chem,* 284**,** 8797-811.
BUCHHOLZ, D. E., HIKITA, S. T., ROWLAND, T. J., FRIEDRICH, A. M., HINMAN, C. R., JOHNSON, L. V. & CLEGG, D. O. 2009. Derivation of functional retinal pigmented epithelium from induced pluripotent stem cells. *Stem Cells,* 27**,** 2427-34.
BUDHU, A. S. & NOY, N. 2002. Direct channeling of retinoic acid between cellular retinoic acid-binding protein II and retinoic acid receptor sensitizes mammary carcinoma cells to retinoic acid-induced growth arrest. *Mol Cell Biol,* 22**,** 2632-41.
CAI, J., NELSON, K. C., WU, M., STERNBERG, P., JR. & JONES, D. P. 2000. Oxidative damage and protection of the RPE. *Prog Retin Eye Res,* 19**,** 205-21.
CALDERON, G. D., JUAREZ, O. H., HERNANDEZ, G. E., PUNZO, S. M. & DE LA CRUZ, Z. D. 2017. Oxidative stress and diabetic retinopathy: development and treatment. *Eye (Lond),* 31**,** 1122-1130.
CAMBY, I., LE MERCIER, M., LEFRANC, F. & KISS, R. 2006. Galectin-1: a small protein with major functions. *Glycobiology,* 16**,** 137r-157r.
CANDAS, D. & LI, J. J. 2014. MnSOD in oxidative stress response-potential regulation via mitochondrial protein influx. *Antioxid Redox Signal,* 20**,** 1599-617.
CAO, W., TOMBRAN-TINK, J., ELIAS, R., SEZATE, S., MRAZEK, D. & MCGINNIS, J. F. 2001. In vivo protection of photoreceptors from light damage by pigment epithelium-derived factor. *Invest Ophthalmol Vis Sci,* 42**,** 1646-52.
CARR, A. J., VUGLER, A. A., HIKITA, S. T., LAWRENCE, J. M., GIAS, C., CHEN, L. L., BUCHHOLZ, D. E., AHMADO, A., SEMO, M., SMART, M. J., HASAN, S., DA CRUZ, L., JOHNSON, L. V., CLEGG, D. O. & COFFEY, P. J. 2009. Protective effects of human iPS-derived retinal pigment epithelium cell transplantation in the retinal dystrophic rat. *PLoS One,* 4**,** e8152.
CARTER, D. A. & DICK, A. D. 2004. CD200 maintains microglial potential to migrate in adult human retinal explant model. *Curr Eye Res,* 28**,** 427-36.

CARTER, D. A., SMART, M. J., LETTON, W. V., RAMSDEN, C. M., NOMMISTE, B., CHEN, L. L., FYNES, K., MUTHIAH, M. N., GOH, P., LANE, A., POWNER, M. B., WEBSTER, A. R., DA CRUZ, L., MOORE, A. T., COFFEY, P. J. & CARR, A. F. 2016. Mislocalisation of BEST1 in iPSC-derived retinal pigment epithelial cells from a family with autosomal dominant vitreoretinochoroidopathy (ADVIRC). *Sci Rep,* 6**,** 33792.

CHAMBERS, S. M., TCHIEU, J. & STUDER, L. 2013. Build-a-brain. *Cell Stem Cell,* 13**,** 377-8.

CHANG, Z. Y., LU, D. W., YEH, M. K. & CHIANG, C. H. 2012. A novel high-content flow cytometric method for assessing the viability and damage of rat retinal ganglion cells. *PLoS One,* 7**,** e33983.

CHANG, Z. Y., YEH, M. K., CHIANG, C. H., CHEN, Y. H. & LU, D. W. 2013. Erythropoietin protects adult retinal ganglion cells against NMDA-, trophic factor withdrawal-, and TNF-alpha-induced damage. *PLoS One,* 8**,** e55291.

CHATTERJEE, A. & GUPTA, S. 2018. The multifaceted role of glutathione S-transferases in cancer. *Cancer Lett,* 433**,** 33-42.

CHATTOPADHYAY, K., RAMAGOPAL, U. A., MUKHOPADHAYA, A., MALASHKEVICH, V. N., DILORENZO, T. P., BRENOWITZ, M., NATHENSON, S. G. & ALMO, S. C. 2007. Assembly and structural properties of glucocorticoid-induced TNF receptor ligand: Implications for function. *Proc Natl Acad Sci U S A,* 104**,** 19452-7.

CHAU, K. Y., SIVAPRASAD, S., PATEL, N., DONALDSON, T. A., LUTHERT, P. J. & CHONG, N. V. 2008. Plasma levels of matrix metalloproteinase-2 and -9 (MMP-2 and MMP-9) in age-related macular degeneration. *Eye (Lond),* 22**,** 855-9.

CHEN, C. L., LIANG, C. M., CHEN, Y. H., TAI, M. C., LU, D. W. & CHEN, J. T. 2012. Glucosamine modulates TNF-alpha-induced ICAM-1 expression and function through O-linked and N-linked glycosylation in human retinal pigment epithelial cells. *Invest Ophthalmol Vis Sci,* 53**,** 2281-91.

CHEN, J. W., DODIA, C., FEINSTEIN, S. I., JAIN, M. K. & FISHER, A. B. 2000. 1-Cys peroxiredoxin, a bifunctional enzyme with glutathione peroxidase and phospholipase A2 activities. *J Biol Chem,* 275**,** 28421-7.

CHEN, Q., ZHUO, Y., KIM, M., HANSON, S. M., FRANCIS, D. J., VISHNIVETSKIY, S. A., ALTENBACH, C., KLUG, C. S., HUBBELL, W. L. & GUREVICH, V. V. 2014. Self-association of arrestin family members. *Handb Exp Pharmacol,* 219**,** 205-23.

CHEN, S. D., WU, C. L., HWANG, W. C. & YANG, D. I. 2017. More Insight into BDNF against Neurodegeneration: Anti-Apoptosis, Anti-Oxidation, and Suppression of Autophagy. *Int J Mol Sci,* 18.

CHEN, Y., STEVENS, B., CHANG, J., MILBRANDT, J., BARRES, B. A. & HELL, J. W. 2008. NS21: re-defined and modified supplement B27 for neuronal cultures. *J Neurosci Methods,* 171**,** 239-47.

CHENG, Y. & RONG, J. 2017. Therapeutic Potential of Heme Oxygenase-1/carbon Monoxide System Against Ischemia-Reperfusion Injury. *Curr Pharm Des,* 23**,** 3884-3898.

CHERNOFF, E. A., O'HARA, C. M., BAUERLE, D. & BOWLING, M. 2000. Matrix metalloproteinase production in regenerating axolotl spinal cord. *Wound Repair Regen,* 8**,** 282-91.

CHIAO, P. J., MIYAMOTO, S. & VERMA, I. M. 1994. Autoregulation of I kappa B alpha activity. *Proceedings of the National Academy of Sciences,* 91**,** 28-32.

CHITU, V. & STANLEY, E. R. 2006. Colony-stimulating factor-1 in immunity and inflammation. *Curr Opin Immunol,* 18**,** 39-48.

CLOSE, J. L., GUMUSCU, B. & REH, T. A. 2005. Retinal neurons regulate proliferation of postnatal progenitors and Muller glia in the rat retina via TGF beta signaling. *Development,* 132**,** 3015-26.

COLLIN, J., QUEEN, R., ZERTI, D., DORGAU, B., HUSSAIN, R., COXHEAD, J., COCKELL, S. & LAKO, M. 2019a. Deconstructing Retinal Organoids: Single Cell RNA-Seq Reveals the Cellular Components of Human Pluripotent Stem Cell-Derived Retina. *Stem Cells,* 37**,** 593-598.

COLLIN, J., ZERTI, D., QUEEN, R., SANTOS-FERREIRA, T., BAUER, R., COXHEAD, J., HUSSAIN, R., STEEL, D., MELLOUGH, C., ADER, M., SERNAGOR, E., ARMSTRONG, L. & LAKO, M. 2019b. CRX Expression in Pluripotent Stem Cell-Derived Photoreceptors Marks a Transplantable Subpopulation of Early Cones. *Stem Cells,* 37**,** 609-622.

CONNER, C., ACKERMAN, K. M., LAHNE, M., HOBGOOD, J. S. & HYDE, D. R. 2014. Repressing Notch Signaling and Expressing TNFα Are Sufficient to Mimic Retinal Regeneration by Inducing Müller Glial Proliferation to Generate Committed Progenitor Cells. *The Journal of Neuroscience,* 34**,** 14403-14419.

CORREDOR, R. G., TRAKHTENBERG, E. F., PITA-THOMAS, W., JIN, X., HU, Y. & GOLDBERG, J. L. 2012. Soluble adenylyl cyclase activity is necessary for retinal ganglion cell survival and axon growth. *J Neurosci,* 32**,** 7734-44.

COSTA, V., APRILE, M., ESPOSITO, R. & CICCODICOLA, A. 2013. RNA-Seq and human complex diseases: recent accomplishments and future perspectives. *Eur J Hum Genet,* 21**,** 134-42.

CRAIG, S. E. L., THUMMEL, R., AHMED, H., VASTA, G. R., HYDE, D. R. & HITCHCOCK, P. F. 2010. The Zebrafish Galectin Drgal1-L2 Is Expressed by Proliferating Müller Glia and Photoreceptor Progenitors and Regulates the Regeneration of Rod Photoreceptors. *Investigative Ophthalmology & Visual Science,* 51**,** 3244-3252.

CURCIO, C. A. & ALLEN, K. A. 1990. Topography of ganglion cells in human retina. *J Comp Neurol,* 300**,** 5-25.

DA CRUZ, L., FYNES, K., GEORGIADIS, O., KERBY, J., LUO, Y. H., AHMADO, A., VERNON, A., DANIELS, J. T., NOMMISTE, B., HASAN, S. M., GOOLJAR, S. B., CARR, A. F., VUGLER, A., RAMSDEN, C. M., BICTASH, M., FENSTER, M., STEER, J., HARBINSON, T., WILBREY, A., TUFAIL, A., FENG, G., WHITLOCK, M., ROBSON, A. G., HOLDER, G. E., SAGOO, M. S., LOUDON, P. T., WHITING, P. & COFFEY, P. J. 2018. Phase 1 clinical study of an embryonic stem cell-derived retinal pigment epithelium patch in age-related macular degeneration. *Nat Biotechnol,* 36**,** 328-337.

DANIAS, J., SHEN, F., GOLDBLUM, D., CHEN, B., RAMOS-ESTEBAN, J., PODOS, S. M. & MITTAG, T. 2002. Cytoarchitecture of the retinal ganglion cells in the rat. *Invest Ophthalmol Vis Sci,* 43**,** 587-94.

DAS, K. C., LEWIS-MOLOCK, Y. & WHITE, C. W. 1995. Activation of NF-kappa B and elevation of MnSOD gene expression by thiol reducing agents in lung adenocarcinoma (A549) cells. *Am J Physiol,* 269**,** L588-602.

DAVIS, B. M., TIAN, K., PAHLITZSCH, M., BRENTON, J., RAVINDRAN, N., BUTT, G., MALAGUARNERA, G., NORMANDO, E. M., GUO, L. & CORDEIRO, M. F. 2017. Topical Coenzyme Q10 demonstrates mitochondrial-mediated neuroprotection in a rodent model of ocular hypertension. *Mitochondrion,* 36**,** 114-123.

DE LA PAZ, M. & ANDERSON, R. E. 1992. Region and age-dependent variation in susceptibility of the human retina to lipid peroxidation. *Invest Ophthalmol Vis Sci,* 33**,** 3497-9.

DE MELO, J., MIKI, K., RATTNER, A., SMALLWOOD, P., ZIBETTI, C., HIROKAWA, K., MONUKI, E. S., CAMPOCHIARO, P. A. & BLACKSHAW, S. 2012. Injury-independent induction of reactive gliosis in retina by loss of function of the LIM homeodomain transcription factor Lhx2. 109**,** 4657-4662.

DE SOUSA ABREU, R., PENALVA, L. O., MARCOTTE, E. M. & VOGEL, C. 2009. Global signatures of protein and mRNA expression levels. *Mol Biosyst,* 5**,** 1512-26.

DE SOUSA, P. A., TYE, B. J., BRUCE, K., DAND, P., RUSSELL, G., COLLINS, D. M., GREENSHIELDS, A., MCDONALD, K., BRADBURN, H., CANHAM, M. A., KUNATH, T., DOWNIE, J. M., BATEMAN, M. & COURTNEY, A. 2016. Derivation of the clinical grade human embryonic stem cell line RCe013-A (RC-9). *Stem Cell Res,* 17**,** 36-41.

DEBERNARDI, J., HOLLVILLE, E., LIPINSKI, M., WIELS, J. & ROBERT, A. 2018. Differential role of FL-BID and t-BID during verotoxin-1-induced apoptosis in Burkitt's lymphoma cells. *Oncogene,* 37**,** 2410-2421.

DING, V., CHIN, A., PEH, G., MEHTA, J. S. & CHOO, A. 2014. Generation of novel monoclonal antibodies for the enrichment and characterization of human corneal endothelial cells (hCENC) necessary for the treatment of corneal endothelial blindness. *MAbs,* 6**,** 1439-52.

DINKOVA-KOSTOVA, A. T., HOLTZCLAW, W. D., COLE, R. N., ITOH, K., WAKABAYASHI, N., KATOH, Y., YAMAMOTO, M. & TALALAY, P. 2002. Direct evidence that sulfhydryl groups of Keap1 are the sensors regulating induction of phase 2 enzymes that protect against carcinogens and oxidants. *Proc Natl Acad Sci U S A,* 99**,** 11908-13.

DISTEFANO, T., CHEN, H. Y., PANEBIANCO, C., KAYA, K. D., BROOKS, M. J., GIESER, L., MORGAN, N. Y., POHIDA, T. & SWAROOP, A. 2018. Accelerated and Improved Differentiation of Retinal Organoids from Pluripotent Stem Cells in Rotating-Wall Vessel Bioreactors. *Stem Cell Reports,* 10**,** 300-313.

DJAVAHERI-MERGNY, M., JAVELAUD, D., WIETZERBIN, J. & BESANCON, F. 2004. NF-kappaB activation prevents apoptotic oxidative stress via an increase of both thioredoxin and MnSOD levels in TNFalpha-treated Ewing sarcoma cells. *FEBS Lett,* 578**,** 111-5.

DONATO, L., BRAMANTI, P., SCIMONE, C., RINALDI, C., GIORGIANNI, F., BERANOVA-GIORGIANNI, S., KOIRALA, D., D'ANGELO, R. & SIDOTI, A. 2018. Corrigendum to: miRNA

expression profile of retinal pigment epithelial cells under oxidative stress conditions. *FEBS Open Bio,* 8**,** 1884.
DRAGANOV, D. I., TEIBER, J. F., SPEELMAN, A., OSAWA, Y., SUNAHARA, R. & LA DU, B. N. 2005. Human paraoxonases (PON1, PON2, and PON3) are lactonases with overlapping and distinct substrate specificities. *J Lipid Res,* 46**,** 1239-47.
DRAPER, J. S., PIGOTT, C., THOMSON, J. A. & ANDREWS, P. W. 2002. Surface antigens of human embryonic stem cells: changes upon differentiation in culture. *J Anat,* 200**,** 249-58.
DRUKKER, M., KATCHMAN, H., KATZ, G., EVEN-TOV FRIEDMAN, S., SHEZEN, E., HORNSTEIN, E., MANDELBOIM, O., REISNER, Y. & BENVENISTY, N. 2006. Human embryonic stem cells and their differentiated derivatives are less susceptible to immune rejection than adult cells. *Stem Cells,* 24**,** 221-9.
DUARTE, D. A., PAPADIMITRIOU, A., GILBERT, R. E., THAI, K., ZHANG, Y., ROSALES, M. A., LOPES DE FARIA, J. B. & LOPES DE FARIA, J. M. 2016. Conditioned Medium from Early-Outgrowth Bone Marrow Cells Is Retinal Protective in Experimental Model of Diabetes. *PLoS One,* 11**,** e0147978.
DUONG, H. Q., YOU, K. S., OH, S., KWAK, S. J. & SEONG, Y. S. 2017. Silencing of NRF2 Reduces the Expression of ALDH1A1 and ALDH3A1 and Sensitizes to 5-FU in Pancreatic Cancer Cells. *Antioxidants (Basel),* 6.
DURSTON, A. J., TIMMERMANS, J. P., HAGE, W. J., HENDRIKS, H. F., DE VRIES, N. J., HEIDEVELD, M. & NIEUWKOOP, P. D. 1989. Retinoic acid causes an anteroposterior transformation in the developing central nervous system. *Nature,* 340**,** 140-4.
DYER, M. A. & CEPKO, C. L. 2000. Control of Muller glial cell proliferation and activation following retinal injury. *Nat Neurosci,* 3**,** 873-80.
EASTLAKE, K., HEYWOOD, W. E., BANERJEE, P., BLISS, E., MILLS, K., KHAW, P. T., CHARTERIS, D. & LIMB, G. A. 2018. Comparative proteomic analysis of normal and gliotic PVR retina and contribution of Muller glia to this profile. *Exp Eye Res,* 177**,** 197-207.
EASTLAKE, K., LUIS, J. & LIMB, G. A. 2019a. Potential of Muller Glia for Retina Neuroprotection. *Curr Eye Res***,** 1-10.
EASTLAKE, K., WANG, W., JAYARAM, H., MURRAY-DUNNING, C., CARR, A. J. F., RAMSDEN, C. M., VUGLER, A., GORE, K., CLEMO, N., STEWART, M., COFFEY, P., KHAW, P. T. & LIMB, G. A. 2019b. Phenotypic and Functional Characterization of Muller Glia Isolated from Induced Pluripotent Stem Cell-Derived Retinal Organoids: Improvement of Retinal Ganglion Cell Function upon Transplantation. *Stem Cells Transl Med*.
EDERVEEN, T. H., MANDEMAKER, I. K. & LOGIE, C. 2011. The human histone H3 complement anno 2011. *Biochim Biophys Acta,* 1809**,** 577-86.
EDWARDS, M. M. & ROBINSON, S. R. 2006. TNF alpha affects the expression of GFAP and S100B: implications for Alzheimer's disease. *J Neural Transm,* 113**,** 1709-15.
EICHLER, W., SAVKOVIC-CVIJIC, H., BURGER, S., BECK, M., SCHMIDT, M., WIEDEMANN, P., REICHENBACH, A. & UNTERLAUFT, J. D. 2017. Muller Cell-Derived PEDF Mediates Neuroprotection via STAT3 Activation. *Cell Physiol Biochem,* 44**,** 1411-1424.
EIRAKU, M. & SASAI, Y. 2011. Mouse embryonic stem cell culture for generation of three-dimensional retinal and cortical tissues. *Nat Protoc,* 7**,** 69-79.
EISMANN, T., HUBER, N., SHIN, T., KUBOKI, S., GALLOWAY, E., WYDER, M., EDWARDS, M. J., GREIS, K. D., SHERTZER, H. G., FISHER, A. B. & LENTSCH, A. B. 2009. Peroxiredoxin-6 protects against mitochondrial dysfunction and liver injury during ischemia-reperfusion in mice. *Am J Physiol Gastrointest Liver Physiol,* 296**,** G266-74.
ELLIOTT, J., JOLICOEUR, C., RAMAMURTHY, V. & CAYOUETTE, M. 2008. Ikaros confers early temporal competence to mouse retinal progenitor cells. *Neuron,* 60**,** 26-39.
ELSHATORY, Y., EVERHART, D., DENG, M., XIE, X., BARLOW, R. B. & GAN, L. 2007. Islet-1 controls the differentiation of retinal bipolar and cholinergic amacrine cells. *J Neurosci,* 27**,** 12707-20.
EMMRICH, S., STRELTSOV, A., SCHMIDT, F., THANGAPANDI, V. R., REINHARDT, D. & KLUSMANN, J. H. 2014. LincRNAs MONC and MIR100HG act as oncogenes in acute megakaryoblastic leukemia. *Mol Cancer,* 13**,** 171.
ERICKSON, P. A., FISHER, S. K., GUÉRIN, C. J., ANDERSON, D. H. & KASKA, D. D. 1987. Glial fibrillary acidic protein increases in Müller cells after retinal detachment. *Experimental Eye Research,* 44**,** 37-48.
ESCHER, P., COTTET, S., AONO, S., OOHIRA, A. & SCHORDERET, D. F. 2008. Differential neuroglycan C expression during retinal degeneration in Rpe65-/- mice. *Mol Vis,* 14**,** 2126-35.

EVERSE, J. & COATES, P. W. 2009. Neurodegeneration and peroxidases. *Neurobiol Aging,* 30**,** 1011-25.
EWELS, P., MAGNUSSON, M., LUNDIN, S. & KALLER, M. 2016. MultiQC: summarize analysis results for multiple tools and samples in a single report. *Bioinformatics,* 32**,** 3047-8.
FANG, J. H., WANG, X. H., XU, Z. R. & JIANG, F. G. 2010. Neuroprotective effects of bis(7)-tacrine against glutamate-induced retinal ganglion cells damage. *BMC Neurosci,* 11**,** 31.
FANG, L., HUANG, T. & TSILFIDIS, C. 2018. Immunopanning purification and culture of retinal ganglion cells from mouse. *J Neurosci Methods,* 303**,** 81-85.
FARKAS, M. H., GRANT, G. R., WHITE, J. A., SOUSA, M. E., CONSUGAR, M. B. & PIERCE, E. A. 2013. Transcriptome analyses of the human retina identify unprecedented transcript diversity and 3.5 Mb of novel transcribed sequence via significant alternative splicing and novel genes. *BMC Genomics,* 14**,** 486.
FATMA, N., KUBO, E., SEN, M., AGARWAL, N., THORESON, W. B., CAMRAS, C. B. & SINGH, D. P. 2008. Peroxiredoxin 6 delivery attenuates TNF-alpha-and glutamate-induced retinal ganglion cell death by limiting ROS levels and maintaining Ca2+ homeostasis. *Brain Res,* 1233**,** 63-78.
FATMA, N., KUBO, E., SHARMA, P., BEIER, D. R. & SINGH, D. P. 2005. Impaired homeostasis and phenotypic abnormalities in Prdx6-/-mice lens epithelial cells by reactive oxygen species: increased expression and activation of TGFbeta. *Cell Death Differ,* 12**,** 734-50.
FATMA, N., KUBO, E., TAKAMURA, Y., ISHIHARA, K., GARCIA, C., BEEBE, D. C. & SINGH, D. P. 2009a. Loss of NF-kappaB control and repression of Prdx6 gene transcription by reactive oxygen species-driven SMAD3-mediated transforming growth factor beta signaling. *J Biol Chem,* 284**,** 22758-72.
FATMA, N., KUBO, E., TORIS, C. B., STAMER, W. D., CAMRAS, C. B. & SINGH, D. P. 2009b. PRDX6 attenuates oxidative stress- and TGFbeta-induced abnormalities of human trabecular meshwork cells. *Free Radic Res,* 43**,** 783-95.
FATMA, N., SINGH, P., CHHUNCHHA, B., KUBO, E., SHINOHARA, T., BHARGAVAN, B. & SINGH, D. P. 2011. Deficiency of Prdx6 in lens epithelial cells induces ER stress response-mediated impaired homeostasis and apoptosis. *Am J Physiol Cell Physiol,* 301**,** C954-67.
FAUSETT, B. & GOLDMAN, D. 2006. A role for alpha1 tubulin-expressing Muller glia in regeneration of the injured zebrafish retina. *J Neurosci,* 26**,** 6303 - 6313.
FENDERSON, B. A., ANDREWS, P. W., NUDELMAN, E., CLAUSEN, H. & HAKOMORI, S. 1987. Glycolipid core structure switching from globo- to lacto- and ganglio-series during retinoic acid-induced differentiation of TERA-2-derived human embryonal carcinoma cells. *Dev Biol,* 122**,** 21-34.
FENG, L., ZHAO, Y., YOSHIDA, M., CHEN, H., YANG, J. F., KIM, T. S., CANG, J., TROY, J. B. & LIU, X. 2013. Sustained ocular hypertension induces dendritic degeneration of mouse retinal ganglion cells that depends on cell type and location. *Invest Ophthalmol Vis Sci,* 54**,** 1106-17.
FERNANDEZ-BUENO, I., GARCIA-GUTIERREZ, M. T., SRIVASTAVA, G. K., GAYOSO, M. J., GONZALO-ORDEN, J. M. & PASTOR, J. C. 2013. Adalimumab (tumor necrosis factor-blocker) reduces the expression of glial fibrillary acidic protein immunoreactivity increased by exogenous tumor necrosis factor alpha in an organotypic culture of porcine neuroretina. *Mol Vis,* 19**,** 894-903.
FIERS, W., BEYAERT, R., DECLERCQ, W. & VANDENABEELE, P. 1999. More than one way to die: apoptosis, necrosis and reactive oxygen damage. *Oncogene,* 18**,** 7719-30.
FIMBEL, S. M., MONTGOMERY, J. E., BURKET, C. T. & HYDE, D. R. 2007. Regeneration of Inner Retinal Neurons after Intravitreal Injection of Ouabain in Zebrafish. *The Journal of Neuroscience,* 27**,** 1712-1724.
FISCHER, A., HENDRICKSON, A. & REH, T. 2001. Immunocytochemical characterization of cysts in the peripheral retina and pars plana of the adult primate. *Invest Ophthalmol Vis Sci,* 42**,** 3256 - 3263.
FISCHER, A. J. 2005. Neural regeneration in the chick retina. *Progress in Retinal and Eye Research,* 24**,** 161-182.
FISCHER, A. J., FOSTER, S., SCOTT, M. A. & SHERWOOD, P. 2008. Transient expression of LIM-domain transcription factors is coincident with delayed maturation of photoreceptors in the chicken retina. *J Comp Neurol,* 506**,** 584-603.
FISCHER, A. J. & REH, T. A. 2003. Potential of Müller glia to become neurogenic retinal progenitor cells. *Glia,* 43**,** 70-76.

FLANAGAN, L. A., JU, Y. E., MARG, B., OSTERFIELD, M. & JANMEY, P. A. 2002. Neurite branching on deformable substrates. *Neuroreport,* 13**,** 2411-5.
FONNUM, F. 1984. Glutamate: a neurotransmitter in mammalian brain. *J Neurochem,* 42**,** 1-11.
FONTAINE, V., MOHAND-SAID, S., HANOTEAU, N., FUCHS, C., PFIZENMAIER, K. & EISEL, U. 2002. Neurodegenerative and neuroprotective effects of tumor Necrosis factor (TNF) in retinal ischemia: opposite roles of TNF receptor 1 and TNF receptor 2. *J Neurosci,* 22**,** Rc216.
FORMAN, H. J., ZHANG, H. & RINNA, A. 2009. Glutathione: overview of its protective roles, measurement, and biosynthesis. *Mol Aspects Med,* 30**,** 1-12.
FOXTON, R. H., FINKELSTEIN, A., VIJAY, S., DAHLMANN-NOOR, A., KHAW, P. T., MORGAN, J. E., SHIMA, D. T. & NG, Y. S. 2013. VEGF-A is necessary and sufficient for retinal neuroprotection in models of experimental glaucoma. *Am J Pathol,* 182**,** 1379-90.
FRANZE, K., GERDELMANN, J., WEICK, M., BETZ, T., PAWLIZAK, S., LAKADAMYALI, M., BAYER, J., RILLICH, K., GOGLER, M., LU, Y. B., REICHENBACH, A., JANMEY, P. & KAS, J. 2009. Neurite branch retraction is caused by a threshold-dependent mechanical impact. *Biophys J,* 97**,** 1883-90.
FRANZE, K., GROSCHE, J., SKATCHKOV, S. N., SCHINKINGER, S., FOJA, C., SCHILD, D., UCKERMANN, O., TRAVIS, K., REICHENBACH, A. & GUCK, J. 2007. Müller cells are living optical fibers in the vertebrate retina. *Proceedings of the National Academy of Sciences,* 104**,** 8287-8292.
FRENKEL, S., GOSHEN, G., LEACH, L., PE'ER, J., MIMOUNI, M. & BLUMENTHAL, E. Z. 2018. Peripapillary distribution of Muller cells within the retinal nerve fiber layer in human eyes. *Exp Eye Res,* 166**,** 91-95.
FURUKAWA, T., MUKHERJEE, S., BAO, Z. Z., MORROW, E. M. & CEPKO, C. L. 2000. rax, Hes1, and notch1 promote the formation of Muller glia by postnatal retinal progenitor cells. *Neuron,* 26**,** 383-94.
GADDINI, L., VARANO, M., MATTEUCCI, A., MALLOZZI, C., VILLA, M., PRICCI, F. & MALCHIODI-ALBEDI, F. 2016. Müller glia activation by VEGF-antagonizing drugs: An in vitro study on rat primary retinal cultures. *Exp Eye Res,* 145**,** 158-163.
GAGLIARDI, G., BEN M'BAREK, K., CHAFFIOL, A., SLEMBROUCK-BREC, A., CONART, J. B., NANTEAU, C., RABESANDRATANA, O., SAHEL, J. A., DUEBEL, J., ORIEUX, G., REICHMAN, S. & GOUREAU, O. 2018. Characterization and Transplantation of CD73-Positive Photoreceptors Isolated from Human iPSC-Derived Retinal Organoids. *Stem Cell Reports,* 11**,** 665-680.
GALINDO, L. T., MUNDIM, M., PINTO, A. S., CHIARANTIN, G. M. D., ALMEIDA, M. E. S., LAMERS, M. L., HORWITZ, A. R., SANTOS, M. F. & PORCIONATTO, M. 2018. Chondroitin Sulfate Impairs Neural Stem Cell Migration Through ROCK Activation. *Mol Neurobiol,* 55**,** 3185-3195.
GALLAGHER, B. M. & PHELAN, S. A. 2007. Investigating transcriptional regulation of Prdx6 in mouse liver cells. *Free Radic Biol Med,* 42**,** 1270-7.
GALVAO, J., IWAO, K., APARA, A., WANG, Y., ASHOURI, M., SHAH, T. N., BLACKMORE, M., KUNZEVITZKY, N. J., MOORE, D. L. & GOLDBERG, J. L. 2018. The Kruppel-Like Factor Gene Target Dusp14 Regulates Axon Growth and Regeneration. *Invest Ophthalmol Vis Sci,* 59**,** 2736-2747.
GAO, F., LI, T., HU, J., ZHOU, X., WU, J. & WU, Q. 2016. Comparative analysis of three purification protocols for retinal ganglion cells from rat. *Mol Vis,* 22**,** 387-400.
GARBER, K. 2015. RIKEN suspends first clinical trial involving induced pluripotent stem cells. *Nat Biotechnol,* 33**,** 890-1.
GARCIA, M. & VECINO, E. 2003. Role of Muller glia in neuroprotection and regeneration in the retina. *Histol Histopathol,* 18**,** 1205-18.
GAUTHIER, A. C. & LIU, J. 2017. Epigenetics and Signaling Pathways in Glaucoma. *Biomed Res Int,* 2017**,** 5712341.
GHAI, K., ZELINKA, C. & FISCHER, A. J. 2010. Notch signaling influences neuroprotective and proliferative properties of mature Muller glia. *J Neurosci,* 30**,** 3101-12.
GHANEM AA, A. L., ELEWA AM 2010. Tumor Necrosis Factor-α and Interleukin-6 Levels in Patients with Primary Open-Angle Glaucoma. *J Clinic Experiment Ophthalmol*.
GHOSH, A. & HESTON, W. D. 2003. Effect of carbohydrate moieties on the folate hydrolysis activity of the prostate specific membrane antigen. *Prostate,* 57**,** 140-51.
GIARDINO, I., FARD, A. K., HATCHELL, D. L. & BROWNLEE, M. 1998. Aminoguanidine inhibits reactive oxygen species formation, lipid peroxidation, and oxidant-induced apoptosis. *Diabetes,* 47**,** 1114-20.

GLOIRE, G., LEGRAND-POELS, S. & PIETTE, J. 2006. NF-kappaB activation by reactive oxygen species: fifteen years later. *Biochem Pharmacol,* 72**,** 1493-505.
GOLDMAN, D. 2014. Muller glial cell reprogramming and retina regeneration. *Nat Rev Neurosci,* 15**,** 431-442.
GOTTLIEB, Y., TRUMAN, M., COHEN, L. A., LEICHTMANN-BARDOOGO, Y. & MEYRON-HOLTZ, E. G. 2012. Endoplasmic reticulum anchored heme-oxygenase 1 faces the cytosol. *Haematologica,* 97**,** 1489-93.
GOTZ, M. & BARDE, Y. 2005. Radial glial cells defined and major intermediates between embryonic stem cells and CNS neurons. *Neuron,* 46**,** 369 - 372.
GROSCHE, A., HAUSER, A., LEPPER, M. F., MAYO, R., VON TOERNE, C., MERL-PHAM, J. & HAUCK, S. M. 2016. The Proteome of Native Adult Muller Glial Cells From Murine Retina. *Mol Cell Proteomics,* 15**,** 462-80.
GUENZI, E., TÖPOLT, K., CORNALI, E., LUBESEDER-MARTELLATO, C., JÖRG, A., MATZEN, K., ZIETZ, C., KREMMER, E., NAPPI, F., SCHWEMMLE, M., HOHENADL, C., BARILLARI, G., TSCHACHLER, E., MONINI, P., ENSOLI, B. & STÜRZL, M. 2001. The helical domain of GBP-1 mediates the inhibition of endothelial cell proliferation by inflammatory cytokines. *Embo j,* 20**,** 5568-77.
GUENZI, E., TÖPOLT, K., LUBESEDER-MARTELLATO, C., JÖRG, A., NASCHBERGER, E., BENELLI, R., ALBINI, A. & STÜRZL, M. 2003. The guanylate binding protein-1 GTPase controls the invasive and angiogenic capability of endothelial cells through inhibition of MMP-1 expression. *Embo j,* 22**,** 3772-82.
HAHN, J. S., AIZENMAN, E. & LIPTON, S. A. 1988. Central mammalian neurons normally resistant to glutamate toxicity are made sensitive by elevated extracellular Ca2+: toxicity is blocked by the N-methyl-D-aspartate antagonist MK-801. *Proc Natl Acad Sci U S A,* 85**,** 6556-60.
HANUS, J., ANDERSON, C. & WANG, S. 2015. RPE necroptosis in response to oxidative stress and in AMD. *Ageing Res Rev,* 24**,** 286-98.
HARADA, T., HARADA, C., KOHSAKA, S., WADA, E., YOSHIDA, K., OHNO, S., MAMADA, H., TANAKA, K., PARADA, L. F. & WADA, K. 2002. Microglia-Muller glia cell interactions control neurotrophic factor production during light-induced retinal degeneration. *J Neurosci,* 22**,** 9228-36.
HARADA, T., HARADA, C., NAKAMURA, K., QUAH, H. M., OKUMURA, A., NAMEKATA, K., SAEKI, T., AIHARA, M., YOSHIDA, H., MITANI, A. & TANAKA, K. 2007. The potential role of glutamate transporters in the pathogenesis of normal tension glaucoma. *J Clin Invest,* 117**,** 1763-70.
HARUTA, M., SASAI, Y., KAWASAKI, H., AMEMIYA, K., OOTO, S., KITADA, M., SUEMORI, H., NAKATSUJI, N., IDE, C., HONDA, Y. & TAKAHASHI, M. 2004. In vitro and in vivo characterization of pigment epithelial cells differentiated from primate embryonic stem cells. *Invest Ophthalmol Vis Sci,* 45**,** 1020-5.
HATAKEYAMA, J. & KAGEYAMA, R. 2004. Retinal cell fate determination and bHLH factors. *Semin Cell Dev Biol,* 15**,** 83-9.
HAUCK, S. M., SCHOEFFMANN, S., AMANN, B., STANGASSINGER, M., GERHARDS, H., UEFFING, M. & DEEG, C. A. 2007. Retinal Mueller glial cells trigger the hallmark inflammatory process in autoimmune uveitis. *J Proteome Res,* 6**,** 2121-31.
HE, K. L. & TING, A. T. 2002. A20 inhibits tumor necrosis factor (TNF) alpha-induced apoptosis by disrupting recruitment of TRADD and RIP to the TNF receptor 1 complex in Jurkat T cells. *Mol Cell Biol,* 22**,** 6034-45.
HEAVNER, W. & PEVNY, L. 2012. Eye development and retinogenesis. *Cold Spring Harb Perspect Biol,* 4.
HENTZE, H., GRAICHEN, R. & COLMAN, A. 2007. Cell therapy and the safety of embryonic stem cell-derived grafts. *Trends Biotechnol,* 25**,** 24-32.
HERRMANN, J. E., IMURA, T., SONG, B., QI, J., AO, Y., NGUYEN, T. K., KORSAK, R. A., TAKEDA, K., AKIRA, S. & SOFRONIEW, M. V. 2008. STAT3 is a critical regulator of astrogliosis and scar formation after spinal cord injury. *J Neurosci,* 28**,** 7231-43.
HICKS, E. A., ZAVERI, M., DESCHAMPS, P. A., NOSEWORTHY, M. D., BALL, A., WILLIAMS, T. & WEST-MAYS, J. A. 2018. Conditional Deletion of AP-2alpha and AP-2beta in the Developing Murine Retina Leads to Altered Amacrine Cell Mosaics and Disrupted Visual Function. *Invest Ophthalmol Vis Sci,* 59**,** 2229-2239.
HIGUCHI, A., KUMAR, S. S., BENELLI, G., ALARFAJ, A. A., MUNUSAMY, M. A., UMEZAWA, A. & MURUGAN, K. 2017. Stem Cell Therapies for Reversing Vision Loss. *Trends Biotechnol*.

HIPPERT, C., GRACA, A. B., BARBER, A. C., WEST, E. L., SMITH, A. J., ALI, R. R. & PEARSON, R. A. 2015. Muller glia activation in response to inherited retinal degeneration is highly varied and disease-specific. *PLoS One,* 10**,** e0120415.
HIRAMI, Y., OSAKADA, F., TAKAHASHI, K., OKITA, K., YAMANAKA, S., IKEDA, H., YOSHIMURA, N. & TAKAHASHI, M. 2009. Generation of retinal cells from mouse and human induced pluripotent stem cells. *Neuroscience Letters,* 458**,** 126-131.
HIRANO, M., YAMAMOTO, A., YOSHIMURA, N., TOKUNAGA, T., MOTOHASHI, T., ISHIZAKI, K., YOSHIDA, H., OKAZAKI, K., YAMAZAKI, H., HAYASHI, S. & KUNISADA, T. 2003. Generation of structures formed by lens and retinal cells differentiating from embryonic stem cells. *Dev Dyn,* 228**,** 664-71.
HOERSTER, R., MUETHER, P. S., VIERKOTTEN, S., HERMANN, M. M., KIRCHHOF, B. & FAUSER, S. 2014. Upregulation of TGF-ss1 in experimental proliferative vitreoretinopathy is accompanied by epithelial to mesenchymal transition. *Graefes Arch Clin Exp Ophthalmol,* 252**,** 11-6.
HOLLBORN, M., JAHN, K., LIMB, G. A., KOHEN, L., WIEDEMANN, P. & BRINGMANN, A. 2004. Characterization of the basic fibroblast growth factor-evoked proliferation of the human Muller cell line, MIO-M1. *Graefes Arch Clin Exp Ophthalmol,* 242**,** 414-22.
HOLTKAMP, G. M., KIJLSTRA, A., PEEK, R. & DE VOS, A. F. 2001. Retinal pigment epithelium-immune system interactions: cytokine production and cytokine-induced changes. *Prog Retin Eye Res,* 20**,** 29-48.
HONDA, K. & TANIGUCHI, T. 2006. IRFs: master regulators of signalling by Toll-like receptors and cytosolic pattern-recognition receptors. *Nat Rev Immunol,* 6**,** 644-58.
HOPKINS, J. M. & BUNGE, R. P. 1991. Regeneration of axons from adult human retina in vitro. *Exp Neurol,* 112**,** 243-51.
HORCH, H. W., KRUTTGEN, A., PORTBURY, S. D. & KATZ, L. C. 1999. Destabilization of cortical dendrites and spines by BDNF. *Neuron,* 23**,** 353-64.
HORIUCHI, T., MITOMA, H., HARASHIMA, S.-I., TSUKAMOTO, H. & SHIMODA, T. 2010. Transmembrane TNF-α: structure, function and interaction with anti-TNF agents. *Rheumatology (Oxford, England),* 49**,** 1215-1228.
HUANG, E. J. & REICHARDT, L. F. 2001. Neurotrophins: roles in neuronal development and function. *Annu Rev Neurosci,* 24**,** 677-736.
HUGHES, G., MURPHY, M. P. & LEDGERWOOD, E. C. 2005. Mitochondrial reactive oxygen species regulate the temporal activation of nuclear factor kappaB to modulate tumour necrosis factor-induced apoptosis: evidence from mitochondria-targeted antioxidants. *Biochem J,* 389**,** 83-9.
HURLEY, J. B., LINDSAY, K. J. & DU, J. 2015. Glucose, lactate, and shuttling of metabolites in vertebrate retinas. *J Neurosci Res,* 93**,** 1079-92.
HUXLIN, K. R. & GOODCHILD, A. K. 1997. Retinal ganglion cells in the albino rat: revised morphological classification. *J Comp Neurol,* 385**,** 309-23.
HUYNH, N., VONMOSS, L., SMITH, D., RAHMAN, I., FELEMBAN, M. F., ZUO, J., RODY, W. J., JR., MCHUGH, K. P. & HOLLIDAY, L. S. 2016. Characterization of Regulatory Extracellular Vesicles from Osteoclasts. *J Dent Res,* 95**,** 673-9.
HWANG, Y. J., LEE, E. W., SONG, J., KIM, H. R., JUN, Y. C. & HWANG, K. A. 2013. MafK positively regulates NF-kappaB activity by enhancing CBP-mediated p65 acetylation. *Sci Rep,* 3**,** 3242.
HYATT, G. A., SCHMITT, E. A., MARSH-ARMSTRONG, N., MCCAFFERY, P., DRAGER, U. C. & DOWLING, J. E. 1996. Retinoic acid establishes ventral retinal characteristics. *Development,* 122**,** 195-204.
ICHIMURA, Y., WAGURI, S., SOU, Y. S., KAGEYAMA, S., HASEGAWA, J., ISHIMURA, R., SAITO, T., YANG, Y., KOUNO, T., FUKUTOMI, T., HOSHII, T., HIRAO, A., TAKAGI, K., MIZUSHIMA, T., MOTOHASHI, H., LEE, M. S., YOSHIMORI, T., TANAKA, K., YAMAMOTO, M. & KOMATSU, M. 2013. Phosphorylation of p62 activates the Keap1-Nrf2 pathway during selective autophagy. *Mol Cell,* 51**,** 618-31.
INARREA, P., ALARCIA, R., ALAVA, M. A., CAPABLO, J. L., CASANOVA, A., INIGUEZ, C., ITURRALDE, M., LARRODE, P., MARTIN, J., MOSTACERO, E. & ARA, J. R. 2014. Mitochondrial complex enzyme activities and cytochrome C expression changes in multiple sclerosis. *Mol Neurobiol,* 49**,** 1-9.
INMAN, D. M., LAMBERT, W. S., CALKINS, D. J. & HORNER, P. J. 2013. alpha-Lipoic acid antioxidant treatment limits glaucoma-related retinal ganglion cell death and dysfunction. *PLoS One,* 8**,** e65389.

INOUE, T., HOJO, M., BESSHO, Y., TANO, Y., LEE, J. E. & KAGEYAMA, R. 2002. Math3 and NeuroD regulate amacrine cell fate specification in the retina. *Development,* 129**,** 831-42.
INOUE, Y., IRIYAMA, A., UENO, S., TAKAHASHI, H., KONDO, M., TAMAKI, Y., ARAIE, M. & YANAGI, Y. 2007. Subretinal transplantation of bone marrow mesenchymal stem cells delays retinal degeneration in the RCS rat model of retinal degeneration. *Exp Eye Res,* 85**,** 234-41.
ISMAIL, S., STURROCK, A., WU, P., CAHILL, B., NORMAN, K., HUECKSTEADT, T., SANDERS, K., KENNEDY, T. & HOIDAL, J. 2009. NOX4 mediates hypoxia-induced proliferation of human pulmonary artery smooth muscle cells: the role of autocrine production of transforming growth factor-{beta}1 and insulin-like growth factor binding protein-3. *Am J Physiol Lung Cell Mol Physiol,* 296**,** L489-99.
ITO, S. I., ONISHI, A. & TAKAHASHI, M. 2017. Chemically-induced photoreceptor degeneration and protection in mouse iPSC-derived three-dimensional retinal organoids. *Stem Cell Res,* 24**,** 94-101.
JAIN, S., GLUBRECHT, D. D., GERMAIN, D. R., MOSER, M. & GODBOUT, R. 2018. AP-2epsilon Expression in Developing Retina: Contributing to the Molecular Diversity of Amacrine Cells. *Sci Rep,* 8**,** 3386.
JAISWAL, A. K. 2004. Nrf2 signaling in coordinated activation of antioxidant gene expression. *Free Radic Biol Med,* 36**,** 1199-207.
JARROUX, J., MORILLON, A. & PINSKAYA, M. 2017. History, Discovery, and Classification of lncRNAs. *Adv Exp Med Biol,* 1008**,** 1-46.
JASNA, J. M., ANANDBABU, K., BHARATHI, S. R. & ANGAYARKANNI, N. 2014. Paraoxonase enzyme protects retinal pigment epithelium from chlorpyrifos insult. *PLoS One,* 9**,** e101380.
JAYARAM, H., JONES, M. F., EASTLAKE, K., COTTRILL, P. B., BECKER, S., WISEMAN, J., KHAW, P. T. & LIMB, G. A. 2014a. Transplantation of photoreceptors derived from human Muller glia restore rod function in the P23H rat. *Stem Cells Transl Med,* 3**,** 323-33.
JAYARAM, H., JONES, M. F., EASTLAKE, K., COTTRILL, P. B., BECKER, S., WISEMAN, J., KHAW, P. T. & LIMB, G. A. 2014b. Transplantation of Photoreceptors Derived From Human Müller Glia Restore Rod Function in the P23H Rat. *Stem Cells Translational Medicine,* 3**,** 323-333.
JIANG, S. M., ZENG, L. P., ZENG, J. H., TANG, L., CHEN, X. M. & WEI, X. 2015. beta-III-Tubulin: a reliable marker for retinal ganglion cell labeling in experimental models of glaucoma. *Int J Ophthalmol,* 8**,** 643-52.
JIN, K., JIANG, H., XIAO, D., ZOU, M., ZHU, J. & XIANG, M. 2015. Tfap2a and 2b act downstream of Ptf1a to promote amacrine cell differentiation during retinogenesis. *Mol Brain,* 8**,** 28.
JOE, M. K., NAKAYA, N., ABU-ASAB, M. & TOMAREV, S. I. 2015. Mutated myocilin and heterozygous Sod2 deficiency act synergistically in a mouse model of open-angle glaucoma. *Hum Mol Genet,* 24**,** 3322-34.
JOHNSEN, E. O., FROEN, R. C., OLSTAD, O. K., NICOLAISSEN, B., PETROVSKI, G., MOE, M. C. & NOER, A. 2018. Proliferative Cells Isolated from the Adult Human Peripheral Retina only Transiently Upregulate Key Retinal Markers upon Induced Differentiation. *Curr Eye Res,* 43**,** 340-349.
JOHNSON, P. T., GELLER, S. F., LEWIS, G. P. & REESE, B. E. 1997. Cellular retinaldehyde binding protein in developing retinal astrocytes. *Exp Eye Res,* 64**,** 759-66.
JONES, D. P., MODY, V. C., JR., CARLSON, J. L., LYNN, M. J. & STERNBERG, P., JR. 2002. Redox analysis of human plasma allows separation of pro-oxidant events of aging from decline in antioxidant defenses. *Free Radic Biol Med,* 33**,** 1290-300.
JU, W. K., KIM, K. Y., NOH, Y. H., HOSHIJIMA, M., LUKAS, T. J., ELLISMAN, M. H., WEINREB, R. N. & PERKINS, G. A. 2015. Increased mitochondrial fission and volume density by blocking glutamate excitotoxicity protect glaucomatous optic nerve head astrocytes. *Glia,* 63**,** 736-53.
JUNYI, L., NA, L. & YAN, J. 2015. Mesenchymal stem cells secrete brain-derived neurotrophic factor and promote retinal ganglion cell survival after traumatic optic neuropathy. *J Craniofac Surg,* 26**,** 548-52.
KAEWKHAW, R., KAYA, K. D., BROOKS, M., HOMMA, K., ZOU, J., CHAITANKAR, V., RAO, M. & SWAROOP, A. 2015. Transcriptome Dynamics of Developing Photoreceptors in Three-Dimensional Retina Cultures Recapitulates Temporal Sequence of Human Cone and Rod Differentiation Revealing Cell Surface Markers and Gene Networks. *Stem Cells,* 33**,** 3504-18.
KAHN, M. A., HUANG, C. J., CARUSO, A., BARRESI, V., NAZARIAN, R., CONDORELLI, D. F. & DE VELLIS, J. 1997. Ciliary neurotrophic factor activates JAK/Stat signal transduction

cascade and induces transcriptional expression of glial fibrillary acidic protein in glial cells. *J Neurochem,* 68**,** 1413-23.
KALANI, A., TYAGI, A. & TYAGI, N. 2014. Exosomes: mediators of neurodegeneration, neuroprotection and therapeutics. *Mol Neurobiol,* 49**,** 590-600.
KAMAO, H., MANDAI, M., OKAMOTO, S., SAKAI, N., SUGA, A., SUGITA, S., KIRYU, J. & TAKAHASHI, M. 2014. Characterization of human induced pluripotent stem cell-derived retinal pigment epithelium cell sheets aiming for clinical application. *Stem Cell Reports,* 2**,** 205-18.
KANAMORI, A., CATRINESCU, M. M., KANAMORI, N., MEARS, K. A., BEAUBIEN, R. & LEVIN, L. A. 2010. Superoxide is an associated signal for apoptosis in axonal injury. *Brain,* 133**,** 2612-25.
KANG, S. W., BAINES, I. C. & RHEE, S. G. 1998. Characterization of a mammalian peroxiredoxin that contains one conserved cysteine. *J Biol Chem,* 273**,** 6303-11.
KARUS, M., BLAESS, S. & BRUSTLE, O. 2014. Self-organization of neural tissue architectures from pluripotent stem cells. *J Comp Neurol,* 522**,** 2831-44.
KATAYAMA, S., TOMARU, Y., KASUKAWA, T., WAKI, K., NAKANISHI, M., NAKAMURA, M., NISHIDA, H., YAP, C. C., SUZUKI, M., KAWAI, J., SUZUKI, H., CARNINCI, P., HAYASHIZAKI, Y., WELLS, C., FRITH, M., RAVASI, T., PANG, K. C., HALLINAN, J., MATTICK, J., HUME, D. A., LIPOVICH, L., BATALOV, S., ENGSTROM, P. G., MIZUNO, Y., FAGHIHI, M. A., SANDELIN, A., CHALK, A. M., MOTTAGUI-TABAR, S., LIANG, Z., LENHARD, B. & WAHLESTEDT, C. 2005. Antisense transcription in the mammalian transcriptome. *Science,* 309**,** 1564-6.
KAWASAKI, A., OTORI, Y. & BARNSTABLE, C. J. 2000. Muller cell protection of rat retinal ganglion cells from glutamate and nitric oxide neurotoxicity. *Invest Ophthalmol Vis Sci,* 41**,** 3444-50.
KERN, T. S. 2007. Contributions of inflammatory processes to the development of the early stages of diabetic retinopathy. *Exp Diabetes Res,* 95103**,** 95103.
KIM, S. H., HAN, S. Y., AZAM, T., YOON, D. Y. & DINARELLO, C. A. 2005. Interleukin-32: a cytokine and inducer of TNFalpha. *Immunity,* 22**,** 131-42.
KIMCHI, A., WANG, X. F., WEINBERG, R. A., CHEIFETZ, S. & MASSAGUE, J. 1988. Absence of TGF-beta receptors and growth inhibitory responses in retinoblastoma cells. *Science,* 240**,** 196-9.
KLASSEN, H., WARFVINGE, K., SCHWARTZ, P. H., KIILGAARD, J. F., SHAMIE, N., JIANG, C., SAMUEL, M., SCHERFIG, E., PRATHER, R. S. & YOUNG, M. J. 2008. Isolation of progenitor cells from GFP-transgenic pigs and transplantation to the retina of allorecipients. *Cloning Stem Cells,* 10**,** 391-402.
KLOCKER, N., KERMER, P., WEISHAUPT, J. H., LABES, M., ANKERHOLD, R. & BAHR, M. 2000. Brain-derived neurotrophic factor-mediated neuroprotection of adult rat retinal ganglion cells in vivo does not exclusively depend on phosphatidyl-inositol-3'-kinase/protein kinase B signaling. *J Neurosci,* 20**,** 6962-7.
KONDKAR, A. A., SULTAN, T., ALMOBARAK, F. A., KALANTAN, H., AL-OBEIDAN, S. A. & ABU-AMERO, K. K. 2018. Association of increased levels of plasma tumor necrosis factor alpha with primary open-angle glaucoma. *Clin Ophthalmol,* 12**,** 701-706.
KOWLURU, R. A., KOWLURU, V., XIONG, Y. & HO, Y. S. 2006. Overexpression of mitochondrial superoxide dismutase in mice protects the retina from diabetes-induced oxidative stress. *Free Radic Biol Med,* 41**,** 1191-6.
KRISHNAMOORTHY, R. R., AGARWAL, P., PRASANNA, G., VOPAT, K., LAMBERT, W., SHEEDLO, H. J., PANG, I. H., SHADE, D., WORDINGER, R. J., YORIO, T., CLARK, A. F. & AGARWAL, N. 2001. Characterization of a transformed rat retinal ganglion cell line. *Brain Res Mol Brain Res,* 86**,** 1-12.
KRISHNAMOORTHY, R. R., CLARK, A. F., DAUDT, D., VISHWANATHA, J. K. & YORIO, T. 2013. A forensic path to RGC-5 cell line identification: lessons learned. *Invest Ophthalmol Vis Sci,* 54**,** 5712-9.
KRITIS, A. A., STAMOULA, E. G., PANISKAKI, K. A. & VAVILIS, T. D. 2015. Researching glutamate - induced cytotoxicity in different cell lines: a comparative/collective analysis/study. *Front Cell Neurosci,* 9**,** 91.
KUBO, E., MIYAZAWA, T., FATMA, N., AKAGI, Y. & SINGH, D. P. 2006. Development- and age-associated expression pattern of peroxiredoxin 6, and its regulation in murine ocular lens. *Mech Ageing Dev,* 127**,** 249-56.

KUBO, E., SINGH, D. P., FATMA, N. & AKAGI, Y. 2009. TAT-mediated peroxiredoxin 5 and 6 protein transduction protects against high-glucose-induced cytotoxicity in retinal pericytes. *Life Sci,* 84**,** 857-64.

KUBO, M., HANADA, T. & YOSHIMURA, A. 2003. Suppressors of cytokine signaling and immunity. *Nat Immunol,* 4**,** 1169-76.

KUGLER, M. C., GERHARD, M., SCHNELZER, A., BORZYM, K., REINHARDT, R., SCHMITT, M. & LENGYEL, E. 2004. Isolation and characterization of Rac1 pseudogenes (psi1Rac1-psi4Rac1) in the human genome. *Gene,* 341**,** 189-97.

KUSE, Y., OGAWA, K., TSURUMA, K., SHIMAZAWA, M. & HARA, H. 2014. Damage of photoreceptor-derived cells in culture induced by light emitting diode-derived blue light. *Sci Rep,* 4**,** 5223.

KUWAHARA, A., OZONE, C., NAKANO, T., SAITO, K., EIRAKU, M. & SASAI, Y. 2015. Generation of a ciliary margin-like stem cell niche from self-organizing human retinal tissue. *Nat Commun,* 6**,** 6286.

LAGOS-QUINTANA, M., RAUHUT, R., YALCIN, A., MEYER, J., LENDECKEL, W. & TUSCHL, T. 2002. Identification of tissue-specific microRNAs from mouse. *Curr Biol,* 12**,** 735-9.

LAMBA, D. A., GUST, J. & REH, T. A. 2009. Transplantation of Human Embryonic Stem Cell-Derived Photoreceptors Restores Some Visual Function in Crx-Deficient Mice. *Cell Stem Cell,* 4**,** 73-79.

LAMBA, D. A., MCUSIC, A., HIRATA, R. K., WANG, P. R., RUSSELL, D. & REH, T. A. 2010. Generation, purification and transplantation of photoreceptors derived from human induced pluripotent stem cells. *PLoS One,* 5**,** e8763.

LANCASTER, M. A. & KNOBLICH, J. A. 2014. Organogenesis in a dish: modeling development and disease using organoid technologies. *Science,* 345**,** 1247125.

LANG, C., SAUTER, M., SZALAY, G., RACCHI, G., GRASSI, G., RAINALDI, G., MERCATANTI, A., LANG, F., KANDOLF, R. & KLINGEL, K. 2008. Connective tissue growth factor: a crucial cytokine-mediating cardiac fibrosis in ongoing enterovirus myocarditis. *J Mol Med (Berl),* 86**,** 49-60.

LANGMANN, T. 2007. Microglia activation in retinal degeneration. *J Leukoc Biol,* 81**,** 1345-51.

LAVAIL, M. M., UNOKI, K., YASUMURA, D., MATTHES, M. T., YANCOPOULOS, G. D. & STEINBERG, R. H. 1992. Multiple growth factors, cytokines, and neurotrophins rescue photoreceptors from the damaging effects of constant light. *Proc Natl Acad Sci U S A,* 89**,** 11249-53.

LAWRENCE, J. M., SINGHAL, S., BHATIA, B., KEEGAN, D. J., REH, T. A., LUTHERT, P. J., KHAW, P. T. & LIMB, G. A. 2007. MIO-M1 Cells and Similar Müller Glial Cell Lines Derived from Adult Human Retina Exhibit Neural Stem Cell Characteristics. *STEM CELLS,* 25**,** 2033-2043.

LEBRUN-JULIEN, F., BERTRAND, M. J., DE BACKER, O., STELLWAGEN, D., MORALES, C. R., DI POLO, A. & BARKER, P. A. 2010. ProNGF induces TNFalpha-dependent death of retinal ganglion cells through a p75NTR non-cell-autonomous signaling pathway. *Proc Natl Acad Sci U S A,* 107**,** 3817-22.

LEBRUN-JULIEN, F., DUPLAN, L., PERNET, V., OSSWALD, I., SAPIEHA, P., BOURGEOIS, P., DICKSON, K., BOWIE, D., BARKER, P. A. & DI POLO, A. 2009. Excitotoxic death of retinal neurons in vivo occurs via a non-cell-autonomous mechanism. *J Neurosci,* 29**,** 5536-45.

LEE, D., KIM, K. Y., SHIM, M. S., KIM, S. Y., ELLISMAN, M. H., WEINREB, R. N. & JU, W. K. 2014a. Coenzyme Q10 ameliorates oxidative stress and prevents mitochondrial alteration in ischemic retinal injury. *Apoptosis,* 19**,** 603-14.

LEE, D., SHIM, M. S., KIM, K. Y., NOH, Y. H., KIM, H., KIM, S. Y., WEINREB, R. N. & JU, W. K. 2014b. Coenzyme Q10 inhibits glutamate excitotoxicity and oxidative stress-mediated mitochondrial alteration in a mouse model of glaucoma. *Invest Ophthalmol Vis Sci,* 55**,** 993-1005.

LEE, H. S., HAN, J., LEE, S. H., PARK, J. A. & KIM, K. W. 2010a. Meteorin promotes the formation of GFAP-positive glia via activation of the Jak-STAT3 pathway. *J Cell Sci,* 123**,** 1959-68.

LEE, J. K., LU, S. & MADHUKAR, A. 2010b. Real-Time dynamics of Ca2+, caspase-3/7, and morphological changes in retinal ganglion cell apoptosis under elevated pressure. *PLoS One,* 5**,** e13437.

LEE, K. Y., NAKAYAMA, M., AIHARA, M., CHEN, Y. N. & ARAIE, M. 2010c. Brimonidine is neuroprotective against glutamate-induced neurotoxicity, oxidative stress, and hypoxia in purified rat retinal ganglion cells. *Mol Vis,* 16**,** 246-51.

LEMMENS, K., BOLLAERTS, I., BHUMIKA, S., DE GROEF, L., VAN HOUCKE, J., DARRAS, V. M., VAN HOVE, I. & MOONS, L. 2016. Matrix metalloproteinases as promising regulators of

axonal regrowth in the injured adult zebrafish retinotectal system. *J Comp Neurol,* 524**,** 1472-93.
LENKOWSKI, J. R., QIN, Z., SIFUENTES, C. J., THUMMEL, R., SOTO, C. M., MOENS, C. B. & RAYMOND, P. A. 2013. Retinal regeneration in adult zebrafish requires regulation of TGFβ signaling. *Glia,* 61**,** 1687-1697.
LENS, A., LANGLEY T., NEMETH, S.C., SHEA, C. 1999. The bony orbit. *In:* LEFORD, J. K., DANIELS, K., CAMPBELL, R. (ed.) *Ocular anatomy and physiology.* Thorofare, USA: SLACK Incoporated.
LEWIS, G. & FISHER, S. 2003. Up-regulation of glial fibrillary acidic protein in response to retinal injury: its potential role in glial remodeling and a comparison to vimentin expression. *Int Rev Cytol,* 230**,** 263 - 290.
LEWIS, G. P. & FISHER, S. K. 2000. Muller cell outgrowth after retinal detachment: association with cone photoreceptors. *Invest Ophthalmol Vis Sci,* 41**,** 1542-5.
LI, G., XIE, B., HE, L., ZHOU, T., GAO, G., LIU, S., PAN, G., GE, J., PENG, F. & ZHONG, X. 2018. Generation of Retinal Organoids with Mature Rods and Cones from Urine-Derived Human Induced Pluripotent Stem Cells. *Stem Cells Int,* 2018**,** 4968658.
LI, L., DU, G., WANG, D., ZHOU, J., JIANG, G. & JIANG, H. 2017. Overexpression of Heme Oxygenase-1 in Mesenchymal Stem Cells Augments Their Protection on Retinal Cells In Vitro and Attenuates Retinal Ischemia/Reperfusion Injury In Vivo against Oxidative Stress. *Stem Cells Int,* 2017**,** 4985323.
LI, L., ZHANG, H., VARRIN-DOYER, M., ZAMVIL, S. S. & VERKMAN, A. S. 2011. Proinflammatory role of aquaporin-4 in autoimmune neuroinflammation. *Faseb j,* 25**,** 1556-66.
LI, P., TIAN, H., LI, Z., WANG, L., GAO, F., OU, Q., LIAN, C., LI, W., JIN, C., ZHANG, J., XU, J. Y., WANG, J., ZHANG, J., WANG, F., LU, L. & XU, G. T. 2016a. Subpopulations of Bone Marrow Mesenchymal Stem Cells Exhibit Differential Effects in Delaying Retinal Degeneration. *Curr Mol Med,* 16**,** 567-81.
LI, Y., SCHLAMP, C. L. & NICKELLS, R. W. 1999. Experimental induction of retinal ganglion cell death in adult mice. *Invest Ophthalmol Vis Sci,* 40**,** 1004-8.
LI, Z., WANG, J., GAO, F., ZHANG, J., TIAN, H., SHI, X., LIAN, C., SUN, Y., LI, W., XU, J. Y., LI, P., ZHANG, J., GAO, Z., XU, J., WANG, F., LU, L. & XU, G. T. 2016b. Human Adipose-Derived Stem Cells Delay Retinal Degeneration in Royal College of Surgeons Rats Through Anti-Apoptotic and VEGF-Mediated Neuroprotective Effects. *Curr Mol Med,* 16**,** 553-66.
LIAO, J. L., YU, J., HUANG, K., HU, J., DIEMER, T., MA, Z., DVASH, T., YANG, X. J., TRAVIS, G. H., WILLIAMS, D. S., BOK, D. & FAN, G. 2010. Molecular signature of primary retinal pigment epithelium and stem-cell-derived RPE cells. *Hum Mol Genet,* 19**,** 4229-38.
LILLIEN, L. 1995. Changes in retinal cell fate induced by overexpression of EGF receptor. *Nature,* 377**,** 158-62.
LIMB, G. A., ALAM, A., EARLEY, O., GREEN, W., CHIGNELL, A. H. & DUMONDE, D. C. 1994. Distribution of cytokine proteins within epiretinal membranes in proliferative vitreoretinopathy. *Curr Eye Res,* 13**,** 791-8.
LIMB, G. A., LITTLE, B. C., MEAGER, A., OGILVIE, J. A., WOLSTENCROFT, R. A., FRANKS, W. A., CHIGNELL, A. H. & DUMONDE, D. C. 1991. Cytokines in proliferative vitreoretinopathy. *Eye (Lond),* 5 (Pt 6)**,** 686-93.
LIMB, G. A., SALT, T. E., MUNRO, P. M., MOSS, S. E. & KHAW, P. T. 2002. In vitro characterization of a spontaneously immortalized human Muller cell line (MIO-M1). *Invest Ophthalmol Vis Sci,* 43**,** 864-9.
LIN, C. C., CHIANG, L. L., LIN, C. H., SHIH, C. H., LIAO, Y. T., HSU, M. J. & CHEN, B. C. 2007. Transforming growth factor-beta1 stimulates heme oxygenase-1 expression via the PI3K/Akt and NF-kappaB pathways in human lung epithelial cells. *Eur J Pharmacol,* 560**,** 101-9.
LIN, Y.-P., OUCHI, Y., SATOH, S. & WATANABE, S. 2009. Sox2 Plays a Role in the Induction of Amacrine and Müller Glial Cells in Mouse Retinal Progenitor Cells. *Investigative Ophthalmology & Visual Science,* 50**,** 68-74.
LIU, G., CUI, X., LI, H. & CAI, L. 2016. Evolutionary direction of processed pseudogenes. *Sci China Life Sci,* 59**,** 839-49.
LIU, G. H., QU, J. & SHEN, X. 2008. NF-kappaB/p65 antagonizes Nrf2-ARE pathway by depriving CBP from Nrf2 and facilitating recruitment of HDAC3 to MafK. *Biochim Biophys Acta,* 1783**,** 713-27.
LIU, H. Y., HUANG, J., XIAO, H., ZHANG, M. J., SHI, F. F., JIANG, Y. H., DU, H., HE, Q. & WANG, Z. Y. 2019. Pseudodominant inheritance of autosomal recessive congenital stationary night

blindness in one family with three co-segregating deleterious GRM6 variants identified by next-generation sequencing. *Mol Genet Genomic Med*, e952.
LIU, R. M. & DESAI, L. P. 2015. Reciprocal regulation of TGF-beta and reactive oxygen species: A perverse cycle for fibrosis. *Redox Biol,* 6, 565-577.
LIVESEY, F. J. & CEPKO, C. L. 2001. Vertebrate neural cell-fate determination: lessons from the retina. *Nat Rev Neurosci,* 2, 109-18.
LOCKSLEY, R. M., KILLEEN, N. & LENARDO, M. J. 2001. The TNF and TNF receptor superfamilies: integrating mammalian biology. *Cell,* 104, 487-501.
LU, X., HUANG, C., HE, X., LIU, X., JI, J., ZHANG, E., WANG, W. & GUO, R. 2017. A Novel Long Non-Coding RNA, SOX21-AS1, Indicates a Poor Prognosis and Promotes Lung Adenocarcinoma Proliferation. *Cell Physiol Biochem,* 42, 1857-1869.
LU, Y.-B., FRANZE, K., SEIFERT, G., STEINHÄUSER, C., KIRCHHOFF, F., WOLBURG, H., GUCK, J., JANMEY, P., WEI, E.-Q., KÄS, J. & REICHENBACH, A. 2006. Viscoelastic properties of individual glial cells and neurons in the CNS. *Proceedings of the National Academy of Sciences of the United States of America,* 103, 17759-17764.
LU, Y.-B., IANDIEV, I., HOLLBORN, M., KÖRBER, N., ULBRICHT, E., HIRRLINGER, P. G., PANNICKE, T., WEI, E.-Q., BRINGMANN, A., WOLBURG, H., WILHELMSSON, U., PEKNY, M., WIEDEMANN, P., REICHENBACH, A. & KÄS, J. A. 2011. Reactive glial cells: increased stiffness correlates with increased intermediate filament expression. *The FASEB Journal,* 25, 624-631.
LUDWIG, P. E., FREEMAN, S. C. & JANOT, A. C. 2019. Novel stem cell and gene therapy in diabetic retinopathy, age related macular degeneration, and retinitis pigmentosa. *Int J Retina Vitreous,* 5, 7.
LUKOWSKI, S. W., LO, C. Y., SHAROV, A. A., NGUYEN, Q., FANG, L., HUNG, S. S., ZHU, L., ZHANG, T., GRUNERT, U., NGUYEN, T., SENABOUTH, A., JABBARI, J. S., WELBY, E., SOWDEN, J. C., WAUGH, H. S., MACKEY, A., POLLOCK, G., LAMB, T. D., WANG, P. Y., HEWITT, A. W., GILLIES, M. C., POWELL, J. E. & WONG, R. C. 2019. A single-cell transcriptome atlas of the adult human retina. *Embo j,* 38, e100811.
LUNA, G., LEWIS, G. P., BANNA, C. D., SKALLI, O. & FISHER, S. K. 2010. Expression profiles of nestin and synemin in reactive astrocytes and Muller cells following retinal injury: a comparison with glial fibrillar acidic protein and vimentin. *Mol Vis,* 16, 2511-23.
LUNDKVIST, A., REICHENBACH, A., BETSHOLTZ, C., CARMELIET, P., WOLBURG, H. & PEKNY, M. 2004. Under stress, the absence of intermediate filaments from Muller cells in the retina has structural and functional consequences. *J Cell Sci,* 117, 3481-8.
LUPIEN, C. B., BOLDUC, C., LANDREVILLE, S. & SALESSE, C. 2007. Comparison between the gene expression profile of human Muller cells and two spontaneous Muller cell lines. *Invest Ophthalmol Vis Sci,* 48, 5229-42.
MA, C. H. & TAYLOR, J. S. 2010. Trophic responsiveness of purified postnatal and adult rat retinal ganglion cells. *Cell Tissue Res,* 339, 297-310.
MA, Q. 2013. Role of nrf2 in oxidative stress and toxicity. *Annu Rev Pharmacol Toxicol,* 53, 401-26.
MA, S., ZHANG, X., ZHENG, L., LI, Z., ZHAO, X., LAI, W., SHEN, H., LV, J., YANG, G., WANG, Q. & JI, J. 2016. Peroxiredoxin 6 Is a Crucial Factor in the Initial Step of Mitochondrial Clearance and Is Upstream of the PINK1-Parkin Pathway. *Antioxid Redox Signal,* 24, 486-501.
MAC NAIR, C. E., FERNANDES, K. A., SCHLAMP, C. L., LIBBY, R. T. & NICKELLS, R. W. 2014. Tumor necrosis factor alpha has an early protective effect on retinal ganglion cells after optic nerve crush. *J Neuroinflammation,* 11, 194.
MADEN, M., ONG, D. E., SUMMERBELL, D. & CHYTIL, F. 1988. Spatial distribution of cellular protein binding to retinoic acid in the chick limb bud. *Nature,* 335, 733-5.
MAINES, M. D. 1988. Heme oxygenase: function, multiplicity, regulatory mechanisms, and clinical applications. *Faseb j,* 2, 2557-68.
MAISONPIERRE, P. C., BELLUSCIO, L., FRIEDMAN, B., ALDERSON, R. F., WIEGAND, S. J., FURTH, M. E., LINDSAY, R. M. & YANCOPOULOS, G. D. 1990a. NT-3, BDNF, and NGF in the developing rat nervous system: parallel as well as reciprocal patterns of expression. *Neuron,* 5, 501-9.
MAISONPIERRE, P. C., BELLUSCIO, L., SQUINTO, S., IP, N. Y., FURTH, M. E., LINDSAY, R. M. & YANCOPOULOS, G. D. 1990b. Neurotrophin-3: a neurotrophic factor related to NGF and BDNF. *Science,* 247, 1446-51.
MANDAI, M., WATANABE, A., KURIMOTO, Y., HIRAMI, Y., MORINAGA, C., DAIMON, T., FUJIHARA, M., AKIMARU, H., SAKAI, N., SHIBATA, Y., TERADA, M., NOMIYA, Y., TANISHIMA, S., NAKAMURA, M., KAMAO, H., SUGITA, S., ONISHI, A., ITO, T., FUJITA,

K., KAWAMATA, S., GO, M. J., SHINOHARA, C., HATA, K. I., SAWADA, M., YAMAMOTO, M., OHTA, S., OHARA, Y., YOSHIDA, K., KUWAHARA, J., KITANO, Y., AMANO, N., UMEKAGE, M., KITAOKA, F., TANAKA, A., OKADA, C., TAKASU, N., OGAWA, S., YAMANAKA, S. & TAKAHASHI, M. 2017. Autologous Induced Stem-Cell-Derived Retinal Cells for Macular Degeneration. *N Engl J Med,* 376**,** 1038-1046.

MANSERGH, F. C., CHADDERTON, N., KENNA, P. F., GOBBO, O. L. & FARRAR, G. J. 2014. Cell therapy using retinal progenitor cells shows therapeutic effect in a chemically-induced rotenone mouse model of Leber hereditary optic neuropathy. *Eur J Hum Genet,* 22**,** 1314-20.

MAO, X., AN, Q., XI, H., YANG, X. J., ZHANG, X., YUAN, S., WANG, J., HU, Y., LIU, Q. & FAN, G. 2019. Single-Cell RNA Sequencing of hESC-Derived 3D Retinal Organoids Reveals Novel Genes Regulating RPC Commitment in Early Human Retinogenesis. *Stem Cell Reports,* 13**,** 747-760.

MARCHETTI, L., KLEIN, M., SCHLETT, K., PFIZENMAIER, K. & EISEL, U. L. 2004. Tumor necrosis factor (TNF)-mediated neuroprotection against glutamate-induced excitotoxicity is enhanced by N-methyl-D-aspartate receptor activation. Essential role of a TNF receptor 2-mediated phosphatidylinositol 3-kinase-dependent NF-kappa B pathway. *J Biol Chem,* 279**,** 32869-81.

MARIONI, J. C., MASON, C. E., MANE, S. M., STEPHENS, M. & GILAD, Y. 2008. RNA-seq: an assessment of technical reproducibility and comparison with gene expression arrays. *Genome Res,* 18**,** 1509-17.

MARSTERS, S. A., AYRES, T. M., SKUBATCH, M., GRAY, C. L., ROTHE, M. & ASHKENAZI, A. 1997. Herpesvirus entry mediator, a member of the tumor necrosis factor receptor (TNFR) family, interacts with members of the TNFR-associated factor family and activates the transcription factors NF-kappaB and AP-1. *J Biol Chem,* 272**,** 14029-32.

MARTÍNEZ-FERNÁNDEZ DE LA CÁMARA, C., OLIVARES-GONZÁLEZ, L., HERVÁS, D., SALOM, D., MILLÁN, J. M. & RODRIGO, R. 2014. Infliximab reduces Zaprinast-induced retinal degeneration in cultures of porcine retina. *Journal of Neuroinflammation,* 11**,** 172.

MASLAND, R. H. 2001. The fundamental plan of the retina. *Nat Neurosci,* 4**,** 877-86.

MASLAND, R. H. 2012. The neuronal organization of the retina. *Neuron,* 76**,** 266-80.

MATHY, N. W. & CHEN, X. M. 2017. Long non-coding RNAs (lncRNAs) and their transcriptional control of inflammatory responses. *J Biol Chem,* 292**,** 12375-12382.

MATSUYAMA, T., YAMADA, A., KAY, J., YAMADA, K. M., AKIYAMA, S. K., SCHLOSSMAN, S. F. & MORIMOTO, C. 1989. Activation of CD4 cells by fibronectin and anti-CD3 antibody. A synergistic effect mediated by the VLA-5 fibronectin receptor complex. *J Exp Med,* 170**,** 1133-48.

MEAD, B., AMARAL, J. & TOMAREV, S. 2018. Mesenchymal Stem Cell-Derived Small Extracellular Vesicles Promote Neuroprotection in Rodent Models of Glaucoma. *Invest Ophthalmol Vis Sci,* 59**,** 702-714.

MEAD, B. & TOMAREV, S. 2017. Bone Marrow-Derived Mesenchymal Stem Cells-Derived Exosomes Promote Survival of Retinal Ganglion Cells Through miRNA-Dependent Mechanisms. *Stem Cells Transl Med,* 6**,** 1273-1285.

MEHTA, A., PRABHAKAR, M., KUMAR, P., DESHMUKH, R. & SHARMA, P. L. 2013. Excitotoxicity: bridge to various triggers in neurodegenerative disorders. *Eur J Pharmacol,* 698**,** 6-18.

MEI, X., ZHANG, T., OUYANG, H., LU, B., WANG, Z. & JI, L. 2019. Scutellarin alleviates blood-retina-barrier oxidative stress injury initiated by activated microglia cells during the development of diabetic retinopathy. *Biochem Pharmacol,* 159**,** 82-95.

MEISTER, A. 1992. Biosynthesis and functions of glutathione, an essential biofactor. *J Nutr Sci Vitaminol (Tokyo),* Spec No**,** 1-6.

MENG, X. M., NIKOLIC-PATERSON, D. J. & LAN, H. Y. 2016. TGF-beta: the master regulator of fibrosis. *Nat Rev Nephrol,* 12**,** 325-38.

MESSMER-BLUST, A. F., BALASUBRAMANIAN, S., GORBACHEVA, V. Y., JEYARATNAM, J. A. & VESTAL, D. J. 2010. The interferon-gamma-induced murine guanylate-binding protein-2 inhibits rac activation during cell spreading on fibronectin and after platelet-derived growth factor treatment: role for phosphatidylinositol 3-kinase. *Mol Biol Cell,* 21**,** 2514-28.

MESTERS, J. R., BARINKA, C., LI, W., TSUKAMOTO, T., MAJER, P., SLUSHER, B. S., KONVALINKA, J. & HILGENFELD, R. 2006. Structure of glutamate carboxypeptidase II, a drug target in neuronal damage and prostate cancer. *Embo j,* 25**,** 1375-84.

MEYER-FRANKE, A., KAPLAN, M. R., PFRIEGER, F. W. & BARRES, B. A. 1995. Characterization of the signaling interactions that promote the survival and growth of developing retinal ganglion cells in culture. *Neuron,* 15**,** 805-19.

MEYER, J. S., KATZ, M. L., MARUNIAK, J. A. & KIRK, M. D. 2006. Embryonic stem cell-derived neural progenitors incorporate into degenerating retina and enhance survival of host photoreceptors. *STEM CELLS,* 24**,** 274-83.
MICHAELOUDES, C., SUKKAR, M. B., KHORASANI, N. M., BHAVSAR, P. K. & CHUNG, K. F. 2011. TGF-beta regulates Nox4, MnSOD and catalase expression, and IL-6 release in airway smooth muscle cells. *Am J Physiol Lung Cell Mol Physiol,* 300**,** L295-304.
MILAM, A. H., DE LEEUW, A. M., GAUR, V. P. & SAARI, J. C. 1990. Immunolocalization of cellular retinoic acid binding protein to Muller cells and/or a subpopulation of GABA-positive amacrine cells in retinas of different species. *J Comp Neurol,* 296**,** 123-9.
MILLER, J. W., LE COUTER, J., STRAUSS, E. C. & FERRARA, N. 2013. Vascular endothelial growth factor a in intraocular vascular disease. *Ophthalmology,* 120**,** 106-14.
MIMURA, T., FUNATSU, H., NOMA, H., SHIMURA, M., KAMEI, Y., YOSHIDA, M., KONDO, A., WATANABE, E. & MIZOTA, A. 2019. Aqueous Humor Levels of Cytokines in Patients with Age-Related Macular Degeneration. *Ophthalmologica,* 241**,** 81-89.
MONGKOLSAPAYA, J., GRIMES, J. M., CHEN, N., XU, X. N., STUART, D. I., JONES, E. Y. & SCREATON, G. R. 1999. Structure of the TRAIL-DR5 complex reveals mechanisms conferring specificity in apoptotic initiation. *Nat Struct Biol,* 6**,** 1048-53.
MONSEL, A., ZHU, Y. G., GUDAPATI, V., LIM, H. & LEE, J. W. 2016. Mesenchymal stem cell derived secretome and extracellular vesicles for acute lung injury and other inflammatory lung diseases. *Expert Opin Biol Ther,* 16**,** 859-71.
MORCOS, Y., HOSIE, M. J., BAUER, H. C. & CHAN-LING, T. 2001. Immunolocalization of occludin and claudin-1 to tight junctions in intact CNS vessels of mammalian retina. *J Neurocytol,* 30**,** 107-23.
MORGAN, J. E., DATTA, A. V., ERICHSEN, J. T., ALBON, J. & BOULTON, M. E. 2006. Retinal ganglion cell remodelling in experimental glaucoma. *Adv Exp Med Biol,* 572**,** 397-402.
MORGAN, M. J., KIM, Y. S. & LIU, Z. G. 2008. TNFalpha and reactive oxygen species in necrotic cell death. *Cell Res,* 18**,** 343-9.
MORGAN, M. J. & LIU, Z. G. 2011. Crosstalk of reactive oxygen species and NF-kappaB signaling. *Cell Res,* 21**,** 103-15.
MORRISON, S. J. & SPRADLING, A. C. 2008. Stem cells and niches: mechanisms that promote stem cell maintenance throughout life. *Cell,* 132**,** 598-611.
MORROW, E. M., FURUKAWA, T., LEE, J. E. & CEPKO, C. L. 1999. NeuroD regulates multiple functions in the developing neural retina in rodent. *Development,* 126**,** 23-36.
MORTAZAVI, A., WILLIAMS, B. A., MCCUE, K., SCHAEFFER, L. & WOLD, B. 2008. Mapping and quantifying mammalian transcriptomes by RNA-Seq. *Nat Methods,* 5**,** 621-8.
MUETHER, P. S., NEUHANN, I., BUHL, C., HERMANN, M. M., KIRCHHOF, B. & FAUSER, S. 2013. Intraocular growth factors and cytokines in patients with dry and neovascular age-related macular degeneration. *Retina,* 33**,** 1809-14.
MUGURUMA, K., NISHIYAMA, A., KAWAKAMI, H., HASHIMOTO, K. & SASAI, Y. 2015. Self-organization of polarized cerebellar tissue in 3D culture of human pluripotent stem cells. *Cell Rep,* 10**,** 537-50.
MURALI, A., RAMLOGAN-STEEL, C. A., ANDRZEJEWSKI, S., STEEL, J. C. & LAYTON, C. J. 2019. Retinal explant culture: A platform to investigate human neuro-retina. *Clin Exp Ophthalmol,* 47**,** 274-285.
MUZYKA, V. V., BROOKS, M. & BADEA, T. C. 2018. Postnatal developmental dynamics of cell type specification genes in Brn3a/Pou4f1 Retinal Ganglion Cells. *Neural Dev,* 13**,** 15.
NAKANO, T., ANDO, S., TAKATA, N., KAWADA, M., MUGURUMA, K., SEKIGUCHI, K., SAITO, K., YONEMURA, S., EIRAKU, M. & SASAI, Y. 2012. Self-formation of optic cups and storable stratified neural retina from human ESCs. *Cell Stem Cell,* 10**,** 771-785.
NAKAYAMA, K., ISHIDA, N., SHIRANE, M., INOMATA, A., INOUE, T., SHISHIDO, N., HORII, I. & LOH, D. Y. 1996. Mice lacking p27(Kip1) display increased body size, multiple organ hyperplasia, retinal dysplasia, and pituitary tumors. *Cell,* 85**,** 707-20.
NAKAZAWA, T., MATSUBARA, A., NODA, K., HISATOMI, T., SHE, H., SKONDRA, D., MIYAHARA, S., SOBRIN, L., THOMAS, K. L., CHEN, D. F., GROSSKREUTZ, C. L., HAFEZI-MOGHADAM, A. & MILLER, J. W. 2006. Characterization of cytokine responses to retinal detachment in rats. *Mol Vis,* 12**,** 867-78.
NAKAZAWA, T., TAKEDA, M., LEWIS, G. P., CHO, K.-S., JIAO, J., WILHELMSSON, U., FISHER, S. K., PEKNY, M., CHEN, D. F. & MILLER, J. W. 2007. Attenuated Glial Reactions and Photoreceptor Degeneration after Retinal Detachment in Mice Deficient in Glial Fibrillary Acidic Protein and Vimentin. *Investigative Ophthalmology & Visual Science,* 48**,** 2760-2768.

NASCHBERGER, E., WERNER, T., VICENTE, A. B., GUENZI, E., TÖPOLT, K., LEUBERT, R., LUBESEDER-MARTELLATO, C., NELSON, P. J. & STÜRZL, M. 2004. Nuclear factor-kappaB motif and interferon-alpha-stimulated response element co-operate in the activation of guanylate-binding protein-1 expression by inflammatory cytokines in endothelial cells. *Biochem J,* 379**,** 409-20.

NAVNEET, S., CUI, X., ZHAO, J., WANG, J., KAIDERY, N. A., THOMAS, B., BOLLINGER, K. E., YOON, Y. & SMITH, S. B. 2019. Excess homocysteine upregulates the NRF2-antioxidant pathway in retinal Muller glial cells. *Exp Eye Res,* 178**,** 228-237.

NEBBIOSO, M., SCARSELLA, G., TAFANI, M. & PESCOSOLIDO, N. 2013. Mechanisms of ocular neuroprotection by antioxidant molecules in animal models. *J Biol Regul Homeost Agents,* 27**,** 197-209.

NELSON, C. M., ACKERMAN, K. M., O'HAYER, P., BAILEY, T. J., GORSUCH, R. A. & HYDE, D. R. 2013. Tumor necrosis factor-alpha is produced by dying retinal neurons and is required for Muller glia proliferation during zebrafish retinal regeneration. *J Neurosci,* 33**,** 6524-39.

NELSON, C. M., GORSUCH, R. A., BAILEY, T. J., ACKERMAN, K. M., KASSEN, S. C. & HYDE, D. R. 2012. Stat3 defines three populations of müller glia and is required for initiating maximal müller glia proliferation in the regenerating zebrafish retina. *The Journal of Comparative Neurology,* 520**,** 4294-4311.

NEUFELD AH, K. S., DAS S, VORA S, GACHIE E 2002. Loss of retinal ganglion cells following retinal ischemia: the role of inducible nitric oxide synthase. *Exp Eye Res* 75**,** 521-528.

NEWMAN, A. M., GALLO, N. B., HANCOX, L. S., MILLER, N. J., RADEKE, C. M., MALONEY, M. A., COOPER, J. B., HAGEMAN, G. S., ANDERSON, D. H., JOHNSON, L. V. & RADEKE, M. J. 2012. Systems-level analysis of age-related macular degeneration reveals global biomarkers and phenotype-specific functional networks. *Genome Med,* 4**,** 16.

NEWMAN, E. & REICHENBACH, A. 1996. The Müller cell: a functional element of the retina. *Trends in Neurosciences,* 19**,** 307-312.

NEWMAN, E. A. 1996. Acid efflux from retinal glial cells generated by sodium bicarbonate cotransport. *J Neurosci,* 16**,** 159-68.

NG, L., HURLEY, J. B., DIERKS, B., SRINIVAS, M., SALTO, C., VENNSTROM, B., REH, T. A. & FORREST, D. 2001. A thyroid hormone receptor that is required for the development of green cone photoreceptors. *Nat Genet,* 27**,** 94-98.

NISHIKAWA, T., EDELSTEIN, D., DU, X. L., YAMAGISHI, S., MATSUMURA, T., KANEDA, Y., YOREK, M. A., BEEBE, D., OATES, P. J., HAMMES, H. P., GIARDINO, I. & BROWNLEE, M. 2000. Normalizing mitochondrial superoxide production blocks three pathways of hyperglycaemic damage. *Nature,* 404**,** 787-90.

NISHINO, J., YAMASHITA, K., HASHIGUCHI, H., FUJII, H., SHIMAZAKI, T. & HAMADA, H. 2004. Meteorin: a secreted protein that regulates glial cell differentiation and promotes axonal extension. *Embo j,* 23**,** 1998-2008.

NITA, M., STRZALKA-MROZIK, B., GRZYBOWSKI, A., MAZUREK, U. & ROMANIUK, W. 2014. Age-related macular degeneration and changes in the extracellular matrix. *Med Sci Monit,* 20**,** 1003-16.

NIWA, H. 2015. A Stepping Stone to Pluripotency. *Cell,* 163**,** 1570-2.

O'DRISCOLL, C., O'CONNOR, J., O'BRIEN, C. J. & COTTER, T. G. 2008. Basic fibroblast growth factor-induced protection from light damage in the mouse retina in vivo. *J Neurochem,* 105**,** 524-36.

OGATA, N., WANG, L., JO, N., TOMBRAN-TINK, J., TAKAHASHI, K., MRAZEK, D. & MATSUMURA, M. 2001. Pigment epithelium derived factor as a neuroprotective agent against ischemic retinal injury. *Curr Eye Res,* 22**,** 245-52.

OGURA, Y., SUTTERWALA, F. S. & FLAVELL, R. A. 2006. The inflammasome: first line of the immune response to cell stress. *Cell,* 126**,** 659-62.

OHNUMA, S., PHILPOTT, A., WANG, K., HOLT, C. E. & HARRIS, W. A. 1999. p27Xic1, a Cdk inhibitor, promotes the determination of glial cells in Xenopus retina. *Cell,* 99**,** 499-510.

OKADA, S., NAKAMURA, M., KATOH, H., MIYAO, T., SHIMAZAKI, T., ISHII, K., YAMANE, J., YOSHIMURA, A., IWAMOTO, Y., TOYAMA, Y. & OKANO, H. 2006. Conditional ablation of Stat3 or Socs3 discloses a dual role for reactive astrocytes after spinal cord injury. *Nat Med,* 12**,** 829-34.

OKU, H., IKEDA, T., HONMA, Y., SOTOZONO, C., NISHIDA, K., NAKAMURA, Y., KIDA, T. & KINOSHITA, S. 2002. Gene expression of neurotrophins and their high-affinity Trk receptors in cultured human Muller cells. *Ophthalmic Res,* 34**,** 38-42.

OOTO, S., AKAGI, T., KAGEYAMA, R., AKITA, J., MANDAI, M., HONDA, Y. & TAKAHASHI, M. 2004. Potential for neural regeneration after neurotoxic injury in the adult mammalian retina. *Proc Natl Acad Sci USA,* 101**,** 13654 - 13659.
ORGANIZATION, W. H. 2017. *Causes of blindness and visual impairment* [Online]. [Accessed 17/8/2017].
OSAFUNE, K., CARON, L., BOROWIAK, M., MARTINEZ, R. J., FITZ-GERALD, C. S., SATO, Y., COWAN, C. A., CHIEN, K. R. & MELTON, D. A. 2008. Marked differences in differentiation propensity among human embryonic stem cell lines. *Nat Biotechnol,* 26**,** 313-5.
OSBORNE, A., HOPES, M., WRIGHT, P., BROADWAY, D. C. & SANDERSON, J. 2016. Human organotypic retinal cultures (HORCs) as a chronic experimental model for investigation of retinal ganglion cell degeneration. *Exp Eye Res,* 143**,** 28-38.
OSBORNE, A., SANDERSON, J. & MARTIN, K. R. 2018. Neuroprotective Effects of Human Mesenchymal Stem Cells and Platelet-Derived Growth Factor on Human Retinal Ganglion Cells. *Stem Cells,* 36**,** 65-78.
OSTER, G. F. & PERELSON, A. S. 1987. The physics of cell motility. *J Cell Sci Suppl,* 8**,** 35-54.
OTORI, Y., WEI, J. Y. & BARNSTABLE, C. J. 1998. Neurotoxic effects of low doses of glutamate on purified rat retinal ganglion cells. *Invest Ophthalmol Vis Sci,* 39**,** 972-81.
OTTO, D., FROTSCHER, M. & UNSICKER, K. 1989. Basic fibroblast growth factor and nerve growth factor administered in gel foam rescue medial septal neurons after fimbria fornix transection. *J Neurosci Res,* 22**,** 83-91.
PACIFICI, F., ARRIGA, R., SORICE, G. P., CAPUANI, B., SCIOLI, M. G., PASTORE, D., DONADEL, G., BELLIA, A., CARATELLI, S., COPPOLA, A., FERRELLI, F., FEDERICI, M., SCONOCCHIA, G., TESAURO, M., SBRACCIA, P., DELLA-MORTE, D., GIACCARI, A., ORLANDI, A. & LAURO, D. 2014. Peroxiredoxin 6, a novel player in the pathogenesis of diabetes. *Diabetes,* 63**,** 3210-20.
PANG, I. H., ZENG, H., FLEENOR, D. L. & CLARK, A. F. 2007. Pigment epithelium-derived factor protects retinal ganglion cells. *BMC Neurosci,* 8**,** 11.
PANNICKE, T., IANDIEV, I., UCKERMANN, O., BIEDERMANN, B., KUTZERA, F., WIEDEMANN, P., WOLBURG, H., REICHENBACH, A. & BRINGMANN, A. 2004. A potassium channel-linked mechanism of glial cell swelling in the postischemic retina. *Mol Cell Neurosci,* 26**,** 493-502.
PARFITT, D. A., LANE, A., RAMSDEN, C., JOVANOVIC, K., COFFEY, P. J., HARDCASTLE, A. J. & CHEETHAM, M. E. 2016. Using induced pluripotent stem cells to understand retinal ciliopathy disease mechanisms and develop therapies. *Biochem Soc Trans,* 44**,** 1245-1251.
PASCOLINI, D. & MARIOTTI, S. P. 2012. Global estimates of visual impairment: 2010. *Br J Ophthalmol,* 96**,** 614-8.
PASTOR, J. C., ROJAS, J., PASTOR-IDOATE, S., DI LAURO, S., GONZALEZ-BUENDIA, L. & DELGADO-TIRADO, S. 2016. Proliferative vitreoretinopathy: A new concept of disease pathogenesis and practical consequences. *Prog Retin Eye Res,* 51**,** 125-55.
PATENAUDE, A., MURTHY, M. R. & MIRAULT, M. E. 2005. Emerging roles of thioredoxin cycle enzymes in the central nervous system. *Cell Mol Life Sci,* 62**,** 1063-80.
PENNOCK, S., HADDOCK, L. J., MUKAI, S. & KAZLAUSKAS, A. 2014. Vascular endothelial growth factor acts primarily via platelet-derived growth factor receptor alpha to promote proliferative vitreoretinopathy. *Am J Pathol,* 184**,** 3052-68.
PERKINS, N. D. 2004. NF-kappaB: tumor promoter or suppressor? *Trends Cell Biol,* 14**,** 64-9.
PERKINS, N. D. & GILMORE, T. D. 2006. Good cop, bad cop: the different faces of NF-kappaB. *Cell Death Differ,* 13**,** 759-72.
PERRY, V. H., MORRIS, R. J. & RAISMAN, G. 1984. Is Thy-1 expressed only by ganglion cells and their axons in the retina and optic nerve? *J Neurocytol,* 13**,** 809-24.
PERSAUD, S. D., LIN, Y. W., WU, C. Y., KAGECHIKA, H. & WEI, L. N. 2013. Cellular retinoic acid binding protein I mediates rapid non-canonical activation of ERK1/2 by all-trans retinoic acid. *Cell Signal,* 25**,** 19-25.
PFEFFER, K. 2003. Biological functions of tumor necrosis factor cytokines and their receptors. *Cytokine Growth Factor Rev,* 14**,** 185-91.
PFEIFFER, R. L., MARC, R. E., KONDO, M., TERASAKI, H. & JONES, B. W. 2016. Muller cell metabolic chaos during retinal degeneration. *Exp Eye Res,* 150**,** 62-70.
PILLING, D., FAN, T., HUANG, D., KAUL, B. & GOMER, R. H. 2009. Identification of markers that distinguish monocyte-derived fibrocytes from monocytes, macrophages, and fibroblasts. *PLoS One,* 4**,** e7475.

PINAZO-DURAN, M. D., ZANON-MORENO, V., GALLEGO-PINAZO, R. & GARCIA-MEDINA, J. J. 2015. Oxidative stress and mitochondrial failure in the pathogenesis of glaucoma neurodegeneration. *Prog Brain Res,* 220**,** 127-53.
PINK, R. C., WICKS, K., CALEY, D. P., PUNCH, E. K., JACOBS, L. & CARTER, D. R. 2011. Pseudogenes: pseudo-functional or key regulators in health and disease? *Rna,* 17**,** 792-8.
PITTALA, V., FIDILIO, A., LAZZARA, F., PLATANIA, C. B. M., SALERNO, L., FORESTI, R., DRAGO, F. & BUCOLO, C. 2017. Effects of Novel Nitric Oxide-Releasing Molecules against Oxidative Stress on Retinal Pigmented Epithelial Cells. *Oxid Med Cell Longev,* 2017**,** 1420892.
POCHE, R. A., FURUTA, Y., CHABOISSIER, M. C., SCHEDL, A. & BEHRINGER, R. R. 2008. Sox9 is expressed in mouse multipotent retinal progenitor cells and functions in Muller glial cell development. *J Comp Neurol,* 510**,** 237-50.
PRASAD, A., TEH, D. B., SHAH JAHAN, F. R., MANIVANNAN, J., CHUA, S. M. & ALL, A. H. 2017. Direct Conversion Through Trans-Differentiation: Efficacy and Safety. *Stem Cells Dev,* 26**,** 154-165.
PRICE, R. D., MILNE, S. A., SHARKEY, J. & MATSUOKA, N. 2007. Advances in small molecules promoting neurotrophic function. *Pharmacol Ther,* 115**,** 292-306.
PUTTFARCKEN, P. S., HANDEN, J. S., MONTGOMERY, D. T., COYLE, J. T. & WERLING, L. L. 1993. N-acetyl-aspartylglutamate modulation of N-methyl-D-aspartate-stimulated [3H]norepinephrine release from rat hippocampal slices. *J Pharmacol Exp Ther,* 266**,** 796-803.
QIU, G., SEILER, M. J., THOMAS, B. B., WU, K., RADOSEVICH, M. & SADDA, S. R. 2007. Revisiting nestin expression in retinal progenitor cells in vitro and after transplantation in vivo. *Exp Eye Res,* 84**,** 1047-59.
QUINLAN, C. L., PEREVOSHCHIKOVA, I. V., HEY-MOGENSEN, M., ORR, A. L. & BRAND, M. D. 2013. Sites of reactive oxygen species generation by mitochondria oxidizing different substrates. *Redox Biol,* 1**,** 304-12.
RAGGE, N. K., LORENZ, B., SCHNEIDER, A., BUSHBY, K., DE SANCTIS, L., DE SANCTIS, U., SALT, A., COLLIN, J. R., VIVIAN, A. J., FREE, S. L., THOMPSON, P., WILLIAMSON, K. A., SISODIYA, S. M., VAN HEYNINGEN, V. & FITZPATRICK, D. R. 2005. SOX2 anophthalmia syndrome. *Am J Med Genet A,* 135**,** 1-7; discussion 8.
RALAT, L. A., MANEVICH, Y., FISHER, A. B. & COLMAN, R. F. 2006. Direct evidence for the formation of a complex between 1-cysteine peroxiredoxin and glutathione S-transferase pi with activity changes in both enzymes. *Biochemistry,* 45**,** 360-72.
RAMACHANDRAN, R., ZHAO, X. F. & GOLDMAN, D. 2011. Ascl1a/Dkk/beta-catenin signaling pathway is necessary and glycogen synthase kinase-3beta inhibition is sufficient for zebrafish retina regeneration. *Proc Natl Acad Sci U S A,* 108**,** 15858-63.
RAMESH, G., MACLEAN, A. G. & PHILIPP, M. T. 2013. Cytokines and chemokines at the crossroads of neuroinflammation, neurodegeneration, and neuropathic pain. *Mediators Inflamm,* 2013**,** 480739.
RAMOS-GOMEZ, M., KWAK, M. K., DOLAN, P. M., ITOH, K., YAMAMOTO, M., TALALAY, P. & KENSLER, T. W. 2001. Sensitivity to carcinogenesis is increased and chemoprotective efficacy of enzyme inducers is lost in nrf2 transcription factor-deficient mice. *Proc Natl Acad Sci U S A,* 98**,** 3410-5.
RANGA, A., GIRGIN, M., MEINHARDT, A., EBERLE, D., CAIAZZO, M., TANAKA, E. M. & LUTOLF, M. P. 2016. Neural tube morphogenesis in synthetic 3D microenvironments. *Proc Natl Acad Sci U S A,* 113**,** E6831-e6839.
RAO, C. N., MOHANAM, S., PUPPALA, A. & RAO, J. S. 1999. Regulation of ProMMP-1 and ProMMP-3 activation by tissue factor pathway inhibitor-2/matrix-associated serine protease inhibitor. *Biochem Biophys Res Commun,* 255**,** 94-8.
RAPAPORT, D. H., WONG, L. L., WOOD, E. D., YASUMURA, D. & LAVAIL, M. M. 2004a. Timing and topography of cell genesis in the rat retina. *J Comp Neurol,* 474**,** 304-24.
RAPAPORT, D. H., WONG, L. L., WOOD, E. D., YASUMURA, D. & LAVAIL, M. M. 2004b. Timing and topography of cell genesis in the rat retina. *The Journal of Comparative Neurology,* 474**,** 304-324.
RASIER, R., GORMUS, U., ARTUNAY, O., YUZBASIOGLU, E., ONCEL, M. & BAHCECIOGLU, H. 2010. Vitreous levels of VEGF, IL-8, and TNF-alpha in retinal detachment. *Curr Eye Res,* 35**,** 505-9.
RATTNER, A. & NATHANS, J. 2005. The genomic response to retinal disease and injury: evidence for endothelin signaling from photoreceptors to glia. *J Neurosci,* 25**,** 4540-9.

RAVI, M., PARAMESH, V., KAVIYA, S. R., ANURADHA, E. & SOLOMON, F. D. 2015. 3D cell culture systems: advantages and applications. *J Cell Physiol,* 230**,** 16-26.
REESE, B. E. & COLELLO, R. J. 1992. Neurogenesis in the retinal ganglion cell layer of the rat. *Neuroscience,* 46**,** 419-29.
REICHENBACH, A. & BRINGMANN, A. 2010. *Müller Cells in the Healthy and Diseased Retina,* New York, Dordrecht, Heidelberg, London, Springer.
REICHMAN, S., SLEMBROUCK, A., GAGLIARDI, G., CHAFFIOL, A., TERRAY, A., NANTEAU, C., POTEY, A., BELLE, M., RABESANDRATANA, O., DUEBEL, J., ORIEUX, G., NANDROT, E. F., SAHEL, J. A. & GOUREAU, O. 2017. Generation of Storable Retinal Organoids and Retinal Pigmented Epithelium from Adherent Human iPS Cells in Xeno-Free and Feeder-Free Conditions. *Stem Cells,* 35**,** 1176-1188.
REZANEJAD, H., SOHEILI, Z. S., HADDAD, F., MATIN, M. M., SAMIEI, S., MANAFI, A. & AHMADIEH, H. 2014. In vitro differentiation of adipose-tissue-derived mesenchymal stem cells into neural retinal cells through expression of human PAX6 (5a) gene. *Cell Tissue Res,* 356**,** 65-75.
RHEAUME, B. A., JEREEN, A., BOLISETTY, M., SAJID, M. S., YANG, Y., RENNA, K., SUN, L., ROBSON, P. & TRAKHTENBERG, E. F. 2018. Single cell transcriptome profiling of retinal ganglion cells identifies cellular subtypes. *Nat Commun,* 9**,** 2759.
ROBERTS, A. B. 1998. Molecular and cell biology of TGF-beta. *Miner Electrolyte Metab,* 24**,** 111-9.
ROBINSON, M. B., BLAKELY, R. D., COUTO, R. & COYLE, J. T. 1987. Hydrolysis of the brain dipeptide N-acetyl-L-aspartyl-L-glutamate. Identification and characterization of a novel N-acetylated alpha-linked acidic dipeptidase activity from rat brain. *J Biol Chem,* 262**,** 14498-506.
RODRIGUES, M., XIN, X., JEE, K., BABAPOOR-FARROKHRAN, S., KASHIWABUCHI, F., MA, T., BHUTTO, I., HASSAN, S. J., DAOUD, Y., BARANANO, D., SOLOMON, S., LUTTY, G., SEMENZA, G. L., MONTANER, S. & SODHI, A. 2013. VEGF secreted by hypoxic Muller cells induces MMP-2 expression and activity in endothelial cells to promote retinal neovascularization in proliferative diabetic retinopathy. *Diabetes,* 62**,** 3863-73.
RODRIGUEZ, A. R., DE SEVILLA MULLER, L. P. & BRECHA, N. C. 2014. The RNA binding protein RBPMS is a selective marker of ganglion cells in the mammalian retina. *J Comp Neurol,* 522**,** 1411-43.
ROESCH, K., JADHAV, A. P., TRIMARCHI, J. M., STADLER, M. B., ROSKA, B., SUN, B. B. & CEPKO, C. L. 2008. The transcriptome of retinal Muller glial cells. *J Comp Neurol,* 509**,** 225-38.
ROYCE, T. E., ROZOWSKY, J. S. & GERSTEIN, M. B. 2007. Toward a universal microarray: prediction of gene expression through nearest-neighbor probe sequence identification. *Nucleic Acids Res,* 35**,** e99.
RUULS, S. R., HOEK, R. M., NGO, V. N., MCNEIL, T., LUCIAN, L. A., JANATPOUR, M. J., KORNER, H., SCHEERENS, H., HESSEL, E. M., CYSTER, J. G., MCEVOY, L. M. & SEDGWICK, J. D. 2001. Membrane-bound TNF supports secondary lymphoid organ structure but is subservient to secreted TNF in driving autoimmune inflammation. *Immunity,* 15**,** 533-43.
RUZAFA, N., PEREIRO, X., LEPPER, M. F., HAUCK, S. M. & VECINO, E. 2018. A Proteomics Approach to Identify Candidate Proteins Secreted by Muller Glia that Protect Ganglion Cells in the Retina. *Proteomics,* 18**,** e1700321.
SAADOUN, S., PAPADOPOULOS, M. C., WATANABE, H., YAN, D., MANLEY, G. T. & VERKMAN, A. S. 2005. Involvement of aquaporin-4 in astroglial cell migration and glial scar formation. *J Cell Sci,* 118**,** 5691-8.
SAARI, J. C. 2016. Vitamin A and Vision. *Subcell Biochem,* 81**,** 231-259.
SAARI, J. C. & BREDBERG, D. L. 1988. Purification of cellular retinaldehyde-binding protein from bovine retina and retinal pigment epithelium. *Exp Eye Res,* 46**,** 569-78.
SABIO, G. & DAVIS, R. J. 2014. TNF and MAP kinase signalling pathways. *Semin Immunol,* 26**,** 237-45.
SAHA, R. N., LIU, X. & PAHAN, K. 2006. Up-regulation of BDNF in astrocytes by TNF-alpha: a case for the neuroprotective role of cytokine. *J Neuroimmune Pharmacol,* 1**,** 212-22.
SAKAGUCHI, H., KADOSHIMA, T., SOEN, M., NARII, N., ISHIDA, Y., OHGUSHI, M., TAKAHASHI, J., EIRAKU, M. & SASAI, Y. 2015. Generation of functional hippocampal neurons from self-organizing human embryonic stem cell-derived dorsomedial telencephalic tissue. *Nat Commun,* 6**,** 8896.
SAKON, S., XUE, X., TAKEKAWA, M., SASAZUKI, T., OKAZAKI, T., KOJIMA, Y., PIAO, J. H., YAGITA, H., OKUMURA, K., DOI, T. & NAKANO, H. 2003. NF-kappaB inhibits TNF-induced

accumulation of ROS that mediate prolonged MAPK activation and necrotic cell death. *Embo j,* 22**,** 3898-909.
SALOMON, B. L., LECLERC, M., TOSELLO, J., RONIN, E., PIAGGIO, E. & COHEN, J. L. 2018. Tumor Necrosis Factor alpha and Regulatory T Cells in Oncoimmunology. *Front Immunol,* 9**,** 444.
SANES, J. R. & MASLAND, R. H. 2015. The types of retinal ganglion cells: current status and implications for neuronal classification. *Annu Rev Neurosci,* 38**,** 221-46.
SANTOS-FERREIRA, T., LLONCH, S., BORSCH, O., POSTEL, K., HAAS, J. & ADER, M. 2016. Retinal transplantation of photoreceptors results in donor-host cytoplasmic exchange. *Nat Commun,* 7**,** 13028.
SANTOS, R., VADODARIA, K. C., JAEGER, B. N., MEI, A., LEFCOCHILOS-FOGELQUIST, S., MENDES, A. P. D., ERIKSON, G., SHOKHIREV, M., RANDOLPH-MOORE, L., FREDLENDER, C., DAVE, S., OEFNER, R., FITZPATRICK, C., PENA, M., BARRON, J. J., KU, M., DENLI, A. M., KERMAN, B. E., CHARNAY, P., KELSOE, J. R., MARCHETTO, M. C. & GAGE, F. H. 2017. Differentiation of Inflammation-Responsive Astrocytes from Glial Progenitors Generated from Human Induced Pluripotent Stem Cells. *Stem Cell Reports,* 8**,** 1757-1769.
SARMA, V., WOLF, F. W., MARKS, R. M., SHOWS, T. B. & DIXIT, V. M. 1992. Cloning of a novel tumor necrosis factor-alpha-inducible primary response gene that is differentially expressed in development and capillary tube-like formation in vitro. *J Immunol,* 148**,** 3302-12.
SATO, S., NAGAOKA, T., HASEGAWA, M., TAMATANI, T., NAKANISHI, T., TAKIGAWA, M. & TAKEHARA, K. 2000. Serum levels of connective tissue growth factor are elevated in patients with systemic sclerosis: association with extent of skin sclerosis and severity of pulmonary fibrosis. *J Rheumatol,* 27**,** 149-54.
SCHMID, S. & GUENTHER, E. 1996. Developmental regulation of voltage-activated Na+ and Ca2+ currents in rat retinal ganglion cells. *Neuroreport,* 7**,** 677-81.
SCHRAERMEYER, U., THUMANN, G., LUTHER, T., KOCIOK, N., ARMHOLD, S., KRUTTWIG, K., ANDRESSEN, C., ADDICKS, K. & BARTZ-SCHMIDT, K. U. 2001. Subretinally transplanted embryonic stem cells rescue photoreceptor cells from degeneration in the RCS rats. *Cell Transplant,* 10**,** 673-80.
SEANDEL, M., NOACK-KUNNMANN, K., ZHU, D., AIMES, R. T. & QUIGLEY, J. P. 2001. Growth factor-induced angiogenesis in vivo requires specific cleavage of fibrillar type I collagen. *Blood,* 97**,** 2323-32.
SEDGER, L. M. & MCDERMOTT, M. F. 2014. TNF and TNF-receptors: From mediators of cell death and inflammation to therapeutic giants – past, present and future. *Cytokine & Growth Factor Reviews,* 25**,** 453-472.
SEKI, M. & LIPTON, S. A. 2008. Targeting excitotoxic/free radical signaling pathways for therapeutic intervention in glaucoma. *Prog Brain Res,* 173**,** 495-510.
SEMRAU, S., GOLDMANN, J. E., SOUMILLON, M., MIKKELSEN, T. S., JAENISCH, R. & VAN OUDENAARDEN, A. 2017. Dynamics of lineage commitment revealed by single-cell transcriptomics of differentiating embryonic stem cells. *Nat Commun,* 8**,** 1096.
SENA, D. F. & LINDSLEY, K. 2017. Neuroprotection for treatment of glaucoma in adults. *Cochrane Database Syst Rev,* 1**,** Cd006539.
SERNAGOR, E., EGLEN, S. J. & WONG, R. O. 2001. Development of retinal ganglion cell structure and function. *Prog Retin Eye Res,* 20**,** 139-74.
SETHI, C. S., LEWIS, G. P., FISHER, S. K., LEITNER, W. P., MANN, D. L., LUTHERT, P. J. & CHARTERIS, D. G. 2005. Glial Remodeling and Neural Plasticity in Human Retinal Detachment with Proliferative Vitreoretinopathy. *Investigative Ophthalmology & Visual Science,* 46**,** 329-342.
SHARMA, P., FATMA, N., KUBO, E., SHINOHARA, T., CHYLACK, L. T., JR. & SINGH, D. P. 2003. Lens epithelium-derived growth factor relieves transforming growth factor-beta1-induced transcription repression of heat shock proteins in human lens epithelial cells. *J Biol Chem,* 278**,** 20037-46.
SINGH, R., CUZZANI, O., BINETTE, F., STERNBERG, H., WEST, M. D. & NASONKIN, I. O. 2018. Pluripotent Stem Cells for Retinal Tissue Engineering: Current Status and Future Prospects. *Stem Cell Rev,* 14**,** 463-483.
SINGH, R. K., MALLELA, R. K., CORNUET, P. K., REIFLER, A. N., CHERVENAK, A. P., WEST, M. D., WONG, K. Y. & NASONKIN, I. O. 2015. Characterization of Three-Dimensional Retinal Tissue Derived from Human Embryonic Stem Cells in Adherent Monolayer Cultures. *Stem Cells Dev,* 24**,** 2778-95.

SINGHAL, S., BHATIA, B., JAYARAM, H., BECKER, S., JONES, M. F., COTTRILL, P. B., KHAW, P. T., SALT, T. E. & LIMB, G. A. 2012. Human Müller Glia with Stem Cell Characteristics Differentiate into Retinal Ganglion Cell (RGC) Precursors In Vitro and Partially Restore RGC Function In Vivo Following Transplantation. *Stem Cells Translational Medicine,* 1**,** 188-199.
SINN, R. & WITTBRODT, J. 2013. An eye on eye development. *Mech Dev,* 130**,** 347-58.
SIPPL, C. & TAMM, E. R. 2014. What is the nature of the RGC-5 cell line? *Adv Exp Med Biol,* 801**,** 145-54.
SIQUEIRA, R. C., MESSIAS, A., MESSIAS, K., ARCIERI, R. S., RUIZ, M. A., SOUZA, N. F., MARTINS, L. C. & JORGE, R. 2015. Quality of life in patients with retinitis pigmentosa submitted to intravitreal use of bone marrow-derived stem cells (Reticell -clinical trial). *Stem Cell Res Ther,* 6**,** 29.
SIQUEIRA, R. C., MESSIAS, A., VOLTARELLI, J. C., MESSIAS, K., ARCIERI, R. S. & JORGE, R. 2013. Resolution of macular oedema associated with retinitis pigmentosa after intravitreal use of autologous BM-derived hematopoietic stem cell transplantation. *Bone Marrow Transplant,* 48**,** 612-3.
SIREN, A. L. & EHRENREICH, H. 2001. Erythropoietin--a novel concept for neuroprotection. *Eur Arch Psychiatry Clin Neurosci,* 251**,** 179-84.
SMITH, C. A. & CHAUHAN, B. C. 2015. Imaging retinal ganglion cells: enabling experimental technology for clinical application. *Prog Retin Eye Res,* 44**,** 1-14.
SMITH, J. W., VESTAL, D. J., IRWIN, S. V., BURKE, T. A. & CHERESH, D. A. 1990. Purification and functional characterization of integrin alpha v beta 5. An adhesion receptor for vitronectin. *J Biol Chem,* 265**,** 11008-13.
SNIDER, W. D. & JOHNSON, E. M., JR. 1989. Neurotrophic molecules. *Ann Neurol,* 26**,** 489-506.
SNODGRASS, S. R. 1992. Vitamin neurotoxicity. *Mol Neurobiol,* 6**,** 41-73.
SOMASUNDARAM, R. & SCHUPPAN, D. 1996. Type I, II, III, IV, V, and VI collagens serve as extracellular ligands for the isoforms of platelet-derived growth factor (AA, BB, and AB). *J Biol Chem,* 271**,** 26884-91.
SONG, G., SHEN, Y., ZHU, J., LIU, H., LIU, M., SHEN, Y. Q., ZHU, S., KONG, X., YU, Z. & QIAN, L. 2013. Integrated analysis of dysregulated lncRNA expression in fetal cardiac tissues with ventricular septal defect. *PLoS One,* 8**,** e77492.
SONG, H. Y., ROTHE, M. & GOEDDEL, D. V. 1996. The tumor necrosis factor-inducible zinc finger protein A20 interacts with TRAF1/TRAF2 and inhibits NF-kappaB activation. *Proc Natl Acad Sci U S A,* 93**,** 6721-5.
SRIDHAR, A., HOSHINO, A., FINKBEINER, C. R., CHITSAZAN, A., DAI, L., HAUGAN, A. K., ESCHENBACHER, K. M., JACKSON, D. L., TRAPNELL, C., BERMINGHAM-MCDONOGH, O., GLASS, I. & REH, T. A. 2020. Single-Cell Transcriptomic Comparison of Human Fetal Retina, hPSC-Derived Retinal Organoids, and Long-Term Retinal Cultures. *Cell Rep,* 30**,** 1644-1659.e4.
ST LAURENT, G., SHTOKALO, D., TACKETT, M. R., YANG, Z., EREMINA, T., WAHLESTEDT, C., URCUQUI-INCHIMA, S., SEILHEIMER, B., MCCAFFREY, T. A. & KAPRANOV, P. 2012. Intronic RNAs constitute the major fraction of the non-coding RNA in mammalian cells. *BMC Genomics,* 13**,** 504.
STEKETEE, M. B., OBOUDIYAT, C., DANEMAN, R., TRAKHTENBERG, E., LAMOUREUX, P., WEINSTEIN, J. E., HEIDEMANN, S., BARRES, B. A. & GOLDBERG, J. L. 2014. Regulation of intrinsic axon growth ability at retinal ganglion cell growth cones. *Invest Ophthalmol Vis Sci,* 55**,** 4369-77.
SUGA, A., SADAMOTO, K., FUJII, M., MANDAI, M. & TAKAHASHI, M. 2014. Proliferation potential of Muller glia after retinal damage varies between mouse strains. *PLoS One,* 9**,** e94556.
SULTAN, M., SCHULZ, M. H., RICHARD, H., MAGEN, A., KLINGENHOFF, A., SCHERF, M., SEIFERT, M., BORODINA, T., SOLDATOV, A., PARKHOMCHUK, D., SCHMIDT, D., O'KEEFFE, S., HAAS, S., VINGRON, M., LEHRACH, H. & YASPO, M. L. 2008. A global view of gene activity and alternative splicing by deep sequencing of the human transcriptome. *Science,* 321**,** 956-60.
SUN, C., ZHANG, J., ZHENG, D., WANG, J., YANG, H. & ZHANG, X. 2018. Transcriptome variations among human embryonic stem cell lines are associated with their differentiation propensity. *PLoS One,* 13**,** e0192625.
SUN, C. C., LI, S. J., LI, G., HUA, R. X., ZHOU, X. H. & LI, D. J. 2016. Long Intergenic Noncoding RNA 00511 Acts as an Oncogene in Non-small-cell Lung Cancer by Binding to EZH2 and Suppressing p57. *Mol Ther Nucleic Acids,* 5**,** e385.

SUN, W., LI, N. & HE, S. 2002. Large-scale morophological survey of rat retinal ganglion cells. *Vis Neurosci,* 19**,** 483-93.
SUN, Y., WANG, D., YE, F., HU, D. N., LIU, X., ZHANG, L., GAO, L., SONG, E. & ZHANG, D. Y. 2013. Elevated cell proliferation and VEGF production by high-glucose conditions in Muller cells involve XIAP. *Eye (Lond),* 27**,** 1299-307.
SUN, Z., CHIN, Y. E. & ZHANG, D. D. 2009. Acetylation of Nrf2 by p300/CBP augments promoter-specific DNA binding of Nrf2 during the antioxidant response. *Mol Cell Biol,* 29**,** 2658-72.
SURGUCHEVA, I., WEISMAN, A. D., GOLDBERG, J. L., SHNYRA, A. & SURGUCHOV, A. 2008. Gamma-synuclein as a marker of retinal ganglion cells. *Mol Vis,* 14**,** 1540-8.
SURZENKO, N., CROWL, T., BACHLEDA, A., LANGER, L. & PEVNY, L. 2013. SOX2 maintains the quiescent progenitor cell state of postnatal retinal Muller glia. *Development,* 140**,** 1445-56.
SUSAIMANICKAM, P. J., MADDILETI, S., PULIMAMIDI, V. K., BOYINPALLY, S. R., NAIK, R. R., NAIK, M. N., REDDY, G. B., SANGWAN, V. S. & MARIAPPAN, I. 2017. Generating minicorneal organoids from human induced pluripotent stem cells. *Development,* 144**,** 2338-2351.
SUZUKI, Y., NAKAZAWA, M., SUZUKI, K., YAMAZAKI, H. & MIYAGAWA, Y. 2011. Expression profiles of cytokines and chemokines in vitreous fluid in diabetic retinopathy and central retinal vein occlusion. *Jpn J Ophthalmol,* 55**,** 256-263.
SWANSON, K. I., SCHLIEVE, C. R., LIEVEN, C. J. & LEVIN, L. A. 2005. Neuroprotective effect of sulfhydryl reduction in a rat optic nerve crush model. *Invest Ophthalmol Vis Sci,* 46**,** 3737-41.
SWEENEY, N. T., JAMES, K. N., NISTORICA, A., LORIG-ROACH, R. M. & FELDHEIM, D. A. 2019. Expression of transcription factors divides retinal ganglion cells into distinct classes. *J Comp Neurol,* 527**,** 225-235.
SYMEONIDIS, C., PAPAKONSTANTINOU, E., ANDROUDI, S., ROTSOS, T., DIZA, E., BRAZITIKOS, P., KARAKIULAKIS, G. & DIMITRAKOS, S. A. 2011. Interleukin-6 and the matrix metalloproteinase response in the vitreous during proliferative vitreoretinopathy. *Cytokine,* 54**,** 212-7.
TAKAHASHI, K. & YAMANAKA, S. 2006. Induction of pluripotent stem cells from mouse embryonic and adult fibroblast cultures by defined factors. *Cell,* 126**,** 663-76.
TAKAHASHI, K. & YAMANAKA, S. 2016. A decade of transcription factor-mediated reprogramming to pluripotency. *Nat Rev Mol Cell Biol,* 17**,** 183-93.
TAKAHASHI, M. & HARUTA, M. 2006. Derivation and characterization of lentoid bodies and retinal pigment epithelial cells from monkey embryonic stem cells in vitro. *Methods Mol Biol,* 330**,** 417-29.
TAKEBE, T., ZHANG, R. R., KOIKE, H., KIMURA, M., YOSHIZAWA, E., ENOMURA, M., KOIKE, N., SEKINE, K. & TANIGUCHI, H. 2014. Generation of a vascularized and functional human liver from an iPSC-derived organ bud transplant. *Nat Protoc,* 9**,** 396-409.
TAKEDA, A., SHINOZAKI, Y., KASHIWAGI, K., OHNO, N., ETO, K., WAKE, H., NABEKURA, J. & KOIZUMI, S. 2018. Microglia mediate non-cell-autonomous cell death of retinal ganglion cells. *Glia,* 66**,** 2366-2384.
TALALAY, P., FAHEY, J. W., HOLTZCLAW, W. D., PRESTERA, T. & ZHANG, Y. 1995. Chemoprotection against cancer by phase 2 enzyme induction. *Toxicol Lett,* 82-83**,** 173-9.
TANG, G., MINEMOTO, Y., DIBLING, B., PURCELL, N. H., LI, Z., KARIN, M. & LIN, A. 2001. Inhibition of JNK activation through NF-kappaB target genes. *Nature,* 414**,** 313-7.
TANWAR, M., DADA, T., SIHOTA, R. & DADA, R. 2010. Mitochondrial DNA analysis in primary congenital glaucoma. *Mol Vis,* 16**,** 518-33.
TEZEL, G. 2008. TNF-alpha signaling in glaucomatous neurodegeneration. *Prog Brain Res,* 173**,** 409-21.
TEZEL, G., LI, L. Y., PATIL, R. V. & WAX, M. B. 2001. TNF-α and TNF-α Receptor-1 in the Retina of Normal and Glaucomatous Eyes. *Investigative Ophthalmology & Visual Science,* 42**,** 1787-1794.
TEZEL, G. & WAX, M. B. 2000. Increased production of tumor necrosis factor-alpha by glial cells exposed to simulated ischemia or elevated hydrostatic pressure induces apoptosis in cocultured retinal ganglion cells. *J Neurosci,* 20**,** 8693-700.
TEZEL, G., YANG, X., YANG, J. & WAX, M. B. 2004. Role of tumor necrosis factor receptor-1 in the death of retinal ganglion cells following optic nerve crush injury in mice. *Brain Res,* 996**,** 202-12.

THAM, Y. C., LI, X., WONG, T. Y., QUIGLEY, H. A., AUNG, T. & CHENG, C. Y. 2014. Global prevalence of glaucoma and projections of glaucoma burden through 2040: a systematic review and meta-analysis. *Ophthalmology,* 121**,** 2081-90.

THANOS, S. 1988. Alterations in the morphology of ganglion cell dendrites in the adult rat retina after optic nerve transection and grafting of peripheral nerve segments. *Cell Tissue Res,* 254**,** 599-609.

THOMAS, J. L., RANSKI, A. H., MORGAN, G. W. & THUMMEL, R. 2016. Reactive gliosis in the adult zebrafish retina. *Exp Eye Res,* 143**,** 98-109.

THOMPSON, J. E., PHILLIPS, R. J., ERDJUMENT-BROMAGE, H., TEMPST, P. & GHOSH, S. 1995. IκB-β regulates the persistent response in a biphasic activation of NF-κB. *Cell,* 80**,** 573-582.

THUMMEL, R., KASSEN, S. C., ENRIGHT, J. M., NELSON, C. M., MONTGOMERY, J. E. & HYDE, D. R. 2008. Characterization of Muller glia and neuronal progenitors during adult zebrafish retinal regeneration. *Exp Eye Res,* 87**,** 433-44.

TIAN, R., LUO, Y., LIU, Q., CAI, M., LI, J., SUN, W., WANG, J., HE, C., LIU, Y. & LIU, X. 2014. The effect of claudin-5 overexpression on the interactions of claudin-1 and -2 and barrier function in retinal cells. *Curr Mol Med,* 14**,** 1226-37.

TOBAR, N., TOYOS, M., URRA, C., MENDEZ, N., ARANCIBIA, R., SMITH, P. C. & MARTINEZ, J. 2014. c-Jun N terminal kinase modulates NOX-4 derived ROS production and myofibroblasts differentiation in human breast stromal cells. *BMC Cancer,* 14**,** 640.

TOBIUME, K., MATSUZAWA, A., TAKAHASHI, T., NISHITOH, H., MORITA, K., TAKEDA, K., MINOWA, O., MIYAZONO, K., NODA, T. & ICHIJO, H. 2001. ASK1 is required for sustained activations of JNK/p38 MAP kinases and apoptosis. *EMBO Rep,* 2**,** 222-8.

TODD, L., PALAZZO, I., SUAREZ, L., LIU, X., VOLKOV, L., HOANG, T. V., CAMPBELL, W. A., BLACKSHAW, S., QUAN, N. & FISCHER, A. J. 2019. Reactive microglia and IL1beta/IL-1R1-signaling mediate neuroprotection in excitotoxin-damaged mouse retina. *J Neuroinflammation,* 16**,** 118.

TOFT-KEHLER, A. K., GURUBARAN, I. S., DESLER, C., RASMUSSEN, L. J., SKYTT, D. M. & KOLKO, M. 2016. Oxidative Stress-Induced Dysfunction of Muller Cells During Starvation. *Invest Ophthalmol Vis Sci,* 57**,** 2721-8.

TRESE, M., REGATIERI, C. V. & YOUNG, M. J. 2012. Advances in Retinal Tissue Engineering. *Materials (Basel),* 5**,** 108-120.

TROUGAKOS, I. P., LOURDA, M., ANTONELOU, M. H., KLETSAS, D., GORGOULIS, V. G., PAPASSIDERI, I. S., ZOU, Y., MARGARITIS, L. H., BOOTHMAN, D. A. & GONOS, E. S. 2009. Intracellular clusterin inhibits mitochondrial apoptosis by suppressing p53-activating stress signals and stabilizing the cytosolic Ku70-Bax protein complex. *Clin Cancer Res,* 15**,** 48-59.

TRYNKA, G., ZHERNAKOVA, A., ROMANOS, J., FRANKE, L., HUNT, K. A., TURNER, G., BRUINENBERG, M., HEAP, G. A., PLATTEEL, M., RYAN, A. W., DE KOVEL, C., HOLMES, G. K., HOWDLE, P. D., WALTERS, J. R., SANDERS, D. S., MULDER, C. J., MEARIN, M. L., VERBEEK, W. H., TRIMBLE, V., STEVENS, F. M., KELLEHER, D., BARISANI, D., BARDELLA, M. T., MCMANUS, R., VAN HEEL, D. A. & WIJMENGA, C. 2009. Coeliac disease-associated risk variants in TNFAIP3 and REL implicate altered NF-kappaB signalling. *Gut,* 58**,** 1078-83.

TSUGE, M., YASUI, K., ICHIYAWA, T., SAITO, Y., NAGAOKA, Y., YASHIRO, M., YAMASHITA, N. & MORISHIMA, T. 2010. Increase of tumor necrosis factor-alpha in the blood induces early activation of matrix metalloproteinase-9 in the brain. *Microbiol Immunol,* 54**,** 417-24.

TUCKER, B. A., ANFINSON, K. R., MULLINS, R. F., STONE, E. M. & YOUNG, M. J. 2013. Use of a synthetic xeno-free culture substrate for induced pluripotent stem cell induction and retinal differentiation. *Stem Cells Transl Med,* 2**,** 16-24.

TUCKER, B. A., PARK, I. H., QI, S. D., KLASSEN, H. J., JIANG, C., YAO, J., REDENTI, S., DALEY, G. Q. & YOUNG, M. J. 2015. Correction: Transplantation of Adult Mouse iPS Cell-Derived Photoreceptor Precursors Restores Retinal Structure and Function in Degenerative Mice. *PLoS One,* 10**,** e0125947.

TULSAWANI, R., KELLY, L. S., FATMA, N., CHHUNCHHA, B., KUBO, E., KUMAR, A. & SINGH, D. P. 2010. Neuroprotective effect of peroxiredoxin 6 against hypoxia-induced retinal ganglion cell damage. *BMC Neurosci,* 11**,** 125.

TURKSEVEN, S., KRUGER, A., MINGONE, C. J., KAMINSKI, P., INABA, M., RODELLA, L. F., IKEHARA, S., WOLIN, M. S. & ABRAHAM, N. G. 2005. Antioxidant mechanism of heme oxygenase-1 involves an increase in superoxide dismutase and catalase in experimental diabetes. *Am J Physiol Heart Circ Physiol,* 289**,** H701-7.

UCHIDA, S., SUZUKI, Y., ARAIE, M., KASHIWAGI, K., OTORI, Y. & SAKURAGAWA, N. 2003. Factors secreted by human amniotic epithelial cells promote the survival of rat retinal ganglion cells. *Neurosci Lett,* 341**,** 1-4.
UEHARA, F., OHBA, N. & OZAWA, M. 2001. Isolation and Characterization of Galectins in the Mammalian Retina. *Investigative Ophthalmology & Visual Science,* 42**,** 2164-2172.
URSCHEL, K. & CICHA, I. 2015. TNF-α in the cardiovascular system: from physiology to therapy. *International Journal of Interferon, Cytokine and Mediator Research,* 7.
VALAPALA, M., EDWARDS, M., HOSE, S., HU, J., WAWROUSEK, E., LUTTY, G. A., ZIGLER, J. S., JR., QIAN, J. & SINHA, D. 2015. βA3/A1-crystallin is a critical mediator of STAT3 signaling in optic nerve astrocytes. *Sci Rep,* 5**,** 8755.
VAN BERGEN, N. J., WOOD, J. P., CHIDLOW, G., TROUNCE, I. A., CASSON, R. J., JU, W. K., WEINREB, R. N. & CROWSTON, J. G. 2009. Recharacterization of the RGC-5 retinal ganglion cell line. *Invest Ophthalmol Vis Sci,* 50**,** 4267-72.
VAN RAAY, T. J. & VETTER, M. L. 2004. Wnt/Frizzled Signaling during Vertebrate Retinal Development. *Developmental Neuroscience,* 26**,** 352-358.
VANDENABEELE, P., DECLERCQ, W., BEYAERT, R. & FIERS, W. 1995. Two tumour necrosis factor receptors: structure and function. *Trends Cell Biol,* 5**,** 392-9.
VANEY, D. I. 2002. Retinal neurons: cell types and coupled networks. *Prog Brain Res,* 136**,** 239-54.
VARDIMON, L., FOX, L. E. & MOSCONA, A. A. 1986. Developmental regulation of glutamine synthetase and carbonic anhydrase II in neural retina. *Proc Natl Acad Sci U S A,* 83**,** 9060-4.
VARFOLOMEEV, E., GONCHAROV, T., FEDOROVA, A. V., DYNEK, J. N., ZOBEL, K., DESHAYES, K., FAIRBROTHER, W. J. & VUCIC, D. 2008. c-IAP1 and c-IAP2 are critical mediators of tumor necrosis factor alpha (TNFalpha)-induced NF-kappaB activation. *J Biol Chem,* 283**,** 24295-9.
VERARDO, M. R., LEWIS, G. P., TAKEDA, M., LINBERG, K. A., BYUN, J., LUNA, G., WILHELMSSON, U., PEKNY, M., CHEN, D.-F. & FISHER, S. K. 2008. Abnormal Reactivity of Müller Cells after Retinal Detachment in Mice Deficient in GFAP and Vimentin. *Investigative Ophthalmology & Visual Science,* 49**,** 3659-3665.
VEREECKE, L., BEYAERT, R. & VAN LOO, G. 2009. The ubiquitin-editing enzyme A20 (TNFAIP3) is a central regulator of immunopathology. *Trends Immunol,* 30**,** 383-91.
VERKMAN, A. S., SMITH, A. J., PHUAN, P. W., TRADTRANTIP, L. & ANDERSON, M. O. 2017. The aquaporin-4 water channel as a potential drug target in neurological disorders. *Expert Opin Ther Targets,* 21**,** 1161-1170.
VERONESI, F., BORSARI, V., SARTORI, M., ORCIANI, M., MATTIOLI-BELMONTE, M. & FINI, M. 2018. The use of cell conditioned medium for musculoskeletal tissue regeneration. *J Cell Physiol,* 233**,** 4423-4442.
VERONI, C., GABRIELE, L., CANINI, I., CASTIELLO, L., COCCIA, E., REMOLI, M. E., COLUMBA-CABEZAS, S., ARICO, E., ALOISI, F. & AGRESTI, C. 2010. Activation of TNF receptor 2 in microglia promotes induction of anti-inflammatory pathways. *Mol Cell Neurosci,* 45**,** 234-44.
VERSLEGERS, M., LEMMENS, K., VAN HOVE, I. & MOONS, L. 2013. Matrix metalloproteinase-2 and -9 as promising benefactors in development, plasticity and repair of the nervous system. *Prog Neurobiol,* 105**,** 60-78.
VITTAL, V., ROSE, A., GREGORY, K. E., KELLEY, M. J. & ACOTT, T. S. 2005. Changes in gene expression by trabecular meshwork cells in response to mechanical stretching. *Invest Ophthalmol Vis Sci,* 46**,** 2857-68.
VOGEL, C. & MARCOTTE, E. M. 2012. Insights into the regulation of protein abundance from proteomic and transcriptomic analyses. *Nat Rev Genet,* 13**,** 227-32.
WAHLIG, S., LOVATT, M. & MEHTA, J. S. 2018. Functional role of peroxiredoxin 6 in the eye. *Free Radic Biol Med,* 126**,** 210-220.
WALDRON, P. V., DI MARCO, F., KRUCZEK, K., RIBEIRO, J., GRACA, A. B., HIPPERT, C., AGHAIZU, N. D., KALARGYROU, A. A., BARBER, A. C., GRIMALDI, G., DURAN, Y., BLACKFORD, S. J. I., KLOC, M., GOH, D., ZABALA ALDUNATE, E., SAMPSON, R. D., BAINBRIDGE, J. W. B., SMITH, A. J., GONZALEZ-CORDERO, A., SOWDEN, J. C., ALI, R. R. & PEARSON, R. A. 2018. Transplanted Donor- or Stem Cell-Derived Cone Photoreceptors Can Both Integrate and Undergo Material Transfer in an Environment-Dependent Manner. *Stem Cell Reports,* 10**,** 406-421.
WALKER, A., KIM, J., WYATT, J., TERLOUW, A., BALACHANDRAN, K. & WOLCHOK, J. 2019. Repeated In Vitro Impact Conditioning of Astrocytes Decreases the Expression and Accumulation of Extracellular Matrix. *Ann Biomed Eng,* 47**,** 967-979.

WALLACE, D. M., MURPHY-ULLRICH, J. E., DOWNS, J. C. & O'BRIEN, C. J. 2014. The role of matricellular proteins in glaucoma. *Matrix Biol,* 37**,** 174-82.
WALSH, N., VALTER, K. & STONE, J. 2001. Cellular and subcellular patterns of expression of bFGF and CNTF in the normal and light stressed adult rat retina. *Exp Eye Res,* 72**,** 495-501.
WAN, J., RAMACHANDRAN, R. & GOLDMAN, D. 2012. HB-EGF Is Necessary and Sufficient for Müller Glia Dedifferentiation and Retina Regeneration. *Developmental Cell,* 22**,** 334-347.
WANG, J. S., ESTEVEZ, M. E., CORNWALL, M. C. & KEFALOV, V. J. 2009a. Intra-retinal visual cycle required for rapid and complete cone dark adaptation. *Nat Neurosci,* 12**,** 295-302.
WANG, K. C. & CHANG, H. Y. 2011. Molecular mechanisms of long noncoding RNAs. *Mol Cell,* 43**,** 904-14.
WANG, M., MA, W., ZHAO, L., FARISS, R. N. & WONG, W. T. 2011. Adaptive Muller cell responses to microglial activation mediate neuroprotection and coordinate inflammation in the retina. *J Neuroinflammation,* 8**,** 173.
WANG, Y., TANG, X., YU, B., GU, Y., YUAN, Y., YAO, D., DING, F. & GU, X. 2012. Gene network revealed involvements of Birc2, Birc3 and Tnfrsf1a in anti-apoptosis of injured peripheral nerves. *PLoS One,* 7**,** e43436.
WANG, Y., WU, T. R., CAI, S., WELTE, T. & CHIN, Y. E. 2000. Stat1 as a component of tumor necrosis factor alpha receptor 1-TRADD signaling complex to inhibit NF-kappaB activation. *Mol Cell Biol,* 20**,** 4505-12.
WANG, Z., GERSTEIN, M. & SNYDER, M. 2009b. RNA-Seq: a revolutionary tool for transcriptomics. *Nat Rev Genet,* 10**,** 57-63.
WARDYN, J. D., PONSFORD, A. H. & SANDERSON, C. M. 2015. Dissecting molecular cross-talk between Nrf2 and NF-kappaB response pathways. *Biochem Soc Trans,* 43**,** 621-6.
WASSLE, H. 2004. Parallel processing in the mammalian retina. *Nat Rev Neurosci,* 5**,** 747-757.
WASSLE, H., PEICHL, L., AIRAKSINEN, M. S. & MEYER, M. 1998. Calcium-binding proteins in the retina of a calbindin-null mutant mouse. *Cell Tissue Res,* 292**,** 211-8.
WATANABE, K., KAMIYA, D., NISHIYAMA, A., KATAYAMA, T., NOZAKI, S., KAWASAKI, H., WATANABE, Y., MIZUSEKI, K. & SASAI, Y. 2005. Directed differentiation of telencephalic precursors from embryonic stem cells. *Nat Neurosci,* 8**,** 288-96.
WATANABE, T., TOTOKI, Y., TOYODA, A., KANEDA, M., KURAMOCHI-MIYAGAWA, S., OBATA, Y., CHIBA, H., KOHARA, Y., KONO, T., NAKANO, T., SURANI, M. A., SAKAKI, Y. & SASAKI, H. 2008. Endogenous siRNAs from naturally formed dsRNAs regulate transcripts in mouse oocytes. *Nature,* 453**,** 539-43.
WEBER, A. J., KAUFMAN, P. L. & HUBBARD, W. C. 1998. Morphology of single ganglion cells in the glaucomatous primate retina. *Invest Ophthalmol Vis Sci,* 39**,** 2304-20.
WEI, N., QUAN, Z., TANG, H. & ZHU, J. 2017. Three-Dimensional Organoid System Transplantation Technologies in Future Treatment of Central Nervous System Diseases. *Stem Cells Int,* 2017**,** 5682354.
WEI, W., NORTON, D. D., WANG, X. & KUSIAK, J. W. 2002. Abeta 17-42 in Alzheimer's disease activates JNK and caspase-8 leading to neuronal apoptosis. *Brain,* 125**,** 2036-43.
WELBY, E., LAKOWSKI, J., DI FOGGIA, V., BUDINGER, D., GONZALEZ-CORDERO, A., LUN, A. T. L., EPSTEIN, M., PATEL, A., CUEVAS, E., KRUCZEK, K., NAEEM, A., MINNECI, F., HUBANK, M., JONES, D. T., MARIONI, J. C., ALI, R. R. & SOWDEN, J. C. 2017. Isolation and Comparative Transcriptome Analysis of Human Fetal and iPSC-Derived Cone Photoreceptor Cells. *Stem Cell Reports,* 9**,** 1898-1915.
WERNIG, M., MEISSNER, A., FOREMAN, R., BRAMBRINK, T., KU, M., HOCHEDLINGER, K., BERNSTEIN, B. E. & JAENISCH, R. 2007. In vitro reprogramming of fibroblasts into a pluripotent ES-cell-like state. *Nature,* 448**,** 318-24.
WEST, E. L., PEARSON, R. A., BARKER, S. E., LUHMANN, U. F., MACLAREN, R. E., BARBER, A. C., DURAN, Y., SMITH, A. J., SOWDEN, J. C. & ALI, R. R. 2010. Long-term survival of photoreceptors transplanted into the adult murine neural retina requires immune modulation. *Stem Cells,* 28**,** 1997-2007.
WHITMORE, S. S., BRAUN, T. A., SKEIE, J. M., HAAS, C. M., SOHN, E. H., STONE, E. M., SCHEETZ, T. E. & MULLINS, R. F. 2013. Altered gene expression in dry age-related macular degeneration suggests early loss of choroidal endothelial cells. *Mol Vis,* 19**,** 2274-97.
WHITMORE, S. S., WAGNER, A. H., DELUCA, A. P., DRACK, A. V., STONE, E. M., TUCKER, B. A., ZENG, S., BRAUN, T. A., MULLINS, R. F. & SCHEETZ, T. E. 2014. Transcriptomic analysis across nasal, temporal, and macular regions of human neural retina and RPE/choroid by RNA-Seq. *Exp Eye Res,* 129**,** 93-106.

WILHELMSSON, U., LI, L., PEKNA, M., BERTHOLD, C.-H., BLOM, S., ELIASSON, C., RENNER, O., BUSHONG, E., ELLISMAN, M., MORGAN, T. E. & PEKNY, M. 2004. Absence of Glial Fibrillary Acidic Protein and Vimentin Prevents Hypertrophy of Astrocytic Processes and Improves Post-Traumatic Regeneration. *The Journal of Neuroscience,* 24**,** 5016-5021.

WILLIAMS, P. A., MORGAN, J. E. & VOTRUBA, M. 2010. Opa1 deficiency in a mouse model of dominant optic atrophy leads to retinal ganglion cell dendropathy. *Brain,* 133**,** 2942-51.

WINZELER, A. & WANG, J. T. 2013a. Culturing hybridoma cell lines for monoclonal antibody production. *Cold Spring Harb Protoc,* 2013**,** 640-2.

WINZELER, A. & WANG, J. T. 2013b. Purification and culture of retinal ganglion cells from rodents. *Cold Spring Harb Protoc,* 2013**,** 643-52.

WISNIEWSKI, H. G., HUA, J. C., POPPERS, D. M., NAIME, D., VILCEK, J. & CRONSTEIN, B. N. 1996. TNF/IL-1-inducible protein TSG-6 potentiates plasmin inhibition by inter-alpha-inhibitor and exerts a strong anti-inflammatory effect in vivo. *J Immunol,* 156**,** 1609-15.

WOOD, Z. A., SCHRODER, E., ROBIN HARRIS, J. & POOLE, L. B. 2003. Structure, mechanism and regulation of peroxiredoxins. *Trends Biochem Sci,* 28**,** 32-40.

WOOTEN, M. W., GEETHA, T., SEIBENHENER, M. L., BABU, J. R., DIAZ-MECO, M. T. & MOSCAT, J. 2005. The p62 scaffold regulates nerve growth factor-induced NF-kappaB activation by influencing TRAF6 polyubiquitination. *J Biol Chem,* 280**,** 35625-9.

WU, D. C., BOYD, A. S. & WOOD, K. J. 2008. Embryonic stem cells and their differentiated derivatives have a fragile immune privilege but still represent novel targets of immune attack. *Stem Cells,* 26**,** 1939-50.

WURZELMANN, M., ROMEIKA, J. & SUN, D. 2017. Therapeutic potential of brain-derived neurotrophic factor (BDNF) and a small molecular mimics of BDNF for traumatic brain injury. *Neural Regen Res,* 12**,** 7-12.

XIA, Y., NIVET, E., SANCHO-MARTINEZ, I., GALLEGOS, T., SUZUKI, K., OKAMURA, D., WU, M. Z., DUBOVA, I., ESTEBAN, C. R., MONTSERRAT, N., CAMPISTOL, J. M. & IZPISUA BELMONTE, J. C. 2013. Directed differentiation of human pluripotent cells to ureteric bud kidney progenitor-like cells. *Nat Cell Biol,* 15**,** 1507-15.

XIANG, M. 2013. Intrinsic control of mammalian retinogenesis. *Cell Mol Life Sci,* 70**,** 2519-32.

XIAO, B. G., LU, C. Z. & LINK, H. 2007. Cell biology and clinical promise of G-CSF: immunomodulation and neuroprotection. *J Cell Mol Med,* 11**,** 1272-90.

XIAO, J., ZHONG, H., ZHOU, Y., YU, F., GAO, Y., LUO, Y., TANG, Z., GUO, Z., GUO, E., GAN, X., ZHANG, M. & ZHANG, Y. 2014. Identification and characterization of microRNAs in ovary and testis of Nile tilapia (Oreochromis niloticus) by using solexa sequencing technology. *PLoS One,* 9**,** e86821.

XIE, J., ZHU, R., PENG, Y., GAO, W., DU, J., ZHAO, L., CHI, Y. & YANG, L. 2017. Tumor necrosis factor-alpha regulates photoreceptor cell autophagy after retinal detachment. *Sci Rep,* 7**,** 17108.

XIONG, W., MACCOLL GARFINKEL, A. E., LI, Y., BENOWITZ, L. I. & CEPKO, C. L. 2015. NRF2 promotes neuronal survival in neurodegeneration and acute nerve damage. *J Clin Invest,* 125**,** 1433-45.

XU, W., WANG, X. T., XU, G. X., GUO, J. & HUANG, L. B. 2014. Stromal cell-derived factor 1alpha-stimulated mesenchymal stem cells confer enhanced protection against light-induced retinal degeneration in rats. *Curr Eye Res,* 39**,** 69-78.

YAFAI, Y., IANDIEV, I., LANGE, J., YANG, X. M., WIEDEMANN, P., BRINGMANN, A. & EICHLER, W. 2013. Basic Fibroblast Growth Factor Contributes to a Shift in the Angioregulatory Activity of Retinal Glial (Müller) Cells. *PLoS ONE,* 8**,** e68773.

YANG, X., LUO, C., CAI, J., POWELL, D. W., YU, D., KUEHN, M. H. & TEZEL, G. 2011. Neurodegenerative and inflammatory pathway components linked to TNF-alpha/TNFR1 signaling in the glaucomatous human retina. *Invest Ophthalmol Vis Sci,* 52**,** 8442-54.

YAO, K. S., HAGEBOUTROS, A., FORD, P. & O'DWYER, P. J. 1997. Involvement of activator protein-1 and nuclear factor-kappaB transcription factors in the control of the DT-diaphorase expression induced by mitomycin C treatment. *Mol Pharmacol,* 51**,** 422-30.

YASUDA, M., TANAKA, Y., RYU, M., TSUDA, S. & NAKAZAWA, T. 2014. RNA sequence reveals mouse retinal transcriptome changes early after axonal injury. *PLoS One,* 9**,** e93258.

YEH, W. C., HAKEM, R., WOO, M. & MAK, T. W. 1999. Gene targeting in the analysis of mammalian apoptosis and TNF receptor superfamily signaling. *Immunol Rev,* 169**,** 283-302.

YONG, P. H., ZONG, H., MEDINA, R. J., LIMB, G. A., UCHIDA, K., STITT, A. W. & CURTIS, T. M. 2010. Evidence supporting a role for N-(3-formyl-3,4-dehydropiperidino)lysine accumulation in Muller glia dysfunction and death in diabetic retinopathy. *Mol Vis,* 16**,** 2524-38.

YOSHIDA, S., SOTOZONO, C., IKEDA, T. & KINOSHITA, S. 2001. Interleukin-6 (IL-6) production by cytokine-stimulated human Müller cells. *Current Eye Research,* 22**,** 341-347.
YOSHIDA, S., YOSHIDA, A. & ISHIBASHI, T. 2004. Induction of IL-8, MCP-1, and bFGF by TNF-alpha in retinal glial cells: implications for retinal neovascularization during post-ischemic inflammation. *Graefes Arch Clin Exp Ophthalmol,* 242**,** 409-13.
YOU, Z., OUYANG, H., LOPATIN, D., POLVER, P. J. & WANG, C. Y. 2001. Nuclear factor-kappa B-inducible death effector domain-containing protein suppresses tumor necrosis factor-mediated apoptosis by inhibiting caspase-8 activity. *J Biol Chem,* 276**,** 26398-404.
YOUNG, R. W. 1984. Cell death during differentiation of the retina in the mouse. *J Comp Neurol,* 229**,** 362-73.
YU, A. L. & WELGE-LUSSEN, U. 2013. Antioxidants reduce TGF-beta2-induced gene expressions in human optic nerve head astrocytes. *Acta Ophthalmol,* 91**,** e92-8.
YU, D. Y. & CRINGLE, S. J. 2005. Retinal degeneration and local oxygen metabolism. *Exp Eye Res,* 80**,** 745-51.
YUAN, J. & YANKNER, B. A. 2000. Apoptosis in the nervous system. *Nature,* 407**,** 802-9.
YUE, F., JOHKURA, K., SHIRASAWA, S., YOKOYAMA, T., INOUE, Y., TOMOTSUNE, D. & SASAKI, K. 2010. Differentiation of primate ES cells into retinal cells induced by ES cell-derived pigmented cells. *Biochem Biophys Res Commun,* 394**,** 877-83.
YURCO, P. & CAMERON, D. A. 2005. Responses of Muller glia to retinal injury in adult zebrafish. *Vision Res,* 45**,** 991-1002.
ZAGOZEWSKI, J. L., ZHANG, Q. & EISENSTAT, D. D. 2014. Genetic regulation of vertebrate eye development. *Clin Genet,* 86**,** 453-60.
ZHA, X., WU, G., ZHAO, X., ZHOU, L., ZHANG, H., LI, J., MA, L. & ZHANG, Y. 2015. PRDX6 Protects ARPE-19 Cells from Oxidative Damage via PI3K/AKT Signaling. *Cell Physiol Biochem,* 36**,** 2217-28.
ZHANG, J., ALCAIDE, P., LIU, L., SUN, J., HE, A., LUSCINSKAS, F. W. & SHI, G. P. 2011. Regulation of endothelial cell adhesion molecule expression by mast cells, macrophages, and neutrophils. *PLoS One,* 6**,** e14525.
ZHANG, L., ZHAO, W., LI, B., ALKON, D. L., BARKER, J. L., CHANG, Y. H., WU, M. & RUBINOW, D. R. 2000. TNF-alpha induced over-expression of GFAP is associated with MAPKs. *Neuroreport,* 11**,** 409-12.
ZHANG, Y., KONG, Z., ZHANG, Y., HUANG, W., WU, H., WAN, X. & LI, Y. 2017. Increased expression of long non-coding RNA GLIDR in prostate cancer. *Cancer Biomark,* 19**,** 145-150.
ZHANG, Z., HARRISON, P. & GERSTEIN, M. 2002. Identification and analysis of over 2000 ribosomal protein pseudogenes in the human genome. *Genome Res,* 12**,** 1466-82.
ZHANG, Z. D., FRANKISH, A., HUNT, T., HARROW, J. & GERSTEIN, M. 2010. Identification and analysis of unitary pseudogenes: historic and contemporary gene losses in humans and other primates. *Genome Biol,* 11**,** R26.
ZHAO, X.-F., WAN, J., POWELL, C., RAMACHANDRAN, R., MYERS, M. G. & GOLDMAN, D. 2014. Leptin and IL-6 Family Cytokines Synergize to Stimulate Müller Glia Reprogramming and Retina Regeneration. *Cell reports,* 9**,** 272-284.
ZHAO, X., LIU, J. & AHMAD, I. 2002. Differentiation of embryonic stem cells into retinal neurons. *Biochem Biophys Res Commun,* 297**,** 177-84.
ZHONG, X., GUTIERREZ, C., XUE, T., HAMPTON, C., VERGARA, M. N., CAO, L. H., PETERS, A., PARK, T. S., ZAMBIDIS, E. T., MEYER, J. S., GAMM, D. M., YAU, K. W. & CANTO-SOLER, M. V. 2014. Generation of three-dimensional retinal tissue with functional photoreceptors from human iPSCs. *Nat Commun,* 5**,** 4047.
ZHOU, Y. & DANBOLT, N. C. 2014. Glutamate as a neurotransmitter in the healthy brain. *J Neural Transm (Vienna),* 121**,** 799-817.
ZUBER, M. E., GESTRI, G., VICZIAN, A. S., BARSACCHI, G. & HARRIS, W. A. 2003. Specification of the vertebrate eye by a network of eye field transcription factors. *Development,* 130**,** 5155-67.
ZUCCHELLI, S., FEDELE, S., VATTA, P., CALLIGARIS, R., HEUTINK, P., RIZZU, P., ITOH, M., PERSICHETTI, F., SANTORO, C., KAWAJI, H., LASSMANN, T., HAYASHIZAKI, Y., CARNINCI, P., FORREST, A. R. R. & GUSTINCICH, S. 2019. Antisense Transcription in Loci Associated to Hereditary Neurodegenerative Diseases. *Mol Neurobiol,* 56**,** 5392-5415.

Appendix

Appendix 1 Antibodies

Protein of interest	Host	Dilution	Source	Catalogue No.
CD29/Integrin B1	Mouse	1:300	Santa Cruz Biotechnology	SC-59829
CD44	Rabbit	1:100	Abcam	Ab157107
Glutamine Synthetase	Rabbit	1:500	Novus Biologicals	NB-110-41404
Vimentin	Rabbit	1:1000	Abcam	Ab92547
CRALBP	Rabbit Mouse	1:100 1:100	Santa Cruz Biotechnology	SC-28193 SC-59487
GFAP	Rabbit	1:100	Dako	Z0334
Sox2	Rabbit	1:200	Abcam	Ab97959
Sox9	Rabbit	1:200	Santa Cruz Biotechnology	SC-20095
Nestin	Mouse	1:750	Millipore	MAB5326
Chx10	Goat	1:250	Santa Cruz Biotechnology	SC-21692
Pax6	Mouse	1:500	Abcam	Ab5790
WNT2B	Mouse	1:750	Santa Cruz Biotechnology	SC-166502
Cleaved Notch1	Goat	1:200	Santa Cruz Biotechnology	SC-6014
PRDX6	Mouse	1:1000	Abcam	Ab16947
HO1	Mouse	1:250	Santa Cruz Biotechnology	SC-136960
NQO1	Mouse	1:750	Santa Cruz Biotechnology	SC-32793
FOLH1	Mouse	1:500	Santa Cruz Biotechnology	SC-514809
SOD2	Mouse	1:500	Santa Cruz Biotechnology	SC-133134
GSR	Mouse	1:500	Santa Cruz Biotechnology	SC-133245
GSS	Mouse	1:500	Santa Cruz Biotechnology	SC-166882
PON2	Mouse	1:500	Santa Cruz Biotechnology	SC-374158
Thy1.1/CD90, clone OX-7	Mouse	1:25	Merck	MAB1406
Beta III tubulin (TUJ)	Rabbit	1:1000	Abcam	Ab18207
BRN3A	Mouse	1:100	Santa Cruz Biotechnology	SC-8429
Alexa Flour 488	Donkey anti-mouse IgG	1:500	ThermoFisher Scientific	A-21202
Alexa Flour 555	Donkey anti-goat IgG	1:500	ThermoFisher Scientific	A-21432
Alexa Flour 555	Donkey anti-rabbit IgG	1:500	ThermoFisher Scientific	A-31572

CD29-VioBright 515, Clone: REA1060	Recombinant human IgG1	1:5	Miltenyi Biotec	130-118-199
CD44-APC, Clone: REA690	Recombinant human IgG1	1:5	Miltenyi Biotec	130-113-900
SSEA-4-VioGreen, Clone: REA101	Recombinant human IgG1	1:2	Miltenyi Biotec	130-098-341
Anti-Cytokeratin 18 antibody [C-04]	Mouse monoclonal IgG1	1:20	Abcam	Ab668
REA Control (S)-VioBright 515	Recombinant human IgG1	1:5	Miltenyi Biotec	130-113-445
REA Control (S)-APC	Recombinant human IgG1	1:5	Miltenyi Biotec	130-113-434
REA Control (S)-VioGreen	Recombinant human IgG1	1:2	Miltenyi Biotec	130-113-444
Brilliant Violet 421™ Donkey anti-rabbit IgG Antibody	Donkey anti-rabbit polyclonal IgG	neat	Biolegend	406410
Alexa Fluor® 647 anti-rat CD45 Antibody	Mouse IgG1, κ	1:100	Biolegend	202212
PE anti-rat CD90/mouse CD90.1 (Thy-1.1) Antibody	Mouse IgG1, κ	1:100	Biolegend	202524

Appendix 2 RT-PCR Primers

Gene of interest	Primer Sequence	Product Size (bp)	Annealing temperature (°C)	Number of cycles
β-actin	**F-**CATGTACGTTGCTATCCAGGC **R-**CTCCTTAATGTCACGCACGAT	250	54	26
Glutamine Synthetase	**F-** TGGGAGCAGACAGAGCCTAT **R-** CAGGAATGGGCTTAGGATCA	240	60	28
CRALBP	**F-** AGGCTGGGAGTTTTCCACAC **R-** TCTCCCAGACAGATGGAGGG	170	60	38
Vimentin	**F-** GAGAACTTTGCCGTTGAAGC **R-** TCCAGCAGCTTCCTGTAGGT	170	58	28
GFAP	**F-** CTGGGCTCAAGCAGTCTACC **R-**GAGTCATCGCTCAGGAGGTC	187	58	36
Notch 1	**F-** GGAGGCATCCTACCCTTTTC **R-** TGTGTTGCTGGAGCATCTTC	118	60	28
Sox2	**F-** GGCAGCTACAGCATGATGC **R-** TCGGACTTGACCACCGAAC	236	60	30
Sox9	**F-**ACGACTACACCGACCACCA **R-**TAGGATCATCTCGGCCATC	256	60	26
Pax6	**F-** AGATGAGGCTCAAATGCGAC **R-** GTTGGTAGACACTGGTGCTG	300	60	30
WNT2B	**F-** GTGTCCTGGCTGGTTCCTTA **R-** GAAGCTGGTGCAAAGGAAAG	188	58	32
Nestin	**F-** CTGCTACCCTTAAGACACTG **R-**GGGTCTGATCTCTGCATCTAC	237	60	30
WNT5B	**F-**TTCTGACAGACGCCAACTC **R-**TGACTCTCCCAAAGACAGATG	188	58	34
Chx10	**F-** AGCAGAGGAGCTGGAGAAG **R-** CATGATGCCATCCTTGGCTG	258	60	36
NR2E3	**F-** CTGGATGGAACCCAGTGTCT **R-** AGACAGGGGTGCCTGTTATG	203	60	36
Recoverin	**F-** AGCTCCTTCCAGACGATGAA **R-** CAAACTGGATCAGTCGCAGA	150	60	30
BRN3B	**F-** CAAGCAGCGACGCATCAAG **R-**GGGTTTGAGCGCGATCATATT	195	58	34
NRF2	**F-**TTCCCGGTCACATCGAGAG **R-**TCCTGTTGCATACCGTCTAAATC	109	58	30
CQ10A	**F-** CCAACGTCCAGGAGTATCGT **R-** TGTGAGGTTTGACCATGGAA	153	64	35
SOD2	**F-**CTTCAGGGTGGTAGGCTGT **R-**TGGCCAGACCTTAATGTTCC	209	64	25
LIAS	**F-** CAGCACTTTAGGAGGCCAAG **R-** CCCGAGTAGCTGGGATTACA	147	64	25
GSS	**F-** GCCTCCTACATCCTCATGGA **R-** ACGGCTTGTTCATCACGAG	158	64	30
GSR	**F-** AGTGGGACTCACGGAAGATG **R-** GTAGGGTGAATGGCGACTGT	270	64	30
PRDX6	**F-** CCAACCATCCCTGAAGAAGA **R-** CTGACATCTCTGGGCTCACA	146	60	30
HO1	**F-** TCTCCGATGGGTCCTTACAC **R-** ATTGCCTGGATGTGCTTTTC	169	64	30
NQO1	**F-** GCCCAGATATTGTGGCTGA **R-** ACCACTGCAGGGGGAACT	187	64	30

PON2	**F-** AATCCTCCCTCGTCAGAGGT **R-** TGGGTCAATGTTGCGGTTA	269	64	30
FOLH1	**F-** CAGGTCTGGAGCGAATTCCA **R-** CGAGTCGGTTTCGTGAAGGA	181	60	35
BDNF	**F-**CTACGAGACCAAGTGCAATCC **R-** AATCGCCAGCCAATTCTCTTT	147	60	27
NGF	**F-**TGTGGGTTGGGGATAAGACCA **R-** GCTGTCAACGGGATTTGGGT	140	60	36
NT3	**F-** CGTGGTGGCGAACAGAACAT **R-** GGCCGATGACTTGTCGGTC	115	60	37
NT4	**F-** CTGTGTGCGATGCAGTCAGT **R-**TGACAGCGGGTTTCAAAGAAGT	142	60	37
PEDF	**F-**TGCAGGAGATGAAGCTGCAA **R-**TCCTCGTTCCACTCAAAGCC	115	62	35

Appendix 3 Taqman qRT-PCR Probes

Gene of interest	Assay ID	Dye	Catalogue no.
18S	Hs99999901_s1	FAM-MGB	4453320
BDNF	Hs02718934_s1	FAM-MGB	4448892
CD29/ITGB1	Hs01127536_m1	FAM-MGB	4331182
CRABP1	Hs01011034_m1	FAM-MGB	4331182
CRABP2	Hs00275636_m1	FAM-MGB	4331182
GLUL	Hs00365928_g1	FAM-MGB	4448892
RLBP1	Hs00165632_m1	FAM-MGB	4331182
GFAP	Hs00909233_m1	FAM-MGB	4453320
SLC1A3	Hs00904823_g1	FAM-MGB	4448892
SOD2	Hs00167309_m1	FAM-MGB	4453320
SOX2	Hs01053049_s1	FAM-MGB	4448892
SOX9	Hs00165814_m1	FAM-MGB	4331182
NES	Hs00707120_s1	FAM-MGB	4453320
PRDX6	Hs00705355_s1	FAM-MGB	4453320
VIM	Hs00958111_m1	FAM-MGB	4448892

Appendix 4 Preparation of stock reagents for isolation of primary RGCs

Appendix 4.1 Basic reagents preparation

1) 10 *N* NaOH
   4 g of NaOH pellet was gradually dissolved into 7 mL of water in a glass beaker. The solution was stirred constantly, and the process was involved in exothermic reaction. The final volume was topped up with water to 3 mL. Sterile filtration is not necessary.
2) 1 *N* NaOH
   1 mL of 10 *N* NaOH was diluted with 9 mL of water.
3) 0.1 *N* NaOH
   1 mL of 1 *N* NaOH was diluted with 9 mL of water.
4) 1 *N* HCl
   8.3 mL of 37% HCL was diluted with 100 mL of water.

5) Tris-HCl (50mM, pH 9.5) (Catalogue no. T2819; Sigma-Aldrich)
   25 mL of Trizma® hydrochloride solution (BioPerformance Certified, pH 9.0, 1 M, suitable for cell culture) was diluted to 475 mL of sterile tissue culture grade water to make a final working concentration of 50mM. pH was adjusted with NaOH to 9.5.
6) 4% BSA stock solution (Catalogue no. A4161; Sigma-Aldrich)
   0.2 g of BSA was dissolved in 3 mL of Dulbecco's phosphate buffered saline (DPBS) (Catalogue no. SH30264.01; HyClone) prewarmed at 37°C. The pH was adjusted to 7.4 with 1 *N* NaOH. The final volume was brought to 5 mL with DPBS. The solution was sterile filtered through a 0.22-µm filter.
7) 0.2 % BSA working solution
   Upon usage, an aliquot of 250 µL of 4% BSA stock solution was defrosted and diluted with 4.75 mL of DPBS to a final concentration of 0.2%.

Appendix 4.2 Reagents used for immunopanning

1) Poly-D-lysine stock (PDL) (1 mg/mL; 100x) (Catalogue no. P6407; Sigma-Aldrich)
   2 mg of PDL powder was dissolved in 2 mL of tissue culture grade sterile water and sterile filtered through a 2-µm filter.
2) Mouse laminin (1 mg/mL) (Catalogue no. 3400-010-02; R&D systems)
   The mouse laminin vial was thawed at 4°C, aliquoted at 10 µL per vial and stored at -80°C.
3) Ovomucoid stock
   Respective amount of BSA and trypsin inhibitor from chick egg white (Catalogue no. T9253; Sigma-Aldrich) were dissolved in the right volume of DPBS to prepare high and low ovomucoid stocks:

Stock	DPBS volume	Reagent	Weight	Final concentration
High-ovomucoid stock (6x)	8 mL	BSA	300 mg	30 mg/mL
		Trypsin inhibitor from chick egg white	300 mg	30 mg/mL
Low-ovomucoid stock (10x)	7.5 mL	BSA	150 mg	15 mg/mL
		Trypsin inhibitor from chick egg white	150 mg	15 mg/mL

   The pH was adjusted to 7.4 with 10 *N* NaOH for high ovomucoid stock and with 1 *N* NaOH for low ovomucoid stock. The final volume was brought to 10 mL with D-PBS. The solution was sterile filtered through a 0.22-µm filter. 1 mL aliquots were stored at -20°C.
4) DNase stock (0.4%) (Catalogue no. LS002007; Worthington biochemicals)
   The Kunitz (U) of DNase per 1 mg of dry weight is 5220 U. To make a final concentration of 125,00 U/1 mL EBSS (Catalogue no. E6267; Sigma-Aldrich), 4.176 mL of EBSS was added to 100 mg of DNase. The solution was mixed well by gentle pipetting and sterile filtered through a 0.22-µm filter. 20 vials of 200 µL aliquots were stored at -20°C.
5) Ovomucoid working solutions

Components	Low ovomucoid	High ovomucoid
DPBS	9 mL	5 mL
1 *N* NaOH	2 µL	2 µL
High Ovomucoid stock (6x)		1 mL
Low Ovomucoid stock (10x)	1 mL	
DNase (0.4%)	100 µL	

6) Trypsin (30,000 U/mL) (Catalogue no. T9935; Sigma-Aldrich)
   The BAEE unit per 1 mg of trypsin is 10316 U/mg. To prepare a final concentration of 30,000 U/mL of trypsin, 11.6 mg of trypsin was dissolved in 4 mL of EBSS. The solution was mixed well by gentle pipetting and sterile filtered through a 0.22-µm filter. 20 vials of 200 µL aliquots were stored at -80°C.
7) Rabbit anti-rat macrophage polyclonal antibody (Catalogue no. CLAD51240; Cedarlane)

2 mL of rabbit anti-rat macrophage polyclonal antibody was defrosted on ice. 25 vials of 80 µL working aliquot were stored at 4°C.

8) Goat anti-rabbit IgG (H + L) stock (2.4 mg/mL) (Catalogue no. 111-005-003; Jackson ImmunoResearch)
   1 mL of goat anti-rabbit IgG (H + L) was aliquoted to 120 µL working aliquot and stored at 4°C.
9) Goat anti-mouse IgM (µ-chain specific) (2.4 mg/mL) (Catalogue no. 115-005-020; Jackson ImmunoResearch)
   Goat anti-mouse IgM (µ-chain specific) was aliquoted to 30 µL working aliquot and stored at 4°C.
10) Panning solutions

Solution	Reagent	Volume
Negative panning solution	Goat anti-rabbit IgG (H + L)	120 µL
	50 mM Tris-HCl (pH 9.5)	40 mL
Positive panning solution	Goat anti-mouse IgM µ-chain specific	30 µL
	50 mM Tris-HCl (pH 9.5)	10 mL

11) Insulin stock (0.5 mg/mL) (Catalogue no. I6634; Sigma-Aldrich)
    1 mg of insulin and 10 µL of 1 *N* HCl was added to 2mL of tissue culture grade sterile water and mixed well. The stock solution was sterile filtered through a 0.22-µm filter and can be stored at 4°C up to 6 weeks.
12) Panning buffer was prepared:

Reagent	Volume
DPBS	18 mL
0.2% BSA	2 mL
Insulin (0.5 mg/mL)	**4**

Appendix 4.3 Supplement factors for RGC growth medium

1) Forskolin stock (4.2 mg/mL) (Catalogue no. F6886; Sigma-Aldrich)
   5 mg of Forskolin was reconstituted in 100 µL of sterile DMSO and the mixture was well mixed by pipetting down and up a few times. The whole mixture was later transferred to a bonjour and topped with another 1.1 mL of sterile DMSO to make a final concentration of 4.2 mg/mL. 12 vials of 80 µL and 24 vials of 20 µL aliquots were stored at -20°C.
2) Human brain derived neurotrophic factor (BDNF) stock (50 µg/mL) (Catalogue no. 450-02; Peprotech)
   10 µg of recombinant human BDNF lyophilised powder was reconstituted in 200 µL of cold 0.2% BSA in DPBS to make a stock of 50 µg/mL. 20 vials of 10 µL working stock were stored at -80°C.
3) Human ciliary neurotrophic factor (CNTF) stock (10 µg/mL) (Catalogue no. 450-13; Peprotech)
   20 µg of recombinant human CNTF lyophilised powder was reconstituted in 2 mL of cold 0.2% BSA in DPBS to make a stock of 10 µg/mL. 20 vials of 10 µL and 18 vials of 100 µL aliquots were stored at -80°C.
4) NS 21 supplement (50x) (Catalogue no. SCM081; Millipore)
   10 mL of NS 21 supplement (50x) were aliquoted to 25 vials of 400 µL working aliquot and stored at -20°C.
5) NAC stock (5 mg/mL) (Catalogue no. A8199; Sigma-Aldrich)
   5 mg of NAC powder was reconstituted in 1mL of Neurobasal medium (Catalogue no. 21103049; Thermo Fisher Scientific). The solution appeared as yellowish and was sterile filtered through a 0.22-µm filter. 10 vials of 20 µL and 10 vials of 80 µL aliquots were stored at -20°C.
6) Thyroxine (T3) stock (4 µg/mL) (Catalogue no. T6397; Sigma-Aldrich)
   0.8 mg of 3,3′,5-triiodo-L-thyronine sodium salt (T3) was reconstituted in 100 µL of 0.1 *N* NaOH. 5 µL of T3 solution was added to 10mL of DPBS and sterile filtered through a 0.22-µm filter. The first 5mL of filtrate was discarded and the rest of 5 mL was stored in 100 µL of aliquots at -20°C.

Appendix 4.4 SATO supplement (100x)

SATO supplement is a combination of hormones and proteins. To prepare SATO supplement 100x stock, the following reagents are made individually and freshly first as the stock solution and combined before sterile filtration. The protocol to prepare individual stock is more than enough to make up a final volume of 5 mL of SATO supplement (100x). The stock solution of 1) and 2) should always be prepared freshly and not reused afterwards.

1) Progesterone stock (Catalogue no. P8783; Sigma-Aldrich)
   1 mg of progesterone was reconstituted in 40 µL of ethanol and mixed well by pipetting.
2) Sodium selenite stock (Catalogue no. S5261; Sigma-Aldrich)
   1 mg of sodium selenite and 2.5 µL of 1 *N* NaOH were dissolved in 2.5 mL of DMEM.
3) Dissolve the following stock reagents in 5mL of DMEM:

Stock Reagent	**Amount**	**Final concentration in 100x**
BSA	50 mg	10 mg/mL
Apo-transferrin (Catalogue no. T1147; Sigma-Aldrich)	50 mg	10 mg/mL
Putrescine (Catalogue no. P5780; Sigma-Aldrich)	6.4 mg	1.6 mg/mL
Progesterone stock	1 µL	6 µg/mL
Sodium selenite stock	40 µL	4 µg/mL

4) 25 vials of 200 µL of SATO supplement (100x) working aliquot was stored at -20°C.

Appendix 4.5 RGC Basal Culture Medium

1) To prepare 10 mL of RGC Basal Culture Medium, the following reagents were mixed:

Reagent	**Volume**	**Final concentration**
Neurobasal medium	4.75 mL	
DMEM	4.75 mL	
Penicillin-streptomycin (100x)	100 µL	100 U/mL
Sodium pyruvate (100 mM)	100 µL	110 µg/mL
L-glutamine (200 mM)	100 µL	292 µg/mL
Insulin stock (0.5 mg/mL)	100 µL	5 µg/mL
SATO supplement (100x)	100 µL	1x
Thyroxine (T3) stock (4 µg/mL)	100 µL	40 ng/mL
NS21 supplement (50x)	200 µL	1x
NAC stock (5 mg/mL)	10 µL	5 µg/mL

2) A 0.22-µm filter was rinsed with PBS before the medium was sterile filtered through.

Appendix 4.6 RGC Complete Culture Medium

1) To prepare 10 mL of RGC Complete Culture Medium, the following reagents were mixed:

Reagent	**Volume**
RGC Basal Medium	10 mL
Forskolin stock (4.2 mg/mL)	10 µL
BDNF stock (50 µg/mL)	10 µL
CNTF stock (10 µg/mL)	10 µL

2) The medium was warmed at 37°C before use. The prepared medium can be stored at 4°C up to 3 days.

Appendix 5 Complete list of DEGs in the transcriptome of MIO-M1 cells treat with TNF-α for 24 hours

Gene	Biotype	Log2 Fold Change	Adjusted p-value
CXCL8	protein_coding	15.12665	6.2E-77
PCDH20	protein_coding	-7.82302	6.56E-67
SOD2	protein_coding	8.523675	4.89E-35
SLC39A14	protein_coding	5.826495	2.63E-31
TNFRSF9	protein_coding	15.02059	4.5E-28
VCAM1	protein_coding	8.511076	3.26E-27
CCL2	protein_coding	9.17267	8.2E-25
NFKBIA	protein_coding	6.095873	1.33E-24
PI15	protein_coding	-7.11302	2.43E-23
LAYN	protein_coding	6.373242	1.21E-22
NRP2	protein_coding	4.737122	1.51E-22
PLPP3	protein_coding	6.376226	2.47E-22
FP565260.3	protein_coding	8.918952	3.06E-21
SESN3	protein_coding	-6.22184	5.3E-20
TNFAIP3	protein_coding	6.497001	6.16E-20
FAM69A	protein_coding	-4.27186	8.22E-20
GBP1	protein_coding	5.902364	1.19E-19
CTSS	protein_coding	8.400115	1.71E-18
BIRC3	protein_coding	10.28948	3.98E-18
TNFAIP2	protein_coding	8.504922	8.68E-18
ICAM1	protein_coding	11.29465	4.79E-17
ZNF436	protein_coding	-4.03758	1.04E-16
ICOSLG	protein_coding	8.978411	1.05E-16
TNFAIP8	protein_coding	5.47726	2.25E-16
GFAP	protein_coding	-7.37623	2.3E-16
CNR1	protein_coding	-4.50917	1.96E-15
CXCL10	protein_coding	11.52222	2.67E-15
IL32	protein_coding	8.402055	4.49E-15
TNFAIP6	protein_coding	5.475082	7.53E-13
CD83	protein_coding	4.848851	2.55E-12
TRAF1	protein_coding	5.343347	2.97E-12
IRF1	protein_coding	5.473701	8.59E-12
SORT1	protein_coding	-4.42982	2.06E-11
MFSD2A	protein_coding	-6.9928	2.66E-11
ID2	protein_coding	-3.84283	3.43E-11
ID4	protein_coding	-4.11936	5.69E-11
GBP4	protein_coding	7.049644	5.72E-11
PTX3	protein_coding	5.70261	1.06E-10
IGFBP3	protein_coding	5.027508	1.25E-10
ALDH1A3	protein_coding	4.765658	2.4E-10
SLN	protein_coding	-5.25784	2.67E-10
C1orf198	protein_coding	-4.86809	4.2E-10
LMO4	protein_coding	4.084022	5.17E-10
H3F3AP4	processed_pseudogene	9.52655	5.51E-10
HIPK3	protein_coding	-4.73461	7.05E-10
SRGN	protein_coding	5.160195	8.12E-10
LGR4	protein_coding	-3.27724	1.67E-09
POU3F2	protein_coding	-4.52431	4.22E-09
FABP7	protein_coding	-5.35783	4.22E-09
CXCL11	protein_coding	9.315761	5.22E-09
THBS1	protein_coding	-3.78578	5.66E-09
RELB	protein_coding	4.476385	8.6E-09
EDNRB	protein_coding	-3.29355	9.29E-09
SCD	protein_coding	-4.36314	1.05E-08
LRRN1	protein_coding	-3.9467	1.09E-08
SCD5	protein_coding	-3.37651	1.3E-08
CCL5	protein_coding	9.479655	1.46E-08
CPNE4	protein_coding	-9.7097	1.59E-08
TNFRSF14	protein_coding	4.144367	1.69E-08
GLDN	protein_coding	-4.14964	2.02E-08
FAM198B	protein_coding	-4.18466	2.04E-08
LMCD1	protein_coding	-3.17045	2.53E-08
IL4I1	protein_coding	7.010217	2.88E-08
TNIP1	protein_coding	3.260926	4.85E-08
NFE2L3	protein_coding	5.863595	5.35E-08
WTAP	protein_coding	3.148432	7.22E-08
AK5	protein_coding	-4.74642	9.18E-08
AUNIP	protein_coding	5.975331	9.87E-08
GBP3	protein_coding	3.058072	1.02E-07
DCLK2	protein_coding	-4.95357	1.44E-07
FAM13C	protein_coding	-3.60421	2.01E-07
CLDN1	protein_coding	8.717916	2.01E-07
AKR1B1	protein_coding	3.469586	2.21E-07
LINC00294	lincRNA	-5.0283	2.71E-07
ARSF	protein_coding	-7.0889	3.4E-07
VCL	protein_coding	-3.3707	3.77E-07
LGALS1	protein_coding	2.78065	3.99E-07
IL7R	protein_coding	4.870776	4.18E-07
ACSL5	protein_coding	4.744826	6.43E-07
ST8SIA4	protein_coding	-5.60144	8.19E-07
BID	protein_coding	3.631264	8.34E-07
ILK	protein_coding	2.910558	1E-06
ATP1B1	protein_coding	-3.89433	1.28E-06
ADORA2A	protein_coding	8.573317	1.28E-06
TTC37	protein_coding	-4.58183	1.38E-06
IFI30	protein_coding	7.16739	1.41E-06
ZZZ3	protein_coding	-2.93486	1.49E-06
CSTF3	protein_coding	-3.71835	1.49E-06
VAMP7	protein_coding	-4.9293	1.52E-06
NUDT4	protein_coding	-4.19016	1.53E-06
PGAM1	protein_coding	2.704386	1.61E-06
TFPI2	protein_coding	7.792233	1.94E-06
SOX2-OT	sense_overlapping	-3.2009	2.07E-06
FAM3C	protein_coding	-3.03675	2.52E-06
DNPEP	protein_coding	2.774782	3.26E-06
VEGFC	protein_coding	5.578402	3.48E-06
BTF3L4P2	processed_pseudogene	8.154486	3.53E-06
POGLUT1	protein_coding	5.297377	3.53E-06
C5orf56	protein_coding	5.730743	3.54E-06
TLR1	protein_coding	4.520698	3.83E-06
CDC42SE1	protein_coding	2.424199	4.31E-06
TRAF2	protein_coding	5.007459	4.62E-06
SOX4	protein_coding	-3.55476	4.98E-06
POLA2	protein_coding	2.840396	5.41E-06
DRAM1	protein_coding	2.689663	5.61E-06
AL139393.2	antisense	-5.54913	6.13E-06
PLPP1	protein_coding	-2.58644	6.36E-06
SYNM	protein_coding	-3.24277	6.72E-06
TRDC	TR_C_gene	-7.80778	6.81E-06
GTF2IP1	transcribed_unprocessed_pseudogene	-3.46105	7.18E-06
TMOD2	protein_coding	-4.13022	8.4E-06
LRRN3	protein_coding	2.317326	9.53E-06
RRAD	protein_coding	7.570004	1.04E-05
CBR3	protein_coding	4.081402	1.08E-05
HLA-E	protein_coding	3.326096	1.22E-05
APLN	protein_coding	-6.09114	1.22E-05
SERPINE2	protein_coding	3.676815	1.24E-05
HMGA1	protein_coding	3.54446	1.36E-05
SLC41A2	protein_coding	3.8202	1.41E-05
TUBA1A	protein_coding	-2.12682	1.63E-05
SNURF	protein_coding	-5.12952	1.66E-05

MPZL1	protein_coding	2.231329	1.74E-05
OAS3	protein_coding	3.575723	2.27E-05
PFN2	protein_coding	-2.33729	2.3E-05
TNFSF10	protein_coding	3.066779	2.38E-05
SLC2A6	protein_coding	4.542932	2.38E-05
FLNB	protein_coding	3.804538	2.42E-05
CXADR	protein_coding	-2.96309	2.42E-05
PRRG4	protein_coding	2.934402	2.53E-05
SLC38A3	protein_coding	-4.64042	2.6E-05
C11orf57	protein_coding	-4.03976	2.92E-05
GPR158	protein_coding	-3.74815	3.29E-05
DTL	protein_coding	3.448792	3.53E-05
IFIT3	protein_coding	3.620545	3.57E-05
ADAMTS1	protein_coding	7.775244	3.76E-05
PML	protein_coding	3.289931	4.03E-05
NLGN4X	protein_coding	-6.12901	4.24E-05
TBC1D32	protein_coding	-4.68907	4.36E-05
OCRL	protein_coding	-3.57865	4.72E-05
H3F3A	protein_coding	-2.67232	4.87E-05
MMP1	protein_coding	8.489017	5.03E-05
ZNF248	protein_coding	-4.0489	5.33E-05
CTGF	protein_coding	-2.68648	5.37E-05
KIAA1549L	protein_coding	-7.2199	5.39E-05
NDRG4	protein_coding	-4.53263	5.4E-05
TLR3	protein_coding	4.310931	5.4E-05
MMAA	protein_coding	4.682168	5.86E-05
TMTC4	protein_coding	-3.56406	5.88E-05
CMC2	protein_coding	2.888689	6.76E-05
SRSF8	protein_coding	-3.70038	6.98E-05
FAM200B	protein_coding	-2.90818	7.13E-05
CRYAB	protein_coding	-2.72203	7.44E-05
RBBP7	protein_coding	2.900821	7.91E-05
TNFRSF10B	protein_coding	3.104475	7.91E-05
C7orf25	protein_coding	4.65335	7.91E-05
BTN3A3	protein_coding	2.734576	7.96E-05
ROBO2	protein_coding	-6.36749	8.21E-05
TRIP6	protein_coding	-2.13662	8.21E-05
RNF152	protein_coding	3.529096	8.52E-05
NOD2	protein_coding	7.181738	9.17E-05
WARS	protein_coding	2.727913	0.000107
RRAGC	protein_coding	-2.8036	0.00011
SOWAHC	protein_coding	-4.30655	0.00011
CKAP4	protein_coding	1.766493	0.000113
SCP2	protein_coding	-2.14195	0.000116
ICA1L	protein_coding	-3.71861	0.000125
PMP2	protein_coding	-5.50429	0.000127
KHDRBS3	protein_coding	-2.98327	0.000134
ST6GAL1	protein_coding	3.600015	0.000135
FAM171B	protein_coding	-2.76616	0.00015
ARNTL2	protein_coding	2.408424	0.000159
SLC2A12	protein_coding	-3.91532	0.000159
GTF2IP4	transcribed_processed_pseudogene	-3.03387	0.000159
NINJ1	protein_coding	3.365814	0.000168
NDUFA4	protein_coding	-2.82484	0.000168
EPHB3	protein_coding	-4.81891	0.000172
STX11	protein_coding	7.848367	0.000172
KDM7A	protein_coding	-3.34304	0.000184
CD70	protein_coding	2.695892	0.00019
FABP5	protein_coding	-4.8482	0.000192
IRAK2	protein_coding	3.539826	0.000192
CIDECP	transcribed_unprocessed_pseudogene	4.561547	0.000192
NFKB2	protein_coding	3.965894	0.000192
CHURC1-FNTB	protein_coding	7.478164	0.000197
ATF5	protein_coding	2.888163	0.000209
PSMB9	protein_coding	4.072074	0.000215
MIR155HG	lincRNA	6.945224	0.000223
GLUL	protein_coding	-1.89574	0.000233
SUSD6	protein_coding	2.629594	0.000239
GJA3	protein_coding	-6.42341	0.000239
ARHGAP12	protein_coding	-2.73233	0.000241
LAMA3	protein_coding	7.207947	0.000252
CSTF2	protein_coding	3.765405	0.000252
UBE2G2	protein_coding	2.916899	0.000254
KCNE4	protein_coding	-2.80426	0.000275
FAM20C	protein_coding	3.283731	0.000276
AKAP12	protein_coding	-5.0583	0.000281
CYP1B1	protein_coding	3.808191	0.000286
MASTL	protein_coding	3.870964	0.000289
SMYD2	protein_coding	2.253132	0.000289
PFN1	protein_coding	2.84138	0.000305
LINC00844	lincRNA	-7.59494	0.000311
KIAA1462	protein_coding	6.002154	0.000316
AC008622.2	antisense	7.426361	0.000319
TRIP10	protein_coding	3.385463	0.000347
FTL	protein_coding	-3.60277	0.00035
STOM	protein_coding	-2.22842	0.000365
TMEM39A	protein_coding	4.57924	0.000368
KAZALD1	protein_coding	-4.7189	0.000368
RIPK2	protein_coding	3.106607	0.000368
RAC1P2	processed_pseudogene	-8.31515	0.00037
EVA1A	protein_coding	2.446137	0.000374
KNTC1	protein_coding	3.26663	0.000374
EDIL3	protein_coding	-2.44537	0.000392
RASSF4	protein_coding	3.316303	0.000402
TIMP4	protein_coding	-3.46667	0.000403
ABHD4	protein_coding	-4.59179	0.000413
FLRT3	protein_coding	-3.81976	0.000417
COL6A1	protein_coding	2.956749	0.000441
ENAH	protein_coding	-2.53335	0.00046
SMARCC1	protein_coding	-2.49562	0.000471
GYPC	protein_coding	2.904402	0.000471
IDO1	protein_coding	6.514265	0.000471
LINC00461	lincRNA	-4.96118	0.000472
TXNIP	protein_coding	-2.8747	0.000477
UFD1	protein_coding	2.297449	0.000478
MIR99AHG	lincRNA	-2.14536	0.000479
ZNF577	protein_coding	-5.94875	0.000483
CD58	protein_coding	-2.51891	0.000497
PPP1CB	protein_coding	-2.66395	0.0005
CASK	protein_coding	3.180073	0.000526
XPNPEP1	protein_coding	2.343912	0.000544
SLC22A4	protein_coding	3.095358	0.000545
BCAT1	protein_coding	2.479555	0.000558
RNF19A	protein_coding	2.911417	0.000565
MMP14	protein_coding	-3.87233	0.000565
ZNF672	protein_coding	-3.15304	0.000567
FTH1P23	processed_pseudogene	3.845448	0.000574
AK4	protein_coding	3.290589	0.000578
CNOT1	protein_coding	1.892256	0.000585
IL15RA	protein_coding	7.319118	0.000585
GALNT5	protein_coding	-2.66073	0.00059
LPAR6	protein_coding	-7.6501	0.000599
OXA1L	protein_coding	-3.82199	0.000624

TLR2	protein_coding	6.650951	0.000642
GCH1	protein_coding	6.740114	0.000668
MRPS36	protein_coding	-2.71324	0.000696
LRP11	protein_coding	-3.6264	0.00073
CENPJ	protein_coding	7.921382	0.00073
PLXDC2	protein_coding	-4.71843	0.000742
SMIM3	protein_coding	2.522898	0.000744
PAMR1	protein_coding	-5.14937	0.000759
SIGMAR1	protein_coding	-2.61487	0.000785
CARD19	protein_coding	-4.51472	0.000785
BDKRB2	protein_coding	7.214646	0.000785
ZNF271P	transcribed_unitary_pseudogene	-2.52121	0.000788
NEMP1	protein_coding	2.298482	0.000803
GPR137	protein_coding	2.76521	0.000803
LONRF1	protein_coding	-3.24268	0.000818
SLC9A7	protein_coding	4.41385	0.000818
AC079465.1	antisense	-6.83164	0.000837
PIGCP1	processed_pseudogene	-4.24254	0.000845
CD82	protein_coding	3.230257	0.00085
PTPRZ1	protein_coding	-3.79518	0.000891
PLCXD3	protein_coding	-3.98145	0.000923
PRKACB	protein_coding	-2.81483	0.000951
SSFA2	protein_coding	-2.38609	0.000967
ZDHHC9	protein_coding	-3.6303	0.000967
EFNB2	protein_coding	2.051377	0.000983
GALNT1	protein_coding	-2.17678	0.001019
SNTB1	protein_coding	-4.94976	0.001019
FZD3	protein_coding	-4.4987	0.001053
APOL3	protein_coding	4.495633	0.001065
CDK2	protein_coding	2.665283	0.001071
PPP1R3C	protein_coding	-2.7868	0.001071
PSME2	protein_coding	2.180276	0.001076
TAP2	protein_coding	2.156816	0.001076
CKB	protein_coding	-2.44694	0.001076
TBX15	protein_coding	-3.2479	0.001076
MEGF6	protein_coding	8.031935	0.001076
MAN1C1	protein_coding	-3.56042	0.001095
PTPN13	protein_coding	-4.2491	0.001123
MAF	protein_coding	-4.69634	0.001143
HEY1	protein_coding	-3.13008	0.001191
MSC	protein_coding	3.113392	0.001191
MANBA	protein_coding	-2.33258	0.001227
LIFR	protein_coding	3.505694	0.001238
DDX60	protein_coding	3.080504	0.001253
GALNT11	protein_coding	-2.04045	0.001253
ZPLD1	protein_coding	-3.74074	0.001264
ASF1B	protein_coding	2.242791	0.001287
GZF1	protein_coding	-2.9496	0.001346
TGFB3	protein_coding	2.439937	0.001366
SLC25A33	protein_coding	-3.54195	0.001366
PRLR	protein_coding	5.244952	0.001412
CENPW	protein_coding	4.81904	0.001416
CXCL5	protein_coding	7.403444	0.001424
IVNS1ABP	protein_coding	-2.70095	0.001433
PLAUR	protein_coding	2.263147	0.001433
PURB	protein_coding	-2.10568	0.00154
CENPX	protein_coding	2.638068	0.001584
ZNF391	protein_coding	-4.0157	0.001751
IKBKAP	protein_coding	-2.99419	0.001764
ANTXR2	protein_coding	2.758136	0.00178
EPHA3	protein_coding	-2.30344	0.00178
UCHL3	protein_coding	2.619199	0.00184
ZW10	protein_coding	2.659025	0.001844
S1PR3	protein_coding	2.579843	0.001873
TMEM56	protein_coding	-3.89784	0.001884
SOCS2	protein_coding	-2.10451	0.001906
TPD52	protein_coding	-4.08022	0.00192
CD47	protein_coding	2.637132	0.001955
SLC16A4	protein_coding	-2.80667	0.001955
CMTM6	protein_coding	3.12056	0.002007
TMSB10	protein_coding	1.733865	0.002029
IGF2R	protein_coding	-3.36603	0.00204
SAP30	protein_coding	-2.80427	0.00204
ASAP3	protein_coding	-2.76473	0.002064
NUB1	protein_coding	1.857749	0.00212
PPP1R12A	protein_coding	-2.21951	0.00212
CXCL2	protein_coding	6.296142	0.00212
FAM212B	protein_coding	-2.21179	0.002125
CD302	protein_coding	-2.80141	0.002127
EIF5A	protein_coding	2.796132	0.002194
NMI	protein_coding	2.672538	0.002194
HEPH	protein_coding	-3.13156	0.002267
ARSD	protein_coding	-4.00458	0.002279
GPR137B	protein_coding	-2.75987	0.002347
CHI3L2	protein_coding	3.063165	0.002375
TAP1	protein_coding	2.141476	0.002465
MCM3	protein_coding	2.681419	0.002476
ARIH2	protein_coding	1.820952	0.002476
HS2ST1	protein_coding	-2.56134	0.00253
MCC	protein_coding	-3.9494	0.002612
STARD4	protein_coding	3.525863	0.002675
GJA1	protein_coding	-1.85417	0.002738
TXN2	protein_coding	-2.97688	0.00283
CLTA	protein_coding	-2.21278	0.002908
TMPRSS2	protein_coding	6.286064	0.002911
USP30-AS1	antisense	6.772524	0.002939
PDE8B	protein_coding	-4.28696	0.00302
LANCL1	protein_coding	-3.28729	0.003024
CYP7B1	protein_coding	7.481329	0.003024
ZCCHC6	protein_coding	2.282404	0.003028
AC107294.2	lincRNA	-7.93664	0.003055
LINC00158	lincRNA	6.148305	0.003189
PDGFC	protein_coding	2.844458	0.003189
RAD51	protein_coding	3.080885	0.003203
COL21A1	protein_coding	-3.5232	0.003257
PBX1	protein_coding	-3.25201	0.003307
SYT13	protein_coding	-3.84904	0.003332
TTC39C	protein_coding	3.457576	0.003332
BRINP1	protein_coding	-6.47785	0.003335
SDC4	protein_coding	2.43706	0.003357
KCTD15	protein_coding	-3.64198	0.003357
HSD3B7	protein_coding	2.510088	0.003357
MRPL35	protein_coding	-2.73107	0.003381
NOL8	protein_coding	2.57659	0.003439
ACAT2	protein_coding	-2.50926	0.003449
G0S2	protein_coding	4.164258	0.00349
C9orf40	protein_coding	2.31059	0.003502
THAP6	protein_coding	-4.17381	0.003759
APIP	protein_coding	-3.05918	0.003759
PEBP1	protein_coding	-2.2013	0.003759
HS3ST1	protein_coding	-3.60359	0.003759
PLK4	protein_coding	3.58429	0.003759
RNF144B	protein_coding	3.643817	0.003759

BTG3	protein_coding	1.568042	0.003867
EIF2B5	protein_coding	2.204227	0.003871
DGCR2	protein_coding	-3.64954	0.003871
ANK1	protein_coding	4.722945	0.003871
SLC27A6	protein_coding	-5.44326	0.003958
GFPT2	protein_coding	1.870648	0.004013
PAPOLA	protein_coding	-1.57195	0.004013
POLD1	protein_coding	3.621792	0.004013
PLA2G12A	protein_coding	3.107932	0.004052
CACNG4	protein_coding	-4.22566	0.004101
BUD13	protein_coding	3.182901	0.004127
BTN3A2	protein_coding	2.965582	0.004154
FGFR2	protein_coding	-3.78255	0.004158
CHMP2B	protein_coding	-2.63449	0.004172
RASAL2	protein_coding	-3.1613	0.00427
MT2A	protein_coding	2.179491	0.004345
DONSON	protein_coding	3.590092	0.004352
BIRC2	protein_coding	3.364203	0.004418
SLC39A8	protein_coding	3.551704	0.004418
FEN1	protein_coding	2.445976	0.004418
CENPN	protein_coding	2.851676	0.00443
S100B	protein_coding	-3.04814	0.004461
TNFSF18	protein_coding	6.449892	0.004567
FP236241.1	lincRNA	4.4222	0.004665
SH3KBP1	protein_coding	3.945296	0.004694
FBXO32	protein_coding	-2.50669	0.004712
HSPB7	protein_coding	-3.28479	0.004729
NRN1	protein_coding	-2.40494	0.004729
GINS2	protein_coding	3.297212	0.005037
SERPINI1	protein_coding	-2.60043	0.005069
IPO4	protein_coding	-2.04928	0.005477
PDCL	protein_coding	-4.05119	0.005586
DACH1	protein_coding	-2.66315	0.005652
HIF1A	protein_coding	-1.61291	0.005675
UG0898H09	lincRNA	-3.86938	0.005704
SDC1	protein_coding	-2.20197	0.005735
TNFRSF1B	protein_coding	5.42141	0.005735
TMEM158	protein_coding	2.944442	0.00574
ARSE	protein_coding	-5.08626	0.006057
SERTAD4-AS1	antisense	-4.18997	0.00616
FSTL3	protein_coding	2.676284	0.00616
NEDD9	protein_coding	-2.78647	0.006179
TMPO	protein_coding	2.156416	0.006256
ETV7	protein_coding	6.580957	0.006256
GBP2	protein_coding	2.718419	0.006313
AC008966.1	antisense	-3.58781	0.006544
INSIG1	protein_coding	-2.16824	0.006569
TRAFD1	protein_coding	1.996582	0.006669
SLC40A1	protein_coding	-3.3934	0.006789
TMEM53	protein_coding	-4.01088	0.006814
SEL1L	protein_coding	2.62765	0.00708
HIVEP2	protein_coding	3.444655	0.00708
KDM6A	protein_coding	2.190799	0.00709
UBE2W	protein_coding	-1.93738	0.007116
AC241585.2	transcribed_unprocessed_pseudogene	4.262452	0.007157
GSN	protein_coding	-1.91583	0.007328
E2F1	protein_coding	1.898009	0.007349
SORBS1	protein_coding	-4.51159	0.007378
RAD1	protein_coding	2.003959	0.007541
NUP62	protein_coding	2.031971	0.007981
PRKX	protein_coding	-4.24479	0.007981
C8orf46	protein_coding	4.118849	0.007981
SLC19A1	protein_coding	4.566876	0.00805
LIPG	protein_coding	2.917533	0.00805
OPHN1	protein_coding	-2.41932	0.008147
CENPC	protein_coding	4.490874	0.008147
WT1	protein_coding	6.689414	0.008147
IQCJ-SCHIP1	protein_coding	-2.31471	0.008183
FZD7	protein_coding	2.031259	0.008236
BPGM	protein_coding	2.482575	0.008296
LTBP1	protein_coding	3.211118	0.008342
ANGPTL2	protein_coding	-1.69723	0.008468
LINC01158	processed_transcript	-2.91229	0.008503
METTL13	protein_coding	2.41022	0.008503
DESI1	protein_coding	1.978883	0.008503
RPRM	protein_coding	-6.12835	0.008516
ALKBH8	protein_coding	-3.61024	0.00854
PLAA	protein_coding	-2.09992	0.008556
NUDT11	protein_coding	-3.36178	0.008628
SLAMF8	protein_coding	6.431446	0.008728
BEX3	protein_coding	-1.70551	0.008891
FAM3C2	processed_pseudogene	-2.39512	0.008936
DCBLD1	protein_coding	3.107953	0.008936
PHYHIPL	protein_coding	-4.37828	0.008936
ATXN1	protein_coding	-2.5403	0.009009
SLITRK6	protein_coding	-6.21571	0.00908
CXCL3	protein_coding	6.414747	0.00908
PDLIM4	protein_coding	2.209161	0.009178
ARHGEF7	protein_coding	-2.75171	0.009178
GRIN2A	protein_coding	-4.19472	0.009178
MRE11	protein_coding	2.535011	0.009191
FBRS	protein_coding	2.53905	0.009266
CHRM3	protein_coding	-3.71062	0.009266
LINC00511	lincRNA	-2.88551	0.009333
CCNL1	protein_coding	2.530469	0.009333
KCTD12	protein_coding	-2.3872	0.009402
CLIC1	protein_coding	2.033437	0.009436
FNBP1L	protein_coding	-3.06348	0.009496
SLTM	protein_coding	-2.92414	0.009566
PQBP1	protein_coding	1.93327	0.009572
BRCC3	protein_coding	-2.88298	0.009572
BICC1	protein_coding	-2.23984	0.009642
PLPPR4	protein_coding	-2.54663	0.009833
CDH11	protein_coding	-3.06902	0.009867
SLC12A7	protein_coding	3.972747	0.009974
MRPL43	protein_coding	1.80368	0.010089
ADIPOR1	protein_coding	-2.01768	0.010089
NTN1	protein_coding	3.28664	0.010296
B3GNT5	protein_coding	2.593828	0.010296
ERI3	protein_coding	-1.50024	0.010385
INSIG2	protein_coding	3.07602	0.010447
RETREG1	protein_coding	-3.14212	0.010502
GAK	protein_coding	2.962832	0.01054
DAPK2	protein_coding	3.989297	0.0106
KIF18A	protein_coding	3.337843	0.010731
ANPEP	protein_coding	2.686325	0.010738
SVIP	protein_coding	2.8531	0.010846
CDR2	protein_coding	2.517014	0.011015
ITGA5	protein_coding	1.791877	0.011015
TLR7	protein_coding	6.403586	0.011015
SMARCA5	protein_coding	2.992163	0.011078
PSMA2	protein_coding	1.842815	0.011078
AC012184.2	protein_coding	-6.4185	0.011078

ZKSCAN1	protein_coding	-2.21531	0.011078
WDR45	protein_coding	1.892874	0.011078
UNC13A	protein_coding	6.756125	0.011078
FAM19A3	protein_coding	6.73343	0.011078
JOSD2	protein_coding	-2.96677	0.011084
ZKSCAN8	protein_coding	-2.21245	0.011084
MORF4L1	protein_coding	-1.50544	0.011221
SQOR	protein_coding	2.905348	0.011324
CDK1	protein_coding	2.936312	0.01143
HRCT1	protein_coding	-5.03997	0.01149
VPS36	protein_coding	2.458115	0.01149
FAM214B	protein_coding	-3.09658	0.011527
NCBP2	protein_coding	-2.23621	0.011563
ITGA2	protein_coding	2.093439	0.011629
INO80D	protein_coding	3.692942	0.012091
C1QTNF1	protein_coding	2.958987	0.012103
ADCK2	protein_coding	-1.85066	0.0124
ISG20	protein_coding	4.583848	0.0124
CSF1	protein_coding	2.591401	0.012517
MAT2A	protein_coding	-2.59287	0.012517
TMEM189-UBE2V1	protein_coding	7.388972	0.012696
NFKBIZ	protein_coding	3.012183	0.012762
LZTS1	protein_coding	-4.35197	0.012791
PPP1R3F	protein_coding	-4.25603	0.013099
PHKA2	protein_coding	3.562051	0.013099
AL445686.2	lincRNA	-5.90701	0.013119
GPM6B	protein_coding	-2.13869	0.013127
MARCKSL1	protein_coding	2.55638	0.013274
ATRIP	protein_coding	4.24944	0.013401
FBXO44	protein_coding	-3.16788	0.013826
TCF19	protein_coding	2.62717	0.013908
CHCHD3	protein_coding	-2.09313	0.014051
CAPS	protein_coding	-2.56101	0.014092
CREB3L1	protein_coding	3.076689	0.014604
NEK6	protein_coding	-3.70506	0.014608
ISCU	protein_coding	-1.68923	0.014608
SLC26A2	protein_coding	-1.89628	0.014608
MAP4	protein_coding	-2.79662	0.014729
CENPU	protein_coding	2.156513	0.014739
LRP6	protein_coding	-2.66324	0.014739
GPRC5A	protein_coding	-3.47129	0.014739
AGK	protein_coding	2.733947	0.014778
PPIAP22	processed_pseudogene	-3.26642	0.014939
DACT1	protein_coding	-3.15143	0.015027
LMO7	protein_coding	2.416246	0.015169
MMP15	protein_coding	-3.1967	0.015181
LRRC17	protein_coding	-2.16402	0.015412
ENKD1	protein_coding	2.339968	0.015412
RGS16	protein_coding	2.469132	0.015441
ACTC1	protein_coding	-5.59925	0.015441
MXI1	protein_coding	-2.16981	0.015512
CAMK2N1	protein_coding	-1.98267	0.015512
P2RY1	protein_coding	-2.37937	0.015512
SLC35G1	protein_coding	3.392269	0.015564
FAM133B	protein_coding	-2.20043	0.015577
RTP4	protein_coding	4.40059	0.015577
SHROOM1	protein_coding	3.735532	0.016019
ACLY	protein_coding	1.554129	0.016019
TUBB3	protein_coding	-2.03956	0.016019
CAP2	protein_coding	-2.32241	0.016141
ZNF181	protein_coding	-2.31141	0.016174
NT5E	protein_coding	1.670751	0.016174
IMMT	protein_coding	-2.91158	0.016469
CD24	protein_coding	-6.06664	0.016488
GPCPD1	protein_coding	-3.43517	0.016488
ANXA1	protein_coding	-1.56276	0.016646
FAM107B	protein_coding	2.366256	0.016727
KIAA1644	protein_coding	3.74812	0.016727
AGO1	protein_coding	-1.82537	0.017069
AOX1	protein_coding	3.894435	0.017081
RDX	protein_coding	1.285485	0.017125
MITD1	protein_coding	2.637918	0.017132
CEMIP	protein_coding	3.883449	0.01741
ZNF358	protein_coding	3.020286	0.017642
FAM174A	protein_coding	-2.31025	0.017656
S1PR1	protein_coding	-4.00241	0.017656
MSH3	protein_coding	-2.80478	0.017656
MCM7	protein_coding	1.67389	0.017683
DHDDS	protein_coding	-2.53052	0.017683
PFKL	protein_coding	2.492473	0.017738
WDR76	protein_coding	2.400519	0.018213
MKLN1	protein_coding	-2.62611	0.018213
AC120049.1	lincRNA	-6.56156	0.018292
KPNA3	protein_coding	-2.76558	0.018478
LINC01579	lincRNA	-2.41607	0.018566
MICU1	protein_coding	-2.24893	0.018592
PREP	protein_coding	-1.5231	0.018699
AL357060.3	antisense	6.739413	0.01888
ATG4C	protein_coding	-2.20591	0.01888
GPANK1	protein_coding	3.3629	0.018919
MYCBP2	protein_coding	2.768101	0.019525
MEAF6	protein_coding	-1.85167	0.019527
ZNF316	protein_coding	5.154515	0.01958
ZNF37BP	transcribed_processed_pseudogene	4.268502	0.01958
PSMA6	protein_coding	1.368778	0.019615
POC1A	protein_coding	1.93596	0.019673
CAT	protein_coding	-1.69035	0.019767
VPS26B	protein_coding	-1.77043	0.019786
TRMT2B	protein_coding	2.529041	0.019789
FAM181B	protein_coding	-6.65924	0.019821
KIAA1217	protein_coding	2.860802	0.019989
CENPBD1P1	transcribed_processed_pseudogene	-1.96897	0.019989
IRF2BPL	protein_coding	-3.04187	0.020068
FAXDC2	protein_coding	-4.60632	0.020235
MGST2	protein_coding	-3.89399	0.020235
GALNT10	protein_coding	-1.56637	0.020235
UROD	protein_coding	-1.52037	0.020407
RAB13	protein_coding	2.941908	0.020473
RP2	protein_coding	2.416879	0.020473
FAM111B	protein_coding	3.091505	0.020473
SERPINH1	protein_coding	-2.55953	0.020495
MLLT11	protein_coding	-2.38348	0.020523
GTF2E2	protein_coding	3.082674	0.020871
ITPR2	protein_coding	-2.64196	0.021092
ARHGEF17	protein_coding	-2.78454	0.021103
RNLS	protein_coding	-3.91049	0.021103
IL24	protein_coding	7.261391	0.021103
SNAI1	protein_coding	-3.33204	0.021194
RUSC2	protein_coding	-4.68073	0.021299
WASHC4	protein_coding	-2.35518	0.021349
SPPL3	protein_coding	1.680212	0.021432
SENP3-EIF4A1	protein_coding	12.68184	0.021479
RBM15	protein_coding	2.243767	0.02159

CEP89	protein_coding	2.324115	0.021743
SRPRA	protein_coding	-1.56144	0.021764
EMC3-AS1	transcribed_unprocessed_pseudogene	6.474534	0.021767
WDR12	protein_coding	-3.19253	0.021904
PSMB10	protein_coding	2.068308	0.022185
ZNF436-AS1	antisense	-5.83463	0.022319
MAGEA3	protein_coding	3.939745	0.023112
LYN	protein_coding	3.47241	0.02338
AL031056.2	lincRNA	-6.40752	0.023563
PSME4	protein_coding	3.015487	0.023563
BAG5	protein_coding	-1.98524	0.023563
ATP6V0E2-AS1	antisense	5.585533	0.023707
MYLK	protein_coding	-1.91673	0.023851
LTA4H	protein_coding	-2.1035	0.023869
CBWD2	protein_coding	2.073544	0.023912
FBXO30	protein_coding	-2.31609	0.024058
BICD1	protein_coding	-2.44237	0.024058
SOX21-AS1	lincRNA	-3.33851	0.024085
POLB	protein_coding	-3.69124	0.024354
AL590399.1	lincRNA	-6.18742	0.024479
PSMA5	protein_coding	1.277123	0.0245
SH3PXD2B	protein_coding	-2.79154	0.0245
GLRB	protein_coding	2.879802	0.024613
LRP10	protein_coding	-2.27663	0.024639
CX3CL1	protein_coding	2.256269	0.024672
ITGA11	protein_coding	-3.42692	0.024787
P3H2	protein_coding	2.122786	0.024851
TMEM51	protein_coding	4.195708	0.024851
ZBTB11	protein_coding	-2.79725	0.024936
SNHG18	lincRNA	-2.65459	0.025104
TOX	protein_coding	-3.87566	0.025194
AC015912.1	antisense	4.764885	0.025205
LDHA	protein_coding	1.486205	0.025353
KLHL8	protein_coding	-2.88578	0.025353
TNFSF13B	protein_coding	4.039407	0.025353
TSPY26P	transcribed_processed_pseudogene	-3.6798	0.02541
DTX4	protein_coding	4.364762	0.025726
PPID	protein_coding	2.485812	0.025841
ORAOV1	protein_coding	3.609586	0.026064
CBLL1	protein_coding	2.437882	0.026114
LEPR	protein_coding	2.551248	0.026191
SIPA1L1	protein_coding	-2.82754	0.02628
CLSTN3	protein_coding	4.9698	0.026571
ASB3	protein_coding	2.651053	0.026752
CHST10	protein_coding	-4.07059	0.026881
SETD7	protein_coding	-2.32128	0.027151
GIMAP2	protein_coding	3.54559	0.027185
RAMP1	protein_coding	-5.86892	0.027734
RRM2	protein_coding	2.075958	0.028202
NR2F1	protein_coding	-2.15306	0.028202
NDFIP1	protein_coding	-1.59146	0.028202
ANGPT2	protein_coding	-2.17093	0.028202
OXSR1	protein_coding	3.000107	0.028228
GLIDR	lincRNA	-3.19578	0.028265
JMJD6	protein_coding	2.521143	0.028265
CBLB	protein_coding	2.924375	0.02839
FMO5	protein_coding	2.913858	0.02839
AFF3	protein_coding	3.879151	0.02839
SLC35A1	protein_coding	-1.90855	0.028549
MITF	protein_coding	-2.86694	0.028556
HSCB	protein_coding	-3.04136	0.028556
FAM126B	protein_coding	-2.72512	0.028807
AC016876.2	processed_transcript	12.23002	0.028969
HOMEZ	protein_coding	-5.0621	0.028969
EDC4	protein_coding	2.245227	0.029007
PRDM5	protein_coding	-2.94345	0.029007
ALK	protein_coding	-5.46032	0.029007
ZFAND5	protein_coding	-2.02376	0.029007
EMP3	protein_coding	1.569118	0.029007
ASPSCR1	protein_coding	2.280098	0.029007
PLLP	protein_coding	3.357818	0.029014
PUDP	protein_coding	-3.55692	0.029014
BTN3A1	protein_coding	1.894422	0.029032
MXRA8	protein_coding	-2.58714	0.029032
SMARCA1	protein_coding	-2.97207	0.029129
RNF145	protein_coding	1.486143	0.029282
TRAK1	protein_coding	-2.28905	0.029312
FADS1	protein_coding	1.998718	0.029786
SLC7A5	protein_coding	1.848789	0.030057
ZNF446	protein_coding	-3.77863	0.030248
CCT8	protein_coding	1.506924	0.030306
BORCS7-ASMT	protein_coding	-5.89158	0.030316
SLC25A18	protein_coding	-2.41663	0.030628
AC005562.1	processed_transcript	-2.67332	0.030866
AATF	protein_coding	3.042435	0.030867
BRF2	protein_coding	2.56095	0.030877
KIAA1161	protein_coding	-3.04051	0.030877
PTK2	protein_coding	1.405356	0.030896
EFEMP1	protein_coding	-1.4067	0.030971
PATJ	protein_coding	-2.88495	0.030971
AQP1	protein_coding	-4.37884	0.030971
CANX	protein_coding	4.444868	0.030996
LPXN	protein_coding	2.652249	0.031541
UNC13B	protein_coding	-2.60799	0.031637
C4orf33	protein_coding	-3.27197	0.031852
TRIM21	protein_coding	1.763362	0.032012
SCRG1	protein_coding	-2.07709	0.032109
EZH2	protein_coding	2.454306	0.032206
PCDHGB2	protein_coding	-3.72763	0.032206
CYLD	protein_coding	1.777494	0.032261
D21S2088E	lincRNA	-5.21267	0.03242
DENND1B	protein_coding	-3.46321	0.032608
LINC00623	lincRNA	3.639389	0.032671
ABI2	protein_coding	-1.72619	0.03278
KLHL13	protein_coding	-2.71168	0.03278
ZNF615	protein_coding	-4.20748	0.03278
TSC22D1	protein_coding	-2.05784	0.03278
CCDC152	protein_coding	-3.14283	0.03278
RAP1GDS1	protein_coding	1.613485	0.032856
EP300	protein_coding	-3.8306	0.032928
SLC41A3	protein_coding	-2.49561	0.03293
OSTF1	protein_coding	2.403618	0.032965
ZNF680	protein_coding	-3.32713	0.032965
SOX2	protein_coding	-1.94926	0.032965
ARPC5L	protein_coding	1.512933	0.033068
ENDOG	protein_coding	-3.21931	0.033068
CENPQ	protein_coding	2.189947	0.033442
SYNC	protein_coding	-3.5038	0.033495
BDNF	protein_coding	3.761504	0.033495
TGFBR3	protein_coding	1.884485	0.033685
PRKD1	protein_coding	-2.356	0.033702
CERS5	protein_coding	1.690726	0.033717
SRPK1	protein_coding	2.025621	0.033826

CSRNP3	protein_coding	-4.18218	0.033826
FP565260.1	protein_coding	1.406067	0.033949
AC008608.2	lincRNA	-6.32789	0.033966
MATR3	protein_coding	2.783611	0.033966
TSPAN13	protein_coding	-2.28953	0.033966
COPS3	protein_coding	-2.07992	0.033966
QTRT2	protein_coding	-2.10275	0.034263
PSMB7	protein_coding	1.603062	0.034491
NCSTN	protein_coding	-2.51387	0.035105
EPHB2	protein_coding	1.778195	0.035177
CDK19	protein_coding	-1.40271	0.035268
UTRN	protein_coding	-2.25719	0.035268
NFKBIE	protein_coding	2.159142	0.035367
SNHG6	processed_transcript	2.691855	0.035499
TMEM185B	protein_coding	2.612501	0.035499
ZSCAN31	protein_coding	-3.33871	0.035499
TNFSF4	protein_coding	3.15069	0.035499
ZBED3	protein_coding	-3.96392	0.035499
AC009902.3	lincRNA	-6.5055	0.035743
DYNC2H1	protein_coding	3.233626	0.035798
OAS1	protein_coding	3.217841	0.036211
HSPB8	protein_coding	-1.42044	0.036211
CSF2	protein_coding	6.917529	0.036211
TNFRSF21	protein_coding	-2.32831	0.036271
TIPARP	protein_coding	-2.06305	0.036271
PAPD4	protein_coding	1.712069	0.036271
RASA2	protein_coding	3.505008	0.036271
TRIB2	protein_coding	-1.85774	0.036357
LRAT	protein_coding	5.480467	0.036357
UBE2T	protein_coding	2.239134	0.036541
SNX16	protein_coding	-2.67419	0.036541
MSN	protein_coding	1.721691	0.036969
PMEPA1	protein_coding	2.359868	0.037159
ITGB5	protein_coding	-2.35893	0.037254
GDF11	protein_coding	-3.24959	0.03726
S100A3	protein_coding	2.011469	0.037409
CMPK2	protein_coding	3.895471	0.037645
BDH2	protein_coding	-2.33537	0.037767
AQP4	protein_coding	-3.27643	0.038046
APOBEC3G	protein_coding	1.698139	0.03818
PRKCE	protein_coding	-3.14885	0.038207
KDM3B	protein_coding	2.321686	0.038246
PRDX6	protein_coding	1.351725	0.038434
IQCG	protein_coding	2.72638	0.038544
METRN	protein_coding	-1.80278	0.038719
ABLIM1	protein_coding	-3.01174	0.038719
KIAA0368	protein_coding	2.030112	0.038917
MPC2	protein_coding	1.297564	0.038927
BTBD9	protein_coding	3.001876	0.038959
ST8SIA1	protein_coding	4.033442	0.039017
SCFD1	protein_coding	2.106537	0.039068
SEC31A	protein_coding	1.52824	0.039068
PTPA	protein_coding	-1.60726	0.039068
SPTY2D1-AS1	protein_coding	-6.61369	0.039068
PDZRN3	protein_coding	-1.70808	0.039068
FREM2	protein_coding	-1.92897	0.039609
SCUBE3	protein_coding	-4.05593	0.039609
AC098864.1	antisense	-4.89742	0.04023
SERPINE1	protein_coding	2.152826	0.04023
TBCEL	protein_coding	-2.17659	0.04023
NCAPG	protein_coding	2.397601	0.040347
CTSL	protein_coding	-1.41203	0.040347
CCDC150	protein_coding	5.651653	0.040583
TSPAN2	protein_coding	3.397514	0.040698
TPST2	protein_coding	2.440835	0.040801
FANCD2	protein_coding	3.358617	0.040822
WDR53	protein_coding	3.152121	0.040822
SHMT2	protein_coding	1.437893	0.040822
DLAT	protein_coding	-2.20276	0.040822
NFIA	protein_coding	-4.35361	0.040949
FZD4	protein_coding	-2.15968	0.04112
ZFR	protein_coding	-2.35018	0.041129
C1orf112	protein_coding	2.398068	0.041724
ARRDC2	protein_coding	2.760408	0.041724
SLC20A2	protein_coding	-2.47307	0.041921
TRA2A	protein_coding	2.679504	0.041993
RAN	protein_coding	1.476788	0.041993
TWF2	protein_coding	1.638939	0.041993
BTBD3	protein_coding	-1.75702	0.041993
TENM4	protein_coding	-4.26122	0.041993
AL109918.1	transcribed_unprocessed_pseudogene	2.850222	0.042074
DHCR24	protein_coding	-1.49687	0.04222
COLGALT2	protein_coding	-1.45795	0.04231
ELOVL5	protein_coding	-1.74363	0.04231
C1orf216	protein_coding	-2.56097	0.042407
TM2D1	protein_coding	-1.73901	0.042438
SYPL1	protein_coding	-1.59455	0.042438
BCL3	protein_coding	2.268488	0.042483
TRAC	TR_C_gene	-3.78836	0.04255
AP001931.1	protein_coding	6.71383	0.042685
MCM6	protein_coding	1.633153	0.042732
DLD	protein_coding	1.922568	0.042848
SPIN3	protein_coding	-4.16741	0.042904
RCHY1	protein_coding	-3.47397	0.042913
CARF	protein_coding	-2.91879	0.043455
THAP2	protein_coding	-2.34256	0.043612
CADPS	protein_coding	-3.73068	0.043612
CCDC191	protein_coding	-4.50159	0.043612
SLC23A2	protein_coding	-1.68918	0.043612
GCOM1	protein_coding	6.192296	0.043651
ABCA13	protein_coding	-2.7818	0.043787
FN1	protein_coding	3.116739	0.043882
FOS	protein_coding	-3.09944	0.044011
RAPGEF4	protein_coding	6.718654	0.044036
HIPK2	protein_coding	-2.02524	0.044186
SCRN3	protein_coding	-2.64469	0.044186
KCNQ3	protein_coding	5.08117	0.04451
RNF2	protein_coding	2.318739	0.044729
PPARGC1A	protein_coding	-3.25705	0.044729
FKBP9	protein_coding	-1.632	0.044729
SEC61G	protein_coding	-2.46945	0.044729
GPRC5B	protein_coding	-2.26665	0.044734
SLC2A10	protein_coding	-1.90211	0.044743
CEND1	protein_coding	-4.10026	0.044758
SNRNP200	protein_coding	-1.76029	0.044763
MFHAS1	protein_coding	2.622908	0.044794
EIF5B	protein_coding	2.944472	0.044823
NAF1	protein_coding	-2.36422	0.044823
TBKBP1	protein_coding	-4.31044	0.045095
COL1A2	protein_coding	-1.44614	0.045175
SLC25A46	protein_coding	1.523839	0.045175
FRMD3	protein_coding	-3.28565	0.045218
CFLAR	protein_coding	2.2522	0.045246

LDB2	protein_coding	-2.68489	0.045246
LINC02475	lincRNA	-3.17192	0.04556
LRRC41	protein_coding	-2.30827	0.04556
PTPRG	protein_coding	-1.64992	0.046387
MGME1	protein_coding	1.902015	0.046387
EFNA1	protein_coding	2.133112	0.046461
IQGAP1	protein_coding	1.394754	0.046461
TRIM11	protein_coding	-3.6364	0.046461
TRAF3IP2	protein_coding	2.72156	0.046473
TRIL	protein_coding	-3.96943	0.046473
IFITM2	protein_coding	-2.6007	0.046591
ITSN2	protein_coding	2.101112	0.047073
ATF7IP	protein_coding	1.829351	0.047073
NT5DC1	protein_coding	2.596839	0.047961
ACTR1B	protein_coding	1.646808	0.047961
ETS1	protein_coding	1.789483	0.048011
EPB41L4A-AS1	lincRNA	-2.13182	0.048027
ARSK	protein_coding	-2.7033	0.048327
SMAD1-AS1	antisense	6.799161	0.048364
ADAMTS9	protein_coding	2.448779	0.048364
CDCA7	protein_coding	3.66701	0.048364
MCOLN2	protein_coding	5.342591	0.048364
XRCC4	protein_coding	-3.19062	0.048364
SALL1	protein_coding	-3.10391	0.048364
ICK	protein_coding	-2.38211	0.048577
PEPD	protein_coding	-2.32574	0.048914
ZBTB20	protein_coding	-3.74554	0.049033
DRAP1	protein_coding	1.515283	0.049033
RPL39L	protein_coding	2.547045	0.049256
TTLL7	protein_coding	1.55352	0.049353
CLIP3	protein_coding	3.028284	0.049417
ARHGEF11	protein_coding	2.145184	0.049417
LDLRAD4	protein_coding	-2.99033	0.049417
SULF1	protein_coding	-1.85097	0.049417
STK32A	protein_coding	-3.07973	0.049417
COL8A1	protein_coding	-1.63646	0.049811
USP13	protein_coding	1.434353	0.049811
CENPI	protein_coding	3.117856	0.049852
RFC5	protein_coding	1.900023	0.049852
CREBRF	protein_coding	-1.89791	0.049852

Publications

1. Eastlake, K., **Wang, W**., Jayaram, H., Murray-Dunning, C., Carr, A. J. F., Ramsden, C. M., . . . Limb, G. A. (2019). Phenotypic and Functional Characterization of Müller Glia Isolated from Induced Pluripotent Stem Cell-Derived Retinal Organoids: Improvement of Retinal Ganglion Cell Function upon Transplantation. Stem Cells Transl Med. doi:10.1002/sctm.18-0263

2. Eastlake, K., **Wang, W**., Lamb, W. D. B., & Limb, G. A. (2018). CHAPTER 12: Stem Cell Therapies for Retinal Repair and Regeneration. RSC Drug Discovery Series, 2019-January (66), 196-215. doi:10.1039/9781788013666-00196